RECONSTRUCTING OCEANOGRAPHIC CONDITIONS THROUGH THE DEGLACIAL AND HOLOCENE (CA. 15 KA) AT THE SUB-ANTARCTIC ISLAND OF SOUTH GEORGIA

ROWAN DEJARDIN MGeol

Thesis submitted to the University Of Nottingham
for the degree of Doctor of Philosophy

JUNE 2018

Acknowledgments

I would like to thank my supervisors Sev Kender, George Swann, Mel Leng, Vicky Peck, and Claire Allen for providing me with the opportunity to work on this project, and for all their support, guidance, and patience throughout this Ph.D. Thanks also to the captain, crew, and science parties of the RRS *James Clark Ross*, on cruises JR527 and JR15002, for the acquisition of the material that form the basis of this thesis, and for making my trip to the Southern Ocean so memorable. Further thanks goes to all the technical staff, across a range of institutions, who enabled the generation of the data presented in this thesis. Especial thanks to Teresa Needham and Ian Conway at the University of Nottingham, Hillary Sloane and Jack Lacey at the British Geological Survey, and Maria Luisa Sanchez-Montes, Amanda Hayton, and Martin West at the University of Durham. I would also like to thank Erin McClymont for allowing me to come and work in her lab at the University of Durham to generate the alkenone data.

During this PhD I have meet many excellent people, in the department at Nottingham, at conferences, and at summer schools, with whom I have shared lots of fun times! Extra thanks goes to Becca Thorne, for being generally ace, Betsabe de la Barreda Bautista, for teaching me many espanish insults, Teresa (again), Joseph John Bailey, for insight and R (and GIS) support, Nick 'Primsy-Pops' Primmer, and Ginnie Panizz(i)o. Thanks to all my other friends and family who have supported through this endeavour.

This research was possible thanks to a 3.5 year studentship funded by the Centre for Environmental Geochemistry, with additional CASE scholarship from the British Geological Survey. Geochemical analysis was supported by NERC Isotope Geoscience Facility Grant IP/1495/1114 (RCUK). Radiocarbon dating was, in part, funded by the NERC Radiocarbon Facility Steering Committee (Allocation Number 1944.1015). Participation in scientific cruise JR15002 was supported the British Antarctic Survey Collaborative Gearing Scheme.

Abstract

South Georgia is located in the path of the Antarctic Circumpolar Current (ACC) and the Southern Hemisphere Westerly Winds (SWW), south of the Antarctic Polar Front (APF) and surrounded by an anticyclonic loop of the Southern ACC Front (SACCF). The waters surrounding South Georgia are highly productive and variability in the interaction of the SACCF with the island may impact productivity on the shelf. Of wider significance is the large phytoplankton bloom that occurs to the north-west of South Georgia, where the SACCF retroflects to return to its cyclonic circumpolar circulation. This bloom represents one of the largest seasonal sinks of atmospheric CO_2 in the Southern Ocean. Given the likely importance of the Southern Ocean as a carbon sink/source during the transition between glacial and interglacial periods a better understanding of the bloom dynamics could be important to our assessment of the Southern Ocean's role in these transitions. This thesis investigates deglacial and Holocene variability in productivity and sea-surface temperature on the north-eastern shelf of South Georgia, through the development of the first palaeoceanographic records from the island.

To support the palaeoceanographic interpretation a comprehensive taxonomic study of the benthic foraminifera of the South Georgia shelf was developed, and the importance of foraminiferal ecology to test carbon isotope composition was investigated. The taxonomic assessment of the shelf benthic foraminifera resulted in the description of 78 species, assigned to 57 genera from 34 families (of these 58 species are identified to species level, while 20 species are discussed in open nomenclature). The investigation of foraminiferal ecology highlighted the importance of understanding the ecology of the species being utilised for isotope analysis to the application of this data to palaeoceanographic interpretations. In addition, a novel calcification strategy was proposed, in which a most benthic foraminiferal calcification occurs at the sediment-seawater interface.

The palaeoceanographic records presented here support the hypothesis that the ice sheet on South Georgia during the Last Glacial Maximum extended onto the shelf. Potential evidence for the formation of a calving bay re-entrant over Royal Bay trough indicates that grounded ice may have been present on the shallower shelf until ca. 15 cal. kyr BP, having retreated rapidly over the deeper cross shelf troughs after the Last Glacial Maximum. Evidence is also found for the influence of the Antarctic Cold Reversal at South Georgia. During the Holocene, I propose that both sea-surface temperature (SST) and shelf productivity may have been driven by variation in the SWW, except during the early Holocene when sea-ice proximity may play an important role in productivity variability. Changes in the intensity of

the SWW at South Georgia drive SST through their impact of local foehn wind frequency and shelf productivity through variation in coastal upwelling. This interpretation of the variability in shelf SST and productivity indicates that the SWW were more intense at South Georgia during the mid-Holocene, and weaker during the early and late Holocene. Similar patterns of SWW variability have been reported from other locations at the same latitude, although some records have been interpreted to reveal different patterns of SWW change. Variation in SWW intensity at South Georgia may be due to either latitudinal migration of the SWW, or to expansion and contraction of the core SWW band, both of which are linked to Southern Hemisphere temperature change.

Contents

Contents i
List of Figures vii
List of Tables ix
List of Acronyms and Abbreviations xi
Chapter 1 1
Introduction 1
1.1 Motivation 1
1.1.1 Why is palaeoceanography important? 1
1.1.2 The relevance of South Georgia and the Southern Ocean 3
1.1.3 Project aims 4
1.2 South Georgia modern oceanography 4
1.2.1 Remote forcing of South Georgia ocean properties 8
1.2.2 Local forcing of South Georgia shelf-water properties 9
1.3 Southern Hemisphere palaeoclimate 10
1.3.1 Deglaciation and the Antarctic Cold Reversal 10
1.3.2 Holocene climatic periods 12
1.3.3 Southern Hemisphere forcing mechanisms 15
1.4 South Georgia palaeoclimate 16
1.4.1 Deglaciation and the ACR 16
1.4.2 The Holocene 20
1.5 Thesis outline 23
1.5.1 Chapter 2 – Materials, methods, and proxy application 23
1.5.2 Chapter 3 – Systematic taxonomy of Holocene South Georgia benthic foraminifera 23
1.5.3 Chapter 4 - Live (stained) benthic foraminiferal living depths and stable isotopes offshore South Georgia: implications for calcification depths 23
1.5.4 Chapter 5 – Results from gravity cores (GC666 and GC673) 24
1.5.5 Chapter 6 – Deglacial oceanography (~15.2 – 12.3 cal. kyr BP) 24
1.5.6 Chapter 7 – Holocene oceanography (~12.3 cal. kyr BP onwards) 24
1.5.7 Chapter 8 – Summary 24
Chapter 2 25
Materials, methods, and proxy application 25
2.1 Material 25
2.1.1 Sample acquisition 25
2.2 Methods 27
2.2.1 Dating and age/depth model development 27
2.2.1.1 Radiocarbon dating 27
2.2.1.2 Radiocarbon calibration and reservoir correction 28

2.2.1.3 Age/depth modelling 28
2.2.2 Benthic foraminiferal census counts 30
2.2.2.1 Sample preparation and counting protocol 30
2.2.2.2 Rose Bengal staining 31
2.2.2.3 BFA as a palaeoceanographic proxy 32
2.2.3 Foraminiferal stable isotopes 34
2.2.3.1 Sample preparation and analysis 34
2.2.3.2 Application of foraminiferal stable isotopes 36
2.2.4 Geochemistry of organic matter 41
2.2.4.1 Sample preparation and analysis 41
2.2.4.2 Application of organic geochemistry data 42
2.2.5 Biogenic silica analysis 43
2.2.5.1 Sample preparation and analysis 43
2.2.5.2 Application of BSi 44
2.2.6 Alkenone analysis 44
2.2.6.1 Sample preparation and analysis 44
2.2.6.2 Alkenones as a proxy for sea surface temperature 46
2.2.7 Statistical methods 48
2.2.7.1 Diversity 48
2.2.7.2 Dominance 48
2.2.7.3 Cluster analysis 48
2.2.7.4 Detrended correspondence analysis 49
2.3 Summary 49
Chapter 3 51
Systematic taxonomy of Holocene South Georgia benthic foraminifera 51
3.1 Introduction 51
3.1.1 Previous benthic foraminiferal studies 51
3.2 Foraminiferal assemblages 52
3.2.1 Surface samples 52
3.2.2 Box core sub-cores 53
3.2.3 Gravity cores 53
3.3 Comparison to other studies 53
3.4 Systematic taxonomy 54
Chapter 4 97
Live (stained) benthic foraminiferal living depths and stable isotopes offshore South Georgia: implications for calcification depths 97
4.1 Introduction 97
4.2 Results 98
4.2.1 Benthic foraminiferal depth distributions 98
4.3 Discussion 103
4.3.1 Foraminiferal living and calcification depths 103

4.3.2 Foraminiferal calcification strategies 108
4.3.3 Implications of sediment-seawater interface calcification for palaeoenvironmental research 110
4.4 Summary 111
Chapter 5 113
Results from Gravity Cores (GC666 and GC673) 113
5.1 Introduction 113
5.2 Core GC666 113
5.2.1 Age/depth model 113
5.2.1.1 Diagenetic alteration 115
5.2.2 Sedimentology 119
5.2.2.1 Sediment description 119
5.2.2.2 Coarse fraction quantification 120
5.2.3 Diatom assemblage composition 121
5.2.4 Benthic foraminiferal census counts 122
5.2.4.1 Diversity, Dominance and BFAR 122
5.2.4.2 Foraminiferal assemblages 124
5.2.4.3 Fursenkoina Assemblage 125
5.2.4.4 Miliammina Assemblage 128
5.2.4.5 Cassidulinoides/Astrononion Assemblage 130
5.2.5 Geochemistry of organic matter 135
5.2.6 Biogenic opal analysis 136
5.2.7 Foraminiferal stable isotope analysis 137
5.2.7.1 Benthic foraminiferal isotopes 137
5.2.7.2 Planktonic foraminiferal isotopes 139
5.2.8 Alkenone analysis 139
5.2.8.1 Samples with low alkenone concentration 142
5.3 Core GC673 144
5.3.1 Age/depth model 144
5.3.2 Sedimentology 145
5.3.2.1 Sediment description 145
5.3.2.2 Coarse fraction quantification 145
5.3.3 Benthic foraminiferal census counts 147
5.3.3.1 Diversity, dominance and BFAR 147
5.3.3.2 Foraminiferal assemblages 148
5.3.3.3 Group 1/Fursenkoina Assemblage 150
5.3.3.4 Group 2/Transition Assemblage 151
5.3.3.5 Group 3A 152
5.3.4 Geochemistry of organic matter 153
5.3.5 Biogenic opal analysis 154
5.3.6 Foraminiferal stable isotope analysis 155

5.4 Summary 157
5.4.1 GC666 157
5.4.2 GC673 158
Chapter 6 161
Deglaciation and the Antarctic Cold Reversal 161
6.1 Introduction 161
6.2 Discussion 163
6.2.1 Deglaciation at South Georgia 163
6.2.1.1 Laminated sediments (15.2−14.7 cal. kyr BP) 164
6.2.1.2 Productivity between 15.2 and 14.7 cal. kyr BP 169
6.2.2 The ACR at South Georgia (14.7−12.9 cal. kyr BP) 171
6.2.2.1 Post-ACR glacial retreat 174
6.2.3 Variation in ACC frontal location 176
6.3 Summary 178
Chapter 7 181
Holocene oceanography (~12.3 cal. kyr BP onwards) 181
7.1 Introduction 181
7.2 South Georgia shelf productivity during the Holocene 181
7.2.1 Holocene productivity variability in core GC666 184
7.2.2 Holocene productivity variability in core GC673 189
7.3 South Georgia shelf oceanography forcing mechanisms 194
7.3.1 Sea-ice proximity 194
7.3.2 Upwelling circumpolar deep water 197
7.3.3 Southern Hemisphere Westerly Wind variability 199
7.3.3.1 Modes of Holocene SWW variability 205
7.3.3.2 Drivers of Holocene Southern Hemisphere temperature 206
7.3.4 Evidence for a Southern Hemisphere 8.2 kyr event? 211
7.4 Summary 212
Chapter 8 215
Summary and conclusions 215
8.1 Introduction 215
8.2 Holocene South Georgia shelf benthic foraminifera 215
8.3 Foraminiferal ecology: implications for calcification depths 216
8.4 The deglacial and Holocene palaeoceanography of South Georgia 217
8.4.1 Background 217
8.4.2 Summary of multiproxy data from GC666 and GC673 218
8.4.3 Discussion 220
8.4.3.1 Calving bay re-entrant development during deglaciation 220
8.4.3.2 SWW variability as the primary driver of Holocene South Georgia shelf productivity and SST 221
8.5 Conclusions 223

8.6 Future work 224
References 227
Appendix A1 – GC666 Sample list and weights 263
Appendix A2 – GC673 Sample list and weights 271
Appendix A3 – GC666 OxCal Age Model Code 283
Appendix A4 – GC673 CLAM Age Model Settings 287
Appendix A5 – Journal of Micropalaeontology manuscript 289
Appendix A6 – Surface sample BFA census counts 291
Appendix A7 – BC737 and BC738 BFA census counts 295
Appendix A8 – GC666 BFA census counts 301
Appendix A9 – GC673 BFA census counts 309
Appendix A10 – GC666 1 cm resolution interpolated ages 313
Appendix A11 – GC666 sediment data 321
Appendix A12 – GC666 organic geochemistry data 323
Appendix A13 – GC666 biogenic silica data 327
Appendix A14 – GC666 foraminiferal stable isotope data 329
Appendix A15 – GC666 alkenone data 331
Appendix A16 – GC673 1 cm resolution interpolated ages 333
Appendix A17 – GC673 sediment data 343
Appendix A18 – GC673 organic geochemistry data 345
Appendix A19 – GC673 biogenic silica data 347
Appendix A20 – GC673 foraminiferal stable isotope data 349

List of Figures

Figure 1.1 South Georgia location map 2
Figure 1.2 Variability in the position of the Southern ACC Front 6
Figure 1.3 Shelf edge front location 10
Figure 1.4 Synthesis of early Holocene cooling records 14
Figure 1.5 Calculated insolation variability 15
Figure 1.6 Different hypotheses for the LGM ice extent at South Georgia 17
Figure 1.7 South Georgia terrestrial evidence for a mid-Holocene optimum 22
Figure 2.1 Sample location map 27
Figure 2.2 Factors affecting $\delta^{18}O_{foram}$ 38
Figure 2.3 Factors influencing $\delta^{13}C_{foram}$ 39
Figure 2.4 Example GC-FID chromatograms 46
Figure 2.5 Example GC-CIMS chromatogram 47
Figure 3.1 SEM of benthic foraminifera 83
Figure 3.2 SEM of benthic foraminifera 85
Figure 3.3 SEM of benthic foraminifera 87
Figure 3.4 SEM of benthic foraminifera 89
Figure 3.5 SEM of benthic foraminifera 91
Figure 3.6 SEM of benthic foraminifera 93
Figure 3.7 SEM of benthic foraminifera 95
Figure 4.1 Downcore live:dead ratio and live histograms 99
Figure 4.2 Histograms showing dead abundances 100
Figure 4.3 Average and Median Living Depths 102
Figure 4.4 $\delta^{13}C$ vs $\delta^{18}O$ cross-plot. 105
Figure 4.5 Isotopic data plotted against sample depth 106
Figure 4.6 $\delta^{13}C$ vs MLD 107
Figure 5.1 GC666 age/depth model 115
Figure 5.2 SEM images of foraminiferal preservation 118
Figure 5.3 Sedimentological data from core GC666 121
Figure 5.4 GC666 benthic foraminifera data 123
Figure 5.5 GC666 cluster analysis 124
Figure 5.6 GC666 DCA 125
Figure 5.7 GC666 downcore BFA relative abundances 126
Figure 5.8 GC666 organic geochemistry data 135
Figure 5.9 GC666 biogenic silica accumulation rate 137
Figure 5.10 GC666 foraminiferal isotopes 138

Figure 5.11 GC666 SST data 141
Figure 5.12 Examples of GC-CIMS chromatograms 143
Figure 5.13 GC673 age/depth model 144
Figure 5.14 GC673 sedimentological data 146
Figure 5.15 GC673 benthic foraminifera data 147
Figure 5.16 GC673 cluster analysis 149
Figure 5.17 GC673 DCA 149
Figure 5.18 GC666 and GC673 combined DCA 150
Figure 5.19 GC673 downcore BFA relative abundances 151
Figure 5.20 GC673 organic geochemistry data 153
Figure 5.21 GC673 biogenic silica accumulation rate 155
Figure 5.22 GC673 foraminiferal isotopes 156
Figure 6.1 Key proxy records from GC666 (15 to 10 cal. kyr BP) 161
Figure 6.2 Ice sheet extent at South Georgia during deglaciation 164
Figure 6.3 Chaetoceros laminae formation model 165
Figure 6.4 Calving bay re-entrant model 166
Figure 6.5 $\delta^{13}C_{org}$ vs C:N 170
Figure 6.6 Comparison of the ACR extent, arranged by latitude. 172
Figure 6.7 Key productivity proxies (15 to 10 cal. kyr BP) 178
Figure 7.1 Summary of key Holocene proxy records from GC666 183
Figure 7.2 $\delta^{13}C_{org}$ vs C:N 184
Figure 7.3 GC666 marine percentage of bulk organic carbon 187
Figure 7.4 GC666 *Miliammina* spp. properties 188
Figure 7.5 Key Holocene proxy records comparing GC666 and GC673 191
Figure 7.6 GC673 marine percentage of bulk organic carbon 192
Figure 7.7 Accumulation rate comparisons 193
Figure 7.8 Modern SWW extent and seasonal variation 199
Figure 7.9 Hypothetical variation in the SWW 204
Figure 7.10 Comparison southern hemisphere temperature records 207
Figure 7.11 Holocene insolation and summer duration 209
Figure 7.12 Evidence for and 8.2 kyr event? 212
Figure 8.1 Summary of key proxy records from GC666 and GC673 219

List of Tables

Table 2.1 Core locations and coring information. 25
Table 2.2 Radiocarbon age determination of surface sample 28
Table 2.3 Duplicate $\delta^{18}O$ and $\delta^{13}C$ analysis.....35
Table 2.4 Rose Bengal and plasma ashing tests 36
Table 2.5 Organic matter end-member values 42
Table 2.6 Components of lipid internal standard 48
Table 4.1 Isotopic data from "live" (stained) foraminifera. 104
Table 5.1 Radiocarbon age determinations for GC666.....114
Table 5.2 Preliminary diatom assemblage analysis 122
Table 5.3 Ecological interpretation of key species of foraminifera 132
Table 5.4 Radiocarbon age determinations for GC673.....145
Table 6.1 Mean values for deglaciation accumulation rates.....178
Table 7.1 Early Holocene linear correlation (r) values 185
Table 7.2 Mid-Holocene linear correlation (r) values 185
Table 7.3 Late Holocene linear correlation (r) values 189

List of Acronyms and Abbreviations

AABW	Antarctic Bottom Water
ACC	Antarctic Circumpolar Current
ACW	Antarctic Circumpolar Wave
ACR	Antarctic Cold Reversal
ALD	Average Living Depth
AMOC	Atlantic Meridional Overturning Circulation
AP	Antarctic Peninsula
APF	Antarctic Polar Front
AR	Accumulation Rate
AZW	Antarctic Zone Water
B-A	Bølling/Allerød
BAS	British Antarctic Survey
BC	Box Core
BFA	Benthic Foraminiferal Assemblage
BFAR	Benthic Foraminifera Accumulation Rate
BSi AR	Biogenic Silica Accumulation Rate
cal. kyr BP	calibrated kiloyears before present
CCD	Carbonate Compensation Depth
CDW	Circumpolar Deep Water
cmcd	cm core depth
C_{org}	Organic Carbon Accumulation Rate
CRVS	*Chaetoceros* Resting and Vegetative Spores
ΔR	local radiocarbon reservoir correction
$\delta^{13}C$	ratio of stable isotopes ^{13}C to ^{12}C
$\delta^{18}O$	ratio of stable isotopes ^{18}O to ^{16}O
DCA	Detrended Correspondence Analysis
DCM	Dichloromethane
DIC	Dissolved Inorganic Carbon
EHCO	Early Holocene Climate Optimum
ENSO	El Niño-Southern Oscillation
GC	Gravity Core
GC-CIMS	Gas-Chromatography with Chemical Ionisation Mass Spectrometry
GC-FID	Gas-Chromatograph fitted with a Flame Ionisation Detector
GIV	Global Ice Volume
HCl	Hydrochloric Acid

LCDW	Lower Circumpolar Deep Water
LGM	Last Glacial Maximum
LIA	Little Ice Age
LIS	Laurentide Ice Sheet
MAR	Mass Accumulation Rate
MCA	Medieval Climate Anomaly
MeOH	Methanol
MIS	Marine Isotope Stage
MLD	Median Living Depth
NADW	North Atlantic Deep Water
SACCF	Southern ACC Front
SAF	Sub-Antarctic Front
SAM	Southern Annular Mode
SB	Southern Boundary of the ACC
SeaWiFS	Sea-viewing Wide Field-of-View Sensor
SEM	Scanning Electron Microscope
SGSW	South Georgia Shelf Water
SST	Sea-Surface Temperature
SWW	Southern Hemisphere Westerly Winds
TLE	Total Lipid Extract
UCDW	Upper Circumpolar Deep Water
VPDB	Vienna Pee Dee Belemnite
WAIS	West Antarctic Ice Sheet
WSDW	Weddell Sea Deep Water
YD	Younger Dryas

Chapter 1

Introduction

This thesis presents the development and interpretation of multiproxy palaeoceanographic records from two marine sediment cores (core GC666 and core GC673), from the north-eastern shelf of the sub-Antarctic island of South Georgia (Fig. 1.1). Core GC666 provides a complete record of the Holocene and extends into the deglacial, from ca. 15 cal. kyr BP onwards, while core GC673 records the majority of the Holocene, from 9.5 cal. kyr BP onwards (Chapters 5, 6, and 7). To support the palaeoceanographic study a systematic taxonomy of the benthic foraminifera of the South Georgia shelf is presented (Chapter 3). Additionally, the ecology of three species of benthic foraminifera are studied using 'live' specimens recovered from box cores, also from the South Georgia shelf (Chapter 4). This chapter introduces the motivation for studying the palaeoceanography of South Georgia, discusses the modern oceanography and the palaeoclimate of the island, the palaeoceanography of the Southern Hemisphere more generally, and introduces the structure of the thesis.

1.1 Motivation

1.1.1 Why is palaeoceanography important?

It is clear that modern human activity is influencing the global climate system, with the high anthropogenic emissions of greenhouse gases having widespread impacts on human and natural systems (IPCC, 2014). Making reliable predictions about the future of the climate system requires an understanding of this system and how it has changed in the past. A good instrumental record is available for at least the past 100 years, although this was strongly biased towards the Northern Hemisphere before the development of satellites in the second half of the 20th century. However, the period for which instrumental records exist is characterised by relatively small climate variability, in comparison to future climate scenarios. Therefore, it is important to reconstruct past climate using archives that span longer timeframes, such as ice-cores, speleothems, lake sediment cores, and marine sediment cores; the latter represent the longest records available for analysis. Palaeoceanography therefore provides an unparalleled opportunity to understand how the Earth climate system has changed over geological timescales, with the oldest marine sediments extending back into the Cretaceous, informing our understanding of how this system may change in the future in response to anthropogenic influences.

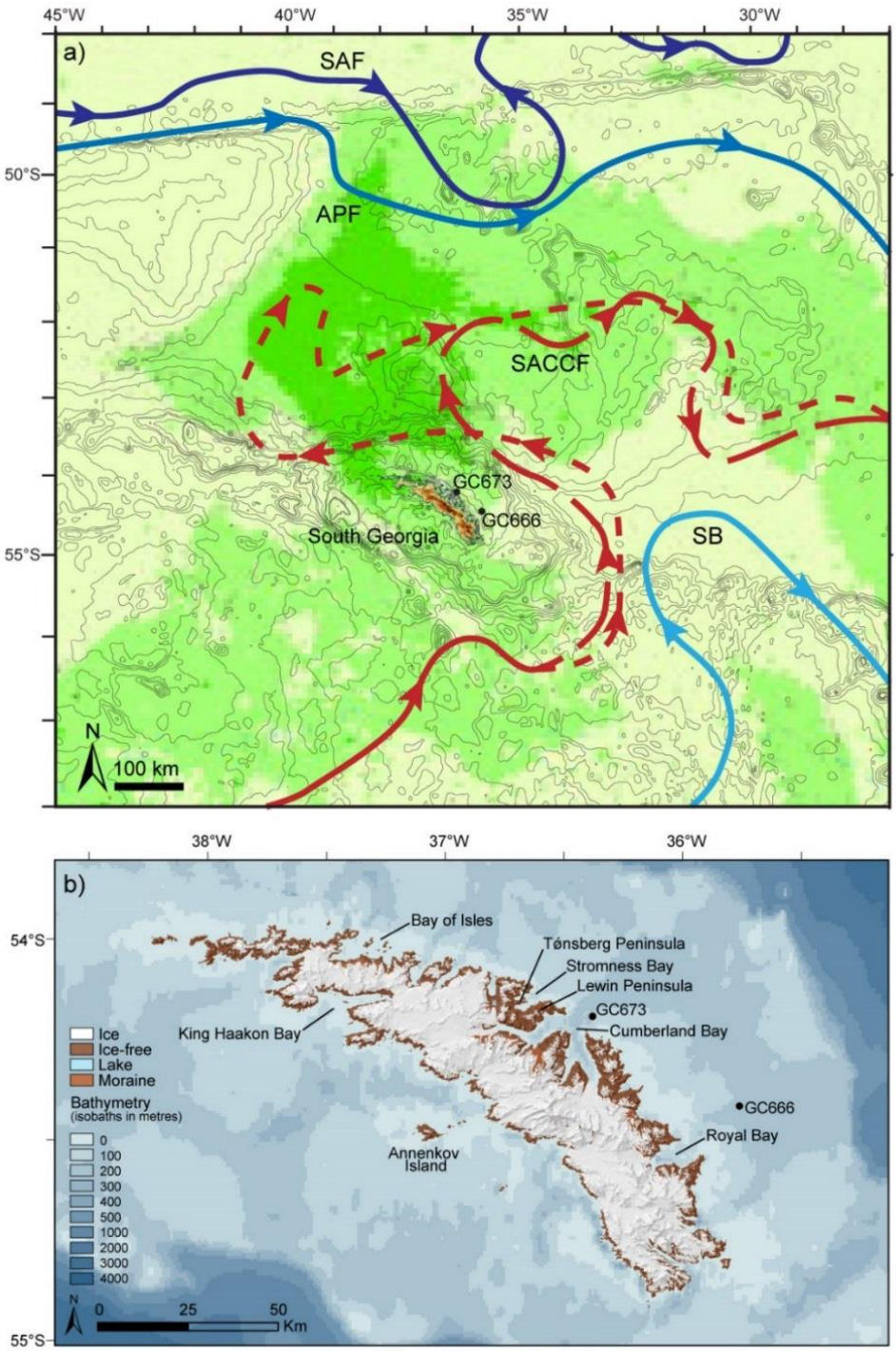


Figure 1.1 South Georgia location map
Topographical maps of South Georgia with surrounding bathymetry. a) The location and average position of the fronts associated with the Antarctic Circumpolar Current are also shown: SACCF - Southern ACC Front (contemporary variation near South Georgia shown by dotted and dashed lines, indicating most easterly and westerly extents (Thorpe et al., 2002)), SB - Southern Boundary of the ACC, APF - Antarctic Polar Front, SAF – Sub-Antarctic Front (Meredith et al., 2003). The mean surface chlorophyll-a concentration (mg m-2) between September and March is shown in green with darker colours indicating higher concentration (SeaWiFS derived satellite data, NASA, means calculated only for cells where 10 values were obtained within a year, from Murphy et al. (2013), illustrating the location of the bloom relative to the SACCF retroflection. b) More detailed map showing the gravity core locations and locations discussed in the thesis (www.sggis.gov.gs).

1.1.2 The relevance of South Georgia and the Southern Ocean

The sub-Antarctic island of South Georgia (57ºS, 54.5ºW) is located at the north-eastern corner of the Scotia Sea in the path of the Antarctic Circumpolar Current (ACC), between the Antarctic Polar Front (APF) and the Southern ACC Front (SACCF) (Fig. 1.1). South Georgia is one of the largest islands in the Sub-Antarctic Zone (SAZ), measuring approximately 180 x 40 km, and is separated from the deep-ocean by a 50–150 km-wide continental shelf. Due to South Georgia's location, oceanographic variation around South Georgia is of particular interest for a number of interrelated reasons. Changes in the Southern Westerly Winds (SWW) intensity and location, and latitudinal variation in the position of the APF can alter water mass circulation around South Georgia, influencing the island's climate. Furthermore, the ACC is a major component of global ocean circulation and South Georgia's location between two of the three main fronts associated with this current (the SACCF and the APF – see Fig. 1.1) mean the island is well situated to inform about variation in the ACC.

The interaction of the SACCF with the South Georgia shelf is believed to be integral to the development of one of the largest phytoplankton blooms in the Southern Ocean, occurring to the north of the island (e.g. Korb et al., 2005; Murphy et al., 2013). The Southern Ocean has been proposed as a potential carbon sink/source during the transition between glacial and interglacial periods (e.g. Sigman et al., 2010). As the South Georgia phytoplankton bloom represents one of the largest seasonal sinks of atmospheric CO_2 in the Southern Ocean (Jones et al., 2012), a better understanding of the bloom dynamics could be important to our assessment of the Southern Ocean's role in the transition between these two climate states. Furthermore, ACC variation may have significant impacts on the South Georgia ecosystem, which is recognised as one of the most diverse in the Southern Ocean and is of ecological and economic importance (Hogg et al., 2011). Interannual variation in the SACCF has been modelled and observed around South Georgia (e.g. Thorpe et al., 2002; Boehme et al., 2008; Young et al., 2014) but, to date, no studies have attempted to place this variability into the context of longer term natural variability through the Holocene and deglacial. New palaeoceanographic records from South Georgia also add to our understanding of the Southern Ocean more generally, providing additional data in this currently underrepresented region. Understanding the Southern Ocean is important because it plays a pivotal role as regulator of the global climate system, particularly because biological and physical carbon pumps operating in the ocean act to buffer atmospheric CO_2 concentration (e.g. Sarmiento and Toggweiler, 1984; Siegenthaler and Wenk, 1984; Watson and Orr, 2003).

1.1.3 Project aims

a) To develop a comprehensive taxonomy of the benthic foraminifera on the South Georgia shelf. Benthic foraminiferal assemblage data is widely used in multi-proxy palaeoclimate studies and the development of a comprehensive taxonomy has not only aided this study but will also provide a resource for any future benthic foraminifera-based work at South Georgia and in the surrounding area.

b) To test the effect of benthic foraminiferal ecology on the carbon isotope ratios of the calcareous test ($\delta^{13}C_{foram}$), specifically how living depth interacts with the well documented carbon isotope gradient in shallow sub-surface marine sediments to impact $\delta^{13}C_{foram}$.

c) To generate multiproxy palaeoceanographic records for two gravity cores (GC666 and GC673). The proxy records generated for the two cores will comprise benthic foraminiferal assemblage and stable isotopes ($\delta^{13}C$ and $\delta^{18}O$), geochemistry of organic matter ($\delta^{13}C$, %C, C:N), biogenic silica content, and alkenone analysis. Age/depth models will be assembled for both cores using radiocarbon dates from benthic foraminifera.

d) To interpret and compare the records in the context of regional and hemispheric/global post-glacial climate change. The development of these new records in the relatively data poor region of the Southern Ocean will help to further our understanding of oceanographic changes through the last ~15 kyr.

1.2 South Georgia modern oceanography

The position of South Georgia, south of the APF, means that the island is always surrounded by polar waters, leading to heavy glaciation of the island and the potential for sea-ice in the surrounding ocean, although the formation of sea-ice around the island is currently extremely rare (Atkinson et al., 2001; Meredith et al., 2003). Two main water masses are found in the open ocean around South Georgia; Circumpolar Deep Water (CDW) and Weddell Sea Deep Water (WSDW). CDW is the warm, saline water mass that occupies most of the deep layers of the ACC, and is split into Upper CDW (UCDW), characterised by low oxygen and high nutrient concentration, and Lower CDW (LCDW), characterised by high salinities (Orsi et al., 1995). CDW is mostly derived from the component of North Atlantic Deep Water (NADW) that becomes incorporated into the ACC (Whitworth and Nowlin, 1987), although UCDW is primarily supplied from the eastern South Pacific and the western Indian Ocean (Orsi et al., 1995). WSDW, formed through the mixing of cold, saline shelf water with warm deep water from Antarctic subpolar gyres (e.g. Gill, 1973), is the densest water found in the Scotia Sea and Georgia Basin and is a

component of Antarctic Bottom Water. The different properties of these two water masses were utilised by Orsi et al. (1995) to define the Southern Boundary of the ACC and to identify the SACCF.

The South Georgia shelf, typically within 200–250 m water depth, is traversed by canyons that connect the island's fjords to the continental slope. The properties of the waters of the shelf itself routinely differ from those of the surrounding ocean, with on-shelf surface waters typically being warmer (2–3ºC on shelf, 1.5–2ºC off shelf; shelf sea surface temperatures (SST) typically range from ~0ºC in winter to ~4ºC in summer) and fresher (salinity 33.4–33.7 psu on shelf, 33.6–33.7 psu off shelf) (Brandon et al., 1999). The main control on these differences is the input of fresh water, from direct runoff, supra- and sub-glacial melt, basal melt where the glacier terminates in the sea, and iceberg calving (Brandon et al., 1999; 2000; Meredith et al., 2005; Young et al., 2011a).

On their passage towards South Georgia, the waters of the SACCF are modified along the margin of the South Scotia Ridge by a combination of vertical mixing and the addition of meltwater in the Weddell-Scotia Confluence (Deacon and Foster, 1977), which extends northwards towards South Georgia (Orsi et al., 1995). The SACCF crosses the Scotia Sea before looping anticyclonically around South Georgia, to the north-west of the island. The front then retroflects back towards the east (Thorpe et al., 2002; Meredith et al., 2003). Meredith et al. (2003) found that, in the region of South Georgia, the SACCF is typically in 2500 m water depth, close to the base of the shelf slope and offset from the shelf edge front identified by Brandon et al. (1999). By combining satellite data with hydrographic and undulating oceanographic recorder data, Meredith et al. (2003) found that the SACCF first interacts with the South Georgia shelf considerably further west than is commonly represented on climatological maps, at least at the time of their survey, which may have important implications for the local ecosystem.

In addition to being integral to the development of large seasonal phytoplankton blooms around South Georgia, the SACCF is also the main route by which Antarctic krill (*Euphasia superba*) reaches the island, the island's krill population not being self-sustaining (Murphy et al., 2007). Antarctic krill supports the diverse ecosystem found on and around South Georgia. The position of the SACCF to the north of South Georgia varies considerably on an interannual scale, potentially affecting local krill abundance (Thorpe et al., 2002); chlorophyll-α concentration in the South Georgia region also varies interannually (Park et al., 2010). Monitoring of large-scale ACC features through Argo data (from sensors on autonomous floats, deployed in the southern Atlantic Ocean) and animal-borne CTD data has revealed both interannual and seasonal variability in the interaction of the

SACCF with the shelf to the south of the island (Boehme et al., 2008) (Fig. 1.2). Temporal and spatial variability in the SACCF has also been reproduced in high resolution modelling conducted by Young et al. (2014). Ward et al. (2007) described water masses approaching the shelf from the southwest as being diverted either through the gap in the North Scotia Ridge, or southeast along the shelf edge. Whitehouse et al. (2008b) observed the occurrence of upwelling, including nutrients, onto the shelf towards the western end of the island and modelling shows increased particle entries onto the shelf where the SACCF meets the shelf (Young et al., 2014).

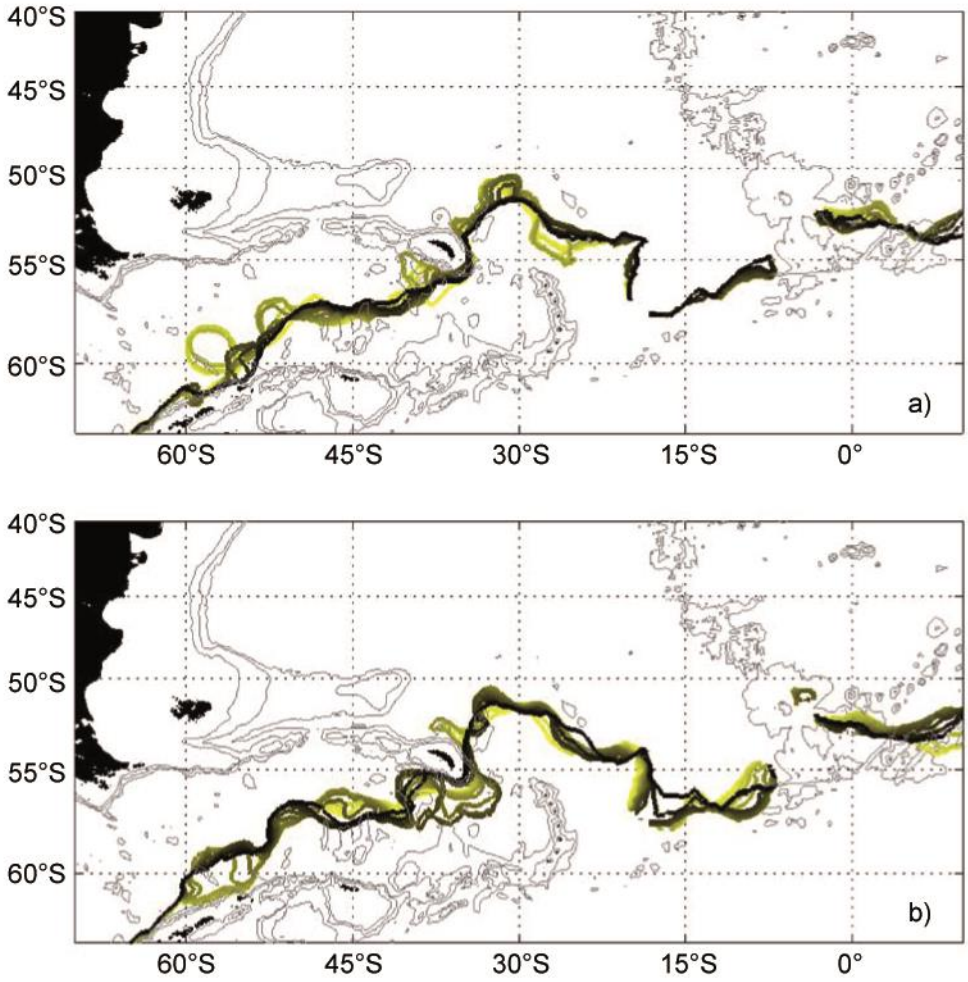


Figure 1.2 Variability in the position of the Southern ACC Front
Interannual and seasonal variability in the position of the Southern ACC Front during 2004 and 2005. Land is shaded black; 1000, 2000, and 3000 m isobaths. (a) Monthly position of the SACCF in 2004 (yellow to black). (b) Monthly position of the SACCF in 2005 (yellow to black). (Reproduced from Boehme et al., 2008)

Variability in the SACCF, therefore, has the potential to affect nutrient availability on the shelf by altering the upwelling of ACC-derived nutrients onto the shelf. When the ACC meets the shelf towards the west any upwelling is likely to be transported north through the gap between the island and Shag Rocks and then

downstream into the ACC, whereas upwelling further east could result in the upwelled water mass and nutrients being transferred to the northern shelf via the anti-clockwise flow that is present on the shelf, evident from both observational data and high resolution modelling (Young et al., 2011a; 2014). The orientation of the SACCF flow in relation to the shelf may also be important; when the SACCF has a stronger northward component on-shelf flow is enhanced while a more eastward component reduces on-shelf flow (Young et al., 2014). Variation in the ACC can potentially be linked to variation in the SWW, which in turn is related to changes in the expression of the Southern Annular Mode (SAM). Recent decades have seen an intensification of the SAM associated with an increase in the strength and a southward shift of the SWW (Thompson and Solomon, 2002). It has been hypothesised that the ACC could respond by also strengthening and shifting southwards (e.g. Fyfe and Saenko, 2006; Cai and Cowan, 2007). However, while the ACC may be able to shift over abyssal plains, rugged bathymetry (as found in the Scotia Sea and around South Georgia) could strongly constrain the path of the ACC (Whitehouse et al., 2008a). Furthermore, Meredith and Hogg (2006) proposed that the hypothesised southward shift of the ACC may be an artefact of the coarse resolution of the models, which fail to accurately model the ACCs interaction with the regions complex bathymetry. This is supported by Boehme et al. (2008) who found that the ACC had actually shifted *northwards* in data from 2004/2005, in comparison to earlier work.

The large phytoplankton blooms regularly present around South Georgia (e.g. Korb et al., 2005; Whitehouse et al., 2008b) are thought to be caused by the relief of iron stress in this area (Holeton et al., 2005). The passage of the ACC past South Georgia, and the North Scotia Ridge, may be the source of this iron (Korb and Whitehouse, 2004; Whitehouse et al., 2008b), with island run-off and flux into the system from the SACCF additional/alternative sources (Whitehouse et al., 1999; 2000; Ward et al., 2002; Korb et al., 2004; Young et al., 2014). This island mass effect results in iron enrichment of the waters near South Georgia, through interaction between water masses and topography, and has been proposed to be the cause of elevated marine productivity downstream of the island (Jones et al., 2012). Recent work has found that glacial meltwater can be an important source of iron and dissolved silica (silicic acid) in the shelf waters of South Georgia (Schlosser et al., 2017). Limitation in these essential elements may be an important factor limiting phytoplankton growth, particularly in northern Antarctic zone waters (Boyd, 2002). Silicic acid has previously been found to be at growth-limiting levels in the waters around South Georgia (Whitehouse et al., 1996; 2000), with Thorpe et al.

(2004) proposing that variation in the influence of the silicic acid-rich Weddell-Scotia Confluence on the ACC could affect marine productivity at South Georgia.

1.2.1 Remote forcing of South Georgia ocean properties

The nature of South Georgia, a small shelf surrounded by deep-ocean and in the path of one of the largest global circulation systems, means that it is potentially subject to both local and more remote influences. A link between South Georgia water temperatures and the duration of fast-ice in the southern Scotia Sea has been proposed by Whitehouse et al. (1996). This link illustrates the potential influence of regional climatic variability on South Georgia, as the fast-ice record in the southern Scotia Sea reflects circumpolar changes (Murphy et al., 1995). Extremes in ocean temperature at South Georgia have been shown to be coincident with local air temperature extremes (Deacon, 1977), which Meredith et al. (2005) interpreted as revealing a link to large-scale atmospheric conditions.

Anomalies in a variety of physical factors (e.g. sea-ice extent, atmospheric pressure, wind stress, sea-surface temperature) are propagated through the Southern Ocean at speeds consistent with the ACC (Murphy et al., 1995; White and Peterson, 1996), described as the Antarctic Circumpolar Wave (ACW). SST variability at South Georgia has been shown to have a four-year periodicity linked to El Niño-Southern Oscillation (ENSO)-related temperature fluctuations in the Pacific, with an approximately three-year temporal lag between South Georgia and the western Pacific, consistent with the ACW pattern (Trathan and Murphy, 2003). Meredith et al. (2005) demonstrated that both off-shelf and shelf water properties at South Georgia can, at times, be more rapidly affected by large-scale remote forcing, potentially linked to the exceptionally strong nature of the 1997/98 El Niño event. They proposed that a cold anomaly at South Georgia in early 1998 was linked to the 1997/98 El Niño event via a combination of ENSO-related atmospheric forcing and the propagation of an ENSO-forced cold anomaly in the southeast Pacific. The potential for more rapid oceanic propagation of SST anomalies was also demonstrated by Murphy et al. (2007), as was the direct influence of the SAM and ENSO-related atmospheric processes on time-scales of less than six months. The importance of ENSO to South Georgia SSTs is further illustrated by Meredith et al. (2008), who demonstrated that ENSO-forced SST anomalies close to the Antarctic Peninsula (AP) could be advected to South Georgia in five to six months. They also elucidated the importance of the SAM in determining South Georgia SST variability through more direct local air-sea interactions. In recent decades both the SAM and ENSO have displayed long-period changes; the SAM exhibiting a trend towards a higher index state (e.g. Thompson et al., 2000) and ENSO showing a higher occurrence of El Niño events (e.g. Kwok and Comiso, 2002).

1.2.2 Local forcing of South Georgia shelf-water properties

South Georgia shelf waters often display markedly different properties to those of the surrounding open ocean, which are strongly influenced by the ACC (Brandon et al., 1999; 2000; Meredith et al., 2005). Along the northern shelf edge, Brandon et al. (1999; 2000) identified separations between shelf waters and open ocean waters, in both eastern and western regions (Fig. 1.3). On-shelf surface waters were fresher (salinity 33.4-33.7 g kg^{-1} on shelf, 33.6-33.7 g kg^{-1} off shelf) and warmer (2-3ºC on shelf, 1.5-2ºC off shelf) and there are consistent differences in chlorophyll *a* concentration (1.1 mg m^{-3} on shelf, 0.27 mg m^{-3} off shelf) and nutrient properties (ammonium and nitrite were significantly higher on-shelf, while silicate, phosphate and nitrate were depleted), indicating higher on-shelf microbial productivity (Brandon et al., 1999). All of these properties tend to merge with depth, indicating deep-water communication between on- and off-shelf waters, suggesting that the separation between on-shelf and off-shelf surface waters is a local feature and not an expression of the SACCF (Brandon et al., 1999). The cause of this surface water disconnect is at least partly due to the microclimate that is present in the lee of South Georgia's high mountains. The orographic disturbance of surface winds, caused by South Georgia's strong topography, has been shown to affect sea surface temperature in the surrounding shelf waters, through the development of complex surface features, such as downwelling or wind-driven gyres (Hosking et al., 2015). In the western region Brandon et al. (2000) identified two water masses, the on-shelf South Georgia Shelf Water (SGSW) and off-shelf Antarctic Zone Water (AZW). SGSW is cooler and fresher than the AZW at the surface, but becomes warmer and more saline below the near-surface temperature minimum, with the differences in properties due to the increased contribution of precipitation and island run-off to the SGSW, and the advection of AZW from higher latitudes (Brandon et al., 2000). The differences in on-shelf and off-shelf water properties are, in part, due to a combination of freshwater release, solar heating, local mixing and water mass retention.

In longer time series data, the separation between shelf and ocean waters is revealed to vary interannually, at times displaying strong differences in on-shelf/off-shelf characteristics while at others there is comparatively little difference (Meredith et al., 2005). Variation in the nature of the on-shelf/off-shelf differences may have important implications for the transfer of water between the shelf and the open ocean. For example, when the on-shelf water is denser, flow around the island is cyclonic, in opposition to the general circulation (including the SACCF), resulting in frontal instability that potentially enables greater exchange between on-shelf and off-shelf waters (Meredith et al., 2005). Meredith et al. (2005) also

established that variation in the eastern and western regions was linked, suggesting that the forcing may be large-scale and remote in origin, although there were still significant differences due to local processes.

It is clear that large-scale, remote processes have the potential to impact the waters around South Georgia. However, a number of shelf-specific processes, such as freshwater run-off, topographically steered circulations, and canyon-induced upwelling (Brandon et al., 1999; 2000; Meredith et al., 2005), are also important influences on the shelf-water properties. For example, Meredith et al. (2005) identified a cyclonic circulation in front of Cumberland Bay, that may be linked to the local bathymetry. This type of circulation has previously been implicated in generating high primary productivity elsewhere in the Southern Ocean, such as on the shelf of Prince Edward Islands, through the retention of nutrient and freshwater run-off from the island (Perissinotto and Duncombe Rae, 1990).

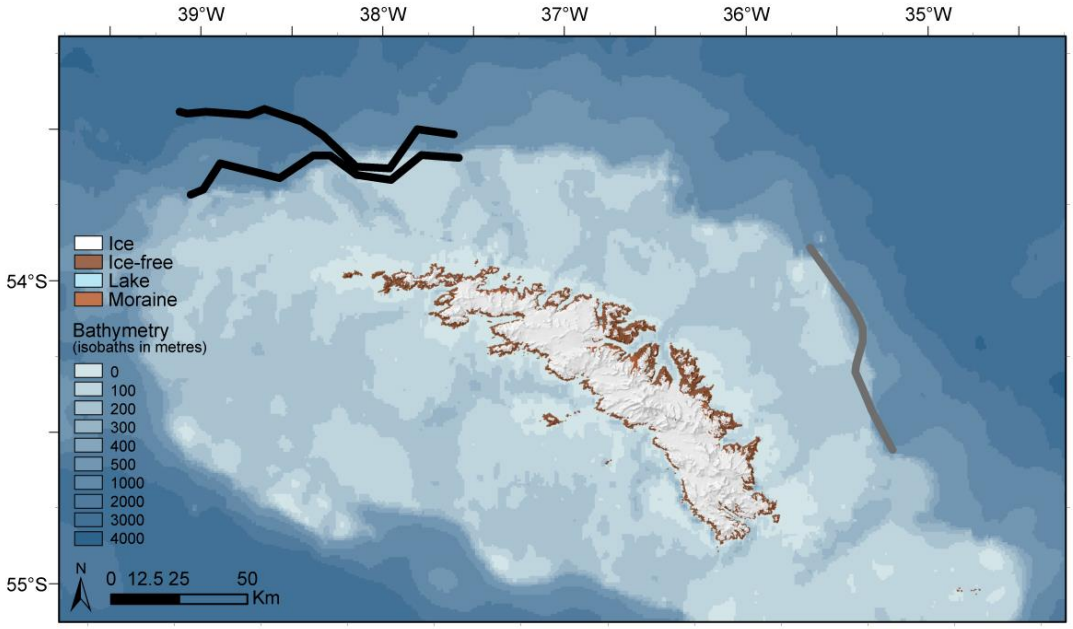


Figure 1.3 Shelf edge front location
Positions of the shelf edge fronts, in the eastern region (dark grey line), and the shelf edge frontal zone, in the northern region (thick black lines), identified by Brandon et al. (1999; 2000), overlain on the local bathymetry (bathymetry data from www.sggis.gov.gs).

1.3 Southern Hemisphere palaeoclimate

1.3.1 Deglaciation and the Antarctic Cold Reversal

During the last glaciation Antarctic ice sheets extended to the continental shelf edge around much of the continent (e.g. Bentley et al., 2014; Larter et al., 2014; Ó Cofaigh et al., 2014), although there are areas where this may not have been the case, such as the Weddell Sea (Hillenbrand et al., 2014), the Ross Sea (Anderson et al., 2014), and Prydz Bay, East Antarctica (Mackintosh et al., 2014).

Retreat from this maximum may have begun as early as 20 kyr BP in certain regions, such as the Bellingshausen Sea (Larter et al., 2014), and the Ross Sea (Anderson et al., 2014). Initial retreat across the Antarctic Peninsula continental shelf began between 18 and 17.5 kyr BP, approximately coincident with the onset of regional warming of the Southern Hemisphere (e.g. Pahnke et al., 2003), becoming progressively later southwards along the peninsula (Bentley et al., 2014; Ó Cofaigh et al., 2014). Retreat from the Antarctic Peninsula continental shelf continued until the present configuration was reached between 10 kyr BP and the mid-Holocene. In the Weddell Sea there is evidence that both the West Antarctic Ice Sheet (WAIS) and the East Antarctic Ice Sheet (EAIS) were retreating by 15 kyr BP, although the extent of this retreat is unclear (Hillenbrand et al., 2014). Elsewhere EAIS retreat was not significant until later; e.g. after 13 kyr BP in the Ross Sea (Anderson et al., 2014).

On the sub-Antarctic islands and in the maritime Antarctic realm, Hodgson et al. (2014a) classified the style of LGM glaciation and subsequent deglaciation into several categories. Islands situated north of the APF can be split into two groups. The first, including the Falkland Islands and Macquarie Island, experienced little or no LGM glaciation (Clapperton, 1971; Selkirk et al., 1990; Clark et al., 1998; Wilson et al., 2008), either due to insufficient moisture supply, insufficient altitude and relief, or to their location within the core band of the SWW causing more wind driven ablation. The second group situated north of the APF, including Campbell Islands and the Auckland Islands, have terrestrial evidence for LGM ice expansion (McGlone, 2002; Quilty, 2007). South of the APF, there are a number of islands that had limited ice extent at the LGM, such as the Kerguelen Islands. Hodgson et al. (2014a) included South Georgia in this group but more recent interpretations (Barnes et al., 2016; Graham et al., 2017; White et al., 2017) suggest LGM ice at South Georgia may have been more extensive (see Section 1.4.1). On islands south of the APF with restricted LGM ice, this limited extent may be due to increased aridity, linked to more northerly sea-ice expansion (Bentley et al., 2007; Allen et al., 2011; Collins et al., 2012). There is evidence that eastern/Argentinian Patagonia, in the Andean rain shadow, was more arid at this time (Recasens et al., 2012) and islands in this group may follow a more Patagonian glacial history with earlier Pleistocene glaciations extending beyond the LGM (Rabassa et al., 2000; Singer et al., 2004). Alternatively, earlier glaciations may have resulted in sufficient erosion to shorten glacial length, with glacier length theoretically decreasing with erosion depth (Anderson et al., 2012). A third class comprises seamounts and volcanoes, such as the South Sandwich Islands and Gough Island, which are unlikely to have accumulated LGM ice due to their low altitudes and steep flanks

that fall rapidly into the deep sea (Hodgson et al., 2014a). Islands on shallow shelves with evidence for extensive LGM glaciation, such as Heard Island, Bouvet Island, Marion Island, Prince Edward Island, the Crozet Islands, the South Orkneys, and Elephant Island, form a fourth class (which could also include South Georgia). On these islands LGM glaciation may have extended as far as the shelf edge, partly facilitated by glacio-eustatic sea level fall, with glaciation initiated by a northward shift of the APF, reducing temperatures and increasing precipitation (Hodgson et al., 2014a).

The Antarctic Cold Reversal (ACR), a period of cooling that interrupted the warming trend during deglaciation, is well-documented in Antarctic ice-cores (e.g. Stenni et al., 2010), occurring between approximately 14.5 and 12.8 kyr BP (Putnam et al., 2010). Evidence from marine cores expands the geographical extent of the ACR to the mid-latitudes of the Southern Hemisphere (e.g. Bianchi and Gersonde, 2004; Lamy et al., 2004; Barker et al., 2009), as do terrestrial records of glacial advance at this time from, for example, New Zealand (Putnam et al., 2010), Patagonia (Kilian and Lamy, 2012), and the Kerguelen Islands (Jomelli et al., 2017). The ACR is considered to be an expression of the bi-polar seesaw, with two possible mechanisms leading to this north-south antiphasing (Putnam et al., 2010). Strengthening of North Atlantic overturning during the warm Bølling/Allerød (B-A) interstadial could have increased northward heat transport across the equatorial Atlantic, resulting in a cooler Southern Ocean (Liu et al., 2009), although it is unclear how this cooling would be spread from southern mid-latitudes to Antarctic ice-core sites (Putnam et al., 2010). Alternatively, the latitudinal migration of global wind-belts may have been the driving mechanism, with warm conditions in the Northern Hemisphere during the B-A shifting wind-belts in both hemispheres northwards (Toggweiler et al., 2006; Denton et al., 2010). A northward shift in the SWW could result in a more northerly location for the sub-tropical front (e.g. Bard and Rickaby, 2009; Sikes et al., 2009; Denton et al., 2010) and a reduction in upwelling (Anderson et al., 2009), leading to a larger, cooler Southern Ocean and to the ACR (Putnam et al., 2010).

1.3.2 Holocene climatic periods

Globally, interglacial conditions were established soon after the start of the Holocene (11.7 kyr BP), but at locations in the high southern latitudes deglaciation may not have commenced until as late as 10.6 kyr, or later (e.g. Sterken et al., 2012; Bentley et al., 2014; Hodgson et al., 2014a; Ó Cofaigh et al., 2014). Subsequent climate has been relatively stable, especially when compared to the transition from glacial to interglacial (Roberts, 2014). However, it is clear that there are detectable changes in climatic conditions throughout the Holocene, especially in

Antarctica (e.g. Mayewski et al., 2004). Four main climatic periods, two warmer and two cooler, are described from a range of high-latitude Southern Hemisphere records (e.g. Masson et al., 2000; Taylor and Sjunneskog, 2002; Crosta et al., 2004; Nielsen et al., 2004; Stenni et al., 2010; Shevenell et al., 2011; Hodgson et al., 2013; Mathiot et al., 2013; Jomelli et al., 2017). The exact timing of the Holocene climatic periods varies between locations and the forcing mechanisms associated with these periods remains open to debate (e.g. Renssen et al., 2005; Renssen et al., 2010; Mathiot et al., 2013).

The Southern Hemisphere 'Early Holocene Climate Optimum' (EHCO) began at ~12.5 kyr BP, is characterised by warming following the ACR (~14.5 to ~12.5 kyr BP), and continued until approximately 9.5 kyr BP. The EHCO overlaps the Northern Hemisphere Younger Dryas cold event (~12.9 to ~11.7 kyr BP) and is present in Antarctic ice-core records (e.g. Masson et al., 2000; Mulvaney et al., 2012), marine and terrestrial records from the AP (reviewed in Bentley et al., 2009), terrestrial records from southern Patagonia (e.g. Unkel et al., 2010; Mansilla et al., 2016), and marine records from the Southern Ocean (e.g. Bianchi and Gersonde, 2004; Xiao et al., 2016). Subsequent to the EHCO, deglaciation on the AP slowed (Bentley et al., 2009) and there is evidence for decreasing temperatures between ~10.0 and ~8.0 kyr BP from a range of high latitude Southern Hemisphere records (see Mathiot et al., 2013 and Fig. 1.4). The term 'climate optimum' is not necessarily useful, as optimal conditions vary for different organisms and climate states, and is therefore only used here, and elsewhere in this thesis, in reference to its use in the literature, not as an indication that I consider these conditions to be 'optimal'.

During the mid-Holocene, the Southern Hemisphere high latitudes experienced a 'climate optimum'; proxy records (e.g. Allen et al., 2010; Stenni et al., 2010; Unkel et al., 2010; Hodgson et al., 2013; Panizzo et al., 2014) suggest the optimum extended from 6 to 3 kyr BP and this is supported by modelling of the period (Renssen et al., 2005). While many records display a distinct climate optimum (as temperature increase, sea-ice reduction, and/or enhanced productivity) in the mid-Holocene, there is variation in the timing of this period, illustrating the spatial heterogeneity of Southern Hemisphere climate. The mid-Holocene climate optimum is followed by a cool period commonly referred to as the neoglacial (e.g. Taylor and Sjunneskog, 2002; Denis et al., 2009; Majewski and Anderson, 2009; Allen et al., 2010; Verleyen et al., 2011; Hodgson et al., 2013; Jomelli et al., 2017). The onset of the neoglacial varies with location, in relation to the relative duration of the mid-Holocene Hypsithermal (MHH) (as early as 5 kyr BP in the southern Andes (Glasser et al., 2004) but as late as 1.5 kyr BP in East Antarctica (Borchers et al., 2016)). During the Antarctic neoglacial period, there are

two short, well-established climatic periods: the warm interval of the Medieval Climate Anomaly (MCA) (~1.0–0.7 kyr BP) and the cooler Little Ice Age (LIA) (~0.6–0.3 kyr BP) (e.g. Mann et al., 2009). In the Northern Hemisphere there is strong evidence for the MCA (e.g. Mann et al., 2009) but Neukom et al. (2014) found no evidence that this was a globally coherent climate event. There is a paucity of strong evidence for the expression of the MCA in Antarctica (e.g. Verleyen et al., 2011), although it is apparently present in some records (e.g. Khim

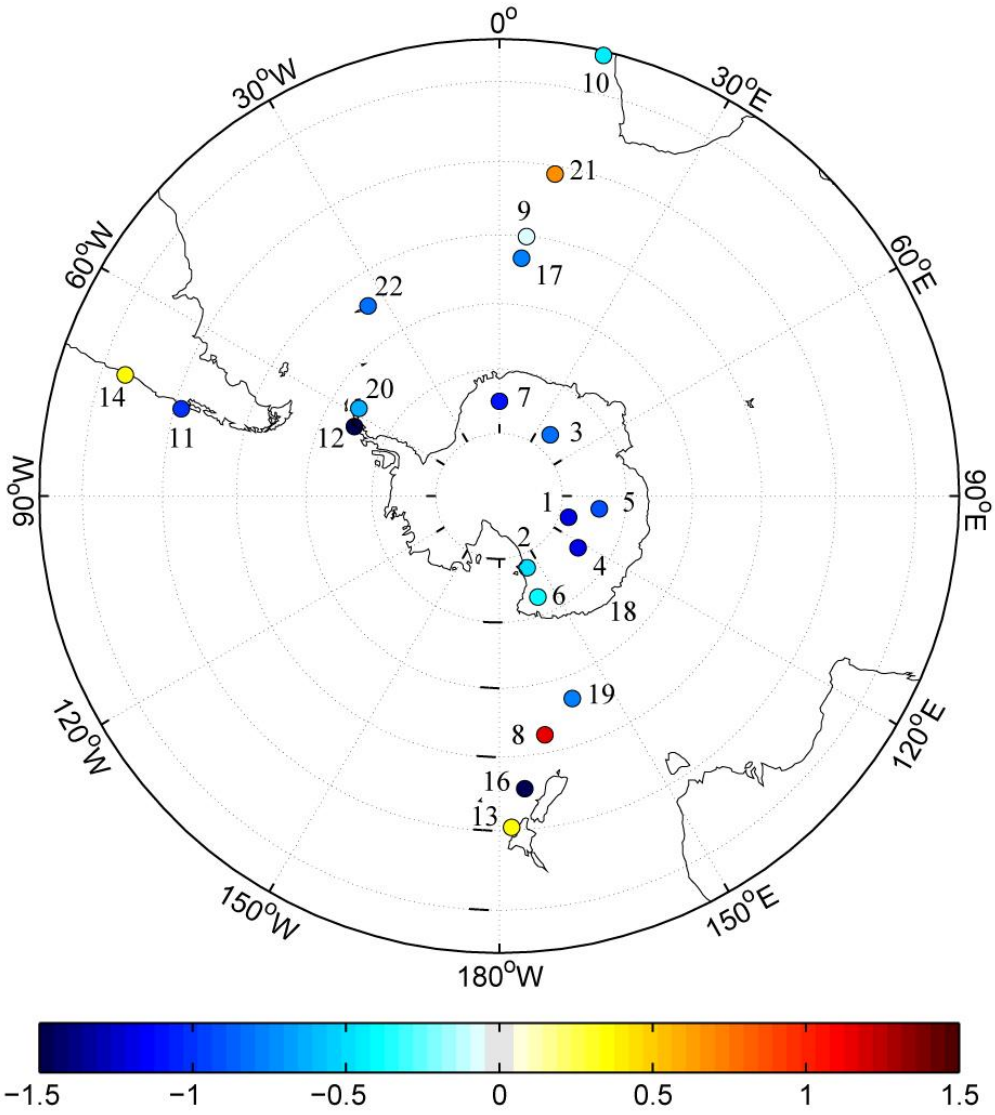


Figure 1.4 Synthesis of early Holocene cooling records
Observed temperature differences between 10 and 8 kyr BP in southern hemisphere palaeo-records. 1 - Vimeux et al. (1999), 2 - Steig et al. (1998), 3 - Watanabe et al. (2003), 4 - Masson-Delmotte et al. (2004), 5 - Nikolaiev et al. (1988), 6 - Stenni et al. (2011), 7 - Barbante et al. (2006), 8 - McGlone et al. (2010), 9 - Nielsen et al. (2004), 10 - Farmer et al. (2005), 11 - Lamy et al. (2002) and Kaiser et al. (2005), 12 - Shevenell et al. (2011), 13 - Pahnke and Sachs (2006), 14 - Kim et al. (2002), 16 - Pahnke and Sachs (2006), 17 - Hodell et al. (2001), 18 - Crosta et al. (2005), 19 - Crosta et al. (2004), 20 - Mulvaney et al. (2012), 21 - Cortese et al. (2007), 22 - this study. Modified from Mathiot et al. (2013).

et al., 2002). In contrast, there is evidence that the LIA is a global climate event (Neukom et al., 2014), and it is present in some Antarctic records (e.g. Masson et al., 2000; Khim et al., 2002; Shevenell and Kennett, 2002).

1.3.3 Southern Hemisphere forcing mechanisms

There are a number of forcing mechanisms that can influence climate in the Southern Hemisphere and that may have been important in causing climate variability through the deglacial and Holocene. Deglaciation was principally driven by changes in insolation, combined with subsequent alteration of the ice sheets, changes to the Atlantic Meridional Overturning Circulation (AMOC), and increases in CO_2 (e.g. Clark et al., 2009; He et al., 2013). The orbitally induced retreat of the Northern Hemisphere ice sheets resulted in weakening of the AMOC, which led to Southern Hemisphere deglaciation, via the bipolar seesaw effect (He et al., 2013). Continuing changes in insolation through the Holocene, in particular during the spring and summer (Fig. 1.5), are likely to have played an important role in controlling Southern Hemisphere climate (e.g. Masson et al., 2000; Renssen et al., 2005; Denis et al., 2010; Pike et al., 2013). One of the mechanisms by which insolation may impact the Southern Hemisphere is through changes to the intensity and/or position of the SWW, due to changes in sea-ice extent (e.g. Etourneau et al., 2013) and/or sea surface temperature (SST) (e.g. Bjorck et al., 2012). Changes to the intensity and/or position of the SWW are commonly cited as the main drivers

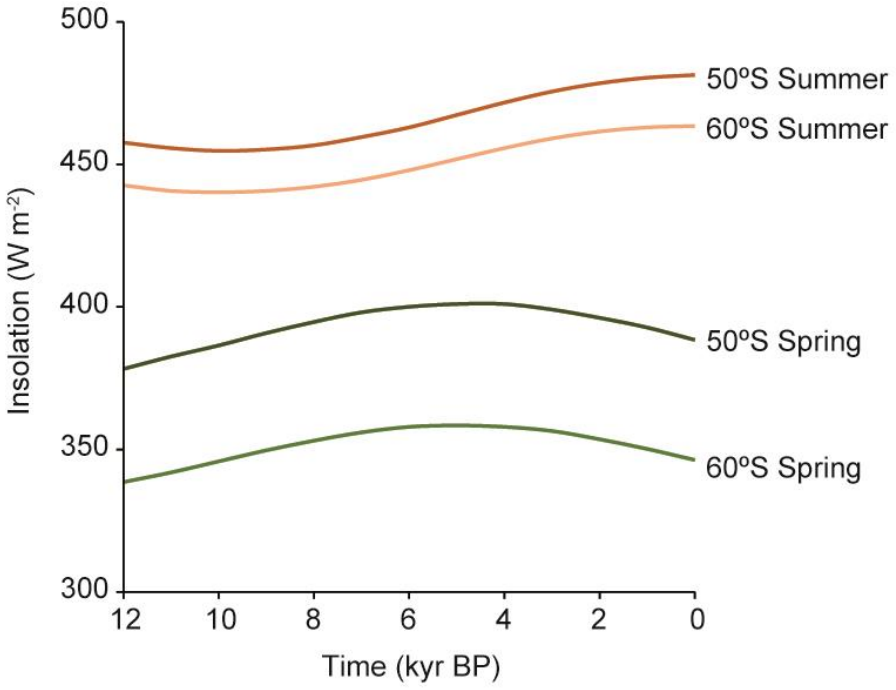


Figure 1.5 Calculated insolation variability
Insolation curves for spring equinox and summer solstice at 50°S and 60°S (Berger and Loutre, 1991).

of climatic change in southern South America (e.g. Lamy et al., 2010; Fernandez et al., 2012; Iglesias et al., 2016; Mansilla et al., 2016).

Large scale changes in oceanographic and atmospheric circulation are also important drivers of Southern Hemisphere climate at local and regional scales. For example, the SAM (also known as the Antarctic Oscillation) is the band of low pressure surrounding Antarctica that moves north or south in its negative or positive phases respectively, and the SWW moves with this band of low pressure. The SAM is currently shifted towards a more positive phase, with the SAM index higher now than at any point in at least the last 1 kyr (Abram et al., 2014), resulting in SWW contraction towards Antarctica. The positive SAM shift is possibly due to increased atmospheric concentration of greenhouse gases and, in recent decades, to depletion of the ozone layer (e.g. Shindell and Schmidt, 2004; Abram et al., 2014). SAM variability may also be the reason for opposing Holocene climate patterns in different regions of the southern high latitudes (Kaplan et al., 2016).

Another pattern of large-scale climate variability is ENSO and the intensification of centennial scale ENSO activity has been implicated in high latitude climate variability/episodic climatic changes in the Southern Hemisphere during the late Holocene (Shevenell et al., 2011; Etourneau et al., 2013; Peck et al., 2015). It has been demonstrated that both SAM and ENSO can affect South Georgia SSTs (Murphy et al., 2007; Meredith et al., 2008), as well as SWW properties (e.g. Thompson and Solomon, 2002). SAM and ENSO variability is linked, with SAM varying in response to ENSO, and vice versa. Positive (negative) SAM phases are dominant during La Niña (El Niño), while SAM can influence the amplitude of ENSO decay (e.g. L'Heureux and Thompson, 2006; Gong et al., 2010; Ding et al., 2012; Zheng et al., 2017). In recent decades the SAM has exhibited a trend towards a higher index state (e.g. Thompson et al., 2000) and El Niño events have become more prevalent in ENSO cyclicity (e.g. Kwok and Comiso, 2002). Global teleconnections are also important earlier in the Holocene, with Renssen et al. (2010) implicating Laurentide ice sheet melting in the early Holocene in cooling of Southern Hemisphere high latitudes, although Mathiot et al. (2013) have proposed this cooling was due to a combination of changes to atmospheric circulation and melting of the WAIS.

1.4 South Georgia palaeoclimate

1.4.1 Deglaciation and the ACR

The glacial history of South Georgia is possibly the best studied of all the sub-Antarctic and maritime islands in the Southern Ocean (see review in Hodgson et al., 2014a), with research on South Georgia extending back over more than 100 years (Gregory, 1915). In recent decades there has been considerable debate about the

extent of the ice sheet at South Georgia during the Last Glacial Maximum (LGM). Some authors propose that there was a large LGM ice sheet, extending as far as the shelf edge (e.g. Clapperton et al., 1989; Graham et al., 2008; Graham et al., 2017), others argue for a much smaller ice sheet, with the maximum extent restricted to the inner fjords (e.g. Rosqvist et al., 1999; Bentley et al., 2007; Hodgson et al., 2014b; 2014a) (Fig. 1.6). Somewhere between these two hypotheses, Barnes et al. (2016) have suggested that a 'little-big ice' scenario best fits the existing evidence, in which grounded ice reaches the shelf edge in most, but not all, areas. The restricted ice hypothesis suggests a glacial history for South Georgia similar to that of Patagonia, where earlier Pleistocene glaciations extended beyond LGM maxima (e.g. Darvill et al., 2015). Both the more extensive ice hypotheses suggest that South Georgia glacial history followed a similar pattern to that seen on the AP, with the outlet glaciers in many areas extending to the shelf edge during the LGM, followed by retreat to its current extent (e.g. Bentley et al., 2014).

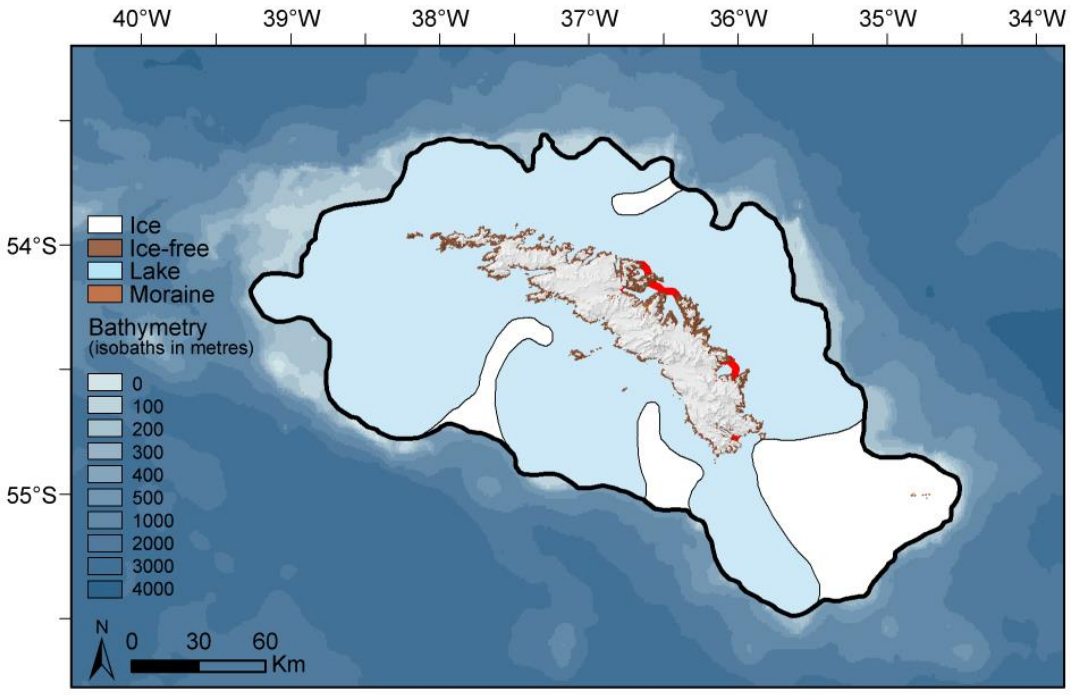


Figure 1.6 Different hypotheses for the LGM ice extent at South Georgia
The continental shelf of South Georgia showing the different estimates of the maximum limit of the grounded ice sheet during the LGM under the three competing hypotheses: Thick black line - ice extended to the shelf edge over the whole shelf (e.g. Graham et al., 2017), light blue area - 'little-big ice' with some ice-free areas on the shelf that act as refugia (Barnes et al., 2016), red line - restricted ice (e.g. Hodgson et al., 2014b).

Based on the analysis of terrestrial glacial geomorphology, but with limited dating constraints, Clapperton et al. (1989) proposed that, prior to 18 kyr BP, the

South Georgia ice-sheet extended to the shelf edge. However, subsequent work combining terrestrial glacial geomorphology with radiocarbon and cosmogenic isotope dating of moraines (Bentley et al., 2007) and the onset of sedimentation in lakes and peat bogs (Rosqvist et al., 1999; Rosqvist and Schuber, 2003; Van der Putten et al., 2004) led Bentley et al. (2007) to propose that glaciation on South Georgia at the LGM was restricted to the inner fjords. Of particular significance is the early onset of sedimentation, at 18.6 kyr BP, in Lake 1 on the Tonsberg Peninsula, Stromness Bay, interpreted by Rosqvist et al. (1999) as indicating that this part of South Georgia was deglaciated by this time. However, radiocarbon dating from sites close to Lake 1 provide much later minimum estimates for deglaciation (~10.9 kyr BP and ~9.2 kyr BP - Van der Putten et al. (2004), ~7.5 kyr BP - Rosqvist and Schuber (2003)). Lake 1 may have become ice-free much earlier due to its location on a ridge between two glaciers (Van der Putten and Verbruggen, 2005), suggesting that the date for deglaciation at this site may not be informative about South Georgia as a whole. Cosmogenic ^{10}Be exposure ages from a moraine representative of the oldest terrestrial ice advance on South Georgia, also from Stromness Bay, reveal a median age for its deposition of ca. 12.2±1.5 kyr BP (Bentley et al., 2007), indicating retreat from this advance occurred much earlier than the onset of sedimentation at most locations but still later than that seen in Lake 1. Hodgson et al. (2014b) have suggested that this offset between glacial retreat and the onset of sedimentation may be linked to increased aridity, due to greater northward extent of sea-ice and strong winds.

Detailed examination of South Georgia fjord submarine geomorphology revealed two sets of moraines within the fjords, one set at the fjord mouths and the other set bounding inner basins within the fjords (Hodgson et al., 2014b). Hodgson et al. (2014b) interpreted the inner moraines as maximum advance grounding lines formed during the LGM, and these moraines may correlate with the terrestrial features identified by Bentley et al. (2007). Hodgson et al. (2014b) proposed that the South Georgia ice-sheet was relatively restricted during the LGM due to a combination of sea-level control, with lower LGM sea-level causing some of the glaciers to ground on land within the fjords, and reduced precipitation. Increased aridity at South Georgia during this period may be linked to the increased northward extent of sea-ice, with winter sea-ice potentially extending north of the island (Gersonde et al., 2005; Allen et al., 2011; Collins et al., 2012), as well as northward migration of the SWW (Toggweiler et al., 2006). At this time the Patagonian climate was similarly arid (Recasens et al., 2012), also due to increased sea-ice extent and SWW migration, with the additional effect of the Andean rain shadow. Alternatively, the restricted ice-sheet extent may not relate to climate but

instead be linked to glacial modification of the underlying topography, with numerous previous glacial cycles eroding the valleys and fjords to sufficient depth to reduce glacier length (Anderson et al., 2012; Hodgson et al., 2014b).

While the above interpretations seem to refute the hypothesis of Clapperton et al. (1989), the possibility of ice extending to the shelf edge is potentially supported by bathymetric data from the wider South Georgia shelf, compiled by Graham et al. (2008), that identified cross-shelf glacial troughs with terminal moraines at the shelf break. The lack of any dating constraint on the formation of these features, beyond Graham et al.'s (2008) proposal that assumed high sedimentation rates would have buried older features, means this evidence cannot be considered conclusive. As the glacial history of South Georgia may extend as far back as the Late Miocene (Graham et al., 2008), there is the possibility that these features formed during more extensive Pleistocene glaciations (MIS 20 and younger). Hodgson et al. (2014b) suggested that the similarity of the South Georgia troughs to those formed during the Pleistocene off the coast of Patagonia supported their restricted LGM ice sheet hypothesis (Rabassa et al., 2000; Singer et al., 2004). 'Far-flung' moraines, at the end of cross shelf troughs, may provide further evidence that a restricted LGM ice-sheet relates to glacial alteration of the landscape (Anderson et al., 2012).

Graham et al. (2017) have recently dated the formation of one of the fjord mouth moraines, identified and hypothesised to represent pre-LGM glaciation by Hodgson et al. (2014b), and found that it formed after the LGM (ca. 15 kyr BP), possibly linked to a glacial readvance during the Antarctic Cold Reversal (ACR). Readvance during the ACR may have also generated the oldest terrestrial moraines on South Georgia, dated to 12.2±1.5 kyr BP (Bentley et al., 2007). Furthermore, based on preliminary dating of GC666 and PARASOUND sub-bottom profiler data, Graham et al. (2017) proposed that sedimentation in Royal Bay trough did not commence until ca. 18 kyr BP, with this sediment underlain by glacial diamicton or bedrock, indicating that grounded ice extended over this location prior to 18 kyr BP. That the LGM ice-sheet at South Georgia extended onto the shelf is further supported by the measurement of exposure ages of glacial deposits on the Lewin Peninsula, Cumberland Bay (White et al., 2017). They determined that the ca. 600 m high peaks on the peninsula were glaciated during the LGM and projected that an ice-sheet that covered these peaks would have had a minimum extent reaching to the mid-shelf. A study of the biodiversity of the South Georgia shelf benthos provides additional support for extensive ice at the LGM, revealing that species richness on much of the shelf is significantly poorer that at the shelf edge, as would be expected if the shelf had recently been covered by grounded ice (Barnes et al.,

2016). However, Barnes et al. (2016) did find higher species richness on some areas of the shelf leading them to propose the 'little-big ice' hypothesis, where the ice-sheet extends to the shelf edge on most of the shelf but some areas are left ice free. Graham et al. (2017) also reported areas of shallow sea bed with no record of recent glacial disturbance, further supporting the 'little-big ice' hypothesis. This third hypothesis may also help to explain the high overall diversity of the South Georgia shelf taxa and how endemic species have been able to survive multiple glaciations, with ice-free areas providing refugia during glaciations (Barnes et al., 2016).

1.4.2 The Holocene

There are currently no previously published marine records of the Holocene from South Georgia, with those studies that do consider the marine realm focussed on the deglacial (see previous section). There are however a number of terrestrial records that investigate the Holocene, from lake and peat cores, and from the glacial geomorphology. Utilising these archives, two Holocene glacial advances were identified by Clapperton et al. (1989), the first between >2.2 and 0.9 cal. kyr BP, followed by a series of fluctuations, which they proposed represented a mean annual temperature decrease of ca. 0.5 to 1 ºC. In addition, Clapperton et al. (1989) identified three drier, and possibly warmer, periods at ca. 7.6-6.3, ca. 5.4-2.7, and ca. 0.9-0.7 cal. kyr BP, supported by the analysis of lacustrine cores (Birnie, 1990). A warming trend in the early Holocene was also identified by Rosqvist et al. (1999) from lacustrine isotope data, between 8.4 and 6.5 cal. kyr BP, briefly interrupted by a short cool period between 7800 and 7400 cal. yr BP, possibly related to the 8.2 ka event (Alley et al., 1997). Rosqvist and Schuber (2003) identified a number of glacial advances and cooling events, between 7200 and 7000 yr BP, 5200 and 4400 yr BP, 2400 and 1600 yr BP, and after 1000 yr BP. These cooling events were identified from a lake fed by a cirque glacier, which are known to respond rapidly to changes in climate, with Rosqvist and Schuber (2003) proposing that glacial changes were being driven by shifts in the position and/or intensity of the SWW.

In an analysis of the terrestrial geomorphology, Bentley et al. (2007) identified two Holocene glacial readvances, one mid-Holocene (ca. 3.6±1.1 kyr BP) and one at ca. 1.1 kyr BP. Both these readvances were extensive, reaching, and in some cases exceeding the advance that occurred during the ACR (see Section 1.4.1). That these advances were so extensive may be linked to precipitation: more southerly sea-ice extent during the late Holocene, in comparison to during the ACR, could have resulted in relatively greater precipitation at South Georgia, generating a positive glacier mass balance (Bentley et al., 2007). Bentley et al. (2007)

suggested this may have been especially true of the 3.6 kyr BP advance, hypothesising that the warmth of the MHH (see Section 1.3.2) resulted in less extensive sea-ice upwind of South Georgia. A southward shift in the SWW could also cause increased precipitation on South Georgia, by advecting more sub-tropical warmth southwards (Bentley et al., 2007). South American proxy records suggest that a southward shift in the SWW may have occurred at ca. 4 ka (Thompson et al., 1998; Cross et al., 2000; Lamy et al., 2001) and modelling suggests such a shift during warm periods (Toggweiler et al., 2006), although evidence from macrofossils (Van der Putten et al., 2004; 2009) indicates dry conditions on South Georgia at 3.6 ka. Evidence for temperature, productivity and vegetation changes seen in South Georgia terrestrial records (Rosqvist and Schuber, 2003; Van der Putten et al., 2004; 2009; Strother et al., 2015; summarised in Fig. 1.7) record the influence of the Antarctic MHH on the island.

Rosqvist and Schuber (2003) interpreted their lake core as recording 'major atmospheric and oceanographic changes' at ca. 2500 cal. yr BP, which may represent the onset of neoglacial conditions (see Section 1.3.2). This is also seen in other Southern Hemisphere lacustrine, marine and ice records (Bjorck et al., 1996; Ingolfsson et al., 1998; Domack and Mayewski, 1999; Masson et al., 2000; Hodell et al., 2001). Van der Putten et al. (2004; 2009; 2012) also identified climatic change on South Georgia at this time, to wetter and colder conditions (also identified by Strother et al. (2015)), and linked this to evidence for worldwide climatic change around 2700 cal. yr BP (van Geel et al., 1996; 2000).

The glacial advance identified by Bentley et al. (2007) at ca. 1.1 kyr BP, in the late Holocene, also correlates with periods of increased warmth recorded in South Georgia lake sediments (ca. 1.5 to 1.0 kyr BP (Clapperton et al., 1989) and ca. 1.7 to 0.7 cal. kyr BP (Strother et al., 2015)), and elsewhere in the Southern Hemisphere (Bentley et al., 2009; Kastner et al., 2010; Neukom et al., 2010). Warming around ca. 1.0 kyr BP is coincident with the MCA (~1.0−0.7 kyr BP - Mann et al., 2009) seen in both Northern and Southern Hemispheres, although, due to the wide variation in timing of these events, the MCA is not believed to be a globally synchronous warming (Neukom et al., 2014). Another late Holocene climate event, which is believed to have a global expression (Neukom et al., 2014), is the LIA (~0.6−0.3 kyr BP - Mann et al., 2009). As with the MCA, there is evidence for the LIA in some of the terrestrial records from South Georgia, including moraines identified by Clapperton et al. (1989) and increased glacier activity linked to cooling temperatures (Rosqvist and Schuber, 2003).

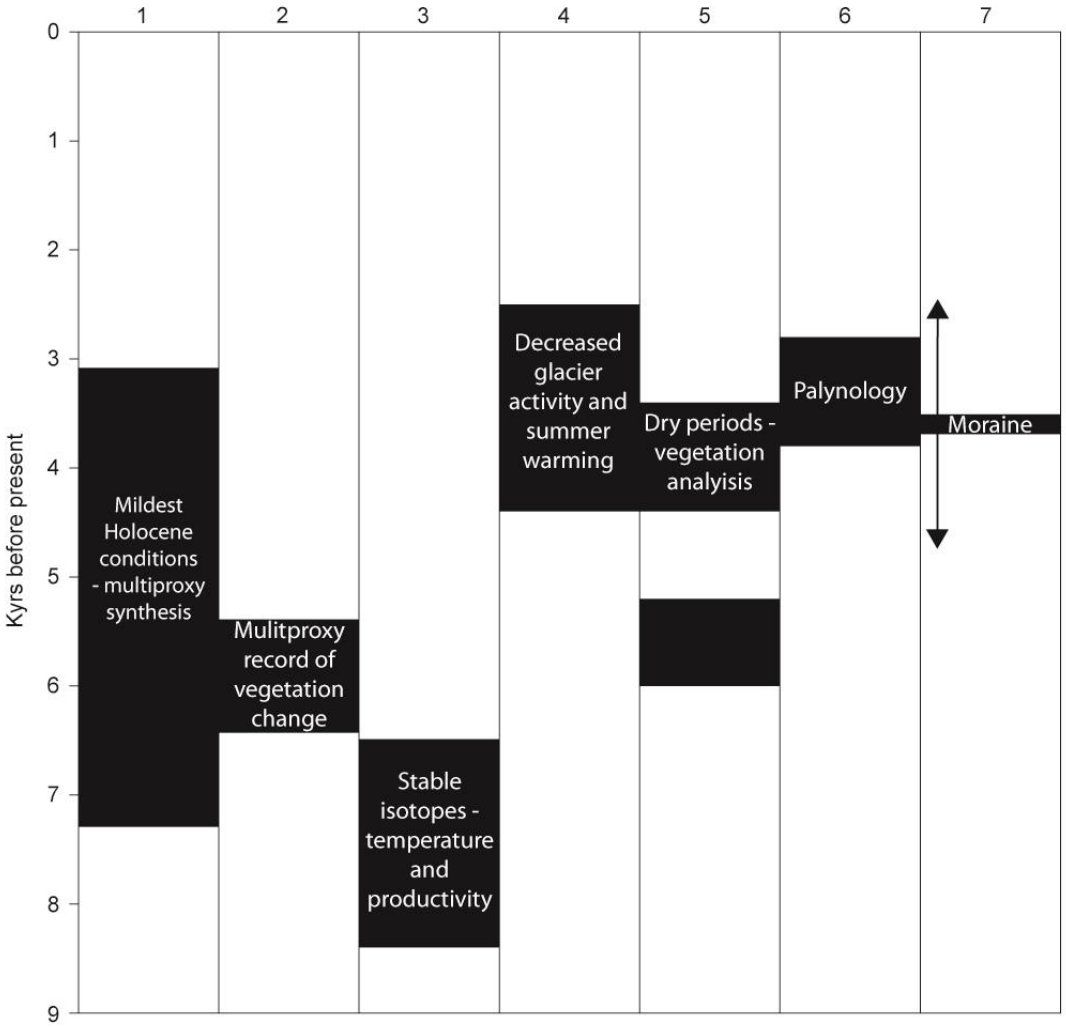


Figure 1.7 South Georgia terrestrial evidence for a mid-Holocene optimum 1 - Clapperton et al. (1989), 2 - Birnie (1990), 3 - Rosqvist et al. (1999), 4 - Rosqvist and Schuber (2003), 5 - Van der Putten et al. (2009), 6 - Strother et al. (2015), 7 - Bentley et al. (2007). Shaded areas represent mid-Holocene climate periods proposed by the authors. With the exception of Bentley et al. (2007) all records were radiocarbon dated. Where these dates have been calibrated the published calibrated dates are used, as any variation due to revised calibration curves will be minimal in the Holocene. Clapperton et al. (1989) and Birnie (1990) published uncalibrated radiocarbon dates, these have been calibrated here using OxCal 4.3 (Bronk Ramsey, 2009) and the SHCal13 calibration curve (Hogg et al., 2013). The errors associated with the cosmogenic dating of the moraine identified by Bentley et al. (2007) are indicated by black arrows.

The multiproxy records presented in this thesis have been generated with the aim of adding to our understanding of South Georgia palaeoclimate and palaeoceanography, and to assess whether this new understanding can further inform comprehension of the climate evolution of the surrounding region. While the record from core GC666 does not extend to the LGM, the early part of this record will provide information about the later part of South Georgia's deglacial history, including the ACR. This has the potential to support one of the competing hypotheses regarding the LGM ice sheet extent on South Georgia, by providing

information about the latter stages of the retreat from this maximum. The Holocene records, from both cores, will add to our understanding of Holocene climate variability in the relatively poorly studied sub-Antarctic region. Investigation of productivity variation of the South Georgia shelf has the potential to aid our assessment of long-term ACC, and SACCF, variability, informing our understanding of the possible impact of such variability on the large phytoplankton blooms recorded in modern South Georgia waters. Multiproxy records of variability in South Georgia shelf water conditions will also support the interpretation of terrestrial palaeoclimatic records.

1.5 Thesis outline

This thesis comprises the results of the multiproxy analysis of two marine gravity cores (GC666 and GC673) from the north-eastern shelf of South Georgia, plus additional data from box cores and surface samples also from the South Georgia shelf. The data presented is discussed in relation to benthic foraminiferal ecology and palaeoceanographic variation at South Georgia through the last ~15 kyrs.

1.5.1 Chapter 2 – Materials, methods, and proxy application

This chapter describes the acquisition of the materials to be analysed, and the main methods used in the generation of the proxy records. The chapter also includes discussion of the palaeoceanographic application of the various proxies.

1.5.2 Chapter 3 – Systematic taxonomy of Holocene South Georgia benthic foraminifera

This chapter comprises a detailed taxonomic appraisal of the Holocene benthic foraminifera of the South Georgia shelf, utilising assemblage data from gravity cores, box cores, and surface samples. The fauna described includes 78 species, assigned to 57 genera from 34 families (of these 58 species were identified to species level, while 20 species are discussed in open nomenclature). The data presented in this chapter has previously been published in Dejardin et al. (2018).

1.5.3 Chapter 4 - Live (stained) benthic foraminiferal living depths and stable isotopes offshore South Georgia: implications for calcification depths

Chapter 4 presents data from the isotope analysis of 'live' (stained with Rose Bengal) benthic foraminifera from two box cores (BC737 and BC738). The data is discussed in relation to the possible impact of the well-established $\delta^{13}C$ gradient that is present in marine sediments, and the possible impact foraminiferal ecology might have on their $\delta^{13}C$ composition. The results presented here further highlight the importance of understanding the ecology of the foraminifera analysed when using their isotopic composition in palaeoclimatic reconstructions. A novel potential

calcification strategy is proposed in this chapter. The data and arguments presented in this chapter have previously been published in Dejardin et al. (2018).

1.5.4 Chapter 5 – Results from gravity cores (GC666 and GC673)

This chapter describes in detail the results of the multiproxy analysis of the two gravity cores (GC666 and GC673). The analyses conducted were: the development of age/depth models for both cores from radiocarbon dating, sedimentological description and coarse fraction quantification, benthic foraminiferal assemblage analysis, organic carbon and nitrogen concentration, isotopic analysis of organic carbon ($\delta^{13}C$), quantification of biogenic opal, isotopic analysis of benthic and planktonic (GC666 only) foraminifera ($\delta^{13}C$ and $\delta^{18}O$), and bulk sediment alkenone analysis (GC666 only).

1.5.5 Chapter 6 – Deglacial oceanography (~15.2 – 12.3 cal. kyr BP)

Chapter 6 comprises discussion of the evolution of the South Georgia shelf oceanography from ~15.2 cal. kyr BP until ~12.3 cal. kyr BP, during the transition from glacial to interglacial conditions. This section of the GC666 core includes the latter part of the first stage of deglaciation, the Antarctic Cold Reversal (ACR), and the post ACR ice retreat. The discussion utilises the multi-proxy records described in Chapter 5, with these proxy records primarily interpreted in terms of changes in primary productivity, and sediment supply. The interpretation of the multi-proxy records has been divided between Chapters 6 and 7, with the chapters being split at 12.3 cal. kyr BP. This date was chosen as the point to divide the two chapters as my interpretation indicates that this is the point at which grounded/glacial ice no longer has a strong influence on the oceanography at GC666, following retreat from the ACR advance.

1.5.6 Chapter 7 – Holocene oceanography (~12.3 cal. kyr BP onwards)

This chapter comprises discussion of the evolution of the South Georgia shelf oceanography from ~12.3 cal. kyr BP onwards, utilising the multi-proxy records described in Chapter 5. These proxy records are interpreted in terms of changes in primary productivity, sediment supply, and sea surface temperature, and are considered in comparison to other palaeoceanographic and palaeoclimatic records from the southern high latitudes, including South Georgia.

1.5.7 Chapter 8 – Summary

Chapter 8 summarises the findings presented in Chapters 3 to 7, presents the key finding from this research, and proposes some possible avenues for future work.

Chapter 2

Materials, methods, and proxy application

This chapter comprises an introduction to the sediments, from gravity cores, box cores, and surface samples, which form the basis of this thesis (Section 2.1). In the second part of the chapter (Section 2.2), the main methodologies that have been utilised to generate proxy records from these sediment samples are described. This second section also comprises justification for the use of these proxies.

2.1 Material

2.1.1 Sample acquisition

Gravity cores (GC) 666 and 673 (Table 2.1 and Fig. 2.1) were collected during British Antarctic Survey (BAS) scientific cruise JR-257, in April 2012 on the RRS *James Clark Ross* (Allen et al., 2012). The two cores are located on the South Georgia shelf, at the proximal ends of the cross-shelf troughs that propagate from Royal Bay and Cumberland Bay. These gravity cores were collected, along with other cores collected during JR-257, to enable detailed regional climate reconstructions of ice and ocean conditions, to complement existing lake and ice records. GC666 is part of a transect of cores spanning the South Georgia continental shelf that were recovered with the aim of reconstructing the local glaciological history, including former grounded ice cap extent.

Table 2.1 Core locations and coring information.

Core	Latitude (ºN)	Longitude (ºE)	Depth (mbsl)	Cruise	Date recovered	Recovery (m)
GC666	-54.42060	-35.74148	254	JR-257	17/04/12	8.13
GC673	-54.20237	-36.37451	239	JR-257	19/04/12	8.84
BC656	-53.78168	-37.95855	303	JR-257	16/04/12	0.19
BC660	-53.78188	-38.12847	354	JR-257	16/04/12	0.18
BC667	-54.42063	-35.74152	252	JR-257	17/04/12	0.18
BC671	-54.20237	-36.37451	239	JR-257	18/04/12	0.25
BC737	-53.99709	-36.82012	260	JR-15002	27/11/15	0.15
BC738	-53.85504	-37.65095	287	JR-15002	28/11/15	0.20

The gravity cores were collected using the BAS gravity corer, which comprises a combination of 3 m and 6 m long steel barrels with a bomb-weight at the top end, allowing barrel configurations with a range of lengths to be deployed (GC666 was recovered from a 12 m deployment and GC673 was recovered from a 15 m

deployment). Pre-labelled core liners were inserted into the barrels, followed by a polythene bag lined core catcher. The complete corer assembly was deployed to the seafloor by the midship winch. After recovery the core was cut into approximately 1 m sections, each section was capped at both ends, cleaned, and then transferred to the cool store.

Core sections from GC666 and GC673 were split into archive and working halves at the Alfred Wegener Institute in Bremerhaven, Germany (GC666) and at the British Antarctic Survey in Cambridge, UK (GC673). To provide the samples that form the basis of this study 1 cm thick quarter core samples were taken from the first six sections of GC666 (and at 64 cm intervals in sections seven to nine) and from the whole of GC673. These samples were bagged, freeze-dried with a Thermo Moduloyd freeze drier at the University of Nottingham, and weighed (Appendices A1 and A2). An initial pilot study sampled GC666 at 64 cm intervals; subsequent sampling, once the age model had been developed, increased the temporal resolution to ca. 200 years (16 cm intervals – 319-383 cmcd; 12 cm intervals – 0-33 cmcd, 199-247 cmcd, and 383-516 cmcd; 8 cm intervals – 57-97 cmcd, 127-199 cmcd, and 247-319 cmcd; 4 cm intervals – 33-57 cmcd; 1 cm intervals – 97-127 cmcd). The organic geochemistry record was generated prior to age model development and has a resolution of 4 cm in the upper 5 m of the core. Samples from core GC673 were analysed at 32 cm resolution, except for organic geochemistry which was sampled at 16 cm resolution. In addition the sampling resolution was increased to 4 cm between 304 and 336 cmcd after the age model for this core indicated a slower sedimentation rate for this interval.

Surface sediment samples (0–2 cm sediment depth) were collected from six locations on the South Georgia shelf. Four of these samples (BC656, BC660, BC667, and BC671) were collected during cruise JR-257, when the box-corer was deployed to assess the locations suitability for gravity coring, prior to deploying the gravity corer (Table 2.1 and Fig. 2.1). BC667 and BC671 were recovered from the locations of GC666 and GC673, respectively, while BC656 and BC660 are associated with additional gravity cores that are being studied elsewhere. A further two surface samples (BC737 and BC738) were collected during cruise JR-15002, in November 2015 (Stowasser et al., 2015), along with 2 sub-cores (BC737 (D) and BC738 (D)) (Table 2.1 and Fig. 2.1), from locations in a similar oceanographic setting to the other four surface samples studied here, to investigate spatial variation in the foraminiferal assemblage across the South Georgia shelf.

Box coring was undertaken using the BAS box corer (JR-257) and the BAS giant box corer (JR-15002 - which has a larger box), both of which were deployed using the midship winch. After recovery, water was allowed to drain from the

collection box, the surface sediment was then photographed and sub-core liners pushed into the sediment. Surface sediment (upper ~2 cm) was transferred to two to six sample bags. Sub-cores were capped at each end and either frozen or stored in the cool store. Four sub-cores were recovered from BC737 and BC738, 15 cm in length from BC737 and 20 cm in length from BC738. Two of these sub-cores were frozen, with one being cut into 1 cm slices that were then wrapped in aluminium foil to prevent plastic contamination that can adversely affect biomarker analysis. The remaining two sub-cores were retained in the cold store (+4 °C), one being cut into 1 cm samples which were then washed through a 63 µm sieve and the top 15 samples dyed with Rose Bengal.

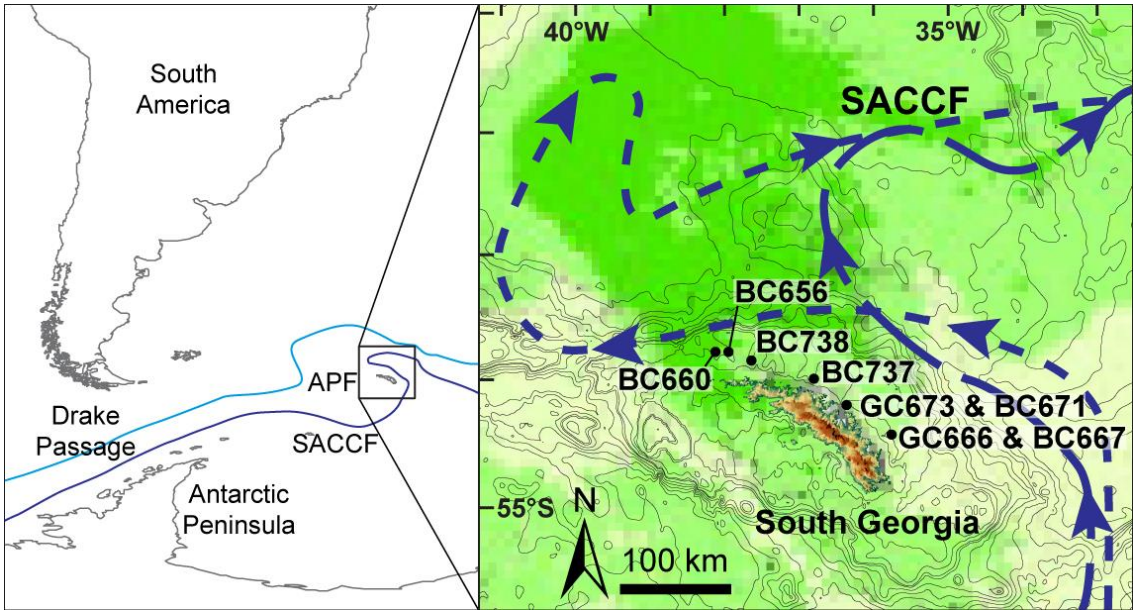


Figure 2.1 Sample location map
Map of South Georgia and sampling locations. The location of South Georgia in relation to the Antarctic Peninsula and South America showing the approximate location of the Antarctic Polar Front (APF – light blue) and the Southern Antarctic Circumpolar Current Front (SACCF – dark blue). The inset shows a topographical map of South Georgia with surrounding bathymetry with the sampling locations indicated. The dark blue lines represent the location and average position of the SACCF (contemporary variation near South Georgia shown by dashed lines, indicating most easterly and westerly extents (Thorpe et al., 2002). The mean surface chlorophyll-α concentration (mg m^{-2}) between September and March is shown in green with darker colours indicating higher concentration (SeaWiFS derived satellite data, NASA, means calculated only for cells where 10 values were obtained within a year, from Murphy et al. (2013)).

2.2 Methods

2.2.1 Dating and age/depth model development

2.2.1.1 Radiocarbon dating

A total of 19 radiocarbon dates, from GC666, GC673 and BC671, were acquired to develop the age/depth models that are utilised in this study (Tables 5.2 and 5.2). Five dates were previously published in Graham et al. (2017), all from

GC666, analysed at the Ion Beam Laboratory, ETH Zurich, Switzerland, using a gas ion source equipped 'mini radiocarbon dating−accelerator mass spectrometry system' that allows the analysis of exceptionally small samples (Wacker et al., 2013; Bard et al., 2015). The nine further samples from GC666 were all graphitised and analysed at the Poznan Radiocarbon Laboratory, A. Mickiewicz University, Poland, using a 1.5 SDH-Pelletron Model "Compact Carbon AMS" system with an MC-SNICS ion source. The four samples from GC673 and the sample from BC671 were graphitised and analysed at the NERC Radiocarbon Facility, East Kilbride, UK, using an NEC accelerator mass spectrometer.

For the horizons analysed as part of this study, samples (4-12 µg) of mixed assemblage benthic foraminifera were picked from the >125 µm sediment fraction. For some samples it was necessary to combine benthic foraminifera from two to four adjacent samples in order to have enough material to generate accurate dates.

2.2.1.2 Radiocarbon calibration and reservoir correction

The ^{14}C ages generated were calibrated to calendar ages (cal. yr BP) using OxCal v4.3 (Bronk Ramsey, 2009) with the Marine13 calibration curve (Reimer et al., 2013). A local reservoir correction (ΔR) of 433 ± 41 yr was applied, in addition to the standard global reservoir correction of 400 years that OxCal operates with. This ΔR was based on the age of surface sediments from BC671 (Table 2.2), used in preference to the ΔR of 708 ± 61 yr applied by Graham et al. (2017), as there is more confidence that the sediment from BC671 represents surface deposition.

Table 2.2 Radiocarbon age determination of surface sample
Samples analysed at the NERC RCF – min and max values represent 2 standard deviations)

Sample details			**Conventional Ages**			**Calibrated Ages**		
Core	Depth (cm)	Carbonate Source	^{14}C Age (yr)	Error (± yr)	Reservoir effect (yr)	Min (cal. yr BP)	Max (cal. yr BP)	Median (cal. yr BP)
BC671	0†	Benthic forams	797	35	NA	332	500	433

2.2.1.3 Age/depth modelling

The age/depth model for GC666 was generated using the deposition model function in OxCal v4.3 (Bronk Ramsey, 2008; 2009 - see Appendix A3 for model specification), with interpolated dates generated at 1 cm resolution. OxCal uses a Bayesian statistical approach to generate a best fit model for the core. Given the errors inherent in radiocarbon dating, in the dating technique, the calibration, and the reservoir correction, a Bayesian approach is advantageous as it can quantitatively assess outlying radiocarbon measurements. OxCal uses Markov Chain

Monte Carlo sampling to build a distribution of possible ages and runs thousands of iterations of potential age/depth models to find the most probable age/depth model for the core (Bronk Ramsey, 2009).

The number of dated horizons available from GC673 means that a Bayesian approach was unsuitable for this core as there is not enough information to generate an accurate model. When this technique was applied to core GC673, the age/depth model generated resembled a simple line of best fit through the four dated horizons which had poor agreement (A_{model} = 24%; A_{model} > 60% would indicate a reliable model). Instead, a locally weighted spline modelling technique was applied to the GC673 dates (see Appendix A4 for settings), using the CLAM age/depth modelling package in R (Blaauw, 2010) with interpolated dates generated at 1 cm resolution. This technique resulted in an age/depth model with a better fit than the other techniques available in this package, relatively small 95% confidence interval ranges and no age reversals. Furthermore, this model fits with hypothesised variation in sedimentation rate, based on variation in the percent coarse sediment in the core and comparison to the impact of similar sedimentological variation on sedimentation rates in core GC666. For consistency between the two cores ideally the same model would then have been applied to the GC666 data. However, when applied to GC666 the locally weighted spline technique resulted in an age depth model with a number of reversals and poor agreement. Therefore the OxCal age depth model has been retained for GC666. Trachsel and Telford (2017) have shown that OxCal and Clam both produce mean age depth models that are close to true ages (based on varve chronologies), although CLAM tends to underestimate the age uncertainties.

When applying the ages generated by these modelling techniques it is important to always consider the associated uncertainties, especially when discussing the relationship between changes in the proxy records developed here and climate events with well-established dates. The 2σ uncertainty in the interpolated modelled ages generated for GC666 ranges from ±120 years to ±2240 years (mean = ±440 years) and the 2σ for GC673 ranges from ±70 years to ± 120 years. There is also uncertainty regarding the accuracy of the local reservoir correction, which has been based on a single sample. Furthermore, it is not possible to quantify how this reservoir effect may have varied through time, a factor that may not be important in the Holocene but can be considerable over the transitions between glacial and interglacials. The introduction of fossil carbon from eroded lithology can also impact radiocarbon ages, particularly in the Southern Ocean (e.g. Pudsey and Evans, 2001), however the use of benthic foraminiferal carbonate, as opposed to acid insoluble organic carbon, should have eliminated this effect.

However, diagenetic alteration of foraminifera, potentially due to methane activity (discussed in detail in Section 5.2.1), has the potential to impact radiocarbon dates. The ages reported for samples where diagenetic alteration has been identified may therefore be older than their true ages. For example, Pohlman et al. (2013) found that authigenic carbonate resulted in ^{14}C ages from foraminifera that were 50−400 years older than their true ages.

2.2.2 Benthic foraminiferal census counts

2.2.2.1 Sample preparation and counting protocol

Eighty-nine quarter core samples from GC666 (giving approximately 200 yr resolution) and 38 quarter core samples from GC673 (at 32 cm resolution, increased to 4 cm resolution between 304 and 336 cmcd) were selected to be analysed for Benthic Foraminiferal Assemblage (BFA). Samples were washed with reverse osmosis deionised water over a 63 μm sieve; both fractions were dried at 40ºC, weighed and retained in plastic vials (>63 μm fraction) or plastic sample bags (<63 μm fraction).

All foraminifera from the >63 μm fraction were counted and identified, using an Olympus SZX10 binocular microscope, to determine downcore changes in BFA. To generate statistically significant assemblage data at least 300 were counted, where possible, in keeping with accepted practice. Where abundance was very high (>500 individuals) samples were split using a microsplitter prior to counting – only counting the first 300 specimens from such a sample would have biased the count, as the samples were split into >250 μm, >125 μm, and 63 μm fractions to ease counting. The species and taxonomic groupings presented in Chapter 3 are arranged in taxonomic order following the suprageneric classifications of Kaminski (2004) for the agglutinated taxa and Loeblich and Tappan (1988) for the calcareous walled taxa. Species identification was largely based on the works of Heron-Allen and Earland (1932a), Earland (1933), Anderson (1975), Mackensen et al. (1990), Ishman and Domack (1994), Violanti (1996), Igarashi et al. (2001), and Majewski (2005, 2013). The specimen images presented in Chapter 3 were generated using the FEI Quanta 600 environmental scanning electron microscope and the LEO 535VP variable pressure scanning electron microscope at the British Geological Survey, Keyworth, UK.

The Benthic Foraminifera Accumulation Rate (BFAR) was also calculated, for use as a semi-quantitative proxy for palaeoproductivity, as developed by Herguera and Berger (1991) and Herguera (1992). BFAR was calculated by summing the benthic foraminifera counted in the >63 μm fraction, adjusted for any sample splitting, and converting this to an accumulation rate using equation 1.1:

$$BFAR = (BFN/100) \times MAR \qquad \text{(Eq. 1.1)}$$

where BFN is the total number of benthic foraminifera in the >63 μm fraction and MAR is the mass accumulation rate, calculated using equation 1.2:

$$\text{MAR} = \text{sedimentation rate} \times \text{dry bulk density} \quad \text{(Eq. 1.2)}$$

Statistical techniques applied to BFA data are described in Section 2.3.7.

2.2.2.2 Rose Bengal staining

Rose Bengal is a non-vital biological stain that is a common technique used to identify 'live' foraminifera (e.g. Bernhard et al., 2006; Figueira et al., 2012; Theodor et al., 2016a). To investigate 'live' abundances in surface samples from the six box cores and samples from sub-cores from BC7373 and BC738 the sediment was washed over a 63 μm sieve, prior to staining with Rose Bengal. The coarse fraction was then soaked in a Rose Bengal/seawater solution (1 g : 1 L) for 24 hrs before being rinsed with seawater from the shipboard underway seawater supply until the water ran clear and dried at 40ºC after a final rinse with MilliQ water. Benthic foraminiferal census counts were then undertaken using the method described in the previous section. Tests where all, or all but one or two, chambers were well stained bright red were considered to be "living" at the time of staining (e.g. Caulle et al., 2015; Fontanier et al., 2016; Wang et al., 2016). For thick-walled agglutinated taxa, where the opaque test wall concealed the extent of the staining, the tests were broken open allowing the staining to be assessed. Tests with a pink tint or isolated spots of red were not included, nor were tests where only a small number of isolated chambers were stained. The Average Living Depth (ALD) (Jorissen et al., 1995) was calculated using equation 1.3, for the 10 taxa with at least five "live" specimens in one or more samples:

$$ALD = \sum_{i=1x} \frac{n_i \times D_i}{N} \quad \text{(Eq. 1.3)}$$

where x is the lower boundary of the deepest sample included in the calculation, n_i is the number of specimens in the interval I, D_i is the midpoint of sample I, and N is the total number of individuals for all levels.

We also calculated Median Living Depth (MLD) (Theodor et al., 2016b) for these taxa using equation 1.4:

$$MLD = \left(\frac{l_m - u_m}{n_m}\right) \times \left(\frac{n}{2 - c_{n-1}}\right) + u_m \quad \text{(Eq. 1.4)}$$

where n is the total number of individuals, n_m is the number of individuals in the median interval, c_{n-1} is the number of individuals shallower than the median depth interval, u_m is the upper limit of the median depth interval, and l_m is the lower limit of the median depth interval. Differences between ALD and MLD are generally small but can be significant for taxa with a wide downcore occurrence range (Theodor et al., 2016b).

It is important to recognize the potential limitations of the Rose Bengal staining technique in identifying truly living specimens. Rose Bengal is adsorbed onto any proteins, whether or not they are alive, and can therefore stain necrotic as well as healthy cytoplasm (e.g. Bernhard, 2000). Where decay rates are slow (due, for example, to low oxygen levels), Rose Bengal may stain foraminifera that have been dead for months to several years (Corliss and Emerson, 1990). It is therefore important to apply criteria that are as strict as possible when categorizing which specimens are living and which are dead (e.g. Caulle et al., 2015; Fontanier et al., 2016) and to bear this limitation in mind when considering live abundances arrived at through Rose Bengal staining. It is also possible for specimens identified as living at a certain depth interval to have been transported there after death by bioturbation (see Bernhard, 2000, and references therein). Furthermore, where decay rates are very slow, specimens that appear live at different depths within the sediment column may be significantly older than the overlying live assemblages. This is dependent on the sedimentation rate being high enough to bury specimens to a significant depth before decay is sufficiently progressed that staining with Rose Bengal will no longer occur. While it is important to recognize the limitations of Rose Bengal staining, it is simple, fairly reliable (depending on the temporal resolution required), and inexpensive to use and is currently the most appropriate technique to apply when, as in this study, the samples are processed immediately upon collection (Bernhard, 2000).

In addition, Murray and Bowser (2000) have proposed that, in oxygenated environments, dead tests are unlikely to retain protoplasm due to predation being the most likely cause of death. While we did not directly measure the oxygenation of the sediments studied here, there was no indication of anoxia or dysoxia from the colour and odour of the sediments on recovery.

2.2.2.3 BFA as a palaeoceanographic proxy

Although BFA does not result in fully quantitative data, it is still widely used in multi-proxy studies, especially in marginal settings, to generate semi-quantitative or qualitative data, especially in combination with geochemical proxy data (carried in the foraminifera tests – stable isotopes, Mg/Ca, Sr/Ca, etc.) (Jorissen et al., 2007). BFA can be used in the reconstruction of several different parameters, including changes in the flux (quantity and seasonality) and type of organic carbon reaching the sea floor, bottom water oxygenation, reconstruction of sea level, salinity, and temperature (Jorissen et al., 1995; Levin et al., 2001; Jorissen et al., 2007). Utilising a large set of surface sediment samples Mackensen et al. (1995) identified four main environmental parameters controlling deep-water benthic foraminiferal assemblage in the Southern Atlantic (including the Atlantic sector of

the Southern Ocean): 1) Bottom water oxygenation, 2) primary productivity and organic carbon flux rates, 3) bottom water carbonate saturation and 4) the hydrodynamic properties of the benthic environment. As with many proxies interpretation of foraminiferal assemblage may be hindered by a number of problems, including the interdependency of many parameters in the oceans, the limitation to the reconstruction of modern ecosystems that may not cover past conditions, and an incomplete understanding of taphonomic effects (Jorissen et al., 2007).

Organic flux is recognised as one of the main parameters affecting benthic faunas (Jorissen et al., 2007). Knowledge of changes in primary production and transport of organic matter to the ocean floor is vital to understanding the response of the biological carbon pump to climate change. Rather than reconstructing primary productivity directly, benthic foraminifera are better utilised in reconstructing organic flux to the sea floor which is a function of surface primary productivity (Eppley and Peterson, 1979) at least to ~1000 m (Fischer et al., 2000), and the conversion of this carbon to particulate organic carbon by bacteria (Thomas, 2007). Three different approaches can be applied to utilise benthic foraminifera as a proxy for palaeo-export:

1. Reconstruction based on the relationships between certain faunal compositions and organic flux rates (e.g. Altenbach et al., 1999; De Rijk et al., 2000). However, some taxa do not appear to be particularly dependent on flux regime (e.g. *Epistominella exigua* and *Melonis* spp. (Altenbach et al., 1999)) and inconsistencies between studied areas appear to exist (Schonfeld and Altenbach, 2005).
2. The application of multivariate statistical methods, such as multiple regression function and correspondence analysis, to investigate faunal response to different flux regimes (Jorissen et al., 2007, and refs therein)
3. The Benthic Foraminifera Accumulation Rate (BFAR) which measures the accumulation rate of foraminifera larger than 150 μm and varies linearly for export production values ranging from 40-135 g/m^2/yr (Herguera and Berger, 1991; Herguera, 1992). This is the method applied in this study

The interpretation of benthic foraminiferal assemblage in terms of palaeo-export flux is complicated by the faunal response not being solely dependent on flux variation but also linked to the quality of the organic matter delivered and the timing of this delivery (Jorissen et al., 2007). Benthic foraminifera respond better to more labile organic matter that is easily metabolised; therefore, if the organic matter delivered has a large terrestrial input, which generally comprises more refractory material, the faunal response will be reduced. Benthic foraminifera are

also known to respond strongly to pulses of large phytoplankton deposits (Gooday, 1988, 1993, 1996), with phytodetrivorous taxa responding rapidly such events and likely to go on to comprise a significant proportion of fossil assemblages, potentially allowing the reconstruction of the seasonality of productivity. However, given their small size and delicate tests, these taxa are more likely to be affected by taphonomic processes (Jorissen et al., 2007).

It may be possible to reconstruct bottom-water current velocity using benthic foraminiferal assemblages as intensified currents have been shown to influence benthic assemblages (e.g. Lutze and Thiel, 1989; Linke and Lutze, 1993; Schonfeld, 1997, 2002). Under high current velocities some taxa may inhabit elevated substrate; Schonfeld (2002) showed a linear correlation between taxa thought typical of elevated microhabitats and bottom-water current velocity, and used this to reconstruct bottom-water current velocity through the Holocene. However, the application of this method may be complicated by transportation adding or removing components, which is more likely in higher current regimes, and the poor understanding of the ecology of many taxa (Schonfeld, 1997, 2002).

2.2.3 Foraminiferal stable isotopes

2.2.3.1 Sample preparation and analysis

Oxygen ($\delta^{18}O$) and carbon ($\delta^{13}C$) stable isotopes were measured on benthic foraminifera from GC666 and GC673, planktonic foraminifera from GC666, and Rose Bengal stained benthic foraminifera from BC737 and BC738. From the gravity cores, the benthic species chosen for this analysis was *Cassidulinoides parkerianus*, as this species was present in most of the samples analysed for BFA. *C. parkerianus* is also a heavily calcified form with a large test, such that even where only one specimen was present in a sample this single specimen often provided enough material for analysis. One to four specimens of *C. parkerianus*, from 73 samples from GC666 and 35 samples from GC673, were analysed. The number of specimens analysed from each sample was dependent on the number of specimens available for analysis and size of the specimens, with a target weight of >100 µg.

The planktonic species analysed from GC666 was *Neogloboquadrina pachyderma*, the only planktonic species recorded in this study. One to 25 specimens of *N. pachyderma* were analysed, from 27 samples from GC666 (planktonic foraminifera were only present in 36 samples from GC666, 9 of which did not provide enough carbonate (i.e. <10µg) to analyse). To test the reproducibility of the benthic data a number of duplicates were analysed from both gravity cores (this was not possible for the planktonic data as there was not enough material to repeat the analysis). The results of the duplicate analysis (Table 2.3)

reveal excellent reproducibility, with an average standard deviation (1 S.D.) of 0.33‰ for $\delta^{13}C$ and 0.10‰ for $\delta^{18}O$, the error used for the data in this study.

Table 2.3 Duplicate $\delta^{18}O$ and $\delta^{13}C$ analysis
Results of duplicate $\delta^{18}O$ and $\delta^{13}C$ analysis of benthic foraminifera from GC666 and GC673. All isotope data given as ‰ on the VPDB scale to 2 D.P.

Sample details		Original Sample		Duplicate Sample		$\delta^{13}C$		$\delta^{18}O$	
Core	**No.**	**$\delta^{13}C$**	**$\delta^{18}O$**	**$\delta^{13}C$**	**$\delta^{18}O$**	**Mean**	**1SD**	**Mean**	**1SD**
GC666	033	−0.05	+3.88	+0.61	+4.10	+0.28	0.47	+3.88	0.15
GC666	053	+0.43	+3.72	+0.28	+4.07	+0.35	0.11	+3.89	0.24
GC666	099	+0.87	+3.79	+0.77	+4.02	+0.82	0.07	+3.90	0.16
GC666	223	−2.37	+4.12	−1.83	+4.37	−2.10	0.38	+4.24	0.17
GC666	335	−3.67	+4.45	−3.28	+4.41	−3.27	0.27	+4.43	0.03
GC666	455	−3.41	+5.00	−4.28	+5.06	−3.85	0.62	+5.05	0.04
GC673	032	+0.67	+3.89	+0.48	+3.92	+0.58	0.13	+3.91	0.02
GC673	308	+0.55	+3.77	+0.32	+3.92	+0.44	0.17	+3.84	0.11
GC673	352	−0.78	+3.84	−1.20	+3.95	−0.99	0.30	+3.89	0.08
GC673	768	−6.30	+4.11	−5.25	+4.12	−5.78	0.74	+4.12	0.01
Average SD							**0.18**		**0.10**

To investigate whether stable isotope ratios change with living depth three species from BC737 (*Astrononion echolsi*, *Cassidulinoides porrectus*, and *Buccella* sp. 1) from 10 samples (0–1 cm to 9–10 cm) and two species from BC738 (*A. echolsi* and *C. porrectus*) from 6 samples (0–1 cm to 5–6 cm) were analysed for $\delta^{18}O$ and $\delta^{13}C$. All specimens for isotope analysis were picked from the 125–250 µm fraction to minimise the possible effects of ontogenetic change in fractionation rates. These species were selected because their ALD/MLD revealed different microhabitat preferences and because they were present in high enough abundance to provide sufficient calcite to conduct the analyses (see Chapter 4). Each isotope data point was measured on between 4 and 15 specimens from each sample for *A. echolsi* and *C. porrectus*, and on 3 to 5 specimens from each sample for the more heavily calcified *Buccella* sp. 1. To eliminate contamination by organic carbon remaining in the test (the presence of the stain indicates that organic carbon is present within the tests) the samples were plasma ashed prior to analysis (at the NERC Isotope Geosciences Laboratory (NIGL), British Geological Survey (Keyworth, UK) using an Emitech K1050X Plasma Asher). To test whether the plasma ashing

process had any impact on the isotope composition of the foraminiferal calcite, five standards (KCM) were subjected to the same processing and analysed in parallel. In addition, to test whether the Rose Bengal stain had any impact on the isotope composition, five KCM standards mixed with Rose Bengal and five KCM standards mixed with Rose Bengal and plasma ashed were also analysed. Results from the test isotope samples (KCM plus Rose Bengal, KCM plasma ashed, plasma ashed KCM plus Rose Bengal), run to establish whether these processing methods could have any impact on the foraminiferal isotope results, revealed that the values from the treated standards for both $\delta^{13}C$ and $\delta^{18}O$ were within the normal 'within-run' error (Table 2.4).

All isotope measurements were carried out by Hilary Sloane and Jack Lacey at the NERC Isotope Geosciences Laboratory (NIGL), British Geological Survey (BGS), Keyworth, UK, using an IsoPrime 100 dual inlet mass spectrometer with Multiprep device. Isotope values were calculated to the Vienna Pee Dee Belemnite (VPDB) scale in parts per thousand using a within-run laboratory standard (KCM) calibrated to international NBS standards. Analytical reproducibility was <0.1‰ (1σ) for both $\delta^{18}O$ and $\delta^{13}C$.

Table 2.4 Rose Bengal and plasma ashing tests
Results of Rose Bengal and plasma ashing tests. All isotope data given as ‰ on the VPDB scale to 2 D.P.

KCM + 10% Rose Bengal			KCM + 10% Rose Bengal plasma ashed			KCM plasma ashed		
	$\delta^{13}C$	$\delta^{18}O$		$\delta^{13}C$	$\delta^{18}O$		$\delta^{13}C$	$\delta^{18}O$
RBKCM 1	+1.99	−1.77	RBKCMP 1	+1.92	−1.67	PKCM 1	+1.92	−1.76
RBKCM 2	+1.91	−1.81	RBKCMP 2	+1.88	−1.89	PKCM 2	+2.05	−1.57
RBKCM 3	+1.98	−1.76	RBKCMP 3	+1.91	−1.58	PKCM 3	+2.02	−1.63
RBKCM 4	+1.96	−1.81	RBKCMP 4	+1.93	−1.72	PKCM 4	+2.02	−1.65
RBKCM 5	+1.91	−1.89	RBKCMP 5	+1.91	−1.62	PKCM 5	+1.94	−1.74
MEAN	+1.95	−1.81	**MEAN**	+1.91	−1.69	**MEAN**	+1.99	−1.67
1sd	0.04	0.05	**1sd**	0.02	0.12	**1sd**	0.06	0.08

2.2.3.2 Application of foraminiferal stable isotopes

Stable isotopes, those isotopes which are not subject to radioactive decay but are readily fractionated by environmental processes, enable the reconstruction of a wide range of palaeoceanographic parameters including global ice volume (GIV), circulation patterns, productivity, , surface and bottom temperatures, salinity, etc. The factors that can influence $\delta^{13}C_{foram}$ and $\delta^{18}O_{foram}$ are discussed in this section.

Factors affecting oxygen isotopes in foraminifera

The two main influences on the $\delta^{18}O_{mineral}$ in marine records are: 1) the $\delta^{18}O$ composition of the water ($\delta^{18}O_{sw}$) in which the precipitate forms, which is controlled by global (e.g. ice volume) and local (e.g. freshwater input vs evaporation) factors; and 2) the water temperature at which the mineral (e.g. foraminiferal calcite) precipitates (as temperature increases $\delta^{18}O$ in the precipitate decreases (Fig. 2.2) (Maslin and Swann, 2005)). The primary global influence on $\delta^{18}O_{sw}$ at the centennial timescale with which this study is concerned is the amount of water that is stored as ice at the ice caps at the time of formation (GIV) (Shackleton, 1967) (isotope exchange with oceanic crust also influences $\delta^{18}O_{sw}$, but this occurs over a much longer timescale (hundreds of millions of years) (Muehlenbachs and Clayton, 1976; Gregory and Taylor, 1981)). The impact of GIV on $\delta^{18}O_{sw}$ is due to the preferential evaporation of water containing the lighter isotope, ^{16}O, resulting in lower $\delta^{18}O$ for water vapour, cloud droplets and precipitation, relative to seawater. This difference is then enhanced by the subsequent preferential condensation of water containing the heavier isotope, ^{18}O, which leaves the clouds as precipitation, such that $\delta^{18}O$ of the remaining water vapour increases with latitude and altitude. Therefore, high latitude snowfall is strongly depleted in ^{18}O and the ice-caps that form from it are a reservoir with low $\delta^{18}O$ values. During glacial periods, when GIV increases as ice accumulates at high northern and southern latitudes, the size of this isotopically light reservoir increases, resulting in an increase in the $\delta^{18}O_{sw}$ of the global ocean, with the opposite occurring during interglacials as the isotopically light ice melts. The $\delta^{18}O_{sw}$ of the global ocean at the LGM (ca. 21 ka) was ca. 1.1‰ higher than current values (Adkins et al., 2002).

Local process influencing $\delta^{18}O_{sw}$ are also related to the preferential evaporation of ^{16}O from the surface of the ocean in restricted environments. Evaporation causes the salinity and $\delta^{18}O$ of surface waters to increase, while inflow of high precipitation via rivers and/or glacial melt causes the salinity and $\delta^{18}O$ of surface waters to decrease. The $\delta^{18}O$ of surface waters in near shore environments is therefore inherently linked to the inflow/evaporation (I/E) balance. Values for both $\delta^{18}O$ and salinity in surface waters are correlated with latitude (high at low latitudes where evaporation is greatest and low at high latitudes where inflow of isotopically light freshwater is high; the relationship between the two is roughly 0.5‰/psu although this varies regionally, dependent on the amount of mixing with precipitation (and the $\delta^{18}O$ of that precipitation) (Schmidt et al., 1999; LeGrande and Schmidt, 2006). The I/E balance $\delta^{18}O$ of surface waters can also be affected by the growth and melt of sea-ice, the input of freshwater from rivers, and the advection or upwelling of water masses with different isotopic values. Rivers add

isotopically light freshwater, while ice-sheet growth produces isotopically light brines and the subsequent melting releases isotopically heavy, low salinity water.

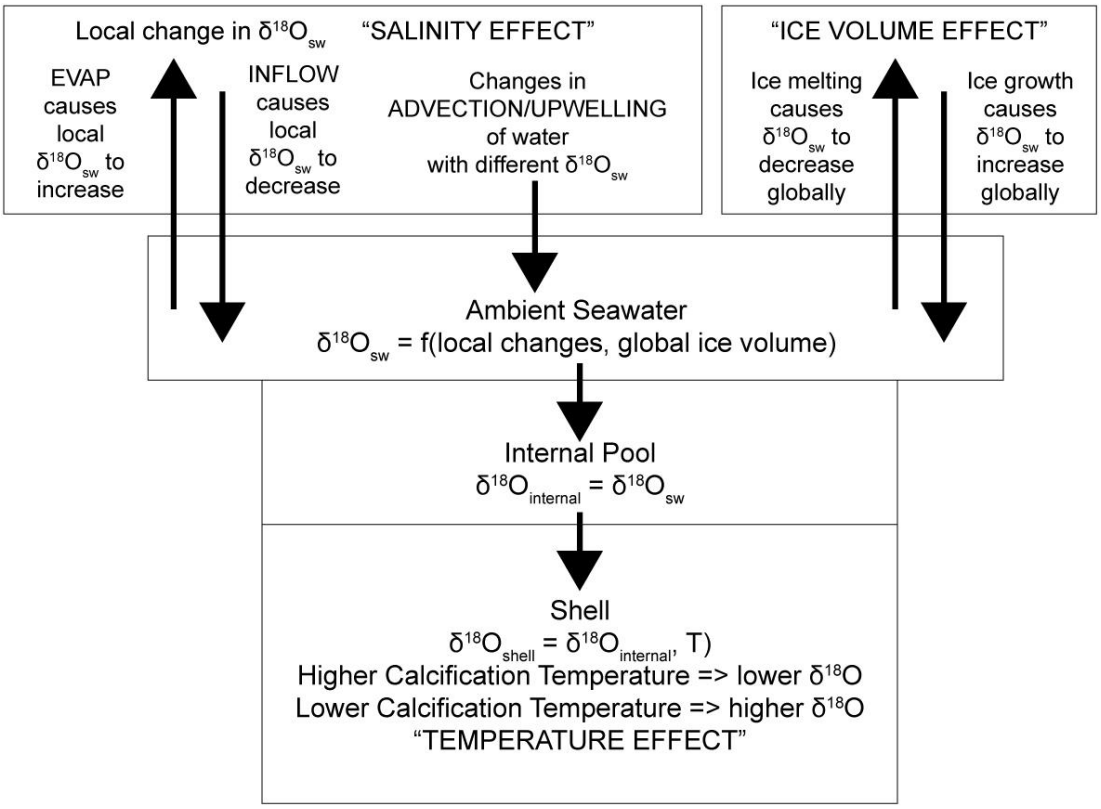


Figure 2.2 Factors affecting $\delta^{18}O_{foram}$
Factors affecting the $\delta^{18}O$ of foraminifera tests, excluding potential vital effects and assuming thermodynamic equilibrium fractionation occurs (redrawn from Ravelo and Hillaire-Marcel, 2007).

In addition, $\delta^{18}O_{foram}$ is offset from $\delta^{18}O_{sw}$ by thermodynamic (equilibrium) isotope fractionation that occurs during carbonate precipitation (Ravelo and Hillaire-Marcel, 2007). When the shell calcite is in oxygen isotopic equilibrium with seawater the $\delta^{18}O$ of the calcite has been found to decrease by ca. 0.23‰ for every 1 ºC temperature increases (Shackleton, 1974). It is therefore possible to use $\delta^{18}O_{foram}$ as a palaeothermometer, provided $\delta^{18}O_{sw}$ at the time of formation can be measured or calculated using another proxy. Given the uncertainty in calculating past $\delta^{18}O_{sw}$ it is more common to apply these values to interpret relative temperature changes rather than to achieve absolute values.

However not all species of foraminifera calcify in isotope equilibrium, due to biological 'vital' effects (e.g. Duplessy et al., 1970), some of which relate to the activity of algal symbionts increasing calcification rates and causing kinetic fractionation (e.g. Ravelo and Fairbanks, 1992; Spero and Lea, 1993). The addition of a gametogenic chamber to some planktonic foraminifera as they sink at the end of their life cycle can result in an increase in $\delta^{18}O_{foram}$, due to the formation of this

chamber at a lower temperature (Lohmann and Schweitzer, 1990). Benthic foraminifera can also exhibit interspecific variation and can be affected by the carbonate ion concentration of their microenvironment, with increasing concentration causing a decrease in $\delta^{18}O_{foram}$ (Spero et al., 1997), possibly due to changes in calcification rates inducing kinetic fractionation. The lower carbonate ion concentration, and lower pH, of porewaters may lead to higher $\delta^{18}O$ values for infaunal species, when compared to epifaunal species.

Factors affecting carbon isotopes in foraminifera

The $\delta^{13}C$ from foraminifera tests ($\delta^{13}C_{foram}$) is strongly influenced by the isotope composition of the dissolved inorganic carbon ($\delta^{13}C_{DIC}$) in the seawater in which they form, although, due to kinetic fractionation and 'vital effects', $\delta^{13}C_{foram}$ is not usually in equilibrium with the $\delta^{13}C_{DIC}$ of seawater (Grossman, 1987; Ravelo and Fairbanks, 1992; Romanek et al., 1992). The variation in $\delta^{13}C_{foram}$ in palaeoceanographic records must be interpreted with regards to a range of parameters (Fig. 2.3) due to the non-uniformity of $\delta^{13}C_{DIC}$ throughout the oceans, and the fact that the average $\delta^{13}C_{DIC}$ of the oceans is not constant with time.

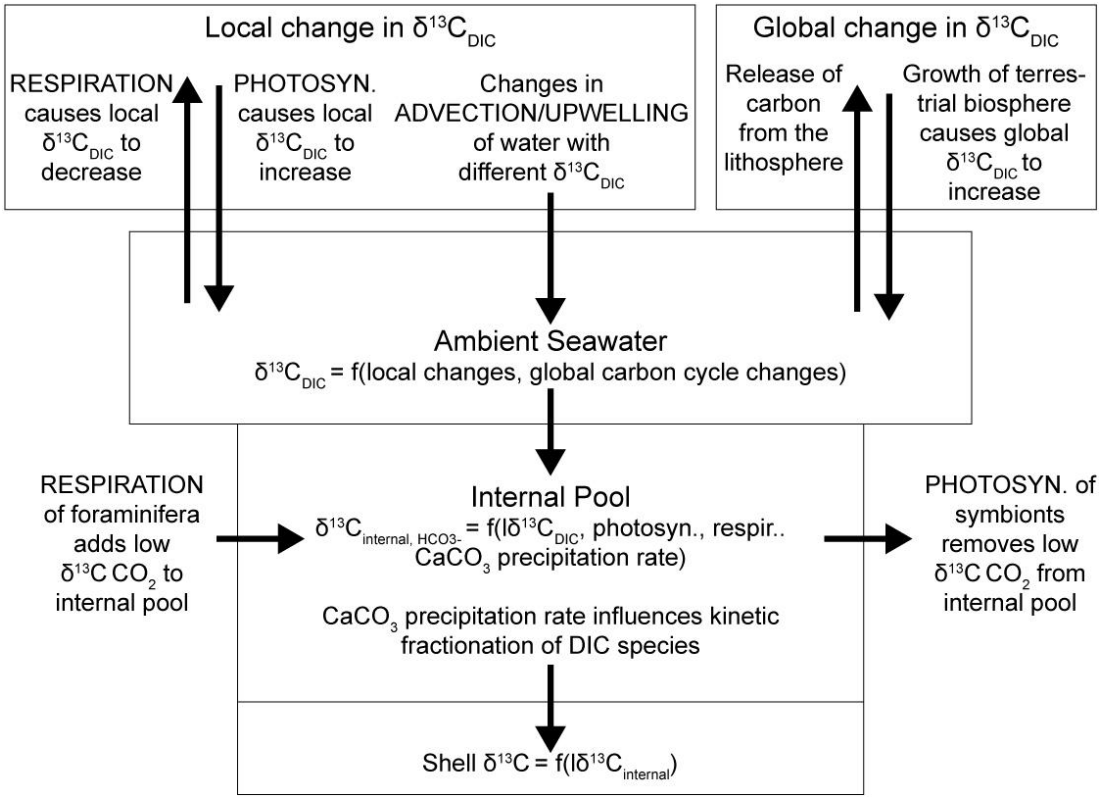


Figure 2.3 Factors influencing $\delta^{13}C_{foram}$
Factors influencing $\delta^{13}C_{foram}$ (redrawn from Ravelo and Hillaire-Marcel, 2007).

The main influence on $\delta^{13}C_{DIC}$ of the ocean is the global carbon cycle, through the division of carbon with different $\delta^{13}C$ values between the three biosphere reservoirs, the ocean, the atmosphere, and the terrestrial (e.g. Ravelo and Hillaire-

Marcel, 2007). This partitioning occurs due to fractionation that occurs during photosynthesis, which preferentially utilises the lighter isotope, ^{12}C, leading to a ^{13}C-depleted terrestrial reservoir (e.g. Park and Epstein, 1960) such that, if the terrestrial biosphere increases in size the ocean and atmosphere reservoirs become enriched in ^{13}C. The $\delta^{13}C$ values of these reservoirs can also be affected by a number of, mainly, geological processes such as: the rate of organic matter sequestration in sediments, volcanic outgassing, the release of gas hydrates, etc. The $\delta^{13}C_{DIC}$ of surface waters is also influenced by temperature, with the isotopic separation between surface waters and atmospheric CO_2 increasing as temperature decreases (e.g. Zhang et al., 1995), although this does not have a significant impact on the $\delta^{13}C_{DIC}$ of the whole ocean due to the ocean carbon reservoir being more than 50 times larger than the atmosphere reservoir.

Site specific factors also influence $\delta^{13}C_{foram}$. The balance between photosynthesis and respiration alters $\delta^{13}C_{DIC}$ in both surface and deep-waters; photosynthesis dominates in surface waters, resulting in high $\delta^{13}C_{DIC}$ values due to the export of ^{13}C-depleted organic matter, while respiration of this depleted organic matter dominates in the deeper ocean, resulting in relatively low $\delta^{13}C_{DIC}$ values (Deines, 1980; Macko et al., 1994). Increases in photosynthesis, by strengthening the biological pump, result in greater differences between surface and deep $\delta^{13}C_{DIC}$ values, such that $\delta^{13}C_{foram}$ can be a proxy for palaeoproductivity changes (once changes to $\delta^{13}C_{DIC}$ caused by variation in the global carbon cycle have been accounted for). It follows that changes to $\delta^{13}C$ in planktonic foraminifera are linked to surface productivity changes (e.g. Ruhlemann et al., 1999), while benthic species will reflect changes in carbon export to the seafloor (the carbon pump), an indirect proxy for surface productivity (e.g. Zahn et al., 1986; Sarnthein et al., 1988).

Additionally, changes in the mixing of water masses, or the original $\delta^{13}C_{DIC}$ of the masses, can impact $\delta^{13}C_{foram}$. For example, North Atlantic Deep-Water (NADW) has relatively high $\delta^{13}C_{DIC}$ values due to its North Atlantic surface water source, while Antarctic Bottom Water (AABW) has relatively low $\delta^{13}C_{DIC}$ values because it is sourced from Southern Ocean surface waters and deep-water from other basins, all of which have low $\delta^{13}C_{DIC}$ values. This means that $\delta^{13}C_{foram}$ from epibenthic species can be used to reconstruct changes in deep-water circulation, such as changes in the location of the mixing zone of NADW and AABW during the Pliocene (Ravelo and Andreasen, 2000).

The $\delta^{13}C$ of foraminifera is also affected by local changes such as seasonal shifts in environmental conditions, changes in habitat during the organism's life cycle (such as migration into deeper sediment), differential dissolution during early

diagenesis, and the deposition of secondary calcite (Ravelo and Hillaire-Marcel, 2007), and by vital effects. The rate of calcification results in abiotic kinetic fractionation, causing an enrichment of the $\delta^{13}C$ of calcite of 1.0±0.2‰ relative to DIC (Romanek et al., 1992), although this offset is subject to wide interspecific variation in both planktonic (Ravelo and Fairbanks, 1992) and benthic (Grossman, 1987) species. In addition $\delta^{13}C_{foram}$ can be affected by the action of algal symbionts which, through their photosynthesis and respiration, alter the pH, DIC concentration, and $\delta^{13}C_{DIC}$ of the microenvironment (Spero et al., 1997; Zeebe et al., 1999). Furthermore, there can be large species-specific differences in the ecological tolerances of both planktonic and benthic species, which can lead to large differences in the $\delta^{13}C_{DIC}$ of the water in which they live (e.g. McCorkle et al., 1997; Mackensen et al., 2000).

2.2.4 Geochemistry of organic matter

2.2.4.1 Sample preparation and analysis

Core GC666 was sampled for organic geochemistry at 4 cm resolution of the upper 5.15 m and at 64 cm resolution between 5.15 and 8.16 m; core GC673 was sampled for organic geochemistry at 16 cm resolution throughout. To prepare the samples for percentage organic carbon (%C), percentage nitrogen (%N), and $\delta^{13}C$ of organic matter ($\delta^{13}C_{org}$) analysis approximately 500 mg of sample was added to 5% HCl, to remove the carbonate. The samples were then rinsed in deionised water, dried at 40ºC, and then ground to a fine powder and homogenised before being transferred to a vial. Samples were analysed using a VG Optima dual inlet mass spectrometer, following combustion using a Costech ECS4010 elemental analyser at 1400ºC, at the NERC Isotope Geosciences Laboratory (NIGL), British Geological Survey (BGS), Keyworth, UK. Isotope values were calculated to the VPDB scale in parts per thousand using a within-run laboratory standards calibrated to international NBS standards. Analytical reproducibility for the within run standards was <0.1‰ for $\delta^{13}C_{org}$, <0.5% for %C, and <0.1% for %N. The %N is reported as a ratio relative to %C (C:N); for many of the samples analysed %N was close to the instrumental tolerances. The %C is reported as the organic carbon accumulation rate (C_{org} AR (g cm^{-2} kyr^{-1})) which was calculated equation 1.5:

$$C_{org}\ AR = (\%C/100) \times MAR \qquad \text{(Eq. 1.5)}$$

To evaluate the potential impact of terrestrial carbon sources on the $\delta^{13}C_{org}$ signal from GC666 and GC673, measurements of $\delta^{13}C_{org}$ were combined with a linear mixing model between potential end member values (Table 2.5) of marine organic matter ($C{:}N_{marine}$) and terrigenous organic matter ($C{:}N_{terr}$), following the method of Knudson and Ravelo (2015) to estimate the minimum and maximum %

marine organic matter ($\%_{marine}$). The $\%_{marine}$ minima and maxima were calculated using equations 1.6 and 1.7:

$$\%_{marine_min} = (C{:}N_{sample} - (C{:}N_{terr} - C{:}N_{terr_error}))/ (C{:}N_{mar} + C{:}N_{mar_error}) - (C{:}N_{terr} - C{:}N_{terr_error}) \quad \text{(Eq. 1.6)}$$

$$\%_{marine_max} = (C{:}N_{sample} - (C{:}N_{terr} + C{:}N_{terr_error}))/ (C{:}N_{mar} - C{:}N_{mar_error}) - (C{:}N_{terr} + C{:}N_{terr_error}) \quad \text{(Eq. 1.7)}$$

The $\%_{marine}$ was then used to calculate the minimum and maximum $\delta^{13}C_{marine}$ for each bulk sample using equations 1.8 and 1.9:

$$\delta^{13}C_{marine_min} = (\delta^{13}C_{org} - ((1 - \%_{marine_max}) \times (\delta^{13}C_{terr} - \delta^{13}C_{terr_error})))/ \%_{marine_max} \quad \text{(Eq. 1.8)}$$

$$\delta^{13}C_{marine_max} = (\delta^{13}C_{org} - ((1 - \%_{marine_min}) \times (\delta^{13}C_{terr} - \delta^{13}C_{terr_error})))/ \%_{marine_min} \quad \text{(Eq. 1.9)}$$

Table 2.5 Organic matter end-member values
Organic matter end-member values used to calculate $\%_{marine}$ and $\delta^{13}C_{marine}$. The terrigenous values are based on analysis of soil samples from South Georgia (Leng, unpublished data) and the marine values are based on analysis of particulate organic matter from the Southern Ocean around South Georgia (Ward et al., 2005).

	Marine	Terrigenous
$\delta^{13}C$ **(‰ VPDB)**		−26.14 ± 0.44 (Leng, unpublished data)
C:N	5.42 ± 0.19 (Ward et al., 2005)	13.01 ± 1.13 (Leng, unpublished data)

2.2.4.2 Application of organic geochemistry data

Photosynthesis is the primary fractionation process in the global carbon cycle, such that carbon isotopes in organic matter can provide information about variation in palaeo-productivity. As discussed in Section 2.2.3.2, a large fractionation occurs during the photosynthetic fixation of carbon, with ^{12}C being preferentially incorporated into organic compounds. The $\delta^{13}C$ of organic matter ($\delta^{13}C_{org}$) in marine plankton ranges between −10‰ and −31‰, with most values constrained between −17‰ and –22‰, influenced by the temperature at which the organic matter forms, in addition to the photosynthetic fractionation (Maslin and Swann, 2005). A proportion of the particulate organic carbon formed by marine phytoplankton will be incorporated and preserved in the sediment and the $\delta^{13}C_{org}$ of this material may reflect primary surface water productivity. However, as with $\delta^{13}C_{foram}$, other factors, such as terrestrial input, variation in atmospheric $\delta^{13}C$, and organic matter diagenesis, must be taken into account for this interpretation to be valid.

As organic carbon represents the largest constituent of organic matter it can provide one of the most direct proxies for palaeoproductivity (Schoepfer et al., 2015). However, only a small fraction of the organic carbon produced at the surface is preserved in the sediment (as low as ~0.1%), with a large proportion being mineralised and recycled within the ocean mixed layer (Schoepfer et al., 2015). While the majority of organic carbon in marine sediments is sourced from the surface ocean, there may also be a component of terrigenous organic carbon (e.g. Goñi et al., 1997; Opsahl and Benner, 1997). The potential influence on terrestrial organic matter can be evaluated using the accompanying C:N data. If marine plankton is the dominant source of the organic matter the C:N ratio would be expected to be below 10, while terrestrial organic matter would result in a higher C:N (e.g. Lamb et al., 2006; and references therein). The proportion of terrestrial organic matter can also be estimated using the technique described in the previous section (2.3.4.1).

2.2.5 Biogenic silica analysis

2.2.5.1 Sample preparation and analysis

65 samples from GC666 and 28 samples from GC673 were analysed for biogenic silica (BSi) at the University of Nottingham, Nottingham, UK, following the method modified by Conley and Schelske (2001) from that of Demaster (1981). For each sample 30 mg of freeze-dried sediment was placed into 125 ml flat-bottomed polypropylene bottles, 40 mL of 1% $NaCO_3$ solution was added to the bottles, and the bottles were placed in a heating bath at 85ºC and agitated every 30 minutes. After five hours 1 mL of liquid was pipetted into centrifuge tubes containing 9 mL of 0.021 N HCl; this subsampling was repeated after six and seven hours.

The subsamples were then analysed for dissolved Si using the UoN Water Chemistry Analysis Procedures: Silicate analysis. Four mL of each sample prepared using the above method was pipetted into a polypropylene centrifuge tube, 0.4 mL of sodium molybdate solution was added, and the tube was well shaken. After 5−15 minutes 1 mL of 50% H_2SO_4 was added and the tube was well shaken again. After 30 minutes the absorbance in a 2 cm^3 cuvette at 365 nm was measured against the reagent blank, using a Thermo-Scientific Helios Omega UV-VIS spectrophotometer. Silicon solution standards at 10 ppm, 5 ppm, 2.5 ppm, 1 ppm, and 0.5 ppm were prepared using the above method and analysed alongside the samples to provide calibration for the spectrophotometer data.

A linear least-squares regression analysis was applied to the increase in BSi extracted versus time, over the three sub-samples for each sample (taking into account the various dilution steps and the amount of sediment used). This was then extrapolated to the intercept, giving the BSi wt. % for each sample, to correct for

any mineral SI that may have also been dissolved during the digestion process. Where there was no increasing trend the mean of the three sub-samples was used; the mean of the three sub-samples was also used where BSi wt. % was greater than 10% (Conley and Schelske, 2001). These values were then converted into an accumulation rate using equation 1.10:

$$BSi\ AR = (\%BSi/100) \times MAR \qquad \text{(Eq. 1.10)}$$

2.2.5.2 Application of BSi

Biogenic silica is a measurement of the amorphous Si content of sediments (Conley and Schelske, 2001). It has been shown to be a reliable proxy for diatom abundance (Conley, 1988), and for the abundance of other siliceous microfossils including phytoliths (Schwandes, 1998) and sponges (Conley and Schelske, 1993). Changes in BSi can therefore be used to infer changes in nutrient enrichment or productivity, via variation in diatom production and sedimentation (e.g. Conley and Schelske, 1993; Ragueneau et al., 2000). The high preservation efficiency of biogenic silica (~3%), approximately 30 times greater than that of organic carbon, means that BSi is a major proxy for export production (Ragueneau et al., 2000; Treguer and De La Rocha, 2013).

However, the robustness of BSi as a palaeoproductivity proxy relies on the assumption that variation in the sediment record is reflective of variation in the overlying surface waters. At the global scale inconsistencies between surface and sedimentary fluxes have been recorded for BSi (e.g. Nelson et al., 1995), as well as for organic carbon (e.g. Jahnke, 1996). Variation in preservation efficiency, lateral advection of water masses, and sediment redistribution all affect the relationship between BSi preserved in the sediment and that produced at the surface (Ragueneau et al., 2000).

2.2.6 Alkenone analysis

2.2.6.1 Sample preparation and analysis

Alkenone analysis was undertaken on 76 samples from core GC666, at approximately 200 year resolution. Samples weighing approximately 4 g were weighed, wrapped in foil and placed in sample bags, with any sediment that had been in contact with the plastic (from the core-liner, cling-film, or packing material) removed. The samples were then freeze-dried before being ground and homogenised using an agate pestle and mortar.

Alkenone analysis was carried out in the Geographical Laboratories at the University of Durham, UK, working with Prof Erin McClymont. Lipids were extracted from the sediment using a CEM microwave system with 12 mL of dichloromethane:methanol (DCM:MeOH – 3:1, v/v). Weighed sediment, magnetic stirrers, and 10 µL of an internal standard (Table 2.6) were placed in Teflon

microwave vessels, to which 12 mL of DCM:MeOH (3:1) was added. The vessels were then placed on a carousel with a microwave optical sensor, the carousel was placed in the microwave and run through a pre-programmed cycle (heat to 70ºC over 2 minutes, hold and 70ºC for 5 minutes, then cool to 35ºC). The solvent/sediment mix was then decanted into screw-cap test tubes before being centrifuged at 3000 rpm for 5 minutes. The supernatant fluid was then decanted into long test tubes, taken to dryness using a Genevac EZ – Envi centrifugal evaporator, transferred to vials and dried using nitrogen blow down, then stored in the freezer until required.

The total lipid extract (TLE) was separated into three fractions using silica column chromatography, with the alkenone containing fraction recovered using 100% DCM. The dried TLE was dissolved with DCM and hexane and transferred to the column. The columns were then rinsed four times with MeOH, four times with DCM, and four times with hexane, separating the TLE into three fractions. The fractions were then dried under nitrogen blow down before being transferred to 2 mL screw top vials and stored in the freezer until required.

The relative abundances of di-, tri-, and tetra-unsaturated C_{37} alkenones were then analysed using two methods. Initially samples were analysed using a gas-chromatograph fitted with a flame ionisation detector (GC-FID).The chromatograms generated by using GC-FID revealed the coelution of other compounds with the C_{37} alkenone peaks, preventing integration of the peaks (Fig. 2.4). The samples were therefore then analysed using gas-chromatography with chemical ionisation mass spectrometry (GC-CIMS), which has the advantage of targeting specific compounds using the relative retention times compared with known standards (Fig. 2.5).

The quantification of relative concentrations of $C_{37:2}$, $C_{37:3}$, and $C_{37:4}$ alkenones were calculated by integrating the area under the compound specific peaks in the GC-CIMS chromatograms using the Xcalibur software (Fig. 2.6). In the majority of samples analysed from GC666 the $C_{37:4}$ peaks are either very poor or not present at all. Therefore, the $U^{K'}_{37}$ index of Muller et al. (1998) was utilised as this is based on $C_{37:2}$ and $C_{37:3}$ alkenones only:

$$U^{k'}_{37} = (C_{37:2})/(C_{37:2} + C_{37:3}) \qquad \text{(Eq. 1.11)}$$

Sea surface temperature estimates were then calculated using the $U^{K'}_{37}$-SST calibrations of Sikes et al. (1997) and Muller et al. (1998):

$$SST = (U^{k'}_{37} + 0.082)/0.038 \text{ (Sikes et al., 1997)} \qquad \text{(Eq. 1.12)}$$

$$SST = (U^{k'}_{37} - 0.044)/0.033 \text{ (Muller et al., 1998)} \qquad \text{(Eq. 1.13)}$$

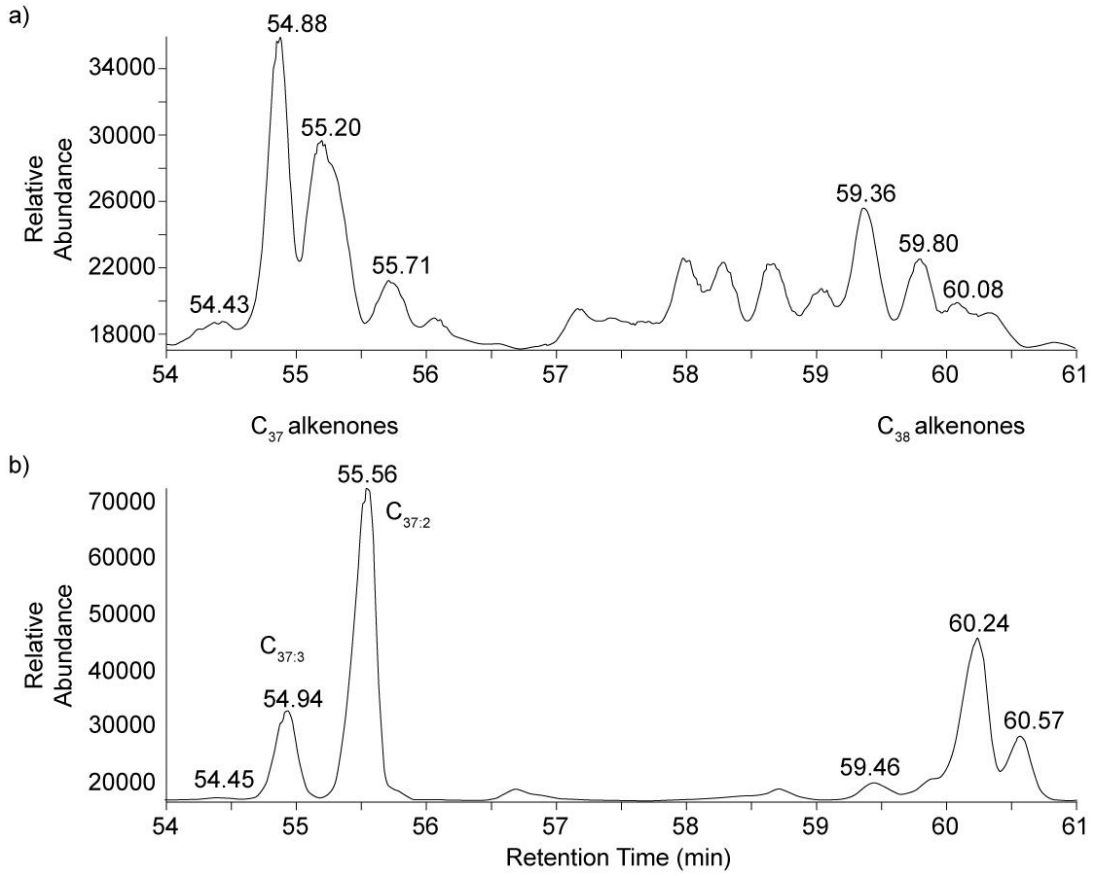


Figure 2.4 Example GC-FID chromatograms
a) GC-FID chromatogram from GC666-108, the complex and muddled peaks show that other chemical species are coeluting with the alkenones making integration of the alkenone peaks difficult. b) Example chromatogram showing clean alkenone peaks that would easily be integrated. This sample, which was known to have good alkenone peaks, was run at the same time as the GC666 samples to aid in the identification of the retention times for the alkenones. The sample comes from warmer tropical seas so the $C_{37:2}$ is much larger than the $C_{37:3}$, unlike in colder seas where the $C_{37:2}$ peak is smaller.

2.2.6.2 Alkenones as a proxy for sea surface temperature

Alkenones are long-chain unsaturated ketones that are produced by coccolithophores, in particular *Emiliana huxleyi* and *Gephyrocapsa oceanica* (e.g. Muller et al., 1998), phytoplankton in the class Prymnesiophyceae (Marlowe et al., 1984). The technique of estimating past SSTs from alkenones was initially developed towards the end of the last century (e.g. Prahl and Wakeham, 1987; Muller et al., 1998). The relative number of unsaturations (the number of carbon-carbon double bonds within the molecule) is the temperature dependent property of alkenones and the U^{K}_{37} and the $U^{K'}_{37}$ indices are both mathematical expressions that show the degree of alkenone unsaturation (Brassell et al., 1986; Prahl and Wakeham, 1987). The U^{K}_{37} index considers three unsaturation states ($C_{37:4}$, $C_{37:3}$, and $C_{37:2}$) while the $U^{K'}_{37}$ index only considers the $C_{37:3}$, and $C_{37:2}$, and was developed because $C_{37:4}$ is often not present in sediments (Brassell et al., 1986;

Prahl and Wakeham, 1987). Initial studies on cultured *E. huxleyi* revealed the strong correlation between C_{37} variation and growth temperature (Marlowe et al., 1984; Prahl and Wakeham, 1987; Prahl et al., 1988) and the calibration study conducted by Muller et al. (1998) further supported the relationship between $U^{K'}_{37}$ and annual mean SST.

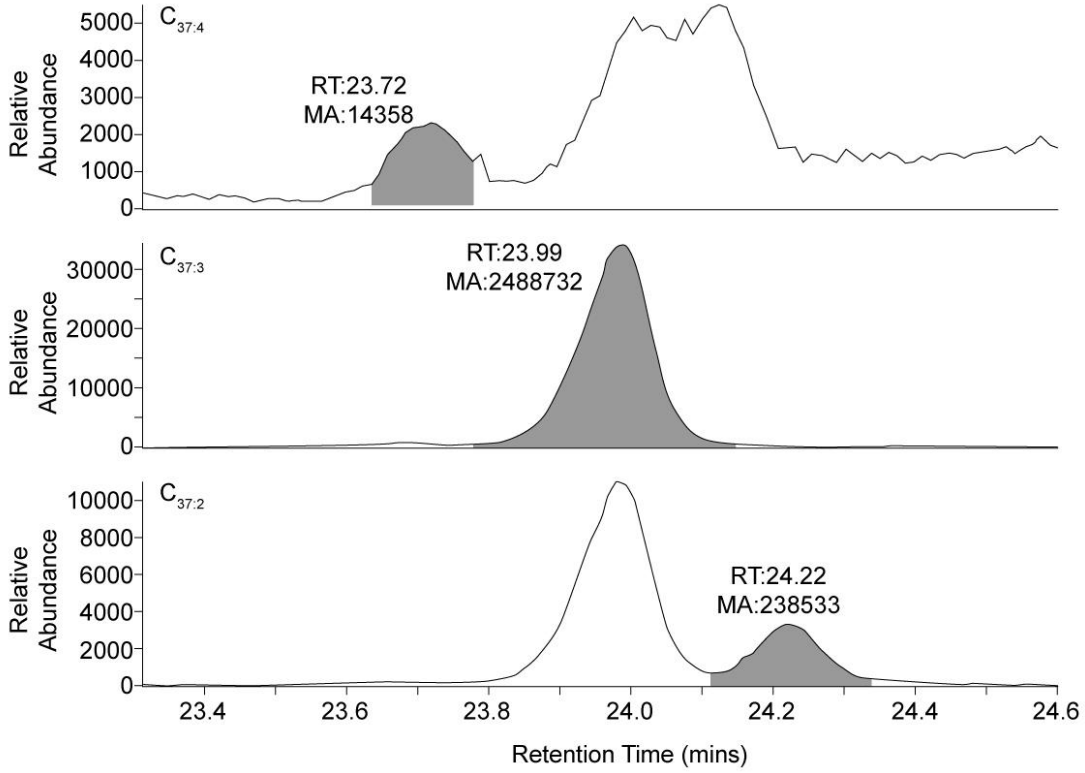


Figure 2.5 Example GC-CIMS chromatogram
An example of a GC-CIMS chromatogram from GC666-021. The GC-CIMS has the advantage of targeting specific compounds using the relative retention times compared with known standards. The di-, tri- and tetra-unsaturated C_{37} alkenones are displayed on separate lines. RT = retention time, MA = area of peak.

Although $U^{K'}_{37}$ is the more commonly used index, due to the low abundance or absence of $C_{37:4}$ in many sediments, $C_{37:4}$ abundance can be high in sediments from the high latitudes of both hemispheres (e.g. Sikes et al., 1997; Sicre et al., 2002; Sikes and Sicre, 2002; Bendle et al., 2005). While high $C_{37:4}$ abundance in northern high latitudes may be associated with deviation between $U^{K'}_{37}$ and SSTs and the U^{K}_{37} index provides more reliable SSTs (e.g. Bendle et al., 2005), in the Southern Ocean $C_{37:4}$ abundance shows a poor relationship to temperature, such that the $U^{K'}_{37}$ is the more appropriate index to use (Sikes et al., 1997).

Table 2.6 Components of lipid internal standard
Components of internal standard, dissolved in 25 mL hexane.

Standard	Weight	Fraction
5-α-cholestane	4.568 mg	F1
Heptatriacontane	2.835 mg	F1
2-nonadecanone	6.168 mg	F2
5α-androstan-3β-ol	2.527 mg	F3

2.2.7 Statistical methods

2.2.7.1 Diversity

The diversity of the benthic foraminiferal assemblage data was estimated using Fisher's alpha (Fisher et al., 1943), as this method takes into account differences in the number of individuals counted in different samples. The Fisher's alpha values were calculated using version 3.18 of the palaeontological statistical package, PAST3 (Hammer et al., 2001), in which Fisher's alpha is defined by the equation:

$$S = a \ln\left(1 + \frac{n}{a}\right) \qquad \text{(Eq. 1.14)}$$

where *S* is the number of taxa, *n* is the number of individuals, and *a* is Fisher's alpha.

2.2.7.2 Dominance

Dominance is a measure of the degree to which a single taxon is more numerous than other taxa within an ecological community. Dominance was calculated for the benthic foraminiferal data in PAST3, which applies the following equation:

$$D = \sum_i \left(\frac{n_i}{n}\right)^2 \qquad \text{(Eq. 1.15)}$$

where n_i is the number of individuals of taxon *i*. Dominance ranges from 0 (all taxa equally present) to 1 (one taxon dominates completely).

2.2.7.3 Cluster analysis

Cluster analysis groups objects such that objects in the same group are more similar than those in other groups and can be used to explore data for similarities. The analysis was applied to the benthic foraminiferal assemblage data to identify whether the analysed samples could be clustered into any statistically supported groupings, and whether these groupings supported down core zonation. The analysis was performed in PAST3 using the chord similarity index applied with an unweighted paired group average (UWPGA) algorithm, with these parameters chosen as they are commonly used to analyse benthic foraminiferal data (Hohenegger pers. comm. 2016). The analysis used the absolute abundance data, after taxa which constituted <1% of total counts in all samples were removed. The

UWPGA algorithm joins clusters based on the average distance of all members in the two groups.

2.2.7.4 Detrended correspondence analysis

Detrended correspondence analysis (DCA) is an ordination technique developed for ecological analysis that converts complex multivariate data into a system of axes. DCA is used in preference to standard correspondence analysis (CA) as it removes the 'horseshoe effect' that commonly occurs when using CA. A unimodal ordination technique (e.g. CA, DCA) was used here in preference to a linear ordination technique, such as principal component analysis, because the length of the longest gradient (DCA Axis 1) was greater than than two (2.18); a gradient length greater than two indicates that unimodal ordination techniques (CA or DCA) are more appropriate (Simpson pers. comm. 2011). Although CA would ideally be used, as it involves fewer assumptions, CA of the BFA data results in an arch, therefore a DCA was applied. The DCA analysis of the benthic foraminiferal assemblage data was undertaken in PAST3, using absolute abundance data after taxa which constituted <1% of total counts in all samples were removed.

2.3 Summary

The methods that were used to generate the data in this thesis are summarised below:

- Benthic foraminifera were picked for radiocarbon analysis, with analysis undertaken at ETH Zurich, the NERC Radiocarbon Facility, and the Poznan Radiocarbon Laboratory. Age/depth models were generated using OxCal and CLAM in R.
- Detailed benthic foraminiferal census counts were carried out on the >63 μm fraction. Samples from box cores BC737 and BC738 were stained with Rose Bengal on collection to allow the identification of 'live' specimens.
- Benthic (*C. parkerianus*) and planktonic (*N. pachyderma*) foraminifera were picked from the >63 μm fraction for stable isotope analysis.
- Organic carbon weight %, $\delta^{13}C$, and nitrogen weight % was determined by acidifying bulk sediment samples with 5% HCl.
- Biogenic silica was digested from bulk sediment samples and the BSi weight % was calculated.
- Alkenones were extracted from freeze-dried samples using a CEM microwave system. Silica columns were used to separate the lipid fractions and the alkenone baring fraction was analysed using gas chromatography (GC-FID and GC-CIMS)

Chapter 3

Systematic taxonomy of Holocene South Georgia benthic foraminifera

3.1 Introduction

Benthic foraminiferal assemblage (BFA) data is widely used in multi-proxy palaeoclimate studies, especially in marginal settings, to generate semi-quantitative or qualitative data. By combining assemblage data with geochemical proxy data (carried in the foraminifera tests – stable isotopes, Mg/Ca, Sr/Ca, etc.) benthic foraminifera have been central to many advances in palaeoclimate research, such as global glacial/interglacial cycles, temperature and salinity changes, and as water mass tracers. As discussed in Section 2.2.2, BFAs can be used in the reconstruction of several different parameters, with the most promising being changes in the flux (quantity and seasonality) and type of organic carbon reaching the sea floor, and bottom water oxygenation, while shallow water assemblages can be applied to the reconstruction of sea level, salinity, and temperature (Jorissen et al., 1995; Levin et al., 2001; Jorissen et al., 2007).

BFAs form part of the palaeoenvironmental investigations discussed in Chapters 6 and 7. To underpin this work, and to provide a resource for any future benthic foraminiferal analyses that may be undertaken in the future, this chapter comprises a detailed taxonomic analysis of benthic foraminifera from two gravity cores (GC666 and GC673), six surface samples from box cores (BC656, BC660, BC667, BC671, BC737, and BC738), and two sub-cores from BC737 and BC738 (for sample locations see Fig. 2.1), the first such study focused on South Georgia since Earland (1933).

The data presented in this chapter has previously been published in Dejardin et al. (2018). The published manuscript is included in Appendix A5. A reference collection of species from South Georgia has been deposited in the European Micropalaeontological Reference Centre at Micropress Europe, Kraków, Poland.

3.1.1 Previous benthic foraminiferal studies

Earland (1933) conducted a survey of the benthic foraminifera of South Georgia, utilising surface sediment samples collected from around the island as part of the *Discovery* Expeditions. Since this study, there has been no further taxonomic work focussed on South Georgia but a number of benthic foraminiferal assemblage studies have been conducted at other Southern Ocean and Antarctic locations. The Antarctic Peninsula (AP) is one of the better studied areas in the region, with

foraminiferal research here commencing in the first half of the 20th century (Earland, 1934; Cushman, 1945), followed by a number of brief US Antarctic Program taxonomic reports (e.g. Lipps et al., 1972). In a more comprehensive study of the AP, Ishman and Domack (1994) analysed a large number of surface sediment samples from three areas on the western side of the peninsula (Bransfield Strait, Marguerite Bay, and Palmer Archipelago). A detailed assessment of the benthic foraminiferal assemblages of Admiralty Bay, King George Island, and the South Shetland Islands has been conducted by Majewski (2005, 2010), again on surface sediment samples. On the eastern side of the AP Majewski and Anderson (2009) examined the palaeoclimatic implications of Holocene foraminiferal assemblages from the Firth of Tay. Further east, Anderson (1975) identified 160 species in surface samples distributed across the Weddell Sea, while Mackensen et al. (1990) focussed on surface samples from the sea's eastern corner.

Herb (1971) described the variation in benthic faunas across the Drake Passage, illustrating the differences between the shelf environments of southern South America and Antarctica. Mackensen et al. (1993) analysed a similar transect of surface samples through the sub-Antarctic zone between 0 and 10º E. Useful studies from Southern Ocean localities more distant from South Georgia include Majewski's (2013) description of benthic foraminifera from core-top samples around Pine Island and Ferrero Bays in the Amundsen Sea, Violanti's (1996) analysis of live and dead foraminifera from surface samples from Terra Nova Bay, Ross Sea, and Igarashi et al.'s (2001) study of samples from sediment cores extending into the Holocene from Lützow-Hom Bay, East Antarctica.

3.2 Foraminiferal assemblages

3.2.1 Surface samples

A total of 1850 benthic foraminifera were identified and counted from the six sample locations, representing 56 taxonomic groupings (see Section 3.4 & Appendix A6). In addition 18 planktonic foraminifera were also identified, all belonging to *Neogloboquadrina pachyderma.* The total benthic abundance ranges from 104 per 30 cm^3 to 818 per 30 cm^3, with agglutinated taxa comprising 59–79% of the fauna.

In the six surface samples five species (*Miliammina earlandi, Reophax, subdentaliniformis, Labrospira scitula, Cassidulinoides porrectus*, and *Astrononion echolsi*) dominate, comprising 36–75% of the total assemblage. The remaining assemblage is largely made up of eight further species; *Lagenammina* cf. *sphaerica, Labrospira* sp. 1., *Glaphyrammina rostrata, Portatrocahmmina antarctica weisneri, Deuterammina scoresbyi, Pseudotrochammina* sp. 1, *Globocassidulina crassa rossensis*, and *Fursenkoina fusiformis*. Together, these 13 species comprise

at least 75% of the total assemblage of the surface samples, with the exception of BC671 in which these 13 species comprise 66% of the assemblage and *Cassidulinoides parkerianus* comprises a further 11% of the total assemblage.

3.2.2 Box core sub-cores

A total of 7686 benthic foraminifera were identified from the sub-core sample sequences, representing 62 taxonomic groupings (see Section 3.4 & Appendix A7). The total abundance for the upper ten samples from the sub-cores ranges from 6 to 16 g^{-1} for BC737, with the highest abundance evident in the 2–3 cm sample, and from 6 to 13 g^{-1} for BC738, with the highest abundance evident in the 0–1 cm sample. The assemblages, down-core variation, and "live" vs dead abundances are discussed in Chapter 4.

3.2.3 Gravity cores

A total of 42452 benthic foraminifera were identified and counted from the two gravity cores (GC666 - 26891, GC673 – 15561) representing 59 taxonomic groupings (see Section 3.4 & Appendix A8 & A9). In addition 223 planktonic foraminifera (GC666 - 185, GC673 – 38) were identified, all belonging to *Neogloboquadrina pachyderma.* The details of the assemblages identified in the two gravity cores are discussed in detail in Sections 5.2.4 and 5.3.3.

3.3 Comparison to other studies

In this study 24 of the 345 species described by Earland (1933) were identified, including 13 of the 24 species identified as being most typical of South Georgia assemblages, and 7 of the 14 species Earland described as being particularly characteristic of the region. The taxa identified as being most abundant by Earland (1933) include many of the more abundant species identified here, such as *M. earlandi*. The majority of species recorded in this study are present at a range of locations around the Southern Ocean but there are 5 species that may be endemic to South Georgia (e.g. *Labrospira* sp. 1, *G. rostrata*, *Recurvoides* sp. 1, *Buccella* sp. 1, and *Buccella* sp. 2). In a comprehensive review of a range a data sources, encompassing a wide diversity of taxa, Hogg et al. (2011) highlighted the significance of endemism within the South Georgia shelf ecosystem and its importance to global biodiversity, and the identification of potentially unidentified species of foraminifera further adds to that diversity. The benthic foraminiferal assemblage documented here suggests that, while there may be partial isolation, the microfauna of South Georgia are connected to those of the rest of the Southern Ocean. A total of 20 species identified in this study were also recorded by Ishman and Domack (1994) in their study of the Bellingshausen Sea margin; 22 of the 105 species identified by Majewski (2005), from King George Island, are also recorded

in this study, as are 11 of the 26 species identified by Majewski and Anderson (2009) from the Firth of Tay. The strong affinity with AP taxa suggests that the position of South Georgia in the path of the ACC downstream of the AP allows for a degree of microfaunal connectivity between the two. The species that are commonly recorded from both the AP and South Georgia include *Portatrochammina antarctica weisneri*, *Reophax subdentaliniformis*, *A. echolsi*, *Spiroplectammina biformis*, *Nonionella bradii*, *N. iridea*, *C. parkerianus*, *C. porrectus*, and *F. fusiformis*, many of which are among the more abundant taxa. A comparable level of similarity is seen with studies of Weddell Sea benthic foraminifera (Anderson, 1975; Mackensen et al., 1990).

There is less similarity between the South Georgia foraminiferal fauna and those recorded from more remote areas of the Southern Ocean. For example, only six of the taxa recorded here were also recorded by Herb (1971) from the Drake Passage. However, this may be due to the open ocean/deep water nature of these locations, rather than proximity, as there are greater levels of connectivity between our sites and more distal locations on the Antarctic shelf including Pine Island Bay and Terra Nova Bay (Violanti, 1996; Majewski, 2013).

A proportion (20 of 78 species; 26%) of the species described here have been left in open nomenclature. While some of this is due to there only being a small number of poor/damaged specimens of certain species preventing accurate identification, a number of these species, for example *Buccella* sp. 1, *Buccella* sp. 2, *Labrospira* sp. 1, and *Recurvoides* sp. 1, may be new to science and previously undescribed. The presence of previously undescribed species would provide evidence for endemism in the microfauna of the South Georgia shelf and confirms the semi-isolated nature of the shelf environment. Given the relatively slow rates of genetic evolution of benthic foraminifera, in comparison to planktonic taxa (Pawlowski et al., 1997; Gooday and Jorissen, 2012), and their long stratigraphic ranges (Kaminski and Gradstein, 2005; Holbourn et al., 2013), the presence of endemic species may indicate that the South Georgia shelf has been isolated for a considerable period of time. A similar pattern of endemism has been identified by Kender and Kaminski (2017) in their study of modern deep-water agglutinated foraminifera in the restricted basin of the Bering Sea. The presence of endemic foraminifera also adds to existing evidence regarding the important biodiversity of South Georgia, as highlighted by Hogg et al. (2011).

3.4 Systematic taxonomy

The following species and taxonomic groupings are arranged in taxonomic order following the suprageneric classifications of Kaminski (2004) for the agglutinated taxa and Loeblich and Tappan (1988) for the calcareous walled taxa.

Species identification are largely based on the works of Heron-Allen and Earland (1932a), Earland (1933), Anderson (1975), Mackensen et al. (1990), Ishman and Domack (1994), Violanti (1996), Igarashi et al. (2001), and Majewski (2005, 2013). Described species are illustrated in Figs. 3.1 to 3.7.

Family **Rhabdamminidae** Brady, 1884
Subfamily **Rhabdammininae** Brady, 1884
Genus *Rhabdammina* M. Sars in Carpenter, 1869

***Rhabdammina* spp.**
(Fig. 3.1:1)

Material. 13 specimens from six samples.
Description. Included in this group are any thick-walled tube fragments comprising coarsely agglutinated material with rough external surface and very smooth internal cavity.

Family **Hippocrepinellidae** Loeblich & Tappan, 1984 emend. Mikhalevich, 1995
Genus *Hippocrepinella* Heron-Allen & Earland, 1932b

Hippocrepinella alba Heron-Allen & Earland, 1932b
(Fig. 3.1:2)

1932b *Hippocrepinella alba* Heron-Allen & Earland: 259, pl. 1, figs 16-18.
1933 *Hippocrepinella alba* Heron-Allen & Earland; Earland: 71, pl. 7, fig. 10-12.

Material. 28 specimens from seven samples.
Description. Unilocular, cylindrical to fusiform test; smooth, thin, white wall constructed of very small particles; aperture round at end of narrow neck, which may have a collar; may also have a secondary basal aperture.
Occurrence. Originally described from the South Atlantic (Heron-Allen and Earland, 1932b) and subsequently recorded from South Georgia (Earland, 1933), both from surface samples.

Family **Rhizamminidae** Wiesner, 1931
Genus *Rhizammina* Brady, 1879

***Rhizammina* spp.**
(Fig. 3.1:3-5)

Material. 49 specimens from nine samples.
Description. Included in this group are any elongate tubular tests with thin, flexible walls; only broken tubes recovered in this study; specimens recorded here mainly composed of diatomaceous material.

Family **Saccamminidae** Brady, 1884
Subfamily **Saccammininae** Brady, 1884
Genus *Lagenammina* Rhumbler, 1911

Lagenammina* cf. *sphaerica Moreman, 1930
(Fig. 3.1:6)

1930 *Lagenammina sphaerica* Moreman: 51, pl. 5, fig. 15.

Material. 70 specimens from 13 samples.

Description. Unilocular, near spherical test; thin agglutinated wall, medium sand grains, rough surface; simple aperture produced at the end of an elongate neck, neck approximately two fifths of test length.
Remarks. As *Lagenammina sphaerica* Moreman was described from Silurian deposits in the USA, this cannot be the same species. However the morphological similarities are uncanny. The species described here does bear some similarity to the extant *Lagenammina arenulata* (Skinner) that is common at other Antarctic localities but this species does not possess an elongate neck. Jones (1994) suggests that specimens similar to *L. arenulata* (Skinner), but with an elongate neck, belong to *L. atlantica* (Cushman). However, the original description of this species reveals that it too does not possess an elongate neck.

Genus *Saccammina* Carpenter, 1869

***Saccammina* spp.**
(Fig. 3.1:8)

Material. Four specimens from three samples.
Description. Included in this group are any forms that have a globular, unilocular test, with a firm, fine to medium agglutinated wall held together with an organic cement, and a round aperture produced on a short neck.

Subfamily **Thuramminінae** Miklukho-Maklay, 1963
Genus *Astrammina* Rhumbler in Wiesner, (1931)

Astrammina rara Rhumbler in Wiesner, (1931)
(Fig. 3.1:9-11)

1931 *Astrammina rara* Rhumbler, in Wiesner: 78, pl. 2, fig. 19.
1932b *Armorella sphaerica* Heron-Allen & Earland: 257, pl. 2, figs 4-11.
1932b *Pelosphaera cornuta* Heron-Allen & Earland: 255, pl. 2, figs 12-15.
1933 *Armorella sphaerica* Heron-Allen & Earland; Earland: 65, pl. 7, figs 16-23.
1933 *Pelosphaera cornuta* Heron-Allen & Earland; Earland, 61, pl. 7, figs 24-27.

Material. 12 specimens from six samples.
Description. Large, near-spherical, unilocular test with a number of narrow 'arms' extending in various directions, often along sponge spicules that are incorporated into the test wall. Wall firmly agglutinated, comprising fine to coarse sand grains, sponge spicules, and diatoms, with a grey to yellowish brown cement.
Occurrence. Originally described from the South Atlantic (Heron-Allen and Earland, 1932b) and subsequently recorded from South Georgia (Earland, 1933), both from surface samples.
Remarks. The synonymy of *Astrammina rara* Rhumbler, *Armorella sphaerica* Heron-Allen & Earland, and *Pelosphaera cornuta* Heron-Allen & Earland was demonstrated by DeLaca (1986) in analysis of live Antarctic specimens.

Family **Psammosphaeridae** Haeckel, 1894
Subfamily **Psammosphaerinae** Haeckel, 1894
Genus *Psammosphaera* Schulze, 1875

Psammosphaera bowmanni Heron-Allen & Earland, 1912
(Fig. 3.1:7)

1912 *Psammosphaera bowmanni* Heron-Allen & Earland: pl. 5, figs 5-6, pl. 6, fig. 5.
2010 *Capsammina bowmanni* (Heron-Allen & Earland); Gooday et al.: 349, pl. 1, figs A & B.

Material. Four specimens from three samples.
Description. Free, monothalamous test, comprising several small flat grains of mica cemented by very fine cement that form an irregular polyhedral chamber. Openings are visible where the flakes meet and cement is absent, which may be the aperture, or accidental.
Occurrence. Originally described from North Sea dredgings (Heron-Allen and Earland, 1912), it was subsequently recorded in the northeast Atlantic (Gooday et al., 2010).
Remarks. Heron-Allen and Earland (1912) were unable to assign a definite oral aperture, recording openings similar to those recorded here on some specimens but not all. Heron-Allen and Earland (1912) also note that this species is difficult to describe, as no two specimens look exactly alike. The flakes are arranged to approximately make an oval or flask shape and the gaps, the size of which may vary considerably, between the flakes are then filled with cement, so that the cemented areas vary from narrow infill to broad flat areas.

Psammosphaera fusca Schulze, 1875
(Fig. 3.2:1-2)

1875 *Psammosphaera fusca* Schulze: 113, pl. 2, fig. 8.
1994 *Psammosphaera fusca* Schulze; R.W. Jones: 31, pl. 18, figs. 1-8.
2003 *Psammosphaera fusca* Schulze; Gazdzicki & Majewski: 7, fig. 3 (1-2).

Material. 46 specimens from 15 samples.
Description. Small spherical test; usually unilocular, occasionally multiple chambers loosely joined. Agglutinated wall comprising medium to coarse grains in a fine cement.
Occurrence. Recorded from several locations in the Atlantic (Jones, 1994) and the Antarctica (Gaździcki and Majewski, 2003), all from Recent sediments.

Family **Ammodiscidae** Reuss, 1862
Subfamily **Ammodiscinae** Reuss, 1862
Genus *Ammodiscus* Reuss, 1862

Ammodiscus incertus (d'Orbigny, 1839a)
(Fig. 3.2:5-6)

1839a *Operculina incerta* d'Orbigny: 49, pl. 6, figs. 16-17.
1996 *Ammodiscus incertus* (d'Orbigny); Violanti: 53, pl. 3, fig. 6.
2001 *Ammodiscus* sp.; Igarashi et al.: 142, pl. 2, fig. 5.
2013 *Ammodiscus incertus* (d'Orbigny); Majewski: 175, fig. 3(4).

Material. 111 specimens from 22 samples.
Description. Small test (ca. 200 µm diameter), generally flat but tending towards irregular coiling in the last whorls. Up to seven whorls in microspheric form and up to six in megalospheric form, sutures between whorls somewhat depressed, proloculus spherical and central. The agglutinated test wall comprises angular grains of sand in a cement matrix that is a yellow-brown colour. Aperture a simple opening at the end of the tubular chamber.
Occurrence. Recorded from a number of locations on the Antarctic shelf (Violanti, 1996; Igarashi et al., 2001; Majewski, 2013), from Recent sediments.

Family **Rzehakinidae** Cushman, 1933
Subfamily **Miliammininae** Saidova, 1981
Genus *Miliammina* Heron-Allen & Earland, 1930

Miliammina earlandi Loeblich & Tappan, 1955

(Fig. 3.2:7-8)

1933 *Miliammina oblonga* (Heron-Allen & Earland); Earland: 92, pl. 3, fig. 17, pl. 5, figs 1-5, 7-8.
1955 *Miliammina earlandi* Loeblich & Tappan: 12, pl. 1, figs. 15-16.
1981 *Miliammina earlandi* Loeblich & Tappan; Milam & Anderson: 304, pl. 2, fig. 4.
1996 *Miliammina earlandi* Loeblich & Tappan; Violanti: 53, pl. 3, figs 10-11.
2004 *Miliammina earlandi* Loeblich & Tappan; Murray & Pudsey: 71, pl. 1, figs 8-9.

Material. 9830 specimens from 153 samples.
Description. Tubular chambers with a rounded peripheral edge, arranged in a quinqueloculine pattern, sutures slightly depressed, increasing as test size increases. Wall comprises very small mineral grains (whose composition is unclear) completely embedded in siliceous cement (insoluble in HCl), smooth/polished surface. Very light grey in colour, and large variation in test size. Crescentiform aperture is at the terminal end of the final chamber, flush or with a slight neck. There is considerable morphological variation within this species due to variation in the roundness of the chambers.
Occurrence. Originally described from the South Atlantic (Heron-Allen and Earland, 1930) and subsequently reported from several locations of the Antarctic shelf (Milam and Anderson, 1981; Violanti, 1996; Murray and Pudsey, 2004), from Recent sediments.
Remarks. Initially included in *Miliammina oblonga* (Chapman) by Heron-Allen and Earland (1930), this South Georgia form was later separated from *Miliammina arenacea* (Chapman) by Earland (1933) due to its more ovate and rounded outline, and was renamed *Miliammina oblonga* Heron & Earland. However, Loeblich and Tappan (1955) recognised that this species name had previously been assigned to *Miliolina oblonga* (Montagu), incorrectly placed in *Miliammina*, and renamed it *Miliammina earlandi* (which is used here). Earland (1933) considered *M. earlandi* to be the most characteristic, and commonest, foraminifera of the South Georgia area.

Miliammina lata Heron-Allen & Earland, 1930
(Fig. 3.2:4)

1930 *Miliammina lata* Heron-Allen & Earland: 43, pl. 1, figs13-17.
1933 *Miliammina lata* Heron-Allen & Earland; Earland: 93, pl. 3, fig. 17, p. 5, figs. 15-19.
1996 *Miliammina lata* Heron-Allen & Earland; Violanti: 52, pl. 3, fig. 12.
2001 *Miliammina lata* Heron-Allen & Earland; Igarashi et al.: 140, pl. 2, fig. 10.
2005 *Miliammina lata* Heron-Allen & Earland; Majewski: 193, fig. 12(8).
2013 *Miliammina lata* Heron-Allen & Earland; Majewski: 176, fig. 4(3).

Material. 472 specimens from 64 samples.
Description. Quinqueloculine test, early chambers often not visible; inflated, broadly rounded chambers, broadening at the base. Slightly depressed sutures, thick, smooth, agglutinated wall comprising very small particles in an excess of siliceous cement. Small crescentiform aperture at the end of the final chamber.
Occurrence. Originally described from the South Atlantic (Heron-Allen and Earland, 1930), it was subsequently recorded from South Georgia (Earland, 1933) and a number of locations on the Antarctic shelf (Violanti, 1996; Igarashi et al., 2001; Majewski, 2005, 2013), all from Recent sediments.

Family **Hormosinellidae** Rauzer-Chernousova & Reytlinger, 1986
Genus *Hormosinella* Shchedrina, 1969

***Hormosinella* sp.**
(Fig. 3.2:3)

Material. Four fragmentary specimens from two samples.
Description. Large, uniserial test, ovate/fusiform chambers separated by long, delicate, necks. Thin, agglutinated wall, rounded terminal aperture on elongate neck.
Remarks. Only recorded here as fragmentary specimens.

Genus *Hormosinelloides* Zheng & Fu, 2001

Hormosinelloides guttifer (Brady, 1881)
(Fig. 3.2:9-10)

1881 *Lituola (Reophax) guttifera* Brady: 49, pl. 31, figs 10-15.
1975 *Reophax guttifer* (Brady); Anderson: 74, pl. 1, fig. 18.
1994 *Hormosinella guttifera* (Brady); R.W. Jones: 38, pl. 31, figs 10-15.
2005 *Hormosinelloides guttifer* (Brady); Kaminski & Gradstein: 249, pl. 46, figs 1-8.

Material. 31 specimens from four samples.
Description. Uniserial test comprising a series of approximately three to five pyriform chambers. Thin, agglutinated wall with a fairly rough finish. Simple, rounded aperture, terminal on an elongated neck.
Occurrence. Originally described from the South Atlantic by Brady (1881) who recorded that it was 'exceedingly rare', it was subsequently recorded from the Weddell Sea (Anderson, 1975), from Recent sediments.
Remarks. Placed in the genus *Hormosinelloides* by Kaminski and Gradstein (2005) because the chambers attach near to the base of the apertural neck of the preceding chamber.

Family **Reophacidae** Cushman, 1927
Genus *Nodulina* Rhumbler, 1895

Nodulina dentaliniformis (Brady, 1881)
(Fig. 3.2:11)

1881 *Lituola (Reophax) dentaliniformis* Brady: 49, pl. 30, figs 21-22.
1994 *Reophax dentaliniformis* (Brady); R.W. Jones: 37, pl. 30, figs 21-22.
2017 *Nodulina dentaliniformis* (Brady); Kender & Kaminski: pl. 8, fig. 1.

Material. Six specimens from one sample.
Description. Slender, elongate test with straight axis, three to six chambers, final chamber significantly larger and tapered; wall comprises sand grains in firm cement, with a smooth finish. Large, round terminal aperture on a short tubular neck of finer grains.
Occurrence. Recorded from the South Pacific, the North Atlantic (Brady, 1881; Jones, 1994), and the Bering Sea (Kender and Kaminski, 2017).
Remarks. *Nodulina dentaliformis* (Brady) is the type species of the genus *Nodulina*, which is distinguished from *Reophax* by its more symmetrical, regular chambers, horizontal sutures, and straighter axis.

Genus *Reophax* de Montfort, 1808

Reophax subdentaliniformis Parr, 1950
(Fig. 3.2:12-13)

1950 *Reophax subdentaliniformis* Parr: 269, pl. 4, fig. 20.
1996 *Nodulina subdentaliniformis* (Parr); Violanti: 53, pl. 3, fig. 18.

2005 *Nodulina subdentaliniformis* (Parr); Majewski: 194, fig. 13(6-7).

Material. 478 specimens from 32 samples.
Description. Slender, elongate test with a slight curvature, usually 4-6 chambers (may be difficult to distinguish), final chamber significantly larger and tapered. Wall comprises poorly sorted sand grains in firm cement, coarsely finished. Large, round terminal aperture on a short neck of finer sand grains.
Occurrence. Recorded from Recent Antarctic sediments (Parr, 1950; Violanti, 1996; Majewski, 2005).
Remarks. In this study this species was placed within the genus *Reophax* on the basis of the curvature of the test.

Reophax subfusiformis Earland, 1933 emend. Höglund, 1947
(Fig. 3.2:14)

1933 *Reophax subfusiformis* Earland: 74, pl. 2, figs 16-19.
1947 *Reophax subfusiformis* Earland; Höglund: 77.
2004 *Reophax subfusiformis* Earland; Murray & Pudsey: 72, pl. 2, fig. 5.
2005 *Reophax subfusiformis* Earland; Kaminski & Gradstein: 275, pl. 54, figs 1-8.

Material. 21 specimens from 12 samples.
Description. Slender, elongate, slightly arched test comprising two to four chambers, final chamber large, tapering and fusiform. Chambers increase rapidly in size, final chamber often comprising the majority of the test, depressed sutures, wall comprises poorly sorted sand grains in firm cement, coarsely finished. Large, round terminal aperture on a short neck.
Occurrence. This species was originally described by Earland (1933) from a number of stations near South Georgia. The description was subsequently emended by Höglund (1947) using specimens from the North Sea. Earland (1934) also reported its occurrence around the Falkland Islands where it is widely distributed but rare at most localities. Kaminski and Gradstein (2005) report *R. subfusiformis* is reported from Recent sediments at high latitude stations throughout the Atlantic and Southern Oceans.

Family **Hormosinidae** Haeckel, 1894
Subfamily **Hormosininae** Haeckel, 1894
Genus *Pseudonodosinella* Saidova, 1970

***Pseudonodosinella* sp.**
(Fig. 3.2:15)

Material. One specimen from one sample.
Description. Elongate, uniserial test, ovate chambers that overlap much of the preceding chamber, including the aperture. Firmly agglutinated, smoothly finished wall, terminal aperture.

Family **Haplophragmoididae** Maync, 1952
Genus *Haplophragmoides* Cushman, 1910

Haplophragmoides bradyi Robertson subsp. ***niigatensis*** Uchio, 1962
(Fig. 3.3:1-2)

1962 *Haplophragmoides bradyi* (Robertson) subsp *niigatensis* Uchio: 385, pl. 18, fig. 6.
1975 *Haplophragmoides bradyi* (Robertson); Anderson: 76, pl. 2, fig. 8.

Material. 18 specimens from seven samples.

Description. Small, subglobose, involute test, becomes slightly evolute and umbilicate in adult tests, rounded periphery, slightly lobulate. Chambers low and broad, somewhat inflated, five in final whorl, gradually increasing in size as added. Distinct, depressed, radiate sutures. Finely agglutinated wall with smooth surface, yellowish colour. Aperture an interiomarginal crescentic slit.
Occurrence. Originally described from Recent sediments from the Sea of Japan (Uchio, 1962), it was subsequently recorded from the Weddell Sea (Anderson, 1975).
Remarks. *Haplophragmoides bradyi niigatensis* Uchio differs from *Haplophragmoides bradyi* (Robertson) in having a less evolute and more inflated test.

Haplophragmoides quadratus Earland, 1934
(Fig. 3.3:5)

1934 *Haplophragmoides quadratus* Earland: 88, pl. 3, figs 7-8.
1960 *Haplophragmoides quadratus* Earland; Uchio: 52, pl. 1, fig. 17, pl. 5, fig. 14.

Material. 38 specimens from seven samples.
Description. Planispiral, compressed test with rounded periphery, approximately square outline with rounded corners. Chambers globose, slightly inflated, four in final whorl. Distinct, depressed sutures. Aperture not clearly visible in the specimens examined here.
Occurrence. Originally described from Bellingshausen Sea, Antarctica (Earland 1932).
Remarks. *Haplophragmoides quadratus* Uchio 1960, described from the Pacific coast of the USA, appears to be the same species and would therefore be a junior synonym

Genus *Labrospira* Höglund, 1947

Labrospira scitula (Brady, 1881)
(Fig. 3.2:16-18)

1881 *Lituola (Haplopragmium) scitulum* Brady: 50, pl. 34, figs 11-13.
1933 *Haplophragmoides scitulum* (Brady); Earland: 78, pl. 3, figs 11-12.
1990 *Labrospira scitula* (Brady); Charnock and Jones: 219, pl. 6, figs 9-10; p. 236, pl. 17, fig. 6.
1994 *Veleroninoides scitulus* (Brady); Jones: 41, pl. 34, fig. 13.
?1996 *Recurvoides contortus* Violanti: 39, pl. 4, fig. 11.
2016 *Veleroninoides scitulus* (Brady); Kender and Kaminski: pl. 8, fig. 10.

Material. 329 specimens from 25 samples.
Description. Planispiral, partially evolute test, comprising three whorls with 8-11 chambers in the final whorl. Some specimens become slightly streptospiral in the final whorl, fairly deep umbilicus on both sides. Sutures slightly curved to straight, radial, and very slightly depressed. Smooth surfaced, thick agglutinated wall comprising coarse grains with yellow-brown cement, colour rapidly fades to white after death. Aperture an elongate oval-shaped areal opening, close to the base of the apertural face, with a fine-grained, raised lip surrounding the aperture.
Occurrence. Originally described from the North Atlantic (Brady, 1881), also recorded from the Bering Sea (Kender and Kaminski, 2017).
Remarks. *Labrospira scitula* (Brady) is also often placed within the genus *Veleroninoides*. However, this designation appears to be incorrect as *L. scitula* (Brady) is not fully evolute – a diagnostic characteristic of *Veleroninoides*.

***Labrospira* sp. 1**
(Fig. 3.3:3-4)

Material. 311 specimens from 35 samples.
Description. Planispiral, slightly evolute test, slightly inflated chambers, six in the final whorl. Small umbilicus, straight, radial, slightly depressed sutures, smooth surface, thick agglutinated wall comprising coarse grains with yellow-brown cement. Aperture an areal, elongate slit, close to the base of the apertural face, with a very fine-grained, raised lip surrounding the aperture.
Remarks. Our material may represent the same species as that recorded by Murray and Pudsey (2004) as *Haplophragmoides canariensis* (d'Orbigny). However, I consider this classification to be incorrect due to the significant differences in apertural characteristics, and that this may be a new species.

Family **Discamminidae** Mikhalevich, 1980
Genus *Glaphyrammina* Loeblich & Tappan, 1984

Glaphyrammina americana (Cushman, 1910)
(Fig. 3.3:6)

1910 *Ammobaculites americanus* Cushman; 117, figs 184-185.
1932a *Ammobaculites americanus* Cushman; Heron-Allen & Earland: 341, pl. 8, figs 15-17.
1994 *Glaphyrammina americana* (Cushman); Jones: 40, pl. 34, fig. 1-4.

Material. Six specimens from four samples.
Description. Very large broad and flattened test, initially planispiral becoming uniserial, spiral section slightly involute, nine chambers in the outer whorl. Wall comprises well-cemented, poorly sorted sand grains and occasional diatom frustules. Long, slit-like aperture extends the width of the final chamber.
Occurrence. Originally described off the west coast of Mexico (Cushman, 1910), later from the South Atlantic (Jones, 1994).

Glaphyrammina rostrata (Heron-Allen and Earland, 1929)
(Fig. 3.3:7)

1929 *Ammobaculites rostratus* Heron-Allen & Earland; 326, pl. 2, figs 14-17.
1933 *Ammobaculites rostratus* Heron-Allen & Earland; Earland: 80, pl. 5, figs 22-25.

Material. 294 specimens from 31 samples.
Description. Thin-walled, flattened, planispiral test. Sutures often indistinct, especially in smaller specimens, approximately six chambers in final whorl, partially evolute. In some specimens the chambers begin to uncoil to have two uniserial chambers, where this uncoiling does not occur the final chamber protrudes at an angle away from the spiral. The test is constructed of fine sand with larger grains distributed throughout this matrix. The final chamber terminates with a narrowing apertural neck, described as 'nipple-like' in Heron-Allen & Earland (1929), that is much more neatly constructed solely comprising fine sand (this structure is very fragile and often partially or completely absent).
Occurrence. This species has been described from the South Georgia region (Heron-Allen and Earland, 1929; Earland, 1933).
Remarks. Originally described by Heron-Allen and Earland (1929) within the genus *Ammobaculites*, here this species is placed in the genus *Glaphyrammina* due to the flattened nature of the test. When the apertural neck is absent the specimens can resemble *Glaphyrammina americana*, but can be separated by the less distinct sutures.

Family **Ammosphaeroidinidae** Cushman, 1927
Subfamily **Recurvoidinae** Alekseychik-Mitskevich, 1973
Genus *Recurvoides* Earland, 1934

***Recurvoides* sp. 1**
(Fig. 3.3:9-10)

Material. Five specimens from three samples.
Description. Involute, subglobose test, streptospirally coiled in early stage, becoming planispiral. Broad, low chambers. Agglutinated wall, with a fairly rough surface. Simple, areal, aperture, just above the base of the final chamber.
Remarks. These specimens are placed in the genus *Recurvoides* on the basis of wall and apertural characteristics. Due to their small size it has not been possible to definitively identify the coiling pattern.

Family **Spiroplectamminidae** Cushman, 1927
Subfamily **Spiroplectammininae** Cushman, 1927
Genus *Spiroplectammina* Cushman, 1927

Spiroplectammina biformis (Parker and Jones, 1865)
(Fig. 3.3:13)

1865 *Textularia agglutinans var. biformis* Parker & Jones: 370, pl. 15, figs 23-24.
1932a *Spiroplectammina biformis* (Parker & Jones); Heron-Allen & Earland: 347, pl. 8, figs 27-31.
1994 *Spiroplectammina biformis* (Parker & Jones); R.W. Jones: 50, pl. 45, figs 25-27.
1994 *Spiroplectammina biformis* (Parker & Jones); Ishman and Domack:150, pl. 1, fig. 4.
2003 *Spiroplectammina biformis* (Parker & Jones); Gazdzicki & Majewski: 8, fig. 4 (5).
2005 *Spiroplectammina biformis* (Parker & Jones); Majewski: 195, fig. 14 (3-5).
2009 *Spiroplectammina biformis* (Parker & Jones); Majewski & Anderson: 138, fig. 3.
2013 *Spiroplectammina biformis* (Parker & Jones); Rodrigues et al.: 214, fig. 3 (9).

Material. One specimen from one sample.
Description. Small test mainly comprising sand grains with a small amount of cement. Initially planispiral, rapidly uncoiling and becoming biserial; coiled section broader than biserial section; biserial chambers are subquadrate. Aperture a low arch at the inner margin of the final chamber.
Occurrence. Originally described from Recent sediments from Greenland (Parker and Jones, 1865) and later from the Arctic (Goes, 1894; Höglund, 1947). More recently this species has been described from the AP (Ishman and Domack, 1994; Majewski, 2005, 2013).
Remarks. The type species of *Spiroplectammina.* The large geographical separation between these two areas suggests that the Antarctic form may be a different species but they are morphologically very similar. Also recorded from the Cretaceous Chalk and Gault of England by Parker and Jones (1865), who suggest it is an abbreviated form of *Textularia annectens*, which is commonly found within the Cretaceous.

Family **Pseudobolivinidae** Wiesner, 1931
Genus *Pseudobolivina* Wiesner, 1931

Pseudobolivina antarctica Wiesner, 1931
(Fig. 3.3:8)

1931 *Pseudobolivina antarctica* Wiesner: 99, pl. 21, figs 257-258.
1975 *Pseudobolivina antarctica* Wiesner; Anderson: 78, pl. 3, fig. 4.
1981 *Pseudobolivina antarctica* Wiesner; Milam & Anderson: 305, pl. 3, fig. 7.
1990 *Pseudobolivina antarctica* Wiesner; Mackensen et al.: 258, pl. 5, fig. 7.
1996 *Pseudobolivina antarctica* Wiesner; Violanti, 55, pl. 4, figs 12-13.

Material. 28 specimens from 16 samples.
Description. Very small biserial test, tapered at the base, chambers rapidly enlarging as they are added to give broad maximum width. Wall comprises fine sand with little cement such that the surface is fairly rough. Sutures clearly visible and slightly depressed. Aperture loop-shaped extending up the face of the final chamber.
Occurrence. Originally described from Antarctica (Wiesner, 1931) and subsequently recorded in Recent sediments from a number of locations on the Antarctic shelf (Anderson, 1975; Milam and Anderson, 1981; Mackensen et al., 1990; Violanti, 1996).
Remarks. *Pseudobolivina antarctica* is also described in Igarashi et al. (2001) and Majewski (2013). However, the slit-like aperture shown by these authors does not agree with the type description suggesting it has been incorrectly assigned (their specimens may be *Textularia antarctica*).

Family **Trochamminidae** Schwager, 1877
Subfamily **Trochammininae** Schwager, 1877
Genus *Portatrochammina* R.J. Echols, 1971

Portatrochammina antarctica weisneri (Parr, 1950)
(Fig. 3.3:14-16)

1950 *Trochammina wiesneri* Parr: 279, pl. 5, fig. 14.
1975 *Portatrochammina wiesneri* (Parr); Anderson: 92, pl. 3, fig. 5.
1988 *Portatrochammina antarctica wiesneri* (Parr); Bronnimann & Whittaker: 68, figs 25D-F, 26 H-K, 27D-I.
1994 *Portatrochammina antarctica* (Parr); Ishman & Domack: 150, pl. 1, fig. 5.
1996 *Portatrochammina antarctica* (Parr); Violanti: 55, pl. 4, figs 14-15.
2001 *Portatrochammina antarctica antarctica* (Parr); Igarashi et al.: 145, pl. 4, fig. 6.
2004 *Portatrochammina antarctica* (Parr); Murray & Pudsey: 71, pl. 1, figs 14-16.
2009 *Portatrochammina antarctica* (Parr); Majewski & Anderson: 138, fig. 3.
2013 *Portatrochammina antarctica* (Parr); Majewski: 178, fig. 6(4).

Material. 462 specimens from 55 samples.
Description. Low, trochospiral test of approximately 17 chambers, slightly convex on the spiral side and shallowly concave on the umbilical side, three whorls with five chambers in the final whorl. Well-defined, moderately depressed sutures producing slightly lobate outline. Periphery sub-acute in edge view. Aperture covered by a large umbilical flap that covers much of the umbilical depression (diagnostic of this genus), parts of the apertural flaps of preceding chambers also visible. Agglutinated, imperforate wall, coarser on spiral side. Yellowish-brown colour that is markedly darker (almost reddish) in earlier chambers.
Occurrence. Originally described from Antarctica (Parr, 1950) and subsequently recorded from around Antarctica (Anderson, 1975; Bronnimann and Whittaker,

1988; Ishman and Domack, 1994; Violanti, 1996; Igarashi et al., 2001; Murray and Pudsey, 2004; Majewski and Anderson, 2009; Majewski, 2013).
Remarks. *Portatrochammina antarctica wiesneri* (Parr) can be distinguished from *Portatrochammina antarctica antarctica* (Parr) by its flatter, smoother test and subacute peripheral margin.

Subfamily **Polystomammininae** Brönnimann & Beurlen, 1977
Genus *Deuterammina* Brönnimann, 1976

Deuterammina scoresbyi Brönnimann & Whittaker, 1988
(Fig. 3.3:11-12)

1988 *Deuterammina scoresbyi* Brönnimann & Whittaker: 116, fig. 43(A-J).

Material. 237 specimens from 34 samples.
Description. Low trochospiral test, becoming planispiral in the final whorl; spiral side slightly depressed centrally; deep wide umbilical depression. Sutures distinct, straight, radial, slightly depressed, 20 chambers including the proloculus arranged in three whorls, six to seven slightly inflated chambers in the final whorl. Primary aperture interiomarginal, sub-peripheral loop-shape that widens towards the spiral side with a lip, secondary aperture at umbilical tip of chamber, may have a lip; both apertures present on every chamber. Agglutinated, imperforate wall.
Occurrence. Originally described from the Bellingshausen Sea and the South Sandwich Islands (Bronnimann and Whittaker, 1988).
Remarks. Bronnimann and Whittaker (1988) describe the wall as being almost entirely composed of barite spherules/ovoids. This is not the case in the specimens described here, although some ovoids were observed. Additionally the specimens described here have 6-7 chambers in the final whorl, rather than the 8 described in Bronnimann and Whittaker (1988).

Subfamily **Trochamminellinae** Brönnimann, Zaninetti & Whittaker, 1983
Genus *Pseudotrochammina* Frerichs, 1969

***Pseudotrochammina* sp. 1**
(Fig. 3.4:1)

Material. 212 specimens from 23 samples.
Description. Low trochospiral test, globular chambers that rapidly increase in size, 4 in final whorl. Depressed sutures, smoothly finished, finely agglutinated wall, areal elongate slit aperture located on the umbilical side but not in the umbilicus.

Family **Cyclamminidae** Marie, 1941
Subfamily **Cyclammininae** Marie, 1941
Genus *Cyclammina* Brady, 1879

Cyclammina* cf. *contorta Pearcey, 1914
(Fig. 3.4:2)

1914 *Cyclammina contorta* Pearcey: 1009, pl. 2, figs 5-7.

Material. One specimen from one sample.
Description. Very large, planispiral, involute, somewhat compressed test, rounded periphery, very slightly lobulate margin. Numerous chambers (ca. 15) in the final whorl, sutures straight. Finely agglutinated, surface smooth, slightly iridescent. Aperture appears to be an interiomarginal, equatorial low arch, although this is poorly preserved on the only specimen found in this study. Apertural face of the

final chambers much more coarsely agglutinated with a rough surface, no evidence for additional apertures.
Occurrence. *Cyclammina contorta* Pearcey was originally described from the Weddell Sea, Antarctica.
Remarks. The species described here differs only in its sutural characteristics, being straighter and less dark in colour.

Family **Textulariidae** Ehrenberg, 1838
Subfamily **Textulariinae** Ehrenberg, 1838
Genus *Textularia* Defrance, 1824

Textularia earlandi Parker, 1952
(Fig. 3.4:3-4)

1933 *Textularia tenuissima* Earland: 95, pl. 3, figs 21-30.
1952 *Textularia earlandi* Parker: 458, (see synonymy)
1996 *Textularia earlandi* Parker; Violanti: 57, pl. 5, figs 13-14.
2010 *Textularia tenuissima* Earland; Majewski: 65, fig. 2(2).

Material. 77 specimens from 27 samples.
Description. Very small, delicate, elongate test. Initial chambers coiled in both microspheric (tapered end) and megalospheric (rounded end) forms, becoming biserial. Numerous subquadrate, rounded chambers that enlarge slightly towards the terminal end. Distinct, slightly depressed sutures. Aperture a low interiomarginal arch on the face of the final chamber. Fairly smooth wall comprising fine grains with little cement visible.
Occurrence. Originally described from South Georgia (Earland, 1933), subsequently recorded from the Ross Sea (Violanti, 1996) and the AP (Majewski, 2010).
Remarks. Originally described from South Georgia as *Textularia tenuissima* Earland, this was however preoccupied by *Textularia tenuissima* Häusler 1881. Therefore, Parker (1952) proposed the new name *Textularia earlandi*. Morphologically it is very similar to *Textularia elegans* Lacroix, found in the Mediterranean.

Family **Cornuspiridae** Schultze, 1854
Subfamily **Cornuspirinae** Schultze, 1854
Genus *Cornuspira* Schultze, 1854

Cornuspira antarctica Rhumbler in Wiesner, (1931)
(Fig. 3.4:6-7)

1931 *Cornuspira antarctica* Rhumbler in Wiesner: 101, pl. 14, figs.164-166.

Material. Four specimens from four samples.
Description. Discoidal test comprising two chambers, the globular proloculus and the planispirally enrolled, undivided, near evolute second chamber. Calcareous, imperforate, porcellaneous wall with transverse growth lines. Aperture simple opening at end of tube.
Occurrence. Originally described from Antartica (Wiesner, 1931).

Family **Hauerinidae** Schwager, 1876
Subfamily **Hauerininae** Schwager, 1876
Genus *Quinqueloculina* d'Orbigny, 1826

Quinqueloculina* cf. *occidentalis Bailey, 1851
(Fig. 3.4:5 & 8-9)

1851 *Quinqueloculina occidentalis* Bailey: 13, figs 46-48.
2013 *Quinqueloculina* sp. Majewski: 179, fig. 7 (6).
2013 *Quinqueloculina seminula* (Linnaeus); Rodrigues et al.: 214, fig. 3 (6-7).

Material. 22 specimens from seven samples.
Description. Small, elongate, subovate test, quinqueloculine chamber arrangement, rounded periphery, long, narrow chambers that rapidly increase in size as added. Calcareous, smooth, thin, porcellaneous wall, distinct, somewhat depressed sutures, aperture a terminal high arch with a small tooth.
Occurrence. *Quinqueloculina occidentalis* Bailey was originally described from the North Atlantic. Similar specimens have been recorded from Antarctica (Majewski, 2013; Rodrigues et al., 2013) but never previously assigned to *Q. occidentalis* Bailey.
Remarks. The specimens described here appear quite similar to *Quinqueloculina occidentalis* Bailey, although the very brief original description hinders any certainty in this designation. The specimens also share a number of features with *Triloculinella antarctica* Kennett but the absence of a broad apertural flap indicates that this species does not belong within the genus *Triloculinella*; it's placement within this genus by Majewski (2005) is therefore incorrect.

Quinqueloculina seminula (Linnaeus, 1758)
(Fig. 3.4:10-11)

1758 *Serpula seminulum* Linnaeus: 786, pl. 2, fig. 1.
1932a *Miliolina seminulum* (Linnaeus); Heron-Allen & Earland: 313, pl. 6, figs 25-40.
1981 *Quinqueloculina seminulum* (Linnaeus); Milam and Anderson: 307, pl. 5, fig. 5.
1994 *Quinqueloculina seminulum* (Linnaeus); Jones: 21, pl. 5, fig. 6, text figs 2-3.
2013 *Quinqueloculina seminulum* (Linnaeus); Rodrigues et al.: 214, fig. 3 (6-7).

Material. Three specimens from three samples.
Description. Slightly compressed ovate test, rounded at base, more angular at apertural end, rounded triangular in section. Quinqueloculine coiling, five chambers visible in final whorl, four from one side and three from the other, more convex on the four-chambered side. Calcareous, imperforate, porcellaneous wall, smooth surface. Large, terminal, horseshoe-shaped aperture with a small bifid tooth.
Occurrence. Recorded from the North Atlantic in the Challenger material (Jones, 1994) and from Antarctica by Milam and Anderson (1981).

Quinqueloculina* cf. *sublineata (Brady, 1884)
(Fig. 3.4:12)

1884 *Miliolina circularis* var. *sublineata* Brady: 169, pl. 4, fig. 7.
1994 *Triloculinella sublineata* (Brady); R.W. Jones: 20, pl. 4, fig. 7.

Material. One specimen from one sample.
Description. Test near-circular in outline, compressed, rounded section. Quinqueloculine coiling, five chambers visible in final whorl, calcareous, imperforate, porcellaneous wall, terminal, low, broad, arch-shaped aperture. Surface ornamented with very delicate, longitudinal striae and large pits.
Remarks. The absence of an apertural flap in the specimen described here, and in the image of Jones (1994), plus the presence of five chambers in the final whorl, suggests affiliation with *Quinqueloculina*. This specimen differs from the specimen figured in Brady (1884) and Jones (1994) in the presence of large pits that cover its surface.

Genus *Pyrgo* Defrance, 1824

Pyrgo* cf. *subpisum Parr, 1950
(Fig. 3.4:14)

1950 *Pyrgo subpisum* Parr: 297, pl. 7, figs 5-6.

Material. One specimen from one sample.
Description. Large, subglobular test, near-circular from front, rounded periphery; two chambers visible in final whorl (biloculine). Calcareous, imperforate, porcellaneous wall, large, ovate, terminal aperture, surrounded by a thickened, raised rim, unusual large tooth with three lobes.
Occurrence. *Pyrgo subpisum* Parr was described from a number of locations in the southern Indian Ocean.
Remarks. The specimen described here is very similar to *Pyrgo subpisum* Parr, differing only in the unusual tooth characteristics.

Pyrgo patagonica (d'Orbigny, 1839b)
(Fig. 3.4:13)

1839b *Biloculina patagonica* d'Orbigny: 65, pl. 3, figs 15-17.
1932a *Biloculina patagonica* d'Orbigny; Heron-Allen & Earland: 311, pl. 6, figs 4-6.
2004 *Pyrgo patagonicum* (d'Orbigny); Mikhalevich: 188, pl. 3, figs 6-7.

Material. One specimen from one sample.
Description. Large, subglobular test, ovate from front, rounded periphery, two inflated chambers visible in final whorl (biloculine). Calcareous, imperforate, porcellaneous, think wall, with a smooth, shiny surface, medium, round, terminal aperture, surrounded by a small, thickened, raised rim; bifid tooth.
Occurrence. Originally described from the Patagonian coast (d'Orbigny, 1839a).

Genus *Triloculina* d'Orbigny, 1826

***Triloculina* sp.**
(Fig. 3.4:15)

Material. 18 specimens from 10 samples.
Description. Ovate text, triangular in section with rounded corners, triloculine, three chambers visible in final whorl. Chambers slightly inflated, sutures somewhat depressed, calcareous, imperforate, porcellaneous wall, smooth surface. Terminal, rounded aperture, no tooth visible.

Family **Nodosariidae** Ehrenberg, 1838
Subfamily **Nodosariinae** Ehrenberg, 1838
Genus *Laevidentalina* Loeblich & Tappan, 1986

Laevidentalina communis (d'Orbigny, 1826)
(Fig. 3.4:17-18)

1826 *Nodosaria (Dentalina) communis* d'Orbigny: 254, (no type figure).
1996 *Dentalina communis* (d'Orbigny); Violanti: 59, pl. 6, fig. 11.
2005 *Dentalina communis* (d'Orbigny); Majewski: 201, fig. 20(2-3).
2013 *Laevidentalina communis* (d'Orbigny); Majewski: 181, fig. 9(2).

Material. Two specimens from two samples.

Description. Elongate, slightly arcuate test, fusiform, apiculate proloculus, followed by a number of uniserially arranged chambers, straight, horizontal sutures. Calcareous, hyaline, finely perforate wall, smooth surface, multilammellar, terminal aperture damaged in our specimens.
Occurrence. Recorded from Antarctica in Recent sediments (Violanti, 1996; Majewski, 2005, 2013)
Remarks. Placed within the genus *Laevidentalina* due to the absence of costae.

Genus *Lotostomoides* Hayward & Kawagata, 2012

Lotostomoides calomorphum (Reuss, 1866)
(Fig. 3.5:1-2)

1866 *Nodosaria (Nodosaria) calomorpha* Reuss: 129, pl. 1, figs 15-19.
1933 *Nodosaria calomorpha* Reuss; Earland: 117, pl. 4, fig. 19.
1994 *Glandulonodosaria calomorpha* (Reuss); Jones: 72, pl. 61, figs 23–26.
2012 *Lotostomoides calomorphum* (Reuss); Hayward et al.: 125, pl. 6, figs 24-29.

Material. 27 specimens from nine samples.
Description. Small, elongate, slightly arcuate test comprising 2-4 sausage-shaped chambers. Simple, round, terminal aperture. Thin, hyaline, calcareous wall, with smooth surface; sutures straight and horizontal.
Occurrence. Reported from South Georgia (Earland, 1933) and the South Atlantic (Jones, 1994).

Genus *Nodosaria* Lamarck, 1812

Nodosaria simplex Silvestri, 1872
(Fig. 3.5:3-4)

1872 *Nodosaria simplex* Silvestri: 95, pl. 11, figs 268-272.
1994 *Nodosaria simplex* Silvestri; Jones: 73, pl. 62, figs 4-5.

Material. Two specimens from two samples.
Description. Small, slightly elongate test comprising two spherical/ovate chambers of approximately the same size; straight, depressed suture between the chambers. Both chambers narrow terminally, the upper towards the aperture, while the lower becomes apicate. Calcareous, hyaline, perforate wall, smooth and unornamented. Terminal, rounded aperture with radiating grooves.

Family **Vaginulinidae** Reuss, 1860
Subfamily **Lenticulininae** Chapman, Parr & Collins, 1934
Genus *Lenticulina* Lamarck, 1804

Lenticulina asterizans Parr, 1950
(Fig. 3.5:5)

1950 *Lenticulina (Robulus) asterizans* Parr: 322, pl. 11, figs 9-10.

Material. One specimen from one sample.
Description. Planispiral, involute, lenticular test, narrow rounded keel on periphery, eight chambers in final whorl. Limbate, flush sutures, triangular, slightly rounded apertural face; calcareous, hyaline, smooth wall. Aperture damaged in the specimen described here.
Occurrence. Originally described from Antarctica (Parr, 1950).

Subfamily **Marginulininae** Wedekind, 1937
Genus *Astacolus* de Montfort, 1808

***? Astacolus* sp.**
(Fig. 3.4:16)

Material. One specimen from one sample.
Description. Elongate, flattened test; low, broad chambers added on a slightly curved axis; strongly oblique, curved sutures; rounded periphery; smooth, perforate, calcareous wall; terminal, radiate aperture.

Family **Lagenidae** Reuss, 1862
Genus *Lagena* Walker & Jacob in Kanmacher, 1798

Lagena substriata Williamson, 1848
(Fig. 3.5:6-7)

1848 *Lagena substriata* Williamson: 15, pl. 2, fig.12.
1994 *Lagena substriata* Williamson; Loeblich & Tappan: 79, pl. 138, figs 1-5.
2001 *Lagena substriata elegantula* R.W. Jones; Igarashi et al.: 148, pl. 7, fig. 5.
2009 *Lagena weisneri* Parr; Majewski & Anderson: 139, fig. 4.

Material. 26 specimens from 15 samples.
Description. Unilocular, ovate test that may be significantly elongated. Calcareous, hyaline wall ornamented with numerous delicate, parallel, longitudinal costae. Simple aperture with phialine lip at the end of a long neck. Some of the costae continue up the neck, either straight up or spiralling around the neck. Some specimens also present a honeycomb pattern on the base of the test.
Occurrence. Originally described from the Recent of England (Williamson, 1848), this species has also been described from the Timor Sea (Loeblich and Tappan, 1994) and Antarctica (Igarashi et al., 2001; Majewski and Anderson, 2009).

Lagena multilatera McCulloch, 1977
(Fig. 3.5:8)

1977 *Lagena multilatera* McCulloch: 40, pl. 50, fig. 5.
1994 *Lagena multilatera* McCulloch; Jones: 65, pl. 58, figs 2-3, 7-8, 22-24.

Material. 23 specimens from 14 samples.
Description. Unilocular, fusiform test. Calcareous, hyaline wall, approximately eight longitudinal costae, high, narrow, tapering, some of which continue onto neck. Small, round, terminal aperture produced on a long delicate neck.
Occurrence. McCulloch (1977) described this species from deep water off Bikini Atoll, Pacific Ocean, subsequently recorded from the South Pacific and Southern Ocean (Jones, 1994).

Genus *Hyalinonetrion* Patterson & Richardson, 1987

Hyalinonetrion* cf. *gracillimum (Seguenza, 1862)
(Fig. 3.5:9)

1862 *Amphorina gracillima* Seguenza: 51, pl. 1, fig. 37.
1994 *Procerolagena gracillima* (Seguenza); Jones: 62, pl. 56, figs 19-22, 24-29.
2005 *Hyalinonetrion gracillima* (Seguenza); Majewski: 201, fig. 20(7).
2015 *Procerolagena gracillima* (Seguenza); Setoyama & Kaminski: 23, fig. 8(28).

Material. 149 specimens from 55 samples.

Description. Fusiform, elongate, unilocular test that slowly tapers at the base. Hyaline, calcareous, unornamented wall. Simple aperture with a phialine lip, at the end of a long, tapering neck.
Occurrence. Originally described from the Miocene of Italy (Seguenza, 1862), subsequently recorded from Recent sediments from Antarctica (Majewski, 2005), the Southern Ocean (Jones, 1994) and the Bering Sea (Setoyama and Kaminski, 2015).
Remarks. Jones (1994) retained this species in *Procerolagena,* as he considered *Hyalinonetrion* to be a junior synonym of *Procerolagena*, but here it is placed in *Hyalinonetrion* due to the absence of any longitudinal ornamentation (Loeblich and Tappan, 1988).

Genus *Procerolagena* Puri, 1954

Procerolagena distoma (Parker & Jones M. S. in Brady, 1864)
(Fig. 3.5:10)

1864 *Lagena distoma* Parker & Jones in Brady: 467, pl. 48, fig. 6.
?1981 *Lagena sulcata var. distoma-polita* Milam & Anderson: 308, pl. 6, fig. 2.
1994 *Hyalinonetrion distoma* (Parker & Jones); Loeblich & Tappan: 77, pl. 137, fig. 9.

Material. 26 specimens from 19 samples.
Description. Unilocular, elongate test with nearly parallel sides in the central part of the test which tapers towards apiculate ends. Calcareous wall ornamented by delicate longitudinal striae.
Occurrence. Originally described from the Shetlands (Brady, 1864), subsequently recorded from Antarctica (Milam and Anderson, 1981) and the Timor Sea (Loeblich and Tappan, 1994).
Remarks. Loeblich and Tappan (1994) assign this species to the genus *Hyalinonetrion*. However, this designation is in conflict with the genus description in Loeblich and Tappan (1988) defining *Hyalinonetrion* as unornamented.

Genus *Pygmaeoseistron* Patterson & Richardson, 1987

Pygmaeoseistron hispidulum (Cushman, 1913)
(Fig. 3.5:11)

1913 *Lagena hispidula* Cushman: 14, pl. 5, figs 2-3.
2013 *Pygmaeoseistron hispidulum* (Cushman 1913); Majewski: 180, fig. 8(11).

Material. 13 specimens from 10 samples.
Description. Unilocular flask-shaped/ovoid test that rapidly narrows to a tubular neck (delicate and often broken, as in figured specimen), evenly covered in fine hispid ornamentation.
Occurrence. Originally described from the North Pacific (Cushman, 1913), also recorded from the Amundsen Sea (Majewski, 2013).

***Pygmaeoseistron* sp.**
(Fig. 3.5:12)

Material. One specimen from one sample.
Description. Unilocular, ovoid test with a narrow, tubular neck; sporadic pustulose ornamentation.
Remarks. Bears some similarity to *Pygmaeoseistron islandicum* (Jones, 1994).

Family **Ellipsolagenidae** A. Silvestri, 1923
Subfamily **Oolininae** Loeblich & Tappan, 1961
Genus *Oolina* d'Orbigny, 1839b

Oolina globosa (Montagu, 1803)
(Fig. 3.5:16-17)

1803 *Vermiculum globosum* Montagu: 523, pl. 1, fig. 8.
1994 *Oolina globosa* (Montagu); Jones: 62, pl. 56, figs 1-3, 15-16.

Material. Two specimens from two samples.
Description. Unilocular, tear-drop shaped test, may have apiculate base. Calcareous, hyaline, smooth wall. Terminal, simple, round aperture, with an entosolenian tube that extends over half the length of the chamber and flares dramatically at the end.
Occurrence. Recorded from the Southern Ocean (Jones, 1994).
Remarks. Following Jones (1994), specimens with an apiculate base are not considered to be distinct from *Oolina globosa* (Montagu).

Oolina squamosa (Montagu, 1803)
(Fig. 3.5:15)

1803 *Vermiculum squamosum* Montagu: 526, pl. 14, fig. 2.
1994 *Oolina squamosa* (Montagu); Jones: 66, pl. 58, figs 28-32.
2015 *Oolina squamosa* (Montagu); Setoyama & Kaminski: 23, figs 7(14), 8(31).

Material. Four specimens from four samples.
Description. Unilocular, ovate test, circular in section, narrowing towards the apertural end. Calcareous, hyaline wall, ornamented with roughly perpendicular vertical costae. Horizontal costae join the vertical to form loosely hexagonal shapes. Round aperture, terminal on a short neck with a rounded lip.
Occurrence. Originally described from Britain (Montagu, 1803), also recorded from the South Pacific (Jones, 1994) and the Bering Sea (Setoyama and Kaminski, 2015).
Remarks. The specimens figured here most closely resemble the specimen from Plate 58, fig. 32 of Jones (1994) from the Challenger material that has previously been variously assigned to *Lagena hexagona* (Williamson) by Brady (1881) and Thalmann (1932), and *Oolina hexagona* (Williamson) by Barker (1960), Hermelin (1989), and Van Marle (1991). The ornamentation on our specimens form roughly perpendicular lines, a feature not seen in *Oolina hexagona* (Williamson), and has therefore been assigned to *Oolina squamosa* (Montagu), following Knight (1986).

***Oolina* spp.**
(Fig. 3.5:13)

Material. 14 specimens from nine samples.
Description. Included in this group any unilocular, ovate tests with calcareous, hyaline, smooth walls, an apiculate base and a rounded terminal aperture, that have not been assigned to *Oolina globosa* (Montagu).

Genus *Vasicostella* Patterson & Richardson, 1987

Vasicostella striatopunctata (Parker & Jones, 1865)
(Fig. 3.5:18)

1865 *Lagena sulcata* Walker & Jones var. *striatopunctata* Parker & Jones: 350, pl. 13, figs 25-27.

2001 *Vasicostella striatopunctata* (Parker & Jones); Igarashi et al.: 148, pl. 8, fig. 5.
2013 *Vasicostella* sp. Majewski: 180, fig. 8 (8).

Material. One specimen from one sample.
Description. Unilocular, flask-like, compressed test, carinate periphery. Calcareous, hyaline wall, ornamented with strong longitudinal costae that appear striped, perpendicular to their length, due to differences in the optical properties of their calcite (only visible with light microscopy). Rounded, terminal aperture, with a slight lip and a short, centrally placed entosolenian tube.
Occurrence. Parker and Jones (1865) originally described this species from Greenland, the Red Sea, the South Atlantic and the Indian Ocean. Igarashi et al. (2001) subsequently described it from Antarctica.
Remarks. Le Coze and Hayward (2017) places *Lagena striatopunctata* Parker & Jones within the genus *Cushmanina.* However, based on the type figures, this classification appears to be incorrect. The compressed nature of the test and the lack of an elongate neck suggest that this species should be placed within the genus *Vasicostella.* The specimen described here and that of Igarashi et al. (2001) also reveal the carinate nature of this species, further supporting this classification.

Subfamily **Ellipsolageninae** A. Silvestri, 1923
Genus *Fissurina* Reuss, 1850

Fissurina subformosa Parr, 1950
(Fig. 3.5:19)

1950 *Fissurina subformosa* Parr: 313, pl. 9, fig. 9.
1996 *Lagena subformosa* (Parr); Violanti: 43, pl.7, fig. 3.

Material. Six specimens from five samples.
Description. Small, pyriform test, slightly compressed, tapering towards a long neck; Keel extends from the neck around the test, with two tabulated supplementary keels that create a 'crimped' appearance. Circular, terminal aperture, straight entosolenian tube extends centrally to approximately one third the length of the chamber.
Occurrence. Previously recorded from Antarctica (Parr, 1950; Violanti, 1996).
Remarks. This species can be distinguished from *F. formosa (Lagena Formosa* Schwager) by the supplementary keels.

***Fissurina* sp. 1**
(Fig. 3.5:14)

Material. 22 specimens from 16 samples.
Description. Unilocular, pyriform test, with pointed protuberance towards basal end, circular section. Smooth, hyaline, calcareous wall, terminal, oval aperture within a slightly depressed fissure at the apex of the test.

***Fissurina* sp. 2**
(Fig. 3.5:20)

Material. 132 specimens from 50 samples.
Description. Elongate, compressed test, broadening towards the base, rounded ends, base somewhat produced, oval section. Smooth, hyaline, calcareous wall, terminal, slit-like aperture within a significantly depressed fissure at the apex of the test.

Remarks. Bears some similarity to the Oligocene *Fissurina oblonga* Reuss, and to *Parafissurina lateralis* (Cushman). May have previously been recorded from the Weddell Sea by Anderson (1975) as *Parafissurina lateralis* (Cushman).

Subfamily **Parafissurininae** R. W. Jones, 1984
Genus *Parafissurina* Parr, 1947

Parafissurina fusiformis Wiesner, 1931
(Fig. 3.5:21)

1931 *Parafissurina fusiformis* Wiesner: 126, pl. 24, fig. j.
1996 *Parafissurina fusiformis* Wiesner; Violanti, 62, pl. 8, fig. 8.
2001 *Parafissurina fusiformis* Wiesner; Igarashi: 151, pl. 9, fig 5.
2005 *Parafissurina fusiformis* Wiesner; Majewski: 203, fig. 22(1-2).

Material. 169 specimens from 56 samples.
Description. Small test, ovate in front view, slightly compressed, rounded periphery. Aperture an elongate slit protected by a protruding hood, with a large lip opposite the hood. Entosolenian tube extends centrally along inner surface of chamber, flaring at the end.
Occurrence. Originally described from high southern latitudes (Wiesner, 1931), and later form other Antarctic localities (Violanti, 1996; Majewski, 2005).

Family **Bolivinidae** Glaessner, 1937
Genus *Bolivinellina* Saidova, 1975

Bolivinellina earlandi (Parr, 1950)
(Fig. 3.5:22)

1950 *Bolivina earlandi* Parr: 339, pl. 12, fig. 16.
1996 *Bolivina pseudopunctata* Höglund; Violanti: 65, pl. 9, fig. 1.
2001 *Bolivinellina earlandi* (Parr); Igarashi et al.: 153, pl. 10, fig. 5.
2013 *Bolivinellina earlandi* (Parr); Majewski: 181, fig. 9(4).

Material. 144 specimens from 55 samples (for *Bolivinellina* spp.).
Description. Elongate test, biserial throughout, oval in section. Chambers up to 12 in number, slightly inflated; strongly curved, slightly depressed sutures. Wall calcareous, hyaline, smooth, finely perforate in the lower half of the chamber, imperforate in the upper half. Narrow, comma-shaped aperture starting at the inner margin of the final chamber.
Occurrence. Parr (1950) described this species as widely distributed around Antarctica.
Remarks. Following Igarashi et al. (2001) and Majewski (2013) this species is placed in the genus *Bolivinellina* based on the absence of perforation in the upper half of the chambers.

Bolivinellina pseudopunctata (Höglund, 1947)
(Fig. 3.5:23)

1947 *Bolivina pseudopunctata* Höglund: 273, pl. 24, fig. 5, pl. 32, figs 23-24.
2005 *Bolivina pseudopunctata* Höglund; Majewski: 203, fig. 22(6-7).
2013 *Bolivinellina pseudopunctata* (Höglund); Majewski: 181, fig. 9(3).

Material. 144 specimens from 55 samples (for *Bolivinellina* spp.).
Description. Elongate, gently tapering test, biserial from a large globular proloculus, oval in section. Chambers distinct, up to 23 in number, slightly inflated; sutures strongly curved, slightly depressed. Wall calcareous, hyaline, smooth, finely

perforate in the lower half of the chamber, imperforate in the upper half. Oval-shaped aperture with a double-folded tongue, starting at the inner margin of the final chamber.
Occurrence. Originally described from the Gullmar Fjord, Sweden (Höglund, 1947), this species has subsequently been described from Antarctica (Majewski, 2005, 2013).
Remarks. Following Majewski (2013) this species is placed in the genus *Bolivinellina* based on the lack of perforation in the upper half of the chambers. *B. pseudopunctata* can be distinguished from *B. earlandi* by the greater number of chambers, an oval-shaped aperture with a double-folded tongue, and a large globular proloculus.

Family **Cassidulinidae** d'Orbigny, 1839a
Subfamily **Cassidulininae** d'Orbigny, 1839a
Genus *Cassidulinoides* Cushman, 1927

Cassidulinoides parkerianus (Brady, 1881)
(Fig. 3.5:24-25)

1881 *Cassidulina parkeriana* Brady: 59, pl. 54, figs. 11-16.
1932a *Cassidulina parkeriana* Brady; Heron-Allen & Earland: 359, pl. 9, figs. 22-25.
1975 *Cassidulinoides parkerianus* (Brady); Anderson: 86, pl. 7, fig. 20.
2001 *Cassidulinoides parvus* (Hussey); Igarashi: 153, pl. 10, fig. 12.
2005 *Cassidulinoides parkerianus* (Brady); Majewski: 204, fig. 23(1-2).
2009 *Cassidulinoides parkerianus* (Brady); Majewski & Anderson: 139, fig. 4.
2013 *Cassidulinoides parkerianus* (Brady); Rodrigues et al.: 214, fig. 3 (4).

Material. 3566 specimens from 138 samples.
Description. Crozier-shaped test, initially planispiral, rapidly uncoiling to become biserial, number of chambers in biserial section quite variable, biserial section cylindrical, straight or arcuate. Chambers subglobose, inflated, with small overlap at the periphery; sutures slightly depressed. Thick, calcareous, perforate, hyaline bi-multilamellar wall. Interiomarginal, loop-shaped aperture, subterminal.
Occurrence. Originally described from the South Pacific (Brady, 1881) and subsequently described from various locations around Antarctica (Heron-Allen and Earland, 1932a; Anderson, 1975; Igarashi et al., 2001; Majewski, 2005; Majewski and Anderson, 2009; Rodrigues et al., 2013).

Cassidulinoides porrectus (Heron-Allen and Earland, 1932a)
(Fig. 3.6:1-2)

1932a *Cassidulina crassa* d'Orbigny var. *porrecta* Heron-Allen & Earland, p. 358, pl. 9, figs. 34-37.
1981 *Cassidulinoides porrecta* (Heron-Allen & Earland); Milam & Anderson: 308, pl. 6, fig. 6.
1996 *Cassidulinoides porrectus* (Heron-Allen & Earland): Violanti: 65, pl. 9, fig. 2-3.
2001 *Cassidulinoides porrectus* (Heron-Allen & Earland); Igarashi et al.: 153, pl. 10, fig. 11.
2005 *Cassidulinoides porrectus* (Heron-Allen & Earland); Majewski: 204, fig. 23(3).
2013 *Cassidulinoides porrectus* (Heron-Allen & Earland); Rodrigues et al.: p.214, fig. 3 (3).

Material. 3484 specimens from 126 samples.
Description. Test small, planispirally enrolled in early stages, uncoiling to become biserial, commonly two to four chambers in the biserial part but can be as many as 10. Chambers subglobose, inflated, with small overlap at the periphery, sutures

slightly depressed. Thick, calcareous, perforate, hyaline wall, covered in distinctive large pores. Interiomarginal, loop-shaped aperture, subterminal.
Occurrence. Originally described from various sub-Antarctic locations (Heron-Allen and Earland, 1932a), subsequently in numerous additional Antarctic studies (Milam and Anderson, 1981; Violanti, 1996; Igarashi et al., 2001; Majewski, 2005; Rodrigues et al., 2013).

Genus *Globocassidulina* Voloshinova, 1960

Globocassidulina crassa* (d'Orbigny) subsp. *rossensis Kennett, 1967
(Fig. 3.6:5-7)

1967 *Globocassidulina crassa* (d'Orbigny) subsp. *rossensis* Kennett 134, pl. 11, figs. 4-6.
1981 *Globocassidulina crassa rossensis* Kennett; Milam & Anderson: 312, pl. 10, fig. 1.
1993 *Globocassidulina rossensis* Kennett; Mackensen et al.: 56, pl. 2, figs. 7-8.
1996 *Globocassidulina rossensis* Kennett; Violanti: p.65, pl. 9, fig. 7.
2006 *Globocassidulina rossensis* Kennett; Hromic et al.: 124, pl. 1, fig. 5.

Material. 2193 specimens from 117 samples.
Description. Oval to circular, involute, slightly compressed test, rounded, slightly lobulate, planispiral coil of biserial, inflated chambers that gradually increase in size, four to five pairs in the last whorl. Thin, smooth, calcareous wall. Aperture a narrow, interiomarginal slit with an aerial branch that extends perpendicular to the main slit approximately halfway up the apertural face, surrounded by a narrow rim.
Occurrence. Originally described from the Ross Sea (Kennett 1967), subsequently described from other Antarctic locations (Milam and Anderson, 1981; Mackensen et al., 1993; Violanti, 1996; Hromic et al., 2006).
Remarks. Distinguished from other subspecies of *Globocassidulina crassa* (d'Orbigny) by an aerial branch that extends from the main part of the aperture.

Subfamily **Ehrenbergininae** Cushman, 1927
Genus *Ehrenbergina* Reuss, 1850

Ehrenbergina glabra Heron-Allen & Earland, 1922

1922 *Ehrenbergina hystrix var. glabra* Heron-Allen & Earland: 140, pl. 5, figs. 1-6.
1981 *Ehrenbergina glabra* Heron-Allen & Earland; Milam & Anderson: 311, pl. 9, fig. 7.
1990 *Ehrenbergina glabra* Heron-Allen & Earland; Mackensen et al.: 254, pl. 1, fig. 5-6.
1996 *Ehrenbergina glabra* Heron-Allen & Earland; Violanti: 65, pl. 9, fig. 9.
2001 *Ehrenbergina glabra* Heron-Allen & Earland; Igarashi et al.: 154, pl. 11, fig. 1.
2013 *Ehrenbergina glabra* Heron-Allen & Earland; Majewski: 182, fig. 10(13).

Material. Two specimens from one sample.
Description. Biserial test, initially enrolled rapidly uncoiling; lenticular in section with a convex dorsal side, flatter ventrally side with a median furrow. Chambers are low and broad with considerable overlap at the peripheral midline. Spinose lateral margins, sutures curved, flush. Calcareous, smooth wall. Curved, elongate, slit-like aperture that runs parallel to the peripheral margin, perpendicular to the base of the apertural face.
Occurrence. Recorded from a number of locations around Antarctica (Milam and Anderson, 1981; Mackensen et al., 1990; Violanti, 1996; Igarashi et al., 2001; Majewski, 2013).

Remarks. Heron-Allen and Earland (1922) distinguished this species from *E. hystrix* Brady by the absence of spines on the early chambers, the more flattened oral face, the more marginal position of the aperture, and the near absence of striations around the aperture.

Family **Buliminidae** Jones in Griffith and Henfrey, (1875)
Genus *Bulimina* d'Orbigny, 1826

Bulimina aculeata d'Orbigny, 1826
(Fig. 3.6:3-4)

1826 *Bulimina aculeata* d'Orbigny: 269 (no type figure)
1990 *Bulimina aculeata* d'Orbigny; Mackensen et al.: 255, pl. 2, fig. 1-3.
1993 *Bulimina aculeata* d'Orbigny; Mackensen et al.: 54, pl. 1, figs. 3-4.
1994 *Bulimina aculeata* d'Orbigny; Ishman & Domack: 152, pl. 2, fig. 8.
2001 *Bulimina aculeata* d'Orbigny; Igarashi et al.: 154, pl. 11, fig. 4.
2013 *Bulimina aculeata* d'Orbigny; Majewski: 181, fig. 9(8-9).

Material. 93 specimens from 31 samples.
Description. Elongate, triserial test, strongly tapered towards base. Globular, inflated chambers rapidly increase in size, distinct, depressed sutures. Smooth, finely perforate, calcareous wall. Early chambers ornamented with long, tapering spines that extend dorsally, fragile and often partially or completely broken. Loop-shaped aperture extends up the face of the final chamber from the basal margin, well-developed, elevated rim.
Occurrence. Originally described from the Adriatic (d'Orbigny, 1826) but more recently from various Antarctic localities (Mackensen et al., 1990; Mackensen et al., 1993; Ishman and Domack, 1994; Igarashi et al., 2001; Majewski, 2013).

Bulimina subteres Brady, 1881

1881 *Bulimina subteres* Brady: 55, pl. 50, figs 17-18.

Material. Three specimens from three samples.
Description. Elongate, triserial, ovate test, rounded at the distal end and tapering to a point at the basal end, slightly inflated chambers, depressed sutures, curved, slit-like aperture extending up the face of the terminal chamber.
Occurrence. Originally described from the Recent of Fiji and the Caribbean (Brady, 1881).

***Bulimina* sp. 1**
(Fig. 3.6:9-10)

Material. 255 specimens from 61 samples.
Description. Near spherical test, wider than high, only the three chambers of the final whorl visible. Inflated, globular chambers, depressed sutures. Calcareous, smooth, perforate wall, loop-shaped aperture extending from the base up the face of the final chamber, with a raised rim.

Family **Uvigerinidae** Haeckel, 1894
Subfamily **Angulogerininae** Galloway, 1933
Genus *Trifarina* Cushman, 1923

Trifarina earlandi (Parr, 1950)
(Fig. 3.6:8)

1950 *Angulogerina earlandi* Parr: 341, pl. 12, fig. 21.

2001 *Angulogerina earlandi* Parr; Igarashi et al.: 154, pl. 11, fig. 7.
2005 *Angulogerina earlandi* Parr; Majewski: 203, fig. 22(8-9).
2013 *Angulogerina earlandi* Parr; Majewski: 181, fig. 9(13-14).

Material. 765 specimens from 65 samples.
Description. Elongate, fusiform test, triserial, becoming uniserial, triangular cross-section becoming rectilinear with rounded to sub-acute corners. Base rounded, slightly lobulate margins. Numerous inflated chambers ornamented with narrow, high costae that generally do not cross the sutures; in some specimens final chambers lack ornamentation. Terminal, ovate aperture, with internal hemicylindrical toothplate, produced on a neck with a phialine lip.
Occurrence. Recorded from a number of locations around Antarctica (Parr, 1950; Igarashi et al., 2001; Majewski, 2005, 2013).
Remarks. Parr (1950) placed this species within *Angulogerina*. Loeblich and Tappan (1988) define *Angulogerina* as triserial throughout, however this species is triserial, becoming uniserial, diagnostic of *Trifarina*. The high narrow costae of *Trifarina earlandi* (Parr) distinguish it from the otherwise similar *T. angulosa* (Williamson).

Family **Fursenkoinidae** Loeblich & Tappan, 1961
Genus *Fursenkoina* Loeblich & Tappan, 1961

Fursenkoina fusiformis (Cushman, 1930)
(Fig. 3.6:13-14)

1930 *Virgulina fusiformis* Cushman: 45, pl. 8, fig. 8.
1981 *Fursenkoina fusiformis* (Cushman); Milam & Anderson: 311, pl. 9, fig. 6.
1994 *Fursenkoina fusiformis* (Cushman); Ishman & Domack: 152, pl. 2, fig. 7.
1996 *Fursenkoina fusiformis* (Cushman); Violanti: 65, pl. 9, fig. 14-15.
2005 *Fursenkoina fusiformis* (Cushman); Majewski: 204, fig. 23(9-12).
2009 *Fursenkoina fusiformis* (Cushman); Majewski & Anderson: 139, fig. 4.

Material. 20833 specimens from 129 samples.
Description. Narrow, elongate test, ovate in section. High, narrow, slightly inflated chambers, biserial, twisted around the test axis. Oblique, depressed sutures, calcareous, hyaline, finely perforate wall, with smooth surface. Narrow, elongate aperture, basal part of the aperture may be closed in adult specimens, leaving an areal comma-shaped opening.
Occurrence. Recorded from a range of Antarctic locations (Milam and Anderson, 1981; Ishman and Domack, 1994; Violanti, 1996; Majewski, 2005; Majewski and Anderson, 2009).
Remarks. Very similar to *Stainforthia fusiformis* (Williamson), a species common in the high, northern latitudes. *F. fusiformis* (Cushman) can be distinguished from this species by the shape of the aperture and by being biserial throughout. *F. fusiformis* (Cushman) is common throughout the high, southern latitudes.

Family **Discorbidae** Ehrenberg, 1838
Genus *Discorbis* Lamarck, 1804

Discorbis vilardeboanus (d'Orbigny, 1839b)
(Fig. 3.6:15-16)

1839b *Rosalina vilardeboana* d'Orbigny: 44, pl. 6, figs. 13-15.
1932a *Discorbis vilardeboana* (d'Orbigny); Heron-Allen & Earland: 409, pl. 13, figs 37-39.
1975 *Rosalina vilardeboana* d'Orbigny; Anderson: 88, pl. 8, fig. 10.
2001 *Rosalina globularis* d'Orbigny; Igarashi et al.: 154, pl. 11, fig. 13.

2005 *Rosalina globularis* d'Orbigny; Majewski: 205, fig. 24(1-4).
?2009 *Rosalina* Majewski & Anderson: 139, fig. 4 (14).
2013 *Rosalina globularis* d'Orbigny; Majewski: 183, fig. 11(1).

Material. 60 specimens from 26 samples.
Description. Trochospiral test, spiral side convex, umbilical side flattened, 2.5 whorls, seven chambers in the final whorl, strongly curved, depressed sutures. Small chamberlets formed in umbilical region below triangular alar projections that protrude from the umbilical margin of each chamber. Thin, calcareous, finely perforate wall. Low, interiomarginal, extraumbilical, arch-shaped aperture, with a secondary opening at the posterior margin of the umbilical flap.
Occurrence. Originally described from the Falkland Islands (d'Orbigny, 1839a), subsequently from various locations on the Antarctic shelf (Heron-Allen and Earland, 1932a; Anderson, 1975; Igarashi et al., 2001; Majewski, 2005; Majewski and Anderson, 2009; Majewski, 2013).
Remarks. Chambers less inflated and alar projections more angular than those of *Rosalina globularis* d'Orbigny, with which it may sometimes be confused.

Family **Cibicididae** Cushman, 1927
Subfamily **Cibicidinae** Cushman, 1927
Genus *Cibicides* de Montfort, 1808

***Cibicides* sp. 1**
(Fig. 3.6:11-12)

Material. Four specimens from four samples.
Description. Trochospiral, planoconvex test; flat, slightly involute spiral side with somewhat thickened sutures; strongly convex, completely involute umbilical side. Sutures flush except around final chamber, rounded periphery, calcareous wall, coarsely perforate on spiral side with five large pores in each chamber, pores in earlier chambers filled by lamellar thickening, umbilical side finely perforate, keel and apertural face imperforate. Low, interiomarginal, equatorial aperture extending along the spiral side suture and slightly onto the umbilical side, with a narrow lip.

***Cibicides* sp. 2**

Material. One specimen from one sample.
Description. Trochospiral, planoconvex test; flat, slightly involute spiral side with somewhat thickened sutures; strongly convex, completely involute umbilical side. Calcareous wall, coarsely perforate on spiral side, umbilical side finely perforate, keel and apertural face imperforate, aperture not preserved.

Family **Nonionidae** Schultze, 1854
Subfamily **Nonioninae** Schultze, 1854
Genus *Nonionella* Cushman, 1926

Nonionella bradii (Chapman, 1916)
(Fig. 3.7:2-4)

1916 *Nonionina scapha* (Fichtel & Moll) var. *bradii* Chapman: 71, pl. 5, fig. 42.
1990 *Nonionella bradii* (Chapman); Mackensen et al.: 254, pl. 1, fig. 4.
1994 *Nonionella bradii* (Chapman); Ishman & Domack: 152, pl. 2, figs 10 & 12.
1994 *Nonionella bradii* (Chapman); Jones: 108, pl. 109, fig. 16.
1996 *Nonionella bradii* (Chapman); Violanti: 67, pl. 10, figs. 8, 13, 17.
2001 *Nonionella bradii* (Chapman); Igarashi et al.: 155, pl. 12, fig. 5.
2005 *Nonionella bradii* (Chapman); Majewski: 206, fig. 25(4-5).
2009 *Nonionella bradii* (Chapman); Majewski & Anderson: 139, fig. 4.

Material. 183 specimens from 62 samples.
Description. Low trochospiral, compressed test with rounded periphery, involute umbilical side, partially evolute spiral side. Low, broad chambers that widen towards the periphery, nine to ten in the final whorl, chambers rapidly enlarge in the final whorl to produce a flared test. Flap-like projections from each chamber overhang the umbilicus. Slightly curved, narrow, depressed sutures. Calcareous, hyaline, finely perforate wall with a smooth surface. Aperture a low arch, interiomarginal, equatorial.
Occurrence. First described from the Ross Sea (Chapman, 1916), subsequently reported from numerous other Antarctic localities (Mackensen et al., 1990; Ishman and Domack, 1994; Jones, 1994; Violanti, 1996; Igarashi et al., 2001; Majewski, 2005; Majewski and Anderson, 2009).

Nonionella iridea Heron-Allen & Earland, 1932a
(Fig. 3.7:1 & 5)

1932a *Nonionella iridea* Heron-Allen & Earland: 438, pl. 16, figs 14-16.
1990 *Nonionella iridea* Heron-Allen & Earland; Mackensen et al.: 254, pl. 1, fig. 7-9.
1994 *Nonionella iridea* Heron-Allen & Earland; Ishman & Domack: 152, pl. 2, fig. 11.
1996 *Nonionella iridea* Heron-Allen & Earland; Violanti: 67, pl. 10, figs 9, 14, 18.
2001 *Nonionella iridea* Heron-Allen & Earland; Igarashi et al.: 155, pl. 12, fig. 6.
2005 *Nonionella iridea* Heron-Allen & Earland; Majewski: 206, fig. 25(2-3).
2009 *Nonionella iridea* Heron-Allen & Earland; Majewski & Anderson: 139, fig. 4.
2013 *Nonionella iridea* Heron-Allen & Earland; Majewski: 182, fig. 10(8).

Material. 936 specimens from 85 samples.
Description. Low trochospiral, compressed test, with rounded periphery; involute umbilical side, partially evolute spiral side. Low, broad, somewhat inflated chambers that widen towards the periphery, six to seven in the final whorl. Chambers enlarge in the final whorl to produce a slightly flared test, flap-like projections from each chamber overhang the umbilicus and overlap each other. Slightly curved, narrow, depressed sutures. Calcareous, hyaline, finely perforate wall with a smooth surface. Aperture a low arch, interiomarginal, equatorial, supplementary apertures develop in later chambers along the sutures from the umbilicus approximately halfway to the periphery (not visible in all specimens).
Occurrence. Originally described from the sub-Antarctic, in particular South Georgia and the Falkland Islands (Heron-Allen and Earland, 1932a), subsequently reported from locations around Antarctica (Mackensen et al., 1990; Ishman and Domack, 1994; Violanti, 1996; Igarashi et al., 2001; Majewski, 2005; Majewski and Anderson, 2009; Majewski, 2013).

Subfamily **Astrononioninae** Saidova, 1981
Genus *Astrononion* Cushman and Edwards, 1937

Astrononion echolsi Kennett, 1967
(Fig. 3.7:6-8)

1967 *Astrononion echolsi* Kennett: 134, pl. 11, figs. 7-8.
1981 *Astrononion echolsi* Kennett; Milam & Anderson: 313, pl. 11, fig. 3.
1994 *Astrononion echolsi* Kennett; Ishman & Domack: 152, pl. 2, fig. 3.
1996 *Astrononion echolsi* Kennett; Violanti: 67, pl. 10, fig. 16.
2001 *Astrononion echolsi* Kennett; Igarashi et al.: 155, pl. 12, fig. 11.
2005 *Astrononion echolsi* Kennett; Majewski: 206, fig. 25(6-7).
2009 *Astrononion echolsi* Kennett; Majewski & Anderson: 139, fig. 4
2013 *Astrononion echolsi* Kennett; Majewski: 182, fig. 10(7).

Material. 3877 specimens from 133 samples.
Description. Involute, planispiral, slightly compressed test, with a rounded periphery. Size of chambers gently increases as they are added, eight to nine in the final whorl, somewhat inflated in some specimens but more commonly not. Slightly limbate, curved sutures, slightly depressed to flush. Indistinct, tube-like supplementary chambers extend from the umbilical region, only visible as sunken pits on the sutural lines. Calcareous, hyaline, finely perforate, smooth wall, often with slightly yellow colour. Primary aperture a low, interiomarginal, equatorial arch.
Occurrence. Abundant in the Ross Sea and Scotia Sea, where it was first described (Kennett, 1967), also recorded from various other Antarctic locations (Milam and Anderson, 1981; Ishman and Domack, 1994; Violanti, 1996; Igarashi et al., 2001; Majewski, 2005; Majewski and Anderson, 2009; Majewski, 2013).

Subfamily **Pulleniinae** Schwager, 1877
Genus *Pullenia* Parker & Jones in Carpenter et al., (1862)

Pullenia subcarinata (d'Orbigny, 1839b)
(Fig. 3.7:9-10)

1839b *Nonionina subcarinata* d'Orbigny: 28, pl. 5, figs 23-24.
1932a *Pullenia subcarinata* (d'Orbigny); Heron-Allen & Earland: 403, pl. 13, figs. 14-18.
1981 *Pullenia subcarinata* (d'Orbigny); Milam & Anderson: 313, pl. 11, fig. 5.
1993 *Pullenia subcarinata* (d'Orbigny); Mackensen et al.: 58, pl. 3, figs. 8-9.
?1994 *Pullenia quinqueloba* (Reuss); Jones: 92, pl. 84, figs. 14-15.
1996 *Pullenia subcarinata* (d'Orbigny); Violanti: 48, pl. 10, fig. 19.

Material. 107 specimens from 33 samples.
Description. Involute, planispiral, slightly compressed test with a rounded periphery. Chambers slightly inflated, giving the test a slightly lobulate outline, five to six in the final whorl, face of final chamber has a somewhat triangular shape. Near-radial, slightly depressed sutures. Calcareous, smooth, very finely perforate wall. Aperture a low, interiomarginal, equatorial, crescentic slit, bordered on the upper margin by a raised lip.
Occurrence. Originally described from recent deposits from the Falkland Islands (d'Orbigny, 1839a) , subsequently recorded from around Antarctica (Heron-Allen and Earland, 1932a; Milam and Anderson, 1981; Mackensen et al., 1993; Jones, 1994; Violanti, 1996).
Remarks. *Pullenia quinqueloba* (Reuss) is morphologically very similar to *P. subcarinata* (d'Orbigny) and Jones (1994) assigns the Challenger specimens to *P. quinqueloba* (Reuss). However, *Pullenia quinqueloba* (Reuss) was originally described from German Eocene deposits and these specimens are therefore assigned to *P. subcarinata* (d'Orbigny), which was originally described from Recent deposits from the Falkland Islands.

Family **Chilostomellidae** Brady, 1881
Subfamily **Chilostomellinae** Brady, 1881
Genus *Chilostomella* Reuss, 1849

***Chilostomella* sp. 1**
(Fig. 3.7:13)

Material. One specimen from one sample.
Description. Ovoid, planispiral, involute test, near-circular cross-section. Two strongly embracing, inflated chambers in final whorls, final chamber significantly larger. Calcareous, finely perforate wall, smooth surface, equatorial,

interiomarginal, narrow slit-shaped aperture, with a raised margin. Distinctive spine-like structure on basal end.

Family **Trichohyalidae** Saidova, 1981
Genus *Buccella* Andersen, 1952

***Buccella* sp. 1**
(Fig. 3.7:14-16)

Material. 1397 specimens from 115 samples.
Description. Large, biconvex, carinate, trochospiral test, spiral side low convex and evolute, umbilical side higher and involute. Numerous rhomboidal chambers with curved sides, slightly inflated on the umbilical side, three and a half whorls, eight to ten chambers in the final whorl. Sutures on spiral side flush, slightly limbate, swept back towards periphery, straighter and depressed on the umbilical side. Umbilical region and sutural fissures on umbilical side filled with a mixture of fine and coarse granules, spiral side surface smooth, finely perforate on the chamber faces; periphery very slightly lobate, with a distinct keel. Aperture not visible in any of the specimens examined, may be covered by the abundant granules.
Remarks. Openings at the end of the sutural fissures that are common in members of this genus are not visible in any of the specimens examined here.

***Buccella* sp. 2**
(Fig. 3.7:11-12)

Material. 98 specimens from 43 samples.
Description. Test small for this genus, trochospiral, biconvex, spiral side flatter and evolute, umbilical side convex and involute. Chambers almost semi-circular, two whorls, six to seven chambers in the final whorl, sutures limbate, flush, slightly curved on the spiral side, very depressed on the umbilical side. Umbilical region and sutural fissures on umbilical side filled with granules, spiral side surface smooth, finely perforate on the chamber faces, periphery slightly lobate and thickened but not carinate. Aperture not visible in any of the specimens examined and may be covered by the abundant granules.
Remarks. Bears some similarity to *Epistominella exigua* (Brady), especially in light microscope.

Genus *Neogloboquadrina* Bandy, Frerichs & Vincent, 1967

Neogloboquadrina pachyderma (Ehrenberg, 1861)

1861 *Aristerospira pachyderma* Ehrenberg: 276, 277, 303.
1932a *Globigerina pachyderma* Ehrenberg; Heron-Allen & Earland: 401, pl. 13, figs 9-13.
1975 *Globigerina pachyderma* Ehrenberg; Anderson: 90, pl. 9, fig. 4.
1996 *Neogloboquadrina pachyderma* (Ehrenberg); Violanti: 62, pl. 8, figs 17 & 21.
2001 *Neogloboquadrina pachyderma* (Ehrenberg); Igarashi et al.: 152, pl. 10, figs 8-9.

Material. 209 specimens from 27 samples.
Description. Globular, low trochospiral test, globular chambers that rapidly enlarge as added, five to six in the final whorl. Straight to slightly curved, depressed, radial sutures, rounded periphery, open umbilical region. Calcareous, perforate wall, interiomarginal, extraumbilical to umbilical aperture with bordering lip (may be absent in later stages).

Figure 3.1 SEM of benthic foraminifera
1. *Rhabdammina* spp. (BC738). 2. *Hippocrepinella alba* Heron-Allen and Earland (BC738). 3-5. *Rhizammina* spp. (BC738). 6. *Lagenammina cf. sphaerica* (Moreman) (BC737). 7. *Psammosphaera bowmanni* Heron-Allen and Earland (BC738). 8. *Saccammina* spp. (BC737 (D) 7-8 cm; BC738 (D) 0-1 cm). 9-11. *Astrammina rara* Rhumbler (BC737). (Scale bar 100 μm unless otherwise indicated.) Reproduced from Dejardin et al. (2018).

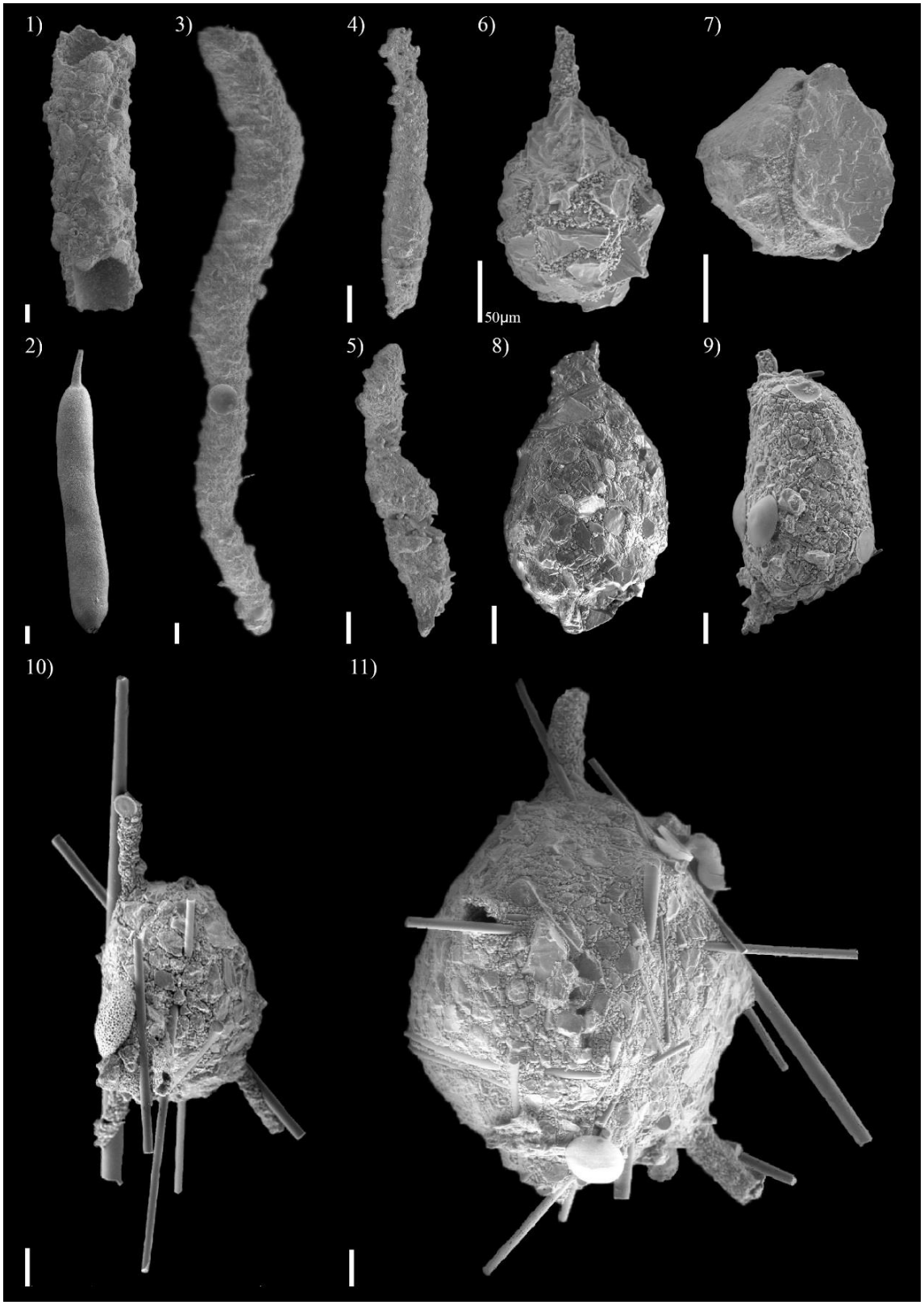


Figure 3.1

Figure 3.2 SEM of benthic foraminifera
1-2. *Psammosphaera fusca* Schulze (BC737 (D) 0-1 cm). 3. *Hormosinella* sp. (BD738). 4. *Miliammina lata* Heron-Allen and Earland (GC666_002). 5-6. *Ammodiscus incertus* (d'Orbigny) (BC737). 7-8. *Miliammina earlandi* Loeblich and Tappan (GC666_002). 9-10. *Hormosinelloides guttifer* (Brady) (BC667). 11. *Nodulina dentaliniformis* (Brady) (BC737 (D) 0-1 cm). 12-13. *Reophax subdentaliniformis* Parr (BC738). 14. *Reophax subfusiformis* Earland emend. Höglund (BC667). 15. *Pseudonodosinella* sp. (BC737 (D) 9-10 cm). 16-18. *Labrospira scitula* (Brady) (BC738). (Scale bar 100 μm unless otherwise indicated.) Reproduced from Dejardin et al. (2018).

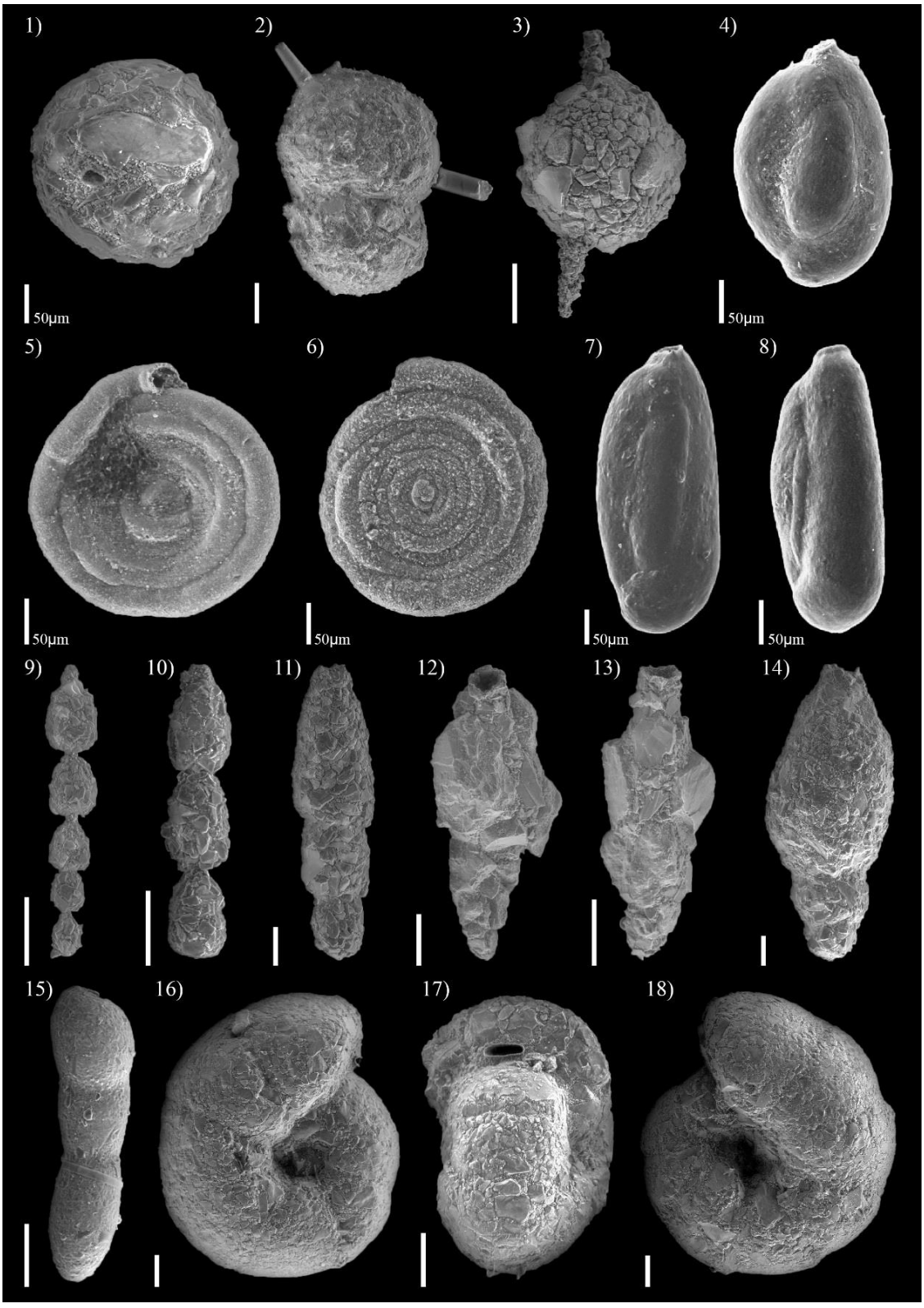

1)
2)
3)
4)
50µm
50µm
5)
6)
7)
8)
50µm
50µm
50µm
50µm
9)
10)
11)
12)
13)
14)
15)
16)
17)
18)

Figure 3.2

Figure 3.3 SEM of benthic foraminifera
1-2. *Haplophragmoides bradyi niigatensis* Uchio 1960 (BC737 (D) 0-1 cm). 3-4. *Labrospira* sp. 1 (GC666_002). 5. *Haplophragmoides quadratus* Earland (GC666_002). 6. *Glaphyrammina americana* (Cushman) (BC738). 7. *Glaphyrammina rostrata* (Heron-Allen and Earland) (BC738). 8. *Pseudobolivina antarctica* Wiesner (BC737 (D) 4-5 cm). 9-10. *Recurvoides* sp. 1 (BC667). 11-12. *Deuterammina scoresbyi* Brönnimann and Whittaker (GC666_002). 13. *Spiroplectammina biformis* (Parker and Jones) (BC738 (D) 9-10 cm). 14-16. *Portatrochammina antarctica weisneri* (Parr) (GC666_002). (Scale bar 100 μm unless otherwise indicated.) Reproduced from Dejardin et al. (2018).

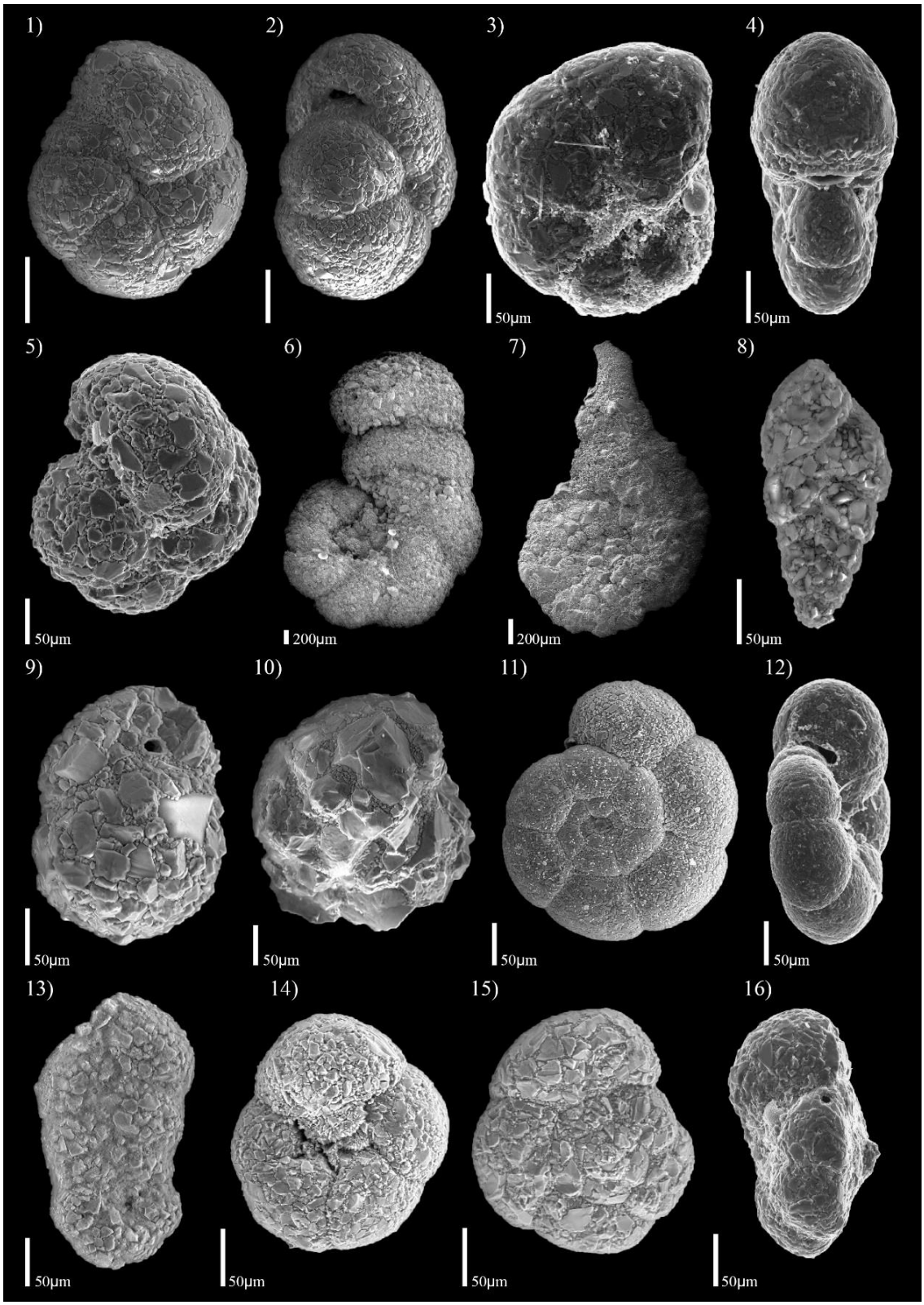

1)
2)
3)
4)
50µm
50µm
5)
6)
7)
8)
50µm
200µm
200µm
50µm
9)
10)
11)
12)
50µm
50µm
50µm
50µm
13)
14)
15)
16)
50µm
50µm
50µm
50µm

Figure 3.3

Figure 3.4 SEM of benthic foraminifera
1. *Pseudotrochammina* sp. 1 (BC737 (D) 0-1 cm). 2. *Cyclammina cf. contorta* Pearcey (BC667). 3-4. *Textularia earlandi* Parker (GC666_002). 5 & 8-9. *Quinqueloculina cf. occidentalis* Bailey (BC738). 6-7. *Cornuspira antarctica* Rhumbler (BC671; GC666_002). 10-11. *Quinqueloculina seminula* (Linnaeus) (BC737 (D) 0-1 cm; BC737 (D) 3-4 cm). 12. *Quinqueloculina cf. sublineata* (Brady) (BC671). 13. *Pyrgo patagonica* (d'Orbigny) (GC673_544). 14. *Pyrgo cf. subpisum* Parr 1950 (GC673_544). 15. *Triloculina* sp. (BC737 (D) 0-1 cm). 16. *?Astacolus* sp. (BC671) 17-18. *Laevidentalina communis* (d'Orbigny) (GC666_002; BC737 (D) 3-4 cm). (Scale bar 100 μm unless otherwise indicated.) Reproduced from Dejardin et al. (2018).

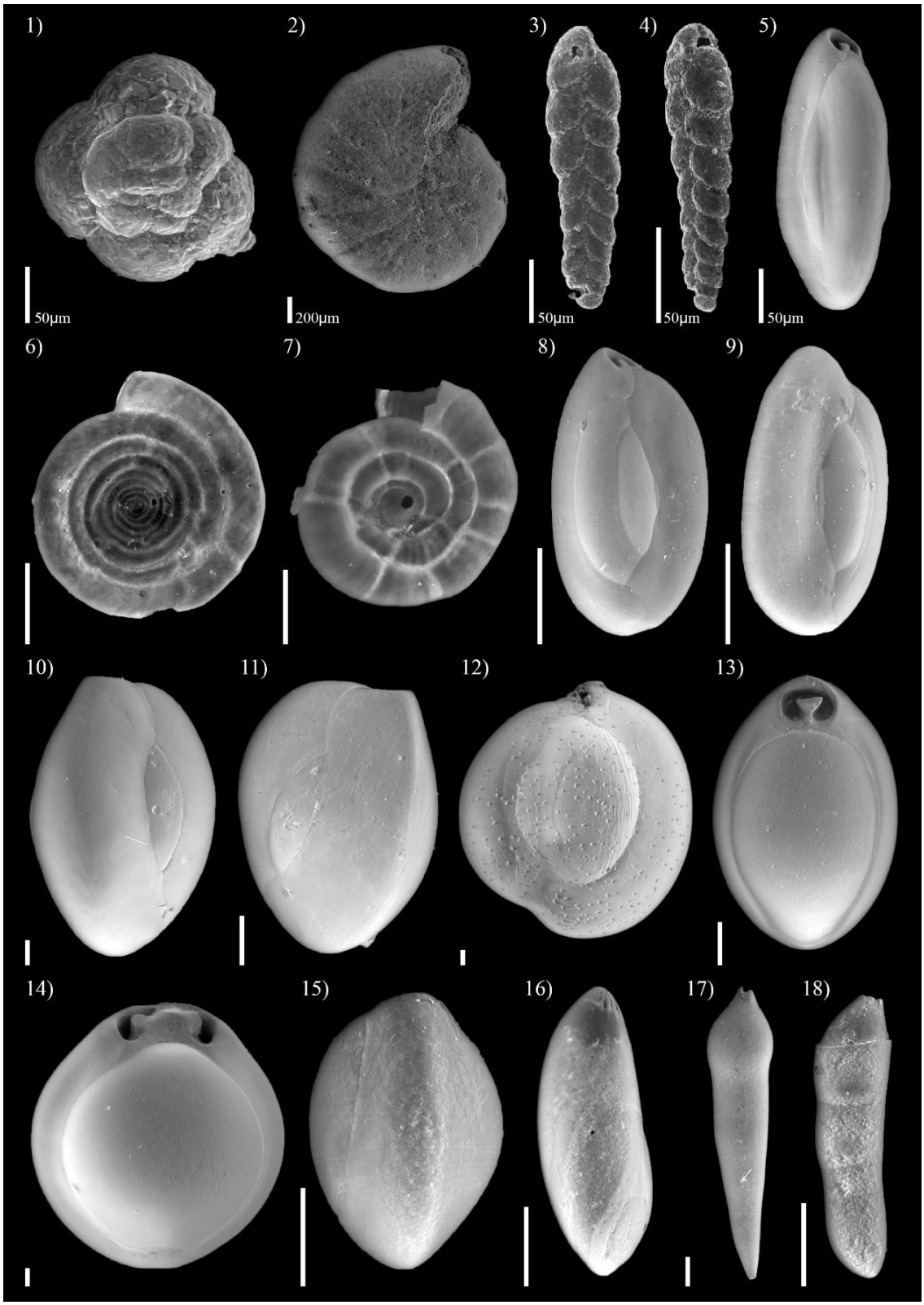


Figure 3.4

Figure 3.5 SEM of benthic foraminifera
1-2. *Lotostomoides calomorphus* (Reuss) (BC737 (D) 2-3 cm). 3-4. *Nodosaria simplex* Silvestri (GC666_119; GC666_159). 5. *Lenticulina asterizans* Parr (GC666_127). 6-7. *Lagena substriata* Williamson (BC737 (D) 4-5 cm; BC738 (D) 5-6 cm). 8. *Lagena multilatera* McCulloch (GC666_002). 9. *Hyalinonetrion cf. gracillima* (Seguenza) (GC666_295). 10. *Procerolagena distoma* (Parker and Jones M.S.) (GC666_127). 11. *Pygmaeoseistron hispidulum* (Cushman) (BC738). 12. *Pygmaeoseistron* sp. (BC738 (D) 2-3cm). 13. *Oolina* spp. (BC738 (D) 8-9 cm). 14. *Fissurina* sp. 1 (GC666_002). 15. *Oolina squamosa* (Montagu) (GC666_124). 16-17. *Oolina globosa* (Montagu) (BC737; BC738 (D) 3-4 cm). 18. *Vasicostella striatopunctata* (Parker and Jones) (BC660). 19. *Fissurina subformosa* Parr (BC737 (D) 2-3 cm). 20. *Fissurina* sp. 2 (GC666_002). 21. *Parafissurina fusiformis* Wiesner (GC666_002). 22. *Bolivinellina earlandi* (Parr) (GC666_002). 23 *Bolivinellina pseudopunctata* (Höglund) (GC666_002). 24-25. *Cassidulinoides parkerianus* (Brady) (GC666_002). (Scale bar 100 μm unless otherwise indicated.) Reproduced from Dejardin et al. (2018).

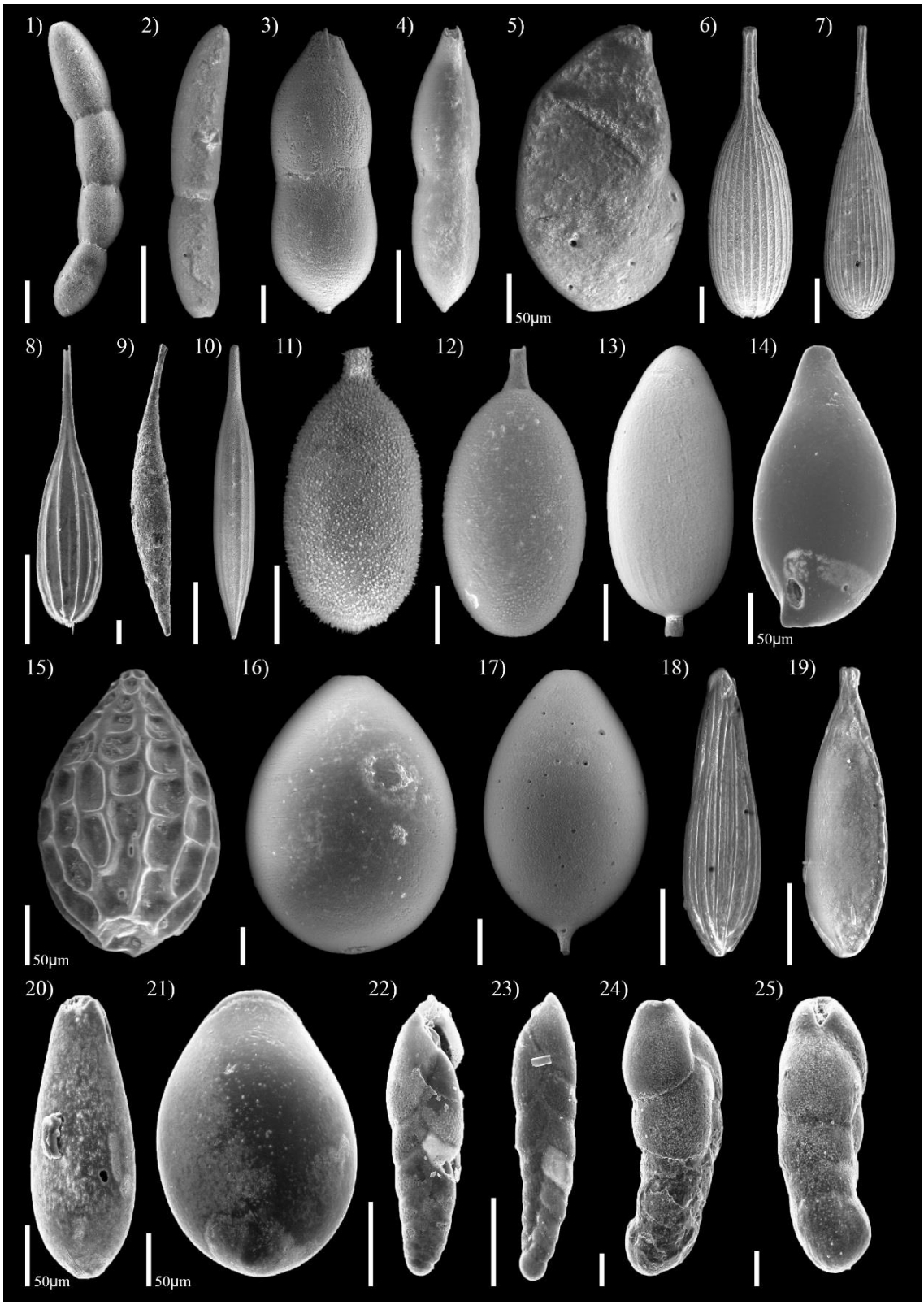

1)
2)
3)
4)
5)
6)
7)
50µm
8)
9)
10)
11)
12)
13)
14)
50µm
15)
16)
17)
18)
19)
50µm
20)
21)
22)
23)
24)
25)
50µm
50µm

Figure 3.5

Figure 3.6 SEM of benthic foraminifera
1-2. *Cassidulinoides porrectus* (Heron-Allen and Earland) (GC666_002). 3-4. *Bulimina aculeata* d'Orbigny (GC666_002). 5-7. *Globocassidulina crassa* (d'Orbigny) *subsp. rossensis* Kennett (GC666_002). 8. *Trifarina earlandi* (Parr (GC666_002)). 9-10. *Bulimina* sp. 1 (GC666_119). 11-12. *Cibicides* sp. 1 (BC737; BC738 (D) 0-1 cm). 13-14. *Fursenkoina fusiformis* (Cushman) (GC666_002). 15-16. *Discorbis vilardeboanus* (d'Orbigny) (GC666_002). 14-16. *Nonionella bradii* (Chapman) (GC666_002). (Scale bar 100 μm unless otherwise indicated.) Reproduced from Dejardin et al. (2018).

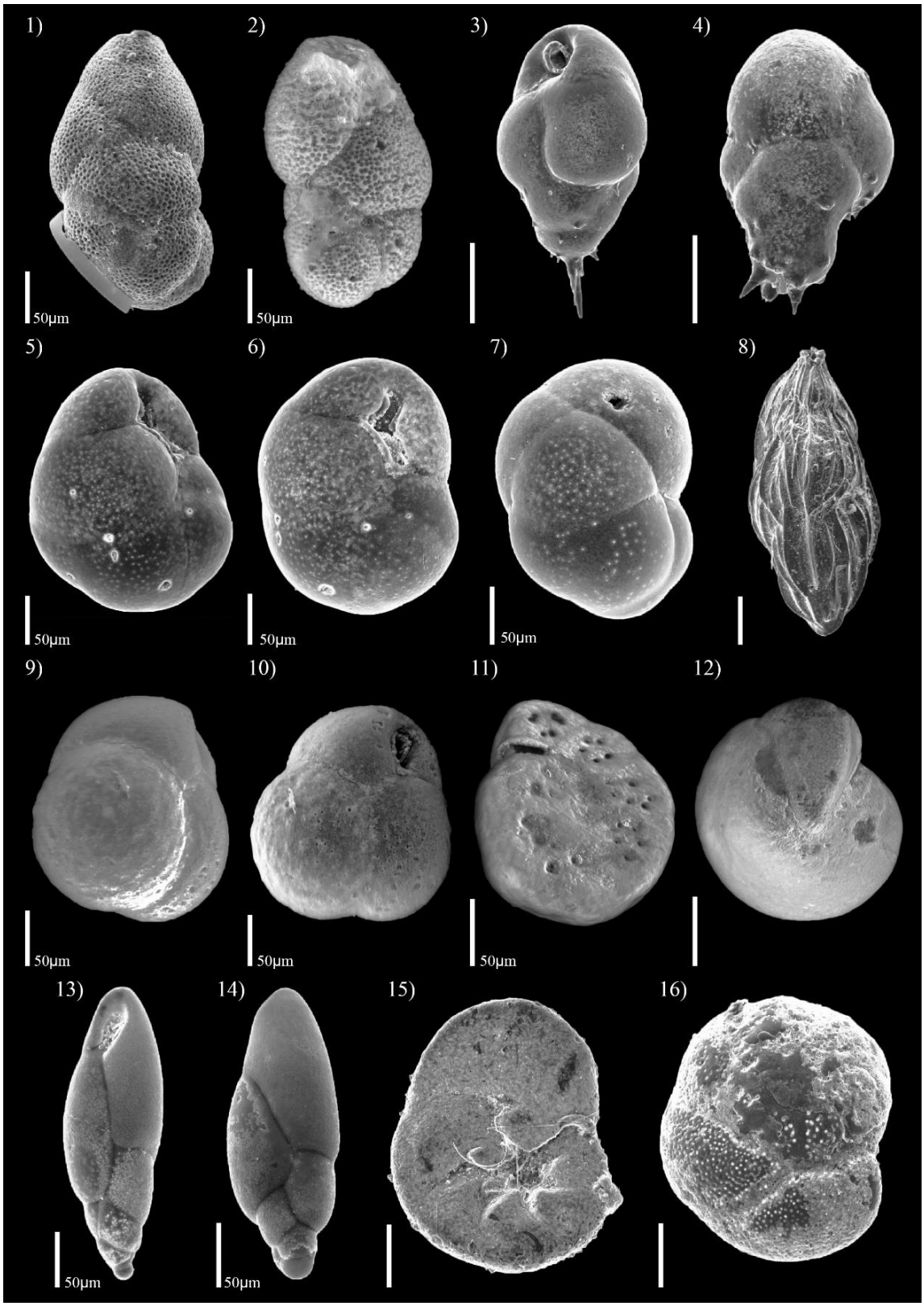

1)
2)
3)
4)
50µm
50µm
5)
6)
7)
8)
50µm
50µm
50µm
9)
10)
11)
12)
50µm
50µm
50µm
13)
14)
15)
16)
50µm
50µm

Figure 3.6

Figure 3.7 SEM of benthic foraminifera
1 & 5. *Nonionella iridea* Heron-Allen and Earland (GC666_002). 2-4. *Nonionella bradii* (Chapman) (GC666_002). 6-8. *Astrononion echolsi* Kennett (GC666_002). 9-10. *Pullenia subcarinata* (d'Orbigny) (GC666_002). 11-12. *Buccella* sp. 2 (GC666_002). 13. *Chilostomella* sp. 1 (BC671). 14-16. *Buccella* sp. 1 (GC666_002). (Scale bar 100 μm unless otherwise indicated.) Reproduced from Dejardin et al. (2018).

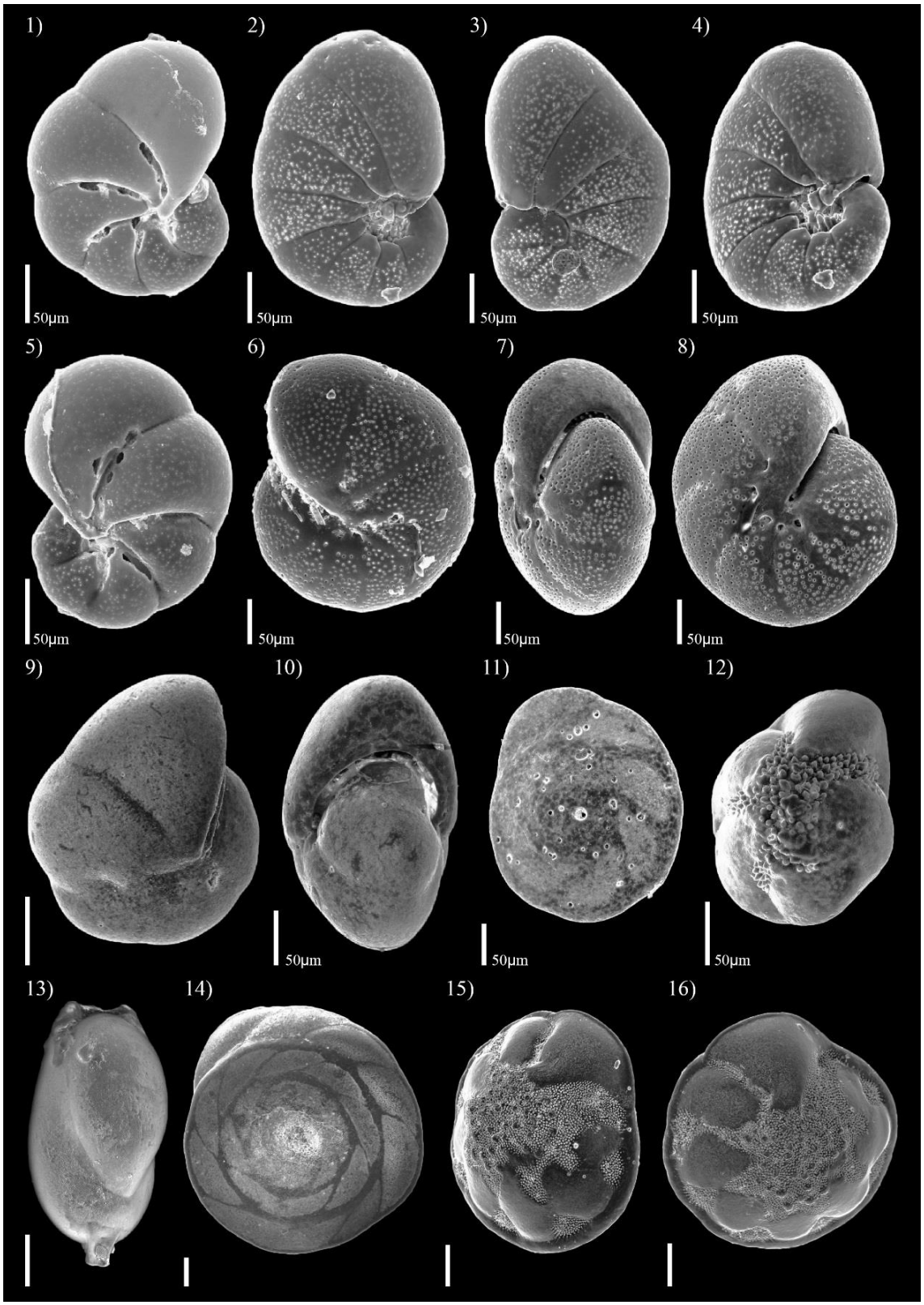


Figure 3.7

Chapter 4

Live (stained) benthic foraminiferal living depths and stable isotopes offshore South Georgia: implications for calcification depths

4.1 Introduction

Benthic foraminifera live both on (epifaunal) and beneath (infaunal) the sediment-seawater interface and their assemblages, stable isotope and trace element compositions are widely utilised as tools in the reconstruction of past oceanographic conditions (see review in Jorissen et al., 2007). Stable isotopes of all species typically exhibit inter-species offsets. In part this offset is accounted for by "vital effects", inter-species differences in the fractionation of stable isotopes due to a range of biological factors (see review in Ravelo and Hillaire-Marcel, 2007). Another consideration, adopted in numerous studies, is that epifaunal and infaunal inter-species isotopic offsets reflect, in part, pore-water chemistry at the preferred depth habitat of each species within the sediment (e.g. Loubere et al., 1995; McCorkle et al., 1997; Theodor et al., 2016b). The carbon isotope composition of pore-water dissolved inorganic carbon ($\delta^{13}C_{DIC}$) has been shown to become lighter (lower $\delta^{13}C$) with sediment depth (e.g. McCorkle et al., 1985), due to the remineralisation (by oxic respiration or denitrification) of organic carbon. The difference between bottom and pore water $\delta^{13}C_{DIC}$ has been shown to increase with bottom water oxygenation (McCorkle and Emerson, 1988). Assuming that infaunal species calcify at preferred depths within the sediment hypothetically allows $\delta^{13}C_{DIC}$ gradients to be reconstructed through the isotope analysis of paired epifaunal and deep infaunal taxa (e.g. *Cibicidoides wuellerstorfi* and *Globobulimina* spp.; Hoogakker et al. 2015). Similarly, the difference in $\delta^{13}C$ between epifaunal and shallow infaunal species (e.g. *Uvigerina* spp.) has been used to reconstruct intensity of organic matter remineralisation, a proxy for the flux of organic matter to the sea floor (Zahn et al., 1986; McCorkle and Emerson, 1988; Schilman et al., 2003). Additionally, Elderfield et al. (2012) used the presence of a constant offset between the $\delta^{13}C$ data from paired epifaunal (*Cibicidoides wuellerstorfi*) and infaunal (*Uvigerina* spp.) foraminifera to negate the suggestion that a negative $\delta^{13}C$ excursion during Marine Isotope Stage 22 was due to productivity changes, and to support their hypothesis that the $\delta^{13}C$ excursion was instead related to global ocean change.

These applications rely on the previously stated assumption that benthic foraminifera inhabit species-specific depth habitats and, more importantly, calcify at that depth, thereby recording the pore-water $\delta^{13}C_{DIC}$ gradient. This assumption has held despite the wide range of sediment depths that individual infaunal species have been observed to live at (e.g. McCorkle et al., 1997). Furthermore, isotope analysis of "live" (Rose Bengal stained) foraminifera reveals a narrow range of isotope values for individuals of the same species despite them having been recovered from a wide range of depths beneath the sediment surface (McCorkle et al., 1990; 1997; Schmiedl et al., 2004; Fontanier et al., 2006a; 2008; Theodor et al., 2016b). A narrow intra-species range of $\delta^{13}C$ composition of "live" specimens recovered from a range of sediment depths argues against individuals having calcified at the depths from which they were recovered (since pore water $\delta^{13}C_{DIC}$ gradients are not reflected in the foraminifera). More recent studies raise further questions about the validity of the assumed calcification depths of infaunal species. For example, it has been assumed that Mg/Ca data from infaunal foraminifera are relatively insulated from the effect of bottom water [CO_3^{2-}] changes (Elderfield et al., 2006; 2010). However, Weldeab et al. (2016) have shown that infaunal *Globobulimina* spp. are sensitive to changes in bottom water [CO_3^{2-}] implying that calcification may not occur exclusively beneath the sediment surface. To extend previous studies of the deep ocean (e.g. McCorkle et al., 1990; 1997; Tachikawa and Elderfield, 2002; Schmiedl et al., 2003; Fontanier et al., 2006a; 2008) onto the shelf environment, and test the assumption that infaunal species calcify at preferred depths and that their $\delta^{13}C$ composition is reflective of pore-water $\delta^{13}C_{DIC}$ (i.e. decreasing $\delta^{13}C_{DIC}$ with increasing calcification depth), this chapter comprises data on the living depths and isotope composition of three as yet unstudied species (*Astrononion echolsi*, *Cassidulinoides porrectus* and *Buccella* sp. 1) from the South Georgia shelf, South Atlantic. The depth ranges of all "living" (Rose Bengal stained) benthic foraminifera recorded from box cores BC737 and BC738 are also reported.

The data presented in this chapter has previously been published in Dejardin et al. (2018). The published manuscript is included in Appendix A5.

4.2 Results

4.2.1 Benthic foraminiferal depth distributions

A total of 1181 "live" (Rose Bengal stained) and 6505 dead specimens were identified from the sub-core sample sequences, representing 62 (36 "living" and 60 dead) taxonomic groupings (See Chapter 3 and Appendix A7). The total abundance for the upper ten samples from the sub-cores ranges from 6 to 16 g^{-1}

for BC737, with the highest abundance evident in the 2–3 cm sample, and from 6 to 13 g^{-1} for BC738, with the highest abundance evident in the 0–1 cm sample. In 0–1 cm samples of the sub-cores the ratio of "live" to dead specimens is 0.42 for BC737 and 0.32 for BC738 (Fig. 4.1). In BC737 this ratio decreases to 0.14 in the 3–4 cm sample before increasing to 0.37 in the 6–7 cm sample, mainly due to the high abundance of "live" *M. earlandi*, and then decreasing to 0.08 in

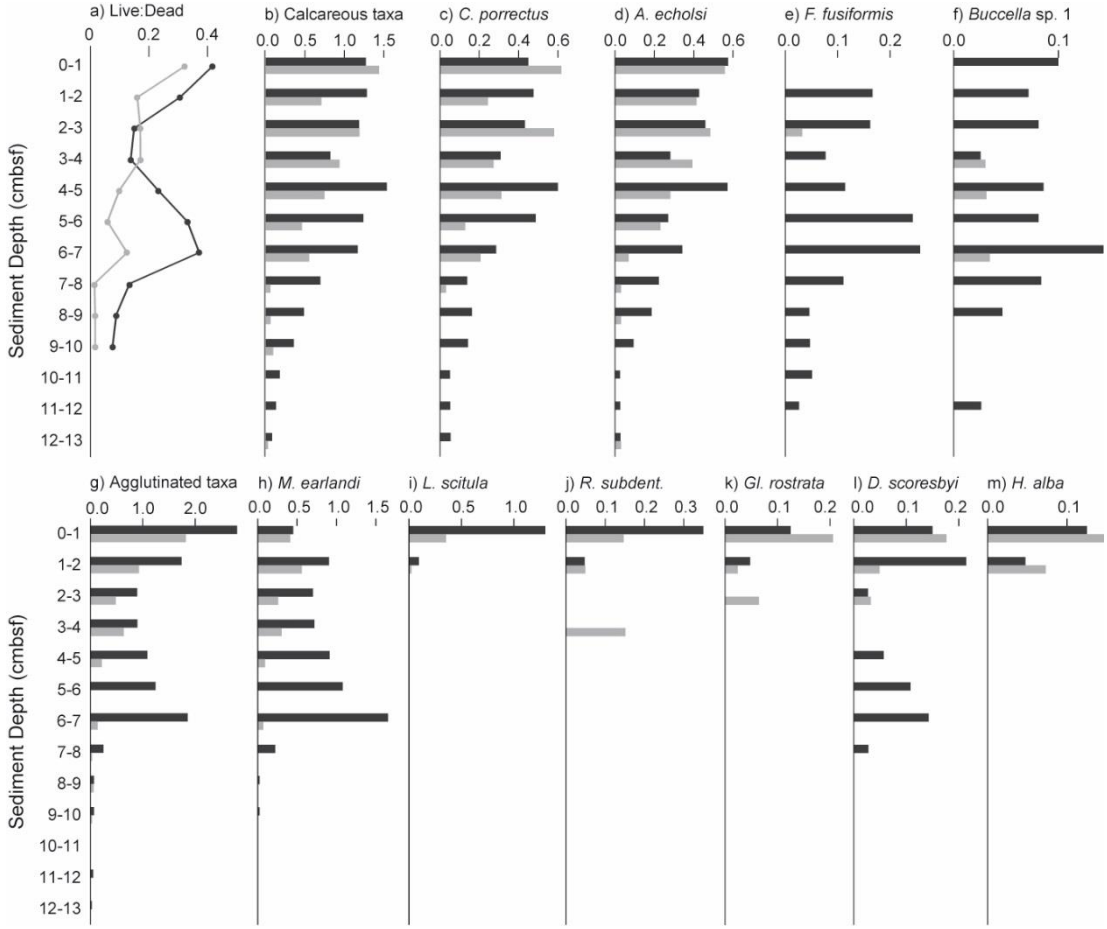


Figure 4.1 Downcore live:dead ratio and live histograms
Downcore live:dead ratio and histograms showing downcore abundance of live (stained) foraminifera. BC7373 (dark grey) and BC738 (light grey) downcore live abundances (g^{-1}): (a) Downcore live:dead ratio (b) total calcareous taxa; (c-f) calcareous taxa with 5 or more live specimens in at least one sample; (g) total agglutinated taxa; (h-m) agglutinated taxa with 5 or more live specimens in at least one sample. Reproduced from Dejardin et al. (2018).

the 9–10 cm sample. In BC738 the "live"/dead ratio decreases steadily throughout the core to 0.02 in the 0–10 cm sample, apart from a small increase to 0.13 in the 6–7 cm sample. A small number of "live" taxa are still present in the 12–13 cm sample of both cores (4 specimens in BC737 and 1 in BC738).

The downcore variation in abundance of the 10 taxa with at least five "live" specimens in one or more samples are shown in Fig. 4.1 (for comparison the

dead abundances of the same taxa are shown in Fig. 4.2). For six of these 10 taxa (*A. echolsi, C. porrectus, F. fusiformis, Buccella* sp. 1, *M. earlandi* and *D. scoresbyi*), "live" specimens were recovered from a wide range of sediment

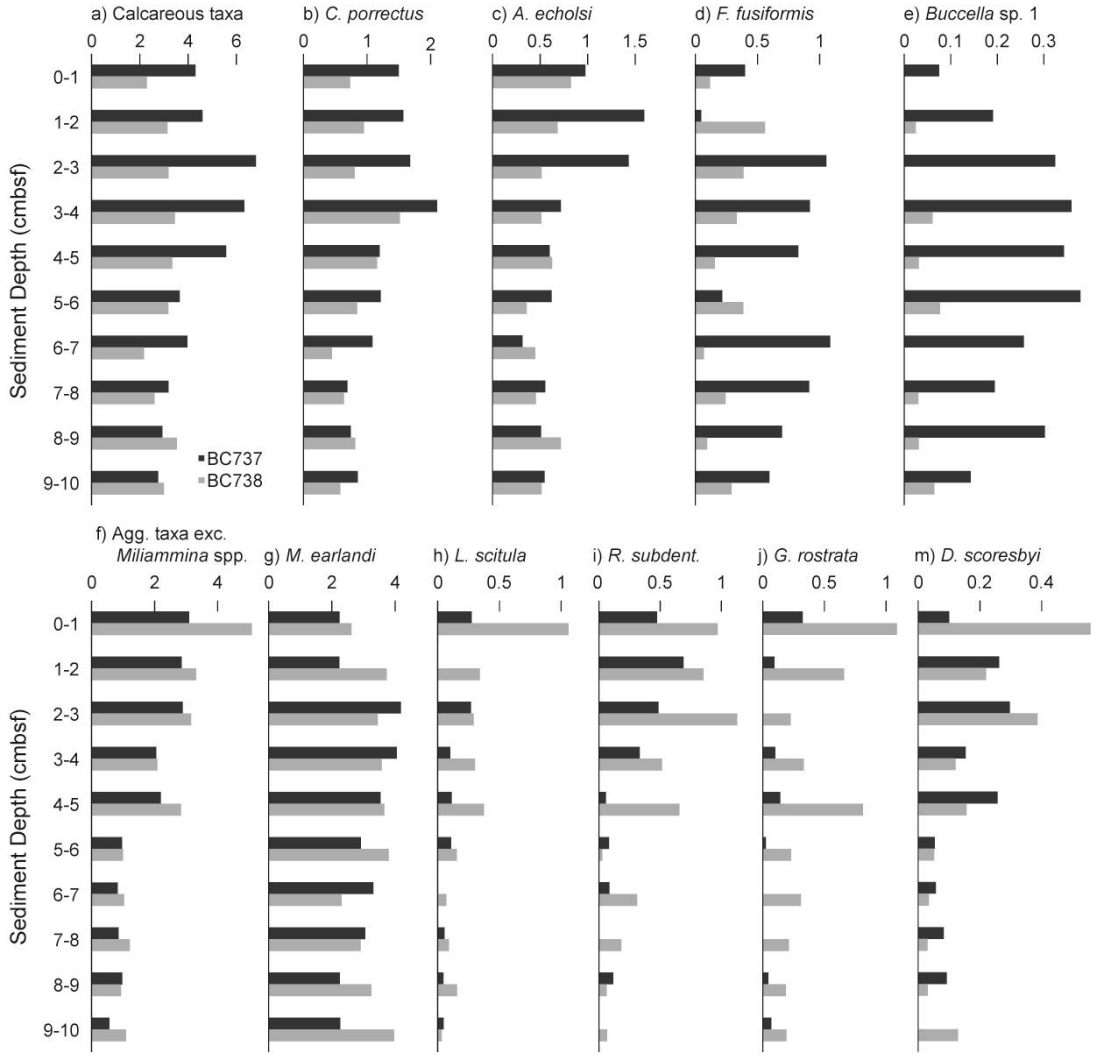


Figure 4.2 Histograms showing dead abundances
Histograms showing downcore abundance of dead foraminifera. BC7373 (dark grey) and BC738 (light grey) downcore live abundances g^{-1}): (a) total calcareous taxa; (b-e) calcareous taxa with 5 or more live specimens in at least one sample; (f) total agglutinated taxa excluding *Miliammina* spp.; (g-m) agglutinated taxa with 5 or more live specimens in at least one sample (*H. alba* has not been plotted in this figure as no dead specimens of this taxa were recorded). Reproduced from Dejardin et al. (2018).

depths, to at least 8 cm, in at least one of the cores. The remaining four taxa (*L. scitula, Reophax subdentaliniformis*, *G. rostrata*, and *Hippocrepinella alba*) were found to be restricted to the upper 0 to 2 cm. The vertical range in living depths for individual species is presented in Fig. 4.3 where the error bars (1SD) reveal a broad depth range of occurrences around the Average Living Depth (ALD) for all species that do not present a restricted epifaunal/shallow infaunal microhabitat

preference. There is a clear separation between the calcareous taxa, which were all found "living" at a range of sediment depths, and the agglutinated taxa, for which the majority were found "living" in the upper 2 cm. The exceptions to this

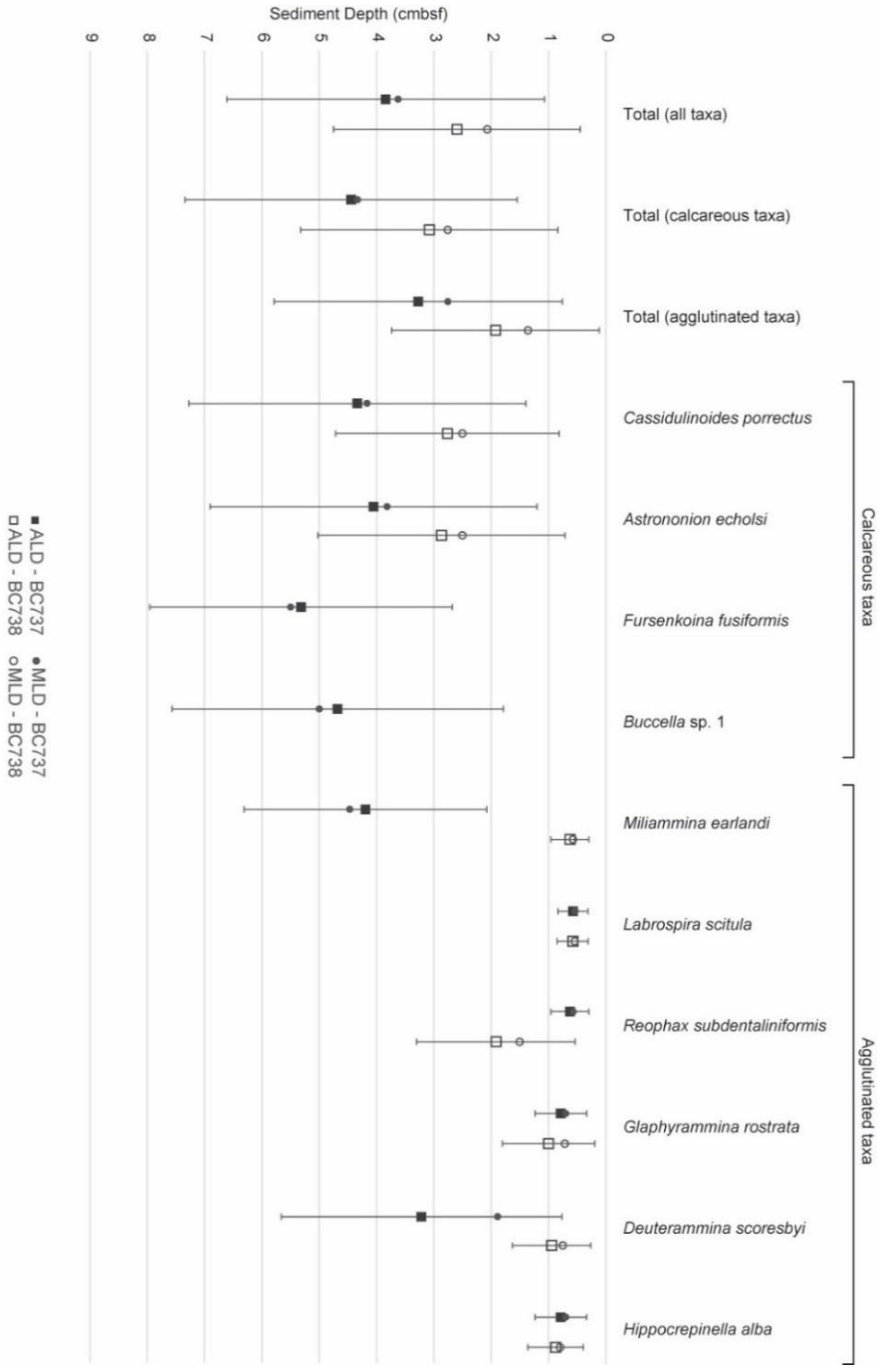


Figure 4.3 Average and Median Living Depths
Average Living Depth (ALD - square symbols), calculated following Jorissen et al. (1995), and Median Living Depth (MLD - circular symbols), calculated following Theodor et al. (2016), plotted for all taxa, all calcareous taxa, all agglutinated taxa, and individually for the 10 taxa with 5 or more "live" specimens in at least one sample. Error bars represent the standard deviation about the ALD (1SD). Closed symbols represent BC737 and open symbols represent BC738. Note that ALD and MLD have not been calculated for *F. fusiformis* and *Buccella* sp. 1 for BC738 as the "live" abundance of these taxa in this core were too low. Reproduced from Dejardin et al. (2018).

are *M. earlandi* and *D. scoresbyi*, which were recorded "living" at a range of depths in BC737, as was *R. subdentaliniformis* in BC738. The agreement

between ALD and Median Living Depth (MLD) is generally good, with a mean difference of 0.21 cm. However, in BC737 the difference between ALD and MLD for *D. scoresbyi* is 1.33 cm, with this difference due to the bimodal depth distribution of "live" occurrences of this species. Although MLD and ALD are generally close within the same box core, there is a systematic difference between the living depths calculated for BC7373 and those calculated for BC738. For four of the five taxa where the difference is >0.5 cm both ALD and MLD are shallower in BC738, relative to BC737, with the exception being *R. subdentaliniformis*, which is shallower in BC737.

The dead abundance of calcareous taxa in BC738 is stable throughout the core; in BC737 this abundance peaks between 2 and 4 cm before becoming stable below this depth. This is in marked contrast to the dead abundance of agglutinated taxa (excluding *Miliammina* spp.) which shows a steady decline with depth in both cores such that, while agglutinated taxa are equal to or exceed calcareous taxa in dead assemblages in the upper core, calcareous taxa come to dominate dead assemblages as sediment depth increases. This trend appears linked to the preservation of taxa with epifaunal/shallow infaunal microhabitat preference as *L. scitula*, *R. subdentaliniformis,* and *G. rostrata* all exhibit a steep decline with depth in the number of dead specimens.

4.2.2 Stable isotopes (δ13C & δ18O) from *Astrononion echolsi, Cassidulinoides porrectus* and *Buccella* sp. 1

The stable isotope compositions of "live" specimens display a relatively wide range of values, from –1.20 to +0.72‰ for $\delta^{13}C$ and from +2.55 to +3.56‰ for $\delta^{18}O$ (Table 4.1). Mean $\delta^{13}C$ values for *Astrononion echolsi, Cassidulinoides porrectus*, and *Buccella* sp. 1 are –0.84±0.15‰, –0.34±0.15‰, and +0.54±0.16‰ respectively; mean $\delta^{18}O$ values are +2.85±0.20‰, +3.40±0.09‰, and +3.49±0.06‰. When plotted on a $\delta^{13}C/\delta^{18}O$ cross-plot (Fig. 4.4) samples from the same species cluster together, irrespective of the living depth. When $\delta^{13}C$ is plotted against depth it is clear that there is no systematic variation with depth (Fig. 4.5). Similarly, no trends with depth are observed in $\delta^{18}O$.

4.3 Discussion

4.3.1 Foraminiferal living and calcification depths

Many of the most abundant infaunal taxa recorded in BC737 and BC738 do not appear to have a clear preference for a specific living depth. However, it is important to recognise the potential limitations of the Rose Bengal staining technique in identifying truly living specimens. Where decay rates are slow, Rose Bengal may stain foraminifera that have been dead for months to several years

(Corliss and Emerson, 1990). It is therefore important to apply as strict a criteria as possible when categorising which specimens are living and which are dead (e.g. Caulle et al., 2015; Fontanier et al., 2016) and to bear this limitation in mind when considering "live" abundances arrived at through Rose Bengal staining. It is also possible for specimens identified as "living" at a certain depth interval to have been transported there after death by bioturbation (see Bernhard, 2000, and references therein). If bioturbation were controlling the distribution of specimens within our data, it might be expected to affect all taxa such that it would not be possible to identify any depth-restricted habitat preferences. The restricted distribution of *L. scitula, R. subdentaliniformis* and *G. rostrata* to epifaunal/very shallow infaunal environments contradicts bioturbation being prevalent at our sites.

Table 4.1 Isotopic data from "live" (stained) foraminifera.
Isotopic data from "live" (stained) foraminifera

		A. echolsi		***C. porrectus***		***Buccella* sp. 1**	
Core	Depth	**$\delta^{13}C$ PDB**	**$\delta^{18}O$ PDB**	**$\delta^{13}C$ PDB**	**$\delta^{18}O$ PDB**	**$\delta^{13}C$ PDB**	**$\delta^{18}O$ PDB**
BC737	0-1 cm	-0.87	3.06	-0.45	3.42	0.72	3.56
BC737	1-2 cm	-1.20	2.77	-0.52	3.45	0.42	3.48
BC737	2-3 cm	-0.98	2.81	-0.45	3.36	0.52	3.47
BC737	3-4 cm	-0.65	2.92	-0.31	3.46	NA	NA
BC737	4-5 cm	-0.93	2.55	NA	NA	0.78	3.48
BC737	5-6 cm	-0.73	2.76	-0.51	3.46	0.60	3.43
BC737	6-7 cm	-0.90	2.58	-0.59	3.14	0.48	3.39
BC737	7-8 cm	-0.78	2.73	NA	NA	0.31	3.48
BC737	8-9 cm	-0.73	2.78	-0.73	3.29	0.46	3.59
BC737	9-10 cm	-0.79	2.76	-0.46	3.50	NA	NA
	Mean	-0.86	2.77	-0.50	3.38	0.54	3.49
	1SD	0.16	0.15	0.12	0.12	0.16	0.06
BC738	0-1 cm	-0.86	2.88	-0.33	3.42	NA	NA
BC738	1-2 cm	-0.82	2.84	-0.20	3.41	NA	NA
BC738	2-3 cm	-0.81	2.88	-0.37	3.41	NA	NA
BC738	3-4 cm	-0.83	2.88	-0.19	3.49	NA	NA
BC738	4-5 cm	-1.03	3.13	-0.56	3.37	NA	NA
BC738	5-6 cm	-0.56	3.34	-0.38	3.39	NA	NA
	Mean	-0.82	2.99	-0.34	3.41	NA	NA
	1SD	0.15	0.20	0.14	0.04	NA	NA

Where decay rates are very slow, specimens that appear "live" at different depths within the sediment column may be significantly older than the overlying

"live" assemblages. This is dependent on the sedimentation rate being high enough to bury specimens to a significant depth before decay is sufficiently progressed that staining with Rose Bengal will no longer occur, and such age control is not available for the samples studied here. While it is important to recognise the limitations of Rose Bengal staining, it is simple, reliable, and inexpensive to use, and is currently the most appropriate technique to apply when, as in this research, the samples are processed immediately upon collection (Bernhard, 2000). In addition, Murray and Bowser (2000) have proposed that, in oxygenated environments, dead tests are unlikely to retain protoplasm due to predation being the most likely cause of death. The oxygenation of the sediments studied here has not been directly measured, but there was no indication of anoxia or dysoxia from the colour and odour of the sediments on recovery.

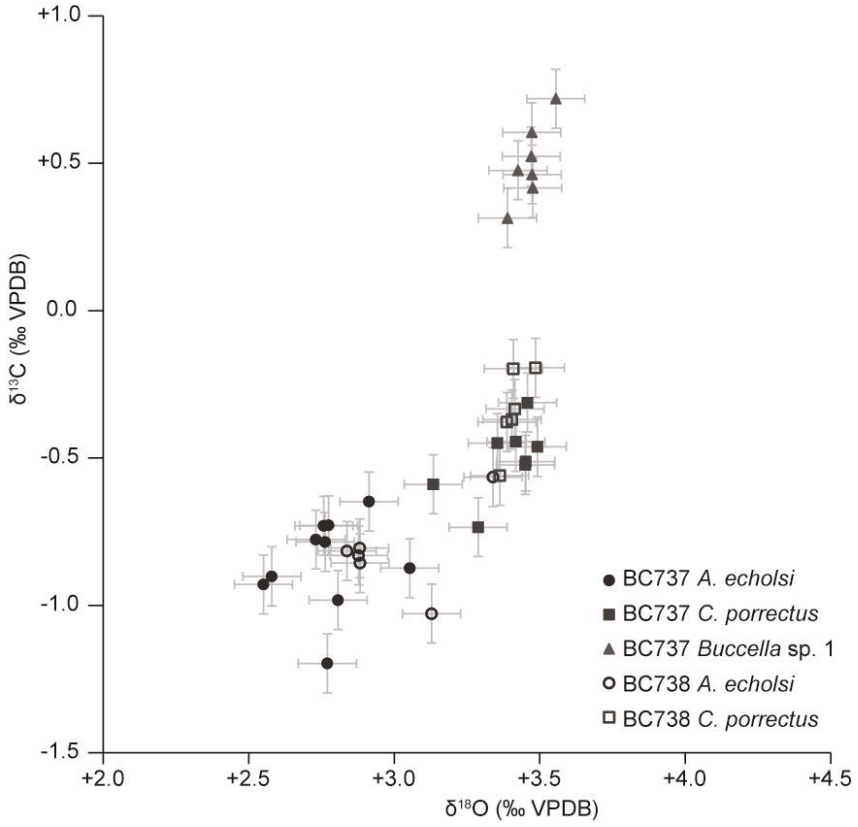


Figure 4.4 $\delta^{13}C$ vs $\delta^{18}O$ cross-plot.
Cross-plot of carbon and oxygen isotopic ratios for all samples analysed in this study. *Astrononion echolsi* - circular symbols, *Cassidulinoides porrectus* - square symbols, *Buccella* sp. 1 - triangular symbols (closed symbols - BC737, open symbols - BC738). Reproduced from Dejardin et al. (2018).

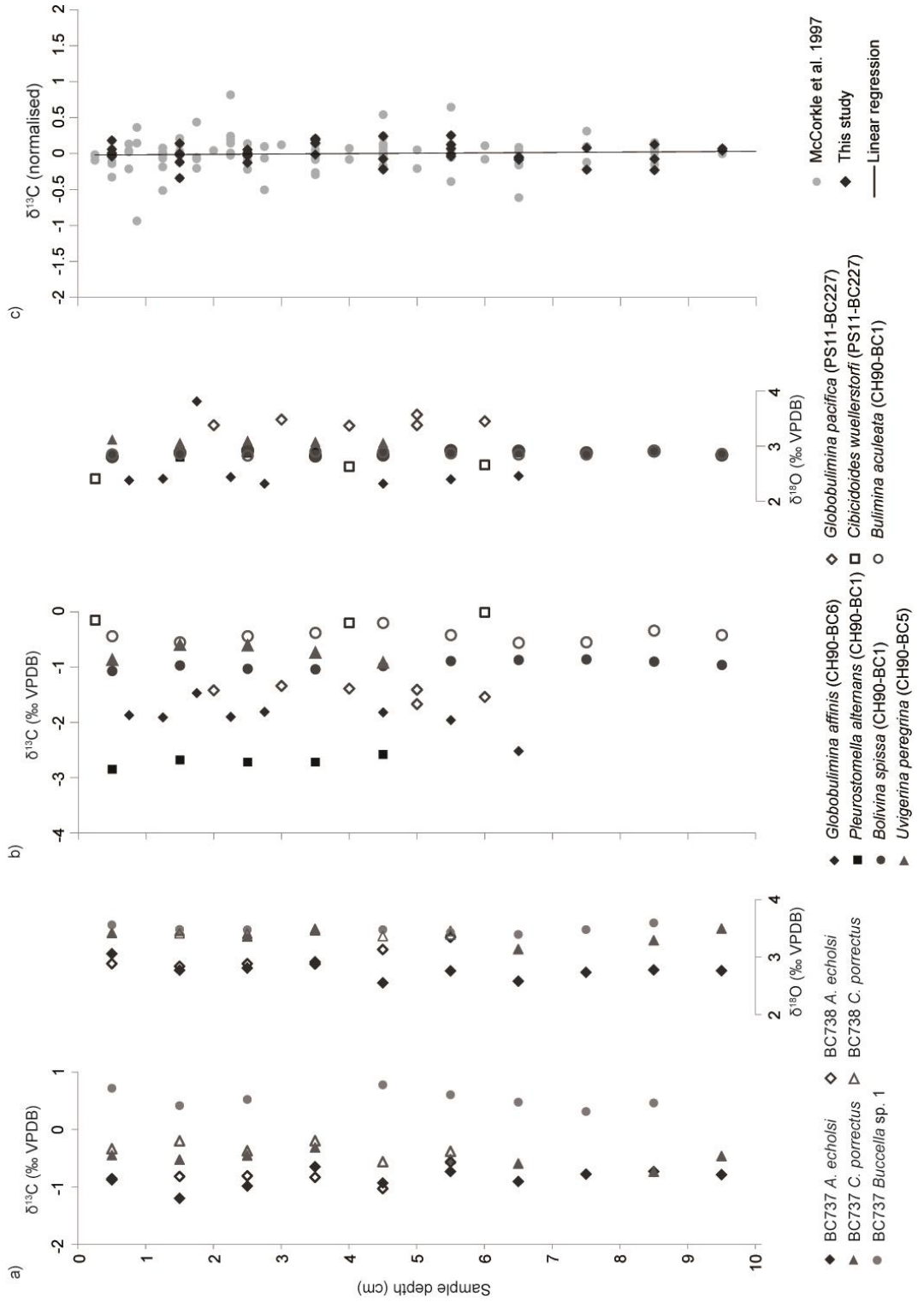


Figure 4.5 Isotopic data plotted against sample depth
(a) Carbon and oxygen isotopic values for species analysed in this study. (b) Carbon and oxygen isotopic values for seven species analysed in McCorkle et al. (1997). (c) Carbon and oxygen isotopic values for species analysed in this study and in McCorkle et al. (1997) normalised by subtracting the mean value for each species from the individual value. There is no systematic variation in either $\delta 13C_{foram}$ or $\delta 18O_{foram}$ with sample depth in any of these three plots. Reproduced from Dejardin et al. (2018).

As discussed in the Section 4.1, it is commonly assumed that foraminifera calcify at their living depth and record the pore water $\delta^{13}C_{DIC}$ in their test isotopic composition, or an isotopic composition offset from that of pore water by species-specific 'vital effects'. Downcore pore water $\delta^{13}C_{DIC}$ data are not available for the cores studied here but records from various other locations consistently report that pore water $\delta^{13}C_{DIC}$ decreases (becomes more negative) with increased sediment depth (e.g. McCorkle et al., 1997; Holsten et al., 2004; Loubere et al., 2011; Luo et al., 2013), before stabilising below the oxygen penetration depth. Furthermore, Gehlen et al. (1999) have modelled how the interaction of oxic organic matter decay and $CaCO_3$ dissolution generate this gradient within marine sediments. It can therefore be assumed that a negative gradient of some kind will be present in sediments from the South Georgia shelf. The observed increase in $\delta^{13}C_{foram}$ with increased MLD (Fig. 4.6) is the opposite of the expected trend were each species calcifying at their respective MLDs. However, there are multiple 'vital-effect' factors that lead to different inter-species $\delta^{13}C$ offsets despite specimens calcifying from waters with the same $\delta^{13}C_{DIC}$ (see review in Ravelo and Hillaire-Marcel, 2007) and without prior knowledge of the impact of these "vital effects" for each species it is not possible to use this as evidence that these species do not calcify at their MLD.

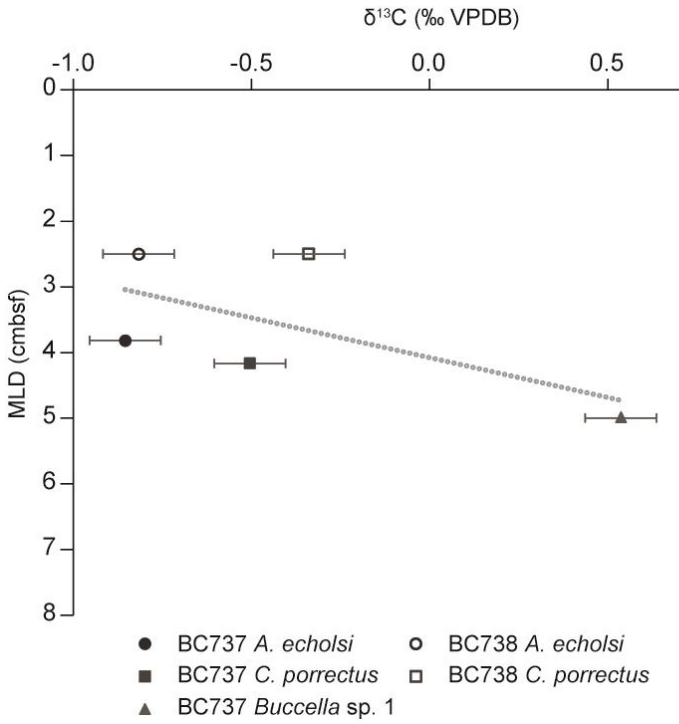


Figure 4.6 $\delta^{13}C$ vs MLD
Mean $\delta^{13}C_{foram}$ values for the three species analysed here plotted against MLD. *A. echolsi* - circular symbols, *C. porrectus* - square symbols, *Buccella* sp. 1 -

triangular symbols (closed symbols - BC737, open symbols - BC738). Error bars = 1SD. Reproduced from Dejardin et al. (2018).

The intra-species isotope data from the three species analysed here do not display the depth-$\delta^{13}C_{foram}$ relationship that would be anticipated, were the foraminifera calcifying with the pore-water $\delta^{13}C_{DIC}$ at the depth from which they were recovered, i.e. intra-species $\delta^{13}C$ does not decrease with depth (Fig. 4.5). The range of inter-species $\delta^{13}C$ and $\delta^{18}O$ compositions considerably exceeds the intra-species range (Fig. 4.4). Other studies that have reported isotope data from "live" foraminifera at a range of living depths have also noted limited variability in the intra-species stable isotope composition. For example, *Bolivina spissa*, *Bulimina aculeate, Cibicidoides wuellerstorfi, Uvigerina peregrina, Pleurostomella alternans*, *Globobulimina affinis* and *G. pacifica* (McCorkle et al., 1997) from mid-latitude continental margins in the Atlantic and Pacific Oceans show no systematic down-core isotope variations (Fig. 4.5), even though the isotopic composition of the same species can vary significantly between locations (e.g. *G. affinis*) (for further examples see McCorkle et al., 1990; Tachikawa and Elderfield, 2002; Schmiedl et al., 2003; Fontanier et al., 2006a; 2008). When the $\delta^{13}C_{foram}$ data presented here, and the data of McCorkle et al. (1997), is normalised, by subtracting the mean for each species at each sample location, there is no trend away from that mean with depth (Fig. 4.5) even though all pore water $\delta^{13}C_{DIC}$ values in those locations (where measured) exhibit a $\delta^{13}C$ gradient.

If the individual foraminifera were calcifying at the depth at which they were found living (as inferred by Fontanier et al., 2006a; Theodor et al., 2016b, amongst others) the intra-species $\delta^{13}C$ data would be expected to reflect a decreasing $\delta^{13}C_{DIC}$ gradient with depth, which they do not. The consistency of intra-species isotope data (Fig. 4.5), despite their broad range of living depths (Figs. 4.1 & 4.5), is good evidence that benthic foraminifera calcify at a *fixed depth location*, and possibly within a specific season, because they fail to capture the variability of pore-water $\delta^{13}C_{DIC}$ that their observed living depth would expose them to.

4.3.2 Foraminiferal calcification strategies

Many have concluded that the observed inter-species differences in $\delta^{13}C$ are due to species preferences for different depth microhabitats, and their position on the $\delta^{13}C_{DIC}$ gradient, implying that calcification occurs infaunally at a specific, restricted depth for each species (e.g. McCorkle et al., 1990; Schmiedl et al., 2004; Theodor et al., 2016b). To account for fixed intra-species $\delta^{13}C$ compositions of infaunal taxa requires calcification to only occur at certain times

during the organism's life when it is exposed to a fixed $\delta^{13}C_{DIC}$ value. Two previously proposed calcification strategies of infaunal species are discussed below: calcification at a specific depth within the sediment, and calcification within macro-/meio-faunal burrows; and a third novel strategy, of calcification at the sediment-seawater interface, is proposed.

In the first strategy, calcification only occurs at a specific depth within the sediment and this depth relates to the preferred microhabitat of the species, broadly speaking epifaunal, shallow infaunal, or deep infaunal. There is evidence for this strategy in some species: for example Holsten et al. (2004) found that the $\delta^{13}C_{foram}$ in three species (*Bolivina argentea, B. subadvena*, and *Buliminella tenuata*) matched the pore water $\delta^{13}C_{DIC}$ at their maximum live abundance depth. However, if the species studied here calcified at a preferred depth within the sediment, what is controlling/determining the narrow calcification depth range (in contrast to the observed wide living depth range), and why it is apparently not the ALD/MLD. On the South Georgia shelf species with deeper ALD/MLD have heavier $\delta^{13}C$ compositions (Fig. 4.6), while pore waters are assumed to change (e.g. become isotopically lighter) with depth.

The second strategy involves calcification in association with the burrows of larger fauna, where voids within the sediment allow pore-water isotopic composition to be homogenous across a range of depths (Loubere et al., 1995; Schmiedl et al., 2004) meaning that calcification within a burrow would result in the same $\delta^{13}C_{foram}$ composition regardless of depth. Loubere et al. (2011) have proposed that all calcareous foraminifera use this strategy, with the activities of macro-/meio-fauna allowing foraminifera to choose micro-habitats with particular geochemical conditions within the complex 'bio-irrigation' systems the larger fauna create.

The third hypothesis, that calcification occurs at the sediment-seawater interface, is supported, in principal, by the presence of "live" specimens of many of the infaunal calcareous taxa recorded in this study (and e.g. McCorkle et al., 1997) within the top 2 cm of the sediment. Foraminifera are known to be capable of migrating throughout the sediment column (e.g. Linke and Lutze, 1993; Geslin et al., 2004) and the occurrence of infaunal species at these shallow depths within the sediment demonstrates their ability to migrate to the sediment-seawater interface. Weldeab et al. (2016) have recorded the presence of a steep $[CO_3^{2-}]$ gradient between bottom water and pore-water, and also within the sediment column. This $[CO_3^{2-}]$ gradient suggests that the sediment-seawater interface may provide the most energy-efficient location for calcification, due to the greater availability of carbonate ions. In addition, food

(phytodetrital matter from the overlying water column) availability and/or quality is greatest at the sediment-seawater interface. While, from the stable isotope data on "living" specimens published here and elsewhere, it is not possible to prove that the species were calcifying at the sediment-seawater interface this may be the simplest explanation for the stability of inter-species isotopic composition.

Alternatively, there may be no requirement to calcify at a specific depth, or within specific geochemical conditions, and foraminifera may be capable of calcifying at a range of sediment depths, and a corresponding range of pore water $\delta^{13}C_{DIC}$ compositions. Calcification across a range of sediment depths could result in foraminiferal calcite recording an average of the range in pore water $\delta^{13}C_{DIC}$ compositions, with any inter-species variation accounted for by species-specific 'vital effects'. The presence of "living" specimens of the species studied here at a range of sediment depths, and the absence of a clear maximum "live" abundance depth, is not inconsistent with this calcification strategy.

4.3.3 Implications of sediment-seawater interface calcification for palaeoenvironmental research

Were foraminiferal calcification only to occur at the sediment-seawater interface, why do inter-species $\delta^{13}C$ offsets vary on annual, decadal, centennial, and longer timescales? As discussed above (see Introduction), $\delta^{13}C$ offsets between epifaunal and infaunal taxa, assumed to be indicative of the pore-water $\delta^{13}C_{DIC}$ gradient, have been used to reconstruct past changes in organic matter flux and sea floor oxygenation (e.g. Zahn et al., 1986; McCorkle and Emerson, 1988; Schilman et al., 2003; Hoogakker et al., 2015). Considering the hypothesis that infaunal species migrate to the sediment-seawater interface to calcify, I propose that changes in epifaunal-infaunal offsets are controlled by the timing of calcification; epifaunal and shallow infaunal taxa calcify persistently, even during periods of relatively low C_{org} availability (oligotrophic/mesotrophic conditions) and infaunal taxa calcify only during periods of high C_{org} availability (eutrophic conditions). Deeper infaunal taxa may be opportunistic, potentially "hibernating", or at least not calcifying new chambers, at depth during oligotrophic periods when food is scarce, and migrating to the sediment-seawater interface to feed and calcify during eutrophic periods.

Supporting this hypothesis, Ohga and Kitazato (1997) observed that, at their study site in Sagami Bay, Japan, all foraminifera where found living in the uppermost part of the sediment column during the peak of phytodetrital flux. Kitazato et al. (2000) have proposed that deep-infaunal taxa may migrate to the sediment-seawater interface to take advantage of phytodetrital input and to

reproduce. Furthermore, in laboratory experiments Nomaki et al. (2005) recorded that many infaunal foraminifera, especially the taxa they classified as shallow or intermediate infauna, migrated upwards through the sediment column in response to an addition of food at the surface. This migration may be quite rapid, with foraminifera capable of moving through several mm of sediment in a day (e.g. Gross, 2000), although Witte et al. (2003) found that foraminifera took eight days to respond to a phytodetritus pulse. In a simulated phytodetritus event Sweetman et al. (2009) found that the uptake of added carbon, labelled with ^{13}C, was confined to surface-living specimens of the deep-infaunal *Globobulimina turgida*. However, Enge et al. (2011) did not record a significant response by deeper infaunal taxa to a simulated phytodetritus pulse, although this may be due to the short duration (4 days) of their experiment. It is also important to note that it has been hypothesised that deep-infaunal taxa may have a preference for degraded organic matter (Caralp, 1989; Fontanier et al., 2003), which if correct may further delay their response to influxes of labile organic matter from phytodetrital pulses. While these studies are consistent with our hypothesis that infaunal taxa migrate to the sediment-seawater interface during eutrophic conditions and calcify, no studies have yet recorded when calcification occurs.

In the scenario described above, infaunal $\delta^{13}C$ records are therefore biased towards eutrophic conditions (even if this is just a brief seasonal pulse of C_{org} to the sea floor), while epifaunal/shallow infaunal $\delta^{13}C$ records are more reflective of mean annual conditions at the sea floor. Since deep infaunal $\delta^{13}C$ is biased towards periods of enhanced C_{org} flux to the sea floor, down core records from the $\delta^{13}C$ of these taxa are potentially less sensitive to variability in C_{org} flux. The abundance of opportunistic infaunal species, however, can increase dramatically by accelerating growth and/or reproduction during eutrophic episodes (e.g. Gooday, 1988; Gooday and Hughes, 2002; Fontanier et al., 2006b; Peck et al., 2015) due to greater organic carbon availability and their tolerance of lower oxygen concentrations (Piña-Ochoa et al., 2010). Down-core epifaunal $\delta^{13}C$ is potentially a more sensitive indicator of variable C_{org} flux and bottom water conditions (oxygenation). During periods of exceptionally high productivity, epifaunal $\delta^{13}C$ may converge with infaunal $\delta^{13}C$ records, reflecting a prolonged abundance of C_{org} at the seafloor throughout the year.

4.4 Summary

There is little intra-species variation in $\delta^{13}C$ of the tests of the "living" benthic foraminiferal species analysed here (*Astrononion echolsi, Cassidulinoides porrectus*, *Buccella* sp. 1), despite them being recovered from a range of depths

(and assumed pore-water isotopic compositions) below the sea floor. The failure of $\delta^{13}C_{foram}$ from depth restricted samples to document the pore water $\delta^{13}C_{DIC}$ gradient common to marine sediments, suggests that infaunal taxa calcify at a fixed $\delta^{13}C_{DIC}$ and therefore depth (e.g. McCorkle et al., 1990; Schmiedl et al., 2004; Theodor et al., 2016b). While it is not possible to conclusively state that the species studied here calcify at the sediment-seawater interface, this hypothesis is consistent with: i) the presence of "live" individuals of all the most abundant taxa in the upper 1-2 cm of sediment in this study (and other studies), ii) the documented ability of foraminifera to migrate through the sediment column (e.g. Linke and Lutze, 1993; Geslin et al., 2004), iii) the absence of a strong living depth preference in this study (and other studies), and iv) the sediment-seawater interface being the most energetically-favourable location for calcification (greatest C_{org} and $[CO_3^{2-}]$ availability).

It is therefore proposed that epifaunal taxa live and calcify at the sediment-seawater interface throughout a wide range of organic carbon availability scenarios (oligotrophic to eutrophic). Infaunal species, however, may only calcify when the concentration of organic carbon at the seafloor is high and they migrate to the sediment-seawater interface to feed. In this scenario, temporal (down-core) variability in the offsets between epifaunal and infaunal $\delta^{13}C$ would reflect changing fluxes of organic carbon to the seafloor, causing variation in $\delta^{13}C_{DIC}$ between oligotrophic and eutrophic conditions. This hypothesis, therefore, has important implications for the use of benthic foraminiferal $\delta^{13}C$ offsets as proxies of productivity and oxygenation, and for the use of trace metal ratios (Mg/Ca, B/Ca) in reconstructing pore water temperature and $\Delta[CO_3^{2-}]$. However, it is evident that changes in epifaunal-infaunal foraminiferal $\delta^{13}C$ offsets through time may reflect the evolution of phytoplankton blooms and watermass chemistry (cf. Hoogakker et al., 2015). This study further highlights the need for a good understanding of foraminiferal ecology when utilising isotopic composition in interpret palaeoenvironmental change. Further work is needed to investigate the timing and depth of calcification in calcareous benthic foraminifera, and the test-forming depths for agglutinated benthic foraminifera.

Chapter 5

Results from Gravity Cores (GC666 and GC673)

5.1 Introduction

This chapter comprises the multiproxy results from the various analyses conducted on sediment samples from two cores from the South Georgia shelf, GC666 (Section 5.2) and GC673 (Section 5.3), including: the development of age/depth models for both cores from radiocarbon dating; sedimentological description and coarse fraction quantification; benthic foraminiferal assemblage analysis; organic carbon and nitrogen concentration; isotopic analysis of organic carbon ($\delta^{13}C$); quantification of biogenic opal; stable isotope analyses of benthic and planktonic (GC666 only) foraminifera ($\delta^{13}C$ and $\delta^{18}O$) and bulk sediment alkenone analysis (GC666 only). For detailed discussion of the methodologies applied in these analyses and their potential interpretation see Chapter 2 – Materials and Methods.

5.2 Core GC666

5.2.1 Age/depth model

A total of 14 radiocarbon-dates were used to generate the age/depth model for GC666 (Table 5.1). Five of these dates have previously been published (Graham et al., 2017) (three from benthic foraminifera, one from a gastropod and one from bivalve shell fragments). Nine further dates were acquired specifically for this project, all from mixed assemblage benthic foraminifera. Dates were calibrated and the age/depth model was calculated using OxCal 4.3 with the standard settings (Bronk Ramsey, 2008; Bronk Ramsey and Lee, 2013; Bronk Ramsey, 2016) and utilising the Marine13 calibration curve (Reimer et al., 2013) with a local reservoir correction of 433 ± 41 years. This correction is based on dating of benthic foraminifera from a surface sample recovered from the same location as GC673, dated as part of this study (see Section 2.2.1). The modelled ages at 1 cm resolution, interpolated linearly between the dated horizons, are presented in Appendix A10. The uncertainties associated with this modelled ages are discussed in Section 2.2.1.3.

The age model sedimentation rates were calculated for the whole core (Fig. 5.1), with values ranging over three orders of magnitude from 4 to 638 cm kyr^{-1}. The sedimentation rate is highest in the basal three metres of the core (815 – 510 cmcd), at 638 cm kyr^{-1}. While this sedimentation rate is high it is not uncommon for cores from the Southern Ocean from shelf environments where there is a strong glacial influence (e.g. in the Palmer Deep (Leventer et al.,

2002)). Between 510 and 115 cm the sedimentation rate is much lower than this, with a mean sedimentation rate of 71 cm kyr^{-1}, ranging from 19 to 122 cm kyr^{-1}. This is followed by an order of magnitude decrease to 4 cm kyr^{-1} between 115 and 97 cm. From 97 cm to the top of the core the sedimentation rate is similar to that calculated between 510 and 115 cm, ranging from 21 to 63 cm kyr^{-1}.

Table 5.1 Radiocarbon age determinations for GC666
(* - samples previously published in Graham et al. (2017); ǂ - samples analysed at the Poznan Radiocarbon Laboratory – min and max values represent 2 standard deviations)

Sample details		Conventional Ages			Calibrated Ages		
Depth (cmcd)	**Carbonate Source**	**^{14}C Age (yr)**	**Error (± yr)**	**Reservoir effect (yr)**	**Min (cal. yr BP)**	**Max (cal. yr BP)**	**Median (cal. yr BP)**
0*	Benthic forams	1097	43	433 ± 41	146	448	317
33ǂ	Benthic forams	1715	30	433 ± 41	710	926	826
57ǂ	Benthic forams	2775	35	433 ± 41	1829	2109	1963
97ǂ	Benthic forams	3590	35	433 ± 41	2790	3108	2945
115ǂ	Benthic forams	7520	50	433 ± 41	7440	7677	7565
127ǂ	Benthic forams	8180	60	433 ± 41	8038	8359	8216
192ǂ	Benthic forams	9750	50	433 ± 41	9763	10132	9901
245ǂ	Benthic forams	10160	50	433 ± 41	10462	10838	10629
324ǂ	Benthic forams	11370	60	433 ± 41	12183	12640	12477
384ǂ	Benthic forams	11780	60	433 ± 41	12652	12988	12811
388*	Gastropod	11856	65	433 ± 41	12706	13091	12889
490*	Benthic forams	13291	74	433 ± 41	14189	15040	14599
510*	Shell fragments	13301	135	433 ± 41	14113	15146	14626
815*	Benthic forams	13572	211	433 ± 41	14226	15800	15111

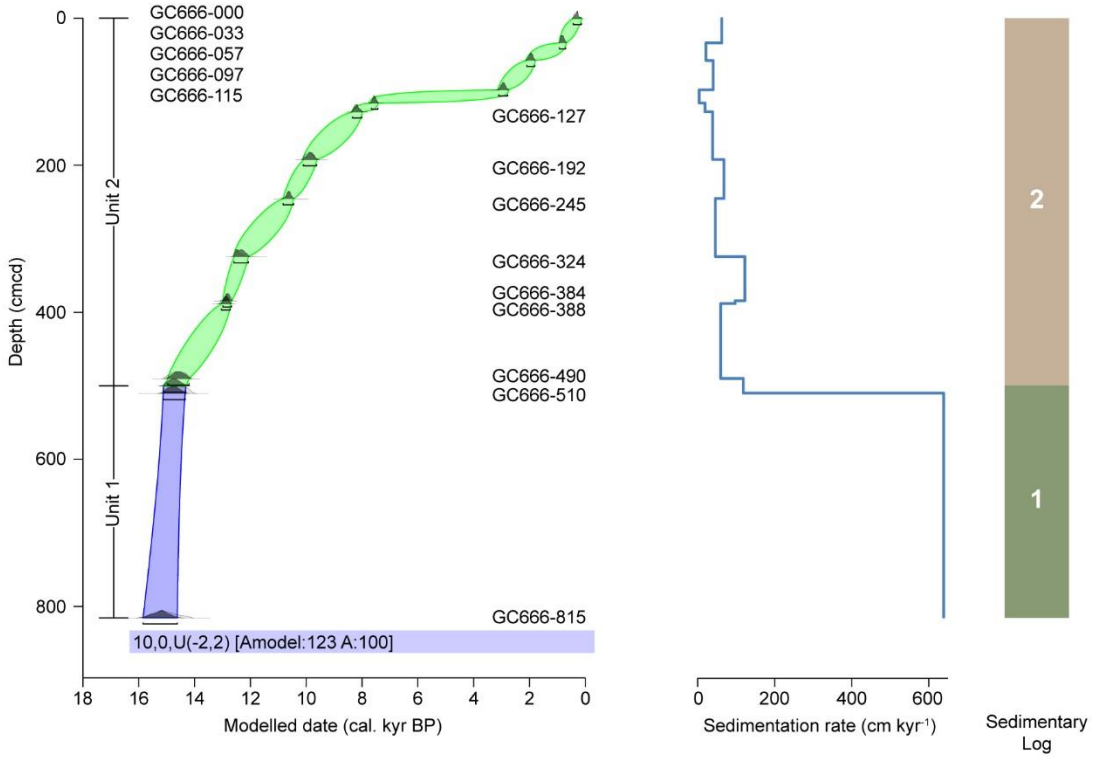


Figure 5.1 GC666 age/depth model
GC666 age/depth model, generated using the deposition model function in OxCal v4.3 (Bronk Ramsey, 2008; 2009; see Appendix A3 for model specification). Sedimentation rates, calculated using dates calibrated in OxCal. The simplified sedimentary log illustrates the extent on the two main sedimentary units (Unit 1 – laminated diatomaceous mud; Unit 2 - homogenous sandy diatomaceous mud; see Section 5.2.2.1).

5.2.1.1 Diagenetic alteration

The preservation of the benthic foraminifera is good in the upper part of the core GC666, however 27 of the samples between 211 and 704 cmcd show varying degrees of diagenetic alteration, evident from discolouration and sugar-like overgrowth covering the tests. This overgrowth is similar in appearance to overgrowth by methane derived authigenic carbonate reported elsewhere (e.g. Cook et al., 2011; Schneider et al., 2017). The overgrowth of authigenic carbonate has the potential to impact the radiocarbon dates generated here and by Graham et al. (2017). In the following discussion I propose that the precipitation of the authigenic carbonate was a result of methane formed deeper in the core, this precipitation may have incorporated older carbon onto the foraminiferal tests analysed for radiocarbon dating. The ages reported for samples where diagenetic alteration has been identified may therefore be older than their true ages. For example, Pohlman et al. (2013) found that authigenic carbonate resulted in ^{14}C ages from foraminifera that were 50−400 years older than their true ages. It is therefore important to take this additional dating uncertainty into account when discussing the proxy records from GC666,

especially when comparing them to other records and to established climate events. That the dates derived from samples containing altered foraminifera are consistent with dates from the unaltered samples may indicate that a thermogenic source for the methane can be excluded, as contamination with fossil carbon from deep reservoirs would result in anomalously old radiocarbon dates.

In addition to potentially altering radiocarbon dates, diagenetic alteration may have also impacted the foraminiferal isotope ratios, presented in Section 5.2.7. The amount of overgrowth varied between specimens within the same sample and care was taken to select for isotope analysis the specimens of *C. parkerianus* that were least altered, based on light microscope analysis. All of the *C. parkerianus* samples identified as having been diagenetically altered also had carbon isotopic ratios more negative than −0.3 ‰, with the exception of the sample from 704 cmcd (+1.1 ‰). The $\delta^{13}C_{foram}$ for the altered *C. parkerianus* samples ranges from −7.9 ‰ to −0.3 ‰ with a mean of −3.4±1.8 ‰. Diagenetically altered samples accounted for all, with the exception of two, of the $\delta^{13}C_{foram}$ values more negative than −0.3 ‰. Diagenetic alteration also affected the planktonic isotopic data, with all the altered samples with planktonic isotope data being more negative than −3.0 ‰, again with the exception of the sample from 704 cmcd (+3.74 ‰). The $\delta^{13}C_{foram}$ for the altered *N. pachyderma* samples ranges from −3.0 ‰ to −11.4 ‰ with a mean of −7.8±2.4 ‰. For both benthic and planktonic data there are no obvious impacts on the $\delta^{18}O$ values, with the offset from the LR04 data (Lisiecki and Raymo, 2005) consistent between altered and unaltered samples.

The large benthic negative $\delta^{13}C_{foram}$ excursions could represent strong ^{12}C enrichment of pore waters within the sediment during the foraminiferal ontogeny. Such strong ^{12}C enrichment can be caused by enhanced oxidation of organic matter (generating $\delta^{13}C_{DIC}$ of approximately −20 ‰ (Berger and Vincent, 1986)) or methane (generating $\delta^{13}C_{DIC}$ of approximately −50 ‰ (Torres et al., 2003)). However, the presence of planktonic negative $\delta^{13}C_{foram}$ excursions in the same samples cannot be explained by pore water ^{12}C enrichment during ontogeny (Blanchet et al., 2012). Combined with the encrusting of the specimens, this suggests that the isotopic excursions are more likely related to diagenetic processes.

The SEM images (Fig. 5.2) show the presence of a crystalline overgrowth on the surfaces of the benthic foraminifera, which is interpreted to be inorganic (authigenic) calcite, based on its dissolution in HCl and the observed crystal shape. The growth of this calcite has resulted in the adherence of diatom

material and other sediment onto the foraminiferal test. The isotopic signature of fossil foraminifera can be modified by the precipitation of authigenic calcite on the tests (e.g. Hill et al., 2003; Reuning et al., 2005; Blanchet et al., 2012; Magalhaes et al., 2012). This process can have a larger effect on planktonic foraminifera as they are more porous than benthic taxa, providing a larger area for precipitation (Pearson et al., 2001). The precipitation of inorganic carbonate in marine sediments is related to the anaerobic oxidation of either organic matter or of methane (formed in organic rich sediments, or released from seeps), both of which have been shown to impact the isotopic composition of foraminifera (Torres et al., 2003; Treude et al., 2005; Cook et al., 2011; Blanchet et al., 2012). The $\delta^{13}C$ of the inorganic calcite formed by these processes ranges from ~−6 ‰ from the anaerobic oxidation of organic matter (Blanchet et al., 2012), to ~−15 ‰ from the anaerobic oxidation of methane in organic-rich sediments (Treude et al., 2005), to −22 ‰ to −51 ‰ from the anaerobic oxidation of methane from methane seeps (Torres et al., 2003; Cook et al., 2011).

Inorganic (authigenic) carbonate was detected throughout Unit 1 of GC666 by Meisel (2013), but not in Unit 2 where the majority of the diagenetically altered foraminifera samples were found in this study. This discrepancy may be due to the low resolution sampling and restricted foraminiferal analysis carried out by Meisel (2013). Isotopic analysis was undertaken by Meisel (2013) on carbonate cemented sediment from 501 to 504 cmcd; the sediment had an average $\delta^{13}C$ of −10.0 ‰ and an average $\delta^{18}O$ of +5.3 ‰. The $\delta^{13}C$ of the carbonate cemented sediment (−10.0 ‰) lies within the range of values reported by Lein (2004) for diagenetic carbonate formation from the anaerobic oxidation of organic matter (−15.6 ‰ to −3.6 ‰). However, there is no indication of exceptionally high organic content, a parameter that favours inorganic carbonate precipitation due to the anaerobic oxidation of organic matter (Blanchet et al., 2012), in the section of Unit 2 where much of the alteration of foraminifera occurs.

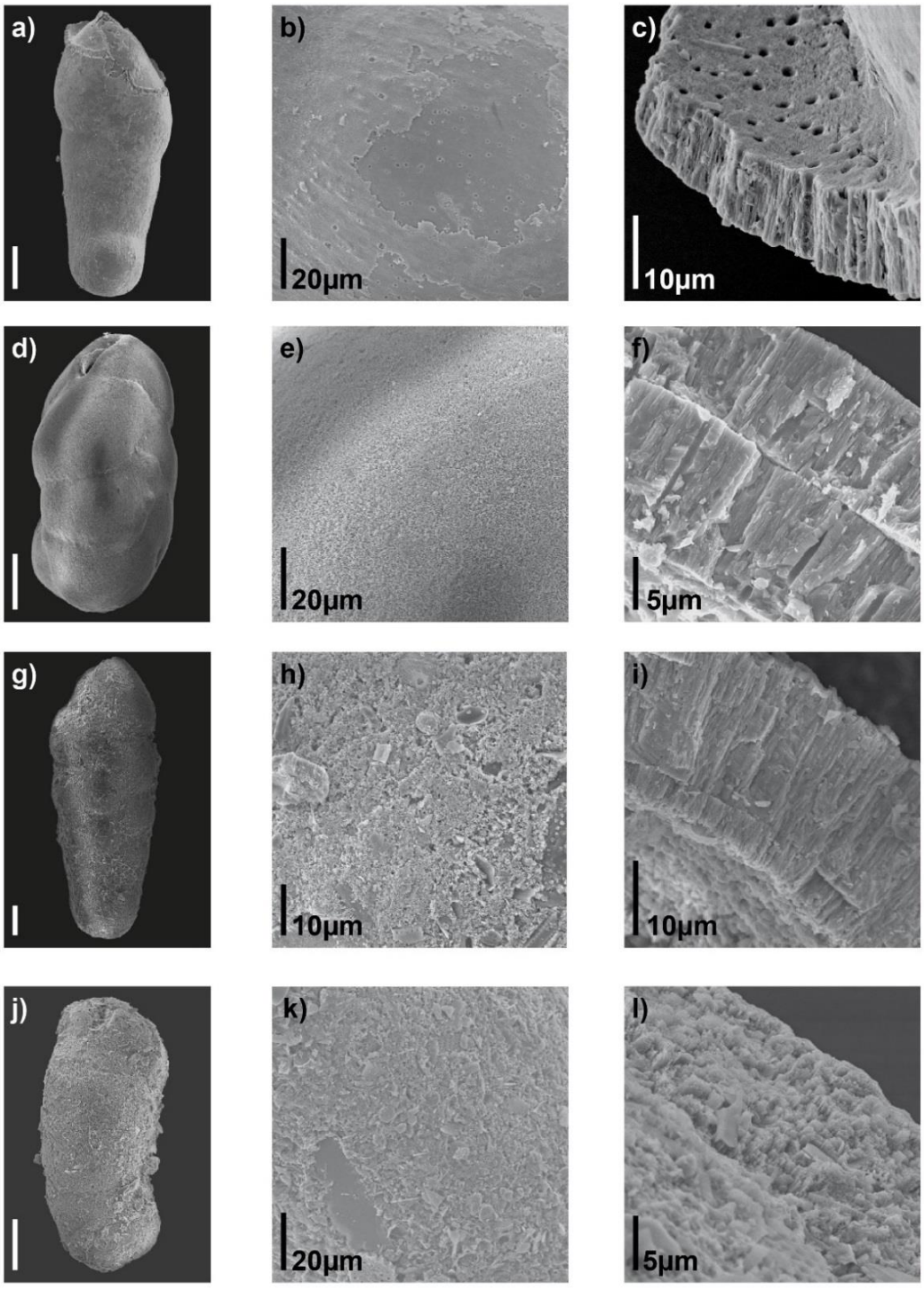


Figure 5.2 SEM images of foraminiferal preservation
Scanning electron micrographs showing examples of the different preservation qualities observed in the *C. parkerianus* specimens that were analysed for stable isotopes. For each preservation example the whole specimen, a detail of the surface texture, and a cross-section through the test is illustrated. a-c) Specimen from a surface sample (BC671) with very good ('glassy') preservation. d-f) Example of the preservation typical of samples from GC666 and GC673 that have not been diagenetically altered. g-i) Example of preservation with some diagenetic overgrowth. j-l) Example of preservation with heavier diagenetic overgrowth and discolouration, and possible alteration of internal structure (l). Scale bars 100 µm unless stated.

Meisel (2013) proposed that the inorganic carbonates found on GC666 were linked to methane, supported by the identification of widespread methane seepage on the South Georgia shelf, including in the Royal Bay trough (Römer et al., 2014). The $\delta^{13}C$ of the inorganic carbonate in GC666 is much less negative than the range reported by Lein (2004) for methane derived authigenic carbonates (−47.5 ‰ to −26.8 ‰), however Malone et al. (2002) constrain this range to −16.4 ‰ to −8.8 ‰. Rapid sedimentation, such as that recorded in Unit 1, favours biogenic methane production (e.g. Hein et al., 1979), and methane may have continued to form in this unit while the overlying sediments were deposited, migrating vertically and causing the diagenetic alteration of the foraminifera. That foraminifera above 211 cmcd (10.1 cal. kyr BP) do not appear to have been altered by inorganic carbonate precipitation may indicate that methane formation in the underlying sediments had ceased by this time. Alternatively, deeply buried reservoirs of thermogenic gas could be the methane source fuelling the precipitation of authigenic carbonate. Graham et al. (2008) proposed that the South Georgia cross-shelf troughs may have developed along lines of structural weakness related to fault zones, which could enable the migration of thermogenic hydrocarbons. Unfortunately the current absence of deep seismic imaging of the South Georgia shelf means that this hypothesis cannot be tested at present (Römer et al., 2014).

That biogenic methane formed in Unit 1 may be further supported by the positive $\delta^{13}C_{foram}$ values recorded in benthic and planktonic data from sample GC666_704, and in authigenic carbonate grains from 808 cmcd analysed by Meisel (2013) (+12.2 ‰). Biochemically formed methane preferentially incorporates ^{12}C, leading to negative $\delta^{13}C$ values in the gas, while the source from which the methane is formed becomes depleted in ^{12}C resulting in a more positive $\delta^{13}C$ signature (Hein et al., 1979; Malone et al., 2002). Authigenic carbonates that precipitate from methane formed from ^{12}C depleted carbon sources can have $\delta^{13}C$ as high as +20 ‰ (Meisel, 2013). Therefore, authigenic carbonate formed in the lower part of GC666 may record the latter stages of biogenic methane formation, from a ^{12}C depleted reservoir.

5.2.2 Sedimentology

5.2.2.1 Sediment description

The sedimentology of GC666 comprises two main units (see Fig. 5.1). Unit 1 comprises laminated diatomaceous mud. Unit 1 forms the basal section of the core (816 – 500 cmcd) and is laminated throughout, has a high sedimentation rate (638 cm kyr^{-1}) and is capped by a ca. 5 cm carbonate cemented mud. Laminae are present throughout the entirety of Unit 1 but the nature of the

lamination varies. In the most basal part of the core (815 – 750 cmcd) the laminae are variously wavy, bent, tilted, disrupted, and discontinuous, possibly due to disruption during the coring process. Above this, between 750 and 654 cmcd, the core is continuously laminated with laminae generally undisturbed and ranging from 1 mm to 1 cm thick. The lamination continues into the upper part of Unit 1 (654 – 500 cmcd) but gradually becomes more intermittent, with sections of homogenous sediment becoming more dominant up core. The laminae comprise light grey-green, dense, clay-rich layers alternating with darker green-black layers of diatom ooze with a cotton wool-like texture. Unit 2 (500 – 0 cmcd) comprises homogenous sandy diatomaceous mud through its entirety, grey/olive green colour with dark mottles, with dropstones occasionally present. The sedimentation rate for this unit ranges from 4 to 122 cm kyr^{-1}.

5.2.2.2 Coarse fraction quantification

Light microscope analysis of the >63 μm fraction revealed that it contains foraminifera, large centric diatoms, and sponge spicules, but that clastic material forms the main component of this fraction. Sediment % >63 μm ranges from 1.3% to 21.9% (Fig. 5.3 & Appendix A11). Between 15.2 and 7.6 cal. kyr BP % >63 μm is below 10% apart from three peaks, between 14.0 and 13.6 cal. kyr BP (max. = 15.2%), at 10.3 cal. kyr BP (11.9%), and between 9.2 and 8.8 cal. kyr BP (max. = 20.8%). After 7.5 cal. kyr BP % >63 μm rises to 20.1% by 6.5 cal. kyr BP and remains >10% until 3.3 cal. kyr BP (mean = 16.2 ± 2.9%); after 3.3 cal. kyr BP % 63 μm remains <10%.

An accumulation rate was also calculated for the >63 μm fraction (>63 μm AR), using the sedimentation rates discussed above. The three peaks recorded between 15.1 and 7.5 cal. kyr BP are also present as peaks where >63 μm AR is >5 g cm^{-1} kyr^{-1}. In addition, >63 μm AR is high (>5 g cm^{-1} kyr^{-1}) prior to 14.8 cal. kyr BP and between 12.8 and 12.4 cal. kyr BP. The high % >63 μm values recorded between 7.5 and 3.3 cal. kyr BP are not translated into high >63 μm AR. Instead the >63 μm AR is lowest during this period (0.74 ± 0.22 g cm^{-1} kyr^{-1}).

The number of coarse clastic grains with a diameter >250 μm were counted under light microscopy, at 40x magnification, during foraminifera picking (Fig. 5.3). Throughout the core, the number of coarse grains is generally <15 g^{-1}, with the exception of two peaks, between 14.0 and 13.6 cal. kyr BP (max. = 35 g^{-1}), and between 7.6 and 6.5 cal. kyr BP (max. = 73 g^{-1}). Conversion of these data to accumulation rates (>250 μm AR), using the calculated mass accumulation rate, reveals that >250 μm AR is high (>250 cm^{-1} kyr^{-1}) in sediments older than 13.6 cal. kyr BP, with >250 μm AR >1000 cm^{-1}

kyr^{-1} prior to 14.9 cal. kyr BP and between 14.0 and 13.6 cal. kyr BP. There is also a smaller >250 µm AR peak between 7.6 and 6.5 cal. kyr BP (>200 cm^{-1} kyr^{-1}).

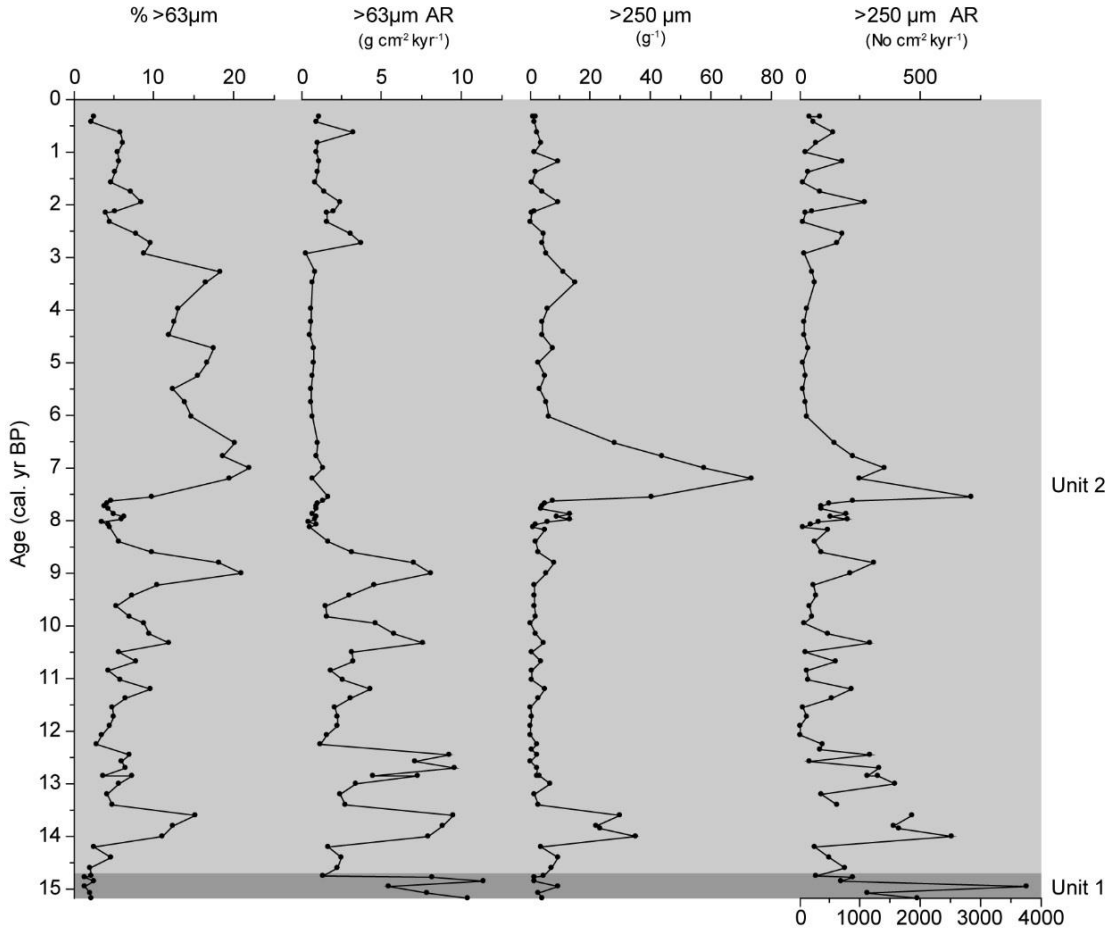


Figure 5.3 Sedimentological data from core GC666
Percentage of the sample that comprises the >63 µm fraction, the >63 µm fraction accumulation rate, number of >250 µm diameter clasts per gram, the >250 µm diameter clast accumulation rate (note the split scale for this plot). Shaded areas represent the two sedimentary units discussed in the text.

5.2.3 Diatom assemblage composition

To test whether the diatom assemblage differed between the light and dark layers, preliminary assemblage analysis was undertaken. Three couplets of light and dark laminae were sampled using a toothpick, and smear slides were made by suspending the sampled sediment in deionised water and pipetting approximately 0.5 mL onto a 19 mm diameter coverslip. After drying the coverslip was then mounted on a microscope slide using Naphrax. Diatoms were counted using a Euromex Bioblue binocular microscope at 1000x magnification and split into two classification groups; *Chaetoceros* (*Hyalochaete*) resting and vegetative spores (CRVS) and non-CRVS, with 100 non-CRVS counted in each sample analysed. This analysis revealed that, while CRVS were very abundant in both light and dark layers, their abundance relative to non-CRVS was much

higher in the dark layers (Table 5.2). The CRVS in the dark layers were mainly resting spores and these layers also contained a lot of thin fibre-like material, interpreted to be the delicate setae of *Chaetoceros* spp., while the lighter layers contained more clastic material.

Table 5.2 Preliminary diatom assemblage analysis
Preliminary diatom assemblage analysis of three dark and light couplets from core GC666.

Sample details		Diatom counts		
Depth (cm)	**Light/Dark**	**CRVS**	**Non-CRVS**	**CRVS:nonCRVS**
539	Light	1918	100	19
538	Dark	7582	102	74
581	Light	1857	100	19
582	Dark	8457	100	85
591	Light	2181	100	22
592	Dark	6048	100	60

5.2.4 Benthic foraminiferal census counts

A total of 26,891 benthic foraminiferal specimens from 47 taxonomic groupings (see Chapter 3 & Appendix A8) were recorded in the 89 samples analysed from GC666, plus 185 specimens of the planktonic taxa *Neogloboquadrina pachyderma* (present in 37 samples). Three hundred or more benthic specimens were present in 41 samples, and a further 26 samples contained between 100 and 299 specimens. Down core diversity, dominance and Benthic Foraminifera Accumulation Rate (BFAR) were also calculated.

5.2.4.1 Diversity, Dominance and BFAR

Diversity (Fisher's alpha – Fig. 5.4) varies through the core with the lowest diversity (0.20) recorded in the oldest sample analysed (15.2 cal. kyr BP). Diversity increases through the deglacial and into the early Holocene, reaching a peak of 4.8 at 8.6 cal. kyr BP, before decreasing to 0.37 by 6.5 cal. kyr BP. The mid-Holocene (6.5 to 3.0 cal. kyr BP) is characterised by low diversity until 3.9 cal. kyr BP (mean diversity during this period is 0.67±0.4). Diversity increases through the late Holocene to a peak of 7.1 in the youngest sample analysed (0.3 cal. kyr BP).

Dominance (Fig. 5.4) follows the inverse of the trends seen in diversity, with the highest value recorded in the oldest sample (15.1 cal. kyr BP). Dominance declines, from a peak of 1.0 at 15.2 cal. kyr BP, through the deglacial and early Holocene to 0.19 at 10.3 cal. kyr BP, remaining low until 7.2 cal. kyr BP (mean = 0.16±0.03). Dominance then increases to 0.79 at 6.0 cal.

kyr BP before decreasing through the mid to late Holocene to 0.13 at 0.4 cal. kyr BP.

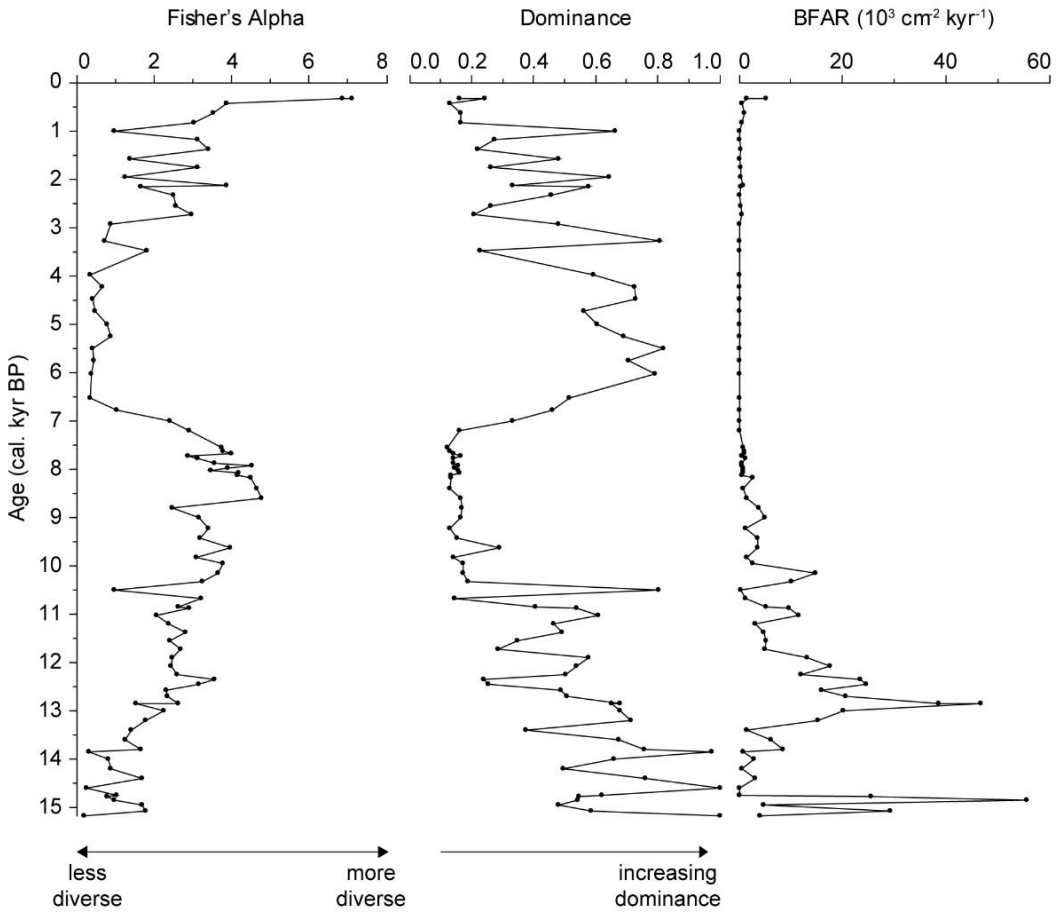


Figure 5.4 GC666 benthic foraminifera data
Benthic foraminiferal diversity (Fisher's alpha) and dominance data, and the accumulation rate of benthic foraminifera, from core GC666.

Between 15.2 and 14.8 cal. kyr BP BFAR is elevated (>4000 cm^{-2} kyr^{-1}) and highly variable, ranging from 4000 to 55700 cm^{-2} kyr^{-1}. After 14.8 cal. kyr BP BFAR remains low (<4000 cm^{-2} kyr^{-1}) until 14.0 cal. kyr BP, when BFAR starts to increase to a peak of 46800 cm^{-2} kyr^{-1} by 12.8 cal. kyr BP. After this peak, BFAR then decreases steeply to 5100 cm^{-2} kyr^{-1} by 11.7 cal. kyr BP, and then decreases further to 700 cm^{-2} kyr^{-1} by 8.1 cal. kyr BP, with this decrease interrupted by peaks at 11.0 cal. kyr BP and 10.1 cal. kyr BP. BFAR then remains low (<1200 cm^{-2} kyr^{-1}) until 7.2 cal. kyr BP when it decreases to <100 cm^{-2} kyr^{-1} remaining at this level until 2.9 cal. kyr BP. BFAR subsequently increases slightly but remains <1000 cm^{-2} kyr^{-1} until the two youngest samples (both 0.3 cal. kyr BP) where it increases to 1400 and 5100 cm^{-2} kyr^{-1}.

5.2.4.2 Foraminiferal assemblages

To assess whether statistically significant groupings of similar assemblages are present, a cluster analysis was applied to the benthic foraminiferal data (Fig. 5.5), performed in PAST3 using the chord similarity index applied with an unweighted paired group average (UWPGA) algorithm (Section 2.3.7). From this analysis three groupings of samples occur at the 0.96 level of similarity. One of these groups (containing 30 samples) comprises samples in which *Fursenkoina fusiformis* is the dominant benthic foraminifera, the second grouping comprises 33 samples in which *Miliammina* spp. are the dominant foraminifera. The foraminiferal assemblage in the remaining 26 samples that form the third group is more diverse, with *Cassidulinoides* spp. and *Astrononion echolsi* among the dominant taxa. To further test the significance of these groupings, Detrended Correspondence Analysis (DCA) was applied to the same data (Fig. 5.6).

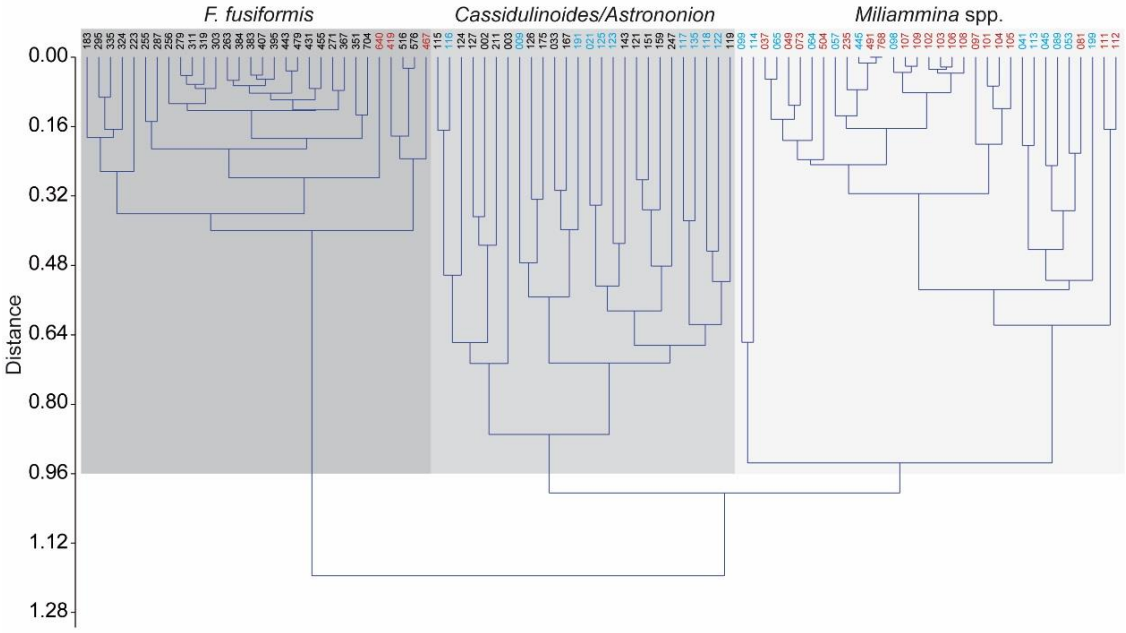


Figure 5.5 GC666 cluster analysis
Cluster analysis carried out in PAST3 (Hammer et al., 2001) using the paired group algorithm and the chord similarity measure. Blue samples have 100-300 benthic specimens, red samples <100.

The eigenvalues for Axis 1 and Axis 2 of the DCA are 0.46 and 0.17 respectively, and when these axes are plotted against one another the DCA supports the three groupings identified by the cluster analysis. While the three groupings plot in different areas of DCA space, there is some overlap of their respective 95% confidence ellipses. Of the 10 most abundant taxa (that collectively represent 96% of the total benthic foraminiferal abundance and named in Figure 5.6) *F. fusiformis* plots in association with the grouping of samples with high *F. fusiformis* abundance, *Miliammina earlandi* plots in

association with the second grouping identified in the cluster analysis, and *Astrononion echolsi*, *Cassidulinoides parkerianus*, and *C. porrectus* plot in association with the third grouping. From this point forward these groupings will be referred to as the *Fursenkoina* Assemblage, the *Miliammina* Assemblage, and the *Cassidulinoides/Astrononion* Assemblage.

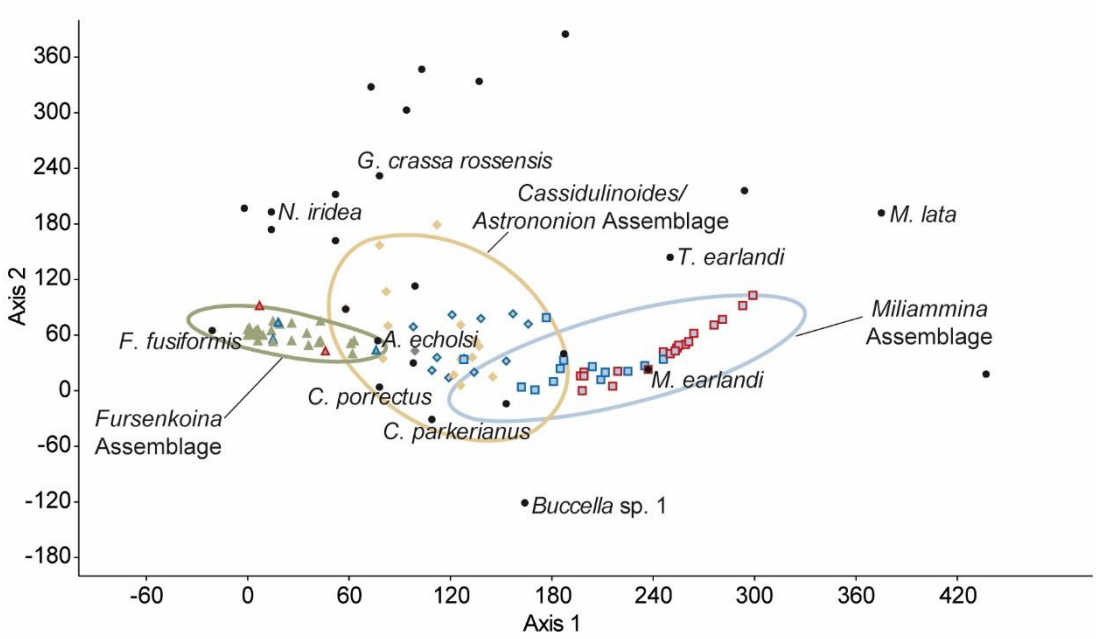


Figure 5.6 GC666 DCA
GC666 DCA Axes 1 & 2. Blue square symbols/ellipse - *Miliammina* Assemblage; green triangle symbols/ellipse - *Fursenkoina* assemblage; yellow diamond symbols/ellipse – *Cassidulinoides/Astrononion* Assemblage. Red borders - <100 specimens, Blue border - <300 specimens. 95% confidence ellipses. Black circles - taxa (ten most abundant named in the plot: *Astrononion echolsi, Buccella* sp. 1, *Cassidulinoides parkerianus, Cassidulinoides porrectus, Fursenkoina fusiformis, Globocassidulina crassa rossensis, Miliammina earlandi, Miliammina lata, Nonionella iridea, Trifarina earlandi*).

In the following three sections (5.2.3.3, 5.2.3.4, and 5.2.3.5) the composition of each of the three assemblages identified is described; in addition there is a discussion of the documented ecological preferences of the dominant species, with published ecological interpretations summarised in Table 5.3.

5.2.4.3 Fursenkoina *Assemblage*

Fursenkoina Assemblage is dominant through the deglacial and into the early Holocene, between 15.1 cal. kyr BP and 10.8 cal. kyr BP, interrupted by the *Miliammina* Assemblage between 14.7 and 14.6 cal. kyr BP and at 13.8 cal. kyr BP (Fig. 5.7). The *Fursenkoina* Assemblage also occurs between 10.3 and 10.1 cal. kyr BP and between 9.6 and 9.4 cal. kyr BP. The *Fursenkoina* Assemblage is diverse (mean Fisher-alpha = 2.2±0.8) but dominated by *F. fusiformis*, which comprises an average of 68.1±13.3% of the assemblage (mean dominance = 0.5±0.2). Other species in the assemblage include

Miliammina earlandi (8.2±8.5%), *C. parkerianus* (4.9±3.6%), *A. echolsi* (4.8±4.2%), and *C. porrectus* (4.7±4.2%), in addition to smaller abundances of *G. crassa rossensis* (2.6±2.2%), and *Nonionella iridea* (2.4±2.3%). Mean BFAR is high in the *Fursenkoina* Assemblage but with a large variation about the mean (14800±13400 cm^{-2} kyr^{-1}).

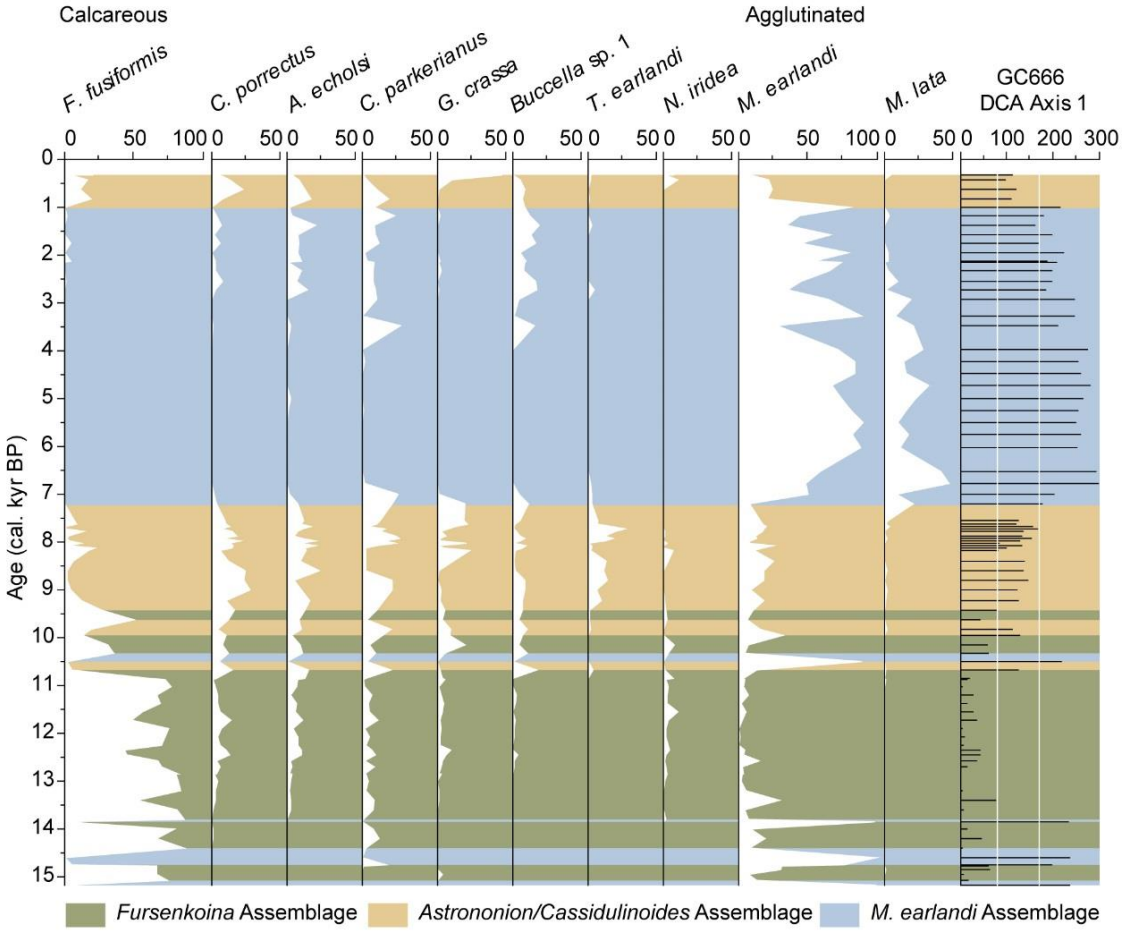


Figure 5.7 GC666 downcore BFA relative abundances
Downcore relative abundances of the 10 most abundant taxa in core GC666, in order of abundance (left to right), separated into calcareous and agglutinated taxa. DCA Axis 1 values plotted in the right-hand column. Coloured bands indicate the different assemblages.

F. fusiformis, and *Nonionella* spp. (the latter of which only peak in samples with high *F. fusiformis* abundance) are typical of sediments rich in organic material and are therefore common throughout the Antarctic Peninsula (AP) and Weddell Sea shelf, where sediments have comparatively high organic carbon concentrations (>0.3 weight %) relative to deeper water Antarctic sediments (Ishman and Domack, 1994). Species in the *Fursenkoina* genus have also been found to be tolerant of the reduced oxygen conditions that often accompany organic enrichment of the substrate (Sen Gupta and Machain-Castillo, 1993). *F. fusiformis* is recorded in a number studies of foraminiferal taxonomy from

Antarctic shelf sediments (e.g. Milam and Anderson, 1981; Violanti, 1996; Majewski, 2005).

The *Fursenkoina* Assemblage identified here comprises similar species to those that constitute the *Fursenkoina* Assemblage identified by Ishman and Domack (1994), from the Bransfield Strait and Marguerite Bay area of the AP, in depths of 50 to 2200 m. Additionally, high *F. fusiformis* abundance during the deglacial and early Holocene have been recorded at several Antarctic Peninsula (AP) locations including Marguerite Bay (Kilfeather et al., 2011; Peck et al., 2015), Palmer Deep (Ishman and Sperling, 2002), the Firth of Tay (Majewski and Anderson, 2009), and Vega Drift, where it was classified as *Stainforthia fusiformis* (Szymcek et al., 2007). Ishman and Domack (1994) proposed that the *Fursenkoina* assemblage they identified tracked the extent of Weddell Sea Transitional Water. Domack et al. (1995) suggest that *Fursenkoina* abundance in the Lallemand Fjord on the AP may be indicative of CDW occupying the fjord, stimulating high productivity. More recent interpretations have indicated the importance of increased productivity and organic carbon flux in generating *F. fusiformis*-dominated assemblages during the deglacial and early Holocene (Ishman and Sperling, 2002; Szymcek et al., 2007; Kilfeather et al., 2011; Peck et al., 2015). This high productivity has been variously linked to proximity of ice-edge conditions (Ishman and Sperling, 2002), ice shelf break-up (Kilfeather et al., 2011), or the influence of nutrient-rich modified Upper Circumpolar Deep Water (m-UCDW) (Domack et al., 1995; Peck et al., 2015). Szymcek et al. (2007) also suggested that *F. fusiformis* abundance at Vega Drift was indicative of non-corrosive bottom water and Majewski and Anderson (2009) proposed that elevated sedimentation rates favoured the preservation of thin-walled calcareous foraminifera, with both characteristics linked to glacier proximal conditions. Where *F. fusiformis*-dominated assemblages are found in surface sediments from coastal West Antarctica they are associated with intense diatom blooms and periods of high terrigenous sedimentation in glacier-proximal settings (Majewski et al., 2016).

F. fusiformis is also reported from locations outside the Southern Ocean, however in all such studies the *F. fusiformis* reported appears to be a junior synonym for *Stainforthia fusiformis* (Mojtahid et al., 2009; Leiter and Altenbach, 2010). *S. fusiformis* is, in some ways, morphologically similar to *F. fusiformis* but there are important differences: *S. fusiformis* is triserial, at least in the early stages, while *F. fusiformis* is biserial throughout, and the apertural shape differs. It is therefore not possible to make inferences about the ecology of *F. fusiformis*

based on the wide literature and experimental data concerning *S. fusiformis* (e.g. Alve, 1995; Gooday and Alve, 2001; Duffield et al., 2015).

In summary the *Fursenkoina* Assemblage is dominant through much of the deglacial, between 15.0 cal. kyr BP and 10.8 cal. kyr BP. *F. fusiformis* is the dominant species in the assemblage, with *A. echolsi*, *C. parkerianus*, *C. porrectus* and *M. earlandi* accessory species in varying proportions. *Fursenkoina fusiformis* can be considered to be typical of conditions of reduced oxygenation and organic enrichment, possibly operating as a phytodetritivore, taking advantage of pulses of organic carbon flux to the sea floor. High *F. fusiformis* abundance has been recorded from a number of other locations in the Southern Ocean, where it is generally thought to be indicative of high productivity, linked to changes in ice conditions, water mass changes, or increased preservation potential.

5.2.4.4 Miliammina *Assemblage*

The *Miliammina* Assemblage occurs at 15.2 cal. kyr BP, between 14.7 and 14.6 cal. kyr BP, at 13.8 cal. kyr BP, at 10.5 cal. kyr BP, and between 7.2 and 1.0 cal. kyr BP (Fig. 5.7). The diversity of *Miliammina* Assemblage is low (mean Fisher-alpha = 1.47±1.15), becoming mono-specific at times, combined with high dominance (mean dominance = 0.55±0.24). The dominant species in the *Miliammina* Assemblage are *M. earlandi* (66.6±22.8%) and *M. lata* (10.9±12.4%). Mean BFAR is two orders of magnitude lower in the *Miliammina* Assemblage, relative to the *Fursenkoina* Assemblage (300±500 cm^{-2} kyr^{-1} (sample GC666_768 is considered to be an outlier and excluded from this calculation)).

Species from the genus *Miliammina* are commonly found in shelf sediments throughout the Southern Ocean and are often considered, with other agglutinated taxa that are less commonly preserved, indicative of the cold, saline waters typical of these shelf environments (e.g. Anderson, 1975; Milam and Anderson, 1981). In particular, *M. arenacea*, a species that is morphologically very similar and may be considered as analogous to *M. earlandi*, has been recorded from numerous locations on the Antarctic shelf. *Miliammina earlandi* is generally considered to be more restricted in distribution, originally being described as endemic to the South Georgia region where it is the commonest and most characteristic foraminifera (Earland, 1933). *Miliammina earlandi* has also been recorded from East Antarctica (Milam and Anderson, 1981), the Ross Sea (Violanti, 1996) and the Weddell Sea (Murray and Pudsey, 2004).

Assemblages in which *Miliammina* spp. are the dominant component have been recorded at a number of locations around the AP during the early to mid-

Holocene (Ishman and Sperling, 2002; Szymcek et al., 2007; Majewski and Anderson, 2009; Kilfeather et al., 2011; Peck et al., 2015). The agglutinated nature of *Miliammina* spp. mean they are unaffected by carbonate dissolution and the siliceous cement that binds their tests (Earland, 1933) is more robust than the organic cements commonly employed by other agglutinated taxa. A number of authors consider that this unique preservation potential, plus their tolerance of salinity fluctuations, mean that *Miliammina* spp.-dominated assemblages are indicative of bottom water regimes where saline shelf water is a major component (Ishman and Sperling, 2002; Szymcek et al., 2007; Peck et al., 2015). However, Kilfeather et al. (2011) interpret the dominance of *M. arenacea*, in combination with *Bulimina aculeata*, as indicative of oceanographic warming and warm Circumpolar Deep Water. Alternatively, *Miliammina* spp.-dominated assemblages may be caused by increases in the corrosivity of bottom water and/or pore water due to increased decomposition of organic matter (linked to enhanced carbon flux to the substrate) (Majewski and Anderson, 2009). In a study of surface sediments from coastal West Antarctica, Majewski et al. (2016) reported a *Miliammina*-dominated assemblage associated with organic-rich, diatomaceous sediments (as do Melis and Salvi (2009) in Holocene sediments from the Ross Sea), which they interpret as being due to local conditions (although these conditions are not specified), as sites with similar oceanographic conditions have abundant calcareous foraminifera. Melis and Salvi (2009) attribute the dominance of agglutinated taxa in late Pleistocene sediments from the Ross Sea to corrosive waters, linked to either water mass change or an increase in productivity causing the Carbonate Compensation Depth (CCD) to shallow, or to fluctuating ice conditions leading to ecological changes that favour the most opportunistic agglutinated taxa. High *M. arenacea* abundance is considered to be indicative of strong carbonate dissolution by Li et al. (2000) and, where this abundance occurs in shallow waters, of a shallow lysocline and CCD. Li et al. (2000) propose that carbonate dissolution is enhanced by high organic flux to the sea floor, leading to increased CO_2 accumulation in the pore-waters due to bacterial degradation of organic matter.

M. earlandi is considered to be endemic to the Southern Ocean (Pudsey et al., 2006), however the species is also reported from estuaries and coastal lakes from a number of lower latitude locations (e.g. Asseez et al., 1974; Debenay et al., 1998; Usera et al., 2002). Based on differences in surface texture and apertural characteristics this is likely to be a misclassification, possibly of a morphotype of *M. fusca*.

In summary the *Miliammina* Assemblage is dominant through the mid-Holocene, between 7.2 and 1.0 cal. kyr BP. *Miliammina earlandi* is the dominant species in the assemblage, accompanied by *M. lata* in the *M. lata* Sub-assemblage and by *A. echolsi*, *C. parkerianus*, and *Buccella* sp. 1 in the *M. earlandi* Sub-assemblage. *Miliammina* spp. are considered to be indicative of the cold saline waters found on the Antarctic shelf. *Miliammina earlandi* (and *M. lata*) are resistant to corrosion and where dominant may be indicative of complete or partial dissolution of calcareous taxa (see Section 7.2.1).

5.2.4.5 Cassidulinoides/Astrononion *Assemblage*

The *Cassidulinoides/Astrononion* Assemblage occurs at 10.7 cal. kyr BP, between 10.0 and 9.8 cal. kyr BP, and between 9.4 and 7.6 cal. kyr BP (Fig. 5.7). The *Cassidulinoides/Astrononion* Assemblage is also the dominant assemblage in the latest Holocene (<1.0 cal. kyr BP). The average diversity of the *Cassidulinoides/Astrononion* Assemblage is high (3.9±1.1), and the average dominance is correspondingly low (0.15±0.02). The major components of the *Cassidulinoides/Astrononion* Assemblage are *M. earlandi* (15.7±5.6%), *C. porrectus* (13.6±6.3%), *C. parkerianus* (12.7±8.1%), *A. echolsi* (12.5±4.9%), and *G crassa rossensis* (10.6±11.2%). Subsidiary species include *F. fusiformis* (10.9±8.5%), *Buccella* sp. 1 (5.6±4.1%), and *Tr. earlandi* (7.8±7.2%). Mean BFAR is an order of magnitude lower than in the *Fursenkoina* Assemblage, with large variation about the mean (2000±2900 cm^{-2} kyr^{-1}).

The species that comprise the major components of the *Cassidulinoides/Astrononion* Assemblage have been recorded in shelf sediments from a wide range of Antarctic locations (e.g. Milam and Anderson, 1981; Ishman and Domack, 1994; Violanti, 1996; Igarashi et al., 2001; Majewski, 2005; Majewski and Anderson, 2009; Majewski, 2013; Rodrigues et al., 2013). High diversity calcareous assemblages featuring some of the same dominant species (*A. echolsi*, *C. porrectus*, and *G. crassa*) have previously been linked to the occurrence of warm fresh shelf water in the Weddell Sea (Anderson, 1975) and East Antarctica (Milam and Anderson, 1981), the formation of which is linked to mixing with summer surface waters. However, *G. crassa, C. parkerianus,* and *C. porrectus* have also been associated with colder waters in the Weddell Sea (Mackensen et al., 1990; Ishman and Domack, 1994; Rodrigues et al., 2010).

Both *C. parkerianus* and *C. porrectus* may be endemic to the Antarctic/sub-Antarctic (Mikhalevich, 2004), although *C. parkerianus* is considered by Holbourn et al. (2013) to have a worldwide distribution (but all studies that discuss ecology are from the Southern Ocean). *C. parkerianus* has been suggested to be

indicative of near shore/glacier conditions on the AP (Majewski et al., 2012) and the South Shetland Islands, in association with *C. porrectus* (Rodrigues et al., 2010). Rodrigues et al. (2013) found a correlation between *C. porrectus* abundance and coarse sediment deposition. In both experimental and field studies *C. porrectus* was found to be tolerant of anoxia and hydrogen sulphide (Bernhard, 1989, 1993), although there is no suggestion that this species is indicative of such conditions.

While *A. echolsi* is a common feature of Southern Ocean shelf assemblages, it is also a cosmopolitan species that has been reported from a range of locations, including the North Atlantic (Belanger et al., 2016), north-west Africa (Jorissen et al., 1998), and the Mediterranean (Murray, 2013). In the Gulf of Aden, where it is also associated with the lowest primary productivity in the area (Almogi-Labin et al., 2000) and in the Arabian Sea (Schmiedl and Leuschner, 2005) *A. echolsi* is interpreted as being indicative of well oxygenated water. This interpretation is linked to the association of *A. echolsi* with the oxygen-rich, saline core of North Atlantic Deep Water (NADW) in the south-west Indian Ocean (Corliss, 1983) and the south Atlantic Ocean (Schmiedl et al., 1997). On the AP *A. echolsi* has been found to be indicative of a distal glacimarine environment (Kilfeather et al., 2011; Majewski et al., 2016) or near open sea conditions (in association with *C. porrectus*) (Majewski, 2005). Elsewhere on the AP, Majewski and Anderson (2009) have suggested that a diverse calcareous assemblage that includes *A. echolsi, Globocassidulina* spp., and *C. parkerianus* is representative of the most glacier-proximal conditions at this site, although this interpretation is strongly dependent on the high abundance of *F. fusiformis* in the assemblage. Majewski et al. (2016) have proposed that *A. echolsi* may be indicative of conditions where food supply is stable, phytodetritus events are uncommon, and sediments are less organic rich. Similarly, *G. rossensis* may be indicative of low productivity, based on its distribution on the Iberian continental margin (Alves Martins et al., 2006).

Trifarina angulosa, a morphologically similar species to *Tr. earlandi*, has been associated with high energy/strong currents (e.g. Mackensen et al., 1990; Hayward et al., 2007; Melis and Salvi, 2009; Hayward et al., 2013), generally in association with sandy/coarse substrates. Although the morphology of *Tr. earlandi* is very similar to that of *Tr. angulosa* it is not associated with sandy sediments in core GC666 suggesting any analogy between the ecology of the two species is not supported. *Globocassidulina* spp. have also been linked to increased bottom current velocities in Southern Ocean shelf environments, although only in association with sandy sediments and generally where they

dominate the assemblage (e.g. Violanti, 1996; Li et al., 2000; Hromic et al., 2006).

In summary the *Cassidulinoides/Astrononion* Assemblage is dominant through early to mid-Holocene, between 9.4 and 7.6 cal. kyr BP, and during the last ~1.0 kyrs. This is a diverse, calcareous assemblage; *A. echolsi*, *C. parkerianus*, *C. porrectus*, *G crassa rossensis,* and *M. earlandi* comprise the dominant taxa, with *F. fusiformis*, *Buccella* sp. 1, and *Tr. earlandi* as subsidiary species. *Astrononion echolsi* may be indicative of well oxygenated conditions, stable, but low, productivity, and a glacier-distal environment. Conflicting interpretation of many of the other key species may indicate that they are cosmopolitan in their environmental preferences, and not representative of any particular conditions. The ecological preferences of *F. fusiformis* and *Miliammina* spp. are discussed in the two preceding sections.

Table 5.3 Ecological interpretation of key species of foraminifera
Summary of the key species and potential ecological interpretation of each assemblage, with associated references and locations of the referenced studies.

Key Species	**Previous ecological interpretation**	**Reference**	**Location**
F. fusiformis	Typical of sediments rich in organic matter (>0.3 weight %) Track Weddell Sea Deep Water	Ishman and Domack (1994)	Antarctic Peninsula
	Tolerant of reduced oxygen (*Fursenkoina* spp.)	Sen Gupta and Machain-Castillo (1993)	California continental margin
	Reflect high productivity and organic carbon flux (linked to ice-edge conditions, ice-shelf break up, influx of nutrient rich waters)	Domack et al. (1995); Ishman and Sperling (2002); Kilfeather et al. (2011); Peck et al. (2015); Majewski et al. (2016)	Antarctic Peninsula; West Antarctica
	Indicative of non-corrosive bottom waters/elevated sedimentation rates	Szymcek et al. (2007); Majewski and Anderson (2009)	Antarctic Peninsula
Miliammina spp.	Typical of the cold, saline waters that characterise the Antarctic shelf – indicative of saline shelf water	Anderson (1975); Milam and Anderson (1981); Ishman and	Weddell Sea; East Antarctica; Antarctic Peninsula

		Sperling (2002); Szymcek et al. (2007); Peck et al. (2015)	
	Indicative of warming and warm CDW	Kilfeather et al. (2011)	Antarctic Peninsula
	Increased corrosivity of bottom water (linked to increased productivity, water mass change)	Li et al. (2000); Majewski and Anderson (2009); Melis and Salvi (2009)	Antarctic Peninsula; Ross Sea
	Association with organic-rich, diatomaceous Holocene sediments	Melis and Salvi (2009); Majewski et al. (2016)	Ross Sea; West Antarctica
A. echolsi	Link to warm Fresh Shelf Water	Anderson (1975); Milam and Anderson (1981)	Weddell Sea; East Antarctica
	Well oxygenated	Corliss (1983); Schmiedl et al. (1997); Almogi-Labin et al. (2000); Schmiedl and Leuschner (2005)	Indian Ocean; South Atlantic Ocean; Gulf of Aden; Arabian Sea
	Indicative of distal glacimarine environment	Kilfeather et al. (2011); Majewski et al. (2016)	Antarctic Peninsula; West Antarctica
	Near open sea conditions	Majewski (2005)	Antarctic Peninsula
	Stable food supply, limited phytodetritus events	Majewski et al. (2016)	West Antarctica
C. parkerianus	Near shore/glacier conditions	Rodrigues et al. (2010); Majewski et al. (2012)	Antarctic Peninsula
C. porrectus	Link to warm Fresh Shelf Water	Anderson (1975); Milam and Anderson (1981)	Weddell Sea; East Antarctica
	Near shore/glacier conditions	Rodrigues et al. (2010)	Antarctic Peninsula
	Correlation with coarse sediment	Rodrigues et al. (2013)	Antarctic Peninsula

	Tolerant of anoxia and hydrogen sulphide	Bernhard (1989, 1993)	Ross Sea
	Near open sea conditions	Majewski (2005)	Antarctic Peninsula

5.2.5 Geochemistry of organic matter

Bulk sediment organic carbon and nitrogen concentration and carbon isotope data are shown in Figure 5.8 and Appendix A12. Organic carbon accumulation rates (C_{org} AR – calculated from % C, reported to 2SF) range from 0.025 to 6.0 g cm^{-2} kyr^{-1} with the highest value recorded at 15.2 cal. kyr BP. C_{org} AR remains high (>4.3 g cm^{-2} kyr^{-1}) until 14.7 cal. kyr BP then decreases to 0.40 g cm^{-2} kyr^{-1} by 14.5 cal. kyr BP, staying below 0.5 g cm^{-2} kyr^{-1} until 12.9 cal. kyr BP. C_{org} AR then increases to 1.1 g cm^{-2} kyr^{-1} by 12.5 cal. kyr BP until 12.3 cal. kyr BP, before decreasing to 0.33 g cm^{-2} kyr^{-1} and remaining below 0.5 g cm^{-2} kyr^{-1} until 10.6 cal. kyr BP. C_{org} AR then increases to 0.77 g cm^{-2} kyr^{-1} before gradually decreasing to 0.026 g cm^{-2} kyr^{-1} by 7.2 cal. kyr BP, after which C_{org} AR remains below 0.05 cm^{-2} kyr^{-1} until 2.9 cal. kyr BP. C_{org} AR then increases to 0.45 g cm^{-2} kyr^{-1} before gradually decreasing to 0.15 g cm^{-2} kyr^{-1} by 0.8 cal. kyr

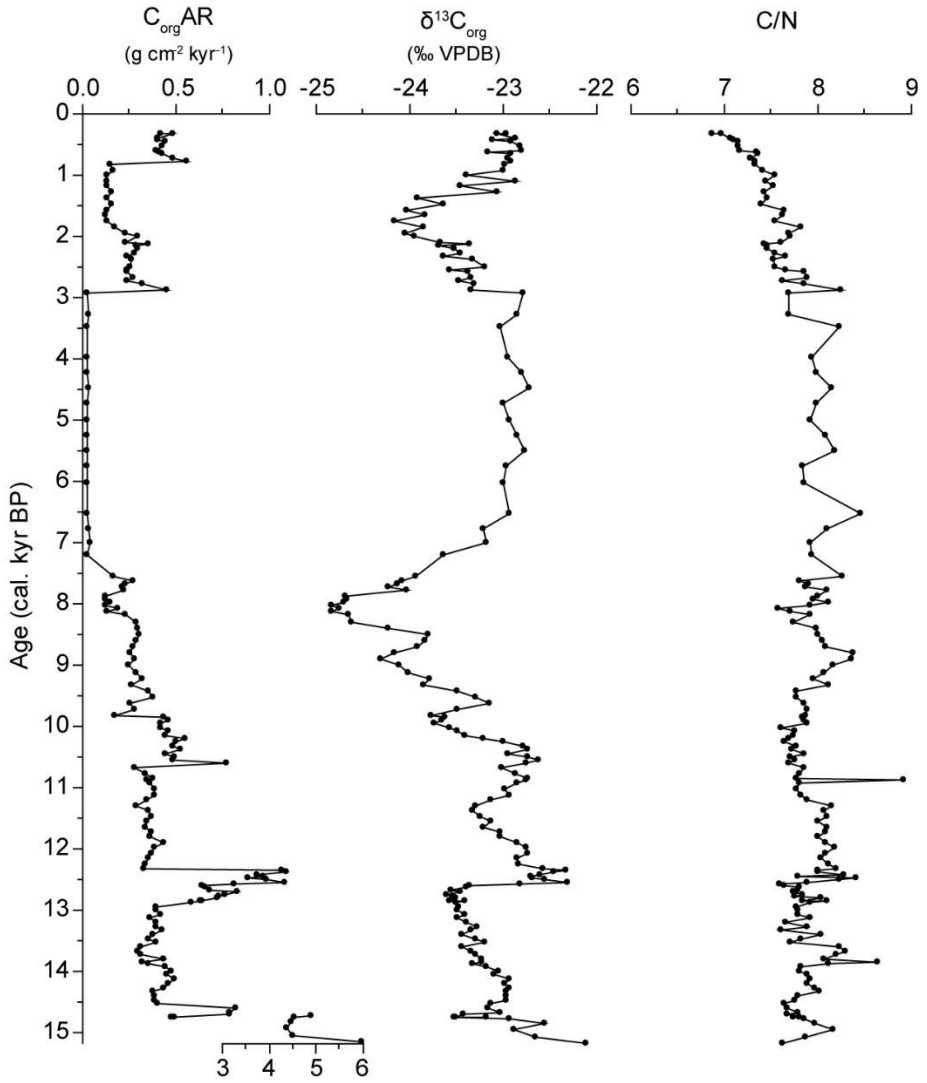


Figure 5.8 GC666 organic geochemistry data
Organic geochemistry data from GC666: organic carbon accumulation rate, $\delta^{13}C_{org}$, the ratio of carbon to nitrogen.

BP, before increasing to 0.56 cm^{-2} kyr^{-1} and remaining above 0.4 g cm^{-2} kyr^{-1} for the youngest part of the record.

The carbon stable isotopic composition of organic carbon ($\delta^{13}C_{org}$) ranges between −24.8 and −22.1 ‰ (mean = −23.3±0.53 ‰). Between 15.2 and 12.7 cal. kyr $\delta^{13}C_{org}$ decreases from −22.1 ‰ to −23.6 ‰, with a brief negative excursion of ~0.5 ‰ at 14.6 cal. kyr BP. By 12.5 cal. kyr BP $\delta^{13}C_{org}$ has increased to −22.3 ‰ before decreasing to −24.8 ‰ by 8.0 cal. kyr BP. Subsequently $\delta^{13}C_{org}$ increases to −22.9 ‰ by 6.5 cal. kyr BP and remains between −22.7 ‰ and −23.0 ‰ until 2.9 cal. kyr BP. Then $\delta^{13}C_{org}$ decreases to −24.1 ‰ by 1.7 cal. kyr BP before increasing to −23.0 ‰ by 0.9 cal. kyr and remaining at the level through the rest of the core.

The weight ratio of carbon to nitrogen (C:N) does not exceed 9 at any point in the core, ranging from 6.87 to 8.93, with a mean value of 7.84±0.30. Between 15.2 and 2.9 cal. kyr BP C:N fluctuates about a mean of 7.94, with a standard deviation of 0.22 and no clear trends in the data. Subsequent to 2.9 cal. kyr BP C:N decreases to 6.87 by 0.3 cal. kyr BP.

5.2.6 Biogenic opal analysis

The biogenic opal accumulation rate (BSi AR, reported to 2SF) was calculated from the biogenic opal weight % and is shown in Figure 5.9 and Appendix A13. The BSi AR follows similar patterns and trends to those recorded in C_{org} AR; BSi AR ranges across several orders of magnitude, from 0.16 to 93 g cm^{-2} kyr^{-1} with the highest value recorded at 15.2 cal. kyr BP. BSi AR remains high (>60 g cm^{-2} kyr^{-1}) until 14.7 cal. kyr BP then decreases to 4.1 g cm^{-2} kyr^{-1} by 13.6 cal. kyr BP, before increasing to 12 g cm^{-2} kyr^{-1} by 12.7 cal. kyr BP. BSi AR then decreases and remains below 4.5 g cm^{-2} kyr^{-1} until 10.7 cal. kyr BP. BSi AR then increases to 9.7 g cm^{-2} kyr^{-1} at 10.0 cal. kyr BP before gradually decreasing to 0.24 g cm^{-2} kyr^{-1} by 7.2 cal. kyr BP, after which BSi AR remains below 0.5 cm^{-2} kyr^{-1} until 2.9 cal. kyr BP. BSi AR then increases to 6.8 g cm^{-2} kyr^{-1} at 2.1 cal. kyr BP before decreasing and remaining below 4.0 g cm^{-2} kyr^{-1} until 0.6 cal. kyr BP, when it increases to 13 cm^{-2} kyr^{-1} and remains above 9.5 g cm^{-2} kyr^{-1} for the rest of the record.

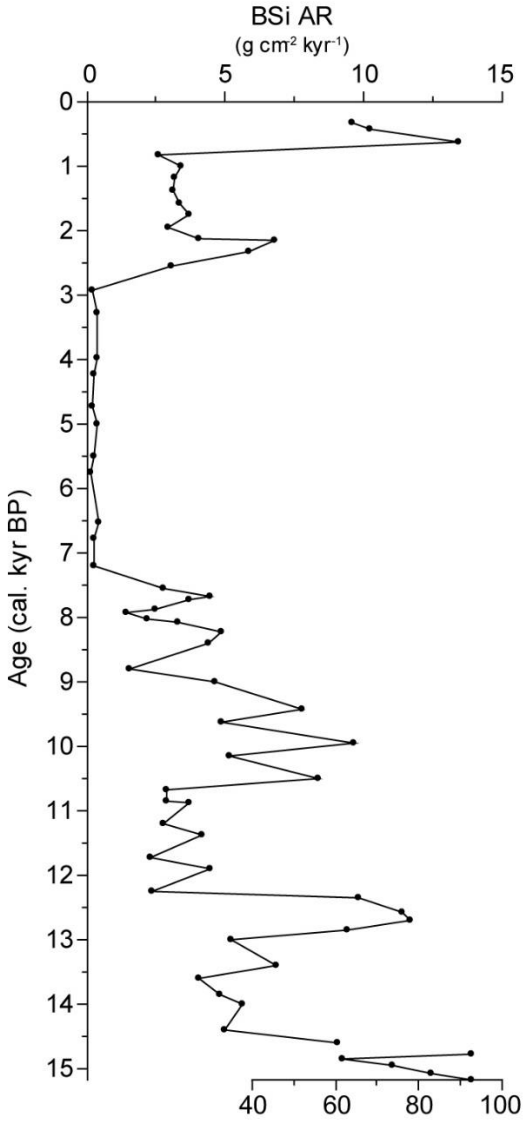


Figure 5.9 GC666 biogenic silica accumulation rate

5.2.7 Foraminiferal stable isotope analysis

The carbon and oxygen isotope data ($\delta^{13}C$ and $\delta^{18}O$) from both benthic and planktonic foraminifera are given in Figure 5.10 and Appendix A14, and described below.

5.2.7.1 Benthic foraminiferal isotopes

Benthic foraminiferal $\delta^{13}C$ ranges from −7.90 ‰ to +1.07 ‰. Values below −1 ‰ only occur between 14.8 and 10.3 cal. yr BP, with the exception of the sample at 4.2 cal. kyr BP. The $\delta^{13}C$ values between 14.8 and 10.3 cal. yr BP fluctuate widely; the foraminifera analysed from this period appear to have been diagenetically altered. They are yellow/brown in colour compared to pristine white or glassy specimens and are covered with varying degrees of sugary crystal overgrowths (see Section 5.2.7.3). After 10.3 cal. kyr BP $\delta^{13}C$ increases from −2.10 to +0.81 ‰ by 8.8 cal. kyr BP before decreasing to −0.23 ‰ by

8.1 cal. kyr BP, then increasing to +0.70 ‰ by 7.0 cal. kyr BP. There are no benthic isotope data between 6.8 and 3.5 cal. kyr BP, with the exception of the sample at 4.2 cal. kyr BP, due to the absence of calcareous foraminifera in this part of the core. The absence of calcareous foraminifera through this period may be due to dissolution of these taxa, linked to the low sedimentation rate, with the implication that the remaining benthic foraminiferal assemblage is a dissolution assemblage, discussed in more detail in Section 7.2.1. Subsequently, $\delta^{13}C$ decreases from +0.82 ‰ to −0.22 ‰ by 0.3 cal. kyr BP, although the values fluctuate between +1.01 ‰ and −0.39 ‰ around this trend.

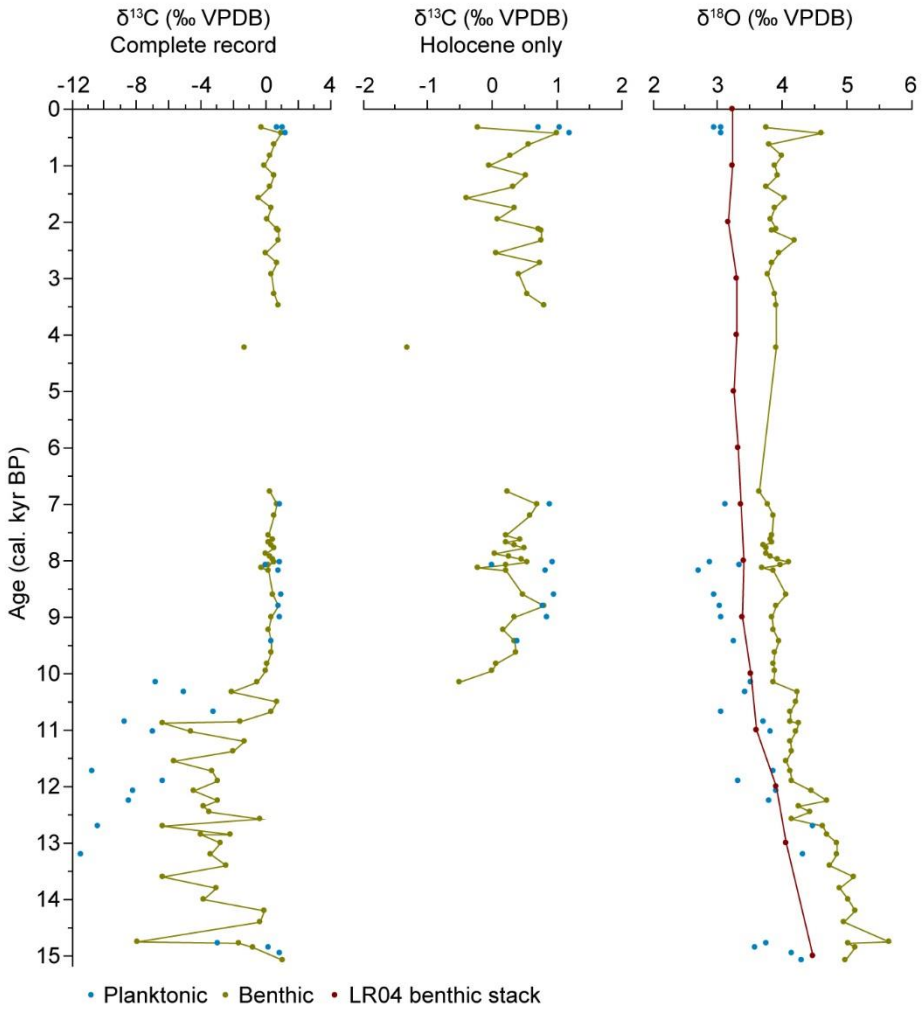


Figure 5.10 GC666 foraminiferal isotopes
Foraminiferal stable isotope data from GC666: green - benthic data, blue - planktonic data, red - LR04 global benthic isotope stack (Lisiecki and Raymo, 2005).

Benthic $\delta^{18}O$ values range from +3.64 ‰ to +5.66 ‰, although the peak value, at 14.7 cal. kyr BP, may be an outlier as it is >0.5 ‰ higher than the surrounding values. Benthic $\delta^{18}O$ values follow the trend seen in the LR04 benthic stack (Lisiecki and Raymo, 2005), although offset by approximately +0.5

‰. Benthic $\delta^{18}O$ decreases from +4.98 ‰ at 15.1 cal. kyr BP to +3.87 ‰ by 10.1 cal. kyr BP. Subsequent to 10.1 cal. kyr BP benthic $\delta^{18}O$ remains between +3.64 ‰ and +4.20 ‰ throughout the rest of the core, with the exception of the sample at 0.4 cal. kyr BP (+4.62 ‰). As with benthic $\delta^{13}C$, there are no benthic $\delta^{18}O$ data between 6.8 and 3.5 cal. kyr BP, with the exception of the sample at 4.2 cal. kyr BP.

5.2.7.2 Planktonic foraminiferal isotopes

The planktonic foraminiferal stable isotope data are at a lower resolution than the benthic record and completely absent between 8.0 and 0.4 cal. kyr BP, with the exception of a sample at 7.0 cal. kyr BP. In planktonic foraminifera, $\delta^{13}C$ ranges from −11.43 ‰ to +1.07 ‰. As with the benthic data, values below −1 ‰ only occur in the early part of the record, between 14.8 and 10.1 cal. kyr BP. Again these negative values appear in the diagenetically altered samples, with the even lower values yielded from the planktonic foraminifera, potentially due to their smaller size and greater surface area, resulting in proportionally larger amount of authigenic carbonate coating. Where planktonic data is present after 10.1 cal. kyr BP it is similar to the benthic data, with an average offset of +0.29 ‰ (from nine samples which have both planktonic and benthic data after 10.1 cal. kyr BP).

Planktonic $\delta^{18}O$ values range from +2.71 ‰ to +4.47 ‰. Planktonic $\delta^{18}O$ values also follow the trend seen in the LR04 benthic stack (Lisiecki and Raymo, 2005), although offset by approximately −0.2 ‰ (based on the comparison of 2nd order polynomial best fit lines for both data sets). There does not appear to have been any diagenetic alteration of the $\delta^{18}O$ signal from either benthic or planktonic foraminifera.

5.2.8 Alkenone analysis

Analysis of alkenones in sediment samples from GC666 intended to generate a SST record for the whole of the core. However, very low alkenone concentration in some of the samples meant that the SST record extends from 0.3 to 11.2 cal. kyr BP, with the data older than 9.0 cal. kyr BP being potentially unreliable, due to low alkenone concentration (Fig. 5.11 & Appendix A15). In addition there are three SST values between 13.2 and 12.8 cal. kyr BP, all of which are also potentially unreliable, due to low alkenone concentration. SSTs using two calibrations are presented in Figure 5.11: the global calibration of Muller et al. (1998), and the Southern Ocean calibration of Sikes et al. (1997). The temperature trends are comparable between the two calibrations, with an average offset of 3.0±0.1ºC; the range between minimum and maximum values

is greater using the Muller et al. (1998) calibration (Fig. 5.11b). The Muller et al. (1998) calibration has a standard error of ±0.032 $U^{k'}_{37}$ units, or ±1.0ºC; comparison of duplicates reveal an analytical error of ±0.003 $U^{k'}_{37}$ units, or ±0.08ºC. The SST data generated using the Muller et al. (1998) calibration is described below and applied to the discussion in Chapter 7. This data was chosen in preference to the SSTs generated using the Sikes et al. (1997) calibration because the range of SSTs are in closer agreement with modern SSTs, with shelf SST typically ranging from ~0ºC in winter to ~4ºC in summer (e.g. Brandon et al., 1999).

The reconstructed SSTs range from 1.1 ºC (at 9.4 and 1.6 cal. kyr BP) to 5.6 ºC (at 11.5 cal. kyr BP). The peak value is from a sample with low alkenone concentration and is therefore considered an outlier and excluded from subsequent discussion and calculations, as is the SST of 4.1 ºC at 11.0 cal. kyr BP. Between 13.2 and 10.8 cal. kyr BP SST averages 2.8±0.4 ºC. SST decreases 1.9 ºC by 10.5 cal. kyr BP and averages 1.8±0.3 ºC between 10.5 and 7.8 cal. kyr BP. SST then increases to 3.5 ºC at 7.2 cal. kyr BP, although this peak may be unreliable as is comes from a sample with low alkenone concentration. Between 7.6 and 4.5 cal. kyr BP SST averages 2.5±0.4 ºC, then gradually decreases to a minimum of 1.1 ºC at 1.6 cal. kyr BP. Subsequently SST increases to 1.8 ºC after 1.0 cal. kyr BP, with a cooler period between 0.6 and 0.4 cal. kyr BP (1.3 ºC). Much of the variability SST described above lies within the margin of error of the calibration and it is therefore important to take this into consideration when interpreting the SST variation.

It is also important to consider the possible impact of changes in seasonality on the alkenone-derived SST record from GC666. In the Southern Hemisphere longer summer duration, at aphelion, results in a higher average annual SST, while the shorter perihelion summers lead to higher peak temperatures during the warm season (Huybers and Denton, 2008). Huybers and Denton (2008) calculated that austral summer duration decreased through the Holocene. Therefore, if alkenone-derived temperatures are representative of spring/summer (as proposed for the Southern Ocean by Sikes et al. (1997)), the GC666 SSTs may be higher during the late Holocene, relative to the actual annual mean SST. However, this is not the case if alkenone-derived SSTs are considered to represent average annual temperatures, as proposed by Muller et al. (1998) in their global calibration of the alkenone SST proxy. Caniupan et al. (2014) concluded that coccolithophore abundance in the Southern Ocean peaks during the austral summer but more work is required to establish whether

alkenone-derived temperatures from the South Georgia region represent summer peaks or annual averages.

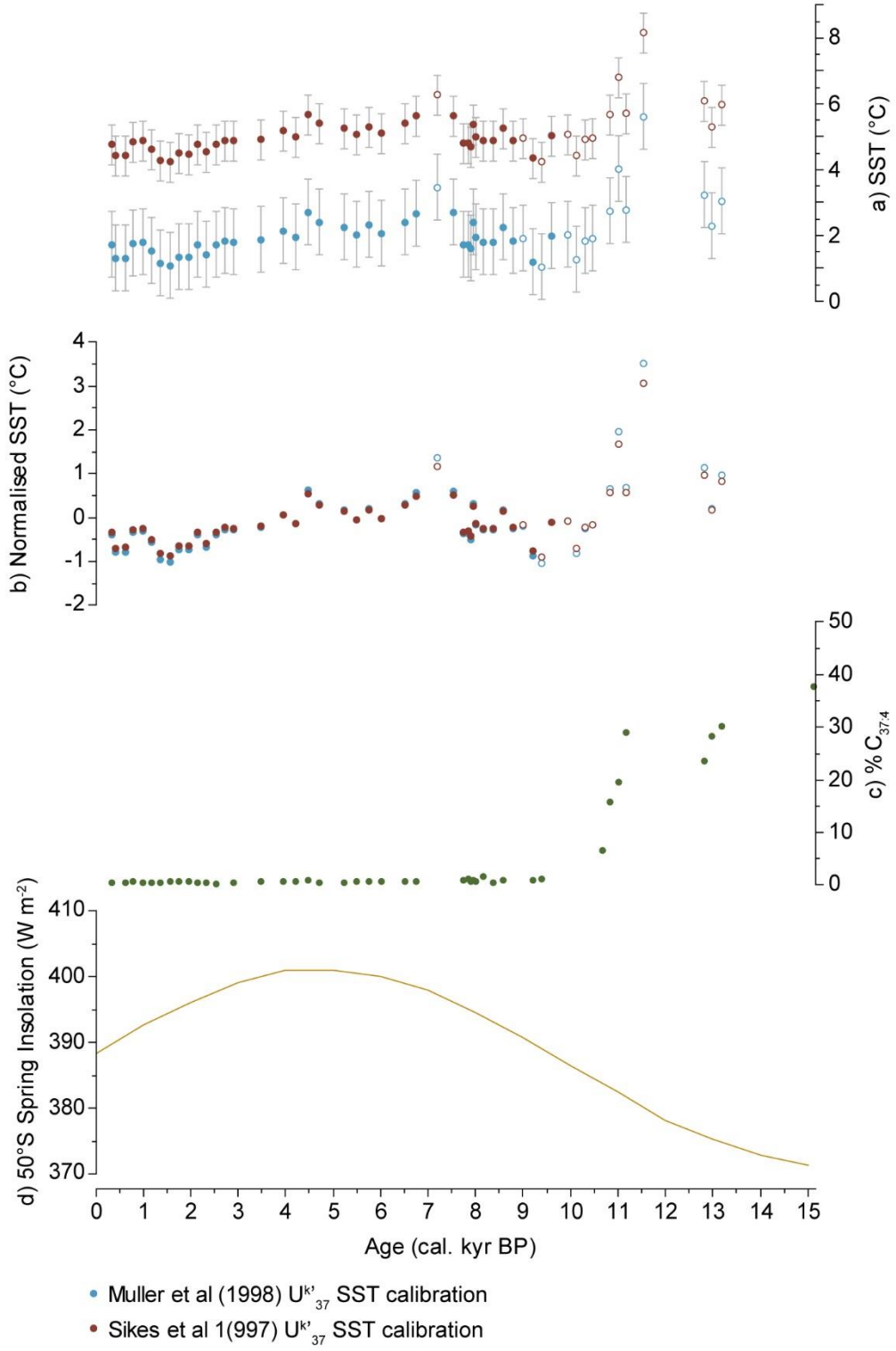


Figure 5.11 GC666 SST data
Alkenone based SST data for GC666. a) Annual mean shelf water SSTs calculated from Uk'37 using two different calibrations, the Muller et al. (1998) global calibration for annual mean temperatures and the Sikes et al. (1997) calibration from the Southern Ocean. Open circles indicates samples where low

alkenone abundance (indicated by very small peaks) has resulted in poor quality chromatograms and potentially unreliable SST estimates. Error bars = calibration standard error. b) SSTs from both calibrations normalised by subtracting their mean SST values. c) The percentage of C37 alkenones that comprises C37:4 alkenones. d) Austral spring insolation for 50°S (Berger and Loutre, 1991).

5.2.8.1 Samples with low alkenone concentration

For 24 of the samples analysed it was not possible generate a $U^{K'}_{37}$ value due to the absence of the $C_{37:2}$ peak in their chromatograms (Fig 5.12a). It was therefore not possible to generate SST data for these samples. In these samples the $C_{37:3}$ peaks, generally the largest peak in samples from GC666, was much smaller than in samples where the $C_{37:2}$ peak was present; the $C_{37:4}$ peak was also reduced or absent. In addition, there were 14 samples with weak $C_{37:2}$ peaks (Fig 5.12b); the SST data generated from these samples is potentially unreliable, as indicated in Fig. 5.11.

All the samples which have no $C_{37:2}$ peak occur below 247 cmcd, coincident with the part of the core where the benthic foraminifera show varying degrees of diagenetic alteration (potentially related to biogenic methane – Section 5.2.7.3). It is possible that, if biogenic methane was present in this part of the core, it may have resulted in the degradation of the alkenones in these samples, resulting in low alkenone abundance. While the degradation of C_{37} alkenones in the water column (e.g. Kaiser et al., 2014) and at the sediment/seawater interface (e.g. Hoefs et al., 1998) has been studied, there does not appear to be any published studies on possible post-burial degradation by biogenic methane.

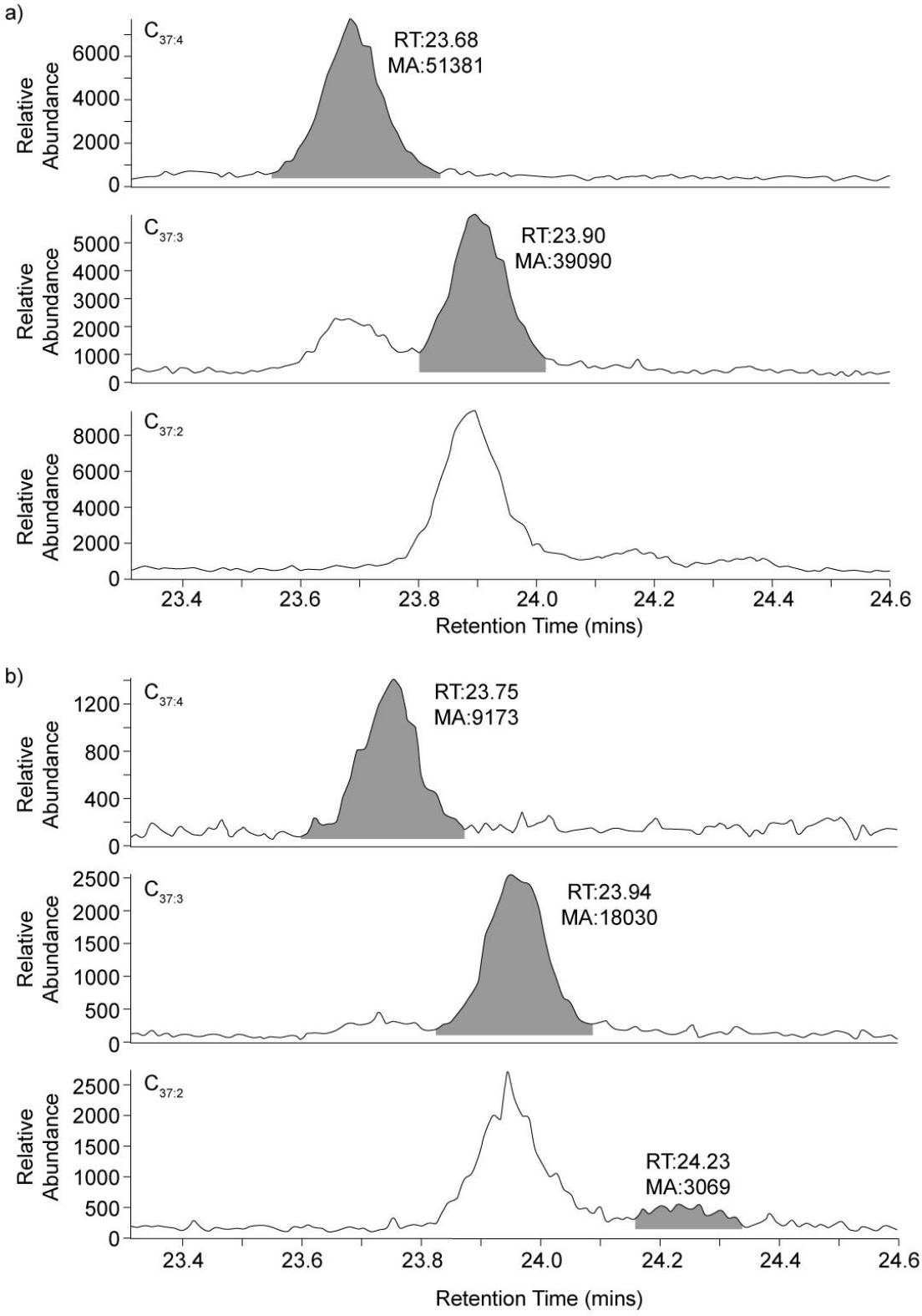


Figure 5.12 Examples of GC-CIMS chromatograms
Examples of GC-CIMS chromatograms from samples with no or weak C37:2 peaks. a) GC666-704, b) GC666-407.

5.3 Core GC673

5.3.1 Age/depth model

Four radiocarbon dated horizons were used to generate the age/depth model for GC673, three used mixed assemblage benthic foraminifera and one from an unidentified bivalve (Table 5.4 and Fig. 5.13). Due to the small number of dated horizons modelling age/depth using OxCal was not possible. Instead the CLAM calibration package in R was applied to the dates, using the weighted spline modelling technique. The Marine13 calibration curve was applied (Reimer et al., 2013). This model replicates the hypothesised changes in sedimentation rate, based on the changes in sedimentology recorded in GC673 and through comparison to the effect of similar sedimentological changes seen in GC666. The model illustrated in Figure 5.13 utilises a local reservoir correction of 433 ± 41 years. Interpolated ages at 1 cm resolution are presented in Appendix A16. For a complete discussion of the methodology used in generating the radiocarbon dates and the age/depth models see Chapter 2 - Material and Methods.

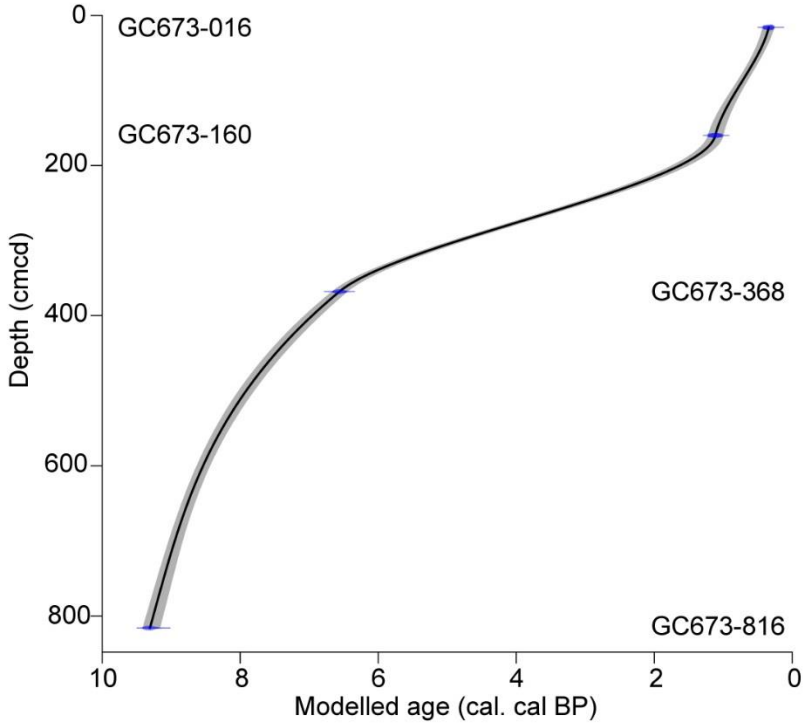


Figure 5.13 GC673 age/depth model
GC673 age/depth model, generated using the locally weighted spline model function in the CLAM age/depth modelling package in R (Blaauw, 2010).

Using the age model, sedimentation rates have been calculated for the whole core, and found to vary greatly between different sections of the core. The sedimentation rate is highest in the basal three metres of the core (815 – 490 cm), where it exceeds 570 cm kyr^{-1}. Between 490 and 115 cm the sedimentation rate is an order of magnitude slower than this ranging from 19.1 cm kyr^{-1} to 79.2 cm kyr^{-1}. This is followed by another order of magnitude decrease to 3.9 cm

kyr^{-1} between 115 and 97 cm kyr^{-1}. From 97 cm to the top of the sedimentation rate is similar to that calculated between 490 and 115 cm, ranging from 21.4 to 62.7 cm kyr^{-1}.

Table 5.4 Radiocarbon age determinations for GC673
(Samples analysed at the NERC RCF – min and max values represent 2 standard deviations)

Sample details		Conventional Ages			Calibrated Ages		
Depth (cm)	**Carbonate Source**	**^{14}C Age (yr)**	**Error (± yr)**	**Reservoir effect (yr)**	**Min (cal. yr BP)**	**Max (cal. yr BP)**	**Median (cal. yr BP)**
16	Benthic forams	1120	37	433 ± 41	240	465	341
160	Benthic forams	1990	37	433 ± 41	977	1243	1115
368	Benthic forams	6567	38	433 ± 41	6424	6704	6564
816	Bivalve (UnID)	9072	39	433 ± 41	9130	9439	9308

5.3.2 Sedimentology

5.3.2.1 Sediment description

Core GC673 comprises grey-olive green sandy bioturbated diatomaceous mud, with no notable sedimentological changes. As in GC666, darker lens-shaped patches are present throughout. Occasional thin dark green or orange laminae, interpreted as comprising diatomaceous ooze, are also recorded in the core, in particular between 0 and 210 cmcd and 620 and 883 cmcd. Dropstones are also intermittently present. Inclusions of carbonate cemented mud several cm in diameter were recorded at 672 and 760 cmcd. The % >63 μm in GC673 is relatively stable during the early and late Holocene but, as in GC666, increases in the mid-Holocene between ca. 4 and 6 cal. kyr BP. A similar pattern is seen in the abundance of clastic grains >250 μm, with an additional peak at ca. 8.25 cal. kyr BP.

5.3.2.2 Coarse fraction quantification

As for core GC666, the percentage of sediment that is >63 μm in diameter (% >63 μm) was calculated for samples analysed from GC673 (Fig. 5.14 & Appendix A17). The % >63 μm ranges from 1.8% to 45.1%.

Throughout the record the % >63 μm is below 10%, with the exception of three peaks. These peaks are at 7.6 cal. kyr BP (12.9%), between 6.6 and 5.1 cal. kyr BP (max. = 45.1%), and between 3.3 and 2.7 cal. kyr BP (max. = 16.4%).

An accumulation rate (>63 μm AR) was also calculated for the >63 μm fraction, using the sedimentation rates calculated with the age model. Two of the

peaks identified in the >63 μm % are still present the peak between 3.3 and 2.7 cal. kyr BP is not evident. In addition to the two previously identified peaks higher >63 μm ARs (>10 g cm^{-2} kyr^{-1}) also occur between 9.3 and 8.8 cal. kyr BP, and between 0.4 and 0.3 cal. kyr BP.

The number of coarse clastic grains with a diameter >250 μm were also quantified, by counting under light microscopy during foraminifera picking (Fig. 5.14). Between 9.5 and 6.7 cal. kyr BP the number of grains >250 μm is below 10 g^{-1} except for two peaks at 8.6 cal. kyr BP (36 g^{-1}) and 8.2 cal. kyr BP (50 g^{-1}).There are then two large peaks at 6.6 cal. kyr BP (134 g^{-1}) and 5.6 cal. kyr BP (186 g^{-1}) before the number of >250 μm grains decreases to 1 g^{-1} at 4.4 cal. kyr BP. Subsequently, the number of >250 μm grains remains below 50 g^{-1}. The >250 μm AR records peaks at the same times (with the AR exceeding 50 cm^{-2} kyr^{-1} for all these previously identified peaks). In addition, the >250 μm AR also exceeds 50 cm^{-2} kyr^{-1} at 1.0 cal. kyr BP (76 cm^{-2} kyr^{-1}) and at 0.4 cal. kyr BP (83 cm^{-2} kyr^{-1}).

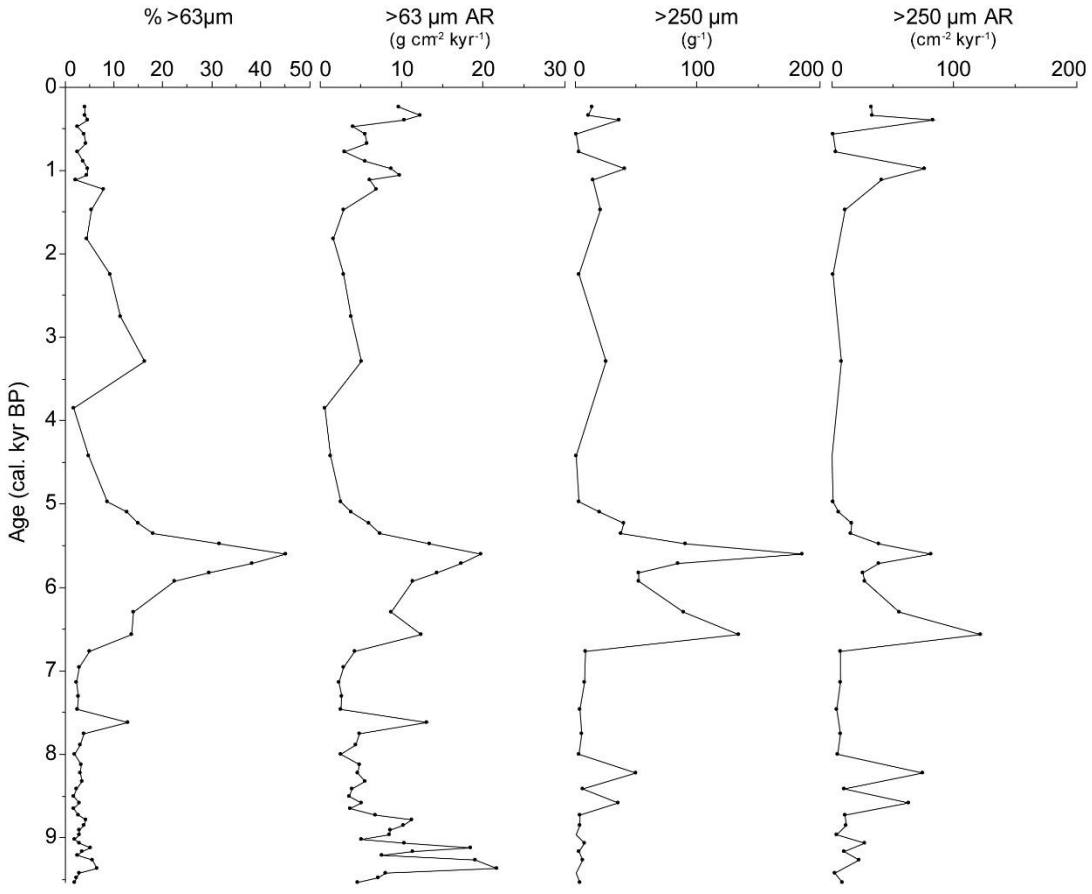


Figure 5.14 GC673 sedimentological data
Sedimentological data from core GC673: percentage of the sample that comprises the >63 μm fraction, the >63 μm fraction accumulation rate, number of >250 μm diameter clasts per gram, the >250 μm diameter clast accumulation rate.

5.3.3 Benthic foraminiferal census counts

5.3.3.1 Diversity, dominance and BFAR

A total of 15561 benthic foraminiferal specimens from 48 taxonomic groupings (see Chapter 3 & Appendix A9) were recorded in the 38 samples analysed from GC673, plus 45 specimens of *N. pachyderma* (present in 13 samples). 300 or more specimens were counted from 25 samples and between 100 and 299 specimens were counted from a further 11 samples.

Diversity (Fisher α – Fig. 5.15) ranges from 0.99 to 5.6, a smaller range than that recorded in core GC666. In the majority of samples (30) this range is further restricted to between 1.0 and 3.0. The mid-Holocene period of very low diversity recorded in GC666 is not present in GC673, but diversity is stable during this period in GC673. Dominance (Fig. 5.15) ranges from 0.13 to 0.91, and is also stable during the mid-Holocene (mean for 6.5 – 3 cal. kyr BP = 0.31±0.07).

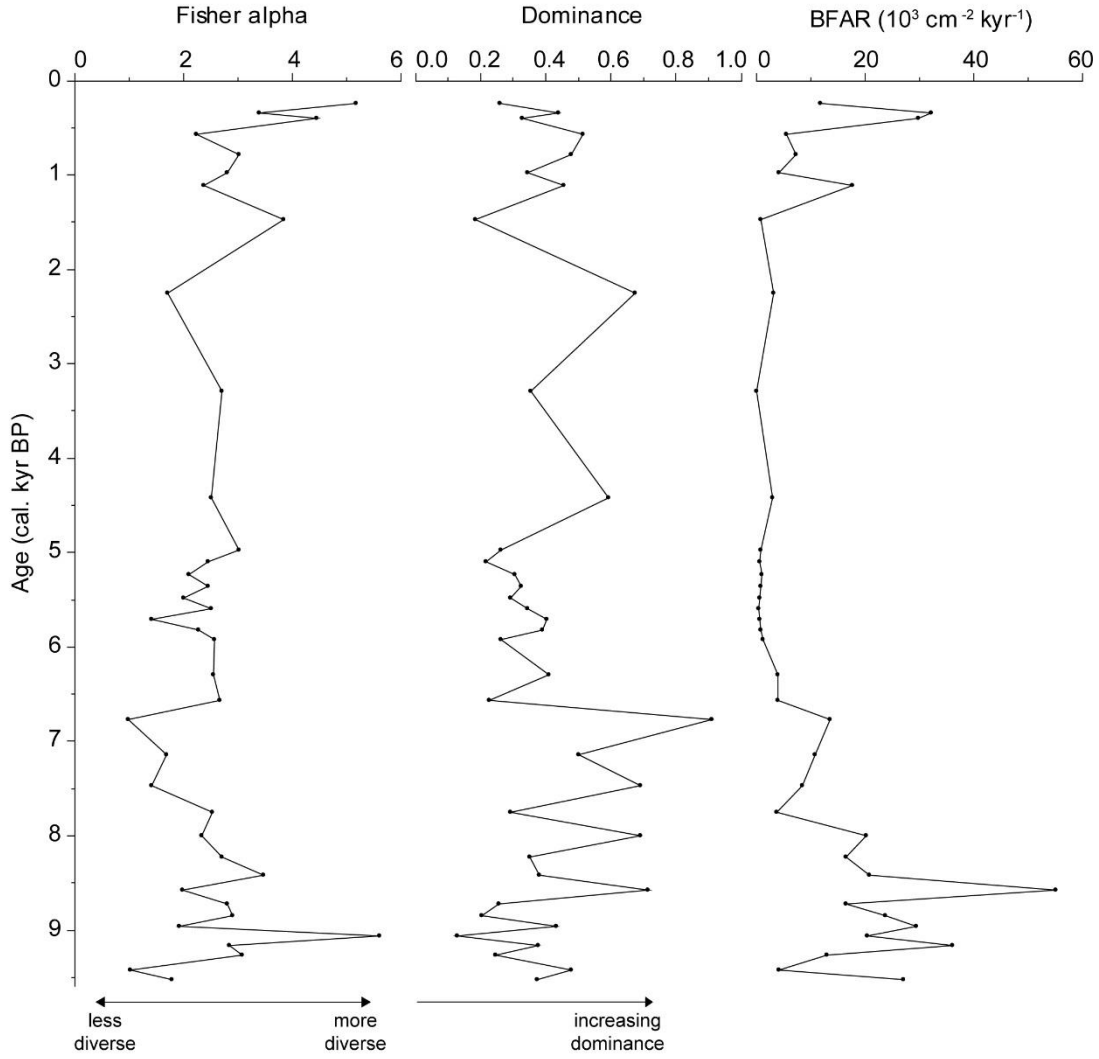


Figure 5.15 GC673 benthic foraminifera data
Benthic foraminiferal diversity (Fisher's alpha) and dominance data, and the accumulation rate of benthic foraminifera, from core GC673.

In core GC673 BFAR is higher values during the early and late Holocene # (>15000 cm^{-2} kyr^{-1} and >4000 # cm^{-2} kyr^{-1}, respectively) and lower (<3000 # cm^{-2} kyr^{-1}) during the mid-Holocene (5.9 – 3.3 cal. kyr BP – Fig. 5.15). The BFAR was highest during the early Holocene, with a peak value of 55300 # cm^{-2} kyr^{-1} at 8.6 cal. kyr BP, before declining to 1300 # cm^{-2} kyr^{-1} by 5.9 cal. kyr BP. Subsequently BFAR remains below 3000 # cm^{-2} kyr^{-1} until 3.3 cal. kyr BP, before increasing to 32300 # cm^{-2} kyr^{-1} at 0.3 cal. kyr BP.

5.3.3.2 Foraminiferal assemblages

As for GC666, a cluster analysis (UWPGA algorithm; chord similarity matrix) was applied to the benthic foraminiferal data to assess whether statistically significant groupings of similar assemblages are present. From this analysis (Fig. 5.16), it was possible to separate the data into four potential groupings (labelled 1, 2, 3 and 4) at the 0.39 similarity level, plus four samples that did not group with any other samples. To further test the significance of these groupings the same data was then analysed using DCA (Fig. 5.17); as discussed in Section 5.2.4 DCA was considered to be the most appropriate ordination technique, based on analysis of the BFA data. The eigenvalues for Axis 1 and Axis 2 of the DCA are 0.23 and 0.08 respectively; when these axes are plotted against one another the DCA supports the identification of group 1. Group 2 samples plot together in DCA space but with some overlap with group 1. Groups 3 and 4 and the ungrouped samples plot in a similar area of DCA space but the 95% confidence ellipse for this group overlaps all the group 2 samples (groups 3 and 4 are now grouped together as group 3A).

The benthic foraminiferal data from GC666 and GC673 were combined and DCA was applied to the complete dataset to test whether the grouping identified in GC673 corresponded to the previously defined assemblages present in GC666 (Fig 5.18). This DCA revealed that Group 1 plots in the same DCA space as the previously identified GC666 *Fursenkoina* Assemblage and can therefore be considered part of the same assemblage. Group 2 plots between the GC666 *Fursenkoina* Assemblage and Group 3A, and may be a transitionary assemblage between these two groupings. Group 3A in part overlaps the GC666 *Miliammina* Assemblage and may by a version of this assemblage that has been less modified by dissolution; Group 3A also partially overlaps the GC666 *Cassidulinoides/Astrononion* Assemblage, suggesting Group 3A has some similarity with this GC666 assemblage, although with a higher proportion of *M. earlandi*. This may indicate that the GC666 *Miliammina* Assemblage comprises what remains of the GC666 *Cassidulinoides/Astrononion* Assemblage following

dissolution of the calcareous taxa and that the separation between Group 2 and Group 3A in GC673 is also due to the effect of dissolution, which is less pronounced than in GC666. The composition of these assemblages is discussed below; possible ecological implications of the key species are discussed in Section 5.2.4.

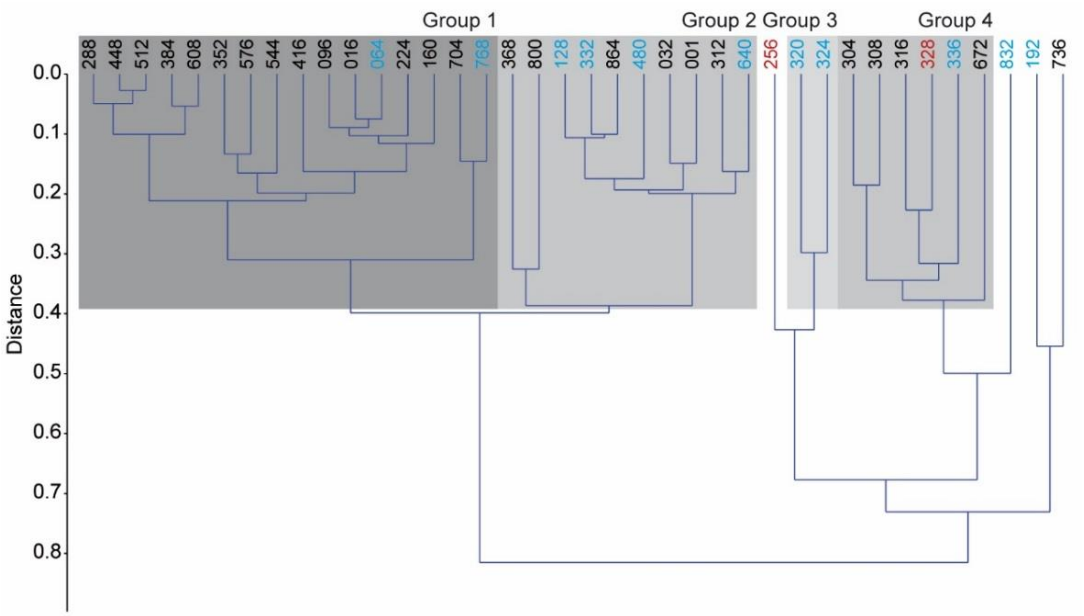


Figure 5.16 GC673 cluster analysis
Cluster analysis carried out in PAST3 (Hammer et al., 2001) using the paired group algorithm and the chord similarity measure. Blue samples have 100-300 benthic specimens, red samples <100.

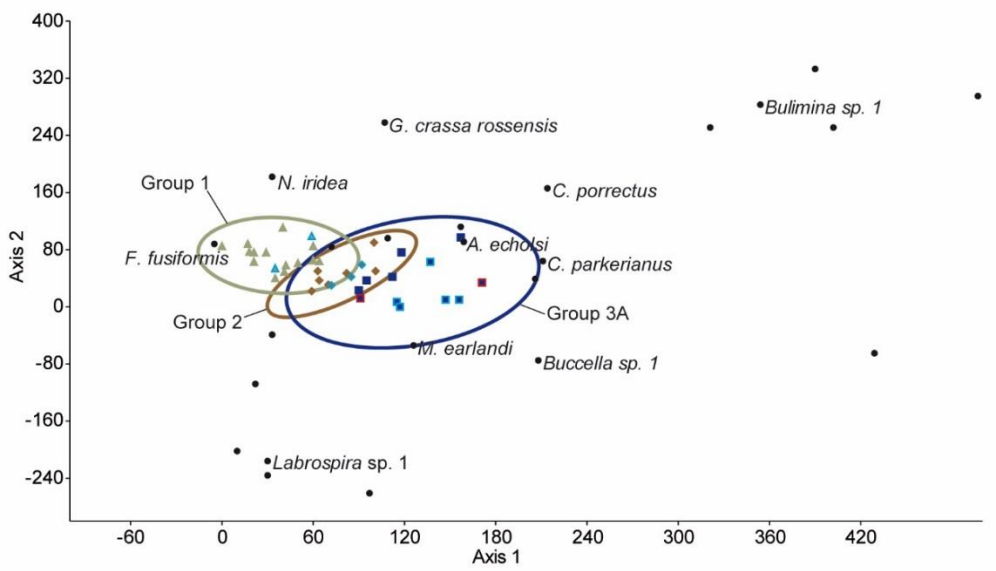


Figure 5.17 GC673 DCA
GC673 DCA Axes 1 & 2. Green triangle symbols/ellipse – Group 1; brown diamond symbols/ellipse – Group 2; blue square symbols/ellipse – Group 3A. Red borders - <100 specimens, Blue border - <300 specimens. 95% confidence ellipses. Black circles - taxa (ten most abundant named in the plot: *Astrononion echolsi, Buccella* sp. 1, *Bulimina* sp. 1, *Cassidulinoides parkerianus, Cassidulinoides porrectus, Fursenkoina fusiformis, Globocassidulina crassa rossensis, Labrospira* sp. 1, *Miliammina earlandi, Nonionella iridea*).

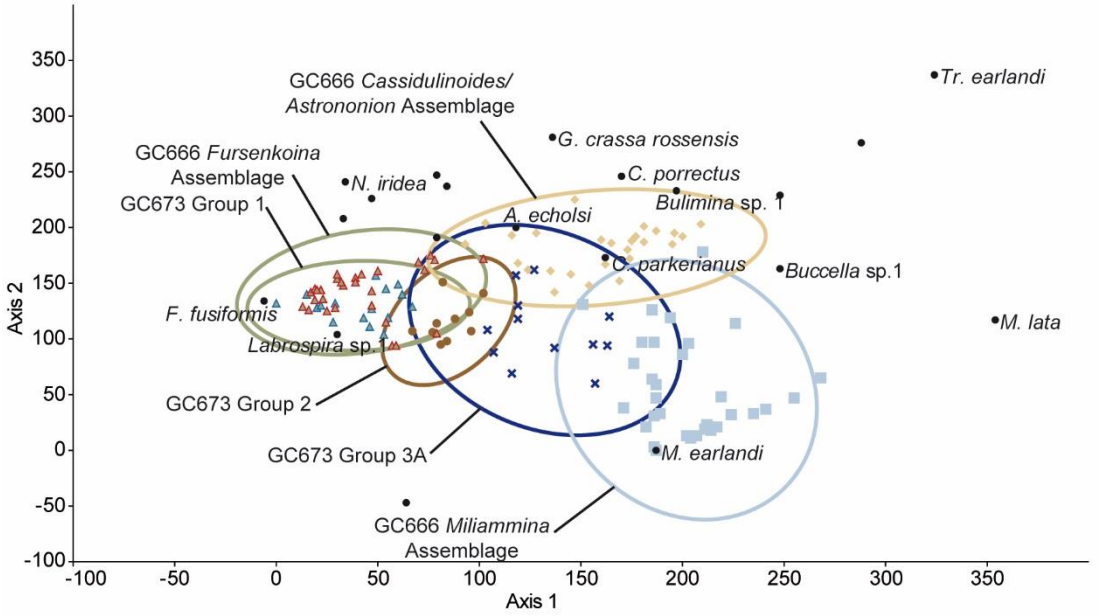


Figure 5.18 GC666 and GC673 combined DCA
GC666 and GC673 combined DCA Axes 1 & 2. Green triangle symbols/ellipse - *Fursenkoina* Assemblage/Group 1 (Red outline = GC666, Blue outline = GC673); yellow diamond symbols/ellipse - GC666 *Cassidulinoides/Astrononion* assemblage; light blue square symbols/ellipse - GC666 *Miliammina* Assemblage; brown circle symbols/ellipse - GC673 Group 2; dark blue crosses/ellipse - GC673 Group 3A. 95% confidence ellipses. Black circles - taxa (ten most abundant from both GC666 and GC673 named in the plot: *Astrononion echolsi, Buccella* sp. 1, *Bulimina* sp. 1, *Cassidulinoides parkerianus, Cassidulinoides porrectus, Fursenkoina fusiformis, Globocassidulina crassa rossensis, Labrospira* sp. 1, *Miliammina earlandi, Miliammina lata, Nonionella iridea, Trifarina earlandi*).

*5.3.3.3 Group 1/*Fursenkoina *Assemblage*

Group 1 is analogous to the GC6666 *Fursenkoina* Assemblage and is subsequently referred using this assemblage name. Unlike in core GC666, where it is only dominant during the deglacial and the very earliest Holocene, the *Fursenkoina* Assemblage dominates much of the early and late Holocene in core GC673. The *Fursenkoina* Assemblage is the most common assemblage between 9.2 and 6.3 cal. kyr BP, interrupted by the *Miliammina* Assemblage at 9.0 and 8.8 cal. kyr BP and the transition assemblage at 8.7, 7.8, and 6.6 cal. kyr BP, and after 1.1 cal. kyr BP, as well as occurring at 4.4 and 2.2 cal. kyr BP (Fig. 5.19). The *Fursenkoina* Assemblage is the least diverse of the three assemblages identified in core GC673 (mean Fisher-alpha = 2.3±0. 7) and is dominated by *F. fusiformis* which comprises an average of 70.4±11.2% of the assemblage (mean dominance = 0.5±0.2), with these values all comparable to those found for this assemblage in core GC666. As in core GC666 other species in the assemblage include *Miliammina earlandi* (12.6±6.1%), *A. echolsi* (4.3±3.3%), *C. parkerianus* (4.1±3.0%), and *G. crassa rossensis* (3.2±5.6%). Mean BFAR is highest in the *Fursenkoina* Assemblage, of the three assemblages in core GC673

(17800±14000 cm^{-2} kyr^{-1}). The ecology of the *Fursenkoina* Assemblage is discussed in detail in Section 5.2.4.3.

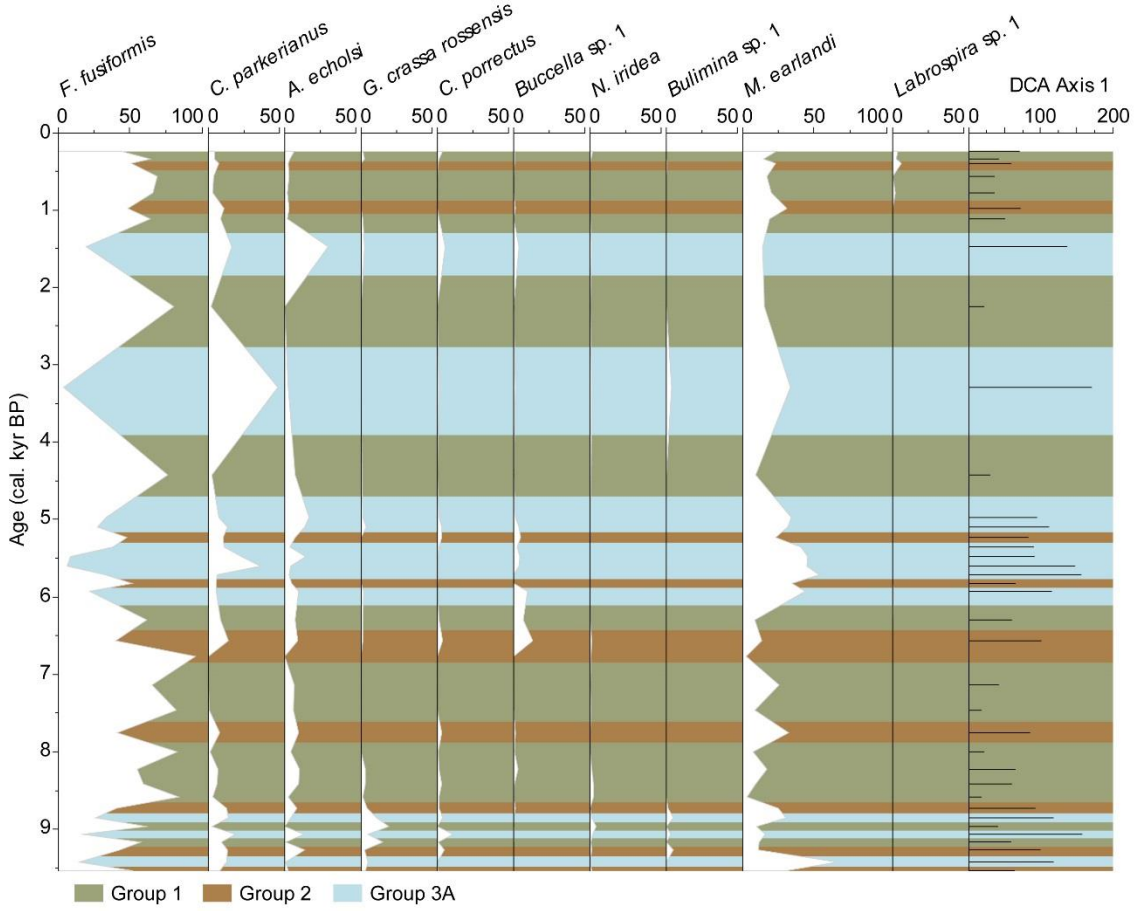


Figure 5.19 GC673 downcore BFA relative abundances
Downcore relative abundances of the 10 most abundant taxa in core GC673, in order of abundance (left to right), separated into calcareous and agglutinated taxa. DCA Axis 1 values plotted in the right-hand column. Coloured bands indicate the different groups.

5.3.3.4 Group 2/Transition Assemblage

The Transition Assemblage occurs intermittently through the GC673 record, at 9.5, 9.3, 8.7, 7.8, 6.6, 5.8, 5.2, 1.0, and 0.4 cal. kyr BP, and only for brief periods, never becoming the dominant assemblage for a sustained period of time (Fig. 5.19). The diversity of the Transition Assemblage is the highest of the three GC673 assemblages (3.0±1.0), and the dominance is correspondingly low (0.3±0.1). The major components of the Transition Assemblage are *F. fusiformis* (46.0±4.4%), *M. earlandi* (24.9±7.3%). Subsidiary species include *C. parkerianus* (9.6±3.1%), *A. echolsi* (7.1±3.5%), *C. porrectus* (2.4±1.7%), *Buccella* sp. 1 (2.6±3.9%), and *G crassa rossensis* (1.5±1.5%). Mean BFAR is 11200±10000 cm^{-2} kyr^{-1}). This assemblage may be indication of a transition between high and more moderate productivity regimes.

5.3.3.5 Group 3A

Group 3A occurs intermittently in the early Holocene (9.4, 9.1, and 8.8 cal. kyr BP), and is the most common assemblage in the mid-Holocene (5.9 and 1.4 cal. kyr BP – Fig. 5.19), roughly coincident with the dominance of the *Miliammina* Assemblage in core GC666 (7.2 and 1.0 cal. kyr BP – Fig. 5.6). The diversity of Group 3A is higher than the *Miliammina* Assemblage in core GC666 (mean Fisher-alpha = 2.7±1.1, in comparison to 1.5±1.2), and dominance is correspondingly lower (0.3±0.1, in comparison to 0.6±0.2). *Miliammina earlandi* is still the dominant species in Group 3A (37.9±14.0%) but *M. lata* is almost completely absent (0.1±0.1%). Other species in the assemblage include *Fursenkoina fusiformis* (20.9±10.7%), *C. parkerianus* (17.9±12.3%), and *A. echolsi* (10.0±8.2%), in addition to smaller abundances of *G. crassa rossensis* (2.8±3.2%), *Buccella* sp. 1 (2.7±2.7%), and *C. porrectus* (2.6±3.0%).Mean BFAR in Group 3A is the lowest of the three assemblages in core GC6723 (4600±7900 cm^{-2} kyr^{-1}).

As discussed in Section 5.2.4.4, *Miliammina* spp. are often considered indicative of the cold, saline waters typical of shelf environments in the Southern Ocean (e.g. Anderson, 1975; Milam and Anderson, 1981). *Miliammina* spp. are unaffected by carbonate dissolution and the siliceous cement that binds their tests (Earland, 1933) is more robust than the organic cements commonly employed by other agglutinated taxa, giving this taxa an exceptional preservation potential. This unique preservation potential, plus their tolerance of salinity fluctuations, means that *Miliammina* spp.-dominated assemblages can be interpreted as being indicative of bottom water regimes where saline shelf water is a major component (Ishman and Sperling, 2002; Szymcek et al., 2007; Peck et al., 2015). Alternatively, increases in the corrosivity of bottom and/or pore water, due to increased organic matter decomposition (related to enhanced carbon flux to the substrate) may result in *Miliammina* spp.-dominated assemblages (e.g. Li et al., 2000; Majewski and Anderson, 2009; Melis and Salvi, 2009; Majewski et al., 2016).

While the dominance of *M. earlandi* in this assemblage indicates its affinity to the GC666 *Miliammina* Assemblage, there are also similarities to the GC666 *Cassidulinoides/Astrononion* Assemblage. As discussed in Section 5.2.4.5, some of the dominant species in this assemblage may be linked to glacial proximity, and to conditions with stable organic flux where phytodetritus events are uncommon (e.g. Majewski and Anderson, 2009; Rodrigues et al., 2010; Majewski et al., 2012; Majewski et al., 2016). The living assemblage of Group 3A may have been equivalent to that of the GC666 *Cassidulinoides/Astrononion*

Assemblage, with the fossil assemblage having been altered by dissolution, although not to the same extent as the GC666 *Miliammina* Assemblage.

5.3.4 Geochemistry of organic matter

Bulk sediment organic carbon and nitrogen concentration and carbon isotope analysis are given in Figure 5.20 and Appendix A18. Organic carbon accumulation rates (C_{org} AR – calculated from % C, reported to 2SF) range from 0.13 to 2.6 g cm^{-2} kyr^{-1} with the highest value recorded at 9.3 cal. kyr BP. Then C_{org} AR decreases to 0.29 g cm^{-2} kyr^{-1} by 5.8 cal. kyr BP and stays below 0.3 g cm^{-2} kyr^{-1} until 1.8 cal. kyr BP before increasing to 2.4 g cm^{-2} kyr^{-1} by 1.1 cal. kyr BP. Subsequently C_{org} AR decreases to 0.83 g cm^{-2} kyr^{-1} by 0.8 cal. kyr BP, before increasing to 2.3 g cm^{-2} kyr^{-1} by 0.3 cal. kyr BP.

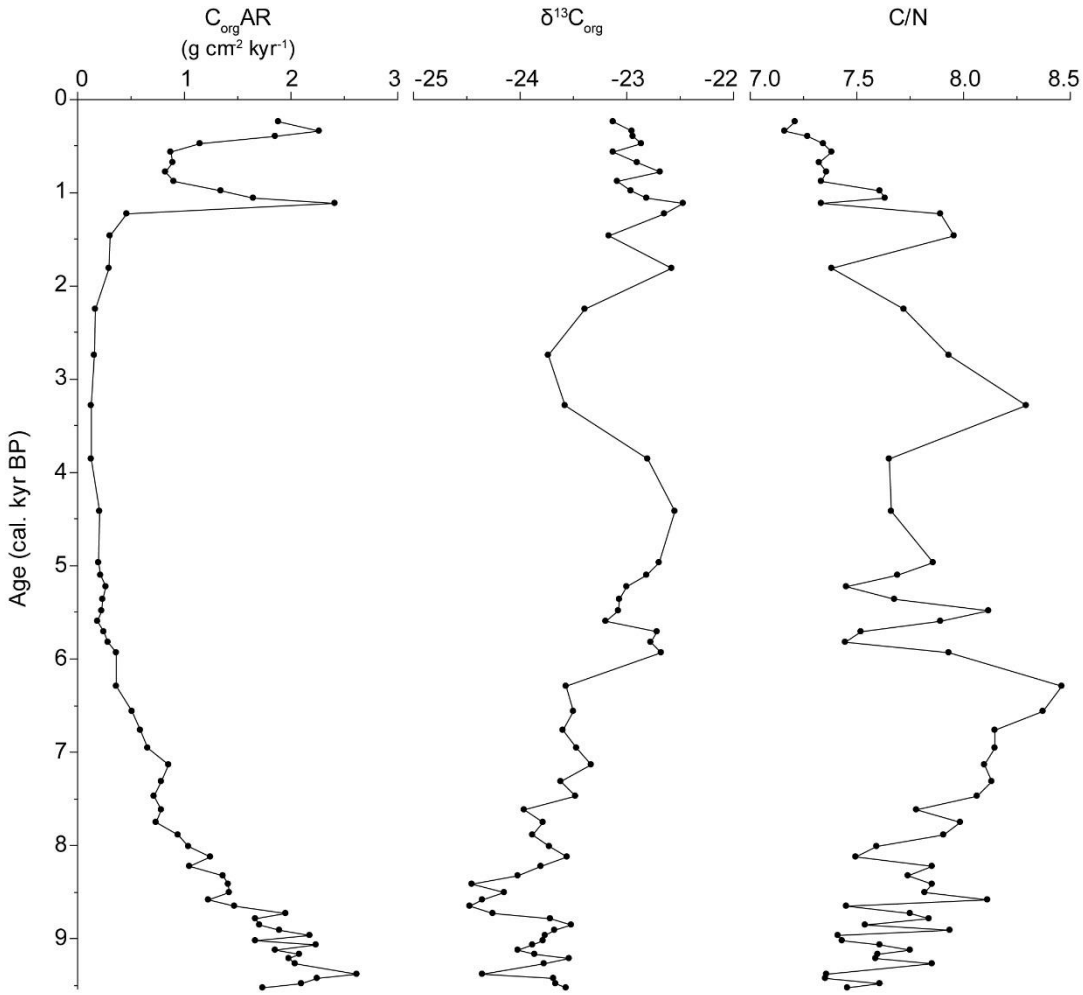


Figure 5.20 GC673 organic geochemistry data
Organic geochemistry data from GC673: organic carbon accumulation rate, $\delta^{13}C_{org}$, the ratio of carbon to nitrogen.

The carbon stable isotope composition of organic carbon ($\delta^{13}C_{org}$) ranges between −24.5 ‰ and −22.5 ‰ (mean = −23.4±0.52 ‰). Between 9.4 and 4.4 cal. kyr $\delta^{13}C_{org}$ increases from −24.3 ‰ to −22.5 ‰, with a negative

excursion between 8.7 and 8.4 cal. kyr BP (max. = −24.4 ‰). The $\delta^{13}C_{org}$ values then decrease to −23.7 ‰ by 2.7 cal. kyr BP, before increasing to −22.6 ‰ by 1.8 cal. kyr BP. This is followed by fluctuation about a slight decreasing trend to −23.1 ‰ by 0.2 cal. kyr BP.

The weight ratio of carbon to nitrogen (C:N) does not exceed 8.5 at any point in the core, ranging from 7.16 to 8.46, with a mean value of 7.71±0.30. Between 9.5 and 6.3 cal. kyr BP C:N fluctuates about an increasing trend from 7.46 to 8.46. This is followed by fluctuation about a decreasing trend to 7.16 by 0.3 cal. kyr BP. The patterns and trends described in all three of the above proxies are broadly similar to the patterns and trends in these proxies recorded in core GC666.

5.3.5 Biogenic opal analysis

The biogenic opal accumulation rate (BSi AR, reported to 2SF) was calculated from the biogenic opal weight % (see Chapter 2 – Materials and Methods) and is presented in Figure 5.21 and Appendix A19. The BSi AR follows similar patterns and trends to those recorded in C_{org} AR, as in core GC666; BSi AR ranges from 3.0 to 51 g cm^{-2} kyr^{-1} with the highest value recorded at 8.9 cal. kyr BP. Then BSi AR decreases to 5.2 g cm^{-2} kyr^{-1} by 6.3 cal. kyr BP, remaining below 10 g cm^{-2} kyr^{-1} until 1.5 cal. kyr BP. Subsequently BSi increases to 35g cm^{-2} kyr^{-1} by 0.2 cal. kyr BP, with a large excursion to 47 g cm^{-2} kyr^{-1} at 1.1 cal. kyr BP.

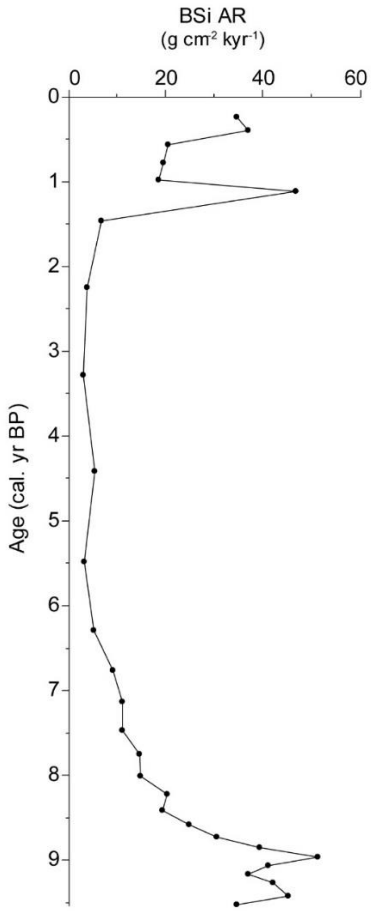


Figure 5.21 GC673 biogenic silica accumulation rate

5.3.6 Foraminiferal stable isotope analysis

In benthic foraminifera from core GC673 $\delta^{13}C$ ranges from −6.27 ‰ to +0.70 ‰ (Fig. 5.22 & Appendix A20). Negative $\delta^{13}C$ values only occur between 9.4 and 6.2 cal. kyr BP and are generally associated with foraminifera that appear to have been diagenetically altered, yellow/brown compared to pristine specimens and covered with varying degrees of sugary crystal overgrowths (see Section 5.2.7.3), as seen in core GC666. Subsequent to 6.4 cal. kyr BP there is little variation in $\delta^{13}C$, with $\delta^{13}C$ values ranging from +0.17 ‰ to +0.70 ‰ (mean = +0.45±0.15 ‰).

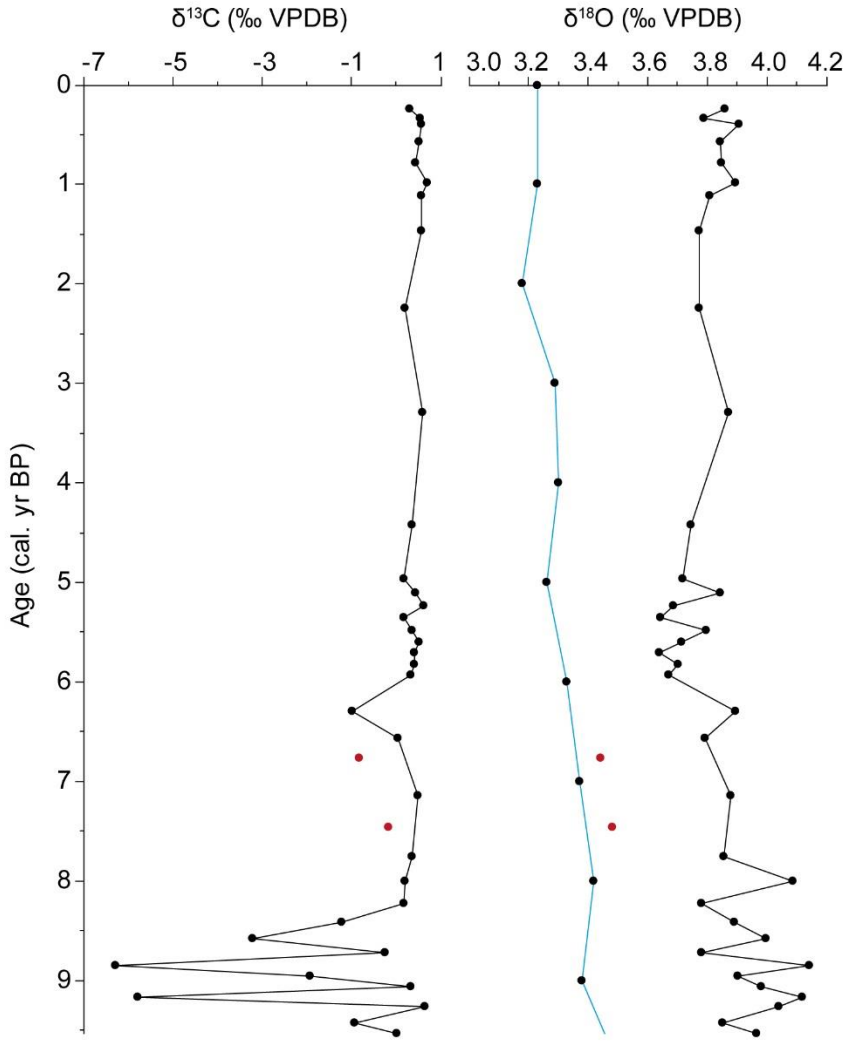


Figure 5.22 GC673 foraminiferal isotopes
Foraminiferal stable isotope data from GC673: blue line - LR04 global benthic isotope stack (Lisiecki and Raymo, 2005).

Benthic $\delta^{18}O$ values range from +3.44 to +4.14 ‰ (Fig. 5.22). As in core GC666 benthic $\delta^{18}O$ values broadly follow the trend seen in the LR04 benthic stack (Lisiecki and Raymo, 2005), although offset by approximately −0.6 ‰. Two samples (red dots in Figure 5.22) that appear to record negative excursions of ca. −0.4 ‰ are considered to be outliers as these samples had low yields during analysis. There is also a smaller negative excursion of ca. −0.2 ‰ between 5.9 and 5.2 cal. kyr BP.

Only three samples from core GC673 displayed similar diagenetic alteration to that discussed in Section 5.2.7.3, all of which have $\delta^{13}C_{foram}$ values more negative than −0.5 ‰. However, unlike in core GC666 where the diagenetically altered samples account for most of the $\delta^{13}C_{foram}$ values more negative than −0.5 ‰, these samples only accounted for 50% (3 of 6) of the $\delta^{13}C_{foram}$ values more negative than −0.5 ‰.

5.4 Summary

5.4.1 GC666

- An age/depth model was developed in OxCal 4.3 for core GC666 utilising 14 radiocarbon dates (5 of which were previously published in Graham et al. (2017)). The Marine13 calibration curve (Reimer et al., 2013) was applied to calibrate the dates and to develop the age model, combined with a local reservoir correction of 433±41 years.
- Two main sedimentological units were identified in core GC666. Unit 1 (816 – 500 cmcd) comprises laminated sediments with a very high sedimentation rate (638 cm kyr^{-1}). Unit 2 comprises grey-olive green sandy diatomaceous mud, with the sedimentation rate ranging from 4 to 122 cm kyr^{-1}.
- The >63 μm AR ranges from 0.74 to >5.00 g cm^{-1} kyr^{-1}, with the lowest values recorded between 7.5 and 3.3 cal. kyr BP. These low values are preceded by a peak in the >250 μm AR.
- Benthic foraminifera from 47 taxonomic groupings were identified, plus a single planktonic taxa (*N. pachyderma*). Statistical analysis separated the benthic data into three assemblages: the *Fursenkoina* Assemblage (dominant prior to ca. 10.0 cal. kyr BP), the *Miliammina* Assemblage (dominant between 7.2 and 1.0 cal. kyr BP), and the *Cassidulinoides/Astrononion* Assemblage (dominant between 10.0 and 7.2 cal. kyr BP, and after 1.0 cal. kyr BP).
- Organic carbon accumulation rates (C_{org} AR) range from 0.025 to 6.0 g cm^{-2} kyr^{-1}, with the highest values in the laminated section of the core and low values in the mid- to late Holocene. The carbon stable isotopic composition of organic carbon ($\delta^{13}C_{org}$) ranges between −24.8 and −22.1 ‰. The weight ratio of carbon to nitrogen (C/N) does not exceed 9 at any point in the core, ranging from 6.87 to 8.93.
- BSi AR ranges across several orders of magnitude, from 0.16 to 93 g cm^{-2} kyr^{-1} with the highest value recorded at 15.2 cal. kyr BP and low values in the mid- to later Holocene.
- Benthic foraminiferal $\delta^{13}C$ ranges from −7.90 ‰ to +1.07 ‰; large negative excursions occur between 14.8 and 10.3 cal. yr BP. Benthic $\delta^{18}O$ values follow the trend seen in the LR04 benthic stack (Lisiecki and Raymo, 2005), although offset by approximately +0.5 ‰. There is a gap the benthic isotope records in GC666 between 6.8 and 3.5 cal. kyr BP.
- The planktonic foraminiferal stable isotope data is at a lower resolution than the benthic record and is completely absent between 8.0 and 0.4

cal. kyr BP. As with the benthic data, values below −1 ‰ only occur in the early part of the record, between 14.8 and 10.1 cal. yr BP. Planktonic $\delta^{18}O$ values also follow the trend seen in the LR04 benthic stack (Lisiecki and Raymo, 2005), although offset by approximately −0.2 ‰.

- The large negative $\delta^{13}C$ excursions may be a result of diagenetic alteration, potentially related to biogenic methane that may have formed in the laminated section of the core.
- The alkenone-based SSTs range from 1.1 ºC (at 1.6 and 9.4 cal. kyr BP) to 5.6 ºC (at 11.5 cal. kyr BP). Prior to 11.2 cal. kyr BP it was not possible to reconstruct SSTs, due to low alkenone concentration possibly linked to biogenic methane activity. SSTs were relatively cool during the early Holocene, warmer during the mid-Holocene, and cooler again in the late Holocene.

5.4.2 GC673

- An age/depth model was developed using the CLAM package in R for core GC673 utilising 4 radiocarbon dates. The Marine13 calibration curve (Reimer et al., 2013) was applied to calibrate the dates and to develop the age model, combined with a local reservoir correction of 433±41 years.
- Core GC673 comprises grey-olive green sandy bioturbated diatomaceous mud, with no notable sedimentological changes. Occasional thin dark green or orange laminae, interpreted as comprising diatomaceous ooze, analogous to the laminae in Unit 1 of core GC666.
- Benthic foraminifera from 48 taxonomic groupings were identified, plus a single planktonic taxa (*N. pachyderma*). Statistical analysis separated the benthic data into three assemblages: the *Fursenkoina* Assemblage (dominant between 9.2 and 6.3 cal. kyr BP and after 1.1 cal. kyr BP), the unmodified *Miliammina* Assemblage (dominant between 5.9 and 1.4 cal. kyr BP), and the Transition Assemblage (occurring intermittently throughout the core).
- Organic carbon accumulation rates (C_{org} AR) range from 0.13 to 2.6 g cm^{-2} kyr^{-1}, with the lowest values in the mid- to late Holocene. The carbon stable isotopic composition of organic carbon ($\delta^{13}C_{org}$) ranges between −24.5 ‰ and −22.5 ‰. The weight ratio of carbon to nitrogen (C/N) does not exceed 8.5 at any point in the core, ranging from 7.16 to 8.46.
- BSi AR ranges from 3.0 to 51 g cm^{-2} kyr^{-1}, with the lowest values recorded in the mid-Holocene.

- Benthic foraminiferal $\delta^{13}C$ ranges from −6.27 ‰ to +0.70 ‰; negative $\delta^{13}C$ values only occur between 9.4 and 6.2 cal. kyr BP and are generally associated with foraminifera that appear to have been diagenetically altered. Benthic $\delta^{18}O$ values follow the trend seen in the LR04 benthic stack (Lisiecki and Raymo, 2005), although offset by approximately +0.5 ‰.

Chapter 6

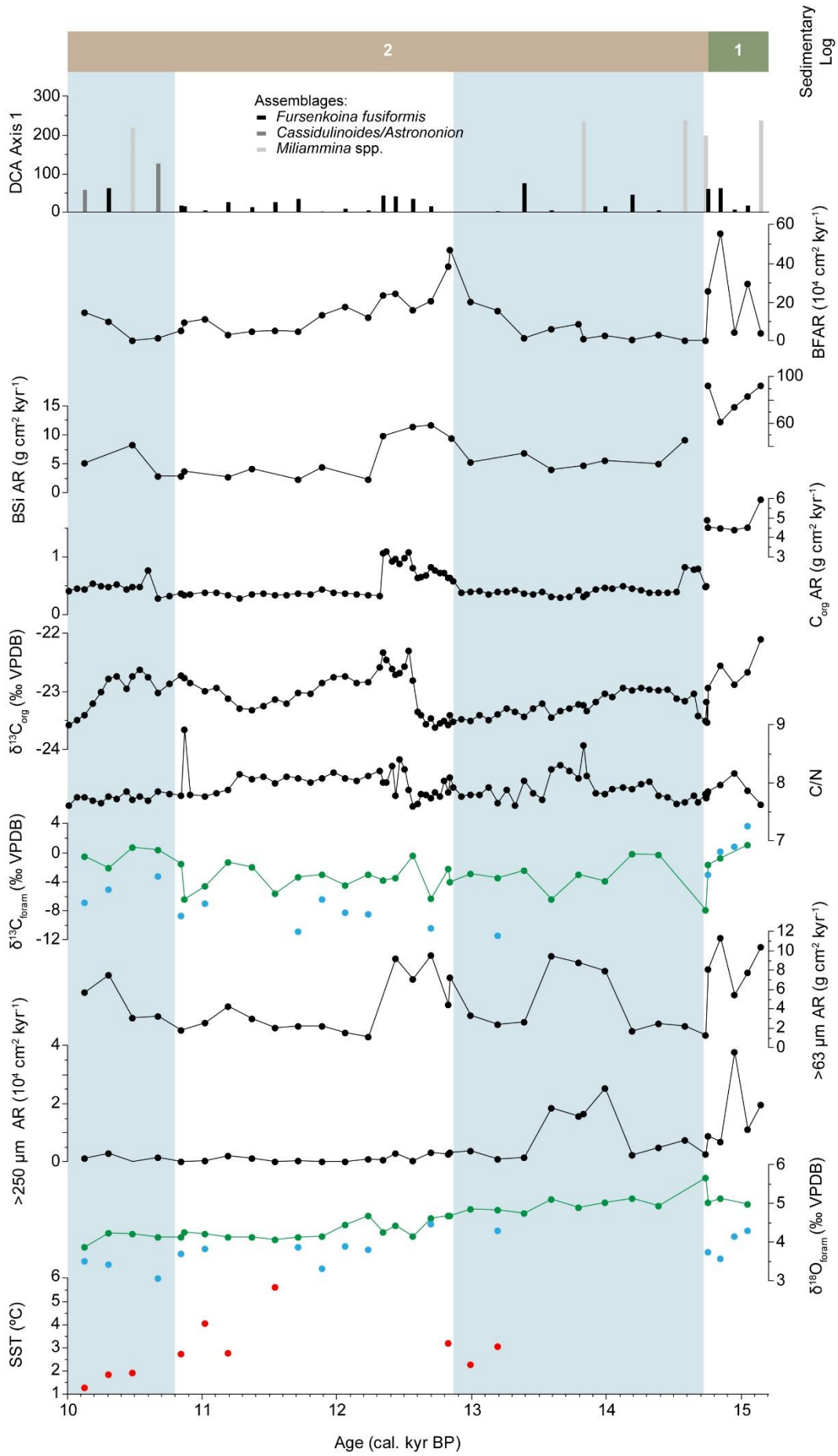
Deglaciation and the Antarctic Cold Reversal

6.1 Introduction

This chapter comprises discussion of the evolution of the South Georgia shelf oceanography from ~15.2 cal. kyr BP until ~12.3 cal. kyr BP, during the transition from glacial to interglacial conditions. This section of the GC666 core includes the latter part of the first stage of deglaciation, the Antarctic Cold Reversal (ACR), and the return to deglaciation that culminates in the establishment of interglacial conditions at South Georgia. Based on my interpretation I consider 12.3 cal. kyr BP to be the point at which grounded/glacial ice no longer has a strong influence on the oceanography at GC666, following retreat from the ACR advance, and it is for this reason that I have divided the records at this point.

The discussion utilises the multi-proxy records described in Chapter 5 (summarised in Fig. 6.1), with these proxy records primarily interpreted in terms of changes in primary productivity, and sediment supply. The proxy records from GC666 are considered in comparison to other palaeoceanographic and palaeoclimatic records from the southern high latitudes (e.g. Leventer et al., 2002; Bianchi and Gersonde, 2004; Leventer et al., 2006; Putnam et al., 2010; Kilian and Lamy, 2012), including South Georgia (e.g. Bentley et al., 2007; Hodgson et al., 2014b; Barnes et al., 2016; Graham et al., 2017); more detailed discussion of these records can be found in Sections 1.3 & 1.4. Potential mechanisms driving the variability recorded at South Georgia are proposed and these mechanisms are compared to those proposed for other high southern latitude records, to assess whether these new records can help to further understand climate forcing in the Southern Hemisphere.

Figure 6.1 Key proxy records from GC666 (15 to 10 cal. kyr BP) $\delta^{13}C_{foram}$ and $\delta^{18}O_{foram}$ - green points = benthic data, blue points = planktonic data. Note the change in scale for BSi AR and C_{org} AR. Data points coloured red in the SST record may be unreliable due to poor quality chromatograms (all samples in this part of the GC666 record). Shaded areas represent the ACR and the early Holocene cool period (discussed in Chapter 7). The sedimentary log shows the two main units identified in core GC666 (see section 5.2.2.1); Unit 1 is the laminated section of the core, Unit 2 is the unlaminated section.


2
1
Sedimentary Log
DCA Axis 1
Assemblages:
Fursenkoina fusiformis
Cassidulinoides/Astrononion
Miliammina spp.
BFAR (10⁴ cm² kyr⁻¹)
BSi AR (g cm² kyr⁻¹)
C_org AR (g cm² kyr⁻¹)
δ¹³C_org (‰ VPDB)
C/N
δ¹³C_foram (‰ VPDB)
>63 µm AR (g cm² kyr⁻¹)
>250 µm AR (10⁴ cm² kyr⁻¹)
δ¹⁸O_foram (‰ VPDB)
SST (°C)
Age (cal. kyr BP)

6.2 Discussion

6.2.1 Deglaciation at South Georgia

Following the Last Glacial Maximum (LGM), occurring between 26.5 and 19.0 kyr BP (Clark et al., 2009), increasing temperatures, principally driven by changes in insolation, resulted in globally recognised deglaciation, between 19.0 and 11.0 kyr BP (Clark et al., 2012). The timing of the onset of deglaciation varies in different regions, occurring between 19.0 and 17.5 kyr BP in southern Patagonia (Kilian and Lamy, 2012) but potentially as late as 14.5 kyr BP in Antarctica (Clark et al., 2009). On South Georgia the onset of deglaciation has been much debated, with this debate linked to uncertainty about the extent of the island's LGM ice-sheet (e.g. Bentley et al., 2007; Hodgson et al., 2014b; Graham et al., 2017). The radiocarbon dating of the onset of sedimentation in a lake on South Georgia to 18.6 kyr BP (Rosqvist et al., 1999) has been proposed as evidence for relatively early deglaciation at South Georgia, and this date, combined with cosmogenic dating of moraines on the island, led Bentley et al. (2007) to propose that the LGM ice-sheet at South Georgia was restricted to within the island's fjords. However, more recent work combining bathymetric data and radiocarbon dating of submarine moraines has indicated that South Georgia had an extensive ice-sheet at the LGM, potentially to the shelf edge (Graham et al., 2017), a hypothesis supported by Barnes et al. (2016) who showed that modern shelf biodiversity was less rich than would be expected if the shelf had been ice-free at the LGM. Moraines on the Lewin Peninsula, Cumberland Bay, South Georgia, dated using geomorphic relationships and rock hardness analysis, also indicate a large ice sheet on South Georgia at the LGM, extending at least to the mid-shelf (White et al., 2017). To fit this large ice-sheet with the early sedimentation onset recorded by Rosqvist et al. (1999), Graham et al. (2017) proposed that the ice-sheet retreated early and rapidly due to early deglacial warming at lower latitudes, combined with a relatively thin South Georgia ice-sheet and the sensitivity of the ice-sheet to external forcing and variation in precipitation supply (Fig. 6.2). The literature regarding the deglacial period around South Georgia and more generally in southern high latitudes has been reviewed in more detail in Sections 1.3.1 and 1.4.1.

Based on this most recent evidence (Barnes et al., 2016; Graham et al., 2017; White et al., 2017), the record from core GC666 will be unsuitable to provide further information about the onset of deglaciation at South Georgia as it starts at 15.2 cal. kyr BP, well into the period of deglaciation. However, GC666 can still inform about the later stages of this first period of deglaciation and this is discussed in the following sections.

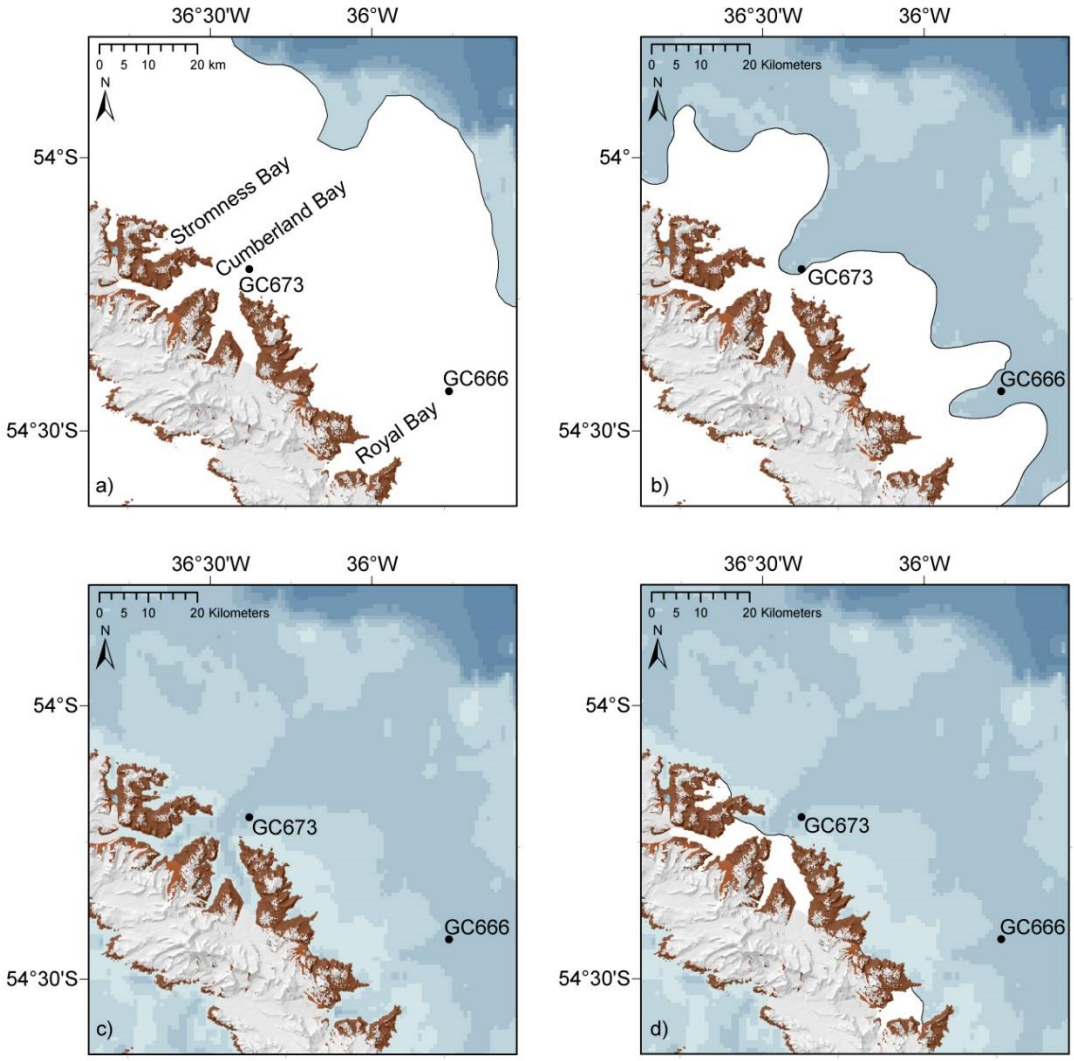


Figure 6.2 Ice sheet extent at South Georgia during deglaciation
a) LGM - Ice sheet extends to the shelf edge (Barnes et al., 2016; Graham et al., 2017; White et al., 2017). b) Calving bay re-entrants form during the first stage of deglaciation, as the ice sheet retreats more rapidly above the cross shelf troughs (Domack et al., 2006; Leventer et al., 2006). c) Maximum retreat during the first stage of deglaciation - ice retreats to at least modern extent (Graham et al., 2017). d) ACR - reversal of warming trend results in glacial readvance to the fjord mouths, evident from moraines at fjord mouths (dated to the ACR in Cumberland Bay (Graham et al., 2017)). The ACR advance is only illustrated in fjords where moraines have been identified. Subsequently to the ACR the ice sheet retreats to, or beyond, the modern extent as interglacial conditions are established.

6.2.1.1 Laminated sediments (15.2–14.7 cal. kyr BP)

As discussed in Section 5.2.2, the basal three metres of core GC666 (816–510 cm core depth (cmcd)) comprise laminated sediments that were rapidly deposited, with a sedimentation rate of 638 cm kyr^{-1}, such that this part of the core represents approximately 0.5 kyrs while the upper ~5 m of the core represent 14.7 kyrs. The dates for this section of the core were acquired by

Graham et al. (2017); it is unclear whether the foraminifera they used had been affected by the diagenetic alteration seen in the foraminifera in the core section above the laminated sediments. The preservation of the samples analysed from the laminated section in the research presented in this thesis show variable preservation, with some showing no signs of alteration.

Initial analysis of smear slides from a small number of laminae couplets from GC666 (see Section 5.2.3) has revealed that the laminae are near-monospecific diatomaceous oozes (comprising mainly *Chaetoceros* Resting and Vegetative Spores (CRVS)) with very little clastic material, alternating with more clastic-dominated sediments containing a more diverse diatom assemblage (but still dominated by CRVS). Rapid deposition of laminated sediments comprising biogenic and terrigenous laminae are also reported from deglacial sediments from the Antarctic Peninsula (AP) (e.g. Leventer et al., 2002; Maddison et al., 2005) and East Antarctica (e.g. Stickley et al., 2005; Leventer et al., 2006; Maddison et al., 2006; Stickley et al., 2006). Leventer et al. (2002) proposed a model for the formation of these laminated couplets, based on analysis of deglacial sediments from Palmer Deep, AP (Fig. 6.3). In this model the biogenic laminae form during the spring, when glacial proximal conditions generate extreme high productivity, and the terrigenous laminae represent the input of

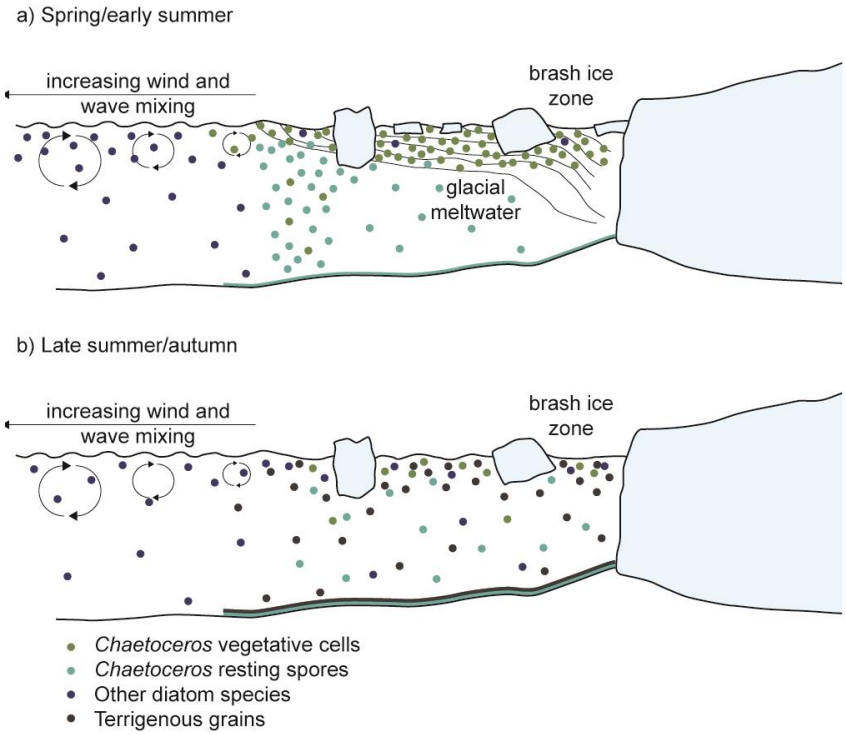


Figure 6.3 Chaetoceros laminae formation model
Model for the processes that result in the formation of laminae of alternating near mono-specific diatomaceous oozes, deposited in spring/early summer, and more terrigenous sediment, with a more diverse diatom assemblage, deposited during late summer/autumn.

ice-rafted material during the summer. The fast-growing *Chaetoceros* are particularly indicative of spring blooms (Grimm et al., 1996, 1997; Kemp et al., 2000), and are preserved as sedimentary laminae due to rapid post-bloom flocculation and mass sinking, linked to sticky exopolymer formation and the growth of more heavily silicified resting spores (Smetacek, 1985; Alldredge and Gotschalk, 1989; Alldredge et al., 1993; Grimm et al., 1997). The dominance of *Chaetoceros* resting spores in the biogenic laminae may also be linked to proximity to the ice-margin, with the break-down of stratification, due to high wind-stress associated with the ice-margin, triggering resting spore formation and the end of the *Chaetoceros* bloom (Leventer et al., 2002).

Following analysis of deglacial laminated sediments from East Antarctica, Leventer et al. (2006), further developed this model to propose that the deposition of laminae was linked to the formation of calving bay re-entrants, as the ice sheet retreated. Calving bay re-entrants form when ice retreats more rapidly over deep troughs (e.g. Domack et al., 2006) and the formation of calving bays could stimulate high productivity and sedimentation by concentrating meltwater run-off into the calving bay (Leventer et al., 2006; Fig. 6.4). While the cross-shelf troughs at South Georgia are shallower than Antarctic shelf troughs and do not have the same reverse slopes, I propose that they

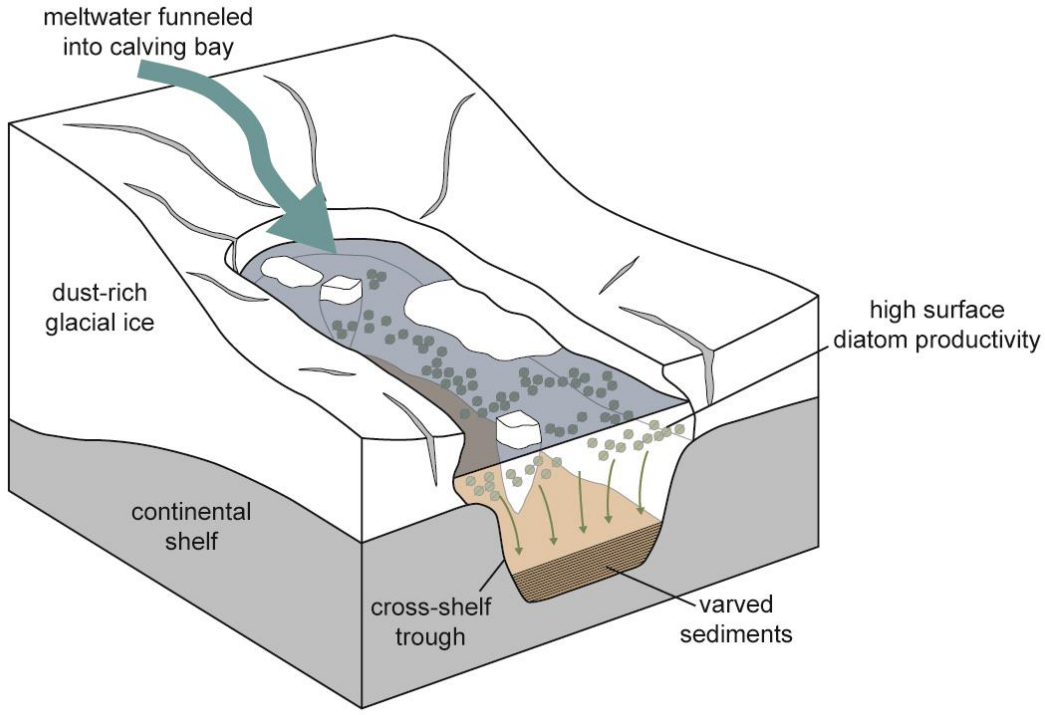


Figure 6.4 Calving bay re-entrant model
Glacial meltwater is concentrated in the restricted bay, leading to extreme spring productivity. More terrigenous material is deposited during the summer and autumn. Redrawn from Leventer et al. (2006).

could still have led to the formation of calving bay re-entrants by allowing the ingress of warm oceanic water under the ice sheet, resulting in a more rapid retreat over the cross-shelf troughs at South Georgia. Therefore, the laminated sediments found in Unit 1 from core GC666 may represent the formation of calving bay re-entrants as the extensive South Georgia LGM ice-sheet retreated. The laminated sediments sampled in this core may only represent the final stages of this style of deposition, with Graham et al. (2017) hypothesising that laminated sediments could extend to a depth of 20 m below the sea floor, based on their analysis of acoustic sub-bottom profile data.

However, *Chaetoceros* dominated laminated sediments from the Gulf of California (e.g. Sancetta, 1995; Grimm et al., 1996; Pike and Kemp, 1996) illustrate that the presence of such laminae alone cannot be considered proof of ice-proximity. For example, the conditions required to trigger the formation of *Chaetoceros* blooms could also have been formed by off-shore winds on the lee-side of South Georgia causing coastal upwelling and resulting in buoyant surface conditions, without the requirement for melt-water input. Further evidence for ice proximity comes from the high accumulation rate of sediment >250 μm in diameter indicating that the terrigenous laminae are composed of ice-rafted material, with deposition of >250 μm grains being an order of magnitude higher in the laminated section, compared to the rest of the core (Fig. 5.2). The accumulation rate of sediment grains >63 μm in diameter is also high in this section of the core, but does not exceed levels recorded later in the deglacial.

Alternatively, the preservation of laminae may indicate that anoxic conditions were present in the bottom water/sediment, inhibiting the benthic activity that would destroy the lamination through bioturbation (e.g. Sturdivant et al., 2012). The development of anoxia could be a result of high productivity and carbon flux, with the degradation of organic matter resulting in low oxygen levels. Reduced oxygen conditions are often held to be a requirement for the preservation of laminae, however the formation of ungrazed diatom mats has been found to have the potential to overwhelm the benthos and result in laminae preservation in oxic environments (Pike and Kemp, 1999). Where the formation of diatom mats capable of restricting benthic activity have been reported the diatom assemblage comprises *Thalassiothrix longissimima* (Kemp and Baldauf, 1993; Boden and Backman, 1996; Pike and Kemp, 1999). While *Thalassiothrix* mats have been reported in the Southern Ocean (Quilty et al., 1985), the diatom assemblage in core GC666 is dominated by *Chaetoceros*. *Chaetoceros* have been shown to aggregate at the end of blooms and the setae can mat in a similar way to *Thalassiothrix* (Alldredge et al., 1993; Grimm et al., 1997), provided

vegetative spores are also present, but whether these aggregations could inhibit benthic activity is unclear.

Variation in the pattern of lamination

The nature of the lamination at GC666 is not consistent throughout the 3 m that contain laminae. Between 816 and 654 cmcd the lamination is nearly continuous, although the structures are disturbed in the final core section below approximately 750 cmcd, potentially due to disturbance during the coring process. Preliminary counting of the laminae in the undisturbed sequence (between 727 and 654 cmcd) indicates that the number of couplets may not be inconsistent with the deposition being varved (69 couplets in 81 cm, with a modelled age of ca. 100 years), but more detailed analysis of the laminae and additional radiocarbon dates bracketing the section containing the undisturbed laminae would be required to further support this. Above 654 cmcd there are sections of continuously laminated sediment interspersed with unlaminated or non-continuously laminated sections which become more dominant as core depth decreases. The continuously laminated section of the core is the most consistent with deposition under conditions generated in a calving bay re-entrant.

Dating of the moraine formed in the mouth of Cumberland Bay indicates that the South Georgia ice sheet had retreated at least to the mouth of the fjords when these continuously laminated sediments were being deposited (Graham et al., 2017), assuming that the ice sheet behaviour is consistent across the shelf and that the moraine in the mouth of Royal Bay was deposited at a similar time. The age of the moraine in Cumberland Bay was used to support the hypothesis that all of the South Georgia ice sheet retreated rapidly after the LGM (Graham et al., 2017). I propose that, rather than the whole ice sheet retreating rapidly, those areas over the cross-shelf troughs retreated but grounded ice was retained on the shallower shelf areas until ca. 15.0 cal. kyr BP. Minimum estimates for deglaciation from lake and peat cores in Stromness Bay and Cumberland Bay (ca. 10.9–9.2 kyr BP (Van der Putten et al., 2004; Van der Putten and Verbruggen, 2005); at 7.5 kyr BP (Rosqvist and Schuber, 2003)) indicate that ice may have been present on land after it had retreated into the fjords, potentially supporting the hypothesis that ice retreated more rapidly over the deeper troughs. The period of more intermittent lamination in core GC666 represents this final retreat from the shallower shelf areas.

However, there is also evidence for terrestrial early deglaciation, in Stromness Bay, South Georgia (approximately 60 km north-west of GC666 - see Fig. 1.1), based on the onset of lacustrine sedimentation at 18.6 kyr BP

(Rosqvist et al., 1999). One possible explanation for this discrepancy could be that the ice sheet responded differently at the two locations, retreating on land faster at Stromness Bay relative to Royal Bay, although the two bays are only separated by ~60 km suggesting that it would be unlikely that the speed of ice retreat would have been markedly different. It is possible that the basal date from the lake analysed by Rosqvist et al. (1999) actually represents the onset of organic sedimentation rather than deglaciation, as proposed by Bentley et al. (2007). Alternatively, the radiocarbon ages of Rosqvist et al. (1999) may be incorrect, although Bentley et al. (2007) reject this possibility on the basis that the dates come from a well dated lake core with several consistent dates and a robust age model. The hypothesis that ice retreated over the troughs first could be tested by collecting cores from the shallower shelf areas between the cross-shelf troughs, or from terrestrial locations in Royal Bay, and dating the onset of sedimentation in these areas, and comparing it to the dates reported by Graham et al. (2017).

6.2.1.2 Productivity between 15.2 and 14.7 cal. kyr BP

A number of proxies from core GC666 indicate that productivity was exceptionally high during the period in which laminated sediments were deposited (15.2−14.7 cal. kyr BP) (Fig. 6.1). Accumulation rates of benthic foraminifera (BFAR), biogenic silica (BSi AR), and organic carbon (C_{org} AR) can all be interpreted as indicative of changes in primary productivity (Conley, 1988; Herguera and Berger, 1991; Herguera, 1992; Schoepfer et al., 2015). All three of these accumulation rates are high during this period, with BSi AR and C_{org} AR an order of magnitude higher than after 14.7 cal. kyr BP. In particular, the extremely high levels of biogenic silica support the hypothesis that diatom productivity was especially high. While BFAR from samples in the laminated section of the core is not as different from samples after 14.7 cal. kyr BP, in comparison to BSi AR and C_{org} AR in the same samples, the dominance of *F. fusiformis* in the foraminiferal assemblage from these samples can also be indicative of high productivity, in association with ice-proximal conditions (e.g. Ishman and Sperling, 2002; Szymcek et al., 2007; Majewski and Anderson, 2009; Kilfeather et al., 2011). The difference between BFAR, in comparison to BSi AR and C_{org} AR may be due to the high flux of organic matter to the sea floor adversely affecting the preservation potential of the thinly calcified *F. fusiformis* tests (with this species being the main driver of BFAR in the cores studied here), by increasing the corrosivity of the pore and bottom water chemistry.

The higher $\delta^{13}C_{org}$ values recorded during the period of laminae deposition may also support the high productivity hypothesis; higher $\delta^{13}C_{org}$ can be interpreted as reflecting increased surface productivity that increases carbon utilisation, resulting in higher $\delta^{13}C_{DIC}$ in the surface water carbon reservoir (relative to periods of low productivity), with these relatively high values then recorded in the $\delta^{13}C_{org}$ of the organic matter exported to the sea-floor. This interpretation is a function of the preferential uptake of ^{12}C by photosynthetic organisms. It is, however, important to note that other factors, such as a change in the proportion of terrestrial carbon, can impact $\delta^{13}C_{org}$, in addition to productivity changes (see Section 2.2.4). For example, the high flux of terrigenous sediment hypothesised to generate the clastic component of the laminae could alter the C:N ratio, if this influx contained terrestrially sourced carbon. There is no shift towards more terrestrial values in either $\delta^{13}C_{org}$ or C:N, suggesting that this terrigenous sediment does not contain significant, or significantly different, amounts of terrestrial carbon, which is unsurprising as South Georgia would have been heavily glaciated, restricting the production of terrestrial carbon (all GC666 samples from the deglacial period plot within the

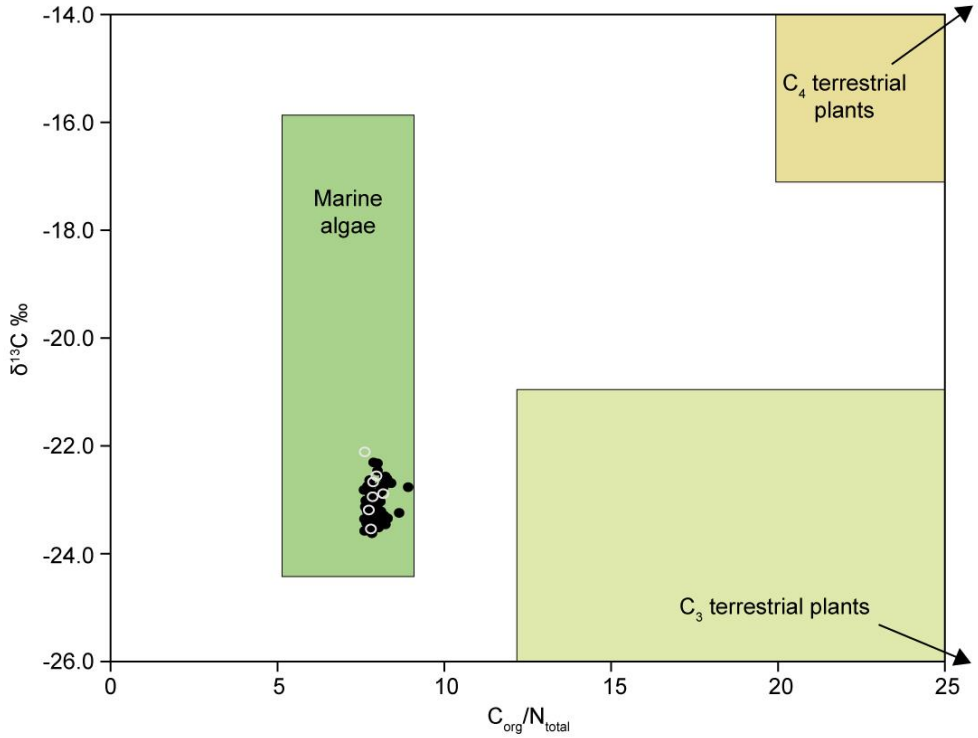


Figure 6.5 $\delta^{13}C_{org}$ vs C:N
Typical $\delta^{13}C$ and C:N ranges for some inputs to coastal environments (simplified from Lamb et al., 2006). Deglacial values from GC666 plotted (black closed = samples from non-laminated core section; grey open circles = samples from laminated core section), showing that all these samples plot within the range expected for marine algae

values expected for marine algae - Fig. 6.5). The negative $\delta^{13}C_{foram}$ from both planktonic and benthic foraminifera in samples above Unit 1 may also provide evidence that productivity was particularly high in Unit 1. As discussed in Section 5.2.7.3, possible diagenetic alteration of foraminifera, as evidenced by discolouration and overgrowth of the tests (Fig. 5.2), could have been caused by biogenic methane generated by the rapid burial of organic rich sediments in Unit 1.

6.2.2 The ACR at South Georgia (14.7−12.9 cal. kyr BP)

The ACR is well-documented in Antarctic ice-cores (e.g. Stenni et al., 2010), occurring between approximately 14.5 and 12.8 kyr BP (Putnam et al., 2010). Evidence from marine cores expands the geographical extent of the ACR to the mid-latitudes of the Southern Hemisphere (e.g. Bianchi and Gersonde, 2004; Lamy et al., 2004; Barker et al., 2009), as do terrestrial records of glacial advance at this time from, for example, New Zealand (Putnam et al., 2010), Patagonia (Kilian and Lamy, 2012), and the Kerguelen Islands (Jomelli et al., 2017) (Fig. 6.6). The ACR is considered to be an expression of the bi-polar seesaw, with two possible mechanisms leading to this north-south antiphasing (Putnam et al., 2010). Strengthening of North Atlantic overturning during the warm Bølling/Allerød (B-A) interstadial could have increased northward heat transport across the equatorial Atlantic, resulting in a cooler Southern Ocean (Liu et al., 2009), although it is unclear how this cooling would be spread from southern mid-latitudes to Antarctic ice-core sites (Putnam et al., 2010). Alternatively, the latitudinal migration of global wind-belts may have been the driving mechanism, with warm conditions in the Northern Hemisphere during the B-A shifting wind-belts in both hemispheres northwards (Toggweiler et al., 2006; Denton et al., 2010). A northward shift in the Southern Hemisphere Westerly Winds (SWW) could result in a more northerly location for the sub-tropical front (e.g. Bard and Rickaby, 2009; Sikes et al., 2009; Denton et al., 2010) and a reduction in upwelling (Anderson et al., 2009), leading to a larger, cooler Southern Ocean and to the ACR (Putnam et al., 2010). The literature regarding the ACR has been reviewed in more detail in Sections 1.3.1 and 1.4.1.

On South Georgia a glacial re-advance during deglaciation was proposed by Clapperton et al. (1989) and this is supported by recent work by Graham et al. (2017), indicating that glaciers re-advanced to the fjord mouth in at least one fjord (Cumberland Bay). The presence of similarly located moraines in many of the fjords of South Georgia (Hodgson et al., 2014b) suggests that this re-advance occurred across the island, as do the outermost terrestrial moraines dated to 12.2±1.5 kyr BP by Bentley et al. (2007). Furthermore, Rosqvist et al.

(1999) identified a period of cooling at South Georgia between 14.8 and 14.2 kyr BP, that was accompanied by wetter conditions. This combination of cooler and wetter climate may have provided ideal conditions for glacial advance at South Georgia (Graham et al., 2017).

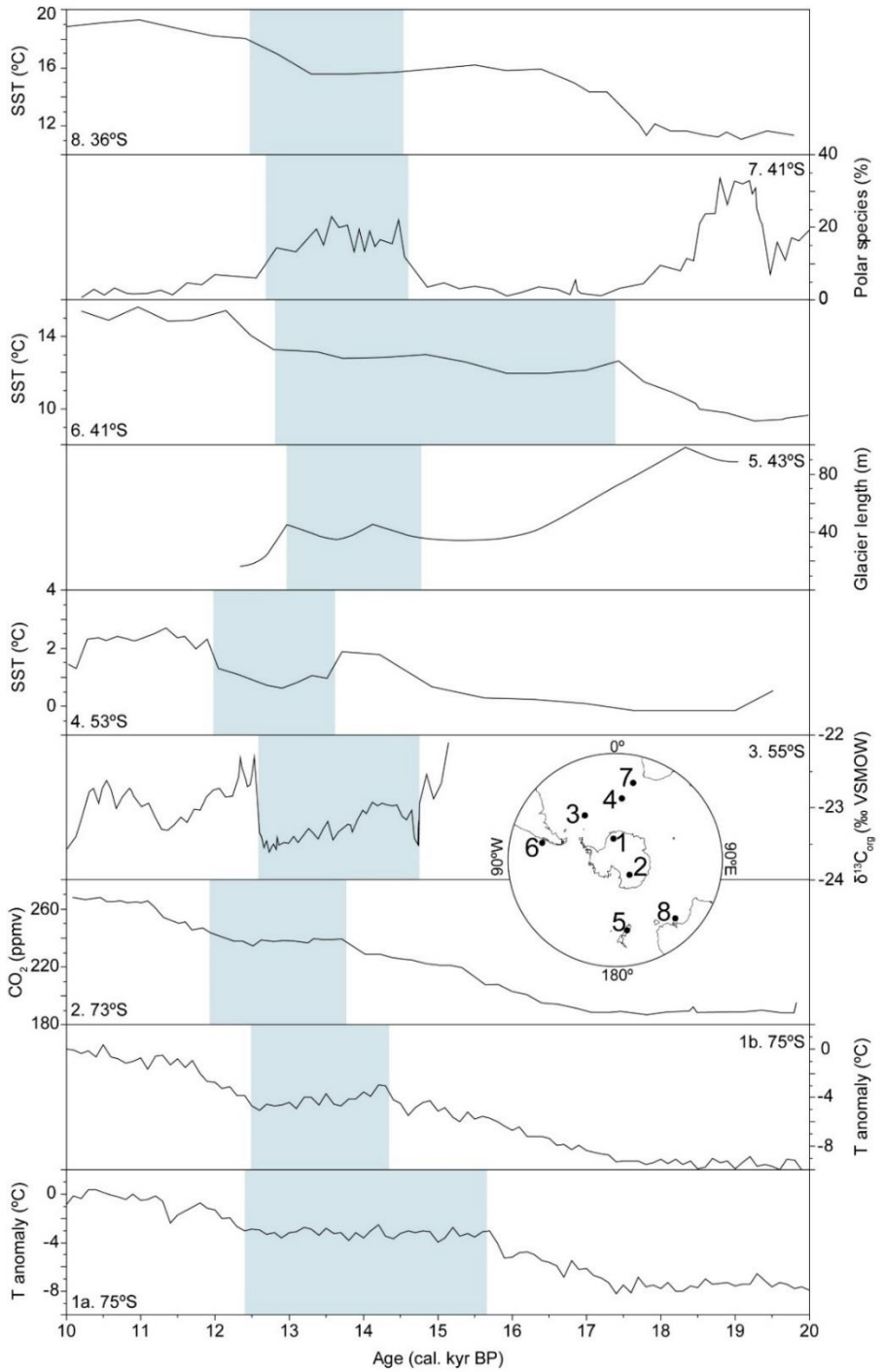


Figure 6.6 Comparison of the ACR extent, arranged by latitude.
1 - Stenni et al. (2010) (1a - EPICA Dome C, 1b - EPICA Dronning Maud Land), 2 - Monnin et al. (2001), 3 - this study, 4 - Bianchi and Gersonde (2004), 5 - Putnam et al. (2010), 6 - Lamy et al. (2004), 7 - Barker et al. (2009), 8 - Calvo et al. (2007). ACR extent indicated by light blue shaded areas. Records are arranged according to latitude, starting with the most southerly (1) through to the most northerly (8).

The end of laminated sedimentation in core GC666, at ~14.7 cal. kyr BP, is approximately coincident with the recognised onset of the ACR (Putnam et al., 2010) , although there is a large uncertainty associated with the modelled ages through this period (±400 years (2σ)). The change in sediment type is accompanied by a decrease in productivity, based on the lower accumulation rates of benthic foraminifera, biogenic silica, and organic carbon, as well as the lower $\delta^{13}C_{org}$ values. Based on acoustic profiler data that identified a regional break/unconformity, Graham et al. (2017) proposed that there may have been a period of marine erosion in the Royal Bay trough at this time. However, there is little difference in the radiocarbon dates either side of this boundary (see Table 5.1) suggesting that little, if any, material was removed from GC666 during this event. The timing of the changes in productivity and sedimentation suggests that they are linked to ACR cooling, with melting/retreating ice during the deglacial causing high productivity, through in-washed nutrients, which then decreases when the glacial readvance and cooler temperatures reduce glacial meltwater flux. Unfortunately, it is not possible to provide evidence for cooler temperatures at South Georgia, as only two samples analysed for alkenones from the ACR period resulted in SST values (3.1ºC at 13.2 cal. kyr BP, and 2.3ºC at 13.0 cal. kyr BP), and these temperatures are unreliable, given the poor quality of the chromatograms (see Section 5.2.8). Similarly, the only sample from the laminated section for which an SST value was generated (1.5ºC at 15.2 cal. kyr BP) was also from a poor quality chromatogram.

In Section 6.2.1 ice-edge proximity was proposed as a driver of the high productivity and sedimentation in the laminated section of core GC666. Proposed glacial readvance to the fjord mouth during the ACR did not result in similarly high productivity and sedimentation, which may be further evidence that the preservation of ice on the shallow areas of the shelf between the cross-shelf troughs during deglaciation resulted in the conditions required to deposit the laminated sediments. This putative ice-sheet configuration may have then completely retreated during the final stages of deglaciation prior to the ACR, during the period when lamination becomes gradually more intermittent, and was not re-established during the ACR. The inferred more proximal ice-edge during the ACR did not result in increased productivity, which may be due to colder conditions resulting in a smaller spring melt and a reduction in the influence of glacial meltwater at GC666. The continued dominance of the *F. fusiformis* Assemblage through the ACR may indicate that carbon flux to the sea-floor continued to have a strong seasonal component through this period, with this opportunistic taxa able to take advantage of the variable conditions (see

Section 5.2.4.2). This suggests that spring meltwater flux, or melting sea-ice, may still have been an important driver of conditions at GC666 during the ACR, but the greatly reduced productivity and sedimentation rate indicates this influence was much lower than during the preceding deglacial period. The seasonality of primary productivity on the South Georgia shelf could be further investigated through future work analysing diatom assemblages through the core.

For a brief period during the ACR at South Georgia, between 14.0 and 13.6 cal. kyr BP, the accumulation rates of both the 63 μm and >250 μm sediment fractions increase. This increase is accompanied by a slight increase in C:N, after 13.9 cal. kyr BP but there is no change in any of the other key proxies (Fig. 6.1). This increase in the accumulation of coarser sediment might represent a temporary reversal of conditions during the ACR, resulting in increased calving and an increase in sediment delivery. Alternatively, the presence of a large, melting iceberg at GC666 for a prolonged period of time could have delivered the coarse sediment. Both of these mechanisms might be expected to also result in an increase in productivity at GC666, through the supply of micronutrients such as Fe (e.g. Lin et al., 2011), but there is no evidence from the productivity proxies for such an increase. The modelled duration of the coarse sediment deposition would suggest that this coarser sediment was being supplied over a 0.4 kyr period. It is not feasible that a single iceberg would endure for such an extended period of time (e.g. Kubat et al., 2007; Wiersma and Jongma, 2010; Smith, 2011), suggesting that an increase in calving from the Cumberland Bay glacier is a better supported hypothesis. Alternatively, the presence of a melting iceberg could have resulted in an increase in the sedimentation rate at this location, with this increase not being identified by the age model generated here due to the absence of dated horizons within the ACR. The current age model could also mask any increase in the accumulation rates of benthic foraminifera, biogenic silica, and organic carbon, which may also explain why there is no evidence for an associated productivity increase.

6.2.2.1 Post-ACR glacial retreat

The hypothesis that cooler conditions during the ACR reduced the influence of glacial meltwater may be supported by the subsequent response of certain proxies. After 12.9 cal. kyr BP there is a marked increase in the accumulation rates of benthic foraminifera, biogenic silica, and organic carbon, with higher levels continuing for ~0.6 kyr, until ~12.3 cal. kyr BP. There is also a marked increase in $\delta^{13}C_{org}$, although this occurs ~0.3 kyrs after the increase in accumulation rates. The increase in BFAR, BSi AR, C_{org} AR, and $\delta^{13}C_{org}$ suggests

that productivity increased during this period, potentially due to increased meltwater flux increasing water column stratification and/or nutrient supply, as the ACR re-advance retreated. Further support for this hypothesis can be found in the coincident increase in >63 μm accumulation rate, which may indicate an increase in the delivery of glacial sediment. There is however no accompanying increase in the accumulation rate of the >250 μm fraction, which may indicate that the coarser sediment is not being delivered as ice-rafted material. A possible explanation for the difference in the timing between the accumulation rate increases and the increase in $\delta^{13}C_{org}$ may be related to the age model: the position of a radiocarbon dated horizon at 388 cmcd, dated to 12.9 cal. kyr BP (see Table 5.1), may have led to an artificially high sedimentation rate during the 0.3 kyrs preceding the increase in $\delta^{13}C_{org}$. This would artificially increase the accumulation rates but would not affect $\delta^{13}C_{org}$, which could therefore be considered the more robust proxy for productivity, suggesting that the ACR at South Georgia continued until ~12.6 cal. kyr BP, approximately coincident with the accepted end of the ACR at 12. 8 cal. kyr BP (e.g. Putnam et al., 2010) especially when the error associated with the modelled age at this point in the record is ±260 years (2σ). This could be further resolved in future work by an additional radiocarbon dated horizon as close to the change in $\delta^{13}C_{org}$ as possible.

The timing of the onset of this change in conditions at South Georgia is coincident with the onset of the Younger Dryas (YD) stadial, at 12.9 kyr BP (Rasmussen et al., 2006), consistent with the view that post-ACR southern warming was linked to the onset of the YD and the bi-polar see-saw (e.g. Denton et al., 2010) , again with the proviso that the modelled ages have a large associated error (±200 years (2σ)). Comparison of high resolution records from Greenland and Antarctic ice-cores has revealed the tight coupling between Northern and Southern Hemisphere climate anomalies (Barbante et al., 2006), as has work investigating the impact of Dansgaard-Oeschger events in the Southern Hemisphere (Gottschalk et al., 2015). The relatively short duration (0.3 to 0.6 kyr) of the high productivity at South Georgia, in comparison to the duration of the YD (~1.2 kyr - Rasmussen et al. (2006)), may support the hypothesis that this productivity increase was driven by the melt of the ACR glacial advance increasing water column stratification and/or nutrient supply, such that the higher productivity was only maintained while the ice retreated and did not continue for the duration of the YD. As with the transition into the ACR it is not possible to reliably define any change in SST, due to the poor quality of the alkenone data for this period. Four samples for which SSTs have been

calculated from either side of the transition (two before and two after) record comparable SSTs (3.1ºC and 2.3ºC before the transition, and 3.2ºC and 2.6ºC after) suggest that there was no temperature change, but the poor quality of the chromatograms means these SSTs are unreliable.

If the above interpretation is correct and the change in conditions does represent the end of the ACR at South Georgia, the timing of this event is 0.3 to 0.6 kyrs later than that proposed by Graham et al. (2017) at 13.3 kyr BP, based on radiocarbon dating of a change in sedimentation style from glacial to sub-glacial in a moraine core from the mouth of Cumberland Bay. This difference can be partially explained by the different local marine reservoir corrections applied when calibrating the radiocarbon dates, with Graham et al. (2017) using a ΔR of 708±61 yr and this study using a ΔR of 433±41 yr, leading to Graham et al.'s (2017) calibrated dates being approximately 0.3 kyrs older. The ΔR used by Graham et al. (2017) is based on dates from core top sediments from core GC666 while the ΔR used here is based on the dating of surface sediment from box core BC671. As it is possible for the surface sediment to be lost during the gravity coring process, resulting in the core top representing older material than the surface sediment, the date from BC671 may be more reliable, as the box core is more likely to preserve the true surface. Even when the difference in ΔR is taken into account the timing of the end of the ACR proposed here is still 0.1 to 0.4 kyrs later than that proposed by Graham et al. (2017). This may be due to local (within-fjord) differences in the timing of glacier response to post-ACR warming, possibly linked to differences in the shape and size of the fjords, and to differences in the location of the respective cores, with the core analysed by Graham et al. (2017) being more proximal. Alternatively, the differences in the timing between the two studies could be an artefact of the inherent uncertainties in the age modelling process, with an error of approximately ±250 years (2σ) being associated with the ages in this section of the record.

6.2.3 Variation in ACC frontal location

Cooling during the ACR may be in part due to a northward shift in the location of the SWW (e.g. Toggweiler et al., 2006; Denton et al., 2010; Putnam et al., 2010). Changes in the SWW have the potential to impact the Antarctic Circumpolar Current (ACC) and, therefore, the oceanographic conditions at South Georgia, as the island is located directly in the path of the ACC (see Section 1.2). A northward shift in the SWW may result in a similar change in the location of the ACC, potentially altering how the SACCF interacts with the South Georgia shelf (e.g. Oke and England, 2004; Fyfe, 2006; Fyfe and Saenko, 2006; Cai and Cowan, 2007), although the rugged bathymetry of the Scotia Sea may

constrain any latitudinal change in the ACC in the South Georgia region (Whitehouse et al., 2008a). However, the nature of the interaction of the SACCF with the shelf does exhibit interannual and seasonal variability, as illustrated by Boehme et al. (2008) and Young et al. (2014), indicating that there is potential for the location of the SACCF in change, in relation to South Georgia, although it is unclear whether this is linked to SWW variability.

Variation in the interaction of the SACCF with the South Georgia shelf may impact productivity on the shelf, including at GC666: Whitehouse et al. (2008b) found evidence for upwelling in the western sector of the South Georgia shelf where the SACCF met the continental shelf, the location of the highest phytoplankton biomass at the time of their study (January 2005). The relatively high temperature and salinity of the upwelled water mass suggests it may have been Circumpolar Deep Water (CDW), which is also nutrient-rich (e.g. Orsi et al., 1995). Furthermore, Whitehouse et al. (2008b) proposed that the ACC is the source of Fe fuelling the high productivity on the shelf. The nature of the circulation patterns around South Georgia would result in water upwelled in the area identified by Whitehouse et al. (2008b) being unlikely to impact the majority of the shelf, as it would be transported north through the gap between the island and Shag Rocks, and then downstream in the ACC (e.g. Young et al., 2014). The SWW may have migrated northwards during the late Holocene (e.g. Toggweiler et al., 2006; Anderson et al., 2009; Bjorck et al., 2012) so the position of the upwelling identified by Whitehouse et al. (2008b) might be analogous to its position during the ACR. We might therefore expect productivity at GC666 to be lower during the ACR than at other times during the deglacial when the SWW are believed to have been in a more southerly position (e.g. Toggweiler et al., 2006; Anderson et al., 2009; Bjorck et al., 2012), as a more southerly position for the interaction of the SACCF could lead to upwelled water being transported to the northern shelf via the anti-clockwise flow that is commonly present on the shelf (Young et al., 2011b; Young et al., 2014). To test this hypothesis the mean values for the main productivity proxies (BFAR, C_{org} AR, BSi AR, and $\delta^{13}C_{org}$) for the ACR (14.7 to 12.9 cal. kyr BP) and the subsequent deglacial period (12.3 to 10.8 cal. kyr BP), with the period hypothesised to be influenced by post-ACR retreat meltwater excluded (12.9 to 12.3 cal. kyr BP), have been calculated (Fig. 6.7 and Table 6.1). This calculation gives a mixed signal: BFAR and $\delta^{13}C_{org}$ are both lower during the ACR, suggesting lower productivity during this period, C_{org} AR and BSi AR are slightly higher during the ACR.

Table 6.1 Mean values for deglaciation accumulation rates
Mean values for BFAR, C_{org} AR, BSi AR, and $\delta^{13}C_{org}$ (to 3 S.F.) from GC666 during deglaciation.

Age range (cal. kyr BP)	**Classification**	**BFAR** (cm^{-2} kyr^{-1})	**C_{org} AR** (g cm^{-2} kyr^{-1})	**BSi AR** (g cm^{-2} kyr^{-1})	**$\delta^{13}C_{org}$** (‰ VPDB)
15.2 – 14.7	Laminated sediment	23900	4.19	80.8	−22.8
14.7 – 12.9	ACR	5410	0.443	5.82	−23.2
12.9 – 12.3	Post-ACR melt	28300	0.798	10.6	−23.1
12.3 – 10.8	Deglaciation stage 2	8750	0.362	3.25	−22.9

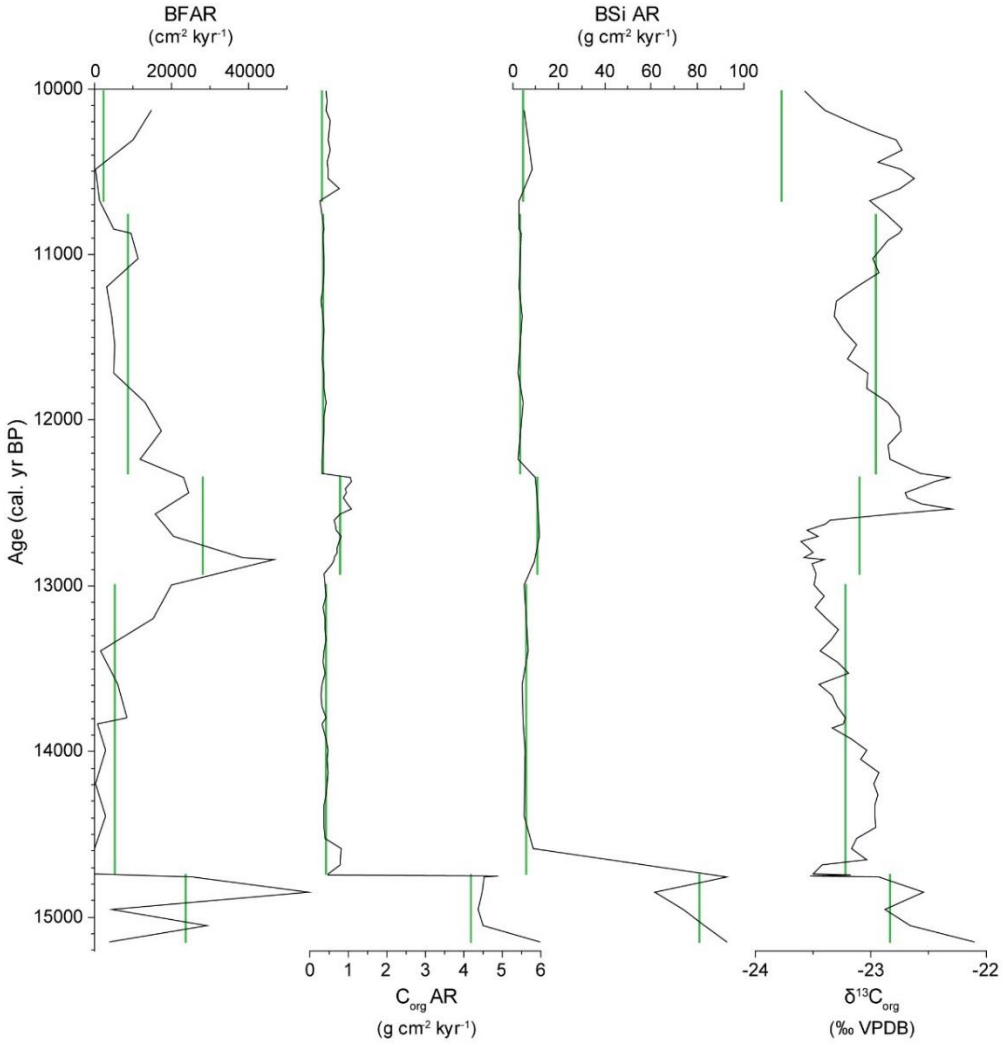


Figure 6.7 Key productivity proxies (15 to 10 cal. kyr BP)
Green lines represent mean values for the different sections of the deglacial: Laminated sediment (15.2-14.7 cal. kyr BP), ACR (14.7-12.9 cal. kyr BP, Post-ACR melt (12.9-12.3 cal. kyr BP), Deglaciation stage 2 (12.3-10.8 cal. kyr BP)

6.3 Summary

This chapter comprised discussion of the evolution of the South Georgia shelf oceanography from 15.2 to 12.3 cal. kyr BP, a record of the latter stages of

the most recent deglaciation. The discussion utilised the multi-proxy records described in Chapter 5, mainly interpreted in terms of changes in primary productivity, and sediment supply.

The earliest part of the record from GC666 (15.2−14.7 cal. kyr BP) represents the final part of the first stage of Southern Hemisphere glaciation, prior to the ACR. This part of the core comprises ~1.6 m of continuously laminated sediment, followed by ~1.5 m where laminae are present but gradually become more intermittent. Based on preliminary diatom assemblage analysis, revealing the dominance of *Chaetoceros*, these laminae are interpreted as being similar to those recorded in Antarctic deglacial sediments (e.g. Leventer et al., 2002; 2006). Productivity (based on $\delta^{13}C_{org}$ and the accumulation rates of benthic foraminifera, organic carbon and biogenic silica) and sedimentation rate are both extremely high during the section of the core containing laminae, relative to the rest of the record. The calving bay re-entrant model for the deposition of this type of lamination (Leventer et al., 2006: Fig. 6.4) is proposed to have generated this sediment sequence. This model is potentially supported by the constraints of the ice-sheet retreat model proposed by Graham et al. (2017) and the proxy response to the ACR advance later in the core.
The gradual transition to completely unlaminated sediments represents the final retreat of the ice sheet from the shallow shelf. The end of lamination is approximately coincident with the established onset of the ACR at 14.5 kyr BP (Putnam et al., 2010). The record of the ACR in GC666 is characterised by relatively low productivity and a decreased sedimentation rate, which are hypothesised to be due to cooler temperatures during this period resulting in decreased influence of glacial meltwater. The ACR at South Georgia continues until 12.9 or 12.6 cal. kyr BP, when there is a marked increase in productivity and sedimentation rate which is interpreted as being due to an increase in glacial meltwater flux, as the ACR advance melts. The variation in the timing of the end of the ACR is due to uncertainty as to whether or not the change in accumulation rates at 12.9 cal. kyr BP is an artefact of the age model, with 12.6 cal. kyr BP being the date at which there is a marked change in $\delta^{13}C_{org}$. The uncertainty about the timing of this event could be resolved with an additional radiocarbon dated horizon at ~350 cmcd. Differences in productivity between the ACR and the final phase of deglaciation at South Georgia are potentially linked to changes in the location of the SACCF, which may be driven by changes to the SWW. However, the evidence for this is mixed and therefore inconclusive.

Chapter 7

Holocene oceanography (~12.3 cal. kyr BP onwards)

7.1 Introduction

This chapter comprises discussion of the evolution of the South Georgia shelf oceanography from ~12.3 cal. kyr BP onwards, utilising the multi-proxy records described in Chapter 5, summarised in Fig. 7.1. These proxy records are interpreted in terms of changes in primary productivity, sediment supply, and sea surface temperature, and are considered in comparison to other palaeoceanographic and palaeoclimatic records from the southern high latitudes, including South Georgia. Palaeo-records from the southern high latitudes and South Georgia are discussed in detail in Sections 1.3 (Southern Hemisphere palaeoclimate and palaeoceanography) and 1.4 (South Georgia palaeoclimate), as are recognised Holocene climate events and their potential driving mechanisms. This chapter will discuss the multiproxy record from ~12.3 cal. kyr BP, initially focussing on core GC666, which is at high resolution and has a well resolved age model, followed by discussion of whether core GC673 supports the initial GC666-based interpretation, or supports alternative hypotheses. Potential mechanisms behind the variability recorded at South Georgia are proposed and these mechanisms are compared to those proposed for other high southern latitude records, to assess whether these new records can help to further understand climate forcing in the Southern Hemisphere.

7.2 South Georgia shelf productivity during the Holocene

Between 12.9 to 12.3 cal. kyr BP, the multiproxy records from core GC666 show higher productivity and increased deposition of coarser sediment, which is interpreted as reflecting increased nutrient availability and sediment supply as the glacial advance associated with the Antarctic Cold Reversal retreats (discussed in Section 6.2.2). Based on visual analysis I have divided the subsequent record from GC666 into four sections: the earliest Holocene (12.3 to 10.8 cal. kyr BP), the early Holocene (10.8 to 7.6 cal. kyr BP), the mid-Holocene (7.6 to 3.0 cal. kyr BP), and the late Holocene (3.0 cal. kyr BP onwards). The Holocene is often divided into early, mid-, and late periods but the dates for these divisions is variable. Although broadly similar the dates used here do differ from the formal division of the Holocene, which defines the Early Holocene as 11.7 to 8.3 cal. kyr BP, the Mid-Holocene as 8.3 to 4.3 cal. kyr BP, and the Late

Holocene as 4.3 cal. kyr BP onwards (Gibbard, 2018). To distinguish the divisions used here from these formal divisions the Holocene prefixes are not capitalised, in keeping with standard geological practice. In this section I will discuss the interpretation of the multiproxy records for each of these sections in turn, compare these records to those from core GC673 and then propose possible forcing mechanisms.

The accumulation rates of benthic foraminifera (BFAR), organic carbon (C_{org} AR), and biogenic silica (BSi AR) are all interpreted as proxies for primary productivity (see Chapter 2). The carbon isotopic composition of organic carbon ($\delta^{13}C_{org}$) can also be used to interpret variation in productivity; lower $\delta^{13}C_{org}$ can be interpreted as reflecting reduced surface productivity that lowers carbon utilisation, resulting in lower $\delta^{13}C_{DIC}$ in the surface water carbon reservoir (relative to periods of high productivity), with these relatively low values then recorded in the $\delta^{13}C_{org}$ of the organic matter exported to the sea-floor. This interpretation is a function of the preferential uptake of ^{12}C by photosynthetic organisms. However, changes in surface $\delta^{13}C_{DIC}$ can also be dependent on the cause of the changes to productivity: for example, if reduced productivity is caused by reduced upwelling then this reduction, in addition to reducing nutrient supply, also reduces the supply of ^{12}C, potentially resulting in no net change in $\delta^{13}C_{DIC}$. Other factors in addition to productivity changes can also impact $\delta^{13}C_{org}$ (see also Section 2.2.4). An increase in the proportion of terrestrial carbon could cause a negative shift in $\delta^{13}C_{org}$, provided that the terrestrial carbon was sourced from plants utilising the C_3 photosynthetic pathway, which usually have $\delta^{13}C$ lower than typical marine algal values (Fig. 7.2).

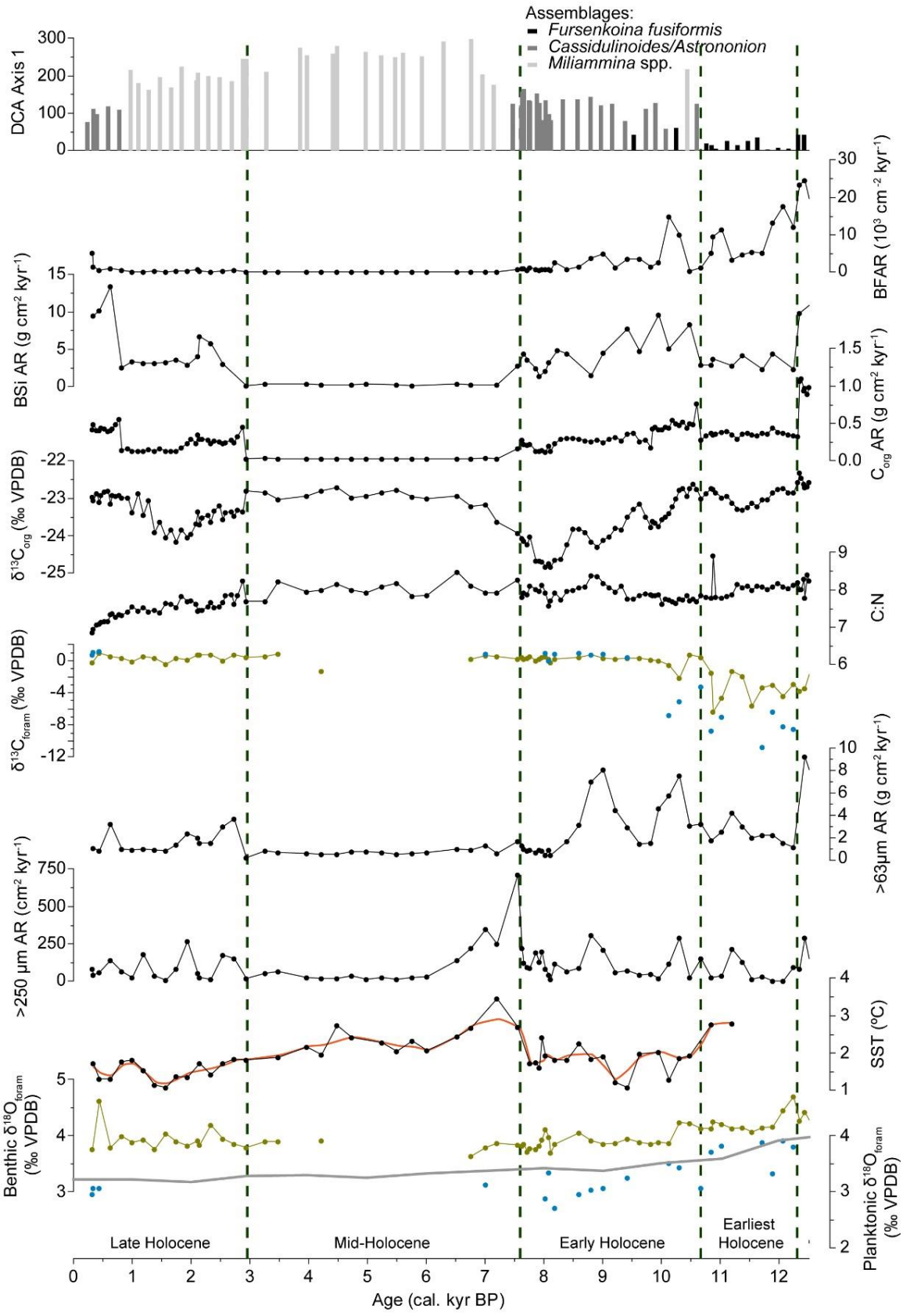


Figure 7.1 Summary of key Holocene proxy records from GC666
Dashed green lines mark the boundary between early mid- and late Holocene. $\delta^{13}C_{foram}$ and $\delta^{18}O_{foram}$ - green points = benthic data, blue points = planktonic data, grey line = LR04 stack (Lisiecki and Raymo, 2005). SST trendline = LOESS (10 %).

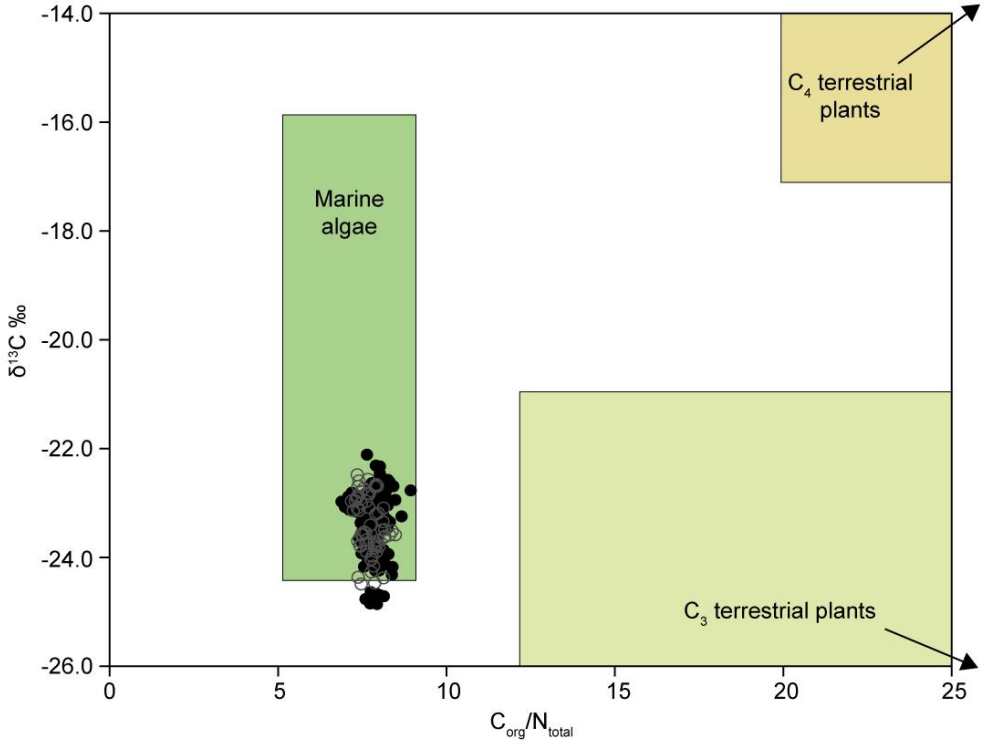


Figure 7.2 $\delta^{13}C_{org}$ vs C:N
Typical $\delta^{13}C$ and C:N ranges for some inputs to coastal environments (simplified from Lamb et al., 2006). GC666 (black closed circles) and GC673 (grey open circles) have also been plotted.

7.2.1 Holocene productivity variability in core GC666

In the earliest Holocene (12.3 to 10.8 cal. kyr BP) interpretation of the productivity signal is complicated, with the individual proxies displaying different responses. Both C_{org} AR and BSi AR were relatively low and stable through this period, while BFAR gradually decreased and $\delta^{13}C_{org}$ initially decreased before increasing again, although the range of variability is small (0.6 ‰) in comparison that seen in the complete record (3.7 ‰). The apparent stability of C_{org} AR and BSi AR may partially be an artefact of changes in sedimentation rate due to the location of radiocarbon dated horizons. A sedimentation rate with smoothed transitions would result in similar pattern of variation to that displayed by $\delta^{13}C_{org}$, with slightly higher productivity at the beginning and end of the earliest Holocene. This suggests that during the earliest Holocene productivity can be interpreted as having been relatively stable, but with a slight decrease centred on ~11.5 cal. kyr BP.

In the transition into the early Holocene, all three accumulation rates show a marked increase, delayed by approximately 200 years in BFAR; $\delta^{13}C_{org}$ is also highest at the start of this period. This is followed by gradually decreasing values in all four proxies until ~8.0 cal. kyr BP, when there is a slight increase in C_{org}

AR, BSi AR, and $\delta^{13}C_{org}$. During the early Holocene there is a significant positive correlation between pairs of $\delta^{13}C_{org}$, BFAR, BSi AR and C_{org} AR (with the exception of BFAR and BSi AR – Table 7.1). The strength of the correlation varies considerably but is strongest between C_{org} AR and BSi AR, and between C_{org} AR and $\delta^{13}C_{org}$. The common trends in all four proxies indicates that productivity peaked at the start of the early Holocene, before gradually decreasing and then starting to increase again after ~8.0 cal. kyr BP.

Table 7.1 Early Holocene linear correlation (r) values
Linear correlation r values (below the shaded cells) and p values (above the shaded cells; $p<0.05$ considered significant) for $\delta^{13}C_{org}$, BFAR, BSi AR and C_{org} AR from GC666 during the early Holocene (~10.8 and 7.6 cal. kyr BP).

	BFAR	**C_{org} AR**	**BSi AR**	**$\delta^{13}C_{org}$**
BFAR		<0.01	0.56	0.03
C_{org} AR	0.46		<0.01	<0.01
BSi AR	0.16	0.82		0.02
$\delta^{13}C_{org}$	0.44	0.82	0.60	

The mid-Holocene was characterised by very low accumulation rates of benthic foraminifera, biogenic silica, and organic carbon, increasing then stable $\delta^{13}C_{org}$, and the dominance of BFA by the *Miliammina* Assemblage (Fig. 7.1). The very low BFAR, BSi AR, and C_{org} AR, which strongly correlate through this period (Table. 7.2), are potentially indicative of low productivity throughout the mid-Holocene. However, between ~6.5 and 3.0 cal. kyr BP, $\delta^{13}C_{org}$ is comparable to that recorded during the productivity peak in the early Holocene, suggesting productivity was higher during this period. While there was a significant positive correlation between $\delta^{13}C_{org}$ and BFAR, C_{org} AR, and BSi AR during the early Holocene (Table. 7.1), during the mid-Holocene a significant strong negative correlation is found between $\delta^{13}C_{org}$ and these accumulation rates (Table 7.2), which is inconsistent with lower productivity during the mid-Holocene. However, this is assuming there is no change in the source of organic carbon, which may not be valid (see below).

Table 7.2 Mid-Holocene linear correlation (r) values
Linear correlation (r) values (below the shaded cells) and p values (above the shaded cells) for $\delta^{13}C_{org}$, BFAR, BSi AR and C_{org} AR from GC666 during the mid-Holocene (~7.6 to 3.0 cal. kyr BP).

	BFAR	**C_{org} AR**	**BSi AR**	**$\delta^{13}C_{org}$**
BFAR		<0.01	<0.01	<0.01
C_{org} AR	0.99		<0.01	<0.01
BSi AR	0.99	0.99		<0.01
$\delta^{13}C_{org}$	–0.76	–0.72	–0.74	

The inconsistencies between the four proxies complicate the interpretation of the productivity signal during the mid-Holocene. One possibility is that the $\delta^{13}C_{org}$ was not reflecting productivity changes during this time, with the higher $\delta^{13}C_{org}$ potentially due to a change in the terrestrial or marine organic carbon source, or by the re-working of older carbon. Variation in the proportion of terrestrial carbon could alter $\delta^{13}C_{org}$, with either a decrease in terrestrial input from C_3 plants, or an increase from C_4 plants, potentially increasing $\delta^{13}C_{org}$. During the mid-Holocene C:N values are slightly higher which may indicate an increase in terrestrial input, although the difference relative to the rest of the Holocene is small and the higher C:N values are still within the range observed for marine algae (Fig. 7.2). The addition of a small amount of terrestrial carbon from C_4 plants with high $\delta^{13}C_{org}$ and relatively low C:N (within the range possible for plants utilising the C_4 pathway) could generate the observed variation in $\delta^{13}C_{org}$ and C:N. However, the present day and palaeo floral assemblages on South Georgia do not include any utilising the C_4 pathway, based on data in the TRY database (Kattge et al., 2011). This is perhaps unsurprising as plants utilising the C_4 pathway are generally those adapted to heat, drought, and/or high salinity (e.g. Sage, 2004). The higher $\delta^{13}C_{org}$ values, if not due to higher productivity, could be caused by a decrease in terrestrial input and C_3 sourced carbon, a hypothesis potentially supported by the low sedimentation rates during the mid-Holocene. However, this is not supported by any decrease in the estimated marine percentage of C_{org} (Fig. 7.3) and the heavily glaciated nature of South Georgia may preclude the development of significant terrestrial vegetation and large variation in the input of terrestrially sourced carbon.

Alternatively, a change in the dominant phytoplankton group could result in a change in marine-sourced $\delta^{13}C_{org}$. Although diatoms are the dominant phytoplankton in the modern South Georgia system (over 80% of biomass - Korb et al., 2005) and appear to be abundant through much of core GC666, the lower BSi AR during the mid-Holocene might be indicative of a phytoplankton change during this period. However, laboratory experiments indicate that $\delta^{13}C$ from phytoplankton groups other than diatoms (e.g. dinoflagellates, coccolithophores, green algae and golden algae) is more negative (Wong and Sackett, 1978). A change to one of these groups being the dominant phytoplankton might be expected to result in a decrease in $\delta^{13}C_{org}$, rather than the observed increase. Another possible cause of increased $\delta^{13}C_{org}$ during lower productivity is the introduction, via re-working, of old carbon with higher $\delta^{13}C_{org}$. The relative stability of $\delta^{13}C_{org}$ between 6.5 and 2.9 cal. kyr BP (−29.9±0.1‰)

could be evidence for the carbon having been reworked with the isotopic signal becoming homogenised.

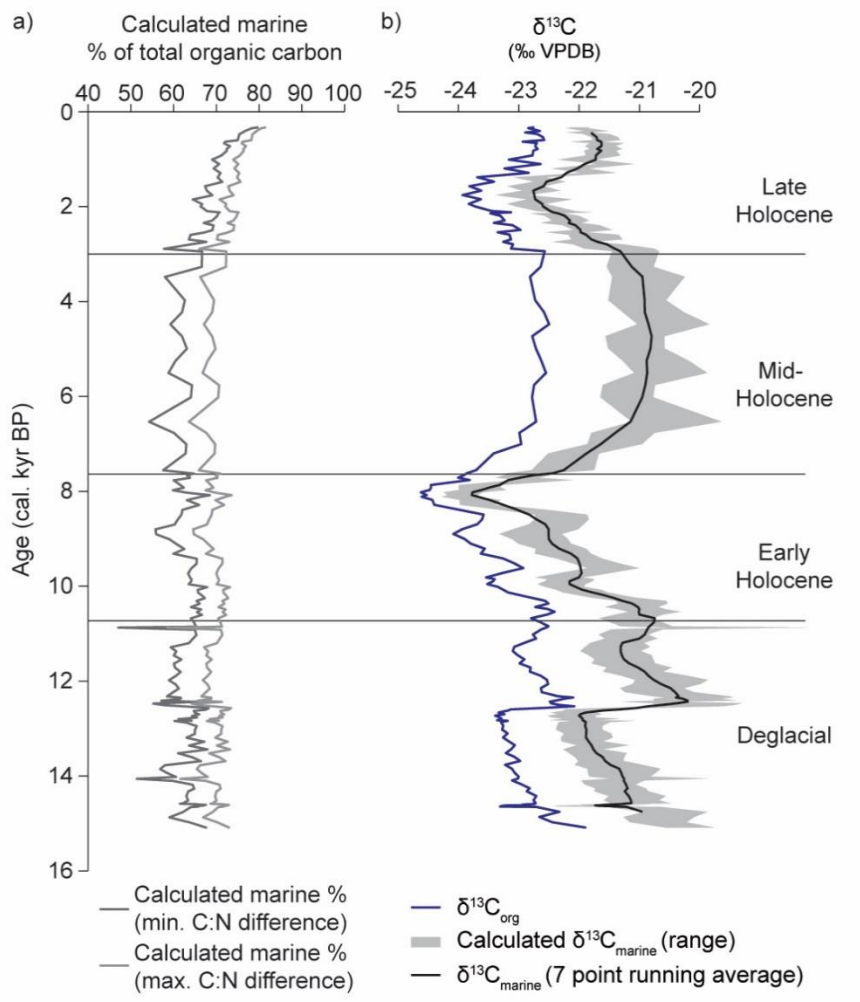


Figure 7.3 GC666 marine percentage of bulk organic carbon
GC666 calculated marine percentage of bulk organic carbon and calculated $\delta^{13}C_{marine}$.

Conversely, if the higher $\delta^{13}C_{org}$ values are considered to be indicative of increased productivity, the low accumulation rates of benthic foraminifera, biogenic silica, and organic carbon could be explained by diagenetic alteration (in the form of dissolution) of the original signal, linked to the very low sedimentation rate during the mid-Holocene. These diagenetic changes are not related to those recorded in the deglacial part of the record, caused by methane activity (Section 5.2.1.1). Changes to BFA during the mid-Holocene may support this hypothesis, with the dominance of the agglutinated taxa *Miliammina* spp. indicating this may be a dissolution assemblage. *Miliammina* spp. are resistant to corrosion and the absence of almost all calcareous taxa throughout much of the mid-Holocene may be due to the low sedimentation rate causing the calcareous fauna to be exposed to slightly corrosive bottom water for longer periods of

time, potentially supported by the observation that *absolute* abundance of *Miliammina* spp. remains relatively stable through the mid-Holocene (Fig. 7.4). High *Miliammina* spp. abundance has previously been interpreted as indicative of high productivity changing the chemistry of bottom and pore waters through increased decomposition of organic matter, causing the local carbonate compensation depth to shallow (Li et al., 2000; Majewski and Anderson, 2009; Melis and Salvi, 2009); the low sedimentation rate could accentuate this effect.

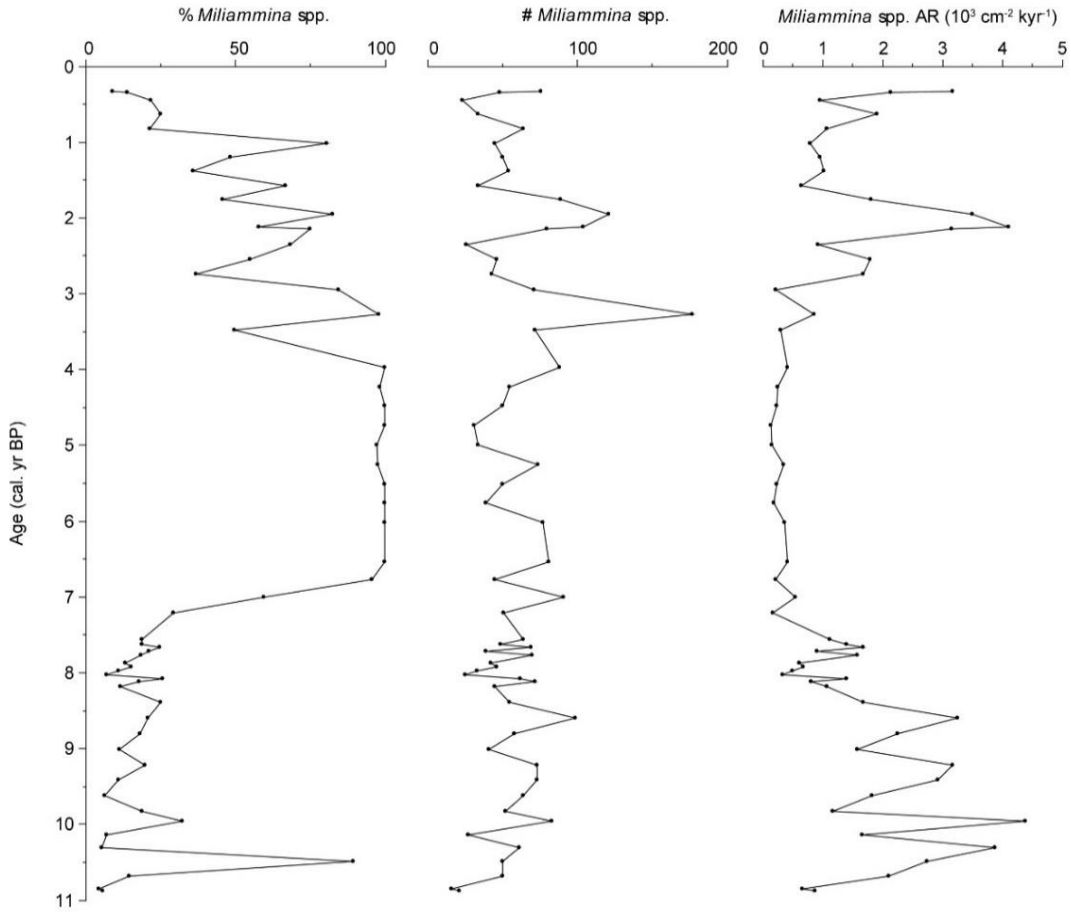


Figure 7.4 GC666 *Miliammina* spp. properties
Comparison of GC666 *Miliammina* spp. relative abundance, absolute abundance and accumulation rate over the past 11 kyr.

The proposed dissolution process that altered the benthic foraminiferal fossil assemblages could have also reduced the amount of organic carbon being preserved. At the same time, the low sedimentation rate could have prolonged access to this carbon for shallow infauna, further reducing preservation. However, anoxic conditions generated by high productivity can also *enhance* the preservation of C_{org} and slow microbial degradation (e.g. Ingall et al., 1993). Whether the same corrosivity could have reduced the biogenic silica (mainly in the form of diatoms) is unclear, but it is possible it could impact diatom preservation. Delayed preservation can also affect $\delta^{13}C_{org}$ values, through the

preferential degradation of more labile marine carbon, increasing the influence of terrestrial carbon on the $\delta^{13}C_{org}$ composition. There is no evidence from C:N ratios, or the calculated terrestrial % of C_{org}, for a shift towards more terrestrially sourced carbon, or for the preferential mineralisation of organic N, known to occur during anoxic conditions triggered by high productivity (e.g. Macko et al., 1993; Koron et al., 2015).

During the late Holocene, as in the early Holocene, there are positive correlations between pairs of $\delta^{13}C_{org}$, BFAR, BSi AR and C_{org} AR, all of which are statistically significant, with the exception of BSi AR with $\delta^{13}C_{org}$ (Table 7.3). These proxies indicate that productivity was highest at the beginning of this period, then gradually decreased to ~1.5 cal. kyr BP before increasing again through the rest of the late Holocene.

In summary, productivity was relatively high and stable during the earliest Holocene, before gradually decreasing through the early Holocene. Given the complexity of the proxy record from the mid-Holocene, it is not possible with the existing dataset to finally conclude that productivity increased, decreased, or even changed at all, during the mid-Holocene. However, if the $\delta^{13}C_{org}$ was not affected by changes in carbon source, this proxy indicates that productivity increased until ~6.5 cal. kyr BP and then remained stable at this level until the late Holocene. The late Holocene was characterised by variable productivity, highest in the early and late part of this period, with lower productivity centred on ~1.5 cal. kyr BP.

Table 7.3 Late Holocene linear correlation (r) values
Linear correlation (r) values (below the shaded cells) and p values (above the shaded cells) for $\delta^{13}C_{org}$, BFAR, BSi AR and C_{org} AR from GC666 during the late Holocene (~3.0 cal. kyr BP onwards). Values highlighted in red do not display a statistically significant correlation ($p < 0.05$).

	BFAR	**C_{org} AR**	**BSi AR**	**$\delta^{13}C_{org}$**
BFAR		<0.01	<0.01	0.03
C_{org} AR	0.84		<0.01	<0.01
BSi AR	0.71	0.89		0.06
$\delta^{13}C_{org}$	0.59	0.57	0.53	

7.2.2 Holocene productivity variability in core GC673

In order to compare the data from core GC666 with that from the second core, GC673, the proxies presented in the GC666 summary figure (Fig. 7.1) are plotted for both cores, for the past 10.0 cal. kyr BP (Fig. 7.5). The broad scale patterns of change in benthic foraminiferal assemblage, $\delta^{13}C_{foram}$, $\delta^{18}O_{foram}$, and the accumulation rates of benthic foraminifera, biogenic silica, organic carbon,

and >250 μm clasts show similarities between the two cores. I will discuss the proxy changes considering the same temporal divides as I applied to GC666. The earliest Holocene is not sampled by GC673, and the early Holocene only extends to 9.6 cal. kyr BP.

As in core GC666, during the early Holocene BFAR, C_{org} AR, and BSi AR were all highest in the earlier part of this period, before gradually decreasing, suggesting that productivity followed a similar pattern to that observed in GC666. However, $\delta^{13}C_{org}$, unlike in core GC666, does not follow the same trend, remaining stable through the early Holocene except for lower values between 8.7 and 8.4 cal. kyr BP. During the mid-Holocene BFAR, C_{org} AR, and BSi AR continue to decrease until ~6.5 cal. kyr BP and then remain low for the rest of this period, potentially indicating that productivity was low at this time. As in GC666, there is a disconnect between the trends in the accumulation rates during the mid-Holocene and those in $\delta^{13}C_{org}$, which increases slightly between 7.6 and ~6.0 cal. kyr BP, remaining at this level until ~4.0 cal. kyr BP, when in $\delta^{13}C_{org}$ decreases slightly towards the end of the mid-Holocene. The higher $\delta^{13}C_{org}$ between 6.0 and 4.0 cal. kyr BP may be indicative of higher productivity at this time, provided the carbon source did not change. As in core GC666, all samples from GC673 plot within the range expected for marine algae (Fig. 7.2) and there is little evidence for a large shift to more terrestrial input (Fig. 7.6). The lower sedimentation rate in GC673 during the mid-Holocene and the increased dominance of *Miliammina* spp. may indicate that the low accumulation rates are an artefact of dissolution and diagenetic alteration, as has been proposed to occur in core GC666 (see Sections 5.2.7.3 and 7.2.1). In the late Holocene BFAR, C_{org} AR, and BSi AR remain low until ca. 1.4 cal. kyr BP when there is a sharp increase, which is likely to be an artefact of the age model due to the position of a radiocarbon dated sample at this point. Unaffected by artificial changes in sedimentation rate, $\delta^{13}C_{org}$ increases through the first part on the late Holocene, peaking at ~1.5 cal. kyr BP, before decreasing slightly through the remaining period.

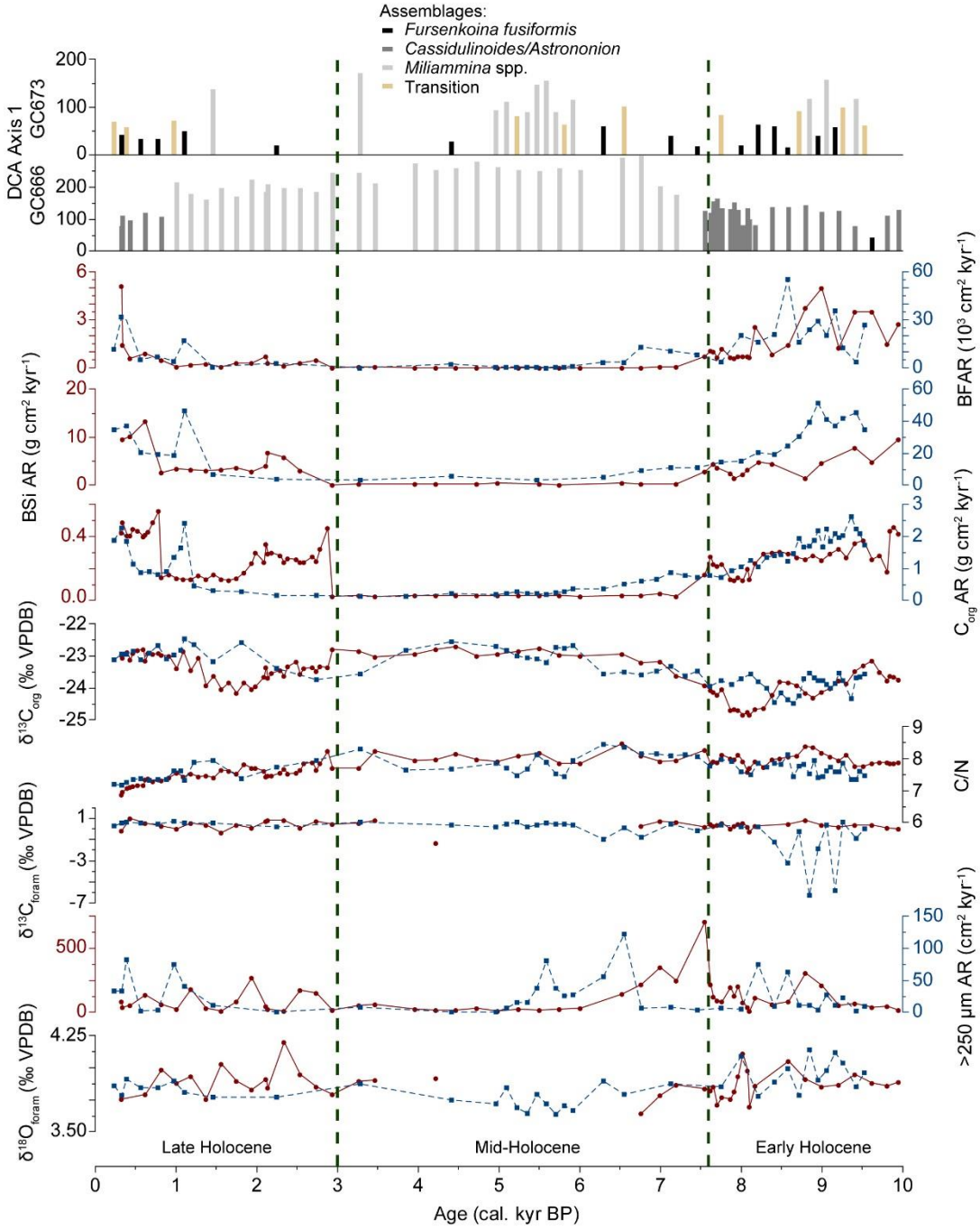


Figure 7.5 Key Holocene proxy records comparing GC666 and GC673
Red lines and circle symbols = GC666, Blue dashed lines and square symbols = GC673. Note the different scales used for BFAR, BSi AR, Corg AR and >250µm AR.

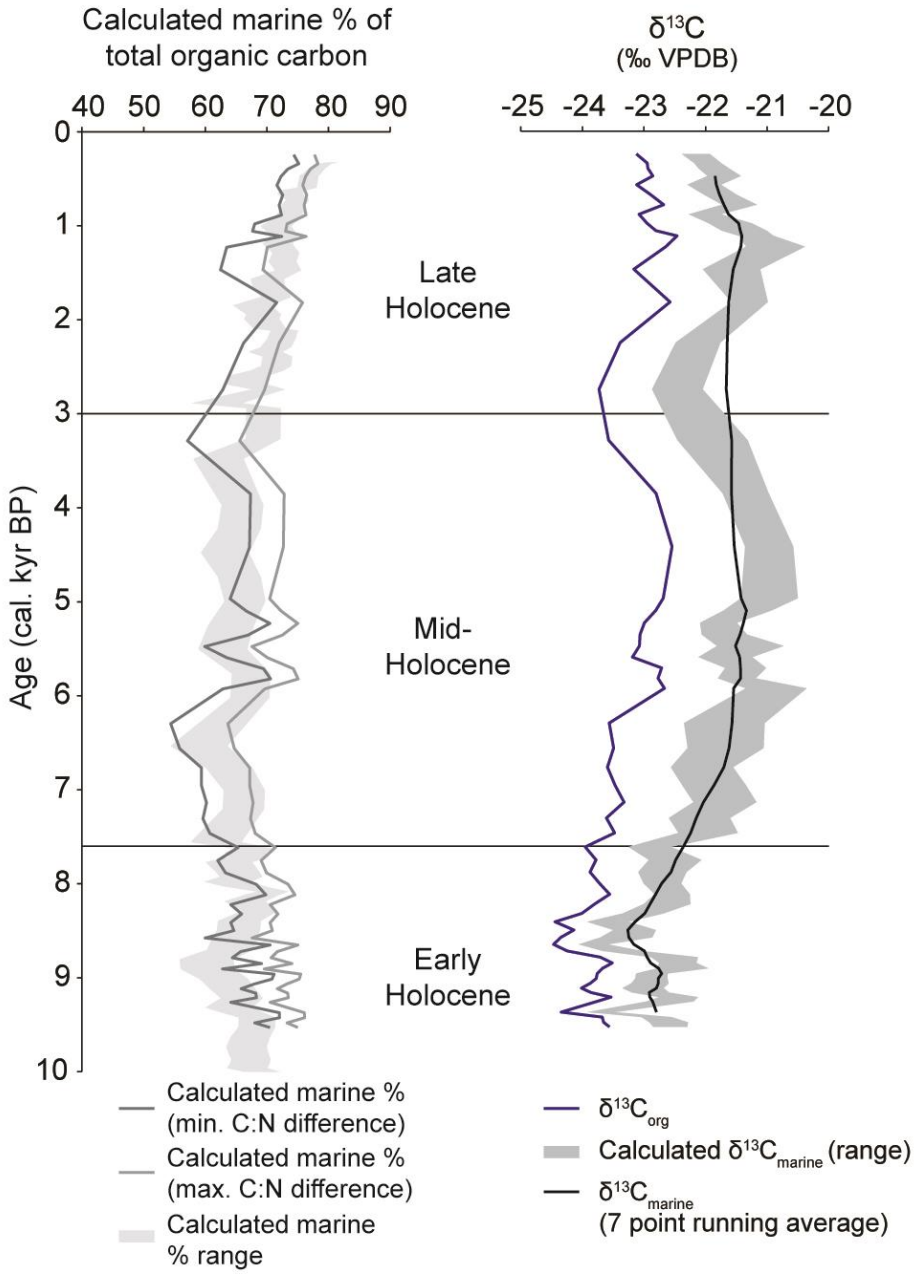


Figure 7.6 GC673 marine percentage of bulk organic carbon
GC673 calculated marine percentage of bulk organic carbon and calculated $\delta^{13}C_{marine}$.

There are some similarities in the patterns of change in BFAR, BSi AR, and C_{org} AR between the two cores, with higher levels in the early and late Holocene and lower in the mid-Holocene. However, while the patterns of change are broadly similar they are not synchronous. Higher ARs were maintained until ~6.0 cal. kyr BP in core GC673, in comparison to ~7.5 cal. kyr BP in core GC666, and low ARs continued deeper into the late Holocene (~1.5 cal. kyr BP) in core GC673 (~2.9 cal. kyr BP in core GC666). Furthermore, unlike in much of core GC666, the patterns of change in accumulation rates in GC673 are not supported

by changes in $\delta^{13}C_{org}$. Part of the reason for the differences between the cores, and the lack of correlation between the accumulation rates and $\delta^{13}C_{org}$, may be the much less well resolved age model of core GC673, leading to inaccuracies in the accumulation rates.

It is therefore difficult to make any strong conclusions about the magnitude and timing of productivity changes in core GC673. It is apparent that productivity is consistently higher at GC673, in comparison to GC666, as illustrated when the three accumulation rates are plotted together at the same scale (Fig. 7.7). The large negative $\delta^{13}C_{foram}$ excursions in core GC673 during the early Holocene may also be indicative of very high productivity, either at this time or in the proceeding period that has not been sampled by this core, generating biogenic methane and resulting in negative $\delta^{13}C_{foram}$ excursions (discussed in Section 5.2.7.3 Diagenetic Alteration). That productivity is higher in GC673 is also supported by the abundance of *F. fusiformis* throughout most of the core, comprising in excess of 25% of the total assemblage in over 80% of the samples analysed (compared to exceeding 25% in 4% of samples from

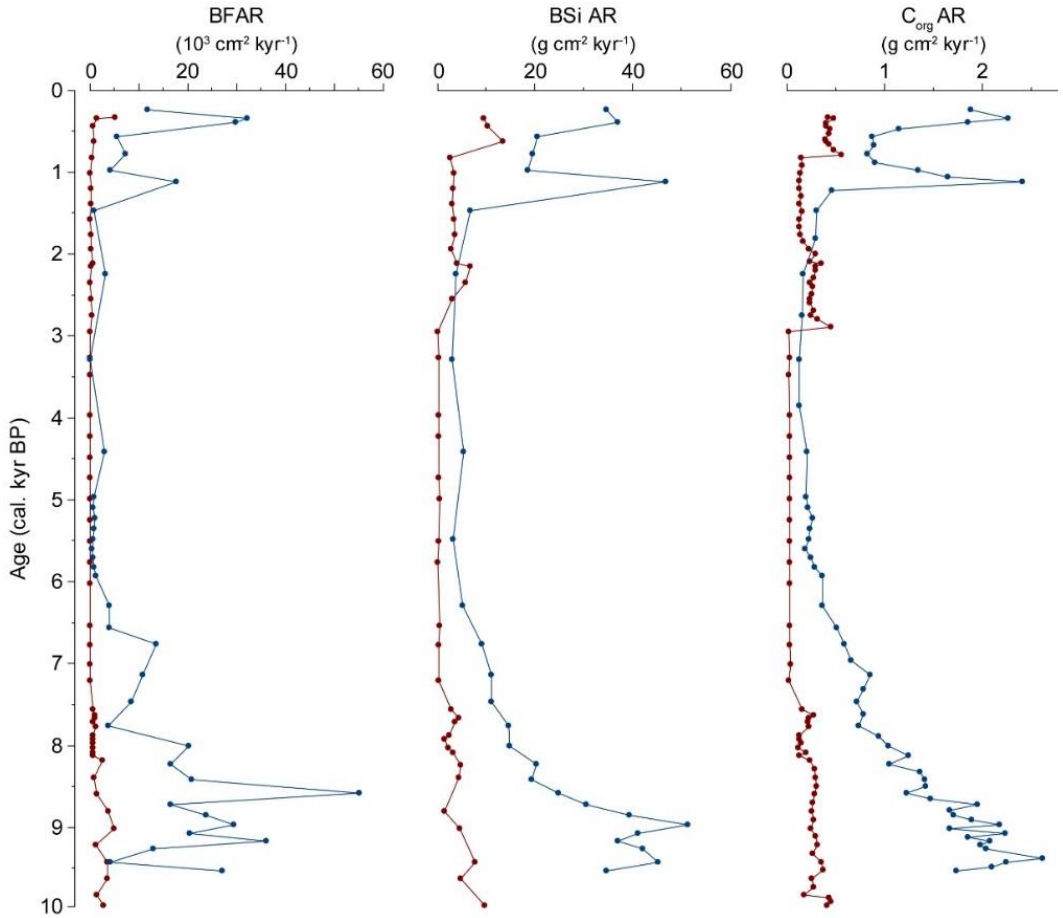


Figure 7.7 Accumulation rate comparisons
BFAR, BSi AR, C_{org} AR from GC666 and GC673 through the Holocene, plotted at the same scale for comparison. Red lines = GC666, Blue lines = GC673.

GC666 for the same time period (9.5 to 0.2 cal. kyr BP)). As discussed previously, *F. fusiformis* is considered to be indicative of high productivity (see Section 5.2.4.2). If $\delta^{13}C_{org}$ is considered to be the more robust proxy for productivity (as it is not affected uncertainties in the sedimentation rate or by potential dissolution effects), there may be less productivity variability at GC673, where $\delta^{13}C_{org}$ ranges from −24.5 ‰ to −22.5 ‰, in comparison to GC666, where $\delta^{13}C_{org}$ ranges from −24.8 ‰ to −22.1 ‰.

7.3 South Georgia shelf oceanography forcing mechanisms

There are a number of factors that can affect primary productivity in marine environments including: nutrient availability (linked to, for example, changes in upwelling, meltwater flux, and/or wind-blown dust), temperature, and sea-ice proximity. Of these factors the main drivers of productivity in high latitude nearshore environments are nutrient availability and/or sea-ice proximity.

7.3.1 Sea-ice proximity

In the previous chapter the importance of meltwater flux as a driver of productivity during deglaciation was discussed and the trend towards decreasing productivity during the early Holocene may have been linked to the final stages of retreat from the Last Glacial Maximum (LGM). Meltwater may be enriched in nutrients such as Fe and DSi via accumulation from atmospheric deposition and by glacial scouring of the underlying geology. Recent work has shown that glacial meltwater, in addition to shelf sediments, can be an important source of DSi and Fe to shelf waters at South Georgia (Schlosser et al., 2017) and on the AP (e.g. Nolting et al., 1991; Loscher et al., 1997; Schlosser et al., 2017). Silicate has been found to be the only macronutrient at growth-limiting levels in the waters around South Georgia (Whitehouse et al., 1996; 2000). Korb and Whitehouse (2004) have discussed the importance of Fe to primary productivity in this area, as do Whitehouse et al. (2008b), although they infer the Antarctic Circumpolar Current (ACC) as the Fe source. Schlosser et al. (2017) also found that surface water maxima of particulate Fe at Cumberland Bay, South Georgia, had a meltwater source which decreased rapidly with increased distance from the coast, which may explain the consistently higher productivity recorded in core GC673. Estimates of surface chlorophyll-a concentration (derived from satellite generated SeaWiFS data) interpreted as showing higher productivity on the South Georgia shelf closer to land (Korb et al., 2004) may support the hypothesis that terrestrially-sourced nutrients are stimulating shelf productivity, although the cross-shelf gradient varies both interannually and seasonally,

potentially linked to nutrients introduced to the South Georgia system by the Southern Antarctic Circumpolar Current Front (SACCF) (Korb et al., 2004).

Due to the rapid retreat of the South Georgia ice sheet (Graham et al., 2017) by the early Holocene meltwater flux may not have been as important a factor in driving productivity on the shelf, compared to the earliest Holocene. This is supported by the lower productivity at GC666 during the early Holocene, relative to the deglacial period. Instead, variation in the influence of sea-ice at South Georgia during the early Holocene may have driven shelf productivity, with this influence gradually decreasing through the early Holocene. Diatom assemblage data has not yet been generated for core GC666 and there is therefore not a direct proxy for sea-ice extent in this record. However, BSi AR (a proxy for diatom abundance) increases after ~10.5 cal. kyr BP before gradually decreasing through the rest of the early Holocene, which may be indirect evidence for increased sea-ice proximity stimulating diatom productivity. There is evidence from diatom sea-ice proxies for decreasing winter sea-ice through the early Holocene at similar latitudes in the Atlantic sector of the Southern Ocean, from open ocean locations (Bianchi and Gersonde, 2004; Xiao et al., 2016).

At high latitudes a prolonged sea-ice season has been implicated in reducing productivity in Antarctic palaeo-records, through light limitation (e.g. Denis et al., 2009). However, sea-ice at lower latitudes, such as South Georgia, is less likely to persist into the growing season. Increased stratification as ice melts in the marginal ice zone could stimulate productivity by stabilising the water column and prolonging the period phytoplankton and nutrients remain in the photic zone (e.g. Korb et al., 2005; Vernet et al., 2008). Evidence for this mechanism has been reported from both open ocean settings (e.g. Korb et al., 2005) and shelf environments, with, for example, Vernet et al. (2008) proposing that primary productivity on the modern western AP shelf is associated with sea-ice retreat forming a shallow summer mixed layer. In an open ocean setting Korb et al. (2005) reported that sea-ice melt-related stratification approximately doubled surface chlorophyll-a values relative to other areas in the Scotia Sea (~2 mg m^{-3} compared to ≤1 mg m^{-3}). On the western AP shelf primary production was approximately double in onshore areas (500-750 mgC m^{-2} d^{-1}), where sea-ice melt has a greater influence, relative to more offshore areas (250-400 mgC m^{-2} d^{-1}) (Vernet et al., 2008). While stratification of the water column could reduce mixing and potentially decrease nutrient availability, in a system with high nutrient availability stratification enhances nutrient availability by prolonging nutrient, and phytoplankton, retention in the photic zone. The

presence of a shallow, well-mixed, nutrient-rich surface layer has been reported from modern South Georgia on the northern shelf (Brandon et al., 1999; Whitehouse et al., 2008b). The increased stratification that forms part of the mechanism that generates high productivity in the marginal sea-ice zone can be generated by other mechanisms such as the influx of low-density glacial meltwater (e.g. Dierssen et al., 2002) or coastal upwelling driven by offshore winds.

If productivity in the early Holocene at GC666 is driven by sea-ice proximity it is unclear why higher productivity would be maintained to a later date at GC673 as this site is further north, and therefore potentially further from any sea-ice effect. It is possible that, given the proximity of GC673 to the mouth of Cumberland Bay, sea-ice forming in the fjord may have influenced productivity at this site. However, Holocene SSTs from GC666 are warmest between ~7.5 and 6.0 cal. kyr BP, potentially precluding sea-ice formation during this period.

The higher productivity at GC673, and the smaller range of variability, in comparison to GC666, may be potentially explained by different mechanisms driving productivity at the two sites. Given the greater proximity of GC673 to South Georgia, and the sites location in close to the mouth of Cumberland Bay, this site may be more closely linked to changes in meltwater flux. As Schlosser et al. (2017) have demonstrated Fe concentration on the South Georgia shelf decreases strongly as the distance from land increases, and the same may be true of DSi concentration, if glacial meltwater is the main source. The greater terrestrial influence on GC673 is further supported by the higher sedimentation rates recorded in this core. However, the C:N values from GC673 plot in the same area of C:N/$\delta^{13}C_{org}$ space as those from GC666 (Fig. 7.2) and do not provide any evidence that terrestrial influence was greater at this site, nor do they show any variation that would support a change in terrestrial influence during the mid-Holocene, although the heavily glaciated nature of Cumberland Bay, up to the present day, may preclude the development of terrestrial vegetation thus negating the use of C:N as a proxy for variation in terrestrial input. Additionally, the calculated estimate for the percentage of C_{org} that is of marine origin in GC673 is similar to that in GC666 (Fig. 7.6). In GC673 the terrestrial percentage of C_{org} increases slightly during the early Holocene and is highest during the mid-Holocene, the opposite of what might be expected if a reduction in the input of terrestrial-sourced nutrients was driving decreased productivity.

Alternatively, the higher productivity at GC673 throughout the Holocene may be due to baroclinically driven cyclonic circulation, evident from doming of isopycnals and linked to local bathymetry, that results in a mesoscale eddy close to Cumberland Bay (Meredith et al., 2005). Mesoscale eddies have been proposed as a mechanism for increased productivity, through the promotion of upward nutrient supply into the euphotic zone (e.g. Romero et al., 2016). Although Meredith et al. (2005) did not report direct evidence for higher productivity associated with this circulation, they suggested that it may generate enhanced productivity through the retention of nutrients and fresh-water run-off, based on the analysis of a similar circulation on the Prince Edward Islands shelf (Perissinotto and Duncombe Rae, 1990). It is unclear whether this circulation is a transient feature (it was not recorded by Brandon et al. (1999), indicating possible interannual variability) or one that would persist long enough to be incorporated into the palaeo-record. Meredith et al.'s (2005) proposal that it is linked to the local bathymetry suggests it may be a persistent feature. Even if it is consistently present throughout the Holocene, productivity variation at GC673 may still be linked to terrestrial variation, as the circulation could amplify the terrestrial signal. Furthermore, the broad scale agreement in productivity variation between GC666 and GC673 suggests they are not responding to site specific forcings, although the later onset of higher productivity in GC673 during the late Holocene might indicate that this circulation was not established at this time.

7.3.2 Upwelling circumpolar deep water

While sea-ice may have been a forcing mechanism driving productivity during the early Holocene the reconstruction of Xiao et al. (2016) indicates that sea-ice did not extend to South Georgia later in the Holocene, although it may reach this latitude elsewhere in the Southern Ocean. Therefore, other mechanisms are required to explain productivity changes on the South Georgia shelf during the mid- and late Holocene.

One possible mechanism could be variation in the upwelling onto the South Georgia shelf of nutrient-rich Upper Circumpolar Deep Water (UCDW), with a reduction (increase) in the influence of UCDW on the north-eastern shelf potentially resulting in lower (higher) productivity in the records from GC666 and GC673. That UCDW can upwell onto the South Georgia shelf is illustrated by Whitehouse et al. (2008b), who found evidence for upwelling where the SACCF met the continental shelf at the time of their study (January 2005). The upwelled water mass had a higher salinity than the shelf waters, possibly indicating that it was UCDW, and the region of the shelf in which the upwelling occurred also

featured the highest phytoplankton biomasses recorded during their study, potentially linking upwelled nutrient-rich UCDW to shelf productivity. In addition to affecting shelf productivity, upwelling of UCDW onto the shelf could also impact SSTs, with UCDW temperature in the South Atlantic (>3.2ºC; Santoso et al., 2006) being slightly higher than that of the South Georgia shelf waters (2 to 3 ºC; Brandon et al., 1999). This difference could be expected to result in slightly higher SSTs on the South Georgia shelf when productivity increases. This was not the pattern during the early Holocene, when gradually decreasing productivity is accompanied by stable, low SSTs. This disconnect between temperature and productivity may be due to productivity being controlled by sea-ice proximity (see Section 7.3.1). Conversely, there is a correlation between $\delta^{13}C_{org}$ (which may be the most robust productivity proxy from GC666, due to the potential for BFAR, BSi AR, and C_{org} AR to be altered by dissolution) and SST in the late Holocene, potentially supporting the hypothesis that SST and productivity were both driven by variation in CDW upwelling, although this correlation is not significant ($r = 0.53$, $p = 0.061$). In the mid-Holocene SST is higher but the productivity record is difficult to interpret (see Section 7.2.1); if the $\delta^{13}C_{org}$ record is considered to reflect higher productivity then SST and productivity variability during this period may support the CDW upwelling hypothesis. The evidence from GC666 for variation in CDW upwelling driving productivity and SST is therefore mixed, but strongest in the late Holocene.

The upwelling identified by Whitehouse et al. (2008b) occurred in the western sector of the South Georgia shelf where the upwelled water mass is likely to have subsequently been transported north through the gap between the island and Shag Rocks, and then downstream into the ACC (e.g. Young et al., 2014), such that the water mass would not have been transported to GC666. However, as shown by Boehme et al. (2008; Fig. 1.2) and Young et al. (2014), the nature of the interaction of the ACC with the South Georgia shelf is interannually and seasonally variable. If upwelling were to occur further south-east, the upwelled water mass could potentially be transferred to the north-eastern shelf via the anti-clockwise flow that is present on the shelf, evident from both observational data and high resolution modelling (Young et al., 2011a; Young et al., 2014). Different downstream pathways can result from small shifts in the location of the ACC impact on the South Georgia shelf, as can be seen in the differing drifter paths illustrated in Young et al. (2011a).

Changes in the interaction of the ACC with the South Georgia shelf could potentially be driven by changes in the Southern Hemisphere Westerly Winds (SWW; Fig. 7.8; drivers of SWW variability are discussed in Section 7.3.3).

Changes in the location and intensity of the SWW have been proposed to impact the ACC, with a stronger, poleward shifted SWW hypothesised to result in an acceleration and southward shift of the ACC (e.g. Oke and England, 2004; Fyfe, 2006; Fyfe and Saenko, 2006; Cai and Cowan, 2007). However, the coarse resolution models that have generated this hypothesis may be unable to replicate the effects of the pronounced bathymetry that constrains the SACCF in the north-eastern Scotia Sea, as the front approaches and interacts with South Georgia, and the position of the SACCF at South Georgia is likely to be strongly constrained by the underlying bathymetry (Boehme et al., 2008; Whitehouse et al., 2008a). Therefore, there are unlikely to be long-term changes in how the SACCF interacts with the South Georgia shelf and the interannual variation observed in modern shelf water productivity would be averaged over the timescales sampled in the data presented here. Further evidence against CDW upwelling as driver of productivity and SST variability is that there is no evidence for change in the water mass on the shelf (as evidenced by the planktonic $\delta^{13}C$ and $\delta^{18}O$), with no systematic change in either $\delta^{13}C_{foram}$ or $\delta^{18}O_{foram}$ that could be associated with water mass change, through the Holocene.

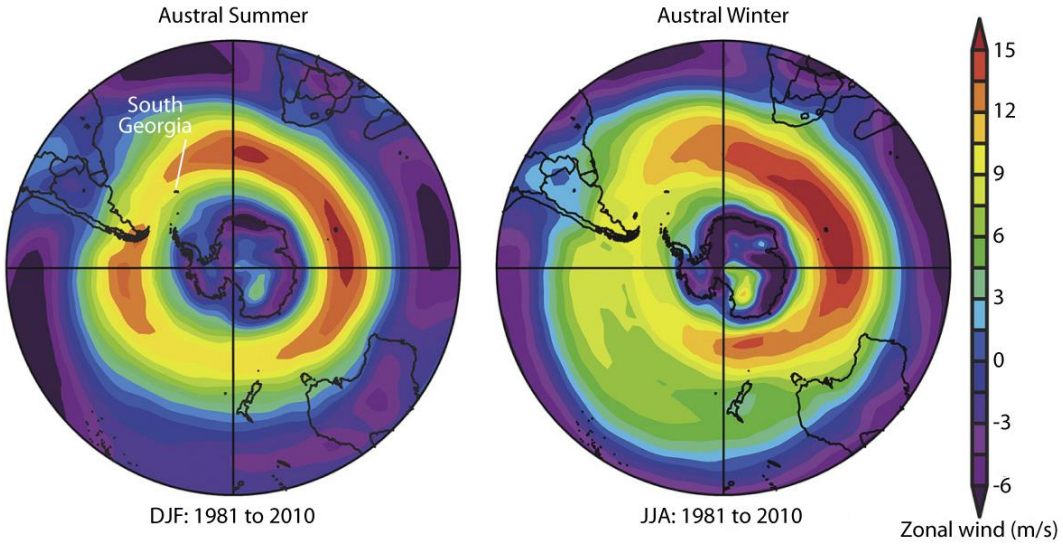


Figure 7.8 Modern SWW extent and seasonal variation
Calculated mean zonal wind strength (m s^{-1}) in summer and winter months 1981 to 2010 based on NCEP/NCAR reanalysis data (Kalnay et al., 1996). Redrawn from Bjorck et al. (2012).

7.3.3 Southern Hemisphere Westerly Wind variability

An alternative mechanism that could have driven both productivity and SST on the South Georgia shelf is variability in the strength and/or position of the SWW, separate to any effect these changes might have had on the ACC. South Georgia's location on the southern edge of the core band of the SWW mean that it may be ideally placed to record such variability. There is a distinct

microclimate on the lee-side of South Georgia, due to the steep orography of the island (e.g. Richards and Tickell, 1968; Brandon et al., 1999). This lee-side microclimate may be sensitive to SWW variability, in part due to the potential for changes in the strength of the SWW to impact the formation of foehn winds. Foehn winds are warm, dry, downslope winds that occur when the approaching wind is sufficiently strong to cause the air mass downwind of the mountain range to ascend, resulting in cooling, condensation, and precipitation which leads to irreversible water loss and latent heating, with increased temperatures transported to the near-surface on the lee-side (e.g. Elvidge and Renfrew, 2016). This suggests that the frequency of foehn events would increase during periods of enhanced SWW strength. However, foehn winds can also form due to 'isentropic drawdown', when winds are too weak for ascent from low levels to occur and the mountains block low-level flow, resulting in the drawdown of higher altitude air that is warmer and drier (e.g. Elvidge and Renfrew, 2016). Therefore, both strengthening and weakening of the SWW at South Georgia have the potential in increase the frequency of foehn events.

The steep orography of South Georgia, combined with the island's position in the path of the SWW, creates ideal conditions for the generation of foehn winds: they are known to be a feature of the climate of the northeast coast of the island and can result in short-term air temperature increases of up to 20ºC (Richards and Tickell, 1968; Stone, 1974; Headland, 1984; Gordon et al., 2008). In addition to the potential for foehn winds to affect temperature, changes in the strength of off-shore winds may result in variability in coastal upwelling. Favourable wind patterns push surface water off-shore allowing the upwelling of more nutrient-rich water into the photic zone, impacting shelf productivity (e.g. Bakun et al., 2010). At South Georgia the importance of wind structure in forcing the surface properties of the surrounding shelf waters has been demonstrated by Hosking et al. (2015), with orography-driven wind disturbances enhancing air-sea heat flux over shelf waters.

If SWW variability was driving South Georgia shelf SST and productivity, the Holocene SST and productivity variability recorded in core GC666 can be interpreted in terms of SWW change. In the following paragraph I discuss the changes in SWW that would be interpreted if stronger winds result in more frequent foehn events, the opposite SWW changes would occur if weaker winds caused higher foehn frequency at South Georgia. During the earliest Holocene (12.3 to 10.8 cal. kyr BP) SST may be higher, suggesting stronger SWW at this latitude. However, the small number of samples (4) that are all calculated from poor quality chromatograms and display a wide SST variability (2.76ºC to

5.63ºC) means that the interpretation of this period as warmer cannot be considered reliable. SSTs during the early Holocene (10.8 to 7.6 cal. kyr BP) are lower, potentially indicative of weaker SWW and lower foehn frequency. Productivity during this period, however, gradually decreases, suggesting that productivity may be disconnected from wind strength at this time: as discussed in Section 7.3.1 productivity decline during the early Holocene may be linked to decreasing sea-ice proximity. Warmer SSTs at the beginning of the mid-Holocene (7.6 to 3.0 cal. kyr BP) could be evidence for stronger SWW, with the gradually decreasing SST representing a decrease in SWW strength. If this interpretation is correct, productivity would also be expected to be higher during the mid-Holocene, indicating that the low BFAR, C_{org} AR, and BSi AR may be artefacts of low sedimentation (see Section 7.2.1) and that $\delta^{13}C_{org}$ is the robust productivity proxy during this period. The glacial advance that peaks at 3.6±1.1 kyr BP (Bentley et al., 2007) is inconsistent with foehn wind-driven higher temperatures. However, this advance occurs when temperatures were decreasing and the advance may represent a period when increased precipitation due to more southerly SWW position/focus combined with low enough temperatures to generate a positive glacier mass balance. During the late Holocene (3.0 cal. kyr BP onwards) there is a correlation between $\delta^{13}C_{org}$ (which may be the most robust productivity proxy from GC666) and SST, although this correlation is not significant ($r = 0.53$, $p = 0.061$). This may indicate that SWW influence at South Georgia was declining to a low centred on ~1.5 cal. kyr BP, before increasing slightly to be similar to the latter part of the mid-Holocene at ~1.0 cal. kyr BP. Bentley et al. (2007) also identified a glacial advance at 1.1 kyr BP, which may be due to a return to the conditions seen in the latter mid-Holocene. In summary, if stronger winds result in higher foehn frequency, the SST and productivity record from GC666 indicates that the SWW were stronger at South Georgia during the earliest Holocene (12.3 to 10.8 cal. kyr BP), weaker during the early Holocene (10.8 to 7.6 cal. kyr BP), strong again at the start of the mid-Holocene (7.6 to 3.0 cal. kyr BP) before gradually weakening through this period and into the late Holocene, and then strengthening again after ~1.5 cal. kyr BP. The opposite pattern of SWW variability would be inferred if weaker winds increase the frequency of foehn events.

Evidence for a similar pattern of SWW variability through the Holocene would support the hypothesis that stronger SWW were driving higher shelf SST and productivity, via increased foehn frequency. Lacustrine and peat records from Isla de los Estados, southern Patagonia (55ºS) have been interpreted in terms of SWW variability (Unkel et al., 2010; Bjorck et al., 2012). These records

were interpreted as showing increased SWW strength between 8.5 and 4.5 cal. kyr BP (Unkel et al., 2010) and between ~7.2 and ~3.5 cal. kyr BP (Bjorck et al., 2012), with the SWW weaker at this latitude in the early and late Holocene, the same pattern of SWW change proposed here. Weakening SWW strength at this latitude during the early Holocene is also supported by the reconstruction by Anderson et al. (2009) in which they propose a northward migration of the SWW, which would result in the core SWW band being further from South Georgia. Further support for this pattern of Holocene SWW variability can be found in the proposed migration of the Brazil-Malvinas Confluence (BMC) in the south western Atlantic, based on the interpretation of changes in $\delta^{18}O$ from planktonic foraminifera linked to water mass change (Voigt et al., 2015). The BMC, which is tightly coupled to the SWW and located north of South Georgia, at ca. 38ºS, migrated southwards during the early Holocene, which could result in the core SWW band being closer to, or over, South Georgia. Subsequent northward migration of the BMC, after ca. 4 kyr BP, peaks at 1.5 kyr BP, coincident with the hypothesised minimum influence of the SWW at South Georgia during the late Holocene. In the earliest Holocene (12.2 to 10.6 cal. kyr BP) Unkel et al. (2010) proposed that the SWW were situated well south of Isla de los Estados; the (potentially unreliable) warmer SSTs at South Georgia at this time would however suggest increased SSW strength. There are two possible explanations for this discrepancy: 1) migration of the SWW is not longitudinally consistent (Fig. 7.9a), 2) the warmer SSTs at South Georgia are not related to foehn winds. Longitudinal variability in SWW would be consistent with modern variability (e.g. Kalnay et al., 1996; Fig. 7.8), in which Isla de los Estados is located more centrally within the core band of the SWW, compared to South Georgia. Alternatively, if the degree of migration was consistent the warmer SSTs at South Georgia could have been caused by increased influence of low latitude, warmer air masses (Fig. 7.9b).

Some of the pattern of SWW variability from Isla de los Estados is also present in records from Campbell Island, New Zealand (52ºS), where McGlone et al. (2010) proposed that SWW influence was stronger between ~9 and ~5 kyr BP, based on their interpretation of pollen-based temperature data. While the data from Isla de los Estados (and, to a lesser extent, Campbell Island) support the pattern of SWW variability hypothesised here, other records present a much different picture. For example, from precipitation proxy records from the west coast of Chile, at ~53ºS, Lamy et al. (2010) proposed that core SWW strength was highest during the early Holocene, until ~8.5 cal. kyr BP, with intermediate conditions present between ~8.5 and ~5.5 cal. kyr BP, and less intense winds

during the late Holocene. Part of the reason for this discrepancy may be the nature of the proxy records used, with Lamy et al. (2010) mainly using precipitation variability as an indirect proxy for the SWW: as Bjorck et al. (2012) utilise direct proxies for wind their interpretation may be more robust. Elsewhere, some Patagonian records appear to indicate a northward expansion/migration of the SWW during the mid-Holocene, for example based on records of glacial advance and retreat (Kaplan et al., 2016) or lake pollen and charcoal records (Moreno and Videla, 2016).

Another mechanism via which changes in the SWW could impact productivity on the South Georgia shelf is through the delivery of aeolian dust. In open ocean regions of the Southern Ocean concentration of micronutrients, such as Fe, may limit productivity (e.g. Martin et al., 1990) and the deposition of aeolian dust is considered to be an important Fe source (Gasso and Stein, 2007; Gabric et al., 2010; Conway et al., 2015). Aeolian dust deposition at South Georgia is estimated to be 1−5 g m^{-2} yr^{-1} (Tegen and Fung, 1995). However, a coupled regional hydrodynamic and biogeochemical model of South Georgia revealed that dust deposition has almost no effect on surface chlorophyll-a concentrations on the South Georgia shelf (Borrione et al., 2014). Additionally, changes in SST driven by SWW variability could drive productivity changes: Korb et al. (2004) reported a correlation between temperature and productivity on the South Georgia shelf. However, the small magnitude of temperature changes recorded in GC666 mean this is unlikely to impact productivity: laboratory experiments have shown that over a much larger temperature change (−1.8 to +4.5ºC) Antarctic phytoplankton increase primary productivity by 30% (Neori and Holm-Hansen, 1982), although in the field temperature effects are harder to quantify (Korb et al., 2004). The potential sensitivity of the South Georgia lee-side microclimate to variability in the SWW means that the SST and productivity record presented here may provide a proxy record for SWW variability at this latitude during the Holocene.

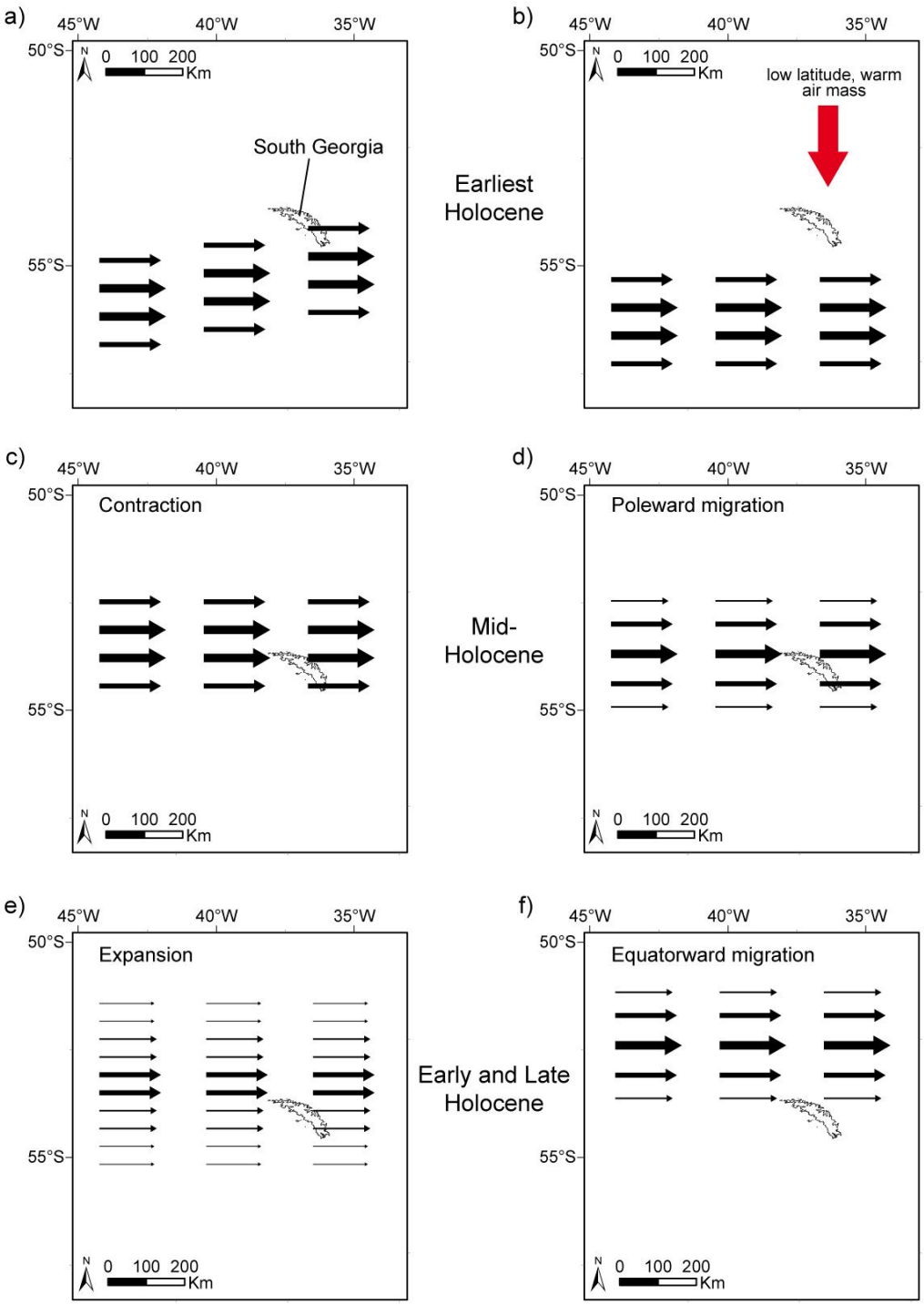


Figure 7.9 Hypothetical variation in the SWW
Simple schematics of possible variation in the position of the SWW in relation to South Georgia. a & b) Hypothetical location of the SWW during the early Holocene climate optimum – a) latitudinal position of SWW varies longitudinally, such that the SWW influence South Georgia but not Isla de los Estado; b) SWW are situated south of South Georgia and the increased SST recorded in GC666 is due to increased influence of warmer low latitude air masses (Bjorck et al., 2012). c & d) Increased SWW intensity at South Georgia during the mid-Holocene – c) SWW contract; d) poleward migration of the SWW. e & f) Reduced SWW intensity at South Georgia during the early and late Holocene – e) SWW expansion; f) equatorward migration of the SWW.

7.3.3.1 Modes of Holocene SWW variability

Changes in SWW strength at a specific location could be due to variability in their intensity/focussing, or meridional migration of the winds, or a combination of both factors. It is not possible to assess whether the SWW shift latitudinally or strengthen using data from a single location; to address this some studies have analysed data across a range of latitudes. For example, using records located in the core and on the northern boundary of the SWW, Lamy et al. (2010) proposed that the main mode of SWW variability through the Holocene was a contraction (with stronger winds in the core band) and expansion (with weaker winds in the core band), analogous to modern seasonal variation (how this could impact South Georgia is illustrated in Figs. 7.9c & 7.9e). These differences are caused by variation in the meridional transport of westerly momentum by transient eddies (Trenberth, 1987), which are in turn driven by meridional SST gradients between mid- and low-latitudes (Gill, 1982). During winter-like conditions, when the temperature gradient is steepest, more eddies form, resulting in greater meridional transport of westerly momentum and more diffuse SWW, with the opposite occurring during summer-like conditions (Lamy et al., 2010). Bjorck et al. (2012) proposed that the mid-Holocene intensification at Isla de los Estados could be the result of increased austral insolation at this time, decreasing the latitudinal SST gradient between mid- and low-latitudes and intensifying the SWW.

Elsewhere, meridional migration of the SWW has been invoked to explain changes in wind strength (Figs. 7.9d & 7.9f). For example, McGlone et al. (2010) proposed that the terrestrial temperature variability they observed at Campbell Island, New Zealand was due to meridional SWW migration, with the SWW south of the island prior to ~9 kyr BP before migrating northwards to more strongly influence the island after ~9 kyr BP. Similarly, Putnam et al. (2010) suggested that glacial advance in the Southern Alps, New Zealand, during the ACR, was related to equator-ward migration of the SWW. Bjorck et al. (2012) also proposed that meridional migration of the SWW drove wind strength variability in the deglacial part of their record, with changes in intensity driving Holocene variability, as do Anderson et al. (2009) in their discussion of variability in the location of Southern Ocean upwelling. The position of SWW may be driven by the index state of the SAM, which is characterised by the difference in atmospheric pressure between the polar cap region (south of 60ºS) and the surrounding zonal ring (centred near 45ºS) (Thompson and Solomon, 2002). In the positive SAM phase, when the pressure difference is higher than normal, the SWW are displaced poleward from their mean position, with the opposite occurring during

the negative phase (Toggweiler et al., 2006). Over the last ~50 years, as the global climate has warmed, there has been a trend towards the positive SAM phase (Thompson and Solomon, 2002), suggesting that the same may have occurred during Holocene warm periods. A southward migration of the SWW, during the mid-Holocene warmth, could have resulted the core band of the SWW having more influence at South Georgia (which is currently on the southern edge of this band). This would have increased the strength of the winds at South Georgia, potentially leading to the stronger foehn winds and the increased SSTs observed at GC666. Alternatively, a poleward migration of the SWW during the mid-Holocene could have resulted in greater influence of lower latitude, warm masses at South Georgia, as proposed by McGlone et al. (2010) as part of the control on temperature at Campbell Island. The positive SAM phase migration of the SWW is also associated with increased northward Ekman drift in the circumpolar ocean, via the intensification of the Westerlies over ca. 60ºS (Hall and Visbeck, 2002). Changes in Ekman transport, related to SWW location and intensity, was proposed by McGlone et al. (2010) to contribute to changes in ocean temperatures in the region of Campbell Island. By increasing northward transport of cool water this might be expected to decrease SSTs at South Georgia: that the opposite pattern of SST change is observed may further support the hypothesis that the SST record from GC666 is primarily driven by foehn wind strength.

7.3.3.2 Drivers of Holocene Southern Hemisphere temperature

Both SAM variability and changes in the temperature gradient between mid and low latitudes in the Southern Hemisphere are driven by changes in the global climate system. A summary of a range of Southern Hemisphere temperature records is presented in Figure 7.10 and the large scale climate processes driving these changes are discussed in this section.

Enhanced freshwater flux from West Antarctic Ice Sheet

Modelling by Mathiot et al. (2013) suggests another possible mechanism that could have caused the early Holocene cooling observed in GC666. They tested the possibility that changes in atmospheric circulation caused the early Holocene cooling observed in Southern Hemisphere palaeo-records (Fig. 1.4) by changing atmospheric meridional heat flow through intensification of the SWW. They found that, while this perturbation of atmospheric circulation generated a cooling of ca. 0.5ºC over Antarctica, atmospheric temperatures over the Southern Ocean increased. Conversely, the simulated impact of enhanced freshwater flux from West Antarctic Ice Sheet (WAIS) generated an appropriate

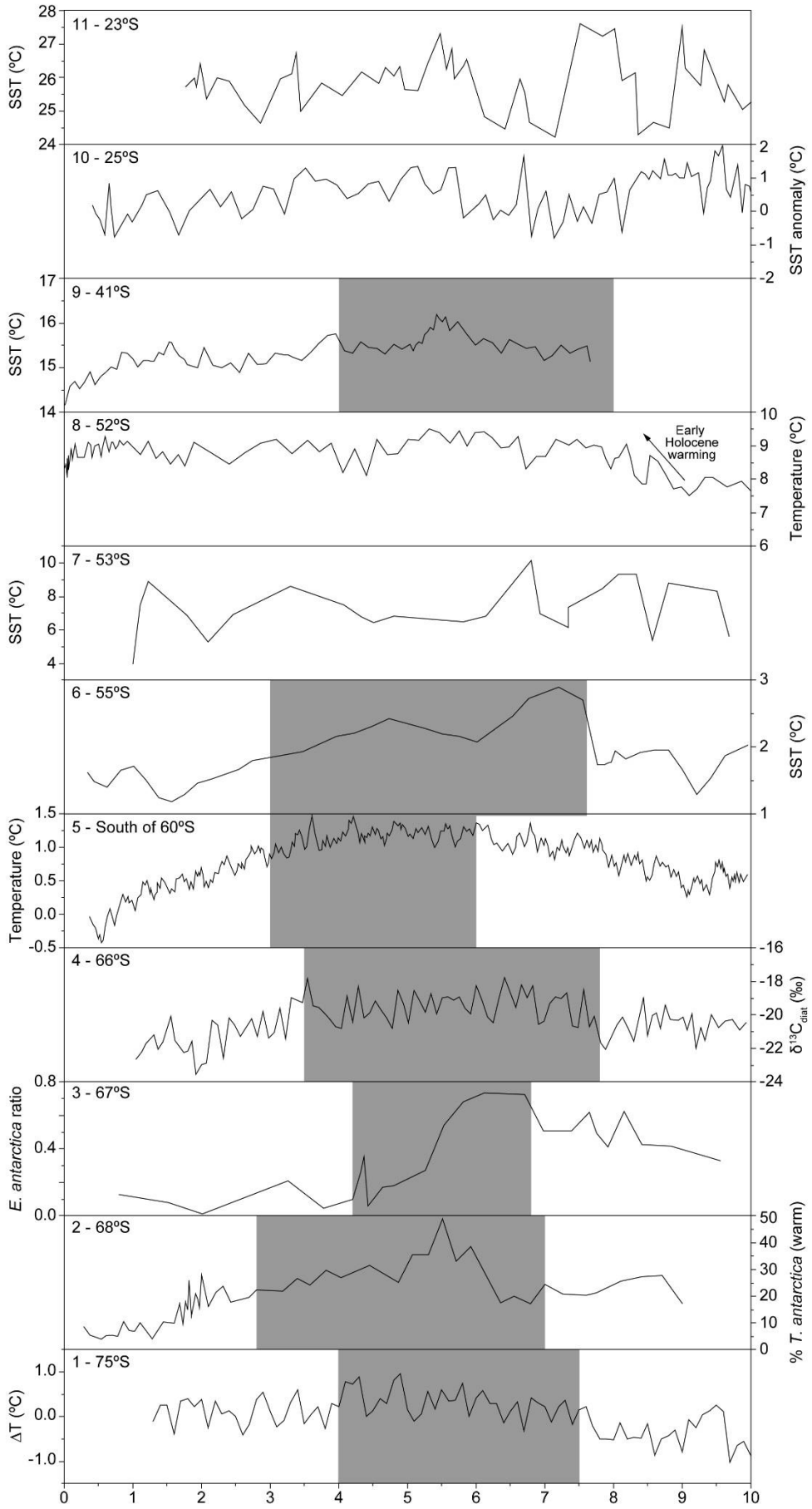
magnitude of cooling over the Southern Ocean (ca. 0.8ºC) but was unable to recreate the observed cooling over Antarctica. When they combined modified atmospheric circulation with enhanced WAIS freshwater flux Mathiot et al. (2013) were able to replicate the observed cooling over both the Southern Ocean (ca. −1.6ºC) and over Antarctica (ca. −0.6ºC), leading them to propose that this combination of mechanisms forced the temperature decrease, with Southern Ocean cooling mainly driven by fresh water release from the WAIS.

Insolation driven temperature change

Southern Hemisphere temperature through the mid- and late Holocene may be driven by changes in spring insolation between 50ºS and 60ºS, which has been linked to decreased austral summer duration (Huybers and Denton, 2008; Shevenell et al., 2011; Xiao et al., 2016; Fig 7.11). After ~5 kyr BP Decreasing temperature through the mid and into the late Holocene is coincident with decreasing spring insolation between 50ºS and 60ºS, which resulted in decreased austral summer duration (Huybers and Denton, 2008; Shevenell et al., 2011; Xiao et al., 2016). Although summer insolation between 50ºS and 60ºS increases after ~7 kyr BP, modelling by Huybers and Denton (2008) has shown that changes in spring insolation have a greater impact on annual temperatures. Variation in spring insolation may therefore be the primary driver of SWW variability during this part of the Holocene, via variation in the latitudinal temperature gradient (causing expansion/contraction) or change in the SAM phase (causing latitudinal migration). The apparent rapid change in conditions at South Georgia after ~7.8 cal. kyr BP may be due to a combination of decreased WAIS freshwater flux and increased spring insolation. While this mechanism may explain SWW variability at South Georgia during the mid-Holocene and into the late Holocene, variability after ~1.5 cal. kyr BP does not fit modelled insolation changes.

It is also important to consider the possible impact of changes in seasonality on the alkenone-derived SST record from GC666. Years with shorter summers have a lower average temperature for the whole year but may have higher peak temperatures during the summer, while longer summer duration

Figure 7.10 Comparison southern hemisphere temperature records
1 - Stenni et al. (2010), 2 - Allen et al. (2010), 3 - Peck et al. (2015), 4 - Panizzo et al. (2014), 5 - Renssen et al. (2005), 6 - this study, 7 - Roberts et al. (2017), 8 - McGlone et al. (2010), 9 - Lamy et al. (2002), 10 - Wainer et al. (2014), 11 - Evangelista et al. (2014), arranged by latitude. Shaded areas represent the extent of the mid-Holocene climate event proposed by the authors.


11 - 23ºS
10 - 25ºS
9 - 41ºS
8 - 52ºS
Early Holocene warming
7 - 53ºS
6 - 55ºS
5 - South of 60ºS
4 - 66ºS
3 - 67ºS
2 - 68ºS
1 - 75ºS
SST (ºC)
SST anomaly (ºC)
Temperature (ºC)
E. antarctica ratio
δ13Cdiat (‰)
% T. antarctica (warm)
ΔT (ºC)

results in higher average temperature but lower peak temperatures (Huybers and Denton, 2008). Therefore, if alkenone-based SSTs are representative of summer temperature, as proposed for the Southern Ocean by Sikes et al. (1997), reconstructed temperatures might be expected to increase as summer duration decreases. That SST at South Georgia decreases as summer duration decreases suggests that the alkenones are recording the annual average temperature, as proposed by Muller et al. (1998), which further supports the use of their $U^{k'}_{37}$ SST calibration in this study. That temperature in the southern high latitudes is primarily driven by insolation changes is supported by modelling of Southern Hemisphere temperature by Renssen et al. (2005).

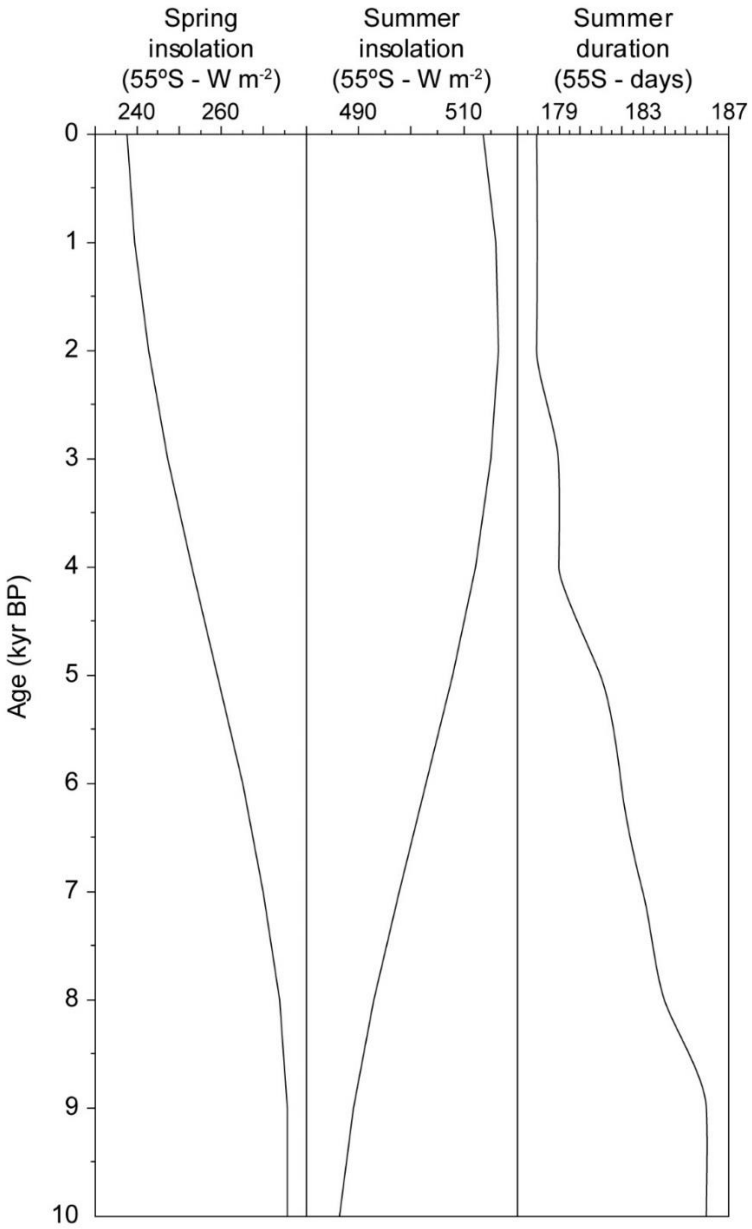


Figure 7.11 Holocene insolation and summer duration
Spring and summer insolation, and summer duration, for 55ºS, calculated following Huybers and Denton (2008).

Variation in Atlantic Meridional Overturning Circulation

Alternatively, Southern Hemisphere temperature may be driven by changes in Atlantic Meridional Overturning Circulation (AMOC). Increases (decreases) in Northern Hemisphere meltwater flux can impact Southern Hemisphere temperatures, by reducing (increasing) meridional heat transfer via AMOC, a mechanism known as the bipolar see-saw (e.g. Crowley, 1992; Broecker, 1998). For example, the early Holocene deglaciation of the Northern Hemisphere Laurentide Ice Sheet (LIS) could be expected to result in a warmer Southern Hemisphere by reducing northward heat transfer. However, modelling by Renssen et al. (2010) found that, because early Holocene melting of the LIS shut down deep convection in the Labrador Sea, the main source of North Atlantic Deep Water (NADW) became the colder Nordic Seas. Renssen et al.'s (2010) model indicates that this change in the temperature of NADW overwhelmed any temperature increase due to the accompanying reduction in the AMOC, cooling the Southern Ocean between 40ºS and 70ºS. They note that proxy evidence supporting this hypothesis is relatively weak; that the cooler SSTs observed at South Georgia during the early Holocene are generated by expansion/northward migration of the SWWs may provide further evidence for this cooling. However, the onset of cooler SSTs in GC666, at ~10.7 cal. kyr BP, is much earlier than the modelled period of cooler temperatures (9−7 kyr BP), although uncertainties about the timing of the LIS collapse could affect the proposed onset and duration of Southern Hemisphere cooling. It is also relevant to consider the fact that the GC666 radiocarbon dates prior ~10 kyr BP may be unreliable due to potential diagenetic alteration of the foraminifera (see discussion in Section 5.2.7.3).

Changes in AMOC have also been proposed as a possible driver for a Southern Hemisphere expression of the Medieval Climate Anomaly (MCA) (Broecker, 2001; Goosse et al., 2004), for which there may be some evidence in the SST record from South Georgia. The warmer conditions between ~1.0−0.8 cal. kyr BP, coincident with the Medieval Climate Anomaly (MCA) (~1.0−0.7 kyr BP - Mann et al. (2009)). SSTs are subsequently cooler by ca. 0.5ºC between ~0.6−0.4 cal. kyr BP, partially overlapping the Little Ice Age (LIA) (~0.6−0.3 kyr BP - Mann et al. (2009)). The LIA appears to be a global climate event (Neukom et al., 2014), is reported from some Antarctic records (e.g. Masson et al., 2000; Khim et al., 2002; Shevenell and Kennett, 2002), and from terrestrial records from South Georgia (Clapperton et al., 1989; Rosqvist and Schuber, 2003). Identification of the MCA and LIA at South Georgia may provide important information to further our understanding of spatial patterns of these changes and the underlying causal factors. However, the identification of these

climate events in GC666 is based on a small number of data points and the error associated with dates in this core during the late Holocene is ±175 yrs so it is not possible to say with any confidence that these observed proxy variation is related to the MCA and LIA.

While the MCA is well supported by evidence from the Northern Hemisphere (e.g. Mann et al., 2009), Neukom et al. (2014) found no evidence for a globally coherent medieval warm period over the past millennium. There are some Antarctic records that show evidence for the MCA (e.g. Khim et al., 2002), however these appear to be anomalous and the general consensus is that there is no strong evidence for the MCA in the Antarctic (e.g. Verleyen et al., 2011). The evidence for the MCA from GC666 suggests that, during the late Holocene, patterns of change in the South Georgia climate switched from following an Antarctic-type climate signal to being more influenced by Northern Hemisphere variation. Further evidence that South Georgia experienced warmer temperatures during this period can be found in terrestrial records from the island (Clapperton et al., 1989; Strother et al., 2015).

7.3.4 Evidence for a Southern Hemisphere 8.2 kyr event?

Benthic $\delta^{18}O_{foram}$ from both GC666 and GC673 broadly follows, offset by ca. +0.5‰, the global composite record of Lisiecki and Raymo (2005), which is used here for comparison in the absence of any local benthic $\delta^{18}O$ records. However, there is a positive excursion of approximately 0.3‰ at ~8.1 cal. kyr BP in benthic $\delta^{18}O_{foram}$ (from GC666 and GC673) and planktonic $\delta^{18}O_{foram}$ (from GC666) (Fig. 7.12). A positive excursion, at approximately the same time (allowing for age model uncertainties), was also reported by Bianchi and Gersonde (2004) in planktonic data from the eastern Atlantic sector of the Southern Ocean, at a similar latitude. The $\delta^{18}O_{foram}$ excursion was preceded by a negative excursion in benthic and planktonic $\delta^{13}C_{foram}$ (from GC666; the lower resolution of the data from GC673 might explain why this is not evident in this core), and a decrease in C:N.

The timing of this excursion may indicate that it is related to the 8.2 kyr event, a one to two century period of cold and dry conditions that represents the most distinct Northern Hemisphere Holocene climate event (Alley and Agustsdottir, 2005) , although it is important to note that the uncertainty associated with the modelled ages through this period of the record is ±250 years (2σ). There is little evidence in the Southern Hemisphere for the 8.2 kyr event, although Ljung et al. (2008) have reported a period of increased precipitation at this time from Tristan da Cunha at 37ºS in the South Atlantic, that they suggest was linked to increased SSTs. On South Georgia Rosqvist et al.

(1999) a 400 year cold event that began at ca. 7.8 cal. kyr BP that they tentatively link to the 8.2 kyr event. A negative $\delta^{18}O$ excursion has been reported at ca. 8 kyr in the Greenland ice core record (Stuiver et al., 1995) and in marine records (e.g. in the western Pacific (Romahn et al., 2015) in the Aegean Sea (Geraga et al., 2010)). The 8.2 kyr event was caused by outburst floods of the ice-damned Lake Agassiz, on the southern margin of the Laurentide ice-sheet, freshening the North Atlantic and greatly reducing or switching off AMOC (Alley and Agustsdottir, 2005 and refs therein). While the proxy records presented here provide an indication of a sub-Antarctic climate event that may be related to the Northern Hemisphere 8.2 kyr event, future work is required to generate higher resolution analysis of the core through this period, to better understand any possible link. If correct, this would be the first evidence for the 8.2 kyr event at such a high southern latitude.

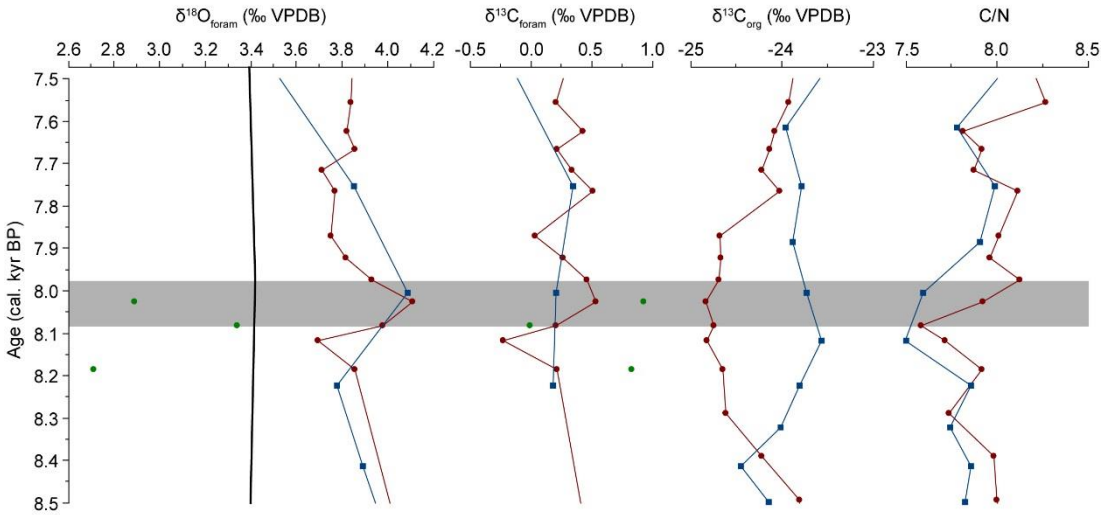


Figure 7.12 Evidence for and 8.2 kyr event?
Summary of selected proxies from GC666 and GC673 between 8.5 and 9.5 cal. kyr BP. Green circles = GC666 planktonic data; Red circles = GC666 benthic data; Blue squares = GC673 benthic data; Black line = LR04 stack (Lisiecki and Raymo, 2005). Shaded area indicates hypothetical evidence for 8.2 kyr event at South Georgia - see text for discussion.

7.4 Summary

This chapter discussed the first Holocene palaeoceanographic record from the South Georgia shelf, using multiproxy records from cores GC666 and GC673 to interpret changes in productivity and sea surface temperature. Sea surface temperature was reconstructed using the relative abundance of C_{37} alkenones to generate a $U^{k'}_{37}$ record, which was converted to SST using the calibration of Muller et al. (1998). The interpretation of productivity change was based variation in the accumulation rates on benthic foraminifera, biogenic silica, and organic carbon, and the carbon isotopic composition of organic carbon.

I propose that the Holocene SST and productivity records presented here were primarily forced by variation in the Southern Hemisphere westerly winds. Variation in foehn wind strength drove SST and productivity was forced by wind-driven coastal upwelling (after sea-ice proximity was no longer an important factor, during the early Holocene). Based on this hypothesis, I propose that SWW intensity at South Georgia was higher during the earliest Holocene (12.3 to 10.8 cal. kyr BP), lower during the early Holocene (10.8 to 7.6 cal. kyr BP), higher at the start of the mid-Holocene (7.6 to 3.0 cal. kyr BP) before gradually decreasing through this period. SWW intensity at South Georgia continues to decrease into the late Holocene (3.0 cal. kyr onwards) to a low centred on ~1.5 cal. kyr BP, before increasing again. Variation in SWW intensity at South Georgia may be either due to latitudinal migration of the SWW (e.g. Anderson et al., 2009), or due to contraction/expansion that intensifies/dissipates (e.g. Lamy et al., 2010). Latitudinal migration of the SWW may be driven by SAM variability, with positive (negative) SAM phase resulting in poleward (equatorward) migration (e.g. Toggweiler et al., 2006). Expansion and contraction of the SWW, analogous to modern seasonal variation, is driven by latitudinal temperature gradients between mid and low latitudes (Lamy et al., 2010). The patterns of SWW variability recorded at South Georgia agree with some interpretations from other locations (e.g. Bjorck et al., 2012; Voigt et al., 2015), but not with others (e.g. Lamy et al., 2010; Kaplan et al., 2016). Interpretation of the variation in the SWW is often vigorously debated (e.g. Kohfeld et al., 2013), in part due to the inability of a single location to record the whole SWW band.

While the SST record from South Georgia cannot add to our understanding of whether SWW variability was due to expansion and contraction or meridional migration, the patterns of variability support those proposed by Bjorck et al. (2012), McGlone et al. (2010), and Voigt et al. (2015). They are also consistent with recognised Southern Hemisphere Holocene temperature variability: early Holocene warmth until ca. 10 kyr BP, a period of cooler temperatures centred on ca. 8 kyr BP, mid-Holocene warmth, and the cooler neoglacial period (e.g. Masson et al., 2000; Renssen et al., 2005; Bentley et al., 2009; Stenni et al., 2010; Mathiot et al., 2013). These temperature variations are consistent with both modes of SWW variability. Increased (decreased) temperature leads to positive (negative) SAM phase, causing poleward (equatorward) SWW migration, but also could result in SWW contraction and intensification (expansion and diffusion). Both these modes would have the same expression in SST and shelf productivity variability at South Georgia, if the foehn wind hypothesis presented here is correct.

Chapter 8

Summary and conclusions

8.1 Introduction

The aim of this thesis was to develop a better understanding of the palaeoceanography of the sub-Antarctic island of South Georgia, over the past ca. 15 kyr, through the generation of multiproxy records from two marine cores from the South Georgia shelf. To support this aim a comprehensive taxonomy of the benthic foraminifera of the South Georgia shelf was developed, and the impact of foraminiferal ecology on the isotope composition of their calcareous tests was investigated. This final chapter summarises the preceding chapters and presents the key findings of this research before discussing possible avenues for future work.

8.2 Holocene South Georgia shelf benthic foraminifera

Taxonomic assessment of benthic foraminifera was conducted on a total of 159 samples, from two gravity cores (GC666 and GC673), two box cores (BC737 and (BC738), and 6 surface samples. The fauna described includes 78 species, assigned to 57 genera from 34 families (of these 58 species are identified to species level, while 20 species are discussed in open nomenclature). Benthic foraminiferal assemblage data is widely used in multi-proxy palaeoclimate studies and the development of a comprehensive taxonomy has not only aided this study but will also provide a resource for any future benthic foraminifera-based work at South Georgia and in the surrounding area.

A key finding from this chapter was the possible presence of endemic benthic foraminifera on the South Georgia shelf. 26% of the species described here have been left in open nomenclature and a number of these species, for example *Buccella* sp. 1, *Buccella* sp. 2, *Labrospira* sp. 1, and *Recurvoides* sp. 1, may be new to science and previously undescribed. This confirms the semi-isolated nature of the shelf environment adding to the existing evidence of the important biodiversity of South Georgia, as highlighted by Hogg et al. (2011).. Given the relatively slow rates of genetic evolution of benthic foraminifera, in comparison to planktonic taxa (Pawlowski et al., 1997; Gooday and Jorissen, 2012), and their long stratigraphic ranges (Kaminski and Gradstein, 2005; Holbourn et al., 2013), the presence of endemic species may indicate that the South Georgia shelf has been isolated for a considerable period of time.

8.3 Foraminiferal ecology: implications for calcification depths

Benthic foraminifera are widely utilised as tools in the reconstruction of past oceanographic conditions, with stable isotope and trace element data from their calcareous tests, as well as assemblage data, being applied in this context (see review in Jorissen et al., 2007). Inter-species differences in the carbon isotopic composition of foraminiferal tests ($\delta^{13}C_{foram}$), between epifaunal and infaunal species, have been utilised to reconstruct the $\delta^{13}C$ gradients that are known to be present within the sediments in which they lived (e.g. Hoogakker et al., 2015). These reconstructed gradients have then been used to interpret changes in bottom water oxygenation (e.g. Hoogakker et al., 2015) and organic matter remineralisation intensity (e.g. Theodor et al., 2016a). This method relies on the assumption that benthic foraminifera inhabit species-specific depth habitats and, more importantly, calcify at that depth, thereby recording the pore-water $\delta^{13}C_{DIC}$ gradient. To investigate whether this depth habitat-stable isotope relationship was present on the South Georgia shelf, the depth distribution and stable isotopes of "living" (Rose Bengal stained) benthic foraminifera of three species (*Astrononion echolsi*, *Cassidulinoides porrectus* and *Buccella* sp. 1) were analysed.

Within each of the species analysed, $\delta^{13}C_{foram}$ was found to be consistent, irrespective of the depth in the sediment at which the specimens were found living, and there were clear differences between the three species. The consistency of intra-species isotope data, despite their broad range of living depths, suggests that benthic foraminifera calcify at a fixed depth location, and possibly within a specific season, because they fail to capture the variability of pore-water $\delta^{13}C_{DIC}$ that their observed living depth would expose them to. In addition, $\delta^{13}C_{foram}$ increased mean living depth (MLD), the opposite of the expected trend were each species calcifying at their respective MLDs (assuming a negative $\delta^{13}C_{DIC}$ gradient was present in the sediment, as is common in marine sediments (e.g. McCorkle et al., 1997; Loubere et al., 2011)). There are multiple 'vital-effect' factors that lead to different inter-species $\delta^{13}C$ offsets despite specimens calcifying from waters with the same DIC (see review in Ravelo and Hillaire-Marcel, 2007) and without prior knowledge of the impact of these "vital effects" for each species it is not possible to use this as evidence that the species studied here do not calcify at their MLD.

Having added to the evidence that benthic foraminifera calcify at a fixed depth, I propose a calcification strategy that has not previously appeared in the literature. In this hypothesis, most benthic foraminifera calcify at the sediment-seawater interface, which may be the most energy efficient location for

calcification to occur as this is where carbonate ions are most abundant (Weldeab et al., 2016). In this scenario changes in epifaunal-infaunal offsets may be controlled by the timing of calcification; epifaunal and shallow infaunal taxa calcify persistently, even during periods of relatively low Corg availability (oligotrophic/mesotrophic conditions) and infaunal taxa calcify only during periods of high Corg availability (eutrophic conditions). Deeper infaunal taxa may be opportunistic, potentially "hibernating", or at least not calcifying new chambers, at depth during oligotrophic periods when food is scarce, and migrating to the sediment-seawater interface to feed and calcify during eutrophic periods. Temporal (down-core) variability in the offsets between epifaunal and infaunal $\delta^{13}C$ would, therefore, reflect changing fluxes of organic carbon to the seafloor, causing variation in $\delta^{13}C_{DIC}$ between oligotrophic and eutrophic conditions. This interpretation further highlights the need for a good understanding of foraminiferal ecology when utilising isotopic composition in interpret palaeoenvironmental change.

8.4 The deglacial and Holocene palaeoceanography of South Georgia

8.4.1 Background

South Georgia is located in the path of the Antarctic Circumpolar Current (ACC), south of the Antarctic Polar Front (APF) and surrounded by an anticyclonic loop of the Southern ACC Front (SACCF) (Fig. 1.1). This location means that palaeoceanographic records from South Georgia, of which this study presents the first, have the potential to provide greater understanding of past variability in the ACC in this regionally-important but under-sampled Southern Ocean sector. The waters surrounding South Georgia are highly productive (e.g. Atkinson et al., 2001) and variability in the interaction of the SACCF with the island (known to occur on seasonal and interannual scales - Boehme et al., 2008) may impact productivity on the shelf (e.g. Korb et al., 2004; Young et al., 2014). Of wider significance is the large phytoplankton bloom that occurs to the north-west of South Georgia, where the SACCF retroflects to return to its cyclonic circumpolar circulation (e.g. Korb et al., 2004; 2008; Murphy et al., 2013). This bloom represents one of the largest seasonal sinks of atmospheric CO_2 in the Southern Ocean (Jones et al., 2012). Given the likely importance of the Southern Ocean as a carbon sink/source during the transition between glacial and interglacial periods (e.g. Sigman et al., 2010) a better understanding of the bloom dynamics could be important to our assessment of the Southern Ocean's role in these transitions.

Palaeoceanographic records from South Georgia may also advance our understanding of large-scale modes of atmospheric variability, such as the Southern Annular Mode (SAM). Changes in the expression of the SAM can impact the Southern Hemisphere Westerly Winds (SWW), with the recent trend towards a more positive SAM phase associated with an increase in the strength, and a southward shift, of the SWW (Thompson and Solomon, 2002). Understanding variation in the SWW is of global importance as they strongly influence Southern Ocean circulation and modify the upwelling of carbon-rich deep water which, combined with ocean biogeochemistry, affects the ocean-atmosphere CO_2 balance (Sigman et al., 2010). Therefore, whether the Southern Ocean acts as a sink or source of atmospheric CO_2 can be affected by changes in the SWW (Le Quere et al., 2007). Reconstructions of palaeo-SST at South Georgia, if they can be shown to reflect atmospheric variability rather than frontal movements, therefore have the potential to inform about long-term changes in these systems.

At a more local scale, deglacial palaeoceanographic records may also further our understanding of the glacial history of South Georgia. In recent decades, whether there was an extensive (e.g. Clapperton et al., 1989; Graham et al., 2017; White et al., 2017) or restricted (Rosqvist et al., 1999; Bentley et al., 2007; Hodgson et al., 2014b) ice sheet at South Georgia during Last Glacial Maximum (LGM) has been debated (Fig. 1.6). The records presented here, while not extending back to the LGM, have the potential to provide useful evidence in this debate. Understanding the glacial history of South Georgia is of wider importance because the island, as a 'sentinel' for environmental change close to the boundary between Northern Hemisphere-type and Antarctic-type climate signals, could be where changes in regional climate are first detected.

8.4.2 Summary of multiproxy data from GC666 and GC673

The multiproxy data from cores GC666 and GC673 that are presented in detail in Chapter 5 are summarised in Figure 8.1. This is done to highlight the key proxies utilised in the interpretation in Chapter 6 and 7, present the complete record in its entirety, and to plot these proxies alongside proximal records of SWW variability (Lamy et al., 2010; Bjorck et al., 2012) and local insolation variability (Berger and Loutre, 1991). BFAR and C_{org} AR from GC666 are both highest in the laminated section of the core and decrease through the rest of the deglacial and early Holocene, except for an increase at ca. 12.5 cal. kyr BP. Both remain low through the mid-Holocene before increasing through the late Holocene. These trends are reflected in the BFAR and C_{org} AR data from GC673, although both are consistently higher. For much of the record the $\delta^{13}C_{org}$

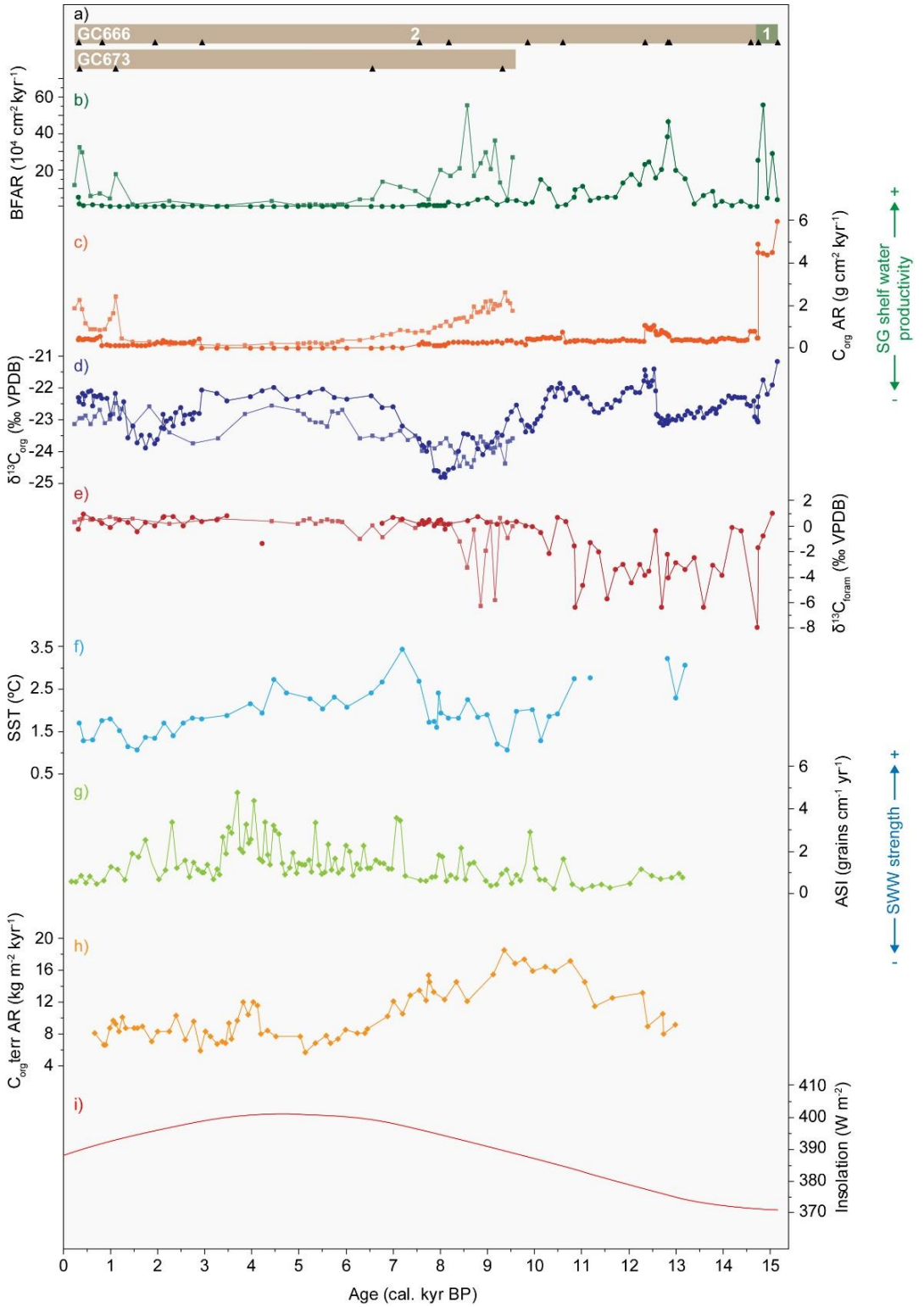


Figure 8.1 Summary of key proxy records from GC666 and GC673
a) Simplified sedimentary logs. Triangles indicate radiocarbon dates. b) Benthic foraminiferal accumulation rate. c) Organic carbon accumulation rate. d) Carbon isotopic composition of organic carbon. e) Carbon isotopic composition of benthic foraminiferal tests. f) $U^{k'}_{37}$ sea surface temperature reconstruction. g) Aeolian sand influx at Isla de los Estados, Patagonia (Bjorck et al., 2012). h) Accumulation rate of terrestrial organic carbon from the Skyring fjord system, Chile (Lamy et al., 2010). i) Insolation at 50ºS during the austral spring (Berger and Loutre, 1991). Circles and darker colour represent GC666, squares and lighter colours represent GC673.

trends are similar to those in BFAR and C_{org} AR, except during the mid-Holocene where $\delta^{13}C_{org}$ is higher while BFAR and C_{org} AR are lower. Where reliable SSTs have been reconstructed they are lowest during the early Holocene, increase to a peak at ca. 7.2 cal. kyr BP, gradually decrease through the mid-Holocene and into the late Holocene.

8.4.3 Discussion

8.4.3.1 Calving bay re-entrant development during deglaciation

While the extent of the ice sheet at South Georgia during the LGM has been the subject of much debate (e.g. Clapperton et al., 1989; Rosqvist et al., 1999; Bentley et al., 2007; Graham et al., 2008; Hodgson et al., 2014b), a number of recent studies appear to be building a consensus that this ice sheet extended over much of the island's shelf (Barnes et al., 2016; Graham et al., 2017; White et al., 2017). Although the cores studied here do not extend as far as the LGM, core GC666 does record the later stages of the deglacial period (from 15.2 cal. kyr BP) and can therefore provide additional understanding of the ice sheet's evolution during this period.

The sequence of laminated sediments at the base of core GC666 may be analogous to sediments deposited during deglaciation in Antarctic shelf settings, specifically in relation to the formation of calving bay re-entrant over cross shelf troughs (Leventer et al., 2006). The location of core GC666 within Royal Bay trough, one of the deep, cross-shelf troughs that characterise the South Georgia shelf, means that the core is ideally situated for such sedimentation to occur during deglaciation. Graham et al. (2017) proposed that, following the LGM, deglaciation at the South Georgia was relatively early and rapid; I propose that these laminated sediments provide further evidence that this hypothesis is correct, except that the rapid retreat occurred over the cross-shelf troughs and that the ice sheet persisted until later in the deglacial period over the shallower shelf areas (Fig. 6.2). That continuous lamination breaks down after ~15.0 cal. kyr BP suggests that by this time the ice sheet on the South Georgia shelf had retreated completely from the shelf, possibly beyond the modern ice extent (Graham et al., 2017), such that a calving bay re-entrant was no longer present. Subsequently, grounded ice on South Georgia may have re-advanced during the ACR, to the fjord mouths (Graham et al., 2017). A peak in productivity and sedimentation rates in core GC666 centred on 12.6 cal. kyr BP may be a result of this ACR advance retreating in response to increases in Southern Hemisphere temperature. The influence of grounded/glacial ice at GC666 is proposed to have ended at 12.3 cal. kyr BP.

8.4.3.2 SWW variability as the primary driver of Holocene South Georgia shelf productivity and SST

During deglaciation productivity on the South Georgia shelf is primarily driven by variation in glacial meltwater flux and the associated changes in nutrient supply. By the earliest Holocene (12.3 to 10.8 cal. kyr BP) grounded ice on South Georgia had retreated at least as far as the modern ice extent, therefore glacial meltwater no longer significantly impacted shelf productivity. Instead, I propose that variation in SWW intensity at South Georgia forced shelf productivity, via coastal upwelling, in addition to driving SST, via variability in foehn wind frequency. While SWW variability may have been the primary forcing mechanism, an additional factor controlling shelf productivity at South Georgia, at least into the early Holocene (10.8 to 7.6 cal. kyr BP), was sea-ice proximity, which became more distal through this period (Bianchi and Gersonde, 2004; Xiao et al., 2016).

The Holocene SST and productivity variability recorded in core GC666 potentially reveals the following patterns of SWW change, assuming foehn frequency increases with increased SWW intensity (Fig. 7.9). During the earliest Holocene (12.3 to 10.8 cal. kyr BP) SST may be higher, suggesting stronger SWW at this latitude. However, the small number of samples (4) that are all calculated for poor quality chromatograms and display a wide SST variability (2.76ºC to 5.63ºC) means that the interpretation of this period as warmer cannot be considered reliable. SSTs during the early Holocene (10.8 to 7.6 cal. kyr BP) are lower, potentially indicative of less intense SWW at South Georgia and weaker foehn wind strength. Productivity during this period is disconnected from wind frequency, instead being driven by decreasing sea-ice proximity, as discussed above. Warmer SSTs at the beginning of the mid-Holocene (7.6 to 3.0 cal. kyr BP) may indicate an intensification of the SWW at South Georgia, with the gradually decreasing SST through this period representing decreasing SWW intensity. The proxy record during the mid-Holocene may indicate productivity was higher during the mid-Holocene but this is not certain, given the apparently contradictory signals from different proxies. During the late Holocene (3.0 cal. kyr BP onwards) there is a correlation between $\delta^{13}C_{org}$ (which may be the most robust productivity proxy from GC666) and SST, although this correlation is not significant ($r = 0.53$, $p = 0.061$). This may indicate that SWW intensity at South Georgia was declining to a low centred on ~1.5 cal. kyr BP, before increasing slightly subsequently to be similar to the latter part of the mid-Holocene after ~1.0 cal. kyr BP.

Similar patterns of Holocene SWW variability are interpreted from lacustrine and peat records from Isla de los Estados, southern Patagonia (Unkel et al., 2010; Bjorck et al., 2012). McGlone et al. (2010) have also proposed that the SWW were more intense between ~9 and ~5 kyr BP at a similar latitude from Campbell Island, south of New Zealand, based on their interpretation of pollen-based temperature data. Northward migration of the SWW in the early Holocene, proposed by Anderson et al. (2009), could also result in weakening of the SWW at South Georgia. Further support for this pattern of Holocene SWW variability can be found in the migration of the Brazil-Malvinas Confluence (BMC) in the south western Atlantic (Voigt et al., 2015). The BMC, which is tightly coupled to the SWW and located north of South Georgia at ca. 38ºS, migrated southwards during the early Holocene, which could result in the core SWW band being closer to, or over, South Georgia. Subsequent northward migration of the BMC, after ca. 4 kyr BP, peaks at 1.5 kyr BP, coincident with the hypothesised minimum influence of the SWW at South Georgia during the late Holocene.

Changes in SWW intensity at a specific location can be caused by contraction/expansion of the core band, or by meridional migration of the winds. Variation in sea surface temperature gradients between mid and low latitudes result in seasonal contraction and expansion of the SWW in the modern climate system. Lamy et al. (2010) propose Holocene variability to be analogous to modern seasonal variability, with the SWW contracting (expanding) during warmer (cooler) periods. At a single site, this contraction and expansion would be evident as changing SWW intensity, with the sign of this change dependent on the sites location within the band. At South Georgia, close to the core SWW band, contraction during warming could result in intensification of the SWW (Fig. 7.9c) and a reduction in intensity during cooler periods (Fig. 7.9e). Alternatively, latitudinal migration of the SWW, caused by temperature-driven changes in the SAM phase (Toggweiler et al., 2006), would also result in SWW intensity changes at a single site. This would result in the same pattern of SWW intensity change at South Georgia as in the expansion/contraction scenario, with intensity increasing during warm periods as the SWW core migrates polewards (Fig. 7.9d) and decreasing during cool periods as the SWW migrate equatorwards (Fig. 7.9f).

While the shelf SST and productivity record from South Georgia cannot add to our understanding of whether SWW variability was due to expansion and contraction or meridional migration, the patterns of variability support those proposed by Bjorck et al. (2012) and McGlone et al. (2010). They are also consistent with recognised Southern Hemisphere Holocene temperature

variability: early Holocene warmth until ca. 10 kyr BP, a period of cooler temperatures centred on ca. 8 kyr BP, mid-Holocene warmth, and the cooler neoglacial period (e.g. Masson et al., 2000; Renssen et al., 2005; Bentley et al., 2009; Stenni et al., 2010; Mathiot et al., 2013). These temperature variations are consistent with both modes of SWW variability. Increased (decreased) temperature leads to positive (negative) SAM phase, causing poleward (equatorward) SWW migration, but also could result in SWW contraction and intensification (expansion and diffusion). Both these modes would have the same expression in SST variability at South Georgia, if the foehn wind hypothesis presented here is correct.

8.5 Conclusions

1. A detailed taxonomy of the benthic foraminifera of the South Georgia shelf revealed that the degree of endemism present in this community was comparable to that of isolated basins such as the Bering Sea. This result indicates that South Georgia has been isolated for a considerable period of time, to allow for the relatively slow evolution of benthic foraminifera to result in new species. It is also further evidence of the biodiversity of the South Georgia ecosystem, previously shown on macrofauna, and the importance of preserving this environment.
2. The investigation of the relationship between benthic foraminiferal $\delta^{13}C$ and the living depth of the specimens analysed led to the proposal of a novel method of calcification, in which calcification mainly occurs at the sediment/water interface. I do not propose that this is the only mode of calcification but the possibility that this may occur highlights the importance of fully understanding the ecology of foraminifera when utilising their test chemistry in palaeoenvironmental reconstruction. That certain taxa were found living at depths in variance with what their morphology might imply indicates that morphology alone is not enough to understand their ecology.
3. The laminated section of the core at the base of GC666 is hypothesised to be indicative of the development of a calving bay re-entrant over cross-shelf troughs on the South Georgia shelf during deglaciation. Evidence for this pattern of ice sheet retreat has been reported from the Antarctic shelf but there are differences in the morphology of these troughs, in comparison to those at South Georgia.
4. Holocene SST and productivity records presented here are hypothesised to have been primarily forced by variation in the Southern Hemisphere westerly winds. Variation in foehn wind strength drove SST and

productivity was forced by wind-driven coastal upwelling (after sea-ice proximity was no longer an important factor, during the early Holocene). Based on this hypothesis, I propose that SWW intensity at South Georgia was higher during the earliest Holocene (12.3 to 10.8 cal. kyr BP), lower during the early Holocene (10.8 to 7.6 cal. kyr BP), higher at the start of the mid-Holocene (7.6 to 3.0 cal. kyr BP) before gradually decreasing through this period. SWW intensity at South Georgia continues to decrease into the late Holocene (3.0 cal. kyr onwards) to a low centred on ~1.5 cal. kyr BP, before increasing again. It will be possible to present a more complete picture of the Holocene palaeoceanography of the South Georgia shelf when data from other cores (currently being analysed elsewhere) in the transect that includes GC666 and GC673 becomes available.

8.6 Future work

1. One of the initial aims of this project was to investigate how the large phytoplankton bloom that occurs to the north-east of South Georgia varied through the last 15 kyr, in comparison to its observed interannual variability, and how this variability may have affected the Southern Ocean in relation to its being a source/sink for atmospheric CO_2. However, as the research progressed it became clear that the cores being studied here would not be appropriate to answer these questions due to their location, being too distal from the bloom and also being strongly influenced by their proximity to South Georgia. Work is underway on a core that is closer to the bloom that may be better able to investigate this variability. Future work could aim to recover cores from the deeper waters directly below the area where the bloom commonly occurs, potentially with the aim of recovering longer cores that would include one or more glacial interglacial cycles.
2. Due to constraints on time and resources the investigation of the laminated section of core GC666 conducted as part of this study was fairly limited in extent. This part of the core likely contains a wealth of data and a detailed analysis of the laminae could be carried out in future. In particular, a more comprehensive characterisation of the nature of the laminae and their diatom assemblages could be undertaken to test the hypothesis that a calving bay re-entrant formed around Royal Bay trough during the deglaciation of South Georgia. If the laminae are confirmed to be varves this offers the potential to develop an annual resolution record of this part of the core. The calving

bay hypothesis could also be further tested through the collection, analysis, and dating of cores from the shallower shelf areas of South Georgia, between the troughs, to test whether there is any evidence for a later retreat of ice from these areas.

3. It would also be useful to develop diatom assemblage records throughout the cores. Such records would have the potential to test hypotheses regarding variation in the influence of sea-ice around South Georgia. Diatom assemblage data could also provide an additional primary productivity proxy, one that is potentially more direct than some of those discussed in this study. Furthermore, diatom assemblage data could be utilised to assess relative SST changes in the part of the record where alkenone data in unreliable, and to support the existing record in the rest of the core.
4. Undertaking higher resolution multiproxy analysis of certain sections of core would also be of interest. For example, higher resolution data from the late Holocene section of the core could be used to test the hypothesis that proxy variability during this period in linked to increased influence of ENSO-type variability, and to investigate the hypothetical evidence for the LIA and the MCA climate events. In addition, higher resolution data from around 8.2 cal. kyr BP could test the hypothesis that there is evidence for this Northern Hemisphere climate event in the cores from South Georgia.

References

Abram, N. J., Mulvaney, R., Vimeux, F., Phipps, S. J., Turner, J., and England, M. H., 2014, Evolution of the Southern Annular Mode during the past millennium: Nature Clim. Change, 4, 7, 564-569.

Adkins, J. F., McIntyre, K., and Schrag, D. P., 2002, The salinity, temperature, and $\delta^{18}O$ of the glacial deep ocean: Science, 298, 5599, 1769-1773.

Alekseychik-Mitskevich, L. S., 1973, Towards the classification of the foraminiferal family Haplophragmiidae: Trudy Vsesoyuzznogo neftyanogo Nauchnoissledovatel'skogo Geologorazvedochnogo Instituta, 343, 12-44.

Alldredge, A. L., and Gotschalk, C. C., 1989, Direct observations of the mass flocculation of diatom blooms - characteristics, settling velocities and formation of diatom aggregates: Deep-Sea Research Part a-Oceanographic Research Papers, 36, 2, 159-171.

Alldredge, A. L., Passow, U., and Logan, B. E., 1993, The abundance and significance of a class of large, transparent organic particles in the ocean: Deep-Sea Research Part I-Oceanographic Research Papers, 40, 6, 1131-1140.

Allen, C. S., Oakes-Fretwell, L., Anderson, J. B., and Hodgson, D. A., 2010, A record of Holocene glacial and oceanographic variability in Neny Fjord, Antarctic Peninsula: The Holocene, 20, 4, 551-564.

Allen, C. S., Pike, J., and Pudsey, C. J., 2011, Last glacial-interglacial sea-ice cover in the SW Atlantic and its potential role in global deglaciation: Quaternary Science Reviews, 30, 19-20, 2446-2458.

Allen, C. S., Peck, V. L., Graham, A. G. C., Blagbrough, H., Robinson, M. W., and McClymont, E., 2012, Collecting records of past oceanographic conditions and calibrating new proxies in the Polar Front Zone of the SW Atlantic (Falkland Plateau, Shag Rocks and South Georgia), Cruise Report, pp. 105.

Alley, R. B., Mayewski, P. A., Sowers, T., Stuiver, M., Taylor, K. C., and Clark, P. U., 1997, Holocene climatic instability: A prominent, widespread event 8200 yr ago: Geology, 25, 6, 483-486.

Alley, R. B., and Agustsdottir, A. M., 2005, The 8k event: cause and consequences of a major Holocene abrupt climate change: Quaternary Science Reviews, 24, 10-11, 1123-1149.

Almogi-Labin, A., Schmiedl, G., Hemleben, C., Siman-Tov, R., Segl, M., and Meischner, D., 2000, The influence of the NE winter monsoon on productivity changes in the Gulf of Aden, NW Arabian Sea, during the last 530 ka as recorded by foraminifera: Marine Micropaleontology, 40, 3, 295-319.

Altenbach, A. V., Pflaumann, U., Schiebel, R., Thies, A., Timm, S., and Trauth, M., 1999, Scaling percentages and distributional patterns of benthic foraminifera with flux rates of organic carbon: Journal of Foraminiferal Research, 29, 3, 173-185.

Alve, E., 1995, Benthic foraminiferal distribution and recolonization of formerly anoxic environments in Drammensfjord, southern Norway: Marine Micropaleontology, 25, 2-3, 169-186.

Alves Martins, V., Patinha, C., Ferreira da Silva, E., Jouanneau, J. M., Weber, O., and Rocha, F., 2006, Holocene record of productivity in the NW Iberian continental shelf: Journal of Geochemical Exploration, 88, 1, 408-411.

Andersen, H. V., 1952, Buccella, a new genus of the rotalid foraminifera: Journal of the Washington Academy of Sciences, 42, 143-151.

Anderson, J. B., 1975, Ecology and distribution of foraminifera in the Weddell Sea of Antarctica: Micropalaeontology, 21, 1, 69-96.

Anderson, J. B., Conway, H., Bart, P. J., Witus, A. E., Greenwood, S. L., McKay, R. M., Hall, B. L., Ackert, R. P., Licht, K., Jakobsson, M., and Stone, J. O.,

2014, Ross Sea paleo-ice sheet drainage and deglacial history during and since the LGM: Quaternary Science Reviews, 100, 31-54.
Anderson, R. F., Ali, S., Bradtmiller, L. I., Nielsen, S. H. H., Fleisher, M. Q., Anderson, B. E., and Burckle, L. H., 2009, Wind-Driven Upwelling in the Southern Ocean and the Deglacial Rise in Atmospheric CO2: Science, 323, 5920, 1443-1448.
Anderson, R. S., Dühnforth, M., Colgan, W., and Anderson, L., 2012, Far-flung moraines: Exploring the feedback of glacial erosion on the evolution of glacier length: Geomorphology, 179, 269-285.
Asseez, L. O., Fayose, E. A., and Omatsola, M. E., 1974, Ecology of the Ogun River estuary, Nigeria: Palaeogeography, Palaeoclimatology, Palaeoecology, 16, 3, 243-260.
Atkinson, A., Whitehouse, M. J., Priddle, J., Cripps, G. C., Ward, P., and Brandon, M. A., 2001, South Georgia, Antarctica: a productive, cold water, pelagic ecosystem: Marine Ecology Progress Series, 216, 279-308.
Bailey, J. W., 1851, Microscopical examination of soundings made by the U. S. Coast Survey of the Atlantic coast of the U. S.: Smithsonian Contributions, 2, 8, 1-48.
Bakun, A., Field, D. B., Redondo-rodriguez, A., and Weeks, S. J., 2010, Greenhouse gas, upwelling-favorable winds, and the future of coastal ocean upwelling ecosystems: Global Change Biology, 16, 4, 1213-1228.
Bandy, O. L., Frerichs, W. E., and Vincent, E., 1967, Origin, development, and geologic significance of *Neogloboquadrina* Bandy, Frerichs, and Vincent, gen. nov.: Contributions from the Cushman Foundation for Foraminiferal Research, 18, 152-157.
Barbante, C., Barnola, J. M., Becagli, S., Beer, J., Bigler, M., Boutron, C., Blunier, T., Castellano, E., Cattani, O., Chappellaz, J., Dahl-Jensen, D., Debret, M., Delmonte, B., Dick, D., Falourd, S., Faria, S., Federer, U., Fischer, H., Freitag, J., Frenzel, A., Fritzsche, D., Fundel, F., Gabrielli, P., Gaspari, V., Gersonde, R., Graf, W., Grigoriev, D., Hamann, I., Hansson, M., Hoffmann, G., Hutterli, M. A., Huybrechts, P., Isaksson, E., Johnsen, S., Jouzel, J., Kaczmarska, M., Karlin, T., Kaufmann, P., Kipfstuhl, S., Kohno, M., Lambert, F., Lambrecht, A., Lambrecht, A., Landais, A., Lawer, G., Leuenberger, M., Littot, G., Loulergue, L., Luthi, D., Maggi, V., Marino, F., Masson-Delmotte, V., Meyer, H., Miller, H., Mulvaney, R., Narcisi, B., Oerlemans, J., Oerter, H., Parrenin, F., Petit, J. R., Raisbeck, G., Raynaud, D., Rothlisberger, R., Ruth, U., Rybak, O., Severi, M., Schmitt, J., Schwander, J., Siegenthaler, U., Siggaard-Andersen, M. L., Spahni, R., Steffensen, J. P., Stenni, B., Stocker, T. F., Tison, J. L., Traversi, R., Udisti, R., Valero-Delgado, F., van den Broeke, M. R., van de Wal, R. S. W., Wagenbach, D., Wegner, A., Weiler, K., Wilhelms, F., Winther, J. G., Wolff, E., and Members, E. C., 2006, One-to-one coupling of glacial climate variability in Greenland and Antarctica: Nature, 444, 7116, 195-198.
Bard, E., and Rickaby, R. E. M., 2009, Migration of the subtropical front as a modulator of glacial climate: Nature, 460, 7253, 380-393.
Bard, E., Tuna, T., Fagault, Y., Bonvalot, L., Wacker, L., Fahrni, S., and Synal, H. A., 2015, AixMICADAS, the accelerator mass spectrometer dedicated to C-14 recently installed in Aix-en-Provence, France: Nuclear Instruments & Methods in Physics Research Section B-Beam Interactions with Materials and Atoms, 361, 80-86.
Barker, R. W., 1960, Taxonomic notes on the species figured by H.B. Brady in his report of the foraminifera dredged by HMS Challenger during the years 1873-1876: American Association of Petroleum Geologists Special Publication, 9, 2-240.

Barker, S., Diz, P., Vautravers, M. J., Pike, J., Knorr, G., Hall, I. R., and Broecker, W. S., 2009, Interhemispheric Atlantic seesaw response during the last deglaciation: Nature, 457, 7233, 1097-1102.
Barnes, D. K. A., Sands, C. J., Hogg, O. T., Robinson, B. J. O., Downey, R. V., and Smith, J. A., 2016, Biodiversity signature of the Last Glacial Maximum at South Georgia, Southern Ocean: Journal of Biogeography, 43, 12, 2391-2399.
Belanger, C. L., Orhun, O. G., and Schiller, C. M., 2016, Benthic foraminiferal faunas reveal transport dynamics and no-analog environments on a glaciated margin (Gulf of Alaska): Palaeogeography, Palaeoclimatology, Palaeoecology, 454, 54-64.
Bendle, J., Rosell-Melé, A., and Ziveri, P., 2005, Variability of unusual distributions of alkenones in the surface waters of the Nordic seas: Paleoceanography, 20, 2, PA2001.
Bentley, M., Evans, D., Fogwill, C., Hansom, J., Sugden, D., and Kubik, P., 2007, Glacial geomorphology and chronology of deglaciation, South Georgia, sub-Antarctic: Quaternary Science Reviews, 26, 5-6, 644-677.
Bentley, M. J., Hodgson, D. A., Smith, J. A., O Cofaigh, C., Domack, E. W., Larter, R. D., Roberts, S. J., Brachfeld, S., Leventer, A., Hjort, C., Hillenbrand, C. D., and Evans, J., 2009, Mechanisms of Holocene palaeoenvironmental change in the Antarctic Peninsula region: Holocene, 19, 1, 51-69.
Bentley, M. J., Cofaigh, C. O., Anderson, J. B., Conway, H., Davies, B., Graham, A. G. C., Hillenbrand, C. D., Hodgson, D. A., Jamieson, S. S. R., Larter, R. D., Mackintosh, A., Smith, J. A., Verleyen, E., Ackert, R. P., Bart, P. J., Berg, S., Brunstein, D., Canals, M., Colhoun, E. A., Crosta, X., Dickens, W. A., Domack, E., Dowdeswell, J. A., Dunbar, R., Ehrmann, W., Evans, J., Favier, V., Fink, D., Fogwill, C. J., Glasser, N. F., Gohl, K., Golledge, N. R., Goodwin, I., Gore, D. B., Greenwood, S. L., Hall, B. L., Hall, K., Hedding, D. W., Hein, A. S., Hocking, E. P., Jakobsson, M., Johnson, J. S., Jomelli, V., Jones, R. S., Klages, J. P., Kristoffersen, Y., Kuhn, G., Leventer, A., Licht, K., Lilly, K., Lindow, J., Livingstone, S. J., Masse, G., McGlone, M. S., McKay, R. M., Melles, M., Miura, H., Mulvaney, R., Nel, W., Nitsche, F. O., O'Brien, P. E., Post, A. L., Roberts, S. J., Saunders, K. M., Selkirk, P. M., Simms, A. R., Spiegel, C., Stolldorf, T. D., Sugden, D. E., van der Putten, N., van Ommen, T., Verfaillie, D., Vyverman, W., Wagner, B., White, D. A., Witus, A. E., Zwartz, D., and Consortium, R., 2014, A community-based geological reconstruction of Antarctic Ice Sheet deglaciation since the Last Glacial Maximum: Quaternary Science Reviews, 100, 1-9.
Berger, A., and Loutre, M. F., 1991, Insolation values for the climate of the last 10 million years: Quaternary Science Reviews, 10, 4, 297-317.
Berger, W. H., and Vincent, E., 1986, Deep-sea carbonates - reading the carbon-isotope signal: Geologische Rundschau, 75, 1, 249-269.
Bernhard, J. M., 1989, The distribution of benthic Foraminifera with respect to oxygen concentration and organic carbon levels in shallow-water Antarctic sediments: Limnology and Oceanography, 34, 6, 1131-1141.
-, 1993, Experimental and field evidence of Antarctic foraminiferal tolerance to anoxia and hydrogen-sulfide: Marine Micropaleontology, 20, 3-4, 203-213.
-, 2000, Distinguishing live from dead foraminifera: Methods review and proper applications: Micropaleontology, 46, 38-46.
Bernhard, J. M., Ostermann, D. R., Williams, D. S., and Blanks, J. K., 2006, Comparison of two methods to identify live benthic foraminifera: A test between Rose Bengal and CellTracker Green with implications for stable isotope paleoreconstructions: Paleoceanography, 21, 4, PA4210.

Bianchi, C., and Gersonde, R., 2004, Climate evolution at the last deglaciation: the role of the Southern Ocean: Earth and Planetary Science Letters, 228, 3-4, 407-424.
Birnie, J., 1990, Holocene environmental-change in South Georgia - evidence from lake-sediments: Journal of Quaternary Science, 5, 3, 171-187.
Bjorck, S., Olsson, S., EllisEvans, C., Hakansson, H., Humlum, O., and deLirio, J. M., 1996, Late Holocene palaeoclimatic records from lake sediments on James Ross Island, Antarctica: Palaeogeography Palaeoclimatology Palaeoecology, 121, 3-4, 195-220.
Bjorck, S., Rundgren, M., Ljung, K., Unkel, I., and Wallin, A., 2012, Multi-proxy analyses of a peat bog on Isla de los Estados, easternmost Tierra del Fuego: a unique record of the variable Southern Hemisphere Westerlies since the last deglaciation: Quaternary Science Reviews, 42, 1-14.
Blaauw, M., 2010, Methods and code for 'classical' age-modelling of radiocarbon sequences: Quaternary Geochronology, 5, 5, 512-518.
Blanchet, C. L., Kasten, S., Vidal, L., Poulton, S. W., Ganeshram, R., and Thouveny, N., 2012, Influence of diagenesis on the stable isotopic composition of biogenic carbonates from the Gulf of Tehuantepec oxygen minimum zone: Geochemistry Geophysics Geosystems, 13, QO4003.
Boden, P., and Backman, J., 1996, A laminated sediment sequence from the northern North Atlantic Ocean and its climatic record: Geology, 24, 6, 507-510.
Boehme, L., Meredith, M. P., Thorpe, S. E., Biuw, M., and Fedak, M., 2008, Antarctic Circumpolar Current frontal system in the South Atlantic: Monitoring using merged Argo and animal-borne sensor data: Journal of Geophysical Research-Oceans, 113, C9, CO9012.
Borchers, A., Dietze, E., Kuhn, G., Esper, O., Voigt, I., Hartmann, K., and Diekmann, B., 2016, Holocene ice dynamics and bottom-water formation associated with Cape Darnley polynya activity recorded in Burton Basin, East Antarctica: Marine Geophysical Research, 37, 1, 49-70.
Borrione, I., Aumont, O., Nielsdottir, M. C., and Schlitzer, R., 2014, Sedimentary and atmospheric sources of iron around South Georgia, Southern Ocean: a modelling perspective: Biogeosciences, 11, 7, 1981-2001.
Boyd, P. W., 2002, Environmental factors controlling phytoplankton processes in the Southern Ocean: Journal of Phycology, 38, 5, 844-861.
Brady, H. B., 1864, Contributions to the knowledge of the foraminifera - On the rhizopodal fauna of the Shetlands: Transactions of the Linnaean Society, 24, 3, 463-476.
-, 1879, Notes on some of the Reticularian Rhizopoda of the "Challenger" Expedition. I. On new or little known arenaceous types: Quarterly Journal of Microscopical Science, 19, 20-62.
-, 1881, Notes on some of the Reticularian Rhizopoda of the "Challenger" Expedition. Part III Quarterly Journal of Microscopical Science, 21, 31-71.
-, 1884, Report on the scientific results of the voyage of H.M.S. Challenger during the years 1873-76, *in* Thompson, C. W., and Murray, J., eds., Zoology of the Challenger Expedition,Volume 9 Neill: Edinburgh, 408.
Brandon, M. A., Murphy, E. J., Whitehouse, M. J., Trathan, P. N., Murray, A. W. A., Bone, D. G., and Priddle, J., 1999, The shelf break front to the east of the sub-Antarctic island of South Georgia: Continental Shelf Research, 19, 6, 799-819.
Brandon, M. A., Murphy, E. J., Trathan, P. N., and Bone, D. G., 2000, Physical oceanographic conditions to the northwest of the sub-Antarctic Island of South Georgia: Journal of Geophysical Research-Oceans, 105, C10, 23983-23996.
Brassell, S. C., Eglinton, G., Marlowe, I. T., Pflaumann, U., and Sarnthein, M., 1986, Molecular stratigraphy: a new tool for climatic assessment: Nature, 320, 6058, 129-133.

Broecker, W. S., 1998, Paleocean circulation during the last deglaciation: A bipolar seesaw?: Paleoceanography, 13, 2, 119-121.
-, 2001, Paleoclimate - Was the medieval warm period global?: Science, 291, 5508, 1497-1499.
Bronk Ramsey, C., 2008, Deposition models for chronological records: Quaternary Science Reviews, 27, 1-2, 42-60.
-, 2009, Bayesian analysis of radiocarbon dates: Radiocarbon, 51, 1, 337-360.
Bronk Ramsey, C., and Lee, S., 2013, Recent and planned developments of the program OxCal: Radiocarbon, 55, 2-3, 720-730.
Bronk Ramsey, C., 2016, Bayesian Analysis of Radiocarbon Dates: Radiocarbon, 51, 1, 337-360.
Bronnimann, P., 1976, Two new genera of Recent Trochamminidae (Foraminiferida): Achives des Sciences, Geneve, 29, 215-218.
Bronnimann, P., and Beurlen, G., 1977, Recent benthonic foraminifera from Brasil. Morphology and ecology. Part I: Achives des Sciences, Geneve, 30, 77-89.
Bronnimann, P., Zaninetti, L., and Whittaker, J. E., 1983, On the classification of the Trochamminacea (Foraminiferida): Journal of Foraminiferal Research, 13, 202-218.
Bronnimann, P., and Whittaker, J. E., 1988, The Trochamminacea of the Discovery Reports, British Museum, London, pp. 152.
Cai, W. J., and Cowan, T., 2007, Trends in Southern Hemisphere circulation in IPCC AR4 models over 1950-99: Ozone depletion versus greenhouse forcing: Journal of Climate, 20, 4, 681-693.
Calvo, E., Pelejero, C., De Deckker, P., and Logan, G. A., 2007, Antarctic deglacial pattern in a 30 kyr record of sea surface temperature offshore South Australia: Geophysical Research Letters, 34, 13, L13707.
Caniupan, M., Lamy, F., Lange, C. B., Kaiser, J., Kilian, R., Arz, H. W., Leon, T., Mollenhauer, G., Sandoval, S., De Pol-Holz, R., Pantoja, S., Wellner, J., and Tiedemann, R., 2014, Holocene sea-surface temperature variability in the Chilean fjord region: Quaternary Research, 82, 2, 342-353.
Caralp, M. H., 1989, Abundance of *Bulimina exilis* and *Melonis barleeanum* - relationship to the quality of marine organic-matter: Geo-Marine Letters, 9, 1, 37-43.
Carpenter, W. B., Parker, W. K., and Jones, T. R., 1862, Introduction to the study of the Foraminifera, Ray Society, London, pp. 440.
Carpenter, W. B., 1869, On the rhizopodal fauna of the deep sea: Proceedings of the Royal Society of London, 18, 59-62.
Caulle, C., Mojtahid, M., Gooday, A. J., Jorissen, F. J., and Kitazato, H., 2015, Living (Rose-Bengal-stained) benthic foraminiferal faunas along a strong bottom-water oxygen gradient on the Indian margin (Arabian Sea): Biogeosciences, 12, 16, 5005-5019.
Chapman, F., 1916, Report on the Foraminifera and Ostracoda from elevated deposits on the shores of the Ross Sea, *in* Benson, W. N., Chapman, F., Cohen, F., Cotton, L. A., Hedley, C., Jensen, H. I., Mawson, D., Skeats, E. W., Thomson, J. A., Walkom, A. B., and Woolnough, W. G., eds., British Antarctic Expedition 1907-9 under the command of Sir E. H. Shackleton, C.V.O.: Reports on the scientific investigations, Geology, Vol. II - Contributions to the palaeontology and petrology of South Victoria Land William Heinemann: London, 25-51.
Chapman, F., Parr, W. J., and Collins, A. C., 1934, Tertiary Foraminifera of Victoria, Australia. The Balcombian deposits of Port Phillip: Journal of the Linnaean Society, 38, 553-576.
Charnock, M. A., and Jones, R. W., 1990, Agglutinated foraminifera from the Palaeogene of the North Sea, *in* Hemleben, C., Kaminski, M. A., Kuhnt, W., and Scott, D. B., eds., Paleoecology , biostratigraphy,

paleoceanography and taxonomy of agglutinated foraminifera Kluwer Academic Publishers: Dordrecht, 139-244.
Clapperton, C. M., 1971, Evidence of cirque glaciation in the Falkland Islands: Journal of Glaciology, 10, 58, 121-125.
Clapperton, C. M., Sugden, D. E., Birnie, J., and Wilson, M. J., 1989, Late-glacial and Holocene glacier fluctuations and environmental-change on South Georgia, Southern-Ocean: Quaternary Research, 31, 2, 210-228.
Clark, P. U., Dyke, A. S., Shakun, J. D., Carlson, A. E., Clark, J., Wohlfarth, B., Mitrovica, J. X., Hostetler, S. W., and McCabe, A. M., 2009, The Last Glacial Maximum: Science, 325, 5941, 710-714.
Clark, P. U., Shakun, J. D., Baker, P. A., Bartlein, P. J., Brewer, S., Brook, E., Carlson, A. E., Cheng, H., Kaufman, D. S., Liu, Z., Marchitto, T. M., Mix, A. C., Morrill, C., Otto-Bliesner, B. L., Pahnke, K., Russell, J. M., Whitlock, C., Adkins, J. F., Blois, J. L., Clark, J., Colman, S. M., Curry, W. B., Flower, B. P., He, F., Johnson, T. C., Lynch-Stieglitz, J., Markgraf, V., McManus, J., Mitrovica, J. X., Moreno, P. I., and Williams, J. W., 2012, Global climate evolution during the last deglaciation: Proceedings of the National Academy of Sciences, 109, 19, E1134-E1142.
Clark, R., Huber, U. M., and Wilson, P., 1998, Late Pleistocene sediments and environmental change at Plaza Creek, Falkland Islands, South Atlantic: Journal of Quaternary Science, 13, 2, 95-105.
Collins, L. G., Pike, J., Allen, C. S., and Hodgson, D. A., 2012, High-resolution reconstruction of southwest Atlantic sea-ice and its role in the carbon cycle during marine isotope stages 3 and 2: Paleoceanography, 27, PA3217.
Conley, D. J., 1988, Biogenic silica as an estimate of siliceous microfossil abundance in Great Lakes sediments: Biogeochemistry, 6, 3, 161-179.
Conley, D. J., and Schelske, C. L., 1993, Potential Role of Sponge Spicules in Influencing the Silicon Biogeochemistry of Florida Lakes: Canadian Journal of Fisheries and Aquatic Sciences, 50, 2, 296-302.
-, 2001, Biogenic Silica, *in* Smol, J. P., Birks, H. J. B., and Last, W. M., eds., Tracking environmental change using lake sediments. Volume 3: Terrestrial, Algal, and Siliceous Indicators Kluwer Academic Publisherd: Dordrecht, The Netherlands, 281-293.
Conway, T. M., Wolff, E. W., Rothlisberger, R., Mulvaney, R., and Elderfield, H. E., 2015, Constraints on soluble aerosol iron flux to the Southern Ocean at the Last Glacial Maximum: Nature Communications, 6, 7850.
Cook, M. S., Keigwin, L. D., Birgel, D., and Hinrichs, K. U., 2011, Repeated pulses of vertical methane flux recorded in glacial sediments from the southeast Bering Sea: Paleoceanography, 26, PA2210.
Corliss, B. H., 1983, Distribution of Holocene deep-sea benthonic foraminifera in the Southwest Indian Ocean: Deep-Sea Research Part a-Oceanographic Research Papers, 30, 2, 95-117.
Corliss, B. H., and Emerson, S., 1990, Distribution of Rose-Bengal stained deep-sea benthic foraminifera from the Nova Scotian continental-margin and Gulf of Maine: Deep-Sea Research Part a-Oceanographic Research Papers, 37, 3, 381-400.
Cortese, G., Abelmann, A., and Gersonde, R., 2007, The last five glacial-interglacial transitions: A high-resolution 450,000-year record from the subantarctic Atlantic: Paleoceanography, 22, 4, PA4203.
Cross, S. L., Baker, P. A., Seltzer, G. O., Fritz, S. C., and Dunbar, R. B., 2000, A new estimate of the Holocene lowstand level of Lake Titicaca, central Andes, and implications for tropical palaeohydrology: Holocene, 10, 1, 21-32.
Crosta, X., Sturm, A., Armand, L., and Pichon, J. J., 2004, Late Quaternary sea ice history in the Indian sector of the Southern Ocean as recorded by diatom assemblages: Marine Micropaleontology, 50, 3-4, 209-223.

Crosta, X., Crespin, J., Billy, I., and Ther, O., 2005, Major factors controlling Holocene $\delta^{13}C_{org}$ changes in a seasonal sea-ice environment, Adelie Land, East Antarctica: Global Biogeochemical Cycles, 19, 4, GB4029.
Crowley, T. J., 1992, North Atlantic deep water cools the southern hemisphere: Paleoceanography, 7, 4, 489-497.
Cushman, J. A., 1910, A monograph of the Foraminifera of the North Pacific Ocean. Part I. Astrorhizidae and Lituolidae: Bulletin of the United States National Museum 71, 1, 1-134.
-, 1913, A monograph of the foraminifera of the North Pacific Ocean. Pt. III. Lagenidae: Bulletin of the United States National Museum, 71, 3, 1-125.
-, 1923, The foraminifera of the Atlantic Ocean, Part 4. Lagenidae: Bulletin United States National Museum, 104, 4, 1-228.
-, 1926, Foraminifera of the typical Monerey of California: Cushman Foundation for Foraminiferal Research Special Publication, 2, 53-69.
-, 1927, An outline of a re-classification of the foraminifera: Contributions from the Cushman laboratory for foraminiferal research, 3, 1-105.
-, 1930, The foraminifera of the Atlantic Ocean, Part 7, Nonionidae, Camerinidae, Peneroplidae and Alveolinellidae: Bulletin United States National Museum, 104, 7, 1-79.
-, 1933, Foraminifera, their classification and economic use Cushman Lab. Foram. Res., Special Publ. No. 4: 1-349.: Special Publications Cushman Laboratory for Foraminiferal Research, 4, 1-349.
Cushman, J. A., and Edwards, P. G., 1937, *Astrononion* a new genus of the foraminifera and its species: Contributions from the Cushman laboratory for foraminiferal research, 13, 29-36.
Cushman, J. A., 1945, Foraminifera of the United States Antarctic Service Expedition 1939–1941: Proceedings, American Philosophical Society, 89, 285-288.
d'Orbigny, A., 1826, Tableau méthodique de la classe des Céphalopodes: Annales des Sciences Naturelles, 7, 245-314.
-, 1839a, Voyage dans l'Amérique Méridionale (le Brésil, la République orientale de l'Uruquay, la République Argentine, la Patagonie, la République du Chili, la République de Bolivia, la République du Pérou) éxécuté pendant les années 1826, 1827, 1832 et 1833 *in* Levrault, S., ed., Foraminifères Bertrand: Paris, 1-86.
-, 1839b, Foraminifères, *in* de la Sagra, R., ed., Histoire Physique, Politique et Naturelle de l'île de Cuba A. Bertrand: Paris, 1-224.
Darvill, C. M., Bentley, M. J., Stokes, C. R., Hein, A. S., and Rodés, Á., 2015, Extensive MIS 3 glaciation in southernmost Patagonia revealed by cosmogenic nuclide dating of outwash sediments: Earth and Planetary Science Letters, 429, Supplement C, 157-169.
de Montfort, P. D., 1808, Conchyliologie systématique et classification méthodique des coquilles, F. Schoell, Paris, pp. 676.
De Rijk, S., Jorissen, F. J., Rohling, E. J., and Troelstra, S. R., 2000, Organic flux control on bathymetric zonation of Mediterranean benthic foraminifera: Marine Micropaleontology, 40, 3, 151-166.
Deacon, G. E. R., and Foster, T. D., 1977, Boundary region between Weddell Sea and Drake Passage currents: Deep-Sea Research, 24, 6, 505-510.
Deacon, G. E. R., 1977, Seasonal and annual variations in water temperature and salinity near South Georgia 1925-1937, Institute of Oceanographic Sciences, Wormley, UK, pp. 21.
Debenay, J.-P., Beck Eichler, B., Duleba, W., Bonetti, C., and Eichler-Coelho, P., 1998, Water stratification in coastal lagoons: its influence on foraminiferal assemblages in two Brazilian lagoons: Marine Micropaleontology, 35, 1–2, 67-89.
Defrance, J. L. M., 1824, Dictionnaire des Sciences Naturelles, F.G. Levrault, Strasbourg, pp.:

Deines, E. T., 1980, The isotopic composition of reduced organic carbon, *in* Fritz, P., and Fontes, J. C., eds., Handbook of environmental isotope geochemistry,Volume 1 Elsevier: New York, 329-406.
Dejardin, R., Kender, S., Allen, C. S., Leng, M. J., Swann, G. E. A., and Peck, V. L., 2018, "Live" (stained) benthic foraminiferal living depths, stable isotopes, and taxonomy offshore South Georgia, Southern Ocean: implications for calcification depths: J. Micropalaeontol., 37, 1, 25-71.
DeLaca, T. E., 1986, The morphology and ecology of *Astrammina rara*: Journal of Foraminiferal Research, 16, 216-233.
Demaster, D. J., 1981, The supply and accumulation of silica in the marine-environment: Geochimica Et Cosmochimica Acta, 45, 10, 1715-1732.
Denis, D., Crosta, X., Schmidt, S., Carson, D. S., Ganeshram, R. S., Renssen, H., Crespin, J., Ther, O., Billy, I., and Giraudeau, J., 2009, Holocene productivity changes off Adelie Land (East Antarctica): Paleoceanography, 24, PA3207.
Denis, D., Crosta, X., Barbara, L., Masse, G., Renssen, H., Ther, O., and Giraudeau, J., 2010, Sea ice and wind variability during the Holocene in East Antarctica: insight on middle-high latitude coupling: Quaternary Science Reviews, 29, 27-28, 3709-3719.
Denton, G. H., Anderson, R. F., Toggweiler, J. R., Edwards, R. L., Schaefer, J. M., and Putnam, A. E., 2010, The Last Glacial Termination: Science, 328, 5986, 1652-1656.
Dierssen, H. M., Smith, R. C., and Vernet, M., 2002, Glacial meltwater dynamics in coastal waters west of the Antarctic peninsula: Proceedings of the National Academy of Sciences of the United States of America, 99, 4, 1790-1795.
Ding, Q. H., Steig, E. J., Battisti, D. S., and Wallace, J. M., 2012, Influence of the Tropics on the Southern Annular Mode: Journal of Climate, 25, 18, 6330-6348.
Domack, E., Amblas, D., Gilbert, R., Brachfeld, S., Camerlenghi, A., Rebesco, M., Canals, M., and Urgeles, R., 2006, Subglacial morphology and glacial evolution of the Palmer Deep outlet system, Antarctic Peninsula: Geomorphology, 75, 1-2, 125-142.
Domack, E. W., Ishman, S. E., Stein, A. B., McClennen, C. E., and Jull, A. J. T., 1995, Late Holocene advance of the Muller Ice Shelf, Antarctic Peninsula - sedimentological, geochemical and paleontological evidence: Antarctic Science, 7, 2, 159-170.
Domack, E. W., and Mayewski, P. A., 1999, Bi-polar ocean linkages: evidence from late-Holocene Antarctic marine and Greenland ice-core records: Holocene, 9, 2, 247-251.
Duffield, C. J., Hess, S., Norling, K., and Alve, E., 2015, The response of *Nonionella iridea* and other benthic foraminifera to "fresh" organic matter enrichment and physical disturbance: Marine Micropaleontology, 120, 20-30.
Duplessy, J. C., Lalou, C., and Vinot, A. C., 1970, Differential isotopic fractionation in benthic foraminifera and paleotemperatures reassessed: Science, 168, 3928, 250-251.
Earland, A., 1933, Foraminifera, Part II, South Georgia, Discovery Reports,Volume 7: London, 27-138.
-, 1934, Foraminifera. Part III. The Falklands sector of the Antarctic (excluding South Georgia), Discovery Reports,Volume 10: London, 1-208.
Echols, R. J., 1971, Distribution of foraminifera in sediments of the Scotia Sea area, Antarctic waters, *in* Reid, J. L., ed., Antarctic Oceanography I,Volume 15 American Geophysical Union: Washington, D. C, 93-168.
Ehrenberg, C. G., 1838, Uber die Bildung der Kreidefelsen und des Kreidemergels durch unsichtbare Organismen: Physikalische

Abhandlungen der Koniglichen Akademie der Wissenschaften zu Berlin, 1838, 59-147.
-, 1861, Elemente des tiefen Meeresgrundes im Mexikanishen Golfstrome bei Florida:uber die Tiefgrund-Verhaltnisse des Oceans am eingange der Davisstrasse und bei Island: Monatsbericht der Koniglichen Preussichen Akademie der Wissenschaften zu Berlin, 1861, 275-315.
Elderfield, H., Yu, J., Anand, P., Kiefer, T., and Nyland, B., 2006, Calibrations for benthic foraminiferal Mg/Ca paleothermometry and the carbonate ion hypothesis: Earth and Planetary Science Letters, 250, 3–4, 633-649.
Elderfield, H., Greaves, M., Barker, S., Hall, I. R., Tripati, A., Ferretti, P., Crowhurst, S., Booth, L., and Daunt, C., 2010, A record of bottom water temperature and seawater $\delta^{18}O$ for the Southern Ocean over the past 440 kyr based on Mg/Ca of benthic foraminiferal *Uvigerina* spp.: Quaternary Science Reviews, 29, 1–2, 160-169.
Elderfield, H., Ferretti, P., Greaves, M., Crowhurst, S., McCave, I. N., Hodell, D., and Piotrowski, A. M., 2012, Evolution of ocean temperature and ice volume through the mid-Pleistocene climate transition: Science, 337, 6095, 704-709.
Elvidge, A. D., and Renfrew, I. A., 2016, The causes of foehn warming in the lee of mountains: Bulletin of the American Meteorological Society, 97, 3, 455-466.
Enge, A. J., Nomaki, H., Ogawa, N. O., Witte, U., Moeseneder, M. M., Lavik, G., Ohkouchi, N., Kitazato, H., Kucera, M., and Heinz, P., 2011, Response of the benthic foraminiferal community to a simulated short-term phytodetritus pulse in the abyssal North Pacific: Marine Ecology Progress Series, 438, 129-142.
Eppley, R. W., and Peterson, B. J., 1979, Particulate organic-matter flux and planktonic new production in the deep ocean: Nature, 282, 5740, 677-680.
Etourneau, J., Collins, L. G., Willmott, V., Kim, J. H., Barbara, L., Leventer, A., Schouten, S., Damste, J. S. S., Bianchini, A., Klein, V., Crosta, X., and Masse, G., 2013, Holocene climate variations in the western Antarctic Peninsula: evidence for sea ice extent predominantly controlled by changes in insolation and ENSO variability: Climate of the Past, 9, 4, 1431-1446.
Evangelista, H., Gurgel, M., Sifeddine, A., Rigozo, N. R., and Boussafir, M., 2014, South Tropical Atlantic anti-phase response to Holocene Bond Events: Palaeogeography Palaeoclimatology Palaeoecology, 415, 21-27.
Farmer, E. C., deMenocal, P. B., and Marchitto, T. M., 2005, Holocene and deglacial ocean temperature variability in the Benguela upwelling region: Implications for low-latitude atmospheric circulation: Paleoceanography, 20, 2, PA2018.
Fernandez, M., Maidana, N., and Rabassa, J., 2012, Palaeoenvironmental conditions during the Middle Holocene at Isla de los Estados (Staaten Island, Tierra del Fuego, 54ºS, Argentina) and their influence on the possibilities for human exploration: Quaternary International, 256, 78-87.
Figueira, B. O., Grenfell, H. R., Hayward, B. W., and Alfaro, A. C., 2012, Comparison of Rose Bengal and CellTracker Green staining for identification of live salt-marsh foraminifera: Journal of Foraminiferal Research, 42, 3, 206-215.
Fischer, G., Ratmeyer, V., and Wefer, G., 2000, Organic carbon fluxes in the Atlantic and the Southern Ocean: relationship to primary production compiled from satellite radiometer data: Deep-Sea Research Part Ii-Topical Studies in Oceanography, 47, 9-11, 1961-1997.
Fisher, R. A., Corbet, A. S., and Williams, C. B., 1943, The relation between the number of species and the number of individuals in a random sample of an animal population: Journal of Animal Ecology, 12, 42-58.

Fontanier, C., Jorissen, F. J., Chaillou, G., David, C., Anschutz, P., and Lafon, V., 2003, Seasonal and interannual variability of benthic foraminiferal faunas at 550 m depth in the Bay of Biscay: Deep-Sea Research Part I-Oceanographic Research Papers, 50, 4, 457-494.
Fontanier, C., Mackensen, A., Jorissen, F. J., Anschutz, P., Licari, L., and Griveaud, C., 2006a, Stable oxygen and carbon isotopes of live benthic foraminifera from the Bay of Biscay: Microhabitat impact and seasonal variability: Marine Micropaleontology, 58, 3, 159-183.
Fontanier, C., Jorissen, F., Anschutz, P., and Chaillou, G., 2006b, Seasonal variability of benthic foraminiferal faunas at 1000 m depth in the Bay of Biscay: Journal of Foraminiferal Research, 36, 1, 61-76.
Fontanier, C., Jorissen, F. J., Michel, E., Cortijo, E., Vidal, L., and Anschutz, P., 2008, Stable oxygen and carbon isotopes of live (stained) benthic foraminifera from Cap-Ferret Canyon (Bay of Biscay): Journal of Foraminiferal Research, 38, 1, 39-51.
Fontanier, C., Garnier, E., Brandily, C., Dennielou, B., Bichon, S., Gayet, N., Eugene, T., Rovere, M., Grémare, A., and Deflandre, B., 2016, Living (stained) benthic foraminifera from the Mozambique Channel (eastern Africa): Exploring ecology of deep-sea unicellular meiofauna: Deep Sea Research Part I: Oceanographic Research Papers, 115, 159-174.
Frerichs, W. E., 1969, Recent arenaceous foraminifers from Gulf of Mexico: Palaeontological Contributions, University of Kansas, 46, 1-2.
Fyfe, J. C., 2006, Southern Ocean warming due to human influence: Geophysical Research Letters, 33, 19, L19701.
Fyfe, J. C., and Saenko, O. A., 2006, Simulated changes in the extratropical Southern Hemisphere winds and currents: Geophysical Research Letters, 33, 6, L06701.
Gabric, A. J., Cropp, R. A., McTainsh, G. H., Johnston, B. M., Butler, H., Tilbrook, B., and Keywood, M., 2010, Australian dust storms in 2002-2003 and their impact on Southern Ocean biogeochemistry: Global Biogeochemical Cycles, 24, GB2005.
Galloway, J. J., 1933, A manual of Foraminifera, Principia Press, Bloomington, pp. 483.
Gasso, S., and Stein, A. F., 2007, Does dust from Patagonia reach the sub-Antarctic Atlantic ocean?: Geophysical Research Letters, 34, 1, L01801.
Gaździcki, A., and Majewski, W., 2003, Recent foraminifera from Goulden Cove of King George Island, Antarctica: Polish Polar Research, 24, 1, 3-12.
Gehlen, M., Mucci, A., and Boudreau, B., 1999, Modelling the distribution of stable carbon isotopes in porewaters of deep-sea sediments: Geochimica Et Cosmochimica Acta, 63, 18, 2763-2773.
Geraga, M., Ioakim, C., Lykousis, V., Tsaila-Monopolis, S., and Mylona, G., 2010, The high-resolution palaeoclimatic and palaeoceanographic history of the last 24,000 years in the central Aegean Sea, Greece: Palaeogeography Palaeoclimatology Palaeoecology, 287, 1-4, 101-115.
Gersonde, R., Crosta, X., Abelmann, A., and Armand, L., 2005, Sea-surface temperature and sea ice distribution of the Southern Ocean at the EPILOG Last Glacial Maximum - A circum-Antarctic view based on siliceous microfossil records: Quaternary Science Reviews, 24, 7-9, 869-896.
Geslin, E., Heinz, P., Jorissen, F., and Hemleben, C., 2004, Migratory responses of deep-sea benthic foraminifera to variable oxygen conditions: laboratory investigations: Marine Micropaleontology, 53, 3-4, 227-243.
Gibbard, P., 2018, Formal subdivision of the Holocene Series/Epoch, Date Accessed: 18/10/18, http://stratigraphy.org/index.php/ics-news-and-meetings/125-formal-subdivision-of-the-holocene-series-epoch.
Gill, A. E., 1973, Circulation and bottom water production in Weddell Sea: Deep-Sea Research, 20, 2, 111-140.
-, 1982, Atmosphere-ocean dynamics, Academic Press, New York, pp. 645.

Glaessner, M. F., 1937, Die Entfaltung der Foraminiferenfamilie Buliminidae: Problemy Palaeontologii, Palaeontologicheskaya Laboratoriya Moskovskogo Gosudarstvennogo Universiteta, 2-3, 411-422.
Glasser, N. F., Harrison, S., Winchester, V., and Aniya, M., 2004, Late Pleistocene and Holocene palaeoclimate and glacier fluctuations in Patagonia: Global and Planetary Change, 43, 1, 79-101.
Goes, A., 1894, A synopsis of the Arctic and Scandinavian Recent marine Foraminifera hitherto discovered: Kongl. svenka vetenskaps-Akademiens handlinger 25, 1-127.
Gong, T. T., Feldstein, S. B., and Luo, D. H., 2010, The impact of ENSO on wave breaking and Southern Annular Mode events: Journal of the Atmospheric Sciences, 67, 9, 2854-2870.
Goñi, M. A., Ruttenberg, K. C., and Eglinton, T. I., 1997, Sources and contribution of terrigenous organic carbon to surface sediments in the Gulf of Mexico: Nature, 389, 275-278.
Gooday, A. J., 1988, A response by benthic foraminifera to the deposition of phytodetritus in the deep-sea: Nature, 332, 6159, 70-73.
-, 1993, Deep-sea benthic foraminiferal species which exploit phytodetritus - characteristic features and controls on distribution: Marine Micropaleontology, 22, 3, 187-205.
-, 1996, Epifaunal and shallow infaunal foraminiferal communities at three abyssal NE Atlantic sites subject to differing phytodetritus input regimes: Deep-Sea Research Part I-Oceanographic Research Papers, 43, 9, 1395-1421.
Gooday, A. J., and Alve, E., 2001, Morphological and ecological parallels between sublittoral and abyssal foraminiferal species in the NE Atlantic: a comparison of *Stainforthia fusiformis* and *Stainforthia* sp.: Progress in Oceanography, 50, 1-4, 261-283.
Gooday, A. J., and Hughes, J. A., 2002, Foraminifera associated with phytodetritus deposits at a bathyal site in the northern Rockall Trough (NE Atlantic): seasonal contrasts and a comparison of stained and dead assemblages: Marine Micropaleontology, 46, 1-2, 83-110.
Gooday, A. J., da Silva, A. A., Koho, K. A., Lecroq, B., and Pearce, R. B., 2010, The 'mica sandwich'; a remarkable new genus of Foraminifera (Protista, Rhizaria) from the Nazare Canyon (Portuguese margin, NE Atlantic): Micropaleontology, 56, 3-4, 345-357.
Gooday, A. J., and Jorissen, F. J., 2012, Benthic Foraminiferal Biogeography: Controls on Global Distribution Patterns in Deep-Water Settings: Annual Review of Marine Science, Vol 4, 4, 237-262.
Goosse, H., Masson-Delmotte, V., Renssen, H., Delmotte, M., Fichefet, T., Morgan, V., van Ommen, T., Khim, B. K., and Stenni, B., 2004, A late medieval warm period in the Southern Ocean as a delayed response to external forcing?: Geophysical Research Letters, 31, 6, L06203.
Gordon, J. E., Haynes, V. M., and Hubbard, A., 2008, Recent glacier changes and climate trends on South Georgia: Global and Planetary Change, 60, 1-2, 72-84.
Gottschalk, J., Skinner, L. C., Misra, S., Waelbroeck, C., Menviel, L., and Timmermann, A., 2015, Abrupt changes in the southern extent of North Atlantic Deep Water during Dansgaard-Oeschger events: Nature Geoscience, 8, 12, 950-955.
Graham, A. G. C., Fretwell, P. T., Larter, R. D., Hodgson, D. A., Wilson, C. K., Tate, A. J., and Morris, P., 2008, A new bathymetric compilation highlighting extensive paleo-ice sheet drainage on the continental shelf, South Georgia, sub-Antarctica: Geochemistry Geophysics Geosystems, 9, Q07011.
Graham, A. G. C., Kuhn, G., Meisel, O., Hillenbrand, C.-D., Hodgson, D. A., Ehrmann, W., Wacker, L., Wintersteller, P., dos Santos Ferreira, C.,

Römer, M., White, D., and Bohrmann, G., 2017, Major advance of South Georgia glaciers during the Antarctic Cold Reversal following extensive sub-Antarctic glaciation: Nature Communications, 8, 14798.
Gregory, J. W., 1915, The physiography of South Georgia as shown by Mr Ferguson's photographs, *in* Ferguson, D., ed., Geological Observations in South Georgia,Volume 50 Transactions of the Royal Society of Edinburgh: Edindurgh, 814-816.
Gregory, R. T., and Taylor, H. P., 1981, An oxygen isotope profile in a section of Cretaceous oceanic-crust, Samail ophiolite, Oman - evidence for $\delta^{18}O$ buffering of the oceans by deep (less-than 5 km) seawater-hydrothermal circulation at mid-ocean ridges: Journal of Geophysical Research, 86, NB4, 2737-2755.
Griffith, J. W., and Henfrey, A., 1875, The Micrographic Dictionary, van Voorst, London, pp. 845.
Grimm, K. A., Lange, C. B., and Gill, A. S., 1996, Biological forcing of hemipelagic sedimentary laminae: Evidence from ODP Site 893, Santa Barbara Basin, California: Journal of Sedimentary Research, 66, 3, 613-624.
-, 1997, Self-sedimentation of phytoplankton blooms in the geologic record: Sedimentary Geology, 110, 3-4, 151-161.
Gross, O., 2000, Influence of temperature, oxygen and food availability on the migrational activity of bathyal benthic foraminifera: evidence by microcosm experiments: Hydrobiologia, 426, 1, 123-137.
Grossman, E. L., 1987, Stable isotopes in modern benthic foraminifera: a study of vital effect: Journal of Foraminiferal Research, 17, 1, 48-61.
Haeckel, E., 1894, Systematische Phylogenie. Entwurf eines Naturlichen Systems der Organismen auf Grund ihrer Stammesgeschichte. Theil 1, Systematische Phylogenie der Protisten und Pflanzen, Georg Reimer, Berlin, pp.:
Hall, A., and Visbeck, M., 2002, Synchronous variability in the southern hemisphere atmosphere, sea ice, and ocean resulting from the annular mode: Journal of Climate, 15, 21, 3043-3057.
Hammer, O., Harper, D. A. T., and Ryan, P. D., 2001, PAST: Paleontological statistics software package for education and data analysis: Palaeontologia Electronica, 4, 1, 4.
Hayward, B. W., Grenfell, H. R., Sabaa, A. T., and Neil, H. L., 2007, Factors influencing the distribution of subantarctic deep-sea benthic foraminifera, Campbell and Bounty Plateaux, New Zealand: Marine Micropaleontology, 62, 3, 141-166.
Hayward, B. W., Kawagata, S., Sabaa, A. T., Grenfell, H. R., van Kerckhoven, L., Johnson, K., and Thomas, E., 2012, The last global extinction (Mid-Pleistocene) of deep-sea benthic foraminifera (Chrysalogoniidae, Ellipsoidinidae, Glandulonodosariidae, Plectofrondiculariidae, Pleursostomellidae, Stilostomellidae), their Late Cretaceous-Cenozoic history and taxonomy: Cushman Foundation for Foraminiferal Research Special Publication, 43, 1-410.
Hayward, B. W., Sabaa, A. T., Grenfell, H. R., Neil, H., and Bostock, H., 2013, Ecological distribution of recent deep-water foraminifera around New Zealand: Journal of Foraminiferal Research, 43, 4, 415-442.
He, F., Shakun, J. D., Clark, P. U., Carlson, A. E., Liu, Z., Otto-Bliesner, B. L., and Kutzbach, J. E., 2013, Northern Hemisphere forcing of Southern Hemisphere climate during the last deglaciation: Nature, 494, 81-85.
Headland, R. K., 1984, The island of South Georgia, Cambridge University Press, Cambridge, pp. 293.
Hein, J. R., Oneil, J. R., and Jones, M. G., 1979, Origin of authigenic carbonates in sediment from the deep Bering Sea: Sedimentology, 26, 5, 681-705.

Herb, R., 1971, Distribution of recent benthonic foraminifera in the Drake Passage, Biology of the Antarctic Seas IV American Geophysical Union, 251-300.
Herguera, J. C., and Berger, W. H., 1991, Paleoproductivity from benthic foraminifera abundance: Glacial to postglacial change in the west-equatorial Pacific: Geology, 19, 12, 1173-1176.
Herguera, J. C., 1992, Deep-sea benthic foraminifera and biogenic opal: Glacial to postglacial productivity changes in the western equatorial Pacific: Marine Micropaleontology, 19, 1-2, 79-98.
Hermelin, J. O. R., 1989, Pliocene benthic foraminifera from the Ontong-Java plateau (western equatorial Pacific Ocean): faunal response to changing paleoenvironments, Cushman Foundation for Foraminiferal Research Special Publication, pp. 143.
Heron-Allen, E., and Earland, A., 1912, On some Foraminifera from the North Sea, etc., dredged by the Fisheries Cruiser 'Goldseeker' (International North Sea Investigations - Scotland). I. On some new Astrorhizidae and their shell-structure.: Journal of the Royal Microscopical Society, 1912, 382-389.
-, 1922, Les Foraminifères des "Sables Rouges" du golfe de Ajaccio (Côte Nord). : Bulletin de la Société des sciences historiques et naturelles de la Corse, 42, 3, 109-149.
-, 1929, XXVII.— Some new Foraminifera from the South Atlantic: Journal of the Royal Microscopical Society, 49, 4, 324-334.
-, 1930, Some new foraminifera from the South Atlantic, Part 3. : Journal of the Royal Microscopical Society, 50, 38-45.
-, 1932a, Foraminifera. Part 1. The ice-free area of the Falkland Islands and adjacent seas., Discovery Reports,Volume 4: London, 291-460.
-, 1932b, Some new foraminifera from the South Atlantic, IV: Journal of the Royal Microscopical Society, 52, 3, 253-261.
Hill, T. M., Kennett, J. P., and Spero, H. J., 2003, Foraminifera as indicators of methane-rich environments: A study of modern methane seeps in Santa Barbara Channel, California: Marine Micropaleontology, 49, 1-2, 123-138.
Hillenbrand, C.-D., Bentley, M. J., Stolldorf, T. D., Hein, A. S., Kuhn, G., Graham, A. G. C., Fogwill, C. J., Kristoffersen, Y., Smith, J. A., Anderson, J. B., Larter, R. D., Melles, M., Hodgson, D. A., Mulvaney, R., and Sugden, D. E., 2014, Reconstruction of changes in the Weddell Sea sector of the Antarctic Ice Sheet since the Last Glacial Maximum: Quaternary Science Reviews, 100, 111-136.
Hodell, D. A., Kanfoush, S. L., Shemesh, A., Crosta, X., Charles, C. D., and Guilderson, T. P., 2001, Abrupt cooling of Antarctic surface waters and sea ice expansion in the South Atlantic sector of the Southern Ocean at 5000 cal yr B.P: Quaternary Research, 56, 2, 191-198.
Hodgson, D. A., Roberts, S. J., Smith, J. A., Verleyen, E., Sterken, M., Labarque, M., Sabbe, K., Vyverman, W., Allen, C. S., Leng, M. J., and Bryant, C., 2013, Late Quaternary environmental changes in Marguerite Bay, Antarctic Peninsula, inferred from lake sediments and raised beaches: Quaternary Science Reviews, 68, 216-236.
Hodgson, D. A., Graham, A. G. C., Roberts, S. J., Bentley, M. J., Cofaigh, C. Ó., Verleyen, E., Vyverman, W., Jomelli, V., Favier, V., Brunstein, D., Verfaillie, D., Colhoun, E. A., Saunders, K. M., Selkirk, P. M., Mackintosh, A., Hedding, D. W., Nel, W., Hall, K., McGlone, M. S., Van der Putten, N., Dickens, W. A., and Smith, J. A., 2014a, Terrestrial and submarine evidence for the extent and timing of the Last Glacial Maximum and the onset of deglaciation on the maritime-Antarctic and sub-Antarctic islands: Quaternary Science Reviews, 100, 137-158.
Hodgson, D. A., Graham, A. G. C., Griffiths, H. J., Roberts, S. J., O Cofaigh, C., Bentley, M. J., and Evans, D. J. A., 2014b, Glacial history of sub-Antarctic

South Georgia based on the submarine geomorphology of its fjords: Quaternary Science Reviews, 89, 129-147.
Hoefs, M. J. L., Versteegh, G. J. M., Rijpstra, W. I. C., de Leeuw, J. W., and Damsté, J. S. S., 1998, Post-depositional oxic degradation of alkenones: Implications for the measurement of palaeo sea surface temperatures: Paleoceanography, 13, 1, 42-49.
Hogg, A. G., Hua, Q., Blackwell, P. G., Niu, M., Buck, C. E., Guilderson, T. P., Heaton, T. J., Palmer, J. G., Reimer, P. J., Reimer, R. W., Turney, C. S. M., and Zimmerman, S. R. H., 2013, SHCal13 southern hemisphere calibration, 0-50,000 years cal BP: Radiocarbon, 55, 4, 1889-1903.
Hogg, O. T., Barnes, D. K. A., and Griffiths, H. J., 2011, Highly diverse, poorly studied and uniquely threatened by climate change: An assessment of marine biodiversity on South Georgia's continental shelf: PLoS One, 6, 5, e19795.
Höglund, H., 1947, Foraminifera in the Gullmar Fjord and the Skagerak. : Zoologiska Bidrag fran Uuppsala, 26, 1-328.
Holbourn, A., Henderson, A. S., and MacLeod, N., 2013, Atlas of benthic foraminifera, John Wiley & Sons, pp. 653.
Holeton, C. L., Nedelec, F., Sanders, R., Brown, L., Moore, C. M., Stevens, D. P., Heywood, K. J., Statham, P. J., and Lucas, C. H., 2005, Physiological state of phytoplankton communities in the Southwest Atlantic sector of the Southern Ocean, as measured by fast repetition rate fluorometry: Polar Biology, 29, 1, 44-52.
Holsten, J., Stott, L., and Berelson, W., 2004, Reconstructing benthic carbon oxidation rates using $\delta^{13}C$ of benthic foraminifers: Marine Micropaleontology, 53, 1–2, 117-132.
Hoogakker, B. A. A., Elderfield, H., Schmiedl, G., McCave, I. N., and Rickaby, R. E. M., 2015, Glacial-interglacial changes in bottom-water oxygen content on the Portuguese margin: Nature Geosci, 8, 1, 40-43.
Hosking, J. S., Bannister, D., Orr, A., King, J., Young, E., and Phillips, T., 2015, Orographic disturbances of surface winds over the shelf waters adjacent to South Georgia: Atmospheric Science Letters, 16, 1, 50-55.
Hromic, T., Ishman, S., and Silva, N., 2006, Benthic foraminiferal distributions in Chilean fjords: 47ºS to 54ºS: Marine Micropaleontology, 59, 2, 115-134.
Huybers, P., and Denton, G., 2008, Antarctic temperature at orbital timescales controlled by local summer duration: Nature Geoscience, 1, 11, 787-792.
Igarashi, A., Numanami, H., Tsuchiya, Y., and Fukucki, M., 2001, Bathymetric distribution of fossil foraminifera within marine sediment cores from the eastern part of Lutzow-Holm Bay, East Antarctica, and its paleoceanographic implications: Marine Micropaleontology, 42, 3-4, 125-162.
Iglesias, V., Markgraf, V., and Whitlock, C., 2016, 17,000 years of vegetation, fire and climate change in the eastern foothills of the Andes (lat. 44ºS): Palaeogeography Palaeoclimatology Palaeoecology, 457, 195-208.
Ingall, E. D., Bustin, R. M., and Van Cappellen, P., 1993, Influence of water column anoxia on the burial and preservation of carbon and phosphorus in marine shales: Geochimica et Cosmochimica Acta, 57, 2, 303-316.
Ingolfsson, O., Hjort, C., Berkman, P. A., Bjorck, S., Colhoun, E., Goodwin, I. D., Hall, B., Hirakawa, K., Melles, M., Moller, P., and Prentice, M. L., 1998, Antarctic glacial history since the Last Glacial Maximum: an overview of the record on land: Antarctic Science, 10, 3, 326-344.
IPCC, 2014, Climate change 2014: Impacts, adaptation, and vulnerability. Part A: Global and sectoral aspects. Contribution of working group II to the fifth assessment report of the Intergovernmental Panel on Climate Change, Cambridge University Press, Cambridge, United Kingdom and New York, NY, USA, pp. 1132.

Ishman, S. E., and Domack, E. W., 1994, Oceanographic controls on benthic foraminifers from the Bellingshausen margin of the Antarctic Peninsula: Marine Micropaleontology, 24, 2, 119-155.
Ishman, S. E., and Sperling, M. R., 2002, Benthic foraminiferal record of Holocene deep-water evolution in the Palmer Deep, western Antarctic Peninsula: Geology, 30, 5, 435-438.
Jahnke, R. A., 1996, The global ocean flux of particulate organic carbon: Areal distribution and magnitude: Global Biogeochemical Cycles, 10, 1, 71-88.
Jomelli, V., Mokadem, F., Schimmelpfennig, I., Chapron, E., Rinterknecht, V., Favier, V., Verfaillie, D., Brunstein, D., Legentil, C., Michel, E., Swingedouw, D., Jaouen, A., Aumaitre, G., Bourlès, D. L., and Keddadouche, K., 2017, Sub-Antarctic glacier extensions in the Kerguelen region (49°S, Indian Ocean) over the past 24,000 years constrained by ^{36}Cl moraine dating: Quaternary Science Reviews, 162, 128-144.
Jones, E. M., Bakker, D. C. E., Venables, H. J., and Watson, A. J., 2012, Dynamic seasonal cycling of inorganic carbon downstream of South Georgia, Southern Ocean: Deep-Sea Research Part Ii-Topical Studies in Oceanography, 59, 25-35.
Jones, R. W., 1984, A revised classification of the unilocular Nodosariida and Buliminida (Foraminifera): Revista Espanola de Micropaleontologia, 16, 91-160.
Jones, R. W., 1994, The Challenger Foraminifera, Oxford University Press, Oxford, pp. 149.
Jorissen, F. J., deStigter, H. C., and Widmark, J. G. V., 1995, A conceptual model explaining benthic foraminiferal microhabitats: Marine Micropaleontology, 26, 1-4, 3-15.
Jorissen, F. J., Wittling, I., Peypouquet, J. P., Rabouille, C., and Relexans, J. C., 1998, Live benthic foraminiferal faunas off Cape Blanc, NW-Africa: Community structure and microhabitats: Deep-Sea Research Part I-Oceanographic Research Papers, 45, 12, 2157-2188.
Jorissen, F. J., Fontanier, C., and Thomas, E., 2007, Paleoceanographical proxies based on deep-sea benthic foraminiferal assemblage characteristics, *in* Hillaire-Marcel, C., and de Vernal, A., eds., Proxies in Late Cenozoic Paleoceanography,Volume 1 Elsevier: Amsterdam, 263-325.
Kaiser, J., Lamy, F., and Hebbeln, D., 2005, A 70-kyr sea surface temperature record off southern Chile (Ocean Drilling Program Site 1233): Paleoceanography, 20, 4, PA4009.
Kaiser, J., Ruggieri, N., Hefter, J., Siegel, H., Mollenhauer, G., Arz, H. W., and Lamy, F., 2014, Lipid biomarkers in surface sediments from the Gulf of Genoa, Ligurian sea (NW Mediterranean sea) and their potential for the reconstruction of palaeo-environments: Deep Sea Research Part I: Oceanographic Research Papers, 89, 68-83.
Kalnay, E., Kanamitsu, M., Kistler, R., Collins, W., Deaven, D., Gandin, L., Iredell, M., Saha, S., White, G., Woollen, J., Zhu, Y., Chelliah, M., Ebisuzaki, W., Higgins, W., Janowiak, J., Mo, K. C., Ropelewski, C., Wang, J., Leetmaa, A., Reynolds, R., Jenne, R., and Joseph, D., 1996, The NCEP/NCAR 40-year reanalysis project: Bulletin of the American Meteorological Society, 77, 3, 437-471.
Kaminski, M. A., 2004, The year 2000 classification of the agglutinated foraminifera, *in* Kaminski, M. A., and Bubik, M., eds., Proceedings of the Sixth International Workshop on Agglutinated Foraminifera (Prague, Czech Republic, September 1-7, 2001),Volume 8 Grzybowski Foundation Special Publication: London, UK, 237-255.
Kaminski, M. A., and Gradstein, F. M., 2005, Atlas of Paleogene cosmopolitan deep-water agglutinated foraminifera, Grzybowski Foundation Special Publication, Krakow, pp. 547.

Kanmacher, F., 1798, Adam's essays on the microscope: The second edition, with considerable additions and improvements, Dillon & Keating, London, pp.:
Kaplan, M. R., Schaefer, J. M., Strelin, J. A., Denton, G. H., Anderson, R. F., Vandergoes, M. J., Finkel, R. C., Schwartz, R., Travis, S. G., Garcia, J. L., Martini, M. A., and Nielsen, S. H. H., 2016, Patagonian and southern South Atlantic view of Holocene climate: Quaternary Science Reviews, 141, 112-125.
Kastner, S., Enters, D., Ohlendorf, C., Haberzettl, T., Kuhn, G., Lucke, A., Mayr, C., Reyss, J. L., Wastegard, S., and Zolitschka, B., 2010, Reconstructing 2000 years of hydrological variation derived from laminated proglacial sediments of Lago del Desierto at the eastern margin of the South Patagonian Ice Field, Argentina: Global and Planetary Change, 72, 3, 201-214.
Kattge, J., Diaz, S., Lavorel, S., Prentice, I. C., Leadley, P., Bonisch, G., Garnier, E., Westoby, M., Reich, P. B., Wright, I. J., Cornelissen, J. H. C., Violle, C., Harrison, S. P., Van Bodegom, P. M., Reichstein, M., Enquist, B. J., Soudzilovskaia, N. A., Ackerly, D. D., Anand, M., Atkin, O., Bahn, M., Baker, T. R., Baldocchi, D., Bekker, R., Blanco, C. C., Blonder, B., Bond, W. J., Bradstock, R., Bunker, D. E., Casanoves, F., Cavender-Bares, J., Chambers, J. Q., Chapin Iii, F. S., Chave, J., Coomes, D., Cornwell, W. K., Craine, J. M., Dobrin, B. H., Duarte, L., Durka, W., Elser, J., Esser, G., Estiarte, M., Fagan, W. F., Fang, J., Fernandez-Mendez, F., Fidelis, A., Finegan, B., Flores, O., Ford, H., Frank, D., Freschet, G. T., Fyllas, N. M., Gallagher, R. V., Green, W. A., Gutierrez, A. G., Hickler, T., Higgins, S. I., Hodgson, J. G., Jalili, A., Jansen, S., Joly, C. A., Kerkhoff, A. J., Kirkup, D., Kitajima, K., Kleyer, M., Klotz, S., Knops, J. M. H., Kramer, K., KÜHn, I., Kurokawa, H., Laughlin, D., Lee, T. D., Leishman, M., Lens, F., Lenz, T., Lewis, S. L., Lloyd, J., LlusiÀ, J., Louault, F., Ma, S., Mahecha, M. D., Manning, P., Massad, T., Medlyn, B. E., Messier, J., Moles, A. T., MÜLler, S. C., Nadrowski, K., Naeem, S., Niinemets, Ü., NÖLlert, S., NÜSke, A., Ogaya, R., Oleksyn, J., Onipchenko, V. G., Onoda, Y., OrdoÑEz, J., Overbeck, G., Ozinga, W. A., et al., 2011, TRY – a global database of plant traits: Global Change Biology, 17, 9, 2905-2935.
Kemp, A. E. S., and Baldauf, J. G., 1993, Vast Neogene laminated diatom mat deposits from the eastern equatorial Pacific Ocean: Nature, 362, 6416, 141-144.
Kemp, A. E. S., Pike, J., Pearce, R. B., and Lange, C. B., 2000, The "Fall dump" - a new perspective on the role of a "shade flora" in the annual cycle of diatom production and export flux: Deep-Sea Research Part Ii-Topical Studies in Oceanography, 47, 9-11, 2129-2154.
Kender, S., and Kaminski, M. A., 2017, Modern deep-water agglutinated foraminifera from IODP Expedition 323, Bering Sea: ecological and taxonomic implications: Journal of Micropalaeontology, 36, 2, 195-218.
Kennett, J. P., 1967, New Foraminifera from the Ross Sea, Antarctica: Contributions from the Cushman Foundation for Foraminiferal Research, 18, 133-135.
Khim, B. K., Yoon, H. I., Kang, C. Y., and Bahk, J. J., 2002, Unstable climate oscillations during the late Holocene in the eastern Bransfield Basin, Antarctic Peninsula: Quaternary Research, 58, 3, 234-245.
Kilfeather, A. A., O Cofaigh, C., Lloyd, J. M., Dowdeswell, J. A., Xu, S., and Moreton, S. G., 2011, Ice-stream retreat and ice-shelf history in Marguerite Trough, Antarctic Peninsula: Sedimentological and foraminiferal signatures: Geological Society of America Bulletin, 123, 5-6, 997-1015.

Kilian, R., and Lamy, F., 2012, A review of Glacial and Holocene paleoclimate records from southernmost Patagonia (49-55ºS): Quaternary Science Reviews, 53, 1-23.
Kim, J. H., Schneider, R. R., Hebbeln, D., Muller, P. J., and Wefer, G., 2002, Last deglacial sea-surface temperature evolution in the Southeast Pacific compared to climate changes on the South American continent: Quaternary Science Reviews, 21, 18-19, 2085-2097.
Kitazato, H., Shirayama, Y., Nakatsuka, T., Fujiwara, S., Shimanaga, M., Kato, Y., Okada, Y., Kanda, J., Yamaoka, A., Masuzawa, T., and Suzuki, K., 2000, Seasonal phytodetritus deposition and responses of bathyal benthic foraminiferal populations in Sagami Bay, Japan: preliminary results from "Project Sagami 1996-1999": Marine Micropaleontology, 40, 3, 135-149.
Knight, R., 1986, Apertural characteristics of certain unilocular foraminifera: methods of study, nomenclature and taxonomic significance. : Journal of Micropaleontology, 5, 37-47.
Knudson, K. P., and Ravelo, A. C., 2015, Enhanced subarctic Pacific stratification and nutrient utilization during glacials over the last 1.2 Myr: Geophysical Research Letters, 42, 22, 9870-9879.
Kohfeld, K. E., Graham, R. M., de Boer, A. M., Sime, L. C., Wolff, E. W., Le Quéré, C., and Bopp, L., 2013, Southern Hemisphere westerly wind changes during the Last Glacial Maximum: paleo-data synthesis: Quaternary Science Reviews, 68, 76-95.
Korb, R. E., Whitehouse, M. J., and Ward, P., 2004, SeaWiFS in the southern ocean: spatial and temporal variability in phytoplankton biomass around South Georgia: Deep-Sea Research Part Ii-Topical Studies in Oceanography, 51, 1-3, 99-116.
Korb, R. E., and Whitehouse, M., 2004, Contrasting primary production regimes around South Georgia, Southern Ocean: large blooms versus high nutrient, low chlorophyll waters: Deep-Sea Research Part I-Oceanographic Research Papers, 51, 5, 721-738.
Korb, R. E., Whitehouse, M. J., Thorpe, S. E., and Gordon, M., 2005, Primary production across the Scotia Sea in relation to the physico-chemical environment: Journal of Marine Systems, 57, 3-4, 231-249.
Korb, R. E., Whitehouse, M. J., Atkinson, A., and Thorpe, S. E., 2008, Magnitude and maintenance of the phytoplankton bloom at South Georgia: a naturally iron-replete environment: Marine Ecology Progress Series, 368, 75-91.
Koron, N., Ogrinc, N., Metzger, E., Riedel, B., and Faganeli, J., 2015, The impact of induced redox transitions on nutrient diagenesis in coastal marine sediments (Gulf of Trieste, northern Adriatic Sea): Journal of Soils and Sediments, 15, 12, 2443-2452.
Kubat, I., Sayed, M., Savage, S. B., Carrieres, T., Crocker, G., and Isope, 2007, An operational iceberg deterioration model, Proceedings of the Seventeenth International Offshore and Polar Engineering Conference, 652-657.
Kwok, R., and Comiso, J. C., 2002, Spatial patterns of variability in antarctic surface temperature: Connections to the Southern Hemisphere Annular Mode and the Southern Oscillation: Geophysical Research Letters, 29, 14, 1705.
L'Heureux, M. L., and Thompson, D. W. J., 2006, Observed relationships between the El Nino-Southern Oscillation and the extratropical zonal-mean circulation: Journal of Climate, 19, 2, 276-287.
Lamarck, J. B., 1804, Suite des mémoires sur les fossiles des environs de Paris: Annales du Muséum d'Histoire Naturelle, 5, 105-115; 179-188.
-, 1812, Extrait du course de zoologie du Museum d'Histoire Naturelle, sur les animaux sans vertebres, d'Hautel, Paris, pp. 150.

Lamb, A. L., Wilson, G. P., and Leng, M. J., 2006, A review of coastal palaeoclimate and relative sea-level reconstructions using $\delta^{13}C$ and C/N ratios in organic material: Earth-Science Reviews, 75, 1, 29-57.
Lamy, F., Hebbeln, D., Rohl, U., and Wefer, G., 2001, Holocene rainfall variability in southern Chile: a marine record of latitudinal shifts of the Southern Westerlies: Earth and Planetary Science Letters, 185, 3-4, 369-382.
Lamy, F., Ruhlemann, C., Hebbeln, D., and Wefer, G., 2002, High- and low-latitude climate control on the position of the southern Peru-Chile Current during the Holocene: Paleoceanography, 17, 2, 1028.
Lamy, F., Kaiser, J., Ninnemann, U., Hebbeln, D., Arz, H. W., and Stoner, J., 2004, Antarctic timing of surface water changes off Chile and Patagonian ice sheet response: Science, 304, 5679, 1959-1962.
Lamy, F., Kilian, R., Arz, H. W., Francois, J.-P., Kaiser, J., Prange, M., and Steinke, T., 2010, Holocene changes in the position and intensity of the southern westerly wind belt: Nature Geoscience, 3, 10, 695-699.
Larter, R. D., Anderson, J. B., Graham, A. G. C., Gohl, K., Hillenbrand, C.-D., Jakobsson, M., Johnson, J. S., Kuhn, G., Nitsche, F. O., Smith, J. A., Witus, A. E., Bentley, M. J., Dowdeswell, J. A., Ehrmann, W., Klages, J. P., Lindow, J., Cofaigh, C. Ó., and Spiegel, C., 2014, Reconstruction of changes in the Amundsen Sea and Bellingshausen Sea sector of the West Antarctic Ice Sheet since the Last Glacial Maximum: Quaternary Science Reviews, 100, 55-86.
Le Coze, F., and Hayward, B., 2017, *Lagena striatopunctata* Parker & Jones, 1865, Date Accessed: 2016-11-25, http://www.marinespecies.org/Foraminifera/aphia.php?p=taxdetails&id=525593.
Le Quere, C., Rodenbeck, C., Buitenhuis, E. T., Conway, T. J., Langenfelds, R., Gomez, A., Labuschagne, C., Ramonet, M., Nakazawa, T., Metzl, N., Gillett, N., and Heimann, M., 2007, Saturation of the Southern Ocean CO_2 sink due to recent climate change: Science, 316, 5832, 1735-1738.
LeGrande, A. N., and Schmidt, G. A., 2006, Global gridded data set of the oxygen isotopic composition in seawater: Geophysical Research Letters, 33, 12, L12604.
Lein, A. Y., 2004, Authigenic carbonate formation in the ocean: Lithology and Mineral Resources, 39, 1, 1-30.
Leiter, C., and Altenbach, A. V., 2010, Benthic foraminifera from the diatomaceous mud belt off Namibia: Characteristic species for severe anoxia: Palaeontologia Electronica, 13, 2.
Leventer, A., Domack, E., Barkoukis, A., McAndrews, B., and Murray, J., 2002, Laminations from the Palmer Deep: A diatom-based interpretation: Paleoceanography, 17, 2, 8002.
Leventer, A., Domack, E., Dunbar, R., Pike, J., Stickley, C. E., Maddison, E. J., Brachfeld, S., Manley, P., and McClennen, C., 2006, Marine sediment record from the East Antarctic margin reveals dynamics of ice sheet recession: GSA Today, 16, 12, 4-10.
Levin, L. A., Etter, R. J., Rex, M. A., Gooday, A. J., Smith, C. R., Pineda, J., Stuart, C. T., Hessler, R. R., and Pawson, D., 2001, Environmental influences on regional deep-sea species diversity: Annual Review of Ecology and Systematics, 32, 51-93.
Li, B. H., Yoon, H. I., and Park, B. K., 2000, Foraminiferal assemblages and $CaCO_3$ dissolution since the last deglaciation in the Maxwell Bay, King George Island, Antarctica: Marine Geology, 169, 1-2, 239-257.
Lin, H., Rauschenberg, S., Hexel, C. R., Shaw, T. J., and Twining, B. S., 2011, Free-drifting icebergs as sources of iron to the Weddell Sea: Deep Sea Research Part II: Topical Studies in Oceanography, 58, 11, 1392-1406.

Linke, P., and Lutze, G. F., 1993, Microhabitat preferences of benthic foraminifera - a static concept or a dynamic adaptation to optimize food acquisition: Marine Micropaleontology, 20, 3-4, 215-234.
Linnaeus, C., 1758, Systema Naturae per Regnia tria Naturae, secundum classes, ordines, genera, species, cum characteribus, differentiis, synonymis, locis, Stockholm, pp. 823.
Lipps, J. H., DeLaca, T. E., Krebs, W. N., and Stockton, W., 1972, Shallow-water foraminifera studies, Antarctic Peninsula, 1971–1972. Foraminiferal ecology, Antarctic Peninsula: Antarctic Journal of the United States, 7, 82.
Lisiecki, L. E., and Raymo, M. E., 2005, A Pliocene-Pleistocene stack of 57 globally distributed benthic $\delta^{18}O$ records: Paleoceanography, 20, 1, PA1003.
Liu, Z., Otto-Bliesner, B. L., He, F., Brady, E. C., Tomas, R., Clark, P. U., Carlson, A. E., Lynch-Stieglitz, J., Curry, W., Brook, E., Erickson, D., Jacob, R., Kutzbach, J., and Cheng, J., 2009, Transient simulation of last deglaciation with a new mechanism for Bolling-Allerod warming: Science, 325, 5938, 310-314.
Ljung, K., Bjorck, S., Renssen, H., and Hammarlund, D., 2008, South Atlantic island record reveals a South Atlantic response to the 8.2 kyr event: Climate of the Past, 4, 1, 35-45.
Loeblich, A. R., and Tappan, H., 1955, Revision of some recent foraminiferal genera: Smithsonian Miscellaneous Collections, 128, 5, 1-37.
-, 1961, Suprageneric classification of the Rhizopodea: Journal of Paleontology, 35, 245-330.
-, 1984, Some new proteinaceous and agglutinated genera of Foraminiferida: Journal of Paleontology, 58, 1158-1163.
-, 1986, Some new and redefined genera and families of Textulariina, Fusulinina, Involutinina and Miliolina (Foraminiferida): Journal of Foraminiferal Research, 16, 334-346.
-, 1988, Foraminiferal genera and their classification, Van Nostrand Reinhold, New York, pp. 970.
-, 1994, Foraminifera of the Sahul Shelf and Timor Sea: Cushman Foundation for Foraminiferal Research Special Publication, 31.
Lohmann, G. P., and Schweitzer, P. N., 1990, *Globorotalia truncatulinoides*' growth and chemistry as probes of the past thermocline: 1. Shell size: Paleoceanography, 5, 1, 55-75.
Loscher, B. M., de Baar, H. J. W., de Jong, J. T. M., Veth, C., and Dehairs, F., 1997, The distribution of Fe in the Antarctic Circumpolar Current: Deep-Sea Research Part Ii-Topical Studies in Oceanography, 44, 1-2, 143-187.
Loubere, P., Meyers, P., and Gary, A., 1995, Benthic foraminiferal microhabitat selection, carbon isotope values, and association with larger animals - a test with *Uvigerina peregrina*: Journal of Foraminiferal Research, 25, 1, 83-95.
Loubere, P., Jacobsen, B., Klitgaard Kristensen, D., Husum, K., Jernas, P., and Richaud, M., 2011, The structure of benthic environments and the paleochemical record of foraminifera: Deep Sea Research Part I: Oceanographic Research Papers, 58, 5, 535-545.
Luo, M., Chen, L. Y., Wang, S. H., Yan, W., Wang, H. B., and Chen, D. F., 2013, Pockmark activity inferred from pore water geochemistry in shallow sediments of the pockmark field in southwestern Xisha Uplift, northwestern South China Sea: Marine and Petroleum Geology, 48, 247-259.
Lutze, G. F., and Thiel, H., 1989, Epibenthic foraminifera from elevated microhabitats: *Cibicidoides wuellerstorfi* and *Planulina ariminensis*: Journal of Foraminiferal Research, 19, 2, 153-158.
Mackensen, A., Grobe, H., Kuhn, G., and Futterer, D. K., 1990, Benthic foraminiferal assemblages from the Eastern Weddell Sea between 68 and

73ºs: Distribution, ecology and fossilisation potential: Marine Micropaleontology, 16, 3-4, 241-283.
Mackensen, A., Futterer, D. K., Grobe, H., and Schmiedl, G., 1993, Benthic foraminiferal assemblages from the eastern South Atlantic Polar Front region between 35 and 57ºS: Distribution, ecology and fossilization potential: Marine Micropaleontology, 22, 1-2, 33-69.
Mackensen, A., Schmiedl, G., Harloff, J., and Giese, M., 1995, Deep-sea foraminifera in the South Atlantic ocean: Ecology and assemblage generation: Micropaleontology, 41, 4, 342-358.
Mackensen, A., Schumacher, S., Radke, J., and Schmidt, D. N., 2000, Microhabitat preferences and stable carbon isotopes of endobenthic foraminifera: clue to quantitative reconstruction of oceanic new production?: Marine Micropaleontology, 40, 3, 233-258.
Mackintosh, A. N., Verleyen, E., O'Brien, P. E., White, D. A., Jones, R. S., McKay, R., Dunbar, R., Gore, D. B., Fink, D., Post, A. L., Miura, H., Leventer, A., Goodwin, I., Hodgson, D. A., Lilly, K., Crosta, X., Golledge, N. R., Wagner, B., Berg, S., van Ommen, T., Zwartz, D., Roberts, S. J., Vyverman, W., and Masse, G., 2014, Retreat history of the East Antarctic Ice Sheet since the Last Glacial Maximum: Quaternary Science Reviews, 100, 10-30.
Macko, S. A., Engel, M. H., and Parker, P. L., 1993, Early diagenesis of organic matter in sediments, *in* Engel, M. H., and Macko, S. A., eds., Organic Geochemistry: Principles and Applications Springer US: Boston, MA, 211-224.
Macko, S. A., Engel, M. H., and Qian, Y. R., 1994, Early diagenesis and organic-matter preservation - a molecular stable carbon-isotope perspective: Chemical Geology, 114, 3-4, 365-379.
Maddison, E. J., Pike, J., Leventer, A., and Domack, E. W., 2005, Deglacial seasonal and sub-seasonal diatom record from Palmer Deep, Antarctica: Journal of Quaternary Science, 20, 5, 435-446.
Maddison, E. J., Pike, J., Leventer, A., Dunbar, R., Brachfeld, S., Domack, E. W., Manley, P., and McClennen, C., 2006, Post-glacial seasonal diatom record of the Mertz Glacier Polynya, East Antarctica: Marine Micropaleontology, 60, 1, 66-88.
Magalhaes, V. H., Pinheiro, L. M., Ivanov, M. K., Kozlova, E., Blinova, V., Kolganova, J., Vasconcelos, C., McKenzie, J. A., Bernasconi, S. M., Kopf, A. J., Diaz-del-Rio, V., Gonzalez, F. J., and Somoza, L., 2012, Formation processes of methane-derived authigenic carbonates from the Gulf of Cadiz: Sedimentary Geology, 243, 155-168.
Majewski, W., 2005, Benthic foraminiferal communities: distribution and ecology in Admiralty Bay, King George Island, West Antarctica: Polish Polar Research, 26, 3, 159-214.
Majewski, W., and Anderson, J. B., 2009, Holocene foraminiferal assemblages from Firth of Tay, Antarctic Peninsula: Paleoclimate implications: Marine Micropaleontology, 73, 3-4, 135-147.
Majewski, W., 2010, Benthic foraminifera from West Antarctic fjord environments: An overview: Polish Polar Research, 31, 1, 61-82.
Majewski, W., Wellner, J. S., Szczuciński, W., and Anderson, J. B., 2012, Holocene oceanographic and glacial changes recorded in Maxwell Bay, West Antarctica: Marine Geology, 326–328, 67-79.
Majewski, W., 2013, Benthic foraminifera from Pine Island and Ferrero bays, Amundsen Sea: Polish Polar Research, 34, 2, 169-200.
Majewski, W., Wellner, J. S., and Anderson, J. B., 2016, Environmental connotations of benthic foraminiferal assemblages from coastal West Antarctica: Marine Micropaleontology, 124, 1-15.
Malone, M. J., Claypool, G., Martin, J. B., and Dickens, G. R., 2002, Variable methane fluxes in shallow marine systems over geologic time - The

composition and origin of pore waters and authigenic carbonates on the New Jersey shelf: Marine Geology, 189, 3-4, 175-196.
Mann, M. E., Zhang, Z., Rutherford, S., Bradley, R. S., Hughes, M. K., Shindell, D., Ammann, C., Faluvegi, G., and Ni, F., 2009, Global signatures and dynamical origins of the Little Ice Age and Medieval Climate Anomaly: Science, 326, 5957, 1256-1260.
Mansilla, C. A., McCulloch, R. D., and Morello, F., 2016, Palaeoenvironmental change in Southern Patagonia during the Lateglacial and Holocene: Implications for forest refugia and climate reconstructions: Palaeogeography Palaeoclimatology Palaeoecology, 447, 1-11.
Marie, P., 1941, La foraminifères de la Craie à Belemnitella mucronata du Bassin de Paris: Mémoires de Museum Nationale d'Histoire Naturelle, 12, 1-296.
Marlowe, I. T., Green, J. C., Neal, A. C., Brassell, S. C., Eglinton, G., and Course, P. A., 1984, Long chain (n-C_{37}–C_{39}) alkenones in the Prymnesiophyceae. Distribution of alkenones and other lipids and their taxonomic significance: British Phycological Journal, 19, 3, 203-216.
Martin, J. H., Gordon, R. M., and Fitzwater, S. E., 1990, Iron in Antarctic waters: Nature, 345, 156-158.
Maslin, M. A., and Swann, G. E. A., 2005, Isotopes in marine sediments, *in* Leng, M. J., ed., Isotopes in Paleoenvironmental Research Springer: The Netherlands, 227-290.
Masson-Delmotte, V., Stenni, B., and Jouzel, J., 2004, Common millennial-scale variability of Antarctic and Southern Ocean temperatures during the past 5000 years reconstructed from the EPICA Dome C ice core: Holocene, 14, 2, 145-151.
Masson, V., Vimeux, F., Jouzel, J., Morgan, V., Delmotte, M., Ciais, P., Hammer, C., Johnsen, S., Lipenkov, V. Y., Mosley-Thompson, E., Petit, J. R., Steig, E. J., Stievenard, M., and Vaikmae, R., 2000, Holocene climate variability in Antarctica based on 11 ice-core isotopic records: Quaternary Research, 54, 3, 348-358.
Mathiot, P., Goosse, H., Crosta, X., Stenni, B., Braida, M., Renssen, H., Van Meerbeeck, C. J., Masson-Delmotte, V., Mairesse, A., and Dubinkina, S., 2013, Using data assimilation to investigate the causes of Southern Hemisphere high latitude cooling from 10 to 8 ka BP: Climate of the Past, 9, 2, 887-901.
Mayewski, P. A., Rohling, E. E., Curt Stager, J., Karlén, W., Maasch, K. A., David Meeker, L., Meyerson, E. A., Gasse, F., van Kreveld, S., Holmgren, K., Lee-Thorp, J., Rosqvist, G., Rack, F., Staubwasser, M., Schneider, R. R., and Steig, E. J., 2004, Holocene climate variability: Quaternary Research, 62, 3, 243-255.
Maync, W., 1952, Critical taxonomic study and nomenclatural revision of the Lituolidae based upon the prototype of the family, *Lituola nautiloidea* Lamarck 1804: Contributions from the Cushman Foundation for Foraminiferal Research, 3, 35-56.
McCorkle, D. C., Emerson, S. R., and Quay, P. D., 1985, Stable carbon isotopes in marine porewaters: Earth and Planetary Science Letters, 74, 1, 13-26.
McCorkle, D. C., and Emerson, S. R., 1988, The relationship between pore water carbon isotopic composition and bottom water oxygen concentration: Geochimica et Cosmochimica Acta, 52, 5, 1169-1178.
McCorkle, D. C., Keigwin, L. D., Corliss, B. H., and Emerson, S. R., 1990, The influence of microhabitats on the carbon isotopic composition of deep-sea benthic foraminifera: Paleoceanography, 5, 2, 161-185.
McCorkle, D. C., Corliss, B. H., and Farnham, C. A., 1997, Vertical distributions and stable isotopic compositions of live (stained) benthic foraminifera from the North Carolina and California continental margins: Deep Sea Research Part I: Oceanographic Research Papers, 44, 6, 983-1024.

McCulloch, I., 1977, Qualitative observations on Recent foraminiferal tests with emphasis on the eastern Pacific, University of Southern California, Los Angeles, pp.:
McGlone, M. S., 2002, The late Quaternary peat, vegetation and climate history of the Southern Oceanic islands of New Zealand: Quaternary Science Reviews, 21, 4, 683-707.
McGlone, M. S., Turney, C. S. M., Wilmshurst, J. M., Renwick, J., and Pahnke, K., 2010, Divergent trends in land and ocean temperature in the Southern Ocean over the past 18,000 years: Nature Geoscience, 3, 9, 622-626.
Meisel, O. H., 2013, Post-LGM climate variability in Sub-Antarctic South Georgia recorded in marine sediments from Royal Bay glacial trough [MSc: University of Bremen, 78.
Melis, R., and Salvi, G., 2009, Late Quaternary foraminiferal assemblages from western Ross Sea (Antarctica) in relation to the main glacial and marine lithofacies: Marine Micropaleontology, 70, 1-2, 39-53.
Meredith, M. P., Watkins, J. L., Murphy, E. J., Ward, P., Bone, D. G., Thorpe, S. E., Grant, S. A., and Ladkin, R. S., 2003, Southern ACC front to the northeast of South Georgia: Pathways, characteristics, and fluxes: Journal of Geophysical Research-Oceans, 108, C5, 3162.
Meredith, M. P., Brandon, M. A., Murphy, E. J., Trathan, P. N., Thorpe, S. E., Bone, D. G., Chernyshkov, P. P., and Sushin, V. A., 2005, Variability in hydrographic conditions to the east and northwest of South Georgia, 1996-2001: Journal of Marine Systems, 53, 1-4, 143-167.
Meredith, M. P., and Hogg, A. M., 2006, Circumpolar response of Southern Ocean eddy activity to a change in the Southern Annular Mode: Geophysical Research Letters, 33, 16, L16608.
Meredith, M. P., Murphy, E. J., Hawker, E. J., King, J. C., and Wallace, M. I., 2008, On the interannual variability of ocean temperatures around South Georgia, Southern Ocean: Forcing by El Nino/Southern Oscillation and the Southern Annular Mode: Deep-Sea Research Part II-Topical Studies in Oceanography, 55, 18-19, 2007-2022.
Mikhalevich, V. I., 1980, Systematics and evolution of foraminifera in the light of new data on their cytology and ultrastructure: Trudy Zoologicheskogo Instituta Akademiya Nauk SSSR, 94, 42-61.
-, 1995, A new classification of the class Astrorhizata: Zoosystematica Rossica, 3, 2, 161-174.
-, 2004, The general aspects of the distribution of Antarctic foraminifera: Micropaleontology, 50, 2, 179-194.
Miklukho-Maklay, A. D., 1963, Upper Palaeozoic of Central Asia, Leningradskiy Universitet, Lenigrad, pp.:
Milam, R. W., and Anderson, J. B., 1981, Distribution and ecology of recent benthonic foraminifera of the Adelie-George-V continental-shelf and slope, Antarctica: Marine Micropaleontology, 6, 3, 297-325.
Mojtahid, M., Jorissen, F., Lansard, B., Fontanier, C., Bombled, B., and Rabouille, C., 2009, Spatial distribution of live benthic foraminifera in the Rhône prodelta: Faunal response to a continental–marine organic matter gradient: Marine Micropaleontology, 70, 3–4, 177-200.
Monnin, E., Indermuhle, A., Dallenbach, A., Fluckiger, J., Stauffer, B., Stocker, T. F., Raynaud, D., and Barnola, J. M., 2001, Atmospheric CO_2 concentrations over the last glacial termination: Science, 291, 5501, 112-114.
Montagu, G., 1803, Testacea Britannica or natural history of British shells, marine, land, and fresh-water, including the most minute, J. S. Hollis, Romsey, England, pp. 183.
Moreman, W. L., 1930, Arenaceous foraminifera from Ordovician and Silurian limestones of Oklahoma: Journal of Paleontology, 4, 1, 42-59.

Moreno, P. I., and Videla, J., 2016, Centennial and millennial-scale hydroclimate changes in northwestern Patagonia since 16,000 yr BP: Quaternary Science Reviews, 149, 326-337.
Muehlenbachs, K., and Clayton, R. N., 1976, Oxygen isotope composition of oceanic-crust and its bearing on seawater: Journal of Geophysical Research, 81, 23, 4365-4369.
Muller, P. J., Kirst, G., Ruhland, G., von Storch, I., and Rosell-Mele, A., 1998, Calibration of the alkenone paleotemperature index $U^{k'37}$ based on core-tops from the eastern South Atlantic and the global ocean (60ºN-60ºS): Geochimica Et Cosmochimica Acta, 62, 10, 1757-1772.
Mulvaney, R., Abram, N. J., Hindmarsh, R. C., Arrowsmith, C., Fleet, L., Triest, J., Sime, L. C., Alemany, O., and Foord, S., 2012, Recent Antarctic Peninsula warming relative to Holocene climate and ice-shelf history: Nature, 489, 7414, 141-144.
Murphy, E. J., Clarke, A., Symon, C., and Priddle, J., 1995, Temporal variation in antarctic sea-ice: Analysis of a long-term fast-ice record from the South Orkney Islands: Deep-Sea Research Part I-Oceanographic Research Papers, 42, 7, 1045-1062.
Murphy, E. J., Trathan, P. N., Watkins, J. L., Reid, K., Meredith, M. P., Forcada, J., Thorpe, S. E., Johnston, N. M., and Rothery, P., 2007, Climatically driven fluctuations in Southern Ocean ecosystems: Proceedings of the Royal Society B-Biological Sciences, 274, 1629, 3057-3067.
Murphy, E. J., Hofmann, E. E., Watkins, J. L., Johnston, N. M., Pinones, A., Ballerini, T., Hill, S. L., Trathan, P. N., Tarling, G. A., Cavanagh, R. A., Young, E. F., Thorpe, S. E., and Fretwell, P., 2013, Comparison of the structure and function of Southern Ocean regional ecosystems: The Antarctic Peninsula and South Georgia: Journal of Marine Systems, 109, 22-42.
Murray, J. W., and Bowser, S. S., 2000, Mortality, protoplasm decay rate, and reliability of staining techniques to recognize 'living' foraminifera: A review: Journal of Foraminiferal Research, 30, 1, 66-70.
Murray, J. W., and Pudsey, C. J., 2004, Living (stained) and dead foraminifera from the newly ice-free Larsen Ice Shelf, Weddell Sea, Antarctica: ecology and taphonomy: Marine Micropaleontology, 53, 1-2, 67-81.
Murray, J. W., 2013, Living benthic foraminifera: biogeographical distributions and the significance of rare morphospecies: Journal of Micropalaeontology, 32, 1, 1-58.
Nelson, D. M., Tréguer, P., Brzezinski, M. A., Leynaert, A., and Quéguiner, B., 1995, Production and dissolution of biogenic silica in the ocean: Revised global estimates, comparison with regional data and relationship to biogenic sedimentation: Global Biogeochemical Cycles, 9, 3, 359-372.
Neori, A., and Holm-Hansen, O., 1982, Effect of temperature on rate of photosynthesis in Antarctic phytoplankton: Polar Biology, 1, 1, 33-38.
Neukom, R., Luterbacher, J., Villalba, R., Kuttel, M., Frank, D., Jones, P. D., Grosjean, M., Esper, J., Lopez, L., and Wanner, H., 2010, Multi-centennial summer and winter precipitation variability in southern South America: Geophysical Research Letters, 37, L14708.
Neukom, R., Gergis, J., Karoly, D. J., Wanner, H., Curran, M., Elbert, J., Gonzalez-Rouco, F., Linsley, B. K., Moy, A. D., Mundo, I., Raible, C. C., Steig, E. J., van Ommen, T., Vance, T., Villalba, R., Zinke, J., and Frank, D., 2014, Inter-hemispheric temperature variability over the past millennium: Nature Climate Change, 4, 5, 362-367.
Nielsen, S. H. H., Koç, N., and Crosta, X., 2004, Holocene climate in the Atlantic sector of the Southern Ocean: Controlled by insolation or oceanic circulation?: Geology, 32, 4, 317-320.

Nikolaiev, V. I., Kotlyakov, V. M., and Smirnov, K. E., 1988, Isotopic studies of the ice core from the Komsomolskaya station, Antarctica: Data of Glaciological Studies of the USSR Academy of Sciences, 66, 97-102.
Nolting, R. F., Debaar, H. J. W., Vanbennekom, A. J., and Masson, A., 1991, Cadmium, copper and iron in the Scotia Sea, Weddell Sea and Weddell Scotia Confluence (Antarctica): Marine Chemistry, 35, 1-4, 219-243.
Nomaki, H., Heinz, P., Hemleben, C., and Kitazato, H., 2005, Behavior and response of deep-sea benthic foraminifera to freshly supplied organic matter: A laboratory feeding experiment in microcosm environments: Journal of Foraminiferal Research, 35, 2, 103-113.
Ó Cofaigh, C., Davies, B. J., Livingstone, S. J., Smith, J. A., Johnson, J. S., Hocking, E. P., Hodgson, D. A., Anderson, J. B., Bentley, M. J., Canals, M., Domack, E., Dowdeswell, J. A., Evans, J., Glasser, N. F., Hillenbrand, C.-D., Larter, R. D., Roberts, S. J., and Simms, A. R., 2014, Reconstruction of ice-sheet changes in the Antarctic Peninsula since the Last Glacial Maximum: Quaternary Science Reviews, 100, 87-110.
Ohga, T., and Kitazato, H., 1997, Seasonal changes in bathyal foraminiferal populations in response to the flux of organic matter (Sagami Bay, Japan): Terra Nova, 9, 1, 33-37.
Oke, P. R., and England, M. H., 2004, Oceanic response to changes in the latitude of the Southern Hemisphere subpolar westerly winds: Journal of Climate, 17, 5, 1040-1054.
Opsahl, S., and Benner, R., 1997, Distribution and cycling of terrigenous dissolved organic matter in the ocean: Nature, 386, 480-482.
Orsi, A. H., Whitworth, T., and Nowlin, W. D., 1995, On the meridional extent and fronts of the Antarctic Circumpolar Current: Deep-Sea Research Part I-Oceanographic Research Papers, 42, 5, 641-673.
Pahnke, K., Zahn, R., Elderfield, H., and Schulz, M., 2003, 340,000-year centennial-scale marine record of Southern Hemisphere climatic oscillation: Science, 301, 5635, 948-952.
Pahnke, K., and Sachs, J. P., 2006, Sea surface temperatures of southern midlatitudes 0-160 kyr BP: Paleoceanography, 21, 2, PA2003.
Panizzo, V., Crespin, J., Crosta, X., Shemesh, A., Masse, G., Yam, R., Mattielli, N., and Cardinal, D., 2014, Sea ice diatom contributions to Holocene nutrient utilization in East Antarctica: Paleoceanography, 29, 4, 328-342.
Park, J., Oh, I. S., Kim, H. C., and Yoo, S., 2010, Variability of SeaWiFs chlorophyll-a in the southwest Atlantic sector of the Southern Ocean: Strong topographic effects and weak seasonality: Deep-Sea Research Part I-Oceanographic Research Papers, 57, 4, 604-620.
Park, R., and Epstein, S., 1960, Carbon isotope fractionation during photosynthesis: Geochimica Et Cosmochimica Acta, 21, 1-2, 110-126.
Parker, F. L., 1952, Foraminiferal distribution in the Long Island Sound - Buzzards Bay area: Bulletin of the Museum of Comparative Zoology, Harvard, 106, 428-473.
Parker, W. K., and Jones, T. R., 1865, On some foraminifera from the North Atlantic and Arctic Oceans, including Davis Straits and Baffin's Bay: Philosophical Transactions of the Royal Society, 155, 325-441.
Parr, W. J., 1947, On *Torrresina*, a new genus of the foraminifera from eastern Australia: Journal of the Royal Microscopical Society, 64, 129-135.
-, 1950, Foraminifera, Reports B.A.N.Z. Antarctic Research Expedition 1929-1931,Volume 5, 232-392.
Patterson, R. T., and Richardson, R. H., 1987, A taxonomic revision of the unilocular Foraminifera: Journal of Foraminiferal Research, 17, 212-226.
Pawlowski, J., Bolivar, I., Fahrni, J. F., deVargas, C., Gouy, M., and Zaninetti, L., 1997, Extreme differences in rates of molecular evolution of foraminifera revealed by comparison of ribosomal DNA sequences and the fossil record: Molecular Biology and Evolution, 14, 5, 498-505.

Pearcey, F. G., 1914, Foraminifera of the Scottish National Antarctic Expedition: Transactions of the Royal Society of Edinburgh, 49, 19, 991-1044.
Pearson, P. N., Ditchfield, P. W., Singano, J., Harcourt-Brown, K. G., Nicholas, C. J., Olsson, R. K., Shackleton, N. J., and Hall, M. A., 2001, Warm tropical sea surface temperatures in the Late Cretaceous and Eocene epochs: Nature, 413, 6855, 481-487.
Peck, V. L., Allen, C. S., Kender, S., McClymont, E. L., and Hodgson, D., 2015, Oceanographic variability on the West Antarctic Peninsula during the Holocene and the influence of upper circumpolar deep water: Quaternary Science Reviews, 119, 0, 54-65.
Perissinotto, R., and Duncombe Rae, C. M., 1990, Occurrence of anticyclonic eddies on the Prince Edward Plateau (Southern Ocean) - effects on phytoplankton biomass and production: Deep-Sea Research Part A-Oceanographic Research Papers, 37, 5, 777-793.
Pike, J., and Kemp, A. E. S., 1996, Records of seasonal flux in Holocene laminated sediments, Gulf of California: Geological Society, London, Special Publications, 116, 1, 157-169.
-, 1999, Diatom mats in Gulf of California sediments: Implications for the paleoenvironmental interpretation of laminated sediments and silica burial: Geology, 27, 4, 311-314.
Pike, J., Swann, G. E. A., Leng, M. J., and Snelling, A. M., 2013, Glacial discharge along the west Antarctic Peninsula during the Holocene: Nature Geoscience, 6, 3, 199-202.
Piña-Ochoa, E., Høgslund, S., Geslin, E., Cedhagen, T., Revsbech, N. P., Nielsen, L. P., Schweizer, M., Jorissen, F., Rysgaard, S., and Risgaard-Petersen, N., 2010, Widespread occurrence of nitrate storage and denitrification among Foraminifera and Gromiida: Proceedings of the National Academy of Sciences, 107, 3, 1148-1153.
Pohlman, J. W., Riedel, M., Bauer, J. E., Canuel, E. A., Paull, C. K., Lapham, L., Grabowski, K. S., Coffin, R. B., and Spence, G. D., 2013, Anaerobic methane oxidation in low-organic content methane seep sediments: Geochimica Et Cosmochimica Acta, 108, 184-201.
Prahl, F. G., and Wakeham, S. G., 1987, Calibration of unsaturation patterns in long-chain ketone compositions for palaeotemperature assessment: Nature, 330, 6146, 367-369.
Prahl, F. G., Muehlhausen, L. A., and Zahnle, D. L., 1988, Further evaluation of long-chain alkenones as indicators of paleoceanographic conditions: Geochimica et Cosmochimica Acta, 52, 9, 2303-2310.
Pudsey, C. J., and Evans, J., 2001, First survey of Antarctic sub-ice shelf sediments reveals mid-Holocene ice shelf retreat: Geology, 29, 9, 787-790.
Pudsey, C. J., Murray, J. W., Appleby, P., and Evans, J., 2006, Ice shelf history from petrographic and foraminiferal evidence, Northeast Antarctic Peninsula: Quaternary Science Reviews, 25, 17-18, 2357-2379.
Puri, H. S., 1954, Contribution to the study of the Miocene of the Florida panhandle: Bulletin Florida State Geological Survey, 36, 1-345.
Putnam, A. E., Denton, G. H., Schaefer, J. M., Barrell, D. J. A., Andersen, B. G., Finkel, R. C., Schwartz, R., Doughty, A. M., Kaplan, M. R., and Schluchter, C., 2010, Glacier advance in southern middle-latitudes during the Antarctic Cold Reversal: Nature Geoscience, 3, 10, 700-704.
Quilty, P. G., Kerry, K. R., and Marchant, H. J., 1985, A seasonally recurrent patch of Antarctic planktonic diatoms: Search, 16, 1-2, 48-48.
Quilty, P. G., 2007, Origin and evolution of the sub-Antarctic islands: the foundation: Papers and Proceedings of the Royal Society of Tasmania, 141, 1, 35-58.
Rabassa, J., Coronato, A., Bujalesky, G., Salemme, M., Roig, C., Meglioli, A., Heusser, C., Gordillo, S., Roig, F., Borromei, A., and Quattrocchio, M.,

2000, Quaternary of Tierra del Fuego, Southernmost South America: an updated review: Quaternary International, 68–71, 217-240.
Ragueneau, O., Tréguer, P., Leynaert, A., Anderson, R. F., Brzezinski, M. A., DeMaster, D. J., Dugdale, R. C., Dymond, J., Fischer, G., François, R., Heinze, C., Maier-Reimer, E., Martin-Jézéquel, V., Nelson, D. M., and Quéguiner, B., 2000, A review of the Si cycle in the modern ocean: recent progress and missing gaps in the application of biogenic opal as a paleoproductivity proxy: Global and Planetary Change, 26, 4, 317-365.
Rasmussen, S. O., Andersen, K. K., Svensson, A. M., Steffensen, J. P., Vinther, B. M., Clausen, H. B., Siggaard-Andersen, M. L., Johnsen, S. J., Larsen, L. B., Dahl-Jensen, D., Bigler, M., Röthlisberger, R., Fischer, H., Goto-Azuma, K., Hansson, M. E., and Ruth, U., 2006, A new Greenland ice core chronology for the last glacial termination: Journal of Geophysical Research: Atmospheres, 111, D6, D06102.
Rauzer-Chernousova, D. M., and Reytlinger, E. A., 1986, On the suprageneric systematics of the Order Hormosinida (Foraminifera): Paleontologicheskiy Zhurnal, 1986, 4, 15-20.
Ravelo, A. C., and Fairbanks, R. G., 1992, Oxygen isotopic composition of multiple species of planktonic foraminifera: Recorders of the modern photic zone temperature gradient: Paleoceanography, 7, 6, 815-831.
Ravelo, A. C., and Andreasen, D. H., 2000, Enhanced circulation during a warm period: Geophysical Research Letters, 27, 7, 1001-1004.
Ravelo, A. C., and Hillaire-Marcel, C., 2007, The use of oxygen and carbon isotopes of foraminifera in paleoceanography, *in* Hillaire-Marcel, C., and De Vernal, A., eds., Proxies in Late Cenozoic Paleoceanography,Volume 1 Elsevier: Amsterdam, 735-764.
Recasens, C., Ariztegui, D., Gebhardt, C., Gogorza, C., Haberzettl, T., Hahn, A., Kliem, P., Lise-Pronovost, A., Lucke, A., Maidana, N., Mayr, C., Ohlendorf, C., Schabitz, F., St-Onge, G., Wille, M., Zolitschka, B., and Team, P. S., 2012, New insights into paleoenvironmental changes in Laguna Potrok Aike, southern Patagonia, since the Late Pleistocene: The PASADO multiproxy record: Holocene, 22, 11, 1323-1335.
Reimer, P. J., Bard, E., Bayliss, A., Beck, J. W., Blackwell, P. G., Ramsey, C. B., Buck, C. E., Cheng, H., Edwards, R. L., Friedrich, M., Grootes, P. M., Guilderson, T. P., Haflidason, H., Hajdas, I., Hatte, C., Heaton, T. J., Hoffmann, D. L., Hogg, A. G., Hughen, K. A., Kaiser, K. F., Kromer, B., Manning, S. W., Niu, M., Reimer, R. W., Richards, D. A., Scott, E. M., Southon, J. R., Staff, R. A., Turney, C. S. M., and van der Plicht, J., 2013, IntCal13 and Marine13 radiocarbon age calibration curves 0-50,000 years cal BP: Radiocarbon, 55, 4, 1869-1887.
Renssen, H., Goosse, H., Fichefet, T., Masson-Delmotte, V., and Koc, N., 2005, Holocene climate evolution in the high-latitude Southern Hemisphere simulated by a coupled atmosphere-sea ice-ocean-vegetation model: Holocene, 15, 7, 951-964.
Renssen, H., Goosse, H., Crosta, X., and Roche, D. M., 2010, Early Holocene Laurentide Ice Sheet deglaciation causes cooling in the high-latitude Southern Hemisphere through oceanic teleconnection: Paleoceanography, 25, PA3204.
Reuning, L., Reijmer, J. J. G., Betzler, C., Swart, P., and Bauch, T., 2005, The use of paleoceanographic proxies in carbonate periplatform settings-opportunities and pitfalls: Sedimentary Geology, 175, 1-4, 131-152.
Reuss, A. E., 1849, Uber zwei neue Arten von Foraminiferen aus dem Tegel van Baden und Mollersdorf, *in* Czjzek, J., ed., Bericht uder die Mittheilungen Freunden der Naturwissenschaften in Wien,Volume 5, 50-56.
Reuss, A. E., 1850, Neues Foraminiferen aus den Schichten des Osterreichischen Tertiarbeckens: Denkschriften der Akademie des Wissenschaften, 1, 365-390.

Reuss, A. E., 1860, Die Foraminiferen der westphälischen Kreideformation: Sitzungsberichte der mathematisch-naturwissenschaflichen Classe der kaiserlichen Akademie der Wissenschaften, 40, 8, 147-238.
-, 1862, Entwurf einer systematischen Zusammenstellung der Foraminiferen: Sitzungsberichte der Kaiserlichen Akademie der Wissenschaften in Wien. Mathematicsch-Naturwissenschaftliche Classe, 1861, 355-396.
-, 1866, Die Foraminiferen, Anthozoen und Bryozoen des deutschen Septarienthones: Denkschriften der Akademie des Wissenschaften. Wien, 25, 117-214.
Rhumbler, L., 1895, Entwurf eines naturlichen systems der Thalamophoren: Nachrichten von der Gesellschaft der Wissenschaften zu Gottingen, Math-Physik Klasse, 1895, 1, 51-98.
Richards, P., and Tickell, W., 1968, Comparison between the weather at Bird Island and King Edward Point, South Georgia: British Antarctic Survey Bulletin, 15, 63-69.
Roberts, J., McCave, I. N., McClymont, E. L., Kender, S., Hillenbrand, C. D., Matano, R., Hodell, D. A., and Peck, V. L., 2017, Deglacial changes in flow and frontal structure through the Drake Passage: Earth and Planetary Science Letters, 474, 397-408.
Roberts, N., 2014, Holocene: An Environmental History, Wiley-Blackwell, Chichester, UK, pp. 378.
Rodrigues, A. R., Maluf, J. C. C., Braga, E. D., and Eichler, B. B., 2010, Recent benthic foraminiferal distribution and related environmental factors in Ezcurra Inlet, King George Island, Antarctica: Antarctic Science, 22, 4, 343-360.
Rodrigues, A. R., Eichler, P. P. B., and Eichler, B. B., 2013, Foraminifera in two inlets fed by a tidewater glacier, King George Island, Antarctic Peninsula: Journal of Foraminiferal Research, 43, 3, 209-220.
Romahn, S., Mackensen, A., Kuhlmann, H., and Patzold, J., 2015, Benthic foraminiferal response to Late Glacial and Holocene sea level rise and rainfall variability off East Africa: Marine Micropaleontology, 119, 34-48.
Romanek, C. S., Grossman, E. L., and Morse, J. W., 1992, Carbon isotopic fractionation in synthetic aragonite and calcite - effects of temperature and precipitation rate: Geochimica Et Cosmochimica Acta, 56, 1, 419-430.
Römer, M., Torres, M., Kasten, S., Kuhn, G., Graham, A. G. C., Mau, S., Little, C. T. S., Linse, K., Pape, T., Geprägs, P., Fischer, D., Wintersteller, P., Marcon, Y., Rethemeyer, J., and Bohrmann, G., 2014, First evidence of widespread active methane seepage in the Southern Ocean, off the sub-Antarctic island of South Georgia: Earth and Planetary Science Letters, 403, 0, 166-177.
Romero, O. E., Fischer, G., Karstensen, J., and Cermeño, P., 2016, Eddies as trigger for diatom productivity in the open-ocean Northeast Atlantic: Progress in Oceanography, 147, 38-48.
Rosqvist, G. C., Rietti-Shati, M., and Shemesh, A., 1999, Late glacial to middle Holocene climatic record of lacustrine biogenic silica oxygen isotopes from a Southern Ocean island: Geology, 27, 11, 967-970.
Rosqvist, G. C., and Schuber, P., 2003, Millennial-scale climate changes on South Georgia, Southern Ocean: Quaternary Research, 59, 3, 470-475.
Ruhlemann, C., Mulitza, S., Muller, P. J., Wefer, G., and Zahn, R., 1999, Warming of the tropical Atlantic Ocean and slowdown of thermohaline circulation during the last deglaciation: Nature, 402, 6761, 511-514.
Sage, R. F., 2004, The evolution of C4 photosynthesis: New Phytologist, 161, 2, 341-370.
Saidova, K. M., 1970, Bentosnye Foraminifery rayona kurilo-Kamchatskogo zheloba (po materianlam 39-go reysa e/s "Vityaz"') [Benthic foraminifera

in the Kurile-Kamchatka region based on the data of the 39th cruise of the R/V "Vityaz."]: Trudy Instituta Okeanologii, 86, 134-161.
-, 1975, Bentosniye foraminifery Tikhogo Okeana, P.P. Shirshov Institute of Oceanology, Academy of Sciences of the USSR, Moscow, pp.:
-, 1981, O sovremennom sostoyanii sistemy nadvidovykh taksonov Kaynozoyskikh bentosnykh foraminifer [On an up-to-date system of supraspecific taxonomy of Cenozoic benthonic foraminifera], Akademiya Nauk SSSR, Moscow, pp.:
Sancetta, C., 1995, Diatoms in the Gulf of California - seasonal flux patterns and the sediment record for the last 15,000 years: Paleoceanography, 10, 1, 67-84.
Santoso, A., England, M. H., and Hirst, A. C., 2006, Circumpolar Deep Water circulation and variability in a coupled climate model: Journal of Physical Oceanography, 36, 8, 1523-1552.
Sarmiento, J. L., and Toggweiler, J. R., 1984, A new model for the role of the oceans in determining atmospheric pCO_2: Nature, 308, 5960, 621-624.
Sarnthein, M., Winn, K., Duplessy, J. C., and Fontugne, M. R., 1988, Global variations of surface ocean productivity in low and mid latitudes: Influence on CO_2 reservoirs of the deep ocean and atmosphere during the last 21,000 years: Paleoceanography, 3, 3, 361-399.
Sars, M., 1869, Fortsatte bemerkinger over det dyriske livs udbredning i havets dybder: Förhandlinger i Videnskabsselskabet i Kristiania, 1869, 246–275.
Schilman, B., Almogi-Labin, A., Bar-Matthews, M., and Luz, B., 2003, Late Holocene productivity and hydrographic variability in the eastern Mediterranean inferred from benthic foraminiferal stable isotopes: Paleoceanography, 18, 3, 1064.
Schlosser, C., Schmidt, K., Aquilina, A., Homoky, W. B., Castrillejo, M., Mills, R. A., Patey, M. D., Fielding, S., Atkinson, A., and Achterberg, E. P., 2017, Mechanisms of dissolved and labile particulate iron supply to shelf waters and phytoplankton blooms off South Georgia, Southern Ocean: Biogeosciences Discuss., 2017, 1-49.
Schmidt, G. A., Bigg, G. R., and Rohling, E. J., 1999, Global Seawater Oxygen-18 Database - v1.22, https://data.giss.nasa.gov/o18data/.
Schmiedl, G., Mackensen, A., and Muller, P. J., 1997, Recent benthic foraminifera from the eastern South Atlantic Ocean: Dependence on food supply and water masses: Marine Micropaleontology, 32, 3-4, 249-287.
Schmiedl, G., Mitschele, A., Beck, S., Emeis, K. C., Hemleben, C., Schulz, H., Sperling, M., and Weldeab, S., 2003, Benthic foraminiferal record of ecosystem variability in the eastern Mediterranean Sea during times of sapropel S-5 and S-6 deposition: Palaeogeography Palaeoclimatology Palaeoecology, 190, 139-164.
Schmiedl, G., Pfeilsticker, M., Hemleben, C., and Mackensen, A., 2004, Environmental and biological effects on the stable isotope composition of recent deep-sea benthic foraminifera, from the western Mediterranean Sea: Marine Micropaleontology, 51, 1-2, 129-152.
Schmiedl, G., and Leuschner, D. C., 2005, Oxygenation changes in the deep western Arabian Sea during the last 190,000 years: Productivity versus deepwater circulation: Paleoceanography, 20, 2, PA2008.
Schneider, A., Crémière, A., Panieri, G., Lepland, A., and Knies, J., 2017, Diagenetic alteration of benthic foraminifera from a methane seep site on the Vestnesa Ridge (NW Svalbard margin): Deep Sea Research Part I: Oceanographic Research Papers, 123, 22-34.
Schoepfer, S. D., Shen, J., Wei, H. Y., Tyson, R. V., Ingall, E., and Algeo, T. J., 2015, Total organic carbon, organic phosphorus, and biogenic barium fluxes as proxies for paleomarine productivity: Earth-Science Reviews, 149, 23-52.

Schonfeld, J., 1997, The impact of the Mediterranean Outflow Water (MOW) on benthic foraminiferal assemblages and surface sediments at the southern Portuguese continental margin: Marine Micropaleontology, 29, 3-4, 211-236.
-, 2002, A new benthic foraminiferal proxy for near-bottom current velocities in the Gulf of Cadiz, northeastern Atlantic Ocean: Deep-Sea Research Part I-Oceanographic Research Papers, 49, 10, 1853-1875.
Schonfeld, J., and Altenbach, A. V., 2005, Late Glacial to Recent distribution pattern of deep-water *Uvigerina* species in the north-eastern Atlantic: Marine Micropaleontology, 57, 1-2, 1-24.
Schultze, M. J. S., 1854, Über den Organismus der Polythalamien (Foraminiferen), nebst Bemerkungen über die Rhizopoden im allgemeinen, Leipzig, Ingelmann, pp.:
Schulze, F. E., 1875, Rhizopodenstudien. III. : Archiv für Mikroskopische Anatomie 11, 94-139.
Schwager, C., 1876, Saggio di una classificazione dei foraminiferi avuto riguardo alle loro famiglie naturali: Bolletino R. Comitato Geologico d'Italia, 7, 475-485.
-, 1877, Quadro del proposto sistema di classificazione dei foraminiferi con guscio: Bolletino R. Comitato Geologico d'Italia, 8, 18-27.
Schwandes, L. P., 1998, Environmental durability of biogenic opal: Soil and Crop Science Society of Florida Proceedings, 57, 36-39.
Seguenza, G., 1862, Dei terreni Terziarii del distretto di Messina: Parte II - Descrizione dei foraminiferi monotalamici delle marne Mioceniche del distretto di Messina, T. Capra, Messina, pp.:
Selkirk, P. M., Seppelt, R. D., and Selkirk, D. R., 1990, Subantarctic Macquarie Island: Environment and Biology, Cambridge University Press, Cambridge, pp.:
Sen Gupta, B. K., and Machain-Castillo, M. L., 1993, Benthic foraminifera in oxygen-poor habitats: Marine Micropaleontology, 20, 3-4, 183-201.
Setoyama, E., and Kaminski, M. A., 2015, Neogene benthic foraminifera from the southern Bering Sea (IODP Expedition 323): Palaeontologia Electronica, 18.2.38A, 1-30.
Shackleton, N., 1974, Attainment of isotopic equilibrium between ocean water and the benthonic foraminifera genus *Uvigerina:* isotopic changes in the ocean during the last glacial, Les methodes quantitatives d'etude des variations du climax au cours du pleistocene Colloques Internationaux du CRNS: Paris, 203-209.
Shackleton, N. J., 1967, Oxygen isotope analyses and Pleistocene temperatures re-assessed: Nature, 215, 5096, 15-17.
Shchedrina, Z. G., 1969, O nekotorykh izmeneniyakh v sisteme semeytv Astrorhizidae i Reophacidae (Foraminifera) [On some changes in the systematics of the families Astrorhizidae and Reopacidae (Foraminifera)]: Voprosy Mikropaleontologii, 11, 157-170.
Shevenell, A. E., and Kennett, J. P., 2002, Antarctic Holocene climate change: A benthic foraminiferal stable isotope record from Palmer Deep: Paleoceanography, 17, 2, 1019.
Shevenell, A. E., Ingalls, A. E., Domack, E. W., and Kelly, C., 2011, Holocene Southern Ocean surface temperature variability west of the Antarctic Peninsula: Nature, 470, 7333, 250-254.
Shindell, D. T., and Schmidt, G. A., 2004, Southern Hemisphere climate response to ozone changes and greenhouse gas increases: Geophysical Research Letters, 31, 18, L18209.
Sicre, M. A., Bard, E., Ezat, U., and Rostek, F., 2002, Alkenone distributions in the North Atlantic and Nordic sea surface waters: Geochemistry Geophysics Geosystems, 3.

Siegenthaler, U., and Wenk, T., 1984, Rapid atmospheric CO_2 variations and ocean circulation: Nature, 308, 5960, 624-626.
Sigman, D. M., Hain, M. P., and Haug, G. H., 2010, The polar ocean and glacial cycles in atmospheric CO_2 concentration: Nature, 466, 7302, 47-55.
Sikes, E. L., Volkman, J. K., Robertson, L. G., and Pichon, J.-J., 1997, Alkenones and alkenes in surface waters and sediments of the Southern Ocean: Implications for paleotemperature estimation in polar regions: Geochimica et Cosmochimica Acta, 61, 7, 1495-1505.
Sikes, E. L., and Sicre, M. A., 2002, Relationship of the tetra-unsaturated C_{37} alkenone to salinity and temperature: Implications for paleoproxy applications: Geochemistry Geophysics Geosystems, 3, 1063.
Sikes, E. L., Howard, W. R., Samson, C. R., Mahan, T. S., Robertson, L. G., and Volkman, J. K., 2009, Southern Ocean seasonal temperature and Subtropical Front movement on the South Tasman Rise in the late Quaternary: Paleoceanography, 24, PA2201.
Silvestri, A., 1923, Lo stipite della Elissoforme e le sue affinita: Memorie della Pontificia Accademia della Scienze. Nouvi Lincei, 6, 231-270.
Silvestri, O., 1872, Saggio di studi sulla fauna microscopia fossile appartenente al terreno subappenino italiano. Mem. I - monografia delle Nodosarie: Academia Gioenia Scienze Naturali Catania 7, 108.
Singer, B. S., Ackert, R. P., and Guillou, H., 2004, $^{40}Ar/^{39}Ar$ and K-Ar chronology of Pleistocene glaciations in Patagonia: Geological Society of America Bulletin, 116, 3-4, 434-450.
Smetacek, V. S., 1985, Role of sinking in diatom life-history cycles: ecological, evolutionary and geological significance: Marine Biology, 84, 3, 239-251.
Smith, K. L., 2011, Free-drifting icebergs in the Southern Ocean: An overview: Deep Sea Research Part II: Topical Studies in Oceanography, 58, 11, 1277-1284.
Spero, H. J., and Lea, D. W., 1993, Intraspecific stable-isotope variability in the planktic foraminifera *Globigerinoides sacculifer*: results from laboratory experiments: Marine Micropaleontology, 22, 3, 221-234.
Spero, H. J., Bijma, J., Lea, D. W., and Bemis, B. E., 1997, Effect of seawater carbonate concentration on foraminiferal carbon and oxygen isotopes: Nature, 390, 6659, 497-500.
Steig, E. J., Brook, E. J., White, J. W. C., Sucher, C. M., Bender, M. L., Lehman, S. J., Morse, D. L., Waddington, E. D., and Clow, G. D., 1998, Synchronous climate changes in Antarctica and the North Atlantic: Science, 282, 5386, 92-95.
Stenni, B., Masson-Delmotte, V., Selmo, E., Oerter, H., Meyer, H., Rothlisberger, R., Jouzel, J., Cattani, O., Falourd, S., Fischer, H., Hoffmann, G., Iacumin, P., Johnsen, S. J., Minster, B., and Udisti, R., 2010, The deuterium excess records of EPICA Dome C and Dronning Maud Land ice cores (East Antarctica): Quaternary Science Reviews, 29, 1-2, 146-159.
Stenni, B., Buiron, D., Frezzotti, M., Albani, S., Barbante, C., Bard, E., Barnola, J. M., Baroni, M., Baumgartner, M., Bonazza, M., Capron, E., Castellano, E., Chappellaz, J., Delmonte, B., Falourd, S., Genoni, L., Iacumin, P., Jouzel, J., Kipfstuhl, S., Landais, A., Lemieux-Dudon, B., Maggi, V., Masson-Delmotte, V., Mazzola, C., Minster, B., Montagnat, M., Mulvaney, R., Narcisi, B., Oerter, H., Parrenin, F., Petit, J. R., Ritz, C., Scarchilli, C., Schilt, A., Schupbach, S., Schwander, J., Selmo, E., Severi, M., Stocker, T. F., and Udisti, R., 2011, Expression of the bipolar see-saw in Antarctic climate records during the last deglaciation: Nature Geoscience, 4, 1, 46-49.
Sterken, M., Roberts, S. J., Hodgson, D. A., Vyverman, W., Balbo, A. L., Sabbe, K., Moreton, S. G., and Verleyen, E., 2012, Holocene glacial and climate history of Prince Gustav Channel, northeastern Antarctic Peninsula: Quaternary Science Reviews, 31, 93-111.

Stickley, C. E., Pike, J., Leventer, A., Dunbar, R., Domack, E. W., Brachfeld, S., Manley, P., and McClennan, C., 2005, Deglacial ocean and climate seasonality in laminated diatom sediments, Mac.Robertson Shelf, Antarctica: Palaeogeography Palaeoclimatology Palaeoecology, 227, 4, 290-310.

Stickley, C. E., Pike, J., and Leventer, A., 2006, Productivity events of the marine diatom *Thalassiosira tumida* (Janisch) Hasle recorded in deglacial varves from the East Antarctic Margin: Marine Micropaleontology, 59, 3-4, 184-196.

Stone, P., 1974, Physiography of the north-east coast of South Georgia.: British Antarctic Survey Bulletin, 38, 17-36.

Stowasser, G., Fielding, S., Tarling, G. A., Manno, C., and Watkins, J., 2015, JR15002 Western Core Box Survey, British Antarctic Survey, Cambridge, UK, BAS Cruise Reports, pp. 1-186.

Strother, S. L., Salzmann, U., Roberts, S. J., Hodgson, D. A., Woodward, J., Van Nieuwenhuyze, W., Verleyen, E., Vyverman, W., and Moreton, S. G., 2015, Changes in Holocene climate and the intensity of Southern Hemisphere Westerly Winds based on a high-resolution palynological record from sub-Antarctic South Georgia: Holocene, 25, 2, 263-279.

Stuiver, M., Grootes, P. M., and Braziunas, T. F., 1995, The GISP2 $\delta^{18}O$ climate record of the past 16,500 years and the role of the sun, ocean, and volcanoes: Quaternary Research, 44, 3, 341-354.

Sturdivant, S. K., Diaz, R. J., and Cutter, G. R., 2012, Bioturbation in a declining oxygen environment, in situ observations from Wormcam: PLoS One, 7, 4, e34539.

Sweetman, A. K., Sommer, S., Pfannkuche, O., and Witte, U., 2009, Retarded response by macrofauna-size foraminifera to phytodetritus in a deep Norwegian fjord: Journal of Foraminiferal Research, 39, 1, 15-22.

Szymcek, P., Ishman, S. E., Domack, E. W., and Leventer, A., 2007, Holocene oceanographic and climatic variability of the Vega Drift deduced through foraminiferal interpretation, 2007-1047-SRP-010.

Tachikawa, K., and Elderfield, H., 2002, Microhabitat effects on Cd/Ca and $\delta^{13}C$ of benthic foraminifera: Earth and Planetary Science Letters, 202, 3–4, 607-624.

Taylor, F., and Sjunneskog, C., 2002, Postglacial marine diatom record of the Palmer Deep, Antarctic Peninsula (ODP Leg 178, Site 1098) 2. Diatom assemblages: Paleoceanography, 17, 3, 8001.

Tegen, I., and Fung, I., 1995, Contribution to the atmospheric mineral aerosol load from land-surface modification: Journal of Geophysical Research-Atmospheres, 100, D9, 18707-18726.

Thalmann, H. E., 1932, Nomenclator (Um- und Neubennungen) zu den Tafeln 1 bis 115 in H. B. Brady's Werk uber die Foraminferen der *Challenger*-Expedition, London 1884: Eclogae Geologicae Helvetiae, 25, 293-312.

Theodor, M., Schmiedl, G., Jorissen, F., and Mackensen, A., 2016a, Stable carbon isotope gradients in benthic foraminifera as proxy for organic carbon fluxes in the Mediterranean Sea: Biogeosciences, 13, 23, 6385-6404.

Theodor, M., Schmiedl, G., and Mackensen, A., 2016b, Stable isotope composition of deep-sea benthic foraminifera under contrasting trophic conditions in the western Mediterranean Sea: Marine Micropaleontology, 124, 16-28.

Thomas, E., 2007, Cenozoic mass extinctions in the deep sea: What perturbs the largest habitat on Earth?: Large Ecosystem Perturbations: Causes and Consequences, 424, 1-23.

Thompson, D. W. J., Wallace, J. M., and Hegerl, G. C., 2000, Annular modes in the extratropical circulation. Part II: Trends: Journal of Climate, 13, 5, 1018-1036.

Thompson, D. W. J., and Solomon, S., 2002, Interpretation of recent Southern Hemisphere climate change: Science, 296, 5569, 895-899.
Thompson, L. G., Davis, M. E., Mosley-Thompson, E., Sowers, T. A., Henderson, K. A., Zagorodnov, V. S., Lin, P. N., Mikhalenko, V. N., Campen, R. K., Bolzan, J. F., Cole-Dai, J., and Francou, B., 1998, A 25,000-year tropical climate history from Bolivian ice cores: Science, 282, 5395, 1858-1864.
Thorpe, S. E., Heywood, K. J., Brandon, M. A., and Stevens, D. P., 2002, Variability of the southern Antarctic Circumpolar Current front north of South Georgia: Journal of Marine Systems, 37, 1-3, 87-105.
Thorpe, S. E., Heywood, K. J., Stevens, D. P., and Brandon, M. A., 2004, Tracking passive drifters in a high resolution ocean model: implications for interannual variability of larval krill transport to South Georgia: Deep-Sea Research Part I-Oceanographic Research Papers, 51, 7, 909-920.
Toggweiler, J. R., Russell, J. L., and Carson, S. R., 2006, Midlatitude westerlies, atmospheric CO_2, and climate change during the ice ages: Paleoceanography, 21, 2, PA2005.
Torres, M. E., Mix, A. C., Kinports, K., Haley, B., Klinkhammer, G. P., McManus, J., and de Angelis, M. A., 2003, Is methane venting at the seafloor recorded by $\delta^{13}C$ of benthic foraminifera shells?: Paleoceanography, 18, 3, 1062.
Trachsel, M., and Telford, R. J., 2017, All age–depth models are wrong, but are getting better: The Holocene, 27, 6, 860-869.
Trathan, P. N., and Murphy, E. J., 2003, Sea surface temperature anomalies near South Georgia: Relationships with the Pacific El Nino regions: Journal of Geophysical Research-Oceans, 108, C4, 8075.
Treguer, P. J., and De La Rocha, C. L., 2013, The world ocean silica cycle, *in* Carlson, C. A., and Giovannoni, S. J., eds., Annual Review of Marine Science, Vol 5,Volume 5, 477-501.
Trenberth, K. E., 1987, The role of eddies in maintaining the westerlies in the southern-hemisphere winter: Journal of the Atmospheric Sciences, 44, 11, 1498-1508.
Treude, T., Niggemann, J., Kallmeyer, J., Wintersteller, P., Schubert, C. J., Boetius, A., and Jorgensen, B. B., 2005, Anaerobic oxidation of methane and sulfate reduction along the Chilean continental margin: Geochimica Et Cosmochimica Acta, 69, 11, 2767-2779.
Uchio, T., 1960 Ecology of living benthonic foraminifera from the San Diego, California area: Special Publications Cushman Laboratory for Foraminiferal Research, 5, 1-72.
Uchio, T., 1962, Influence of the River Shinano on foraminifera and sediment grain size distribution: Publications of the Seto Marine Biological Laboratory, 10, 363-392.
Unkel, I., Fernandez, M., Bjorck, S., Ljung, K., and Wohlfarth, B., 2010, Records of environmental changes during the Holocene from Isla de los Estados (54.4ºS), southeastern Tierra del Fuego: Global and Planetary Change, 74, 3-4, 99-113.
Usera, J., Blázquez, A. M., Guillem, J., and Alberola, C., 2002, Biochronological and paleoenvironmental interest of foraminifera lived in restricted environments: application to the study of the western Mediterranean holocene: Quaternary International, 93–94, 139-147.
Van der Putten, N., Stieperaere, H., Verbruggen, C., and Ochyra, R., 2004, Holocene palaeoecology and climate history of South Georgia (sub-Antarctica) based on a macrofossil record of bryophytes and seeds: The Holocene, 14, 3, 382-392.
Van der Putten, N., and Verbruggen, C., 2005, The onset of deglaciation of Cumberland Bay and Stromness Bay, South Georgia: Antarctic Science, 17, 1, 29-32.

Van der Putten, N., Verbruggen, C., Ochyra, R., Spassov, S., de Beaulieu, J. L., De Dapper, M., Hus, J., and Thouveny, N., 2009, Peat bank growth, Holocene palaeoecology and climate history of South Georgia (sub-Antarctica), based on a botanical macrofossil record: Quaternary Science Reviews, 28, 1-2, 65-79.
Van der Putten, N., Mauquoy, D., Verbruggen, C., and Bjorck, S., 2012, Subantarctic peatlands and their potential as palaeoenvironmental and palaeoclimatic archives: Quaternary International, 268, 65-76.
van Geel, B., Buurman, J., and Waterbolk, H. T., 1996, Archaeological and palaeoecological indications of an abrupt climate change in The Netherlands, and evidence for climatological teleconnections around 2650 BP: Journal of Quaternary Science, 11, 6, 451-460.
van Geel, B., Heusser, C. J., Renssen, H., and Schuurmans, C. J. E., 2000, Climatic change in Chile at around 2700 BP and global evidence for solar forcing: a hypothesis: Holocene, 10, 5, 659-664.
Van Marle, L., 1991, Eastern Indonesia Late Cenozoic smaller benthic foraminifera: Verhandeling Koninklijke Nederlandse Akademie van Wetenschappen. Afdeling Antuurkunde, Eerste Reeks, 34, 1-328.
Verleyen, E., Hodgson, D. A., Sabbe, K., Cremer, H., Emslie, S. D., Gibson, J., Hall, B., Imura, S., Kudoh, S., Marshall, G. J., McMinn, A., Melles, M., Newman, L., Roberts, D., Roberts, S. J., Singh, S. M., Sterken, M., Tavernier, I., Verkulich, S., Van de Vyver, E., Van Nieuwenhuyze, W., Wagner, B., and Vyverman, W., 2011, Post-glacial regional climate variability along the East Antarctic coastal margin-Evidence from shallow marine and coastal terrestrial records: Earth-Science Reviews, 104, 4, 199-212.
Vernet, M., Martinson, D., Iannuzzi, R., Stammerjohn, S., Kozlowski, W., Sines, K., Smith, R., and Garibotti, I., 2008, Primary production within the sea-ice zone west of the Antarctic Peninsula: I-Sea ice, summer mixed layer, and irradiance: Deep-Sea Research Part II-Topical Studies in Oceanography, 55, 18-19, 2068-2085.
Vimeux, F., Masson, V., Jouzel, J., Stievenard, M., and Petit, J. R., 1999, Glacial-interglacial changes in ocean surface conditions in the southern hemisphere: Nature, 398, 6726, 410-413.
Violanti, D., 1996, Taxonomy and distribution of recent benthic foraminifers from Terra Nova Bay (Ross Sea, Antarctica), oceanographic campaign 1987/1988: Palaeontographica Italica, 83, 25-71.
Voigt, I., Chiessi, C. M., Prange, M., Mulitza, S., Groeneveld, J., Varma, V., and Henrich, R., 2015, Holocene shifts of the southern westerlies across the South Atlantic: Paleoceanography, 30, 2, 39-51.
Voloshinova, N. A., 1960, Progress in micropalaeontology in the work of studying the inner structure of Foraminifera: Trudy Pervogo Seminara po Mikrofaune, 48-87.
Wacker, L., Lippold, J., Molnar, M., and Schulz, H., 2013, Towards radiocarbon dating of single foraminifera with a gas ion source: Nuclear Instruments & Methods in Physics Research Section B-Beam Interactions with Materials and Atoms, 294, 307-310.
Wainer, I., Prado, L. F., Khodri, M., and Otto-Bliesner, B., 2014, Reconstruction of the South Atlantic Subtropical Dipole index for the past 12,000 years from surface temperature proxy: Scientific Reports, 4, 5291.
Wang, F., Gao, M., Liu, J., Pei, S., Li, C., Mei, X., and Yang, S., 2016, Distribution and environmental significance of live and dead benthic foraminiferal assemblages in surface sediments of Laizhou Bay, Bohai Sea: Marine Micropaleontology, 123, 1-14.
Ward, P., Whitehouse, M., Meredith, M., Murphy, E., Shreeve, R., Korb, R., Watkins, J., Thorpe, S., Woodd-Walker, R., Brierley, A., Cunningham, N., Grant, S., and Bone, D., 2002, The Southern Antarctic Circumpolar

Current Front: physical and biological coupling at South Georgia: Deep-Sea Research Part I-Oceanographic Research Papers, 49, 12, 2183-2202.
Ward, P., Shreeve, R., Whitehouse, M., Korb, B., Atkinson, A., Meredith, M., Pond, D., Watkins, J., Goss, C., and Cunningham, N., 2005, Phyto- and zooplankton community structure and production around South Georgia (Southern Ocean) during Summer 2001/02: Deep-Sea Research Part I-Oceanographic Research Papers, 52, 3, 421-441.
Ward, P., Whitehouse, M., Shreeve, R., Thorpe, S., Atkinson, A., Korb, R., Pond, D., and Young, E., 2007, Plankton community structure south and west of South Georgia (Southern Ocean): Links with production and physical forcing: Deep-Sea Research Part I-Oceanographic Research Papers, 54, 11, 1871-1889.
Watanabe, O., Jouzel, J., Johnsen, S., Parrenin, F., Shoji, H., and Yoshida, N., 2003, Homogeneous climate variability across East Antarctica over the past three glacial cycles: Nature, 422, 6931, 509-512.
Watson, A., and Orr, J. C., 2003, Carbon dioxide fluxes in the global ocean, *in* Fasham, M. J. R., ed., Ocean biogeochemistry: The role of the ocean carbon cycle in global change Springer-Verlag: Berlin, 123-143.
Wedekind, P. R., 1937, Einfuhrung in die Grundlagen der historischen Geologie. Band II. Mikrobiostratigraphie der Korallen- und Foraminiferenzeit, Ferdinand Enke, Stuttgart, pp.:
Weldeab, S., Arce, A., and Kasten, S., 2016, Mg/Ca-$\Delta CO_3^{2-\ pore\text{-}water}$-temperature calibration for *Globobulimina* spp.: A sensitive paleothermometer for deep-sea temperature reconstruction: Earth and Planetary Science Letters, 438, 95-102.
White, D. A., Bennike, O., Melles, M., Berg, S., and Binnie, S. A., 2017, Was South Georgia covered by an ice cap during the Last Glacial Maximum?: Geological Society, London, Special Publications, 461, 1, 49-59.
White, W. B., and Peterson, R. G., 1996, An Antarctic circumpolar wave in surface pressure, wind, temperature and sea-ice extent: Nature, 380, 6576, 699-702.
Whitehouse, M. J., Priddle, J., and Symon, C., 1996, Seasonal and annual change in seawater temperature, salinity, nutrient and chlorophyll a distributions around South Georgia, South Atlantic: Deep-Sea Research Part I-Oceanographic Research Papers, 43, 4, 425-443.
Whitehouse, M. J., Priddle, J., Brandon, M. A., and Swanson, C., 1999, A comparison of chlorophyll/nutrient dynamics at two survey sites near South Georgia, and the potential role of planktonic nitrogen recycled by land-based predators: Limnology and Oceanography, 44, 6, 1498-1508.
Whitehouse, M. J., Priddle, J., and Brandon, M. A., 2000, Chlorophyll/nutrient characteristics in the water masses to the north of South Georgia, Southern Ocean: Polar Biology, 23, 6, 373-382.
Whitehouse, M. J., Meredith, M. P., Rothery, P., Atkinson, A., Ward, P., and Korb, R. E., 2008a, Rapid warming of the ocean around South Georgia, Southern Ocean, during the 20th century: Forcings, characteristics and implications for lower trophic levels: Deep Sea Research Part I: Oceanographic Research Papers, 55, 10, 1218-1228.
Whitehouse, M. J., Korb, R. E., Atkinson, A., Thorpe, S. E., and Gordon, M., 2008b, Formation, transport and decay of an intense phytoplankton bloom within the High-Nutrient Low-Chlorophyll belt of the Southern Ocean: Journal of Marine Systems, 70, 1–2, 150-167.
Whitworth, T., and Nowlin, W. D., 1987, Water masses and currents of the Southern Ocean at the Greenwich Meridian: Journal of Geophysical Research-Oceans, 92, C6, 6462-6476.
Wiersma, A. P., and Jongma, J. I., 2010, A role for icebergs in the 8.2 ka climate event: Climate Dynamics, 35, 2, 535-549.

Wiesner, H., 1931, Die Foraminiferen der Deutschen Südpolar Expedition 1901-1903. Deutschen Südpolar Expedition: Berlin (Zoology), 20, 53-165.
Williamson, W. C., 1848, On the Recent British species of the genus *Lagena*: Annals and Magazine of Natural History, 2, 1, 1-20.
Wilson, P., Bentley, M., Schnabel, C., Clark, R., and Xu, S., 2008, Stone run (block stream) formation in the Falkland Islands over several cold stages, deduced from cosmogenic isotope (^{10}Be and ^{26}Al) surface exposure dating: Journal of Quaternary Science, 23, 5, 461-473.
Witte, U., Wenzhofer, F., Sommer, S., Boetius, A., Heinz, P., Aberle, N., Sand, M., Cremer, A., Abraham, W. R., Jorgensen, B. B., and Pfannkuche, O., 2003, In situ experimental evidence of the fate of a phytodetritus pulse at the abyssal sea floor: Nature, 424, 6950, 763-766.
Wong, W. W., and Sackett, W. M., 1978, Fractionation of stable carbon isotopes by marine phytoplankton: Geochimica et Cosmochimica Acta, 42, 12, 1809-1815.
Xiao, W., Esper, O., and Gersonde, R., 2016, Last Glacial - Holocene climate variability in the Atlantic sector of the Southern Ocean: Quaternary Science Reviews, 135, 115-137.
Young, E. F., Meredith, M. P., Murphy, E. J., and Carvalho, G. R., 2011a, High-resolution modelling of the shelf and open ocean adjacent to South Georgia, Southern Ocean: Deep-Sea Research Part II-Topical Studies in Oceanography, 58, 13-16, 1540-1552.
Young, E. F., Thorpe, S. E., Banglawala, N., and Murphy, E. J., 2014, Variability in transport pathways on and around the South Georgia shelf, Southern Ocean: Implications for recruitment and retention: Journal of Geophysical Research-Oceans, 119, 1, 241-252.
Young, I. R., Zieger, S., and Babanin, A. V., 2011b, Global trends in wind speed and wave height: Science, 332, 6028, 451-455.
Zahn, R., Winn, K., and Sarnthein, M., 1986, Benthic foraminiferal $\delta^{13}C$ and accumulation rates of organic carbon: *Uvigerina peregrina* group and *Cibicidoides wuellerstorfi*: Paleoceanography, 1, 1, 27-42.
Zeebe, R. E., Bijma, J., and Wolf-Gladrow, D. A., 1999, A diffusion-reaction model of carbon isotope fractionation in foraminifera: Marine Chemistry, 64, 3, 199-227.
Zhang, J., Quay, P. D., and Wilbur, D. O., 1995, Carbon-isotope fractionation during gas-water exchange and dissolution of CO_2: Geochimica Et Cosmochimica Acta, 59, 1, 107-114.
Zheng, F., Li, J. P., and Ding, R. Q., 2017, Influence of the preceding austral summer Southern Hemisphere annular mode on the amplitude of ENSO decay: Advances in Atmospheric Sciences, 34, 11, 1358-1379.
Zheng, S., and Fu, Z., 2001, Fauna Sinica, Phylum Granuloreticulosa, Class Foraminiferea, Agglutinated Foraminifera, Science Press, Beijing, pp. 779.

Appendix A1 – GC666 Sample list and weights

Section	Section depth (cm)	Core depth (cm)	Sample No.	Weight (dry, g)
1	0-1	0-1	000	
1	1-2	1-2	001	
1	2-3	2-3	002	6.8
1	3-4	3-4	003	10.7
1	4-5	4-5	004	9.2
1	5-6	5-6	005	7.7
1	6-7	6-7	006	10.4
1	7-8	7-8	007	8.1
1	8-9	8-9	008	7.7
1	9-10	9-10	009	7.2
1	10-11	10-11	010	
1	11-12	11-12	011	9.6
1	12-13	12-13	012	6.9
1	13-14	13-14	013	9.0
1	14-15	14-15	014	10.8
1	15-16	15-16	015	10.0
1	16-17	16-17	016	9.0
1	17-18	17-18	017	8.4
1	18-19	18-19	018	6.7
1	19-20	19-20	019	9.7
1	20-21	20-21	020	
1	21-22	21-22	021	8.1
1	22-23	22-23	022	9.2
1	23-24	23-24	023	10.4
1	24-25	24-25	024	9.3
1	25-26	25-26	025	8.5
1	26-27	26-27	026	10.5
1	27-28	27-28	027	10.2
1	28-29	28-29	028	8.3
1	29-30	29-30	029	11.9
1	30-31	30-31	030	
1	31-32	31-32	031	9.2
1	32-33	32-33	032	12.2
1	33-34	33-34	033	10.5
1	34-35	34-35	034	12.4
1	35-36	35-36	035	14.2
2	0-1	36-37	036	9.2
2	1-2	37-38	037	11.1
2	2-3	38-39	038	11.2
2	3-4	39-40	039	11.2
2	4-5	40-41	040	
2	5-6	41-42	041	8.6
2	6-7	42-43	042	9.2
2	7-8	43-44	043	9.7
2	8-9	44-45	044	11.0
2	9-10	45-46	045	10.4
2	10-11	46-47	046	11.0
2	11-12	47-48	047	13.1
2	12-13	48-49	048	10.7
2	13-14	49-50	049	11.7
2	14-15	50-51	050	
2	15-16	51-52	051	9.2
2	16-17	52-53	052	9.9
2	17-18	53-54	053	11.9
2	18-19	54-55	054	9.7
2	19-20	55-56	055	11.9
2	20-21	56-57	056	9.2
2	21-22	57-58	057	12.2
2	22-23	58-59	058	9.3
2	23-24	59-60	059	8.7
2	24-25	60-61	060	
2	25-26	61-62	061	8.2
2	26-27	62-63	062	8.8
2	27-28	63-64	063	9.5
2	28-29	64-65	064	9.9
2	29-30	65-66	065	13.2
2	30-31	66-67	066	8.4
2	31-32	67-68	067	8.6
2	32-33	68-69	068	9.1
2	33-34	69-70	069	8.6
2	34-35	70-71	070	
2	35-36	71-72	071	9.2
2	36-37	72-73	072	8.2
2	37-38	73-74	073	10.9
2	38-39	74-75	074	11.3
2	39-40	75-76	075	12.0

Section	Section depth (cm)	Core depth (cm)	Sample No.	Weight (dry, g)
2	40-41	76-77	076	12.1
2	41-42	77-78	077	9.8
2	42-43	78-79	078	9.5
2	43-44	79-80	079	10.6
2	44-45	80-81	080	
2	45-46	81-82	081	9.3
2	46-47	82-83	082	10.7
2	47-48	83-84	083	12.1
2	48-49	84-85	084	10.5
2	49-50	85-86	085	12.3
2	50-51	86-87	086	12.2
2	51-52	87-88	087	10.0
2	52-53	88-89	088	9.4
2	53-54	89-90	089	9.6
2	54-55	90-91	090	
2	55-56	91-92	091	13.5
2	56-57	92-93	092	12.9
2	57-58	93-94	093	9.4
2	58-59	94-95	094	11.2
2	59-60	95-96	095	12.0
2	60-61	96-97	096	12.6
2	61-62	97-98	097	11.3
2	62-63	98-99	098	10.5
2	63-64	99-100	099	10.1
2	64-65	100-101	100	
2	65-66	101-102	101	12.4
2	66-67	102-103	102	9.6
2	67-68	103-104	103	10.4
2	68-69	104-105	104	9.6
2	69-70	105-106	105	10.9
2	70-71	106-107	106	8.5
2	71-72	107-108	107	9.6
2	72-73	108-109	108	10.1
2	73-74	109-110	109	12.5
2	74-75	110-111	110	
2	75-76	111-112	111	12.2
2	76-77	112-113	112	9.1
2	77-78	113-114	113	10.2
2	78-79	114-115	114	8.5
2	79-80	115-116	115	7.9
2	80-81	116-117	116	6.6
2	81-82	117-118	117	6.4
2	82-83	118-119	118	6.6
2	83-84	119-120	119	6.9
2	84-85	120-121	120	
2	85-86	121-122	121	6.7
2	86-87	122-123	122	6.9
2	87-88	123-124	123	6.0
2	88-89	124-125	124	6.4
2	89-90	125-126	125	7.2
2	90-91	126-127	126	6.5
2	91-92	127-128	127	7.0
2	92-93	128-129	128	8.7
2	93-94	129-130	129	8.1
3	0-1	130-131	130	
3	1-2	131-132	131	7.2
3	2-3	132-133	132	8.3
3	3-4	133-134	133	9.3
3	4-5	134-135	134	8.5
3	5-6	135-136	135	8.0
3	6-7	136-137	136	6.9
3	7-8	137-138	137	8.1
3	8-9	138-139	138	8.7
3	9-10	139-140	139	10.3
3	10-11	140-141	140	
3	11-12	141-142	141	10.6
3	12-13	142-143	142	11.4
3	13-14	143-144	143	10.9
3	14-15	144-145	144	10.4
3	15-16	145-146	145	10.3
3	16-17	146-147	146	12.3
3	17-18	147-148	147	11.9
3	18-19	148-149	148	12.0
3	19-20	149-150	149	12.3
3	20-21	150-151	150	
3	21-22	151-152	151	13.0
3	22-23	152-153	152	13.9
3	23-24	153-154	153	12.1

Appendix A1 – GC666 Sample list and weights

Section	Section depth (cm)	Core depth (cm)	Sample No.	Weight (dry, g)
3	24-25	154-155	154	11.2
3	25-26	155-156	155	12.7
3	26-27	156-157	156	15.5
3	27-28	157-158	157	11.6
3	28-29	158-159	158	12.6
3	29-30	159-160	159	11.1
3	30-31	160-161	160	
3	31-32	161-162	161	17.5
3	32-33	162-163	162	13.2
3	33-34	163-164	163	14.9
3	34-35	164-165	164	11.9
3	35-36	165-166	165	12.6
3	36-37	166-167	166	11.2
3	37-38	167-168	167	12.7
3	38-39	168-169	168	9.6
3	39-40	169-170	169	10.4
3	40-41	170-171	170	
3	41-42	171-172	171	13.2
3	42-43	172-173	172	9.4
3	43-44	173-174	173	7.4
3	44-45	174-175	174	7.5
3	45-46	175-176	175	7.4
3	46-47	176-177	176	8.3
3	47-48	177-178	177	7.5
3	48-49	178-179	178	7.2
3	49-50	179-180	179	7.0
3	50-51	180-181	180	
3	51-52	181-182	181	8.6
3	52-53	182-183	182	7.3
3	53-54	183-184	183	8.0
3	54-55	184-185	184	7.5
3	55-56	185-186	185	6.5
3	56-57	186-187	186	8.0
3	57-58	187-188	187	8.1
3	58-59	188-189	188	9.4
3	59-60	189-190	189	9.6
3	60-61	190-191	190	
3	61-62	191-192	191	11.2
3	62-63	192-193	192	6.6
3	63-64	193-194	193	10.8
3	64-65	194-195	194	11.2
3	65-66	195-196	195	9.2
3	66-67	196-197	196	7.9
3	67-68	197-198	197	8.4
3	68-69	198-199	198	10.2
3	69-70	199-200	199	9.8
3	70-71	200-201	200	
3	71-72	201-202	201	10.4
3	72-73	202-203	202	12.5
3	73-74	203-204	203	8.7
3	74-75	204-205	204	10.5
3	75-76	205-206	205	11.0
3	76-77	206-207	206	12.0
3	77-78	207-208	207	11.1
3	78-79	208-209	208	10.7
3	79-80	209-210	209	10.3
3	80-81	210-211	210	
3	81-82	211-212	211	12.5
3	82-83	212-213	212	12.9
3	83-84	213-214	213	12.8
3	84-85	214-215	214	10.5
3	85-86	215-216	215	10.1
3	86-87	216-217	216	13.1
3	87-88	217-218	217	12.4
3	88-89	218-219	218	11.8
3	89-90	219-220	219	13.4
3	90-91	220-221	220	
3	91-92	221-222	221	14.7
3	92-93	222-223	222	13.4
3	93-94	223-224	223	13.8
3	94-95	224-225	224	14.7
3	95-96	225-226	225	13.1
3	96-97	226-227	226	14.6
3	97-98	227-228	227	16.7
3	98-99	228-229	228	12.6
3	99-100	229-230	229	14.8
4	0-1	230-231	230	
4	1-2	231-232	231	

Section	Section depth (cm)	Core depth (cm)	Sample No.	Weight (dry, g)
4	2-3	232-233	232	8.3
4	3-4	233-234	233	8.6
4	4-5	234-235	234	10.0
4	5-6	235-236	235	10.5
4	6-7	236-237	236	8.5
4	7-8	237-238	237	9.0
4	8-9	238-239	238	8.2
4	9-10	239-240	239	7.5
4	10-11	240-241	240	
4	11-12	241-242	241	10.0
4	12-13	242-243	242	9.2
4	13-14	243-244	243	9.9
4	14-15	244-245	244	11.7
4	15-16	245-256	245	10.6
4	16-17	246-247	246	12.4
4	17-18	247-248	247	14.0
4	18-19	248-249	248	15.3
4	19-20	249-250	250	
4	20-21	250-251		
4	21-22	251-252	251	10.5
4	22-23	252-253	252	9.9
4	23-24	253-254	253	11.0
4	24-25	254-255	254	10.0
4	25-26	255-256	255	11.9
4	26-27	256-257	256	6.3
4	27-28	257-258	257	11.7
4	28-29	258-259	258	14.5
4	29-30	259-260	260	
4	30-31	260-261		
4	31-32	261-262	261	10.5
4	32-33	262-263	262	8.3
4	33-34	263-264	263	10.1
4	34-35	264-265	264	9.5
4	35-36	265-266	265	11.4
4	36-37	266-267	266	12.4
4	37-38	267-268	267	10.7
4	38-39	268-269	268	12.5
4	39-40	269-270	270	
4	40-41	270-271		

Section	Section depth (cm)	Core depth (cm)	Sample No.	Weight (dry, g)
4	41-42	271-272	271	10.3
4	42-43	272-273	272	12.2
4	43-44	273-274	273	9.9
4	44-45	274-275	274	10.7
4	45-46	275-276	275	12.8
4	46-47	276-277	276	11.4
4	47-48	277-278	277	10.6
4	48-49	278-279	278	11.4
4	49-50	279-280	279	8.2
4	50-51	280-281	280	
4	51-52	281-282	281	9.1
4	52-53	282-283	282	8.7
4	53-54	283-284	283	10.2
4	54-55	284-285	284	12.2
4	55-56	285-286	285	11.0
4	56-57	286-287	286	11.0
4	57-58	287-288	287	11.2
4	58-59	288-289	288	13.0
4	59-60	289-290	289	8.0
4	60-61	290-291	290	
4	61-62	291-292	291	9.8
4	62-63	292-293	292	11.6
4	63-64	293-294	293	11.1
4	64-65	294-295	294	10.0
4	65-66	295-296	295	12.2
4	66-67	296-297	296	11.8
4	67-68	297-298	297	9.6
4	68-69	298-299	298	10.6
4	69-70	299-300	299	10.3
4	70-71	300-301	300	
4	71-72	301-302	301	11.8
4	72-73	302-303	302	10.8
4	73-74	303-304	303	10.9
4	74-75	304-305	304	9.8
4	75-76	305-306	305	11.1
4	76-77	306-307	306	11.0
4	77-78	307-308	307	11.3
4	78-79	308-309	308	8.9
4	79-80	309-310	309	

Section	Section depth (cm)	Core depth (cm)	Sample No.	Weight (dry, g)
4	80-81	310-311	310	
4	81-82	311-312	311	10.2
4	82-83	312-313	312	8.4
4	83-84	313-314	313	11.9
4	84-85	314-315	314	8.9
4	85-86	315-316	315	12.0
4	86-87	316-317	316	11.1
4	87-88	317-318	317	15.0
4	88-89	318-319	318	9.8
4	89-90	319-320	319	5.1
4	90-91	320-321	320	
4	91-92	321-322	321	11.7
4	92-93	322-323	322	9.2
4	93-94	323-324	323	8.9
4	94-95	324-325	324	8.6
4	95-96	325-326	325	10.8
4	96-97	326-327	326	11.4
4	97-98	327-328	327	10.0
4	98-99	328-329	328	8.8
4	99-100	329-330	329	8.5
5	0-1	330-331	330	
5	1-2	331-332	331	
5	2-3	332-333	332	12.9
5	3-4	333-334	333	12.9
5	4-5	334-335	334	14.6
5	5-6	335-336	335	14.6
5	6-7	336-337	336	12.1
5	7-8	337-338	337	11.7
5	8-9	338-339	338	10.2
5	9-10	339-340	339	11.4
5	10-11	340-341	340	
5	11-12	341-342	341	13.2
5	12-13	342-343	342	13.8
5	13-14	343-344	343	11.4
5	14-15	344-345	344	11.3
5	15-16	345-346	345	13.8
5	16-17	346-347	346	13.2
5	17-18	347-348	347	12.4
5	18-19	348-349	348	13.3

Section	Section depth (cm)	Core depth (cm)	Sample No.	Weight (dry, g)
5	19-20	349-350	349	
5	20-21	350-351	350	
5	21-22	351-352	351	12.4
5	22-23	352-353	352	12.4
5	23-24	353-354	353	13.2
5	24-25	354-355	354	14.9
5	25-26	355-356	355	15.5
5	26-27	356-357	356	13.1
5	27-28	357-358	357	14.5
5	28-29	358-359	358	12.3
5	29-30	359-360	359	
5	30-31	360-361	360	
5	31-32	361-362	361	15.5
5	32-33	362-363	362	14.2
5	33-34	363-364	363	13.2
5	34-35	364-365	364	12.2
5	35-36	365-366	365	13.3
5	36-37	366-367	366	11.5
5	37-38	367-368	367	14.1
5	38-39	368-369	368	13.8
5	39-40	369-370	369	12.3
5	40-41	370-371	370	
5	41-42	371-372	371	12.9
5	42-43	372-373	372	14.5
5	43-44	373-374	373	12.1
5	44-45	374-375	374	11.0
5	45-46	375-376	375	11.9
5	46-47	376-377	376	11.7
5	47-48	377-378	377	12.5
5	48-49	378-379	378	11.4
5	49-50	379-380	379	15.7
5	50-51	380-381	380	
5	51-52	381-382	381	14.5
5	52-53	382-383	382	13.1
5	53-54	383-384	383	14.0
5	54-55	384-385	384	8.5
5	55-56	385-386	385	13.0
5	56-57	386-387	386	16.2
5	57-58	387-388	387	12.3

Section	Section depth (cm)	Core depth (cm)	Sample No.	Weight (dry, g)
5	58-59	388-389	388	13.2
5	59-60	389-390	389	
5	60-61	390-391	390	
5	61-62	391-392	391	16.8
5	62-63	392-393	392	11.7
5	63-64	393-394	393	12.0
5	64-65	394-395	394	11.9
5	65-66	395-396	395	10.9
5	66-67	396-397	396	13.6
5	67-68	397-398	397	10.8
5	68-69	398-399	398	12.0
5	69-70	399-400	399	9.3
5	70-71	400-401	400	
5	71-72	401-402	401	13.2
5	72-73	402-403	402	12.5
5	73-74	403-404	403	11.7
5	74-75	404-405	404	9.9
5	75-76	405-406	405	11.8
5	76-77	406-407	406	12.6
5	77-78	407-408	407	10.7
5	78-79	408-409	408	8.9
5	79-80	409-410	409	7.9
5	80-81	410-411	410	
5	81-82	411-412	411	15.3
5	82-83	412-413	412	17.5
6	0-1	413-414	413	11.8
6	1-2	414-415	414	12.5
6	2-3	415-416	415	13.3
6	3-4	416-417	416	13.3
6	4-5	417-418	417	12.0
6	5-6	418-419	418	12.6
6	6-7	419-420	419	6.9
6	7-8	420-421	420	
6	8-9	421-422	421	12.4
6	9-10	422-423	422	13.7
6	10-11	423-424	423	12.1
6	11-12	424-425	424	13.4
6	12-13	425-426	425	12.6
6	13-14	426-427	426	10.7

Section	Section depth (cm)	Core depth (cm)	Sample No.	Weight (dry, g)
6	14-15	427-428	427	10.3
6	15-16	428-429	428	12.1
6	16-17	429-430	429	10.6
6	17-18	430-431	430	
6	18-19	431-432	431	12.9
6	19-20	432-433	432	13.9
6	20-21	433-434	433	15.2
6	21-22	434-435	434	13.3
6	22-23	435-436	435	15.7
6	23-24	436-437	436	14.5
6	24-25	437-438	437	15.8
6	25-26	438-439	438	12.5
6	26-27	439-440	439	11.9
6	27-28	440-441	440	
6	28-29	441-442	441	18.5
6	29-30	442-443	442	15.5
6	30-31	443-444	443	12.2
6	31-32	444-445	444	13.9
6	32-33	445-446	445	11.6
6	33-34	446-447	446	14.5
6	34-35	447-448	447	12.1
6	35-36	448-449	448	11.2
6	36-37	449-450	449	8.2
6	37-38	450-451	450	
6	38-39	451-452	451	14.6
6	39-40	452-453	452	13.8
6	40-41	453-454	453	13.9
6	41-42	454-455	454	12.4
6	42-43	455-456	455	11.9
6	43-44	456-457	456	10.7
6	44-45	457-458	457	12.5
6	45-46	458-459	458	12.4
6	46-47	459-460	459	
6	47-48	460-461	460	
6	48-49	461-462	461	11.9
6	49-50	462-463	462	10.7
6	50-51	463-464	463	9.4
6	51-52	464-465	464	11.9
6	52-53	465-466	465	10.5

Appendix A1 – GC666 Sample list and weights

Section	Section depth (cm)	Core depth (cm)	Sample No.	Weight (dry, g)
6	53-54	466-467	466	10.5
6	54-55	467-468	467	10.5
6	55-56	468-469	468	10.5
6	56-57	469-470	469	10.6
6	57-58	470-471	470	
6	58-59	471-472	471	11.6
6	59-60	472-473	472	11.7
6	60-61	473-474	473	10.6
6	61-62	474-475	474	10.2
6	62-63	475-476	475	9.9
6	63-64	476-477	476	12.2
6	64-65	477-478	477	9.4
6	65-66	478-479	478	11.9
6	66-67	479-480	479	11.8
6	67-68	480-481	480	
6	68-69	481-482	481	11.8
6	69-70	482-483	482	8.1
6	70-71	483-484	483	10.3
6	71-72	484-485	484	10.3
6	72-73	485-486	485	11.6
6	73-74	486-487	486	11.3
6	74-75	487-488	487	9.9
6	75-76	488-489	488	10.4
6	76-77	489-490	489	
6	77-78	490-491	490	
6	78-79	491-492	491	11.9
6	79-80	492-493	492	9.1
6	80-81	493-494	493	8.0
6	81-82	494-495	494	8.3
6	82-83	495-496	495	8.6
6	83-84	496-497	496	8.3
6	84-85	497-498	497	9.2
6	85-86	498-499	498	
6	86-87	499-500	499	
6	87-88	500-501	500	
6	88-89	501-502	501	
6	89-90	502-503	502	
6	90-91	503-504	503	
6	91-92	504-505	504	9.2
6	92-93	505-506	505	7.8
6	93-94	506-507	506	7.5
6	94-95	507-508	507	8.5
6	95-96	508-509	508	7.1
6	96-97	509-510	509	
6	97-98	510-511	510	
6	98-99	511-512	511	
6	99-100	512-513	512	8.0
7	2-3	515-516	515	9.5
7	3-4	516-517	516	10.2
7	63-64	576-577	576	3.8
8	27-28	640-641	640	5.0
8	91-92	704-705	704	4.0
9	55-56	768-769	768	3.4
9	102-103	815-816	815	

Appendix A2 – GC673 Sample list and weights

Section	Section depth (cm)	Core depth (cm)	Sample No.	Weight (wet. g)	Weight (dry, g)
1	0-1	0-1	000	17.1	
1	1-2	1-2	001	14.5	7.0
1	2-3	2-3	002	28.1	
1	3-4	3-4	003	18.1	
1	4-5	4-5	004	14.7	
1	5-6	5-6	005	17.0	
1	6-7	6-7	006	19.5	
1	7-8	7-8	007	20.8	
1	8-9	8-9	008	21.1	
1	9-10	9-10	009	20.9	
1	10-11	10-11	010	19.5	
1	11-12	11-12	011	20.5	
1	12-13	12-13	012	22.5	
1	13-14	13-14	013	20.5	
1	14-15	14-15	014	19.6	9.0
1	15-16	15-16	015	19.1	8.6
1	16-17	16-17	016	18.5	8.6
1	17-18	17-18	017	20.2	9.8
1	18-19	18-19	018	21.1	10.4
1	19-20	19-20	019	29.9	12.6
1	20-21	20-21	020	20.9	10.7
1	21-22	21-22	021	25.3	
1	22-23	22-23	022	21.6	
1	23-24	23-24	023	20.0	
1	24-25	24-25	024	21.2	
1	25-26	25-26	025	22.6	
1	26-27	26-27	026	22.8	
1	27-28	27-28	027	20.3	
1	28-29	28-29	028	24.4	
1	29-30	29-30	029	18.5	
1	30-31	30-31	030	23.0	
1	31-32	31-32	031	22.6	
1	32-33	32-33	032	19.3	9.4
1	33-34	33-34	033	28.3	
1	34-35	34-35	034	23.6	
1	35-36	35-36	035	21.9	
1	36-37	36-37	036	20.8	

Section	Section depth (cm)	Core depth (cm)	Sample No.	Weight (wet. g)	Weight (dry, g)
1	37-38	37-38	037	24.8	
1	38-39	38-39	038	20.2	
1	39-40	39-40	039	22.0	
1	40-41	40-41	040	22.0	
1	41-42	41-42	041	22.9	
1	42-43	42-43	042	26.0	
1	43-44	43-44	043	26.0	
1	44-45	44-45	044	25.0	
1	45-46	45-46	045	21.9	
1	46-47	46-47	046	25.8	
1	47-48	47-48	047	26.4	
1	48-49	48-49	048	17.0	9.0
1	49-50	49-50	049	28.7	
1	50-51	50-51	050	28.4	
1	51-52	51-52	051	23.0	
1	52-53	52-53	052	26.0	
1	53-54	53-54	053	21.6	
1	54-55	54-55	054	27.4	
1	55-56	55-56	055	26.3	
1	56-57	56-57	056	26.8	
1	57-58	57-58	057		
2	0-1	58-59	058		
2	1-2	59-60	059	18.1	
2	2-3	60-61	060	18.1	
2	3-4	61-62	061	25.0	
2	4-5	62-63	062	21.5	
2	5-6	63-64	063	19.4	
2	6-7	64-65	064	34.2	
2	7-8	65-66	065	18.5	10.2
2	8-9	66-67	066	20.9	
2	9-10	67-68	067	21.3	
2	10-11	68-69	068	17.7	
2	11-12	69-70	069	20.2	
2	12-13	70-71	070	20.3	
2	13-14	71-72	071	24.4	
2	14-15	72-73	072	20.8	
2	15-16	73-74	073	18.6	

Section	Section depth (cm)	Core depth (cm)	Sample No.	Weight (wet. g)	Weight (dry, g)
2	16-17	74-75	074	20.7	
2	17-18	75-76	075	22.9	
2	18-19	76-77	076	20.9	
2	19-20	77-78	077	22.9	
2	20-21	78-79	078	20.5	
2	21-22	79-80	079	21.8	
2	22-23	80-81	080	21.3	
2	23-24	81-82	081	15.8	8.5
2	24-25	82-83	082	22.1	
2	25-26	83-84	083	21.0	
2	26-27	84-85	084	22.5	
2	27-28	85-86	085	24.6	
2	28-29	86-87	086	20.6	
2	29-30	87-88	087	21.9	
2	30-31	88-89	088	17.4	
2	31-32	89-90	089	20.4	
2	32-33	90-91	090	19.9	
2	33-34	91-92	091	21.1	
2	34-35	92-93	092	20.6	
2	35-36	93-94	093	20.0	
2	36-37	94-95	094	18.4	
2	37-38	95-96	095	22.4	
2	38-39	96-97	096	19.7	
2	39-40	97-98	097	13.9	7.1
2	40-41	98-99	098	23.2	
2	41-42	99-100	099	26.0	
2	42-43	100-101	100	28.4	
2	43-44	101-102	101	22.1	
2	44-45	102-103	102	23.5	
2	45-46	103-104	103	24.8	
2	46-47	104-105	104	21.2	
2	47-48	105-106	105	26.5	
2	48-49	106-107	106	21.1	
2	49-50	107-108	107	27.1	
2	50-51	108-109	108	28.4	
2	51-52	109-110	109	24.4	
2	52-53	110-111	110	24.6	
2	53-54	111-112	111	28.6	
2	54-55	112-113	112	32.0	

Section	Section depth (cm)	Core depth (cm)	Sample No.	Weight (wet. g)	Weight (dry, g)
2	55-56	113-114	113	17.2	9.2
2	56-57	114-115	114	23.5	
2	57-58	115-116	115	21.4	
2	58-59	116-117	116	22.2	
2	59-60	117-118	117	20.5	
2	60-61	118-119	118	24.4	
2	61-62	119-120	119	26.3	
2	62-63	120-121	120	24.9	
2	63-64	121-122	121	21.5	
2	64-65	122-123	122	28.3	
2	65-66	123-124	123	24.1	
2	66-67	124-125	124	26.4	
2	67-68	125-126	125	27.5	
2	68-69	126-127	126	30.3	
2	69-70	127-128	127	23.9	
2	70-71	128-129	128	30.7	
2	71-72	129-130	129	16.0	8.7
2	72-73	130-131	130	22.9	
2	73-74	131-132	131	21.4	
2	74-75	132-133	132	27.4	
2	75-76	133-134	133	24.6	
2	76-77	134-135	134	27.5	
2	77-78	135-136	135	18.3	
2	78-79	136-137	136	21.7	
2	79-80	137-138	137	26.1	
2	80-81	138-139	138	18.6	
2	81-82	139-140	139	22.0	
2	82-83	140-141	140	23.3	
2	83-84	141-142	141	21.7	
2	84-85	142-143	142	21.0	
2	85-86	143-144	143	27.8	
2	86-87	144-145	144	23.4	
2	87-88	145-146	145	16.5	8.0
2	88-89	146-147	146	19.6	
2	89-90	147-148	147	21.3	
2	90-91	148-149	148	25.4	
2	91-92	149-150	149		
2	92-93	150-151	150	21.9	
2	93-94	151-152	151	19.5	

Section	Section depth (cm)	Core depth (cm)	Sample No.	Weight (wet. g)	Weight (dry, g)
2	94-95	152-153	152	24.4	
3	0-1	153-154	153	5.1	
3	1-2	154-155	154	13.4	
3	2-3	155-156	155	19.0	
3	3-4	156-157	156	18.3	
3	4-5	157-158	157	23.4	
3	5-6	158-159	158	18.8	
3	6-7	159-160	159	20.0	10.6
3	7-8	160-161	160	12.4	7.8
3	8-9	161-162	161	16.4	8.6
3	9-10	162-163	162	20.9	11.4
3	10-11	163-164	163	23.8	13.0
3	11-12	164-165	164	17.2	9.2
3	12-13	165-166	165	25.2	13.4
3	13-14	166-167	166	19.8	
3	14-15	167-168	167	20.3	
3	15-16	168-169	168	21.4	
3	16-17	169-170	169	19.1	
3	17-18	170-171	170	27.0	
3	18-19	171-172	171	23.2	
3	19-20	172-173	172	24.0	
3	20-21	173-174	173	18.4	
3	21-22	174-175	174	23.4	
3	22-23	175-176	175	24.5	
3	23-24	176-177	176	16.8	
3	24-25	177-178	177	12.5	7.5
3	25-26	178-179	178	24.9	
3	26-27	179-180	179	23.1	
3	27-28	180-181	180	27.3	
3	28-29	181-182	181	22.2	
3	29-30	182-183	182	21.6	
3	30-31	183-184	183	24.6	
3	31-32	184-185	184	26.3	
3	32-33	185-186	185	24.1	
3	33-34	186-187	186	22.4	
3	34-35	187-188	187	27.1	
3	35-36	188-189	188	22.6	
3	36-37	189-190	189	27.1	
3	37-38	190-191	190	21.8	

Section	Section depth (cm)	Core depth (cm)	Sample No.	Weight (wet. g)	Weight (dry, g)
3	38-39	191-192	191	20.7	
3	39-40	192-193	192	20.6	
3	40-41	193-194	193	16.3	10.2
3	41-42	194-195	194	10.1	
3	42-43	195-196	195	26.5	
3	43-44	196-197	196	18.4	
3	44-45	197-198	197	16.0	
3	45-46	198-199	198	20.6	
3	46-47	199-200	199	15.1	
3	47-48	200-201	200	16.2	
3	48-49	201-202	201	11.4	
3	49-50	202-203	202	13.2	
3	50-51	203-204	203	19.1	
3	51-52	204-205	204	26.1	
3	52-53	205-206	205	14.3	
3	53-54	206-207	206	15.5	
3	54-55	207-208	207	17.0	
3	55-56	208-209	208	19.7	
3	56-57	209-210	209	17.4	7.4
3	57-58	210-211	210	25.2	
3	58-59	211-212	211	17.8	
3	59-60	212-213	212	13.4	
3	60-61	213-214	213	24.3	
3	61-62	214-215	214	18.2	
3	62-63	215-216	215	28.2	
3	63-64	216-217	216	24.4	
3	64-65	217-218	217	18.5	
3	65-66	218-219	218	25.4	
3	66-67	219-220	219	23.0	
3	67-68	220-221	220	25.2	
3	68-69	221-222	221	22.8	
3	69-70	222-223	222	28.7	
3	70-71	223-224	223	24.3	
3	71-72	224-225	224	27.5	
3	72-73	225-226	225	18.4	10.4
3	73-74	226-227	226	23.7	
3	74-75	227-228	227	26.6	
3	75-76	228-229	228	21.1	
3	76-77	229-230	229	23.0	

Section	Section depth (cm)	Core depth (cm)	Sample No.	Weight (wet. g)	Weight (dry, g)
3	77-78	230-231	230	27.0	
3	78-79	231-232	231	23.3	
3	79-80	232-233	232	23.7	
3	80-81	233-234	233	22.8	
3	81-82	234-235	234	24.6	
3	82-83	235-236	235	22.9	
3	83-84	236-237	236	18.8	
3	84-85	237-238	237	23.6	
3	85-86	238-239	238	17.9	
3	86-87	239-240	239	24.5	
3	87-88	240-241	240	20.3	
3	88-89	241-242	241	16.9	10.3
3	89-90	242-243	242	27.6	
3	90-91	243-244	243	23.1	
3	91-92	244-245	244	24.3	
3	92-93	245-256	245	22.3	
3	93-94	246-247	246	26.2	
3	94-95	247-248	247	25.7	
3	95-96	248-249	248	20.7	
3	96-97	249-250	249	24.2	
3	97-98	250-251	250	26.6	
4	0-1	251-252	251	22.2	
4	1-2	252-253	252	29.5	
4	2-3	253-254	253	28.7	
4	3-4	254-255	254	30.2	
4	4-5	255-256	255	28.3	
4	5-6	256-257	256	27.5	
4	6-7	257-258	257	19.0	12.2
4	7-8	258-259	258	26.2	
4	8-9	259-260	259	25.9	
4	9-10	260-261	260	27.4	
4	10-11	261-262	261	39.1	
4	11-12	262-263	262	33.2	
4	12-13	263-264	263	27.0	
4	13-14	264-265	264	32.0	
4	14-15	265-266	265	30.3	
4	15-16	266-267	266	32.5	
4	16-17	267-268	267	28.9	
4	17-18	268-269	268	30.0	

Section	Section depth (cm)	Core depth (cm)	Sample No.	Weight (wet. g)	Weight (dry, g)
4	18-19	269-270	269	32.7	
4	19-20	270-271	270	30.3	
4	20-21	271-272	271	25.0	
4	21-22	272-273	272	24.9	
4	22-23	273-274	273	17.3	8.8
4	23-24	274-275	274	23.8	
4	24-25	275-276	275	25.7	
4	25-26	276-277	276	24.7	
4	26-27	277-278	277	23.8	
4	27-28	278-279	278	21.6	
4	28-29	279-280	279	22.0	
4	29-30	280-281	280	24.8	
4	30-31	281-282	281	22.9	
4	31-32	282-283	282	20.5	
4	32-33	283-284	283	22.5	
4	33-34	284-285	284	22.6	
4	34-35	285-286	285	22.3	
4	35-36	286-287	286	25.3	
4	36-37	287-288	287	20.1	
4	37-38	288-289	288	21.0	
4	38-39	289-290	289	15.0	7.9
4	39-40	290-291	290	21.0	
4	40-41	291-292	291	19.6	
4	41-42	292-293	292	22.2	
4	42-43	293-294	293	23.5	
4	43-44	294-295	294	27.9	
4	44-45	295-296	295	21.2	
4	45-46	296-297	296	26.2	
4	46-47	297-298	297	27.1	
4	47-48	298-299	298	23.3	
4	48-49	299-300	299	26.7	
4	49-50	300-301	300	26.6	
4	50-51	301-302	301	20.7	
4	51-52	302-303	302	24.4	
4	52-53	303-304	303	26.5	
4	53-54	304-305	304	26.4	
4	54-55	305-306	305	19.0	11.1
4	55-56	306-307	306	28.4	
4	56-57	307-308	307	21.9	

Section	Section depth (cm)	Core depth (cm)	Sample No.	Weight (wet. g)	Weight (dry, g)
4	57-58	308-309	308	22.2	
4	58-59	309-310	309	23.3	
4	59-60	310-311	310	25.5	
4	60-61	311-312	311	20.7	
4	61-62	312-313	312	25.3	
4	62-63	313-314	313	22.1	
4	63-64	314-315	314	22.8	
4	64-65	315-316	315	26.3	
4	65-66	316-317	316	26.4	
4	66-67	317-318	317	23.1	
4	67-68	318-319	318	25.4	
4	68-69	319-320	319	24.6	
4	69-70	320-321	320	20.9	
4	70-71	321-322	321	16.4	11.3
4	71-72	322-323	322	30.2	
4	72-73	323-324	323	25.0	
4	73-74	324-325	324	30.2	
4	74-75	325-326	325	30.7	
4	75-76	326-327	326	26.7	
4	76-77	327-328	327	17.5	
4	77-78	328-329	328	6.5	
4	78-79	329-330	329	10.3	
4	79-80	330-331	330	17.9	
4	80-81	331-332	331	26.0	
4	81-82	332-333	332	29.2	
4	82-83	333-334	333	23.7	
4	83-84	334-335	334	25.9	
4	84-85	335-336	335	20.1	
4	85-86	336-337	336	21.4	
4	86-87	337-338	337	15.7	10.2
4	87-88	338-339	338	30.0	
4	88-89	339-340	339	25.8	
4	89-90	340-341	340	27.9	
4	90-91	341-342	341	29.5	
4	91-92	342-343	342	36.4	
4	92-93	343-344	343	31.8	
4	93-94	344-345	344	27.7	
4	94-95	345-346	345	26.1	
4	95-96	346-347	346	31.1	

Section	Section depth (cm)	Core depth (cm)	Sample No.	Weight (wet. g)	Weight (dry, g)
4	96-97	347-348	347	24.7	
4	97-98	348-349	348	30.1	
4	98-99	349-350	349	32.4	
4	99-100	350-351	350	35.8	
5	0-1	351-352	351	16.8	
5	1-2	352-353	352	26.4	
5	2-3	353-354	353	18.8	12.1
5	3-4	354-355	354	18.7	
5	4-5	355-356	355	23.3	
5	5-6	356-357	356	22.1	
5	6-7	357-358	357	24.1	
5	7-8	358-359	358	22.5	
5	8-9	359-360	359	21.1	
5	9-10	360-361	360	25.5	
5	10-11	361-362	361	25.3	
5	11-12	362-363	362	22.3	
5	12-13	363-364	363	22.9	
5	13-14	364-365	364	25.1	
5	14-15	365-366	365	41.5	
5	15-16	366-367	366	17.5	
5	16-17	367-368	367	25.0	16.4
5	17-18	368-369	368	22.0	14.2
5	18-19	369-370	369	17.1	11.4
5	19-20	370-371	370	14.9	9.7
5	20-21	371-372	371	17.3	11.2
5	21-22	372-373	372	23.0	
5	22-23	373-374	373	24.7	
5	23-24	374-375	374	23.4	
5	24-25	375-376	375	23.2	
5	25-26	376-377	376	19.7	
5	26-27	377-378	377	25.6	
5	27-28	378-379	378	23.3	
5	28-29	379-380	379	21.5	
5	29-30	380-381	380	23.8	
5	30-31	381-382	381	24.2	
5	31-32	382-383	382	24.2	
5	32-33	383-384	383	23.3	
5	33-34	384-385	384	32.2	
5	34-35	385-386	385	12.9	7.2

Section	Section depth (cm)	Core depth (cm)	Sample No.	Weight (wet. g)	Weight (dry, g)
5	35-36	386-387	386	22.5	
5	36-37	387-388	387	13.9	
5	37-38	388-389	388	35.2	
5	38-39	389-390	389	26.1	
5	39-40	390-391	390	34.5	
5	40-41	391-392	391	32.4	
5	41-42	392-393	392	33.3	
5	42-43	393-394	393	21.2	
5	43-44	394-395	394	22.4	
5	44-45	395-396	395	26.2	
5	45-46	396-397	396	21.4	
5	46-47	397-398	397	26.9	
5	47-48	398-399	398	26.4	
5	48-49	399-400	399	21.4	
5	49-50	400-401	400	31.2	
5	50-51	401-402	401	13.2	7.4
5	51-52	402-403	402	22.8	
5	52-53	403-404	403	28.1	
5	53-54	404-405	404	24.8	
5	54-55	405-406	405	22.9	
5	55-56	406-407	406	20.3	
5	56-57	407-408	407	26.3	
5	57-58	408-409	408	24.2	
5	58-59	409-410	409	24.6	
5	59-60	410-411	410	26.0	
5	60-61	411-412	411	24.4	
5	61-62	412-413	412	18.9	
5	62-63	413-414	413	25.1	
5	63-64	414-415	414	22.9	
5	64-65	415-416	415	24.3	
5	65-66	416-417	416	25.5	
5	66-67	417-418	417	12.8	6.3
5	67-68	418-419	418	18.3	
5	68-69	419-420	419	19.1	
5	69-70	420-421	420	29.2	
5	70-71	421-422	421	25.8	
5	71-72	422-423	422	21.6	
5	72-73	423-424	423	21.8	
5	73-74	424-425	424	24.3	

Section	Section depth (cm)	Core depth (cm)	Sample No.	Weight (wet. g)	Weight (dry, g)
5	74-75	425-426	425	23.4	
5	75-76	426-427	426	24.8	
5	76-77	427-428	427	19.9	
5	77-78	428-429	428	25.4	
5	78-79	429-430	429	23.2	
5	79-80	430-431	430	22.6	
5	80-81	431-432	431	22.0	
5	81-82	432-433	432	16.2	
5	82-83	433-434	433	15.6	8.5
5	83-84	434-435	434	14.0	
5	84-85	435-436	435	15.9	
5	85-86	436-437	436	25.9	
5	86-87	437-438	437	27.5	
5	87-88	438-439	438	33.5	
5	88-89	439-440	439	22.1	
5	89-90	440-441	440	27.8	
5	90-91	441-442	441	20.8	
5	91-92	442-443	442	17.8	
5	92-93	443-444	443	27.1	
5	93-94	444-445	444	24.3	
5	94-95	445-446	445	29.6	
5	95-96	446-447	446	20.2	
5	96-97	447-448	447	25.4	
5	97-98	448-449	448	26.2	
5	98-99	449-450	449	17.1	9.6
5	99-100	450-451	450	26.8	
6	0-1	451-452	451	23.6	
6	1-2	452-453	452	29.5	
6	2-3	453-454	453	21.5	
6	3-4	454-455	454	23.5	
6	4-5	455-456	455	22.4	
6	5-6	456-457	456	22.8	
6	6-7	457-458	457	27.0	
6	7-8	458-459	458	23.8	
6	8-9	459-460	459	23.7	
6	9-10	460-461	460	24.5	
6	10-11	461-462	461	27.8	
6	11-12	462-463	462	24.2	
6	12-13	463-464	463	25.5	

Section	Section depth (cm)	Core depth (cm)	Sample No.	Weight (wet. g)	Weight (dry, g)
6	13-14	464-465	464	26.8	
6	14-15	465-466	465	13.8	7.2
6	15-16	466-467	466	21.6	
6	16-17	467-468	467	22.1	
6	17-18	468-469	468	25.4	
6	18-19	469-470	469	24.1	
6	19-20	470-471	470	24.9	
6	20-21	471-472	471	23.8	
6	21-22	472-473	472	22.1	
6	22-23	473-474	473	25.6	
6	23-24	474-475	474	26.7	
6	24-25	475-476	475	30.6	
6	25-26	476-477	476	30.5	
6	26-27	477-478	477	30.8	
6	27-28	478-479	478	28.9	
6	28-29	479-480	479	28.8	
6	29-30	480-481	480	29.6	
6	30-31	481-482	481	15.6	9.4
6	31-32	482-483	482	28.7	
6	32-33	483-484	483	24.8	
6	33-34	484-485	484	23.9	
6	34-35	485-486	485	28.3	
6	35-36	486-487	486	23.7	
6	36-37	487-488	487	31.0	
6	37-38	488-489	488	23.9	
6	38-39	489-490	489	27.8	
6	39-40	490-491	490	27.2	
6	40-41	491-492	491	26.1	
6	41-42	492-493	492	28.2	
6	42-43	493-494	493	22.6	
6	43-44	494-495	494	27.8	
6	44-45	495-496	495	27.0	
6	45-46	496-497	496	26.6	
6	46-47	497-498	497	17.5	10.2
6	47-48	498-499	498	26.2	
6	48-49	499-500	499	28.0	
6	49-50	500-501	500	26.4	
6	50-51	501-502	501	30.9	
6	51-52	502-503	502	25.8	

Section	Section depth (cm)	Core depth (cm)	Sample No.	Weight (wet. g)	Weight (dry, g)
6	52-53	503-504	503	27.8	
6	53-54	504-505	504	27.5	
6	54-55	505-506	505	31.3	
6	55-56	506-507	506	25.8	
6	56-57	507-508	507	23.3	
6	57-58	508-509	508	24.0	
6	58-59	509-510	509	27.7	
6	59-60	510-511	510	23.9	
6	60-61	511-512	511	25.9	
6	61-62	512-513	512	27.6	
6	62-63	513-514	513	19.0	10.3
6	63-64	514-515	514	26.3	
6	64-65	515-516	515	23.1	
6	65-66	516-517	516	30.0	
6	66-67	517-518	517	26.5	
6	67-68	518-519	518	30.6	
6	68-69	519-520	519	27.9	
6	69-70	520-521	520	29.7	
6	70-71	521-522	521	29.9	
6	71-72	522-523	522	29.1	
6	72-73	523-524	523	29.0	
6	73-74	524-525	524	31.6	
6	74-75	525-526	525	28.7	
6	75-76	526-527	526	27.1	
6	76-77	527-528	527	30.3	
6	77-78	528-529	528	29.0	
6	78-79	529-530	529	16.9	7.3
6	79-80	530-531	530	23.2	
6	80-81	531-532	531	27.5	
6	81-82	532-533	532	16.9	
6	82-83	533-534	533		
6	83-84	534-535	534		
6	84-85	535-536	535		
6	85-86	536-537	536	14.7	
6	86-87	537-528	537	21.5	
6	87-88	538-539	538	22.6	
6	88-89	539-540	539	24.7	
6	89-90	540-541	540	24.3	
6	90-91	541-542	541	29.8	

Section	Section depth (cm)	Core depth (cm)	Sample No.	Weight (wet. g)	Weight (dry, g)
6	91-92	542-543	542	23.4	
6	92-93	543-544	543	24.7	
6	93-94	544-545	544	30.7	
6	94-95	545-546	545	15.4	8.3
6	95-96	546-547	546	26.9	
6	96-97	547-548	547	22.6	
6	97-98	548-549	548	25.3	
6	98-99	549-550	549	25.7	
6	99-100	550-551	550	21.9	
6	100-101	551-552	551	23.7	
7	0-1	552-553	552	22.0	
7	1-2	553-554	553	30.0	
7	2-3	554-555	554	28.8	
7	3-4	555-556	555	37.2	
7	4-5	556-557	556	29.2	
7	5-6	557-558	557	28.2	
7	6-7	558-559	558	25.8	
7	7-8	559-560	559	26.6	
7	8-9	560-561	560	33.1	
7	9-10	561-562	561	19.8	10.7
7	10-11	562-563	562	28.6	
7	11-12	563-564	563	22.4	
7	12-13	564-565	564	23.0	
7	13-14	565-566	565	37.1	
7	14-15	566-567	566	26.3	
7	15-16	567-568	567	27.3	
7	16-17	568-569	568	34.3	
7	17-18	569-570	569	25.4	
7	18-19	570-571	570	28.1	
7	19-20	571-572	571	29.4	
7	20-21	572-573	572	34.3	
7	21-22	573-574	573	30.3	
7	22-23	574-575	574	27.4	
7	23-24	575-576	575	31.5	
7	24-25	576-577	576	31.9	
7	25-26	577-578	577	13.2	7.2
7	26-27	578-579	578	24.2	
7	27-28	579-580	579	26.3	
7	28-29	580-581	580	27.2	

Section	Section depth (cm)	Core depth (cm)	Sample No.	Weight (wet. g)	Weight (dry, g)
7	29-30	581-582	581	28.2	
7	30-31	582-583	582	26.7	
7	31-32	583-584	583	30.0	
7	32-33	584-585	584	30.3	
7	33-34	585-586	585	30.3	
7	34-35	586-587	586	29.2	
7	35-36	587-588	587	33.8	
7	36-37	588-589	588	32.2	
7	37-38	589-590	589	25.3	
7	38-39	590-591	590	31.8	
7	39-40	591-592	591	24.1	
7	40-41	592-593	592	36.1	
7	41-42	593-594	593	14.5	7.9
7	42-43	594-595	594	24.4	
7	43-44	595-596	595	30.2	
7	44-45	596-597	596	30.1	
7	45-46	597-598	597	29.2	
7	46-47	598-599	598	33.5	
7	47-48	599-600	599	29.4	
7	48-49	600-601	600	27.9	
7	49-50	601-602	601	28.4	
7	50-51	602-603	602	29.4	
7	51-52	603-604	603	27.5	
7	52-53	604-605	604	34.5	
7	53-54	605-606	605	23.9	
7	54-55	606-607	606	34.3	
7	55-56	607-608	607	30.6	
7	56-57	608-609	608	28.6	
7	57-58	609-610	609	16.4	8.8
7	58-59	610-611	610	28.0	
7	59-60	611-612	611	31.6	
7	60-61	612-613	612	32.4	
7	61-62	613-614	613	33.9	
7	62-63	614-615	614	34.5	
7	63-64	615-616	615	26.7	
7	64-65	616-617	616	34.2	
7	65-66	617-618	617	28.7	
7	66-67	618-619	618	28.8	
7	67-68	619-620	619	34.8	

Section	Section depth (cm)	Core depth (cm)	Sample No.	Weight (wet. g)	Weight (dry, g)
7	68-69	620-621	620	27.1	
7	69-70	621-622	621	23.2	
7	70-71	622-623	622	33.7	
7	71-72	623-624	623	25.8	
7	72-73	624-625	624	33.5	
7	73-74	625-626	625	23.0	12.3
7	74-75	626-627	626	24.2	
7	75-76	627-628	627	32.9	
7	76-77	628-629	628	31.0	
7	77-78	629-630	629	24.4	
7	78-79	630-631	630	26.5	
7	79-80	631-632	631	33.0	
7	80-81	632-633	632	18.2	
8	0-1	633-634	633	28.8	
8	1-2	634-635	634	24.1	
8	2-3	635-636	635	26.0	
8	3-4	636-637	636	25.9	
8	4-5	637-638	637	30.3	
8	5-6	638-639	638	24.5	
8	6-7	639-640	639	26.3	
8	7-8	640-641	640	31.8	
8	8-9	641-642	641	14.6	8.4
8	9-10	642-643	642	25.4	
8	10-11	643-644	643	25.8	
8	11-12	644-645	644	28.7	
8	12-13	645-646	645	27.7	
8	13-14	646-647	646	27.9	
8	14-15	647-648	647	26.0	
8	15-16	648-649	648	30.0	
8	16-17	649-650	649	30.7	
8	17-18	650-651	650	33.9	
8	18-19	651-652	651	33.9	
8	19-20	652-653	652	26.0	
8	20-21	653-654	653	31.4	
8	21-22	654-655	654	25.1	
8	22-23	655-656	655	24.7	
8	23-24	656-657	656	32.0	
8	24-25	657-658	657	19.5	11.7
8	25-26	658-659	658	32.0	
8	26-27	659-660	659	30.0	
8	27-28	660-661	660	29.4	
8	28-29	661-662	661	28.4	
8	29-30	662-663	662	27.0	
8	30-31	663-664	663	25.2	
8	31-32	664-665	664	26.6	
8	32-33	665-666	665	27.8	
8	33-34	666-667	666	26.7	
8	34-35	667-668	667	27.6	
8	35-36	668-669	668	25.6	
8	36-37	669-670	669	29.1	
8	37-38	670-671	670	21.7	
8	38-39	671-672	671	23.1	
8	39-40	672-673	672	25.9	
8	40-41	673-674	673	17.9	7.9
8	41-42	674-675	674	17.7	
8	42-43	675-676	675	12.8	
8	43-44	676-677	676	19.1	
8	44-45	677-678	677	23.4	
8	45-46	678-679	678	23.0	
8	46-47	679-680	679	25.4	
8	47-48	680-681	680	25.9	
8	48-49	681-682	681	25.9	
8	49-50	682-683	682	25.9	
8	50-51	683-684	683	25.3	
8	51-52	684-685	684	25.1	
8	52-53	685-686	685	27.6	
8	53-54	686-687	686	24.9	
8	54-55	687-688	687	27.8	
8	55-56	688-689	688	28.3	
8	56-57	689-690	689	15.4	8.6
8	57-58	690-691	690	24.5	
8	58-59	691-692	691	21.2	
8	59-60	692-693	692	26.9	
8	60-61	693-694	693	28.6	
8	61-62	694-695	694	22.3	
8	62-63	695-696	695	24.3	
8	63-64	696-697	696	27.3	
8	64-65	697-698	697	20.9	

Section	Section depth (cm)	Core depth (cm)	Sample No.	Weight (wet. g)	Weight (dry, g)
8	65-66	698-699	698	25.3	
8	66-67	699-700	699	25.3	
8	67-68	700-701	700	25.5	
8	68-69	701-702	701	20.9	
8	69-70	702-703	702	28.4	
8	70-71	703-704	703	22.9	
8	71-72	704-705	704	28.8	
8	72-73	705-706	705	14.4	6.9
8	73-74	706-707	706	27.5	
8	74-75	707-708	707	20.6	
8	75-76	708-709	708	25.0	
8	76-77	709-710	709	21.3	
8	77-78	710-711	710	22.9	
8	78-79	711-712	711	20.9	
8	79-80	712-713	712	22.3	
8	80-81	713-714	713	22.2	
8	81-82	714-715	714	24.5	
8	82-83	715-716	715	25.0	
8	83-84	716-717	716	23.0	
8	84-85	717-718	717	19.0	
8	85-86	718-719	718	23.4	
8	86-87	719-720	719	19.5	
8	87-88	720-721	720	23.5	
8	88-89	721-722	721	18.1	8.6
8	89-90	722-723	722	27.5	
8	90-91	723-724	723	18.3	
8	91-92	724-725	724	25.8	
8	92-93	725-726	725	25.7	
8	93-94	726-727	726	22.6	
8	94-95	727-728	727	24.9	
8	95-96	728-729	728	21.8	
8	96-97	729-730	729	22.9	
8	97-98	730-731	730	21.9	
8	98-99	731-732	731	31.0	
8	99-100	732-733	732	33.4	
8	100-101	733-734	733	21.8	
9	0-1	734-735	734	23.3	
9	1-2	735-736	735	29.8	
9	2-3	736-737	736	29.8	

Section	Section depth (cm)	Core depth (cm)	Sample No.	Weight (wet. g)	Weight (dry, g)
9	3-4	737-738	737	14.2	8.1
9	4-5	738-739	738	19.8	
9	5-6	739-740	739	24.4	
9	6-7	740-741	740	27.5	
9	7-8	741-742	741	26.6	
9	8-9	742-743	742	25.0	
9	9-10	743-744	743	25.5	
9	10-11	744-745	744	26.4	
9	11-12	745-746	745	26.1	
9	12-13	746-747	746	30.7	
9	13-14	747-748	747	30.7	
9	14-15	748-749	748	31.0	
9	15-16	749-750	749	26.6	
9	16-17	750-751	750	26.4	
9	17-18	751-752	751	31.1	
9	18-19	752-753	752	24.7	
9	19-20	753-754	753	16.8	9.3
9	20-21	754-755	754	27.2	
9	21-22	755-756	755	25.2	
9	22-23	756-757	756	29.0	
9	23-24	757-758	757	28.2	
9	24-25	758-759	758	26.2	
9	25-26	759-760	759	32.0	
9	26-27	760-761	760	27.2	
9	27-28	761-762	761	29.3	
9	28-29	762-763	762	25.9	
9	29-30	763-764	763	29.2	
9	30-31	764-765	764	19.6	
9	31-32	765-766	765	20.1	
9	32-33	766-767	766	20.3	
9	33-34	767-768	767	30.4	
9	34-35	768-769	768	24.2	
9	35-36	769-770	769	19.3	9.7
9	36-37	770-771	770	19.9	
9	37-38	771-772	771	25.5	
9	38-39	772-773	772	25.0	
9	39-40	773-774	773	23.1	
9	40-41	774-775	774	26.1	
9	41-42	775-776	775	30.1	

Appendix A2 – GC673 Sample list and weights

Section	Section depth (cm)	Core depth (cm)	Sample No.	Weight (wet. g)	Weight (dry, g)
9	42-43	776-777	776	26.3	
9	43-44	777-778	777	28.1	
9	44-45	778-779	778	27.0	
9	45-46	779-780	779	22.2	
9	46-47	780-781	780	27.8	
9	47-48	781-782	781	22.1	
9	48-49	782-783	782	21.8	
9	49-50	783-784	783	22.6	
9	50-51	784-785	784	26.9	
9	51-52	785-786	785	17.5	8.4
9	52-53	786-787	786	26.3	
9	53-54	787-788	787	19.6	
9	54-55	788-789	788	25.2	
9	55-56	789-790	789	27.7	
9	56-57	790-791	790	27.8	
9	57-58	791-792	791	27.2	
9	58-59	792-793	792	28.6	
9	59-60	793-794	793	25.3	
9	60-61	794-795	794	26.3	
9	61-62	795-796	795	26.9	
9	62-63	796-797	796	24.8	
9	63-64	797-798	797	22.8	
9	64-65	798-799	798	27.7	
9	65-66	799-800	799	24.8	
9	66-67	800-801	800	27.5	
9	67-68	801-802	801	17.5	10.4
9	68-69	802-803	802	20.3	
9	69-70	803-804	803	28.2	
9	70-71	804-805	804	34.2	
9	71-72	805-806	805	24.6	
9	72-73	806-807	806	26.3	
9	73-74	807-808	807	24.0	
9	74-75	808-809	808	24.7	
9	75-76	809-810	809	26.7	
9	76-77	810-811	810	29.5	
9	77-78	811-812	811	27.6	
9	78-79	812-813	812	25.3	
9	79-80	813-814	813	30.6	
9	80-81	814-815	814	26.1	
9	81-82	815-816	815	26.3	
9	82-83	816-817	816	24.2	
9	83-84	817-818	817	16.1	6.3
9	84-85	818-819	818	31.1	
9	85-86	819-820	819	31.4	
9	86-87	820-821	820	32.0	
9	87-88	821-822	821	27.8	
9	88-89	822-823	822	25.0	
9	89-90	823-824	823	27.1	
9	90-91	824-825	824	28.9	
9	91-92	825-826	825	25.4	
9	92-93	826-827	826	29.2	
9	93-94	827-828	827	29.1	
9	94-95	828-829	828	29.4	
9	95-96	829-830	829	26.5	
9	96-97	830-831	830	25.7	
9	97-98	831-832	831	22.6	
9	98-99	832-833	832	21.0	
9	99-100	833-834	833	18.4	8.8
9	100-101	834-835	834	24.4	
9	101-102	835-836	835	17.1	
10	0-1	836-867	836	21.9	
10	1-2	837-838	837	20.6	
10	2-3	838-839	838	20.8	
10	3-4	839-840	839	22.2	
10	4-5	840-841	840	24.0	
10	5-6	841-842	841	25.0	
10	6-7	842-843	842	22.7	
10	7-8	843-844	843	20.2	
10	8-9	844-845	844	23.7	
10	9-10	845-846	845	21.4	
10	10-11	846-847	846	20.1	
10	11-12	847-848	847	16.5	
10	12-13	848-849	848	21.3	
10	13-14	849-850	849	17.4	8.9
10	14-15	850-851	850	21.7	
10	15-16	851-852	851	20.3	
10	16-17	852-853	852	23.0	
10	17-18	853-854	853	22.9	

Section	Section depth (cm)	Core depth (cm)	Sample No.	Weight (wet. g)	Weight (dry, g)
10	18-19	854-855	854	24.0	
10	19-20	855-856	855	21.7	
10	20-21	856-857	856	22.3	
10	21-22	857-858	857	23.9	
10	22-23	858-859	858	17.3	
10	23-24	859-860	859	23.8	
10	24-25	860-861	860	21.7	
10	25-26	861-862	861	20.8	
10	26-27	862-863	862	15.9	
10	27-28	863-864	863	26.1	
10	28-29	864-865	864	28.3	
10	29-30	865-866	865	16.1	8.0
10	30-31	866-867	866	20.4	
10	31-32	867-868	867	19.7	
10	32-33	868-869	868	22.1	
10	33-34	869-870	869	20.3	
10	34-35	870-871	870	26.7	
10	35-36	871-872	871	26.7	
10	36-37	872-873	872	13.7	
11	0-1	873-874	873	16.2	
11	1-2	874-875	874	16.3	
11	2-3	875-876	875	17.8	
11	3-4	876-877	876	20.1	
11	4-5	877-878	877	18.1	
11	5-6	878-879	878	16.3	
11	6-7	879-880	879	22.0	
11	7-8	880-881	880	17.3	
11	8-9	881-882	881	14.6	
11	9-10	882-883	882	11.5	

Appendix A3 – GC666 OxCal Age Model Code

```
Plot()
 {
  Curve("Marine13","Marine13.14c");
  Delta_R("LocalMarine",433,41);
  Outlier_Model("General",T(5),U(0,4),"t");
  P_Sequence("",10,1,U(-2,2))
  {
   Boundary();
   R_Date("GC666-815",13572,211)
   {
    Outlier(0.05);
    z=815;
   };
   R_Date("GC666-510",13301,135)
   {
    Outlier(0.05);
    z=510;
   };
   Boundary("sed change")
   {
    z=500;
   };
   R_Date("GC666-490",13291,74)
   {
    Outlier(0.05);
    z=490;
   };
   R_Date("GC666-388",11856,65)
   {
    Outlier(0.05);
    z=388;
   };
   R_Date("GC666-384",11780,60)
   {
    Outlier(0.05);
    z=384;
   };
```

```
R_Date("GC666-324",11370,60)
{
 Outlier(0.05);
 z=324;
};
R_Date("GC666-245", 10160, 50)
{
 Outlier(0.05);
 z=245;
};
R_Date("GC666-192",9570,50)
{
 Outlier(0.05);
 z=192;
};
R_Date("GC666-127",8180,60)
{
 Outlier(0.05);
 z=127;
};
R_Date("GC666-115",7520,50)
{
 Outlier(0.05);
 z=115;
};
R_Date("GC666-097", 3590, 35)
{
 Outlier(0.05);
 z=97;
};
R_Date("GC666-057", 2775, 35)
{
 Outlier(0.05);
 z=57;
};
R_Date("GC666-033", 1715, 30)
{
 Outlier(0.05);
```

```
        z=33;
       };
       R_Date("GC666-000",1097,43)
       {
        Outlier(0.05);
        z=0;
       };
       Boundary();
      };
};
```

Appendix A4 – GC673 CLAM Age Model Settings

Settings (square brackets give names of the constants)

Calibration curve: Marine13.14C
Age-depth model: locally weighted spline [type=5] with span = 0.75 [smooth]
Weighted by the calibrated probabilities [wghts=1]
Calculations at 95% confidence ranges [prob=0.95]
Amount of iterations: 10000 [its]
Calendar age point estimates for depths based on weighted average of all age-depth curves [est=1]
Calendar scale used: cal BP [BCAD=FALSE] at a resolution of 1 yr [yrsteps]
Ages were calculated every 1 [every] cm [depth], from 16 [dmin] to 816 [dmax] cm

Goodness-of-fit (-log, lower is better): 2.87
Any models with age-depth reversals were removed

Appendix A5 – Journal of Micropalaeontology manuscript

Dejardin, R., Kender, S., Allen, C. S., Leng, M. J., Swann, G. E. A., and Peck, V. L.: "Live" (stained) benthic foraminiferal living depths, stable isotopes, and taxonomy offshore South Georgia, Southern Ocean: implications for calcification depths, J. Micropalaeontol., 37, 25-71, https://doi.org/10.5194/jm-37-25-2018, 2018.

J. Micropalaeontology, 37, 25–71, 2018
https://doi.org/10.5194/jm-37-25-2018
© Author(s) 2018. This work is distributed under
the Creative Commons Attribution 4.0 License.

Journal of Micropalaeontology
Open Access

"Live" (stained) benthic foraminiferal living depths, stable isotopes, and taxonomy offshore South Georgia, Southern Ocean: implications for calcification depths

Rowan Dejardin[1], Sev Kender[2,3], Claire S. Allen[4], Melanie J. Leng[1,5], George E. A. Swann[1], and Victoria L. Peck[4]

[1]Centre for Environmental Geochemistry, School of Geography, University of Nottingham, University Park, Nottingham, NG7 2RD, UK
[2]Camborne School of Mines, University of Exeter, Penryn, Cornwall TR10 9FE, UK
[3]British Geological Survey, Keyworth, Nottingham NG12 5GG, UK
[4]British Antarctic Survey, High Cross, Madingley Road, Cambridge, CB3 0ET, UK
[5]NERC Isotope Geosciences Facilities, British Geological Survey, Keyworth, Nottingham, NG12 5GG, UK

Correspondence: Rowan Dejardin (rowan.dejardin@nottingham.ac.uk)

Published: 5 January 2018

Abstract. It is widely held that benthic foraminifera exhibit species-specific calcification depth preferences, with their tests recording sediment pore water chemistry at that depth (i.e. stable isotope and trace metal compositions). This assumed depth-habitat-specific pore water chemistry relationship has been used to reconstruct various palaeoenvironmental parameters, such as bottom water oxygenation. However, many deep-water foraminiferal studies show wide intra-species variation in sediment living depth but relatively narrow intra-species variation in stable isotope composition. To investigate this depth-habitat–stable-isotope relationship on the shelf, we analysed depth distribution and stable isotopes of "living" (Rose Bengal stained) benthic foraminifera from two box cores collected on the South Georgia shelf (ranging from 250 to 300 m water depth). We provide a comprehensive taxonomic analysis of the benthic fauna, comprising 79 taxonomic groupings. The fauna shows close affinities with shelf assemblages from around Antarctica. We find "live" specimens of a number of calcareous species from a range of depths in the sediment column. Stable isotope ratios (δ^{13}C and δ^{18}O) were measured on stained specimens of three species, *Astrononion echolsi*, *Cassidulinoides porrectus*, and *Buccella* sp. 1, at 1 cm depth intervals within the downcore sediment sequences. In agreement with studies in deep-water settings, we find no significant intra-species variability in either $\delta^{13}C_{foram}$ or $\delta^{18}O_{foram}$ with sediment living depth on the South Georgia shelf. Our findings add to the growing evidence that infaunal benthic foraminiferal species calcify at a fixed depth. Given the wide range of depths at which we find "living", "infaunal" species, we speculate that they may actually calcify predominantly at the sediment–seawater interface, where carbonate ion concentration and organic carbon availability is at a maximum.

1 Introduction

Benthic foraminifera live both on (epifaunal) and beneath (infaunal) the sediment–seawater interface, and their assemblages and stable isotope and trace element compositions are widely utilized as tools in the reconstruction of past oceanographic conditions (see review in Jorissen et al., 2007). Stable isotopes of all species typically exhibit inter-species offsets. In part this offset is accounted for by "vital effects", inter-species differences in the fractionation of stable isotopes due to a range of biological factors (see review in Ravelo and Hillaire-Marcel, 2007). Another consideration, adopted in numerous studies, is that epifaunal and infaunal inter-species isotopic offsets reflect, in part, pore water chemistry at the preferred depth habitat of each species within the sediment (e.g. Loubere et al., 1995; McCorkle et

al., 1997; Theodor et al., 2016). The carbon isotope composition of pore water dissolved inorganic carbon ($\delta^{13}C_{DIC}$) has been shown to become lighter (lower $\delta^{13}C$) with sediment depth (e.g. McCorkle et al., 1985), due to the remineralization (by oxic respiration or denitrification) of organic carbon. The difference between bottom and pore water $\delta^{13}C_{DIC}$ has been shown to increase with bottom water oxygenation (McCorkle and Emerson, 1988). Assuming that infaunal species calcify at preferred depths within the sediment hypothetically allows $\delta^{13}C_{DIC}$ gradients to be reconstructed through the isotope analysis of paired epifaunal and deep-infaunal taxa (e.g. *Cibicidoides wuellerstorfi* and *Globobulimina* spp.; Hoogakker et al., 2015). Similarly, the difference in $\delta^{13}C$ between epifaunal and shallow infaunal species (e.g. *Uvigerina* spp.) has been used to reconstruct the intensity of organic matter remineralization, a proxy for the flux of organic matter to the sea floor (Zahn et al., 1986; McCorkle and Emerson, 1988; Schilman et al., 2003). Additionally, Elderfield et al. (2012) used the presence of a constant offset between the $\delta^{13}C$ data from paired epifaunal (*Cibicidoides wuellerstorfi*) and infaunal (*Uvigerina* spp.) foraminifera to negate the suggestion that a negative $\delta^{13}C$ excursion during Marine Isotope Stage 22 was due to productivity changes and to support their hypothesis that the $\delta^{13}C$ excursion was instead related to global ocean change.

These applications rely on the previously stated assumption that benthic foraminifera inhabit species-specific depth habitats and, more importantly, calcify at that depth, thereby recording the pore water $\delta^{13}C_{DIC}$ gradient. This assumption is held despite the wide range of sediment depths that individual infaunal species have been observed to live at (e.g. McCorkle et al., 1997). Furthermore, isotope analysis of "live" (Rose Bengal stained) foraminifera reveals a narrow range of isotope values for individuals of the same species despite them having been recovered from a wide range of depths beneath the sediment surface (McCorkle et al., 1990, 1997; Schmiedl et al., 2004; Fontanier et al., 2006b, 2008; Theodor et al., 2016). A narrow intra-species range of $\delta^{13}C$ composition of "live" specimens recovered from a range of sediment depths argues against individuals having calcified at the depths from which they were recovered (since pore water $\delta^{13}C_{DIC}$ gradients are not reflected in the foraminifera). More recent studies raise further questions about the validity of the assumed calcification depths of infaunal species. For example, it has been assumed that Mg / Ca data from infaunal foraminifera are relatively insulated from the effect of bottom water $[CO_3^{2-}]$ changes (Elderfield et al., 2006, 2010). However, Weldeab et al. (2016) have shown that infaunal *Globobulimina* spp. are sensitive to changes in bottom water $[CO_3^{2-}]$, implying that calcification may not occur exclusively beneath the sediment surface. To extend previous studies of the deep ocean (e.g. McCorkle et al., 1990, 1997; Tachikawa and Elderfield, 2002; Schmiedl et al., 2003; Fontanier et al., 2008, 2006b) onto the shelf environment, and test the assumption that infaunal species calcify at preferred depths and that their $\delta^{13}C$ composition is reflective of pore water $\delta^{13}C_{DIC}$ (i.e. decreasing $\delta^{13}C_{DIC}$ with increasing calcification depth), we measured the living depths and isotope composition of three as yet unstudied species (*Astrononion echolsi*, *Cassidulinoides porrectus*, and *Buccella* sp. 1) from the South Georgia shelf, South Atlantic. We also report the depth ranges of all "living" (Rose Bengal stained) benthic foraminifera. To underpin these and future analyses, we carried out a detailed taxonomic analysis of benthic foraminifera from six surface samples, two box-core downcore sequences, and two gravity cores, the first such study focused on South Georgia since Earland (1933).

1.1 Previous benthic foraminiferal studies

Earland (1933) conducted a survey of the benthic foraminifera of South Georgia, utilizing surface sediment samples collected from around the island as part of the *Discovery* expeditions. Since this study, there has been no further taxonomic work focussed on South Georgia, but a number of benthic foraminiferal assemblage studies have been conducted at other Southern Ocean and Antarctic locations. The Antarctic Peninsula is one of the better-studied areas in the region, with foraminiferal research here commencing in the first half of the 20th century (Earland, 1934; Cushman, 1945), followed by a number of brief US Antarctic Program taxonomic reports (e.g. Lipps et al., 1972). In a more comprehensive study of the Antarctic Peninsula, Ishman and Domack (1994) analysed a large number of surface sediment samples from three areas on the western side of the peninsula (Bransfield Strait, Marguerite Bay, and Palmer Archipelago). A detailed assessment of the benthic foraminiferal assemblages of Admiralty Bay, King George Island, and the South Shetland Islands has been conducted by Majewski (2005, 2010), again on surface sediment samples. On the eastern side of the Antarctic Peninsula, Majewski and Anderson (2009) examined the palaeoclimatic implications of Holocene foraminiferal assemblages from the Firth of Tay. Further east, Anderson (1975) identified 160 species in surface samples distributed across the Weddell Sea, whilst Mackensen et al. (1990) focussed on surface samples from the sea's eastern corner.

Herb (1971) described the variation in benthic faunas across the Drake Passage, illustrating the differences between the shelf environments of southern South America and Antarctica. Mackensen et al. (1993) analysed a similar transect of surface samples through the subantarctic zone between 0 and 10° E. Useful studies from Southern Ocean localities more distant from South Georgia include Majewski's (2013) description of benthic foraminifera from core-top samples around Pine Island and Ferrero Bays in the Amundsen Sea, Violanti's (1996) analysis of live and dead foraminifera from surface samples from Terra Nova Bay, Ross Sea, and Igarashi et al.'s (2001) study of samples from

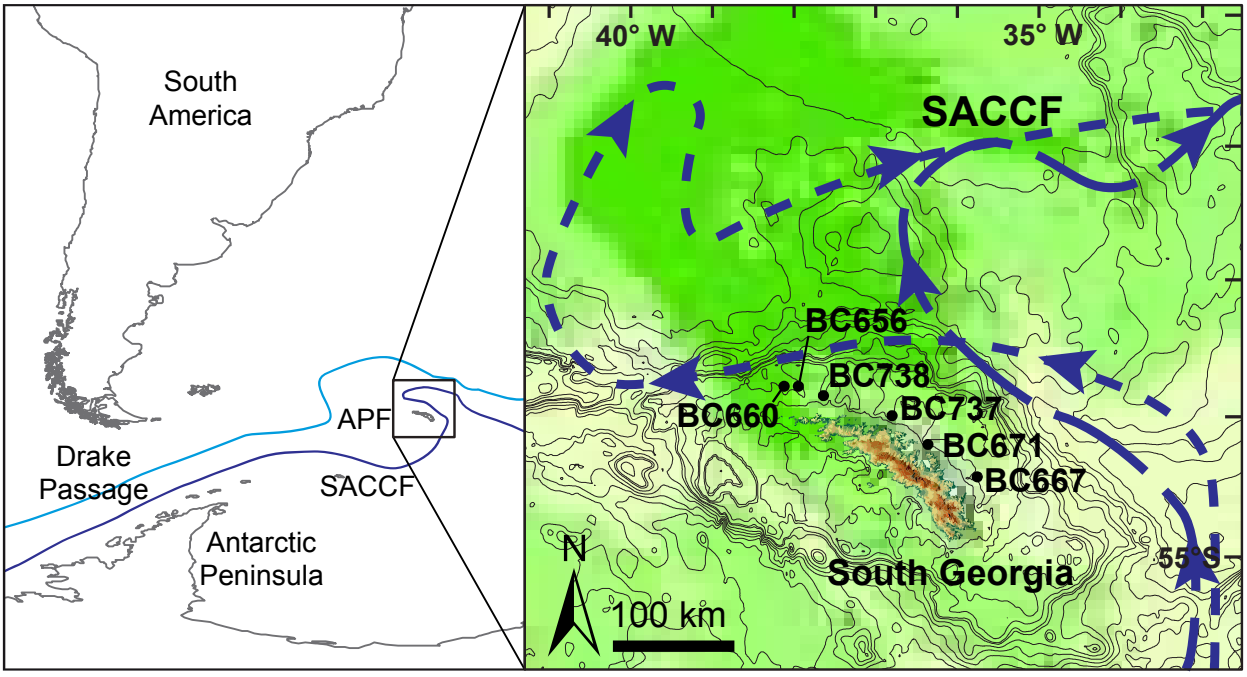


Figure 1. Map of South Georgia and sampling locations. The location of South Georgia in relation to the Antarctic Peninsula and South America showing the approximate location of the Antarctic Polar Front (APF – light blue) and the Southern Antarctic Circumpolar Current Front (SACCF – dark blue). The inset and map on the left show a topographical map of South Georgia and surrounding bathymetry with the sampling locations indicated. The dark blue lines represent the location and average position of the SACCF (contemporary variation near South Georgia shown by the dashed lines, indicating most easterly and westerly extents (Thorpe et al., 2002). The mean surface chlorophyll-α concentration (mg m^{-2}) between September and March is shown in green with darker colours indicating higher concentration (SeaWiFS derived satellite data, NASA; means calculated only for cells where 10 values were obtained within a year; from Murphy et al., 2013).

sediment cores extending into the Holocene from Lützow-Hom Bay, East Antarctica.

1.2 Oceanographic setting

The subantarctic island of South Georgia (54° S, 36° W) is located at the northern edge of the Scotia Sea in the path of the Antarctic Circumpolar Current (ACC), between the Antarctic Polar Front (APF) and the Southern ACC Front (SACCF) (Fig. 1). South Georgia is one of the largest islands in the subantarctic zone (SAZ), measuring approximately 180 × 40 km, and is separated from the deep ocean by a 50–150 km wide continental shelf. The shelf, typically within 200–250 m water depth, is traversed by canyons that connect the island's fjords to the continental slope. The properties of the waters of the shelf itself routinely differ from those of the surrounding ocean, with on-shelf surface waters typically being warmer (2–3 °C on shelf, 1.5–2 °C off shelf) and fresher (salinity 33.4–33.7 psu on shelf, 33.6–33.7 psu off shelf) (Brandon et al., 1999). These differences are caused by a number of shelf-specific processes, such as freshwater run-off and topographically steered circulation (Brandon et al., 1999, 2000; Meredith et al., 2005).

2 Methods

2.1 Sample acquisition and preparation

Two box cores (BC737 and BC738) were collected during British Antarctic Survey scientific cruise JR-15002, in November 2015 (see Table 1 and Fig. 1), from which two sub-cores were collected (BC737 (D) and BC738 (D)). The box cores were collected using the British Antarctic Survey (BAS) box corer, deployed from the RRS *James Clark Ross*. The sub-cores were taken from BC737 (15 cm) and BC738 (20 cm); these cores were cut into 1 cm sections which were weighed to the nearest gram before being washed over a 63 µm sieve. The coarse fraction was then soaked in a Rose Bengal / seawater solution (1 g : 1 L) for 24 h before being rinsed with seawater from the underway seawater supply until the water ran clear and dried at 40° C after a final rinse with MilliQ water. Rose Bengal is a non-vital biological stain that is adsorbed onto any proteins, whether or not they are alive, and can therefore stain necrotic as well as healthy cytoplasm (Bernhard, 2000).

Table 1. Sample locations.

Core no.	Latitude	Longitude	Water depth (m)	Sample
BC656	−53.78168	−37.95855	303	Surface sample
BC660	−53.78188	−38.12847	354	Surface sample
BC667	−54.42063	−35.74152	252	Surface sample
BC671	−54.20237	−36.37451	239	Surface sample
BC737	−53.99709	−36.82012	260	Surface sample
BC737 (D)	−53.99709	−36.82012	260	15 cm sub-core
BC738	−53.85504	−37.65095	287	Surface sample
BC738 (D)	−53.85504	−37.65095	287	20 cm sub-core
GC666*	−54.4206	−35.74148	253	815 cm gravity core
GC673*	−54.20237	−36.37451	238	884 cm gravity core

* Samples with foram species not present in the box cores are included in Sect. 6 and Supplement.

2.2 Benthic foraminiferal assemblage analysis

All "living" (stained) and dead foraminifera were dry picked from each of the 1 cm samples between 0 and 10 cm, and only "living" (stained) foraminifera were dry picked from each of the 1cm samples between 10 and 13 cm, from BC737 and BC738. Tests where all, or all but one or two, chambers were well stained bright red were considered to be "living" at the time of staining (e.g. Caulle et al., 2015; Fontanier et al., 2016; Wang et al., 2016). For thick-walled agglutinated taxa, where the opaque test wall concealed the extent of the staining, the tests were broken open allowing the staining to be assessed. Tests with a pink tint or isolated spots of red were not included, nor were tests where only a small number of isolated chambers were stained. The average living depth (ALD) (Jorissen et al., 1995) was calculated for the 10 taxa with at least five "live" specimens in one or more samples. We also calculated the median living depth (MLD) (Theodor et al., 2016) for these taxa. Differences between ALD and MLD are generally small but can be significant for taxa with a wide downcore occurrence range (Theodor et al., 2016). Foraminiferal abundances are reported as number per gram.

2.3 Stable isotope analysis

Oxygen and carbon isotope analyses were carried out on three species of foraminifera from BC737 (*Astrononion echolsi*, *Cassidulinoides porrectus*, and *Buccella* sp. 1), from 10 samples (0–1 to 9–10 cm), and on two species from BC738 (*Astrononion echolsi* and *Cassidulinoides porrectus*) from 6 samples (0–1 to 5–6 cm). All specimens for isotope analysis were picked from the 125–250 µm fraction to minimize the possible effects of ontogenetic change in fractionation rates. These species were selected because their ALD/MLD revealed different microhabitat preferences and because they were present in high enough abundance to provide sufficient calcite to conduct the analyses. Each isotope data point was measured on between 4 and 15 specimens from each sample for *A. echolsi* and *C. porrectus* and on 3–5 specimens from each sample for the more heavily calcified *Buccella* sp. 1. The measurements were carried out at the NERC Isotope Geosciences Laboratory (NIGL), British Geological Survey (Keyworth, UK) using an IsoPrime 100 dual-inlet mass spectrometer with Multiprep device. Isotope values were calculated according to the Vienna Pee Dee Belemnite (VPDB) scale in parts per thousand using a within-run laboratory standard (KCM) calibrated to international NBS standards. Analytical reproducibility was 0.1 ‰ (1σ) for both $\delta^{18}O$ and $\delta^{13}C$. To eliminate contamination by any organic carbon remaining in the test (the presence of the stain indicates that organic carbon is present within the tests), the samples were plasma ashed prior to analysis (at NIGL using an Emitech K1050X plasma asher). To test whether the plasma ashing process had any impact on the isotope composition of the foraminiferal calcite, five standards (KCM) were subjected to the same processing and analysed in parallel. In addition, to test whether the Rose Bengal stain had any impact on the isotope composition, five standards (KCM) mixed with Rose Bengal and five KCM standards mixed with Rose Bengal and plasma ashed were also analysed.

3 Results

3.1 Benthic foraminiferal assemblage results

A total of 1181 "live" (Rose Bengal stained) and 6505 dead specimens were identified from the sub-core sample sequences, representing 62 (36 "living" and 60 dead) taxonomic groupings (See "Systematic taxonomy" section and the Supplement). The total abundance for the upper 10 samples from the sub-cores ranges from 6 to 16 g^{-1} for BC737, with the highest abundance evident in the 2–3 cm sample, and from 6 to 13 g^{-1} for BC738, with the highest abundance evident in the 0–1 cm sample. In 0–1 cm samples of the sub-cores, the ratio of "live" to dead specimens is 0.42 for BC737 and 0.32 for BC738 (Fig. 2). In BC737 this ratio decreases to 0.14 in the 3–4 cm sample before increasing to 0.37 in the 6–7 cm sample, mainly due to the high abundance of "live" *M.*

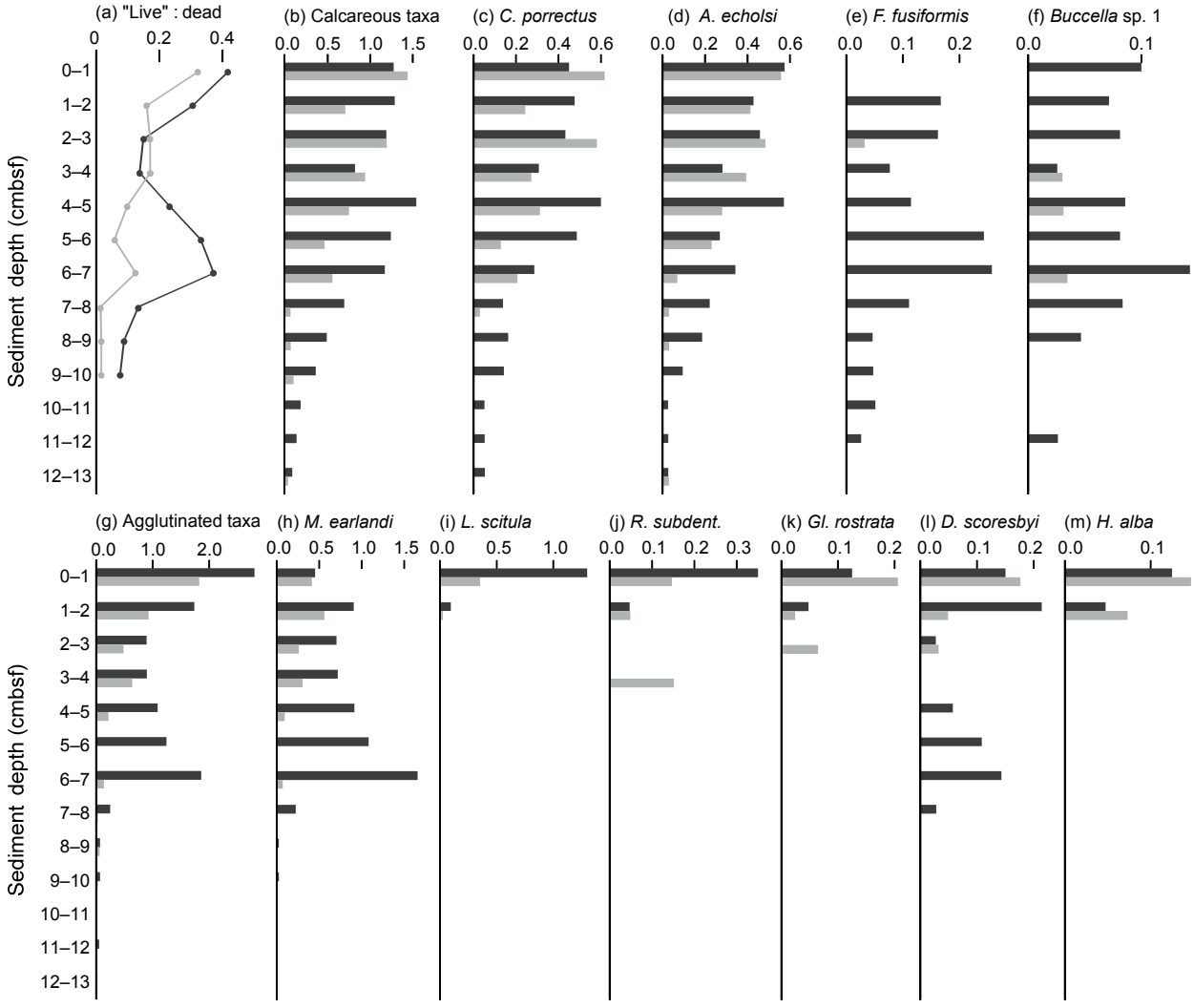


Figure 2. Downcore "live" : dead ratio and histograms showing downcore abundance of "live" (stained) foraminifera. BC7373 (dark grey) and BC738 (light grey) downcore "live" abundances (numbers per gram): **(a)** downcore "live" : dead ratio; **(b)** total calcareous taxa; **(c–f)** calcareous taxa with five or more "live" specimens in at least one sample; **(g)** total agglutinated taxa; **(h–m)** agglutinated taxa with five or more "live" specimens in at least one sample.

earlandi, and then decreasing to 0.08 in the 9–10 cm sample. In BC738 the "live" / dead ratio decreases steadily throughout the core to 0.02 in the 0–10 cm sample, apart from a small increase to 0.13 in the 6–7 cm sample. A small number of "live" taxa are still present in the 12–13 cm sample of both cores (4 specimens in BC737 and one in BC738).

The downcore variation in abundance of the 10 taxa with at least five "live" specimens in one or more samples are shown in Fig. 2 (for comparison the dead abundances of the same taxa are shown in Fig. 3). For six of these 10 taxa (*A. echolsi*, *C. porrectus*, *F. fusiformis, Buccella* sp. 1, *M. earlandi*, and *D. scoresbyi*), live specimens were recovered from a wide range of sediment depths, to at least 8 cm, in at least one of the cores. The remaining four taxa (*L. scitula*, *Reophax subdentaliniformis*, *G. rostrata*, and *Hippocrepinella alba*) were found to be restricted to the upper 0 to 2 cm. The vertical range in living depths for individual species is presented in Fig. 4 where the error bars (1 SD) reveal a broad depth range of occurrences around the ALD for all species that do not present a restricted epifaunal/shallow infaunal microhabitat preference. There is a clear separation between the calcareous taxa, which were all found living at a range of sediment depths, and the agglutinated taxa, for which the majority were found living in the upper 2 cm. The exceptions to this are *M. earlandi* and *D. scoresbyi*, which were recorded "living" at a range of depths in BC737, as was *R. subdentaliniformis* in BC738. The agreement between ALD and MLD is generally good, with a mean difference of 0.21 cm. However, in BC737 the difference between ALD and MLD for *D. scoresbyi* is 1.33 cm, with this difference

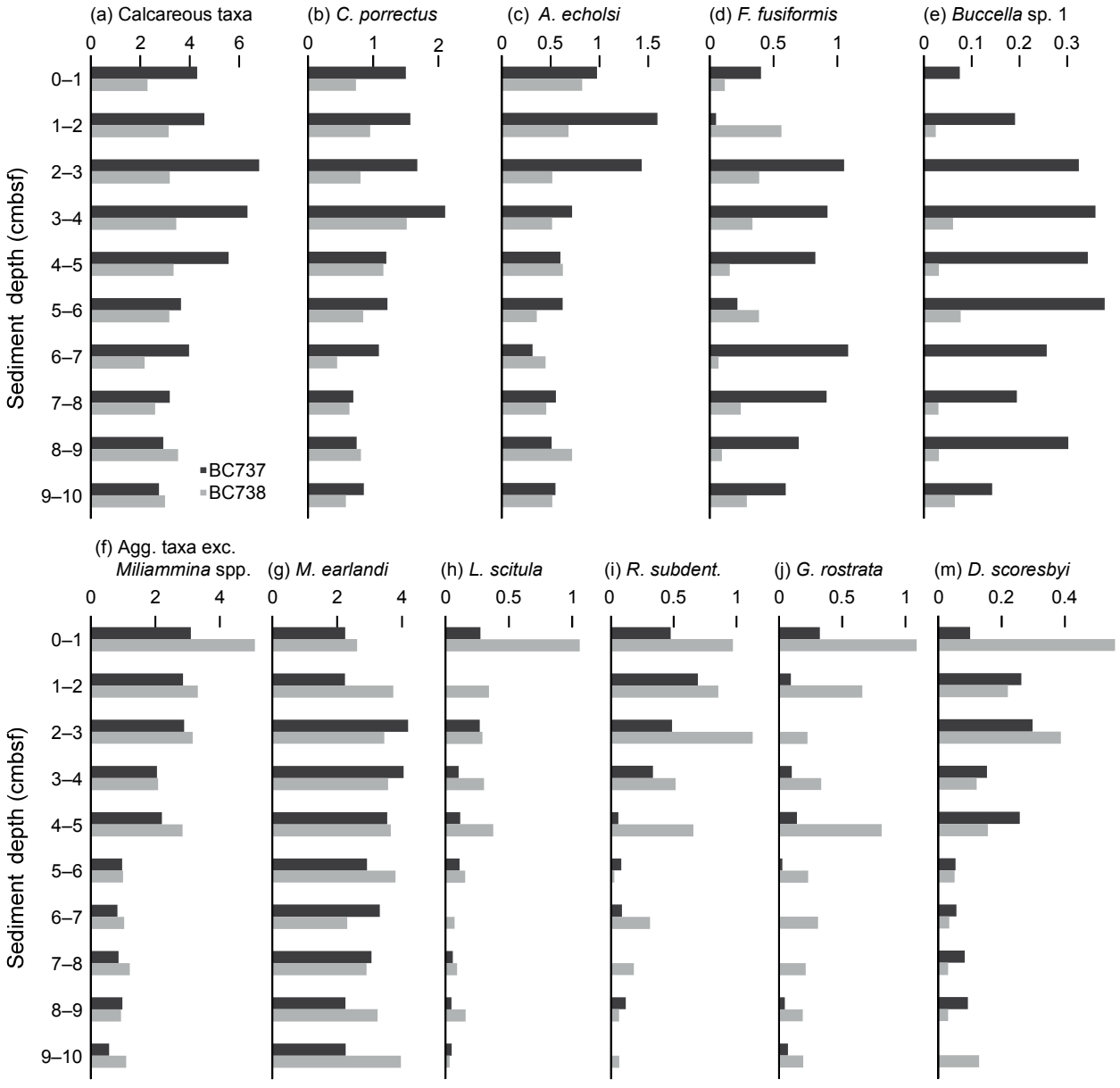


Figure 3. Histograms showing downcore abundance of dead foraminifera. BC7373 (dark grey) and BC738 (light grey) downcore "live" abundances no. g^{-1}): **(a)** total calcareous taxa; **(b–e)** calcareous taxa with five or more "live" specimens in at least one sample; **(f)** total agglutinated taxa excluding *Miliammina* spp.; **(g–m)** agglutinated taxa with five or more "live" specimens in at least one sample (*H. alba* has not been plotted in this figure as no dead specimens of this taxon were recorded).

due to the bimodal depth distribution of "live" occurrences of this species. Whilst MLD and ALD are generally close within the same box core, there is a systematic difference between the living depths calculated for BC7373 and those calculated for BC738. For four of the five taxa where the difference is > 0.5 cm, both ALD and MLD are shallower in BC738, relative to BC737, with the exception being *R. subdentaliniformis*, which is shallower in BC737.

The dead abundance of calcareous taxa in BC738 is stable throughout the core, whilst this abundance peaks between 2 and 4 cm in BC737 before becoming stable below this depth. This is in marked contrast to the dead abundance of agglutinated taxa (excluding *Miliammina* spp.), which shows a steady decline with depth in both cores such that, whilst agglutinated taxa are equal to or exceed calcareous taxa in dead assemblages in the upper core, calcareous taxa come to dominate dead assemblages as sediment depth increases. This trend appears linked to the preservation of taxa with epifaunal/shallow infaunal microhabitat preference as *L. scitula*,

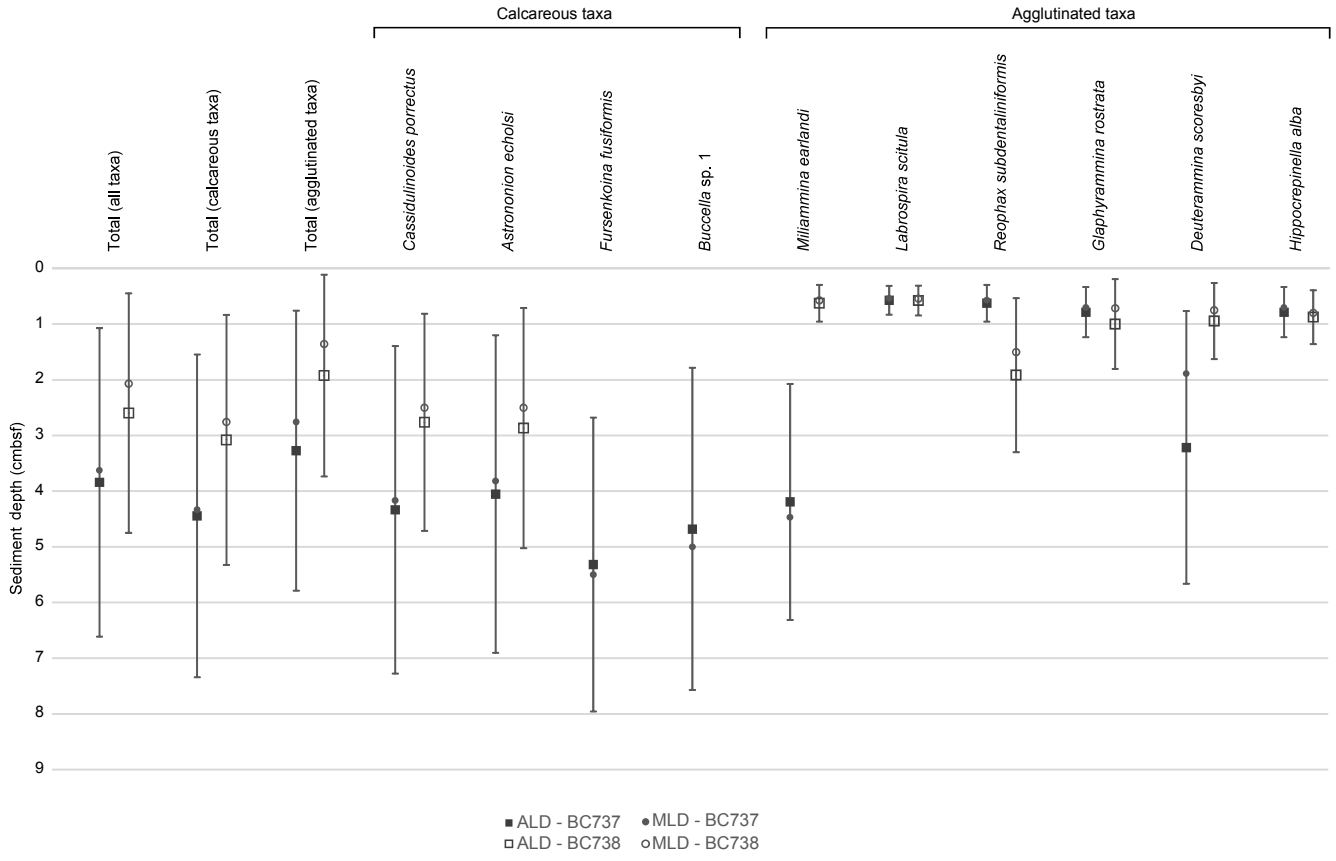


Figure 4. Average and median living depths.ALD (square symbols), calculated following Jorissen et al. (1995), and MLD (circular symbols), calculated following Theodor et al. (2016), plotted for all taxa, all calcareous taxa, all agglutinated taxa, and individually for the 10 taxa with five or more "live" specimens in at least one sample. Error bars represent the standard deviation about the ALD (1 SD). Closed symbols represent BC737 and open symbols represent BC738. Note that ALD and MLD have not been calculated for *F. fusiformis* and *Buccella* sp. 1 for BC738 as the "live" abundance of these taxa in this core was too low.

R. subdentaliniformis, and *G. rostrata* all exhibit a steep decline with depth in the number of dead specimens.

3.2 Stable isotopes

Results from the test isotope samples (KCM plus Rose Bengal, KCM plasma ashed, plasma ashed KCM plus Rose Bengal), run to establish whether these processing methods could have any impact on the foraminiferal isotope results, revealed that the values from the treated standards for both δ^{13}C and δ^{18}O were within the normal "within-run" error (Table 2).

The stable isotope compositions of "live" specimens display a relatively wide range of values, from -1.20 to $+0.72$ ‰ for δ^{13}C and from $+2.55$ to $+3.56$ ‰ for δ^{18}O (Table 3). Mean δ^{13}C values for *Astrononion echolsi*, *Cassidulinoides porrectus*, and *Buccella* sp. 1 are -0.84 ± 0.15 ‰, -0.34 ± 0.15 ‰, and $+0.54 \pm 0.16$ ‰ respectively; mean δ^{18}O values are $+2.85 \pm 0.20$ ‰, $+3.40 \pm 0.09$ ‰, and $+3.49 \pm 0.06$ ‰. When plotted on a δ^{13}C / δ^{18}O cross-plot (Fig. 5), samples from the same species cluster together, irrespective of the living depth. When δ^{13}C is plotted against depth, it is clear that there is no systematic variation with depth (Fig. 6a). Similarly, no trends with depth are observed in δ^{18}O.

4 Discussion

4.1 Benthic foraminiferal distributions

In this study we identified 24 of the 345 species identified by Earland (1933), including 13 of the 24 species identified as being most typical of South Georgia assemblages, and 7 of the 14 species Earland described as being particularly characteristic of the region. The taxa identified as being most abundant by Earland (1933) include many of the more abundant species identified here, such as *M. earlandi*. The majority of species recorded in this study are present at a range of locations around the Southern Ocean, but there are five species that may be endemic to South Georgia (e.g. *Labrospira* sp. 1, *G. rostrata*, *Recurvoides* sp. 1, *Buccella* sp. 1, and *Buccella* sp. 2). In a comprehensive review of a range a data sources, encompassing a wide diversity of taxa, Hogg et al. (2011)

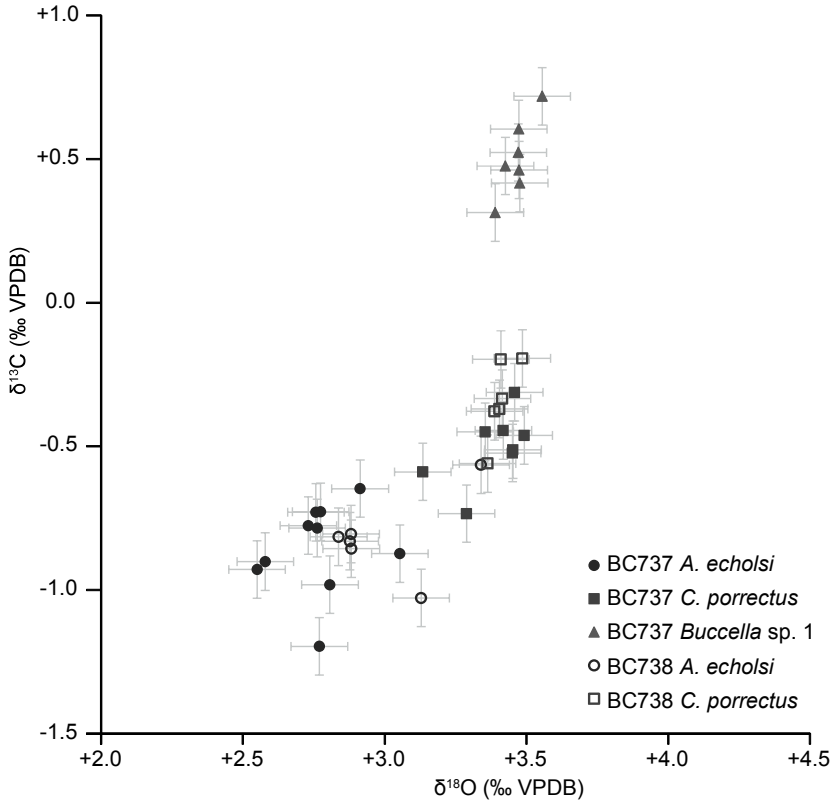


Figure 5. δ^{13}C vs. δ^{18}O cross-plot. Cross-plot of carbon and oxygen isotopic ratios for all samples analysed in this study. *Astrononion echolsi* – circular symbols; *Cassidulinoides porrectus* – square symbols; *Buccella* sp. 1 – triangular symbols (closed symbols – BC737; open symbols - BC738).

Table 2. Isotopic data from Rose Bengal test (STD: laboratory standard)

STD + 10 % Rose Bengal			STD + 10 % Rose Bengal plasma ashed			STD plasma ashed		
	δ^{13}C VPDB	δ^{18}O VPDB		δ^{13}C VPDB	δ^{18}O VPDB		δ^{13}C VPDB	δ^{18}O VPDB
RBKCM 1	1.99	−1.77	RBKCMP 1	1.92	−1.67	PKCM 1	1.92	−1.76
RBKCM 2	1.91	−1.81	RBKCMP 2	1.88	−1.89	PKCM 2	2.05	−1.57
RBKCM 3	1.98	−1.76	RBKCMP 3	1.91	−1.58	PKCM 3	2.02	−1.63
RBKCM 4	1.96	−1.81	RBKCMP 4	1.93	−1.72	PKCM 4	2.02	−1.65
RBKCM 5	1.91	−1.89	RBKCMP 5	1.91	−1.62	PKCM 5	1.94	−1.74
Mean	1.95	−1.81	Mean	1.91	−1.69	Mean	1.99	−1.67
1 SD	0.04	0.05	1 SD	0.02	0.12	1 SD	0.06	0.08

highlighted the significance of endemism within the South Georgia shelf ecosystem and its importance to global biodiversity, and the identification of potentially unidentified species of foraminifera further adds to that diversity. The benthic foraminiferal assemblage documented here suggests that, whilst there may be partial isolation, the microfauna of South Georgia are connected to those of the rest of the Southern Ocean. A total of 20 species identified in this study were also recorded by Ishman and Domack (1994) in their study of the Bellingshausen Sea margin; 22 of the 105 species identified by Majewski (2005), from King George Island, are also recorded in this study, as are 11 of the 26 species identified by Majewski and Anderson (2009) from the Firth of Tay. The strong affinity with Antarctic Peninsula taxa suggests that the position of South Georgia in the path of the ACC downstream of the Antarctic Peninsula (AP) allows for a degree of microfaunal connectivity between the two. The species that are commonly recorded from both the AP and South Georgia in-

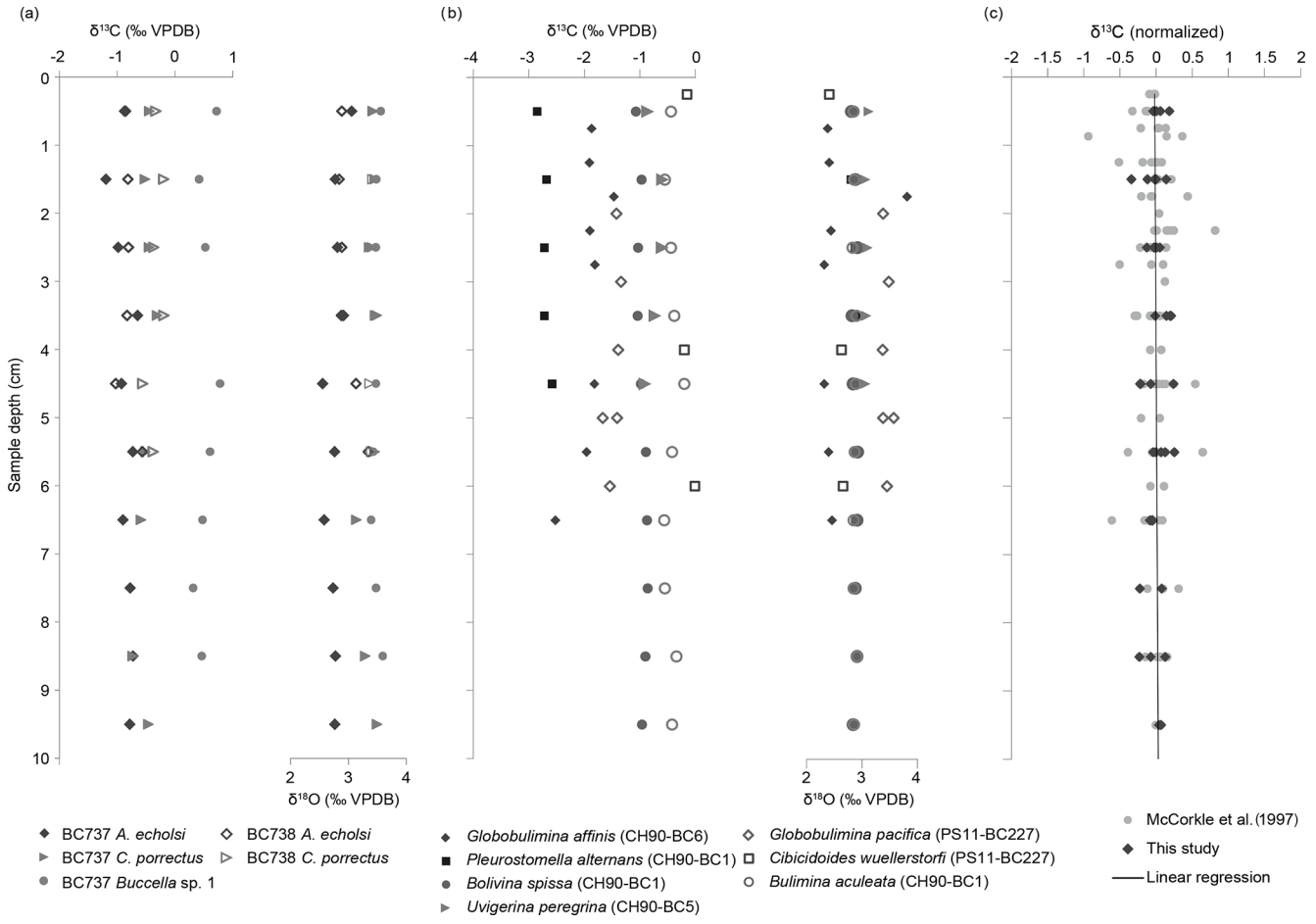


Figure 6. Isotopic data plotted against sample depth. **(a)** Carbon and oxygen isotopic values for species analysed in this study. **(b)** Carbon and oxygen isotopic values for seven species analysed in McCorkle et al. (1997). **(c)** Carbon and oxygen isotopic values for species analysed in this study and in McCorkle et al. (1997), normalized by subtracting the mean value for each species from the individual value. There is no systematic variation in either $\delta^{13}C_{foram}$ or $\delta^{18}O_{foram}$ with sample depth in any of these three plots.

clude *Portatrochammina antarctica weisneri*, *Reophax subdentaliniformis*, *A. echolsi*, *Spiroplectammina biformis*, *Nonionella bradii*, *N. iridea*, *C. parkerianus*, *C. porrectus*, and *F. fusiformis*, many of which are among the more abundant taxa. A comparable level of similarity is seen with studies of Weddell Sea benthic foraminifera (Mackensen et al., 1990; Anderson, 1975).

There is less similarity between the South Georgia foraminiferal fauna and those recorded from more remote areas of the Southern Ocean. For example, only six of the taxa recorded here were also recorded by Herb (1971) from the Drake Passage. However, this may be due to the open-ocean/deep-water nature of these locations, rather than proximity, as there are greater levels of connectivity between our sites and more distal locations on the Antarctic shelf, including Pine Island Bay and Terra Nova Bay (Majewski, 2013; Violanti, 1996).

The decreasing abundance of "live" specimens with depth within the sediment (Fig. 2) reflects well-established gradients in organic carbon and oxygen availability (see Jorissen et al., 2007). The shallower ALD/MLD observed in BC738 across almost all taxa (Fig. 4) may indicate steeper oxygen and organic carbon concentration gradients at this location. Variation in these gradients between the two sites may be linked to differences in sedimentation rate or carbon flux, with the latter potentially linked to BC738's closer proximity to seasonal phytoplankton blooms occurring north-west of South Georgia. The interruption in the decreasing "live" abundance trend seen in the agglutinated taxa in BC737 is the result of a peak in "live" abundance of a single species, *M. earlandi*, between 5 and 7 cm.

Dead abundances in both cores peak around the ALD/MLD for all taxa combined; the decline in dead abundances below this depth can be attributed to the physical and chemical breakdown of the tests. The decrease in dead abundance is more pronounced in the agglutinated taxa, indicating that the organic matrix of agglutinated tests has a greater susceptibility to taphonomic processes. An exception

Table 3. Isotopic data from "live" (stained) foraminifera.

		A. echolsi		*C. porrectus*		*Buccella* sp. 1	
Core	Depth	δ^{13}C VPDB	δ^{18}O VPDB	δ^{13}C VPDB	δ^{18}O VPDB	δ^{13}C VPDB	δ^{18}O VPDB
BC737	0–1 cm	−0.87	3.06	−0.45	3.42	0.72	3.56
BC737	1–2 cm	−1.20	2.77	−0.52	3.45	0.42	3.48
BC737	2–3 cm	−0.98	2.81	−0.45	3.36	0.52	3.47
BC737	3–4 cm	−0.65	2.92	−0.31	3.46	–	–
BC737	4–5 cm	−0.93	2.55	–	–	0.78	3.48
BC737	5–6 cm	−0.73	2.76	−0.51	3.46	0.60	3.43
BC737	6–7 cm	−0.90	2.58	−0.59	3.14	0.48	3.39
BC737	7–8 cm	−0.78	2.73	–	–	0.31	3.48
BC737	8–9 cm	−0.73	2.78	−0.73	3.29	0.46	3.59
BC737	9–10 cm	−0.79	2.76	−0.46	3.50	–	–
	Mean	−0.86	2.77	−0.50	3.38	0.54	3.49
	1 SD	0.16	0.15	0.12	0.12	0.16	0.06
BC738	0–1 cm	−0.86	2.88	−0.33	3.42	NA	NA
BC738	1–2 cm	−0.82	2.84	−0.20	3.41	NA	NA
BC738	2–3 cm	−0.81	2.88	−0.37	3.41	NA	NA
BC738	3–4 cm	−0.83	2.88	−0.19	3.49	NA	NA
BC738	4–5 cm	−1.03	3.13	−0.56	3.37	NA	NA
BC738	5–6 cm	−0.56	3.34	−0.38	3.39	NA	NA
	Mean	−0.82	2.99	−0.34	3.41	NA	NA
	1 SD	0.15	0.20	0.14	0.04	NA	NA

to this is *M. earlandi*, whose dead abundance remains stable in both sub-cores, likely due to its siliceous cement being more resistant to chemical breakdown (Earland, 1933). This enhanced downcore loss of agglutinated taxa, relative to calcareous taxa, illustrates the well-recognized complication of fossil/dead assemblages not truly reflecting living assemblages due to the loss of taxa with poor preservation potential (e.g. Majewski, 2005; Jorissen et al., 2007; Stefanoudis et al., 2017).

4.2 Sediment living and calcification depths

Many of the most abundant infaunal taxa recorded in BC737 and BC738 do not appear to have a clear preference for a specific living depth. However, it is important to recognize the potential limitations of the Rose Bengal staining technique in identifying truly living specimens. Where decay rates are slow, Rose Bengal may stain foraminifera that have been dead for months to several years (Corliss and Emerson, 1990). It is therefore important to apply criteria that are as strict as possible when categorizing which specimens are living and which are dead (e.g. Fontanier et al., 2016; Caulle et al., 2015) and to bear this limitation in mind when considering live abundances arrived at through Rose Bengal staining. It is also possible for specimens identified as living at a certain depth interval to have been transported there after death by bioturbation (see Bernhard, 2000, and references therein). If bioturbation were controlling the distribution of specimens within our data, we would expect to see all taxa affected such that it would not be possible to identify any depth-restricted habitat preferences. The restricted distribution of *L. scitula*, *R. subdentaliniformis*, and *G. rostrata* to epifaunal/very shallow infaunal environments contradicts bioturbation being prevalent at our sites. Furthermore, where decay rates are very slow, specimens that appear live at different depths within the sediment column may be significantly older than the overlying live assemblages. This is dependent on the sedimentation rate being high enough to bury specimens to a significant depth before decay is sufficiently progressed that staining with Rose Bengal will no longer occur, and such age control in not available for the samples studied here. Whilst it is important to recognize the limitations of Rose Bengal staining, it is simple, reliable, and inexpensive to use and is currently the most appropriate technique to apply when, as in this study, the samples are processed immediately upon collection (Bernhard, 2000). In addition, Murray and Bowser (2000) have proposed that, in oxygenated environments, dead tests are unlikely to retain protoplasm due to predation being the most likely cause of death. Whilst we did not directly measure the oxygenation of the sediments studied here, there was no indication of anoxia or dysoxia from the colour and odour of the sediments on recovery.

As discussed in the Introduction, it is commonly assumed that foraminifera calcify at their living depth and record the pore water $\delta^{13}C_{DIC}$ in their test isotopic composition

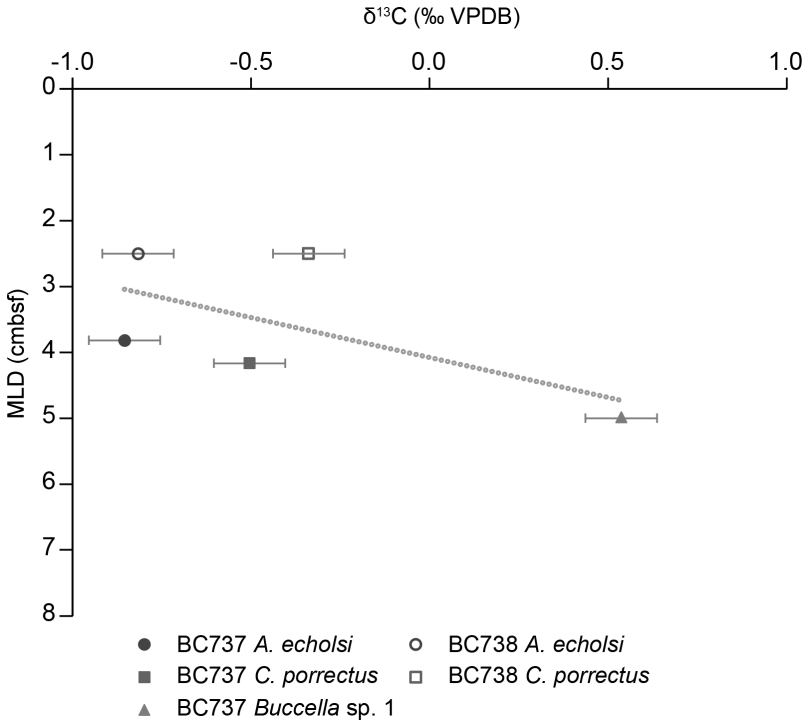


Figure 7. $\delta^{13}C$ vs. MLD. Mean $\delta^{13}C_{foram}$ values for the three species analysed here plotted against MLD. *A. echolsi* – circular symbols; *C. porrectus* – square symbols; *Buccella* sp. 1 – triangular symbols (closed symbols – BC737; open symbols – BC738). Error bars: 1 SD.

or an isotopic composition offset from that of pore water by species-specific vital effects. Whilst downcore pore water $\delta^{13}C_{DIC}$ data are not available for the cores studied here, records from various other locations consistently report that pore water $\delta^{13}C_{DIC}$ decreases (becomes more negative) with increased sediment depth (e.g. McCorkle et al., 1997; Holsten et al., 2004; Loubere et al., 2011; Luo et al., 2013), before stabilizing below the oxygen penetration depth. Furthermore, Gehlen et al. (1999) have modelled how the interaction of oxic organic matter decay and $CaCO_3$ dissolution generate this gradient within marine sediments. We therefore assume that a negative gradient of some kind will be present in sediments from the South Georgia shelf. The observed increase in $\delta^{13}C_{foram}$ with increased MLD (Fig. 7) is the opposite of the expected trend were each species calcifying at their respective MLDs. However, there are multiple vital-effect factors that lead to different inter-species $\delta^{13}C$ offsets despite specimens calcifying from waters with the same $\delta^{13}C_{DIC}$ (see review in Ravelo and Hillaire-Marcel, 2007), and without prior knowledge of the impact of these vital effects for each species, we cannot use this as evidence that these species do not calcify at their MLD.

Assessing the intra-species isotope data from the three species analysed here, we note that the depth–$\delta^{13}C_{foram}$ relationship we would anticipate, were the foraminifera calcifying with the pore water $\delta^{13}C_{DIC}$ at the depth from which they were recovered, does not hold true; i.e. intra-species $\delta^{13}C$ does not decrease with depth (Fig. 6a). The range of inter-species $\delta^{13}C$ and $\delta^{18}O$ compositions considerably exceeds the intra-species range (Fig. 5). Other studies that have reported isotope data from live foraminifera at a range of living depths have also noted limited variability in the intra-species stable isotope composition. For example, *Bolivina spissa*, *Bulimina aculeata*, *Cibicidoides wuellerstorfi*, *Uvigerina peregrina*, *Pleurostomella alternans*, *Globobulimina affinis*, and *G. pacifica* (McCorkle et al., 1997) from midlatitude continental margins in the Atlantic and Pacific oceans show no systematic downcore isotope variations (Fig. 6b), even though the isotopic composition of the same species can vary significantly between locations (e.g. *G. affinis*) (for further examples, see McCorkle et al., 1990; Tachikawa and Elderfield, 2002; Schmiedl et al., 2003; Fontanier et al., 2006b, 2008). When we normalize our $\delta^{13}C_{foram}$ data, and the data of McCorkle et al. (1997), by subtracting the mean for each species at each sample location, there is no trend away from that mean with depth (Fig. 6c) even though all pore water $\delta^{13}C_{DIC}$ values in those locations (where measured) exhibit a gradient.

If the individual foraminifera were calcifying at the depth at which they were found living (as inferred by Fontanier et al., 2006b, and Theodor et al., 2016, amongst others), we would expect our intra-species $\delta^{13}C$ data, and those of other studies (e.g. McCorkle et al., 1997), to reflect a decreasing $\delta^{13}C_{DIC}$ gradient with depth, which they do not. The con-

sistency of intra-species isotope data (Fig. 6), despite their broad range of living depths (Figs. 2 and 6), are good evidence that benthic foraminifera calcify at a *fixed depth location*, and possibly within a specific season, because they fail to capture the variability of pore water $\delta^{13}C_{DIC}$ that their observed living depth would expose them to.

4.3 Foraminiferal calcification strategies

Many have concluded that the observed inter-species differences in $\delta^{13}C$ are due to species preferences for different depth microhabitats, and their position on the $\delta^{13}C_{DIC}$ gradient, implying that calcification occurs infaunally at a specific, restricted depth for each species (e.g. McCorkle et al., 1990; Schmiedl et al., 2004; Theodor et al., 2016). To account for fixed intra-species $\delta^{13}C$ compositions of infaunal taxa requires calcification to only occur at certain times during the organism's life when it is exposed to a fixed $\delta^{13}C_{DIC}$ value. We discuss two previously proposed calcification strategies of infaunal species – at a specific depth within the sediment and within macro-/meio-faunal burrows – and propose a third, novel strategy: calcification at the sediment–seawater interface.

In the first strategy, calcification only occurs at a specific depth within the sediment and this depth relates to the preferred microhabitat of the species: broadly speaking epifaunal, shallow infaunal, or deep infaunal. There is evidence for this strategy in some species: for example Holsten et al. (2004) found that the $\delta^{13}C_{foram}$ in three species (*Bolivina argentea*, *B. subadvena*, and *Buliminella tenuata*) matched the pore water $\delta^{13}C_{DIC}$ at their maximum live abundance depth. However, if the species studied here calcified at a preferred depth within the sediment, we need to question what is controlling/determining the narrow calcification depth range (in contrast to the observed wide living depth range) and why it is apparently not the ALD/MLD. We note that, on the South Georgia shelf, species with deeper ALD/MLD have heavier $\delta^{13}C$ compositions (Fig. 7), whilst pore waters are assumed to change (e.g. become isotopically lighter) with depth.

The second strategy involves calcification in association with the burrows of larger fauna, where voids within the sediment allow pore water isotopic composition to be homogenous across a range of depths (Loubere et al., 1995; Schmiedl et al., 2004), meaning that calcification within a burrow would result in the same $\delta^{13}C_{foram}$ composition regardless of depth. Loubere et al. (2011) have proposed that all calcareous foraminifera use this strategy, with the activities of macro-/meio-fauna allowing foraminifera to choose micro-habitats with particular geochemical conditions within the complex "bio-irrigation" systems the larger fauna create.

Our third hypothesis, that calcification occurs at the sediment–seawater interface, is supported, in principal, by the presence of live specimens of many of the infaunal calcareous taxa recorded in this study (and e.g. McCorkle et al., 1997) within the top 2 cm of the sediment. Foraminifera are known to be capable of migrating throughout the sediment column (e.g. Linke and Lutze, 1993; Geslin et al., 2004) and the occurrence of infaunal species at these shallow depths within the sediment demonstrates their ability to migrate to the sediment–seawater interface. Weldeab et al. (2016) have recorded the presence of a steep $[CO_3^{2-}]$ gradient between bottom water and pore water and also within the sediment column. This $[CO_3^{2-}]$ gradient suggests that the sediment–seawater interface may provide the most energy-efficient location for calcification, due to the greater availability of carbonate ions. In addition, food (phytodetrital matter from the overlying water column) availability and/or type is greatest at the sediment–seawater interface. Whilst from the stable isotope data on living specimens published here and elsewhere, it is not possible to prove that the species were calcifying at the sediment–seawater interface, we conclude that this may be the simplest explanation for the stability of inter-species isotopic composition.

Alternatively, there may be no requirement to calcify at a specific depth, or within specific geochemical conditions, and foraminifera may be capable of calcifying at a range of sediment depths and a corresponding range of pore water $\delta^{13}C_{DIC}$ compositions. Calcification across a range of sediment depths could result in foraminiferal calcite recording an average of the range in pore water $\delta^{13}C_{DIC}$ compositions, with any inter-species variation accounted for by species-specific vital effects. The presence of "living" specimens of the species studied here at a range of sediment depths and the absence of a clear maximum "live" abundance depth are not inconsistent with this calcification strategy.

4.4 Implications of sediment–seawater interface calcification for palaeoenvironmental research

Were foraminiferal calcification only to occur at the sediment–seawater interface, why do inter-species $\delta^{13}C$ offsets vary on annual, decadal, centennial, and longer timescales? As discussed above (see Introduction), $\delta^{13}C$ offsets between epifaunal and infaunal taxa, assumed to be indicative of the pore water $\delta^{13}C_{DIC}$ gradient, have been used to reconstruct past changes in organic matter flux and sea floor oxygenation (e.g. McCorkle and Emerson, 1988; Zahn et al., 1986; Schilman et al., 2003; Hoogakker et al., 2015). Considering our hypothesis that infaunal species migrate to the sediment–seawater interface to calcify, we propose that changes in epifaunal–infaunal offsets are controlled by the timing of calcification; epifaunal and shallow infaunal taxa calcify persistently, even during periods of relatively low C_{org} availability (oligotrophic/mesotrophic conditions), and infaunal taxa calcify only during periods of high C_{org} availability (eutrophic conditions). Deeper infaunal taxa may be opportunistic, potentially "hibernating" or at least not calcifying new chambers, at depth during oligotrophic periods when food is scarce and migrating to the sediment–seawater interface to feed and calcify during eutrophic periods.

Supporting this hypothesis, Ohga and Kitazato (1997) observed that, at their study site in Sagami Bay, Japan, all foraminifera where found living in the uppermost part of the sediment column during the peak of phytodetrital flux. Kitazato et al. (2000) have proposed that deep-infaunal taxa may migrate to the sediment–seawater interface to take advantage of phytodetrital input and to reproduce. Furthermore, in laboratory experiments Nomaki et al. (2005) recorded that many infaunal foraminifera, especially the taxa they classified as shallow or intermediate infauna, migrated upwards through the sediment column in response to an addition of food at the surface. This migration may be quite rapid, with foraminifera capable of moving through several millimetres of sediment in a day (e.g. Gross, 2000), although Witte et al. (2003) found that foraminifera took 8 days to respond to a phytodetritus pulse. In a simulated phytodetritus event Sweetman et al. (2009) found that the uptake of added carbon, labelled with ^{13}C, was confined to surface-living specimens of the deep-infaunal *Globobulimina turgida*. However, we note that Enge et al. (2011) did not record a significant response by deeper infaunal taxa to a simulated phytodetritus pulse, although this may be due to the short duration (4 days) of their experiment. It is also important to note that it has been hypothesized that deep-infaunal taxa may have a preference for degraded organic matter (Caralp, 1989; Fontanier et al., 2003), which if correct may further delay their response to influxes of labile organic matter from phytodetrital pulses. Whilst these studies are consistent with our hypothesis that infaunal taxa migrate to the sediment–seawater interface during eutrophic conditions and calcify, no studies have yet recorded when calcification occurs.

In our scenario, infaunal $\delta^{13}C$ records are therefore biased towards eutrophic conditions (even if this is just a brief seasonal pulse of C_{org} to the sea floor), while epifaunal/shallow infaunal $\delta^{13}C$ records are more reflective of mean annual conditions at the sea floor. Since deep-infaunal $\delta^{13}C$ is biased towards periods of enhanced C_{org} flux to the sea floor, downcore records from the $\delta^{13}C$ of these taxa are potentially less sensitive to variability in C_{org} flux. The abundance of opportunistic infaunal species, however, can increase dramatically by accelerating growth and/or reproduction during eutrophic episodes (e.g. Gooday, 1988; Gooday and Hughes, 2002; Fontanier et al., 2006a; Peck et al., 2015) due to greater organic carbon availability and their tolerance of lower oxygen concentrations (Piña-Ochoa et al., 2010). Downcore epifaunal $\delta^{13}C$ is potentially a more sensitive indicator of variable C_{org} flux and bottom water conditions (oxygenation). During periods of exceptionally high productivity, epifaunal $\delta^{13}C$ may converge with infaunal $\delta^{13}C$ records, reflecting a prolonged abundance of C_{org} at the seafloor throughout the year.

5 Summary

In this study, we show that the diversity of benthic foraminifera does not vary greatly at our study sites across the South Georgia shelf and that there are similarities between the assemblages recorded here and those found on the Antarctic Peninsula and elsewhere on the Antarctica shelf, particularly among the more abundant taxa. We find that for most of the taxa in this study, there is no strong preference for a specific living depth, except for a small number of species that exhibit a preference for an epifaunal/shallow infaunal microhabitat (e.g. *Labrospira scitula* and *Glaphyrammina rostrata*).

We find little intra-species variation in $\delta^{13}C$ of the tests of the "living" benthic foraminiferal species analysed here (*Astrononion echolsi*, *Cassidulinoides porrectus*, *Buccella* sp. 1), despite their recovery from a range of depths (and assumed pore water isotopic compositions) below the sea floor. The failure of $\delta^{13}C_{foram}$ from depth-restricted samples to document the pore water $\delta^{13}C_{DIC}$ gradient common to marine sediments suggests that infaunal taxa calcify at a fixed $\delta^{13}C_{DIC}$ and therefore depth (e.g. McCorkle et al., 1990; Schmiedl et al., 2004; Theodor et al., 2016). Whilst we are not able to conclusively state that the species studied here calcify at the sediment–seawater interface, this hypothesis is consistent with (i) the presence of "live" individuals of all the most abundant taxa in the upper 1–2 cm of sediment in this study (and other studies), (ii) the documented ability of foraminifera to migrate through the sediment column (e.g. Linke and Lutze, 1993; Geslin et al., 2004), (iii) the absence of a strong living depth preference in this study (and other studies), and (iv) the sediment–seawater interface being the most energetically favourable location for calcification (greatest C_{org} and $[CO_3^{2-}]$ availability).

We propose that epifaunal taxa live and calcify at the sediment–seawater interface throughout a wide range of organic carbon availability scenarios (oligotrophic to eutrophic). Infaunal species, however, may only calcify when the concentration of organic carbon at the seafloor is high and they migrate to the sediment–seawater interface to feed. In this scenario, temporal (downcore) variability in the offsets between epifaunal and infaunal $\delta^{13}C$ would reflect changing fluxes of organic carbon to the seafloor, causing variation in $\delta^{13}C_{DIC}$ between oligotrophic and eutrophic conditions. Our hypothesis, therefore, has important implications for the use of benthic foraminiferal $\delta^{13}C$ offsets as proxies of productivity and oxygenation and for the use of trace metal ratios (Mg / Ca, B / Ca) in reconstructing pore water temperature and $\Delta[CO_3^{2-}]$. However, we maintain that changes in epifaunal–infaunal foraminiferal $\delta^{13}C$ offsets through time are likely to reflect the evolution of phytoplankton blooms and water mass chemistry (cf. Hoogakker et al., 2015). This study further highlights the need for a good understanding of foraminiferal ecology when utilizing isotopic composition in interpreting palaeoenvironmental change. Further work is

needed to investigate the timing and depth of calcification in calcareous benthic foraminifera and the test-forming depths for agglutinated benthic foraminifera.

6 Systematic taxonomy

The following species and taxonomic groupings are arranged in taxonomic order following the supra-generic classifications of Kaminski (2004) for the agglutinated taxa and Loeblich and Tappan (1988) for the calcareous walled taxa. Species identification is largely based on the works of Heron-Allen and Earland (1932a), Earland (1933), Anderson (1975), Mackensen et al. (1990), Ishman and Domack (1994), Violanti (1996), Igarashi et al. (2001), and Majewski (2005, 2013). Eleven additional species have been described, recorded in benthic foraminiferal assemblage work on sediment from surface samples from other box cores and gravity cores collected from the South Georgia shelf (Table 1 and Fig. 1) that were not present in the sub-cores. Described species are illustrated in Figs. 8–14.

Family **Rhabdamminidae** Brady, 1884

Subfamily **Rhabdammininae** Brady, 1884

Genus *Rhabdammina* M. Sars in Carpenter, 1869.

***Rhabdammina* spp.**
(Fig. 8:1)

Material. Thirteen specimens from six samples.

Description. Included in this group are any thick-walled tube fragments comprising coarsely agglutinated material with rough external surface and very smooth internal cavity.

Family **Hippocrepinellidae** Loeblich & Tappan, 1984 emend. Mikhalevich, 1995

Genus *Hippocrepinella* Heron-Allen & Earland, 1932b

Hippocrepinella alba Heron-Allen & Earland, 1932b
(Fig. 8:2)

1932b *Hippocrepinella alba* Heron-Allen & Earland: 259, pl. 1, figs. 16–18.
1933 *Hippocrepinella alba* Heron-Allen & Earland; Earland: 71, pl. 7, figs. 10–12.

Material. Twenty-eight specimens from seven samples.

Description. Unilocular, cylindrical to fusiform test; smooth, thin, white wall constructed of very small particles; aperture round at end of narrow neck, which may have a collar; may also have a secondary basal aperture.

Occurrence. Originally described from the South Atlantic (Heron-Allen and Earland, 1932b) and subsequently recorded from South Georgia (Earland, 1933), both from surface samples.

Family **Rhizamminidae** Wiesner, 1931

Genus *Rhizammina* Brady, 1879

***Rhizammina* spp.**
(Fig. 8:3–5)

Material. Forty-nine specimens from nine samples.

Description. Included in this group are any elongate tubular tests with thin, flexible walls; only broken tubes recovered in this study; specimens recorded here mainly composed of diatomaceous material.

Family **Saccamminidae** Brady, 1884

Subfamily **Saccammininae** Brady, 1884

Genus *Lagenammina* Rhumbler, 1911

Lagenammina* cf. *sphaerica Moreman, 1930
(Fig. 8:6)

1930 *Lagenammina sphaerica* Moreman: 51, pl. 5, fig. 15.

Material. Seventy specimens from 13 samples.

Description. Unilocular, near spherical test; thin agglutinated wall; medium sand grains; rough surface; simple aperture produced at the end of an elongate neck; neck approximately two fifths of test length.

Remarks. As *Lagenammina sphaerica* Moreman was described from Silurian deposits in the USA, this cannot be the same species. However the morphological similarities are uncanny. The species described here does bear some similarity to the extant *Lagenammina arenulata* (Skinner) that is common at other Antarctic localities, but this species does not possess an elongate neck. Jones (1994) suggests that specimens similar to *L. arenulata* (Skinner), but with an elongate neck, belong to *L. atlantica* (Cushman). However, the original description of this species reveals that it too does not possess an elongate neck.

Genus *Saccammina* Carpenter, 1869

***Saccammina* spp.**
(Fig. 8:8)

Material. Four specimens from three samples.

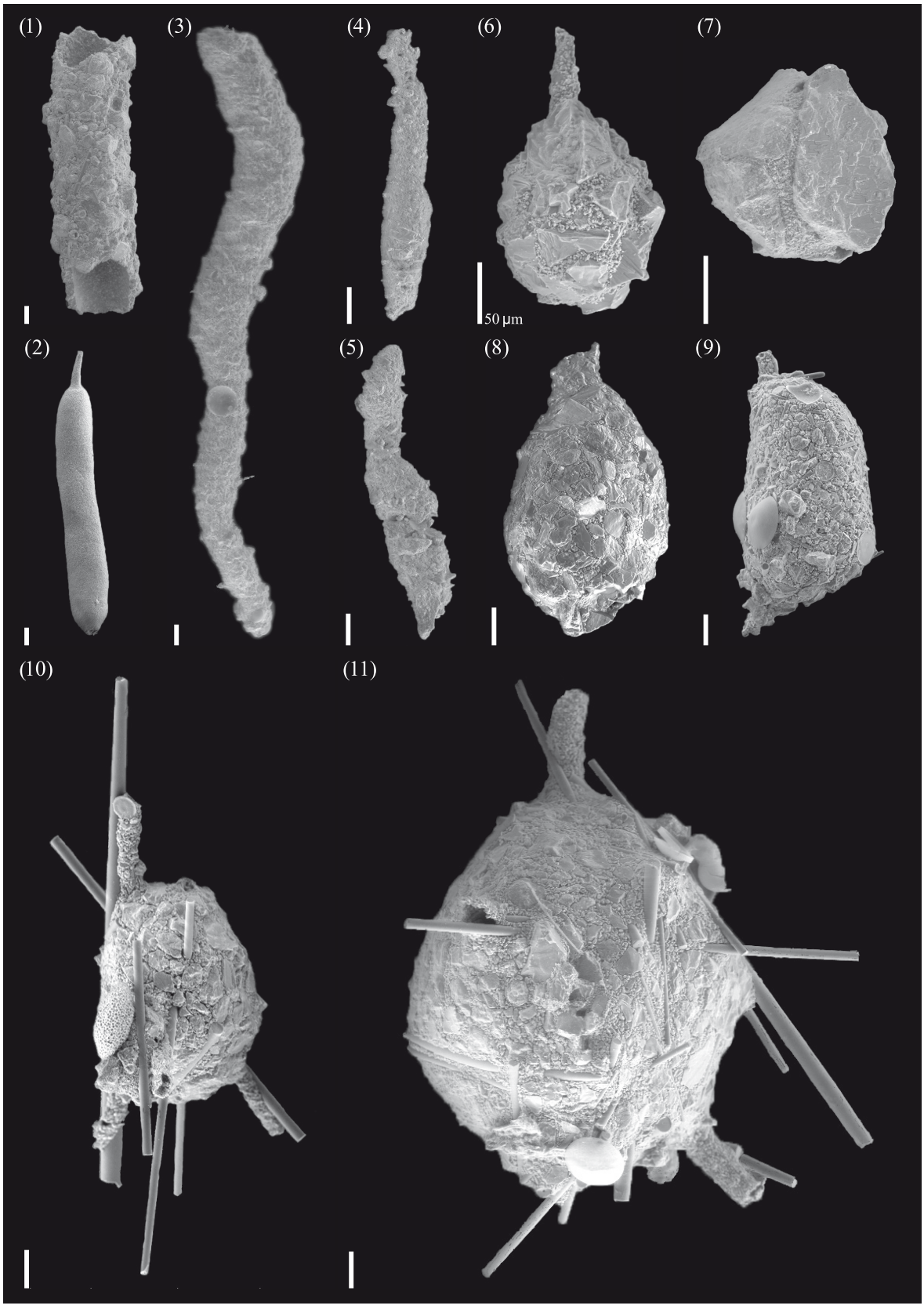


Figure 8. (1) *Rhabdammina* spp. (BC738). (2) *Hippocrepinella alba* Heron-Allen and Earland (BC738). (3–5) *Rhizammina* spp. (BC738). (6) *Lagenammina* cf. *sphaerica* (Moreman) (BC737). (7) *Psammosphaera bowmanni* Heron-Allen and Earland (BC738). (8) *Saccammina* spp. (BC737 (D) 7–8 cm; BC738 (D) 0–1 cm). (9–11) *Astrammina rara* Rhumbler (BC737). (Scale bar 100 µm unless otherwise indicated.)

Description. Included in this group are any forms that have a globular, unilocular test, with a firm, fine to medium agglutinated wall held together with an organic cement, and a round aperture produced on a short neck.

Subfamily **Thuramminininae** Miklukho-Maklay, 1963

Genus *Astrammina* Rhumbler in Wiesner, 1931

Astrammina rara Rhumbler in Wiesner, 1931
(Fig. 8:9–11)

1931 *Astrammina rara* Rhumbler, in Wiesner: 78, pl. 2, fig. 19.
1932b *Armorella sphaerica* Heron-Allen & Earland: 257, pl. 2, figs. 4–11.
1932b *Pelosphaera cornuta* Heron-Allen & Earland: 255, pl. 2, figs. 12–15.
1933 *Armorella sphaerica* Heron-Allen & Earland; Earland: 65, pl. 7, figs. 16–23.
1933 *Pelosphaera cornuta* Heron-Allen & Earland; Earland, 61, pl. 7, figs. 24–27.

Material. Twelve specimens from six samples.

Description. Large, near-spherical, unilocular test with a number of narrow "arms" extending in various directions, often along sponge spicules that are incorporated into the test wall. Wall firmly agglutinated, comprising fine to coarse sand grains, sponge spicules, and diatoms, with a grey to yellowish brown cement.

Occurrence. Originally described from the South Atlantic (Heron-Allen and Earland, 1932b) and subsequently recorded from South Georgia (Earland, 1933), both from surface samples.

Remarks. The synonymy of *Astrammina rara* Rhumbler, *Armorella sphaerica* Heron-Allen & Earland, and *Pelosphaera cornuta* Heron-Allen & Earland was demonstrated by DeLaca (1986) in an analysis of live Antarctic specimens.

Family **Psammosphaeridae** Haeckel, 1894

Subfamily **Psammosphaerinae** Haeckel, 1894

Genus *Psammosphaera* Schulze, 1875

Psammosphaera bowmanni Heron-Allen & Earland, 1912
(Fig. 8:7)

1912 *Psammosphaera bowmanni* Heron-Allen & Earland: pl. 5, figs. 5–6, pl. 6, fig. 5.
2010 *Capsammina bowmanni* (Heron-Allen & Earland); Gooday et al.: 349, pl. 1, figs. A & B.

Material. Four specimens from three samples.

Description. Free, monothalamous test, comprising several small flat grains of mica cemented by very fine cement that form an irregular polyhedral chamber. Openings are visible where the flakes meet and cement is absent, which may be the aperture or accidental.

Occurrence. Originally described from North Sea dredgings (Heron-Allen and Earland, 1912), it was subsequently recorded in the north-east Atlantic (Gooday et al., 2010).

Remarks. Heron-Allen and Earland (1912) were unable to assign a definite oral aperture, recording openings similar to those recorded here on some specimens but not all. Heron-Allen and Earland (1912) also note that this species is difficult to describe, as no two specimens look exactly alike. The flakes are arranged to approximately make an oval or flask shape, and the gaps, the size of which may vary considerably, between the flakes are then filled with cement, so that the cemented areas vary from narrow infill to broad flat areas.

Psammosphaera fusca Schulze, 1875
(Fig. 9:1–2)

1875 *Psammosphaera fusca* Schulze: 113, pl. 2, fig. 8.
1994 *Psammosphaera fusca* Schulze; R. W. Jones: 31, pl. 18, figs. 1–8.
2003 *Psammosphaera fusca* Schulze; Gaździcki & Majewski: 7, fig. 3 (1–2).

Material. Forty-six specimens from 15 samples.

Description. Small spherical test; usually unilocular, occasionally multiple chambers loosely joined. Agglutinated wall comprising medium to coarse grains in a fine cement.

Occurrence. Recorded from several locations in the Atlantic (Jones, 1994) and Antarctica (Gaździcki and Majewski, 2003), all from Recent sediments.

Family **Ammodiscidae** Reuss, 1862

Subfamily **Ammodiscinae** Reuss, 1862

Genus *Ammodiscus* Reuss, 1862

Ammodiscus incertus (d'Orbigny, 1839a)
(Fig. 9:5–6)

1839a *Operculina incerta* d'Orbigny: 49, pl. 6, figs. 16–17.

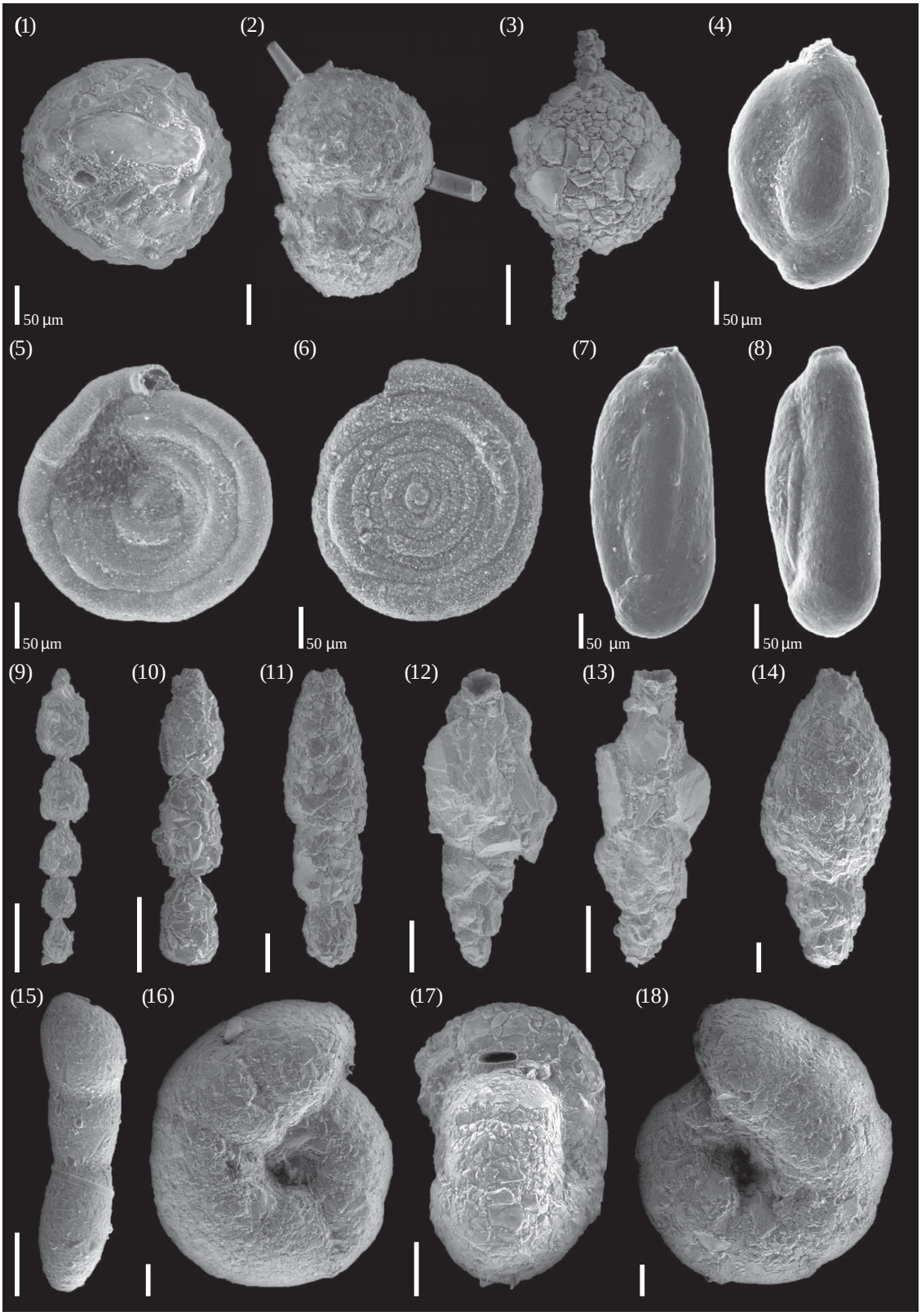


Figure 9. (1–2) *Psammosphaera fusca* Schulze (BC737 (D) 0–1 cm). (3) *Hormosinella* sp. (BD738). (4) *Miliammina lata* Heron-Allen and Earland (GC666_002). (5–6) *Ammodiscus incertus* (d'Orbigny) (BC737). (7–8) *Miliammina earlandi* Loeblich and Tappan (GC666_002). (9–10) *Hormosinelloides guttifer* (Brady) (BC667). (11) *Nodulina dentaliniformis* (Brady) (BC737 (D) 0–1 cm). (12–13) *Reophax subdentaliniformis* Parr (BC738). (14) *Reophax subfusiformis* Earland emend. Höglund (BC667). (15) *Pseudonodosinella* sp. (BC737 (D) 9–10 cm). (16–18) *Labrospira scitula* (Brady) (BC738). (Scale bar 100 µm unless otherwise indicated.)

1996 *Ammodiscus incertus* (d'Orbigny); Violanti: 53, pl. 3, fig. 6.
2001 *Ammodiscus* sp.; Igarashi et al.: 142, pl. 2, fig. 5.
2013 *Ammodiscus incertus* (d'Orbigny); Majewski: 175, fig. 3(4).

Material. Overall, 109 specimens from 22 samples.

Description. Small test (ca. 200 µm diameter), generally flat but tending towards irregular coiling in the last whorls. Up to seven whorls in microspheric form and up to six in megalospheric form; sutures between whorls somewhat depressed; proloculus spherical and central. The agglutinated test wall comprises angular grains of sand in a cement matrix that is a yellow-brown colour. Aperture a simple opening at the end of the tubular chamber.

Occurrence. Recorded from a number of locations on the Antarctic shelf (Violanti, 1996; Igarashi et al., 2001; Majewski, 2013), from Recent sediments.

Family **Rzehakinidae** Cushman, 1933

Subfamily **Miliammininae** Saidova, 1981

Genus *Miliammina* Heron-Allen & Earland, 1930

Miliammina earlandi Loeblich & Tappan, 1955
(Fig. 9:7–8)

1933 *Miliammina oblonga* (Heron-Allen & Earland); Earland: 92, pl. 3, fig. 17, pl. 5, figs. 1–5, 7–8.
1955 *Miliammina earlandi* Loeblich & Tappan: 12, pl. 1, figs. 15–16.
1981 *Miliammina earlandi* Loeblich & Tappan; Milam & Anderson: 304, pl. 2, fig. 4.
1996 *Miliammina earlandi* Loeblich & Tappan; Violanti: 53, pl. 3, figs. 10–11.
2004 *Miliammina earlandi* Loeblich & Tappan; Murray & Pudsey: 71, pl. 1, figs. 8–9.

Material. Overall, 3240 specimens from 34 samples.

Description. Tubular chambers with a rounded peripheral edge, arranged in a quinqueloculine pattern; sutures slightly depressed, increasing as test size increases. Wall comprises very small mineral grains (whose composition is unclear) completely embedded in siliceous cement (insoluble in HCl), smooth/polished surface. Very light grey in colour, and large variation in test size. Crescentiform aperture is at the terminal end of the final chamber, flush or with a slight neck. There is considerable morphological variation within this species due to variation in the roundness of the chambers.

Occurrence. Originally described from the South Atlantic (Heron-Allen and Earland, 1930) and subsequently reported from several locations of the Antarctic shelf (Milam and Anderson, 1981; Violanti, 1996; Murray and Pudsey, 2004), from Recent sediments.

Remarks. Whilst initially included in *Miliammina oblonga* (Chapman) by Heron-Allen and Earland (1930), this South Georgia form was later separated from *Miliammina arenacea* (Chapman) by Earland (1933) due to its more ovate and rounded outline and was renamed *Miliammina oblonga* Heron & Earland. However, Loeblich and Tappan (1955) recognized that this species name had previously been assigned to *Miliolina oblonga* (Montagu), incorrectly placed in *Miliammina*, and renamed it *Miliammina earlandi* (which we use here). Earland (1933) considered *M. earlandi* to be the most characteristic and commonest foraminifera of the South Georgia area.

Miliammina lata Heron-Allen & Earland, 1930
(Fig. 9:4)

1930 *Miliammina lata* Heron-Allen & Earland: 43, pl. 1, figs. 13–17.
1933 *Miliammina lata* Heron-Allen & Earland; Earland: 93, pl. 3, fig. 17, p. 5, figs. 15–19.
1996 *Miliammina lata* Heron-Allen & Earland; Violanti: 52, pl. 3, fig. 12.
2001 *Miliammina lata* Heron-Allen & Earland; Igarashi et al.: 140, pl. 2, fig. 10.
2005 *Miliammina lata* Heron-Allen & Earland; Majewski: 193, fig. 12(8).
2013 *Miliammina lata* Heron-Allen & Earland; Majewski: 176, fig. 4(3).

Material. Sixty specimens from 13 samples.

Description. Quinqueloculine test; early chambers often not visible; inflated, broadly rounded chambers, broadening at the base. Slightly depressed sutures; thick, smooth, agglutinated wall comprising very small particles in an excess of siliceous cement. Small crescentiform aperture at the end of the final chamber.

Occurrence. Originally described from the South Atlantic (Heron-Allen and Earland, 1930), it was subsequently recorded from South Georgia (Earland, 1933) and a number of locations on the Antarctic shelf (Igarashi et al., 2001; Violanti, 1996; Majewski, 2005, 2013), all from Recent sediments.

Family **Hormosinellidae** Rauzer-Chernousova & Reytlinger, 1986

Genus *Hormosinella* Shchedrina, 1969

***Hormosinella* sp.**
(Fig. 9:3)

Material. Three fragmentary specimens from one sample.

Description. Large, uniserial test; ovate/fusiform chambers separated by long, delicate, necks. Thin, agglutinated wall; rounded terminal aperture on elongate neck.

Remarks. Only recorded here as fragmentary specimens.

Genus *Hormosinelloides* Zheng & Fu, 2001

Hormosinelloides guttifer (Brady, 1881)
(Fig. 9:9–10)

1881 *Lituola (Reophax) guttifera* Brady: 49, pl. 31, figs 10–15.
1975 *Reophax guttifer* (Brady); Anderson: 74, pl. 1, fig. 18.
1994 *Hormosinella guttifera* (Brady); R. W. Jones: 38, pl. 31, figs. 10–15.
2005 *Hormosinelloides guttifer* (Brady); Kaminski & Gradstein: 249, pl. 46, figs. 1–8.

Material. Thirty-one specimens from four samples.

Description. Uniserial test comprising a series of approximately three to five pyriform chambers. Thin, agglutinated wall with a fairly rough finish. Simple, rounded aperture; terminal on an elongated neck.

Occurrence. Originally described from the South Atlantic by Brady (1881) who recorded that it was "exceedingly rare", it was subsequently recorded from the Weddell Sea (Anderson, 1975), from Recent sediments.

Remarks. Placed in the genus *Hormosinelloides* by Kaminski and Gradstein (2005) because the chambers attach near the base of the apertural neck of the preceding chamber.

Family **Reophacidae** Cushman, 1927

Genus *Nodulina* Rhumbler, 1895

Nodulina dentaliniformis (Brady, 1881)
(Fig. 9:11)

1881 *Lituola (Reophax) dentaliniformis* Brady: 49, pl. 30, figs. 21–22.
1994 *Reophax dentaliniformis* (Brady); R. W. Jones: 37, pl. 30, figs. 21–22.
2017 *Nodulina dentaliniformis* (Brady); Kender & Kaminski: pl. 8, fig. 1.

Material. Six specimens from one sample.

Description. Slender, elongate test with straight axis; three to six chambers; final chamber significantly larger and tapered; wall comprises sand grains in firm cement, with a smooth finish. Large, round terminal aperture on a short tubular neck of finer grains.

Occurrence. Recorded from the South Pacific, the North Atlantic (Brady, 1881; Jones, 1994), and the Bering Sea (Kender and Kaminski, 2017).

Remarks. *Nodulina dentaliformis* (Brady) is the type species of the genus *Nodulina*, which is distinguished from *Reophax* by its more symmetrical, regular chambers, horizontal sutures, and straighter axis.

Genus *Reophax* de Montfort, 1808

Reophax subdentaliniformis Parr, 1950
(Fig. 9:12–13)

1950 *Reophax subdentaliniformis* Parr: 269, pl. 4, fig. 20.
1996 *Nodulina subdentaliniformis* (Parr); Violanti: 53, pl. 3, fig. 18.
2005 *Nodulina subdentaliniformis* (Parr); Majewski: 194, fig. 13(6–7).

Material. Overall, 457 specimens from 25 samples.

Description. Slender, elongate test with a slight curvature; usually four to six chambers (may be difficult to distinguish); final chamber significantly larger and tapered. Wall comprises poorly sorted sand grains in firm cement, coarsely finished. Large, round terminal aperture on a short neck of finer sand grains.

Occurrence. Recorded from Recent Antarctic sediments (Parr, 1950; Violanti, 1996; Majewski, 2005).

Remarks. We have placed this species within the genus *Reophax* on the basis of the curvature of the test.

Reophax subfusiformis Earland, 1933 emend. Höglund, 1947
(Fig. 9:14)

1933 *Reophax subfusiformis* Earland: 74, pl. 2, figs. 16–19.
1947 *Reophax subfusiformis* Earland; Höglund: 77.
2004 *Reophax subfusiformis* Earland; Murray & Pudsey: 72, pl. 2, fig. 5.
2005 *Reophax subfusiformis* Earland; Kaminiski & Gradstein: 275, pl. 54, figs. 1–8.

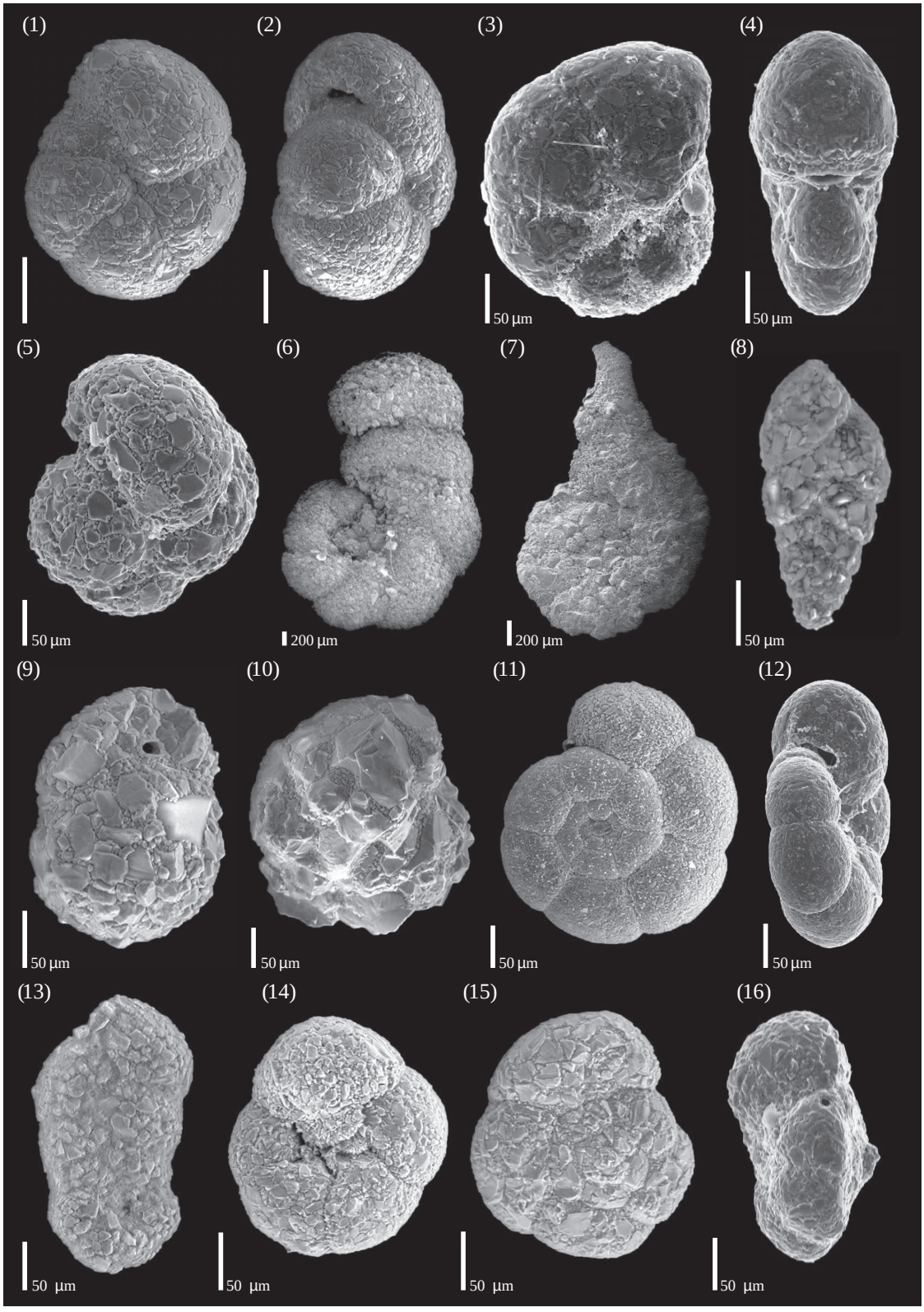


Figure 10. (1–2) *Haplophragmoides bradyi niigatensis* Uchio (1960) (BC737 (D) 0–1 cm). (3–4) *Labrospira* sp. 1 (GC666_002). (5) *Haplophragmoides quadratus* Earland (GC666_002). (6) *Glaphyrammina americana* (Cushman) (BC738). (7) *Glaphyrammina rostrata* (Heron-Allen and Earland) (BC738). (8) *Pseudobolivina antarctica* Wiesner (BC737 (D) 4–5 cm). (9–10) *Recurvoides* sp. 1 (BC667). (11–12) *Deuterammina scoresbyi* Brönnimann and Whittaker (GC666_002). (13) *Spiroplectammina biformis* (Parker and Jones) (BC738 (D) 9–10 cm). (14–16) *Portatrochammina antarctica weisneri* (Parr) (GC666_002). (Scale bar 100 µm unless otherwise indicated.)

Material. Seventeen specimens from 10 samples.

Description. Slender, elongate, slightly arched test comprising two to four chambers; final chamber large, tapering, and fusiform. Chambers increase rapidly in size; final chamber often comprising the majority of the test; depressed sutures; wall comprises poorly sorted sand grains in firm cement, coarsely finished. Large, round terminal aperture on a short neck.

Occurrence. This species was originally described by Earland (1933) from a number of stations near South Georgia. The description was subsequently emended by Höglund (1947) using specimens from the North Sea. Earland (1934) also reported its occurrence around the Falkland Islands, where it is widely distributed but rare at most localities. Kaminski and Gradstein (2005) report that *R. subfusiformis* is reported from Recent sediments at high-latitude stations throughout the Atlantic and Southern Oceans.

Family **Hormosinidae** Haeckel, 1894

Subfamily **Hormosininae** Haeckel, 1894

Genus *Pseudonodosinella* Saidova, 1970

***Pseudonodosinella* sp.**
(Fig. 9:15)

Material. One specimen from one sample.

Description. Elongate, uniserial test; ovate chambers that overlap much of the preceding chamber, including the aperture. Firmly agglutinated, smoothly finished wall; terminal aperture.

Family **Haplophragmoididae** Maync, 1952

Genus *Haplophragmoides* Cushman, 1910

Haplophragmoides bradyi Robertson subsp. ***niigatensis*** Uchio, 1962
(Fig. 10:1–2)

1962 *Haplophragmoides bradyi* (Robertson) subsp. *niigatensis* Uchio: 385, pl. 18, fig. 6.
1975 *Haplophragmoides bradyi* (Robertson); Anderson: 76, pl. 2, fig. 8.

Material. Seventeen specimens from six samples.

Description. Small, subglobose, involute test; becomes slightly evolute and umbilicate in adult tests; rounded periphery, slightly lobulate. Chambers low and broad, somewhat inflated; five in final whorl, gradually increasing in size as added. Distinct, depressed, radiate sutures. Finely agglutinated wall with smooth surface, yellowish colour. Aperture an interiomarginal crescentic slit.

Occurrence. Originally described from Recent sediments from the Sea of Japan (Uchio, 1962), it was subsequently recorded from the Weddell Sea (Anderson, 1975).

Remarks. *Haplophragmoides bradyi niigatensis* Uchio differs from *Haplophragmoides bradyi* (Robertson) in having a less evolute and more inflated test.

Haplophragmoides quadratus Earland, 1934
(Fig. 10:5)

1934 *Haplophragmoides quadratus* Earland: 88, pl. 3, figs. 7–8.
1960 *Haplophragmoides quadratus* Earland; Uchio: 52, pl. 1, fig. 17, pl. 5, fig. 14.

Material. Forty-three specimens from seven samples.

Description. Planispiral, compressed test with rounded periphery; approximately square outline with rounded corners. Chambers globose, slightly inflated; four in final whorl. Distinct, depressed sutures. Aperture not clearly visible in the specimens examined here.

Occurrence. Originally described from Bellingshausen Sea, Antarctica (Earland, 1932).

Remarks. *Haplophragmoides quadratus* Uchio 1960, described from the Pacific coast of the USA, appears to be the same species and would therefore be a junior synonym.

Genus *Labrospira* Höglund, 1947

Labrospira scitula (Brady, 1881)
(Fig. 9:16–18)

1881 *Lituola (Haplopragmium) scitulum* Brady: 50, pl. 34, figs 11–13.
1933 *Haplophragmoides scitulum* (Brady); Earland: 78, pl. 3, figs. 11–12.
1994 *Veleroninoides scitulus* (Brady); Jones: 41, pl. 34, fig. 13.
? 1996 *Recurvoides contortus* Violanti: 39, pl. 4, fig. 11.
2017 *Veleroninoides scitulus* (Brady); Kender and Kaminski: pl. 8, fig. 10.

Material. Overall, 328 specimens from 25 samples.

Description. Planispiral, partially evolute test, comprising three whorls with 8–11 chambers in the final whorl. Some specimens become slightly streptospiral in the final

whorl; fairly deep umbilicus on both sides. Sutures slightly curved to straight, radial, and very slightly depressed. Smooth-surfaced, thick agglutinated wall comprising coarse grains with yellow-brown cement; colour rapidly fades to white after death. Aperture an elongate oval-shaped areal opening, close to the base of the apertural face, with a fine-grained, raised lip surrounding the aperture.

Occurrence. Originally described from the North Atlantic (Brady, 1881); also recorded from the Bering Sea (Kender and Kaminski, 2017).

Remarks. *Labrospira scitula* (Brady) is also often placed within the genus *Veleroninoides*. However, we believe this designation to be incorrect as *L. scitula* (Brady) is not fully evolute – a diagnostic characteristic of *Veleroninoides*.

***Labrospira* sp. 1**
(Fig. 10:3–4)

Material. Overall, 236 specimens from 26 samples.

Description. Planispiral, slightly evolute test; slightly inflated chambers; six in the final whorl. Small umbilicus; straight, radial, slightly depressed sutures; smooth surface; thick agglutinated wall comprising coarse grains with yellow-brown cement. Aperture an areal, elongate slit, close to the base of the apertural face, with a very fine-grained, raised lip surrounding the aperture.

Remarks. Our material may represent the same species as that recorded by Murray and Pudsey (2004) as *Haplophragmoides canariensis* (d'Orbigny). We consider that this classification is incorrect, however, due to the significant differences in apertural characteristics.

Family **Discamminidae** Mikhalevich, 1980

Genus *Glaphyrammina* Loeblich & Tappan, 1984

Glaphyrammina americana (Cushman, 1910)
(Fig. 10:6)

1910 *Ammobaculites americanus* Cushman; 117, figs. 184–185.
1932a *Ammobaculites americanus* Cushman; Heron-Allen & Earland: 341, pl. 8, figs. 15–17.
1994 *Glaphyrammina americana* (Cushman); Jones: 40, pl. 34, figs. 1–4.

Material. Six specimens from four samples.

Description. Very large broad and flattened test, initially planispiral becoming uniserial; spiral section slightly involute; nine chambers in the outer whorl. Wall comprises well-cemented, poorly sorted sand grains and occasional diatom frustules. Long, slit-like aperture extends the width of the final chamber.

Occurrence. Originally described off the west coast of Mexico (Cushman, 1910), later from the South Atlantic (Jones, 1994).

Glaphyrammina rostrata (Heron-Allen and Earland, 1929)
(Fig. 10:7)

1929 *Ammobaculites rostratus* Heron-Allen & Earland; 326, pl. 2, figs. 14–17.
1933 *Ammobaculites rostratus* Heron-Allen & Earland; Earland: 80, pl. 5, figs. 22–25.

Material. Overall, 278 specimens from 23 samples.

Description. Thin-walled, flattened, planispiral test. Sutures often indistinct, especially in smaller specimens; approximately six chambers in final whorl, partially evolute. In some specimens the chambers begin to uncoil to have two uniserial chambers; where this uncoiling does not occur the final chamber protrudes at an angle away from the spiral. The test is constructed of fine sand with larger grains distributed throughout this matrix. The final chamber terminates with a narrowing apertural neck, described as "nipple-like" in Heron-Allen and Earland (1929) that is much more neatly constructed, solely comprising fine sand (this structure is very fragile and often partially or completely absent).

Occurrence. This species has been described from the South Georgia region (Heron-Allen and Earland, 1929; Earland, 1933).

Remarks. Originally described by Heron-Allen and Earland (1929) within the genus *Ammobaculites*, here we place this species in the genus *Glaphyrammina* due to the flattened nature of the test. When the apertural neck is absent the specimens can resemble *Glaphyrammina americana* but can be separated by the less distinct sutures.

Family **Ammosphaeroidinidae** Cushman, 1927

Subfamily **Recurvoidinae** Alekseychik-Mitskevich, 1973

Genus *Recurvoides* Earland, 1934

***Recurvoides* sp. 1**
(Fig. 10:9–10)

Material. Five specimens from three samples.

Description. Involute, subglobose test, streptospirally coiled in early stage, becoming planispiral. Broad, low chambers. Agglutinated wall, with a fairly rough surface. Simple, areal, aperture, just above the base of the final chamber.

Remarks. These specimens are placed in the genus *Recurvoides* on the basis of wall and apertural characteristics. Due to their small size, it has not been possible to definitively identify the coiling pattern.

Family **Spiroplectamminidae** Cushman, 1927

Subfamily **Spiroplectammininae** Cushman, 1927

Genus *Spiroplectammina* Cushman, 1927

Spiroplectammina biformis (Parker and Jones, 1865) (Fig. 10:13)

1865 *Textularia agglutinans* var. *biformis* Parker & Jones: 370, pl. 15, figs. 23–24.
1932a *Spiroplectammina biformis* (Parker & Jones); Heron-Allen & Earland: 347, pl. 8, figs. 27–31.
1994 *Spiroplectammina biformis* (Parker & Jones); R. W. Jones: 50, pl. 45, figs. 25–27.
1994 *Spiroplectammina biformis* (Parker & Jones); Ishman and Domack: 150, pl. 1, fig. 4.
2003 *Spiroplectammina biformis* (Parker & Jones); Gaździcki & Majewski: 8, fig. 4 (5).
2005 *Spiroplectammina biformis* (Parker & Jones); Majewski: 195, fig. 14 (3–5).
2009 *Spiroplectammina biformis* (Parker & Jones); Majewski & Anderson: 138, fig. 3.
2013 *Spiroplectammina biformis* (Parker & Jones); Rodrigues et al.: 214, fig. 3 (9).

Material. One specimen from one sample.

Description. Small test mainly comprising sand grains with a small amount of cement. Initially planispiral, rapidly uncoiling and becoming biserial; coiled section broader than biserial section; biserial chambers are subquadrate. Aperture a low arch at the inner margin of the final chamber.

Occurrence. Originally described from Recent sediments from Greenland (Parker and Jones, 1865) and later from the Arctic (Goes, 1894; Höglund, 1947). More recently this species has been described from the Antarctic Peninsula (Ishman and Domack, 1994; Majewski, 2005, 2013).

Remarks. The type species of *Spiroplectammina.* The large geographical separation between these two areas suggests that the Antarctic form may be a different species but they are morphologically very similar. Also recorded from the Cretaceous Chalk and Gault of England by Parker and Jones (1865), who suggest it is an abbreviated form of *Textularia annectens*, which is commonly found within the Cretaceous.

Family **Pseudobolivinidae** Wiesner, 1931

Genus *Pseudobolivina* Wiesner, 1931

Pseudobolivina antarctica Wiesner, 1931 (Fig. 10:8)

1931 *Pseudobolivina antarctica* Wiesner: 99, pl. 21, figs. 257–258.
1975 *Pseudobolivina antarctica* Wiesner; Anderson: 78, pl. 3, fig. 4.
1981 *Pseudobolivina antarctica* Wiesner; Milam & Anderson: 305, pl. 3, fig. 7.
1990 *Pseudobolivina antarctica* Wiesner; Mackensen et al.: 258, pl. 5, fig. 7.
1996 *Pseudobolivina antarctica* Wiesner; Violanti, 55, pl. 4, figs. 12–13.

Material. Twenty-three specimens from 11 samples.

Description. Very small biserial test, tapered at the base; chambers rapidly enlarging as they are added to give broad maximum width. Wall comprises fine sand with little cement such that the surface is fairly rough. Sutures clearly visible and slightly depressed. Aperture loop-shaped extending up the face of the final chamber.

Occurrence. Originally described from Antarctica (Wiesner, 1931) and subsequently recorded in Recent sediments from a number of locations on the Antarctic shelf (Anderson, 1975; Milam and Anderson, 1981; Mackensen et al., 1990; Violanti, 1996).

Remarks. *Pseudobolivina antarctica* is also described in Igarashi et al. (2001) and Majewski (2013). However, the slit-like aperture shown by these authors does not agree with the type description, suggesting it has been incorrectly assigned (these specimens may be *Textularia antarctica*).

Family **Trochamminidae** Schwager, 1877

Subfamily **Trochammininae** Schwager, 1877

Genus *Portatrochammina* R. J. Echols, 1971

Portatrochammina antarctica weisneri (Parr, 1950) (Fig. 10:14–16)

1950 *Trochammina wiesneri* Parr: 279, pl. 5, fig. 14.
1975 *Portatrochammina wiesneri* (Parr); Anderson: 92, pl. 3, fig. 5.
1988 *Portatrochammina antarctica wiesneri* (Parr); Brönnimann & Whittaker: 68, figs. 25D–F, 26H–K, 27D–I.

1994 *Portatrochammina antarctica* (Parr); Ishman & Domack: 150, pl. 1, fig. 5.
1996 *Portatrochammina antarctica* (Parr); Violanti: 55, pl. 4, figs. 14–15.
2001 *Portatrochammina antarctica antarctica* (Parr); Igarashi et al.: 145, pl. 4, fig. 6.
2004 *Portatrochammina antarctica* (Parr); Murray & Pudsey: 71, pl. 1, figs. 14–16.
2009 *Portatrochammina antarctica* (Parr); Majewski & Anderson: 138, fig. 3.
2013 *Portatrochammina antarctica* (Parr); Majewski: 178, fig. 6(4).

Material. Overall, 383 specimens from 31 samples.

Description. Low, trochospiral test of approximately 17 chambers, slightly convex on the spiral side and shallowly concave on the umbilical side; three whorls with five chambers in the final whorl. Well-defined, moderately depressed sutures producing slightly lobate outline. Periphery sub-acute in edge view. Aperture covered by a large umbilical flap that covers much of the umbilical depression (diagnostic of this genus); parts of the apertural flaps of preceding chambers also visible. Agglutinated, imperforate wall, coarser on spiral side. Yellowish-brown colour that is markedly darker (almost reddish) in earlier chambers.

Occurrence. Originally described from Antarctica (Parr, 1950) and subsequently recorded from around Antarctica (Anderson, 1975; Brönnimann and Whittaker, 1988; Ishman and Domack, 1994; Violanti, 1996; Igarashi et al., 2001; Murray and Pudsey, 2004; Majewski and Anderson, 2009; Majewski, 2013).
Remarks. *Portatrochammina antarctica wiesneri* (Parr) can be distinguished from *Portatrochammina antarctica antarctica* (Parr) by its flatter, smoother test and subacute peripheral margin.

Subfamily **Polystomammininae** Brönnimann & Beurlen, 1977

Genus *Deuterammina* Brönnimann, 1976

Deuterammina scoresbyi Brönnimann & Whittaker, 1988
(Fig. 10:11–12)

1988 *Deuterammina scoresbyi* Brönnimann & Whittaker: 116, fig. 43(A–J).

Material. Overall, 207 specimens from 26 samples.

Description. Low trochospiral test, becoming planispiral in the final whorl; spiral side slightly depressed centrally; deep wide umbilical depression. Sutures distinct, straight, radial, slightly depressed; 20 chambers including the proloculus arranged in three whorls; six to seven slightly inflated chambers in the final whorl. Primary aperture interiomarginal, sub-peripheral loop-shape that widens towards the spiral side with a lip; secondary aperture at umbilical tip of chamber, may have a lip; both apertures present on every chamber. Agglutinated, imperforate wall.

Occurrence. Originally described from the Bellingshausen Sea and the South Sandwich Islands (Brönnimann and Whittaker, 1988).

Remarks. Brönnimann and Whittaker (1988) describe the wall as being almost entirely composed of barite spherules/ovoids. This is not the case in the specimens described here, although some ovoids were observed. Additionally the specimens described here have six to seven chambers in the final whorl, rather than the eight described in Brönnimann and Whittaker (1988).

Subfamily **Trochamminellinae** Brönnimann, Zaninetti & Whittaker, 1983

Genus *Pseudotrochammina* Frerichs, 1969

***Pseudotrochammina* sp. 1**
(Fig. 11:1)

Material. Overall, 182 specimens from 21 samples.

Description. Low trochospiral test; globular chambers that rapidly increase in size; four in final whorl. Depressed sutures; smoothly finished, finely agglutinated wall; areal elongate slit aperture located on the umbilical side but not in the umbilicus.

Family **Cyclamminidae** Marie, 1941

Subfamily **Cyclammininae** Marie, 1941

Genus *Cyclammina* Brady, 1879

Cyclammina* cf. *contorta Pearcey, 1914
(Fig. 11:2)

1914 *Cyclammina contorta* Pearcey: 1009, pl. 2, figs. 5–7.

Material. One specimen from one sample.

Description. Very large, planispiral, involute, somewhat compressed test; rounded periphery; very slightly lobulate margin. Numerous chambers (ca. 15) in the final whorl; sutures straight. Finely agglutinated, surface smooth, slightly iridescent. Aperture appears to be an interiomarginal, equatorial low arch, although this is poorly preserved on the only specimen found in this study. Apertural face of the final

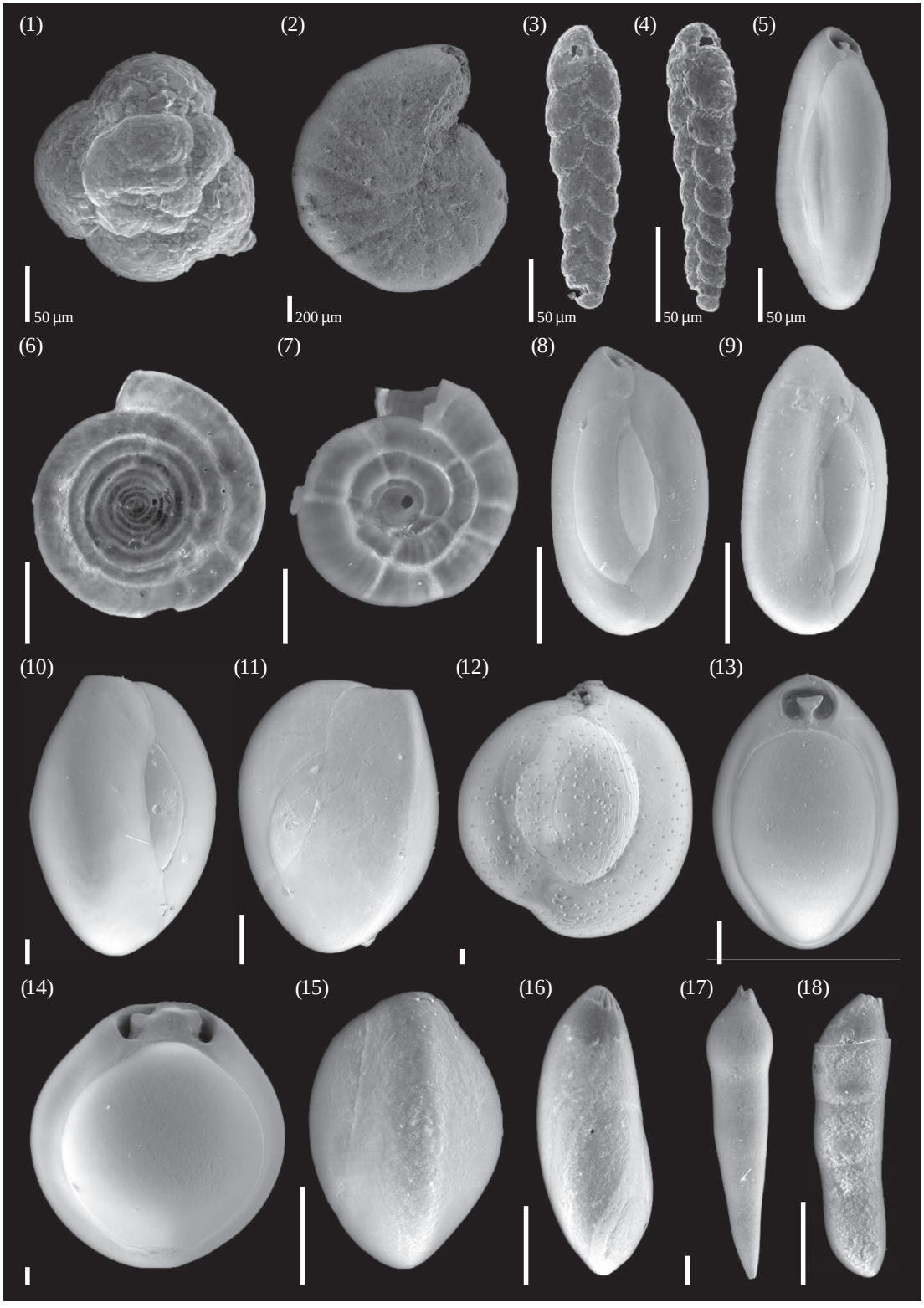


Figure 11. (1) *Pseudotrochammina* sp. 1 (BC737 (D) 0–1 cm). (2) *Cyclammina* cf. *contorta* Pearcey (BC667). (3–4) *Textularia earlandi* Parker (GC666_002). (5 and 8–9) *Quinqueloculina* cf. *occidentalis* Bailey (BC738). (6–7) *Cornuspira antarctica* Rhumbler (BC671; GC666_002). (10–11) *Quinqueloculina seminula* (Linnaeus) (BC737 (D) 0–1 cm; BC737 (D) 3–4 cm). (12) *Quinqueloculina* cf. *sublineata* (Brady) (BC671). (13) *Pyrgo patagonica* (d'Orbigny) (GC673_544). (14) *Pyrgo* cf. *subpisum* Parr (1950) (GC673_544). (15) *Triloculina* sp. (BC737 (D) 0–1 cm). (16) ? *Astacolus* sp. (BC671). (17–18) *Laevidentalina communis* (d'Orbigny) (GC666_002; BC737 (D) 3–4 cm). (Scale bar 100 µm unless otherwise indicated.)

chambers much more coarsely agglutinated with a rough surface; no evidence of additional apertures.

Occurrence. *Cyclammina contorta* Pearcey was originally described from the Weddell Sea, Antarctica.

Remarks. The species described here differs only in its sutural characteristics, being straighter and less dark in colour.

Family **Textulariidae** Ehrenberg, 1838

Subfamily **Textulariinae** Ehrenberg, 1838

Genus *Textularia* Defrance, 1824

Textularia earlandi Parker, 1952
(Fig. 11:3–4)

1933 *Textularia tenuissima* Earland: 95, pl. 3, figs. 21–30.
1952 *Textularia earlandi* Parker: 458 (see synonymy).
1996 *Textularia earlandi* Parker; Violanti: 57, pl. 5, figs. 13–14.
2010 *Textularia tenuissima* Earland; Majewski: 65, fig. 2(2).

Material. Forty-nine specimens from 18 samples.

Description. Very small, delicate, elongate test. Initial chambers coiled in both microspheric (tapered end) and megalospheric (rounded end) forms, becoming biserial. Numerous subquadrate, rounded chambers that enlarge slightly towards the terminal end. Distinct, slightly depressed sutures. Aperture a low interiomarginal arch on the face of the final chamber. Fairly smooth wall comprising fine grains with little cement visible.

Occurrence. Originally described from South Georgia (Earland, 1933); subsequently recorded from the Ross Sea (Violanti, 1996) and the Antarctic Peninsula (Majewski, 2010).

Remarks. Originally described from South Georgia as *Textularia tenuissima* Earland, this was however preoccupied by *Textularia tenuissima* Häusler 1881. Therefore, Parker (1952) proposed the new name *Textularia earlandi*. Morphologically it is very similar to *Textularia elegans* Lacroix, found in the Mediterranean.

Family **Cornuspiridae** Schultze, 1854

Subfamily **Cornuspirinae** Schultze, 1854

Genus *Cornuspira* Schultze, 1854

Cornuspira antarctica Rhumbler in Wiesner, 1931
(Fig. 11:6–7)

1931 *Cornuspira antarctica* Rhumbler in Wiesner: 101, pl. 14, figs. 164–166.

Material. Two specimens from two samples.

Description. Discoidal test comprising two chambers, the globular proloculus and the planispirally enrolled, undivided, near-evolute second chamber. Calcareous, imperforate, porcellaneous wall with transverse growth lines. Aperture simple opening at end of tube.

Occurrence. Originally described from Antarctica (Wiesner, 1931).

Family **Hauerinidae** Schwager, 1876

Subfamily **Hauerininae** Schwager, 1876

Genus *Quinqueloculina* d'Orbigny, 1826

Quinqueloculina* cf. *occidentalis Bailey, 1851
(Fig. 11:5 and 11:8–9)

1851 *Quinqueloculina occidentalis* Bailey: 13, figs. 46–48.
2013 *Quinqueloculina* sp. Majewski: 179, fig. 7 (6).
2013 *Quinqueloculina seminula* (Linnaeus); Rodrigues et al.: 214, fig. 3 (6–7).

Material. Twenty-one specimens from seven samples.

Description. Small, elongate, subovate test, quinqueloculine chamber arrangement, rounded periphery, long, narrow chambers that rapidly increase in size as added. Calcareous, smooth, thin, porcellaneous wall; distinct, somewhat depressed sutures; aperture a terminal high arch with a small tooth.

Occurrence. *Quinqueloculina occidentalis* Bailey was originally described from the North Atlantic. Similar specimens have been recorded from Antarctica (Majewski, 2013; Rodrigues et al., 2013) but never previously assigned to *Q. occidentalis* Bailey.

Remarks. The specimens described here appear quite similar to *Quinqueloculina occidentalis* Bailey, although the very brief original description hinders any certainty in this designation. The specimens also share a number of features with *Triloculinella antarctica* Kennett, but the absence of a broad apertural flap indicates that this species does not belong within the genus *Triloculinella*; its placement within this genus by Majewski (2005) is therefore incorrect.

Quinqueloculina seminula (Linnaeus, 1758)
(Fig. 11:10–11)

1758 *Serpula seminulum* Linnaeus: 786, pl. 2, fig. 1.
1932a *Miliolina seminulum* (Linnaeus); Heron-Allen & Earland: 313, pl. 6, figs. 25–40.
1981 *Quinqueloculina seminulum* (Linnaeus); Milam and Anderson: 307, pl. 5, fig. 5.
1994 *Quinqueloculina seminulum* (Linnaeus); Jones: 21, pl. 5, fig. 6, text figs. 2–3.
2013 *Quinqueloculina seminulum* (Linnaeus); Rodrigues et al.: 214, fig. 3 (6–7).

Material. Two specimens from two samples.

Description. Slightly compressed ovate test, rounded at base, more angular at apertural end, rounded triangular in section. Quinqueloculine coiling; five chambers visible in final whorl, four from one side and three from the other; more convex on the four-chambered side. Calcareous, imperforate, porcellaneous wall; smooth surface. Large, terminal, horseshoe-shaped aperture with a small bifid tooth.

Occurrence. Recorded from the North Atlantic in the *Challenger* material (Jones, 1994) and from Antarctica by Milam and Anderson (1981).

Quinqueloculina* cf. *sublineata (Brady, 1884)
(Fig. 11:12)

1884 *Miliolina circularis* var. *sublineata* Brady: 169, pl. 4, fig. 7.
1994 *Triloculinella sublineata* (Brady); R. W. Jones: 20, pl. 4, fig. 7.

Material. One specimen from one sample.

Description. Test near-circular in outline; compressed, rounded section. Quinqueloculine coiling; five chambers visible in final whorl; calcareous, imperforate, porcellaneous wall; terminal, low, broad, arch-shaped aperture. Surface ornamented with very delicate, longitudinal striae and large pits.

Remarks. The absence of an apertural flap in the specimen described here, and in the image of Jones (1994), plus the presence of five chambers in the final whorl, leads us to place it within *Quinqueloculina*. This specimen differs from the specimen figured in Brady (1884) and Jones (1994) in the presence of large pits that cover its surface.

Genus *Pyrgo* Defrance, 1824

Pyrgo* cf. *subpisum Parr, 1950
(Fig. 11:14)

1950 *Pyrgo subpisum* Parr: 297, pl. 7, figs. 5–6.

Material. One specimen from one sample.

Description. Large, subglobular test, near-circular from front, rounded periphery; two chambers visible in final whorl (biloculine). Calcareous, imperforate, porcellaneous wall; large, ovate, terminal aperture, surrounded by a thickened, raised rim; unusual large tooth with three lobes.

Occurrence. *Pyrgo subpisum* Parr was described from a number of locations in the southern Indian Ocean.

Remarks. The specimen described here is very similar to *Pyrgo subpisum* Parr, differing only in the unusual tooth characteristics.

Pyrgo patagonica (d'Orbigny, 1839b)
(Fig. 11:13)

1839b *Biloculina patagonica* d'Orbigny: 65, pl. 3, figs. 15–17.
1932a *Biloculina patagonica* d'Orbigny; Heron-Allen & Earland: 311, pl. 6, figs. 4–6.
2004 *Pyrgo patagonicum* (d'Orbigny); Mikhalevich: 188, pl. 3, figs. 6–7.

Material. One specimen from one sample.

Description. Large, subglobular test, ovate from front, rounded periphery; two inflated chambers visible in final whorl (biloculine). Calcareous, imperforate, porcellaneous, think wall, with a smooth, shiny surface; medium, round, terminal aperture, surrounded by a small, thickened, raised rim; bifid tooth.

Occurrence. Originally described from the Patagonian coast (d'Orbigny, 1839b).

Genus *Triloculina* d'Orbigny, 1826

***Triloculina* sp.**
(Fig. 11:15)

Material. Twenty-three specimens from 11 samples.

Description. Ovate text, triangular in section with rounded corners; triloculine, three chambers visible in final whorl. Chambers slightly inflated; sutures somewhat depressed; calcareous, imperforate, porcellaneous wall; smooth surface. Terminal, rounded aperture; no tooth visible.

Family **Nodosariidae** Ehrenberg, 1838

Subfamily **Nodosariinae** Ehrenberg, 1838

Genus *Laevidentalina* Loeblich & Tappan, 1986

Laevidentalina communis (d'Orbigny, 1826)
(Fig. 11:17–18)

1826 *Nodosaria (Dentalina) communis* d'Orbigny: 254 (no type figure).
1996 *Dentalina communis* (d'Orbigny); Violanti: 59, pl. 6, fig. 11.
2005 *Dentalina communis* (d'Orbigny); Majewski: 201, fig. 20(2–3).
2013 *Laevidentalina communis* (d'Orbigny); Majewski: 181, fig. 9(2).

Material. Two specimens from two samples.

Description. Elongate, slightly arcuate test; fusiform, apiculate proloculus, followed by a number of uniserially arranged chambers; straight, horizontal sutures. Calcareous, hyaline, finely perforate wall; smooth surface; multilamellar, terminal aperture damaged in our specimens.

Occurrence. Recorded from Antarctica in Recent sediments (Violanti, 1996; Majewski, 2005, 2013)

Remarks. Placed within the genus *Laevidentalina* due to the absence of costae.

Genus *Lotostomoides* Hayward & Kawagata, 2012

Lotostomoides calomorphum (Reuss, 1866)
(Fig. 12:1–2)

1866 *Nodosaria (Nodosaria) calomorpha* Reuss: 129, pl. 1, figs. 15–19.
1933 *Nodosaria calomorpha* Reuss; Earland: 117, pl. 4, fig. 19.
1994 *Glandulonodosaria calomorpha* (Reuss); Jones: 72, pl. 61, figs. 23–26.

Material. Six specimens from four samples.

Description. Small, elongate, slightly arcuate test comprising two to four sausage-shaped chambers. Simple, round, terminal aperture. Thin, hyaline, calcareous wall, with smooth surface; sutures straight and horizontal.

Occurrence. Reported from South Georgia (Earland, 1933) and the South Atlantic (Jones, 1994).

Genus *Nodosaria* Lamarck, 1812

Nodosaria simplex Silvestri, 1872
(Fig. 12:3–4)

1872 *Nodosaria simplex* Silvestri: 95, pl. 11, figs. 268–272.
1994 *Nodosaria simplex* Silvestri; Jones: 73, pl. 62, figs. 4–5.

Material. Two specimens from two samples.

Description. Small, slightly elongate test comprising two spherical/ovate chambers of approximately the same size; straight, depressed suture between the chambers. Both chambers narrow terminally: the upper towards the aperture, whilst the lower becomes apicate. Calcareous, hyaline, perforate wall, smooth and unornamented. Terminal, rounded aperture with radiating grooves.

Family **Vaginulinidae** Reuss, 1860

Subfamily **Lenticulininae** Chapman, Parr & Collins, 1934

Genus *Lenticulina* Lamarck, 1804

Lenticulina asterizans Parr, 1950
(Fig. 12:5)

1950 *Lenticulina (Robulus) asterizans* Parr: 322, pl. 11, figs. 9–10.

Material. One specimen from one sample.

Description. Planispiral, involute, lenticular test; narrow rounded keel on periphery; eight chambers in final whorl. Limbate, flush sutures; triangular, slightly rounded apertural face; calcareous, hyaline, smooth wall. Aperture damaged in the specimen described here.

Occurrence. Originally described from Antarctica (Parr, 1950).

Subfamily **Marginulininae** Wedekind, 1937

Genus *Astacolus* de Montfort, 1808

? ***Astacolus* sp.**
(Fig. 11:16)

Material. One specimen from one sample.

Description. Elongate, flattened test; low, broad chambers added on a slightly curved axis; strongly oblique, curved sutures; rounded periphery; smooth, perforate, calcareous wall; terminal, radiate aperture.

Family **Lagenidae** Reuss, 1862

Genus *Lagena* Walker & Jacob in Kanmacher, 1798

Lagena substriata Williamson, 1848
(Fig. 12:6–7)

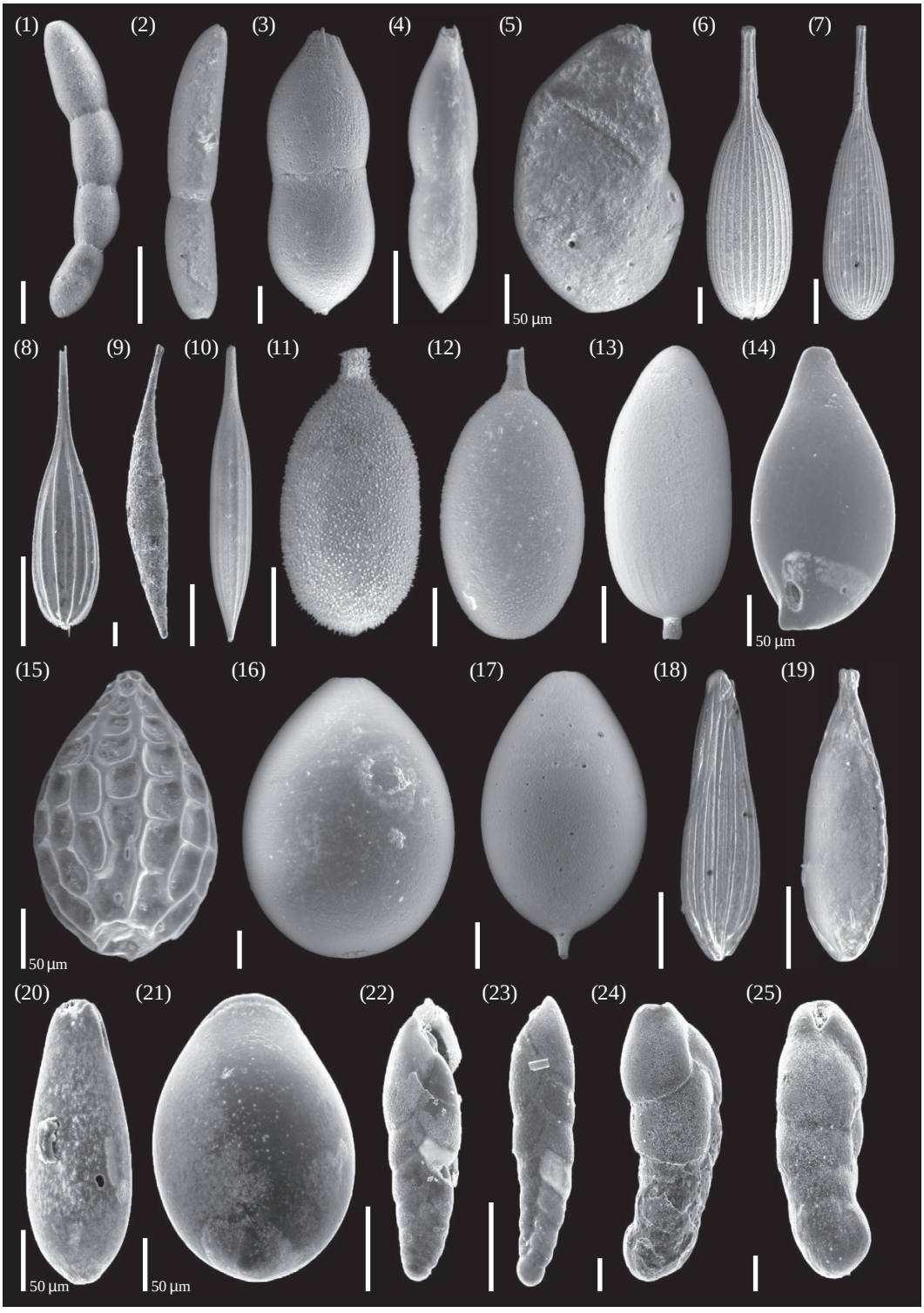


Figure 12. (1–2) *Lotostomoides calomorphum* (Reuss) (BC737 (D) 2–3 cm). (3–4) *Nodosaria simplex* Silvestri (GC666_119; GC666_159). (5) *Lenticulina asterizans* Parr (GC666_127). (6–7) *Lagena substriata* Williamson (BC737 (D) 4–5 cm; BC738 (D) 5–6 cm). (8) *Lagena multilatera* McCulloch (GC666_002). (9) *Hyalinonetrion* cf. *gracillimum* (Seguenza) (GC666_295). (10) *Procerolagena distoma* (Parker and Jones M.S.) (GC666_127). (11) *Pygmaeoseistron hispidulum* (Cushman) (BC738). (12) *Pygmaeoseistron* sp. (BC738 (D) 2–3 cm). (13) *Oolina* spp. (BC738 (D) 8–9 cm). (14) *Fissurina* sp. 1 (GC666_002). (15) *Favulina squamosa* (Montagu) (GC666_124). (16–17) *Oolina globosa* (Montagu) (BC737; BC738 (D) 3–4 cm). (18) *Vasicostella striatopunctata* (Parker and Jones) (BC660). (19) *Fissurina subformosa* Parr (BC737 (D) 2–3 cm). (20) *Fissurina* sp. 2 (GC666_002). (21) *Parafissurina fusiformis* Wiesner (GC666_002). (22) *Bolivinellina earlandi* (Parr) (GC666_002). (23) *Bolivinellina pseudopunctata* (Höglund) (GC666_002). (24–25) *Cassidulinoides parkerianus* (Brady) (GC666_002). (Scale bar 100 µm unless otherwise indicated.)

1848 *Lagena substriata* Williamson: 15, pl. 2, fig. 12.
1994 *Lagena substriata* Williamson; Loeblich & Tappan: 79, pl. 138, figs. 1–5.
2001 *Lagena substriata elegantula* R. W. Jones; Igarashi et al.: 148, pl. 7, fig. 5.
2009 *Lagena weisneri* Parr; Majewski & Anderson: 139, fig. 4.

Material. Four specimens from three samples.

Description. Unilocular, ovate test that may be significantly elongated. Calcareous, hyaline wall ornamented with numerous delicate, parallel, longitudinal costae. Simple aperture with phialine lip at the end of a long neck. Some of the costae continue up the neck, either straight up or spiralling around the neck. Some specimens also present a honeycomb pattern on the base of the test.

Occurrence. Originally described from the Recent of England (Williamson, 1848), this species has also been described from the Timor Sea (Loeblich and Tappan, 1994) and Antarctica (Igarashi et al., 2001; Majewski and Anderson, 2009).

Lagena multilatera McCulloch, 1977
(Fig. 12:8)

1977 *Lagena multilatera* McCulloch: 40, pl. 50, fig. 5.
1994 *Lagena multilatera* McCulloch; Jones: 65, pl. 58, figs. 2–3, 7–8, 22–24.

Material. Five specimens from three samples.

Description. Unilocular, fusiform test. Calcareous, hyaline wall; approximately eight longitudinal costae, high, narrow, tapering, some of which continue onto neck. Small, round, terminal aperture produced on a long delicate neck.

Occurrence. McCulloch (1977) described this species from deep water off Bikini Atoll, Pacific Ocean; subsequently recorded from the South Pacific and Southern Ocean (Jones, 1994).

Genus *Hyalinonetrion* Patterson & Richardson, 1987

Hyalinonetrion* cf. *gracillimum (Seguenza, 1862)
(Fig. 12:9)

1862 *Amphorina gracillima* Seguenza: 51, pl. 1, fig. 37.
1994 *Procerolagena gracillima* (Seguenza); Jones: 62, pl. 56, figs. 19–22, 24–29.
2005 *Hyalinonetrion gracillima* (Seguenza); Majewski: 201, fig. 20(7).
2015 *Procerolagena gracillima* (Seguenza); Setoyama & Kaminski: 23, fig. 8(28).

Material. Eighteen specimens from five samples.

Description. Fusiform, elongate, unilocular test that slowly tapers at the base. Hyaline, calcareous, unornamented wall. Simple aperture with a phialine lip, at the end of a long, tapering neck.

Occurrence. Originally described from the Miocene of Italy (Seguenza, 1862); subsequently recorded from Recent sediments from Antarctica (Majewski, 2005), the Southern Ocean (Jones, 1994), and the Bering Sea (Setoyama and Kaminski, 2015).

Remarks. Whilst Jones (1994) retained this species in *Procerolagena,* as he considered *Hyalinonetrion* to be a junior synonym of *Procerolagena*, here we place it in *Hyalinonetrion* due to the absence of any longitudinal ornamentation (Loeblich and Tappan, 1988).

Genus *Procerolagena* Puri, 1954

Procerolagena distoma (Parker & Jones M. S. in Brady, 1864)
(Fig. 12:10)

1864 *Lagena distoma* Parker & Jones in Brady: 467, pl. 48, fig. 6.
? 1981 *Lagena sulcata* var. *distomapolita* Milam & Anderson: 308, pl. 6, fig. 2.
1994 *Hyalinonetrion distoma* (Parker & Jones); Loeblich & Tappan: 77, pl. 137, fig. 9.

Material. Thirteen specimens from nine samples.

Description. Unilocular, elongate test with nearly parallel sides in the central part of the test which tapers towards apiculate ends. Calcareous wall ornamented by delicate longitudinal striae.

Occurrence. Originally described from the Shetlands (Brady, 1864); subsequently recorded from Antarctica (Milam and Anderson, 1981) and the Timor Sea (Loeblich and Tappan, 1994).

Remarks. Loeblich and Tappan (1994) assign this species to the genus *Hyalinonetrion*. However, this designation is in conflict with the genus description in Loeblich and Tappan (1988) defining *Hyalinonetrion* as unornamented.

Genus *Pygmaeoseistron* Patterson & Richardson, 1987

Pygmaeoseistron hispidulum (Cushman, 1913)
(Fig. 12:11)

1913 *Lagena hispidula* Cushman: 14, pl. 5, figs. 2–3.

2013 *Pygmaeoseistron hispidulum* (Cushman 1913); Majewski: 180, fig. 8(11).

Material. Two specimens from two samples.

Description. Unilocular flask-shaped/ovoid test that rapidly narrows to a tubular neck (delicate and often broken, as in figured specimen), evenly covered in fine hispid ornamentation.

Occurrence. Originally described from the North Pacific (Cushman, 1913); also recorded from the Amundsen Sea (Majewski, 2013).

***Pygmaeoseistron* sp.**
(Fig. 12:12)

Material. One specimen from one sample.

Description. Unilocular, ovoid test with a narrow, tubular neck; sporadic pustulose ornamentation.

Remarks. Bears some similarity to *Pygmaeoseistron islandicum* (Jones, 1994).

Family **Ellipsolagenidae** A. Silvestri, 1923

Subfamily **Oolininae** Loeblich & Tappan, 1961

Genus *Favulina* Patterson & Richardson, 1987

Favulina squamosa (Montagu, 1803)
(Fig. 12:15)

1803 *Vermiculum squamosum* Montagu: 526, pl. 14, fig. 2.
1994 *Oolina squamosa* (Montagu); Jones: 66, pl. 58, figs. 28–32.
2015 *Oolina squamosa* (Montagu); Setoyama & Kaminski: 23, figs. 7(14), 8(31).

Material. Two specimens from two samples.

Description. Unilocular, ovate test, circular in section, narrowing towards the apertural end. Calcareous, hyaline wall, ornamented with roughly perpendicular vertical costae. Horizontal costae join the vertical to form loosely hexagonal shapes. Round aperture, terminal on a short neck with a rounded lip.

Occurrence. Originally described from Britain (Montagu, 1803); also recorded from the South Pacific (Jones, 1994) and the Bering Sea (Setoyama and Kaminski, 2015).

Remarks. The specimens figured here most closely resemble the specimen from Plate 58, fig. 32, of Jones (1994) from the *Challenger* material that has previously been variously assigned to *Lagena hexagona* (Williamson) by Brady (1881) and Thalmann (1932) and *Oolina hexagona* (Williamson) by Barker (1960), Hermelin (1989), and Van Marle (1991). The ornamentation on our specimens forms roughly perpendicular lines, a feature not seen in *Favulina hexagona* (Williamson), and it has therefore been assigned to *Oolina squamosa* (Montagu), following Knight (1986), which is then assigned to the genus *Favulina* following Clark et al. (1994).

Genus *Oolina* d'Orbigny, 1839b

Oolina globosa (Montagu, 1803)
(Fig. 12:16–17)

1803 *Vermiculum globosum* Montagu: 523, pl. 1, fig. 8.
1994 *Oolina globosa* (Montagu); Jones: 62, pl. 56, figs. 1–3, 15–16.

Material. Two specimens from two samples.

Description. Unilocular, tear-drop shaped test; may have apiculate base. Calcareous, hyaline, smooth wall. Terminal, simple, round aperture, with an entosolenian tube that extends over half the length of the chamber and flares dramatically at the end.

Occurrence. Recorded from the Southern Ocean (Jones, 1994).

Remarks. Following Jones (1994), specimens with an apiculate base are not considered to be distinct from *Oolina globosa* (Montagu).

***Oolina* spp.**
(Fig. 12:13)

Material. Eight specimens from four samples.

Description. Included in this group any unilocular, ovate tests with calcareous, hyaline, smooth walls, an apiculate base, and a rounded terminal aperture that have not been assigned to *Oolina globosa* (Montagu).

Genus *Vasicostella* Patterson & Richardson, 1987

Vasicostella striatopunctata (Parker & Jones, 1865)
(Fig. 12:18)

1865 *Lagena sulcata* Walker & Jones var. *striatopunctata* Parker & Jones: 350, pl. 13, figs. 25–27.
2001 *Vasicostella striatopunctata* (Parker & Jones); Igarashi et al.: 148, pl. 8, fig. 5.
2013 *Vasicostella* sp. Majewski: 180, fig. 8 (8).

Material. One specimen from one sample.

Description. Unilocular, flask-like, compressed test; carinate periphery. Calcareous, hyaline wall, ornamented with strong longitudinal costae that appear striped, perpendicular to their length, due to differences in the optical properties of their calcite (only visible with light microscopy). Rounded, terminal aperture, with a slight lip and a short, centrally placed entosolenian tube.

Occurrence. Parker and Jones (1865) originally described this species from Greenland, the Red Sea, the South Atlantic, and the Indian Ocean. Igarashi et al. (2001) subsequently described it from Antarctica.

Remarks. Le Coze and Hayward (2017) places *Lagena striatopunctata* Parker & Jones within the genus *Cushmanina*. However, we believe that, based on the type figures, this classification is incorrect. The compressed nature of the test and the lack of an elongate neck suggest that this species should be placed within the genus *Vasicostella*. The specimen described here and that of Igarashi et al. (2001) also reveal the carinate nature of this species, further supporting this classification.

Subfamily **Ellipsolageninae** A. Silvestri, 1923

Genus *Fissurina* Reuss, 1850

Fissurina subformosa Parr, 1950
(Fig. 12:19)

1950 *Fissurina subformosa* Parr: 313, pl. 9, fig. 9.
1996 *Lagena subformosa* (Parr); Violanti: 43, pl. 7, fig. 3.

Material. Three specimens from three samples.

Description. Small, pyriform test, slightly compressed, tapering towards a long neck; keel extends from the neck around the test, with two tabulated supplementary keels that create a "crimped" appearance. Circular, terminal aperture; straight entosolenian tube extends centrally to approximately one third the length of the chamber.

Occurrence. Previously recorded from Antarctica (Parr, 1950; Violanti, 1996).

Remarks. This species can be distinguished from *F. formosa (Lagena Formosa* Schwager) by the supplementary keels.

***Fissurina* sp. 1**
(Fig. 12:14)

Material. Seven specimens from four samples.

Description. Unilocular, pyriform test, with pointed protuberance towards basal end; circular section. Smooth, hyaline, calcareous wall; terminal, oval aperture within a slightly depressed fissure at the apex of the test.

***Fissurina* sp. 2**
(Fig. 12:20)

Material. Thirty-one specimens from 15 samples.

Description. Elongate, compressed test, broadening towards the base; rounded ends; base somewhat produced; oval section. Smooth, hyaline, calcareous wall; terminal, slit-like aperture within a significantly depressed fissure at the apex of the test.

Remarks. Bears some similarity to the Oligocene *Fissurina oblonga* Reuss and to *Parafissurina lateralis* (Cushman). May have previously been recorded from the Weddell Sea by Anderson (1975) as *Parafissurina lateralis* (Cushman).

Subfamily **Parafissurininae** R. W. Jones, 1984

Genus *Parafissurina* Parr, 1947

Parafissurina fusiformis Wiesner, 1931
(Fig. 12:21)

1931 *Parafissurina fusiformis* Wiesner: 126, pl. 24, fig. j.
1996 *Parafissurina fusiformis* Wiesner; Violanti, 62, pl. 8, fig. 8.
2001 *Parafissurina fusiformis* Wiesner; Igarashi: 151, pl. 9, fig. 5.
2005 *Parafissurina fusiformis* Wiesner; Majewski: 203, fig. 22(1–2).

Material. Thirty-seven specimens from 14 samples.

Description. Small test, ovate in front view; slightly compressed, rounded periphery. Aperture an elongate slit protected by a protruding hood, with a large lip opposite the hood. Entosolenian tube extends centrally along inner surface of chamber, flaring at the end.

Occurrence. Originally described from high southern latitudes (Wiesner, 1931) and later from other Antarctic localities (Violanti, 1996; Majewski, 2005).

Family **Bolivinidae** Glaessner, 1937

Genus *Bolivinellina* Saidova, 1975

Bolivinellina earlandi (Parr, 1950)
(Fig. 12:22)

1950 *Bolivina earlandi* Parr: 339, pl. 12, fig. 16.
1996 *Bolivina pseudopunctata* Höglund; Violanti: 65, pl. 9, fig. 1.
2001 *Bolivinellina earlandi* (Parr); Igarashi et al.: 153, pl. 10, fig. 5.
2013 *Bolivinellina earlandi* (Parr); Majewski: 181, fig. 9(4).

Material. Seventy specimens from 19 samples (for *Bolivinellina* spp.).

Description. Elongate test, biserial throughout, oval in section. Chambers up to 12 in number, slightly inflated; strongly curved, slightly depressed sutures. Wall calcareous, hyaline, smooth; finely perforate in the lower half of the chamber, imperforate in the upper half. Narrow, comma-shaped aperture starting at the inner margin of the final chamber.

Occurrence. Parr (1950) described this species as widely distributed around Antarctica.

Remarks. Following Igarashi et al. (2001) and Majewski (2013), we have placed this species in the genus *Bolivinellina* due the lack of perforation in the upper half of the chambers.

Bolivinellina pseudopunctata (Höglund, 1947)
(Fig. 12:23)

1947 *Bolivina pseudopunctata* Höglund: 273, pl. 24, fig. 5, pl. 32, figs. 23–24.
2005 *Bolivina pseudopunctata* Höglund; Majewski: 203, fig. 22(6–7).
2013 *Bolivinellina pseudopunctata* (Höglund); Majewski: 181, fig. 9(3).

Material. Seventy specimens from 19 samples (for *Bolivinellina* spp.).

Description. Elongate, gently tapering test, biserial from a large globular proloculus, oval in section. Chambers distinct; up to 23 in number; slightly inflated; sutures strongly curved, slightly depressed. Wall calcareous, hyaline, smooth, finely perforate in the lower half of the chamber, imperforate in the upper half. Oval-shaped aperture with a double-folded tongue, starting at the inner margin of the final chamber.

Occurrence. Originally described from the Gullmar Fjord, Sweden (Höglund, 1947), this species has subsequently been described from Antarctica (Majewski, 2005, 2013).

Remarks. Following Majewski (2013) we have placed this species in the genus *Bolivinellina* due the lack of perforation in the upper half of the chambers. *B. pseudopunctata* can be distinguished from *B. earlandi* by the greater number of chambers, an oval-shaped aperture with a double-folded tongue, and a large globular proloculus.

Family **Cassidulinidae** d'Orbigny, 1839a

Subfamily **Cassidulininae** d'Orbigny, 1839a

Genus *Cassidulinoides* Cushman, 1927

Cassidulinoides parkerianus (Brady, 1881)
(Fig. 12:24–25)

1881 *Cassidulina parkeriana* Brady: 59, pl. 54, figs. 11–16.
1932a *Cassidulina parkeriana* Brady; Heron-Allen & Earland: 359, pl. 9, figs. 22–25.
1975 *Cassidulinoides parkerianus* (Brady); Anderson: 86, pl. 7, fig. 20.
2001 *Cassidulinoides parvus* (Hussey); Igarashi: 153, pl. 10, fig. 12.
2005 *Cassidulinoides parkerianus* (Brady); Majewski: 204, fig. 23(1–2).
2009 *Cassidulinoides parkerianus* (Brady); Majewski & Anderson: 139, fig. 4.
2013 *Cassidulinoides parkerianus* (Brady); Rodrigues et al.: 214, fig. 3 (4).

Material. Overall, 713 specimens from 32 samples.

Description. Crozier-shaped test, initially planispiral, rapidly uncoiling to become biserial; number of chambers in biserial section quite variable; biserial section cylindrical, straight or arcuate. Chambers subglobose, inflated, with small overlap at the periphery; sutures slightly depressed. Thick, calcareous, perforate, hyaline bi-multilamellar wall. Interiomarginal, loop-shaped aperture; subterminal.

Occurrence. Originally described from the South Pacific (Brady, 1881) and subsequently described from various locations around Antarctica (Heron-Allen and Earland, 1932a; Anderson, 1975; Igarashi et al., 2001; Majewski, 2005; Majewski and Anderson, 2009; Rodrigues et al., 2013).

Cassidulinoides porrectus (Heron-Allen and Earland, 1932a)
(Fig. 13:1–2)

1932a *Cassidulina crassa* d'Orbigny var. *porrecta* Heron-Allen & Earland, p. 358, pl. 9, figs. 34–37.
1981 *Cassidulinoides porrecta* (Heron-Allen & Earland); Milam & Anderson: 308, pl. 6, fig. 6.
1996 *Cassidulinoides porrectus* (Heron-Allen & Earland): Violanti: 65, pl. 9, figs. 2–3.

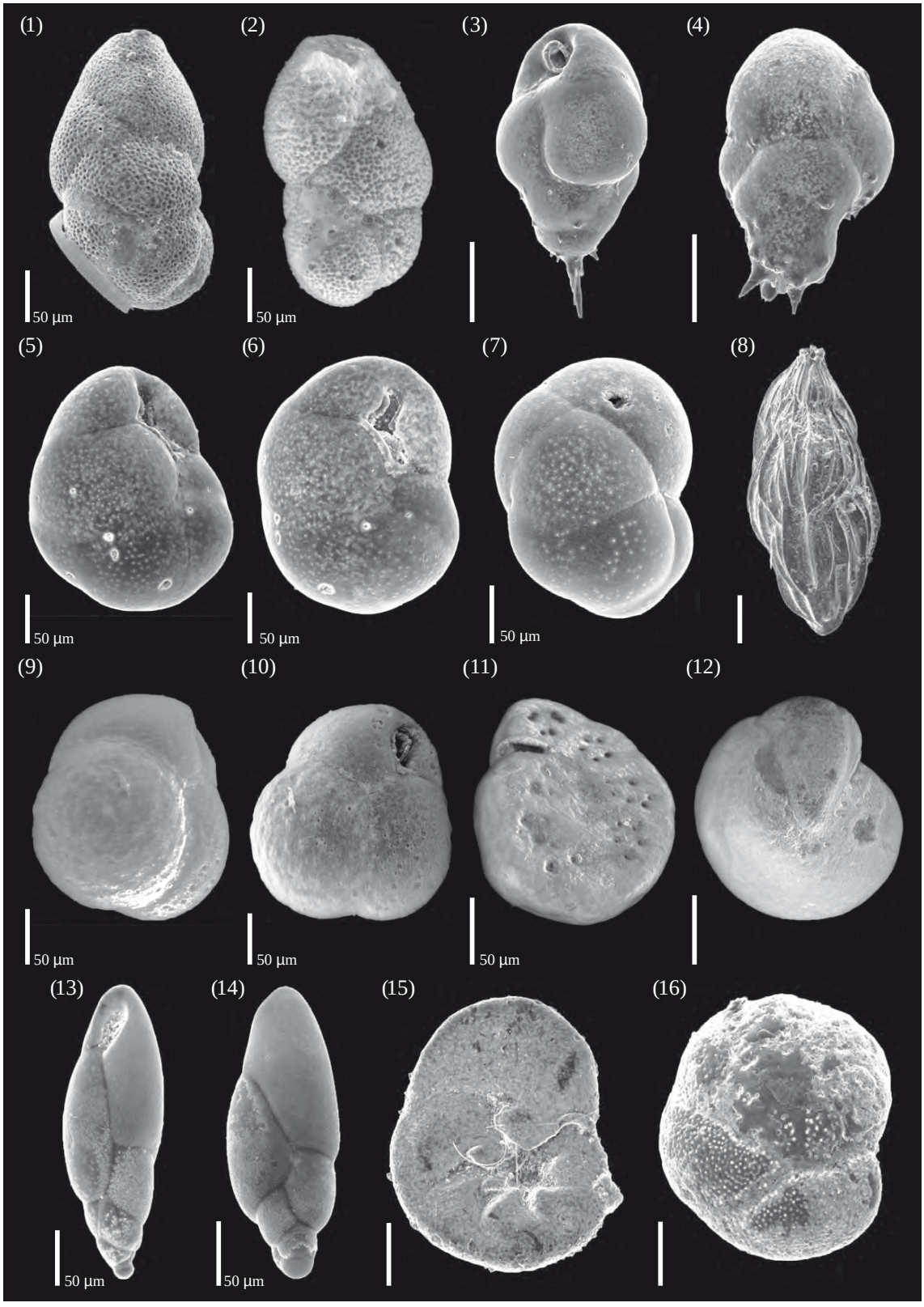


Figure 13. (1–2) *Cassidulinoides porrectus* (Heron-Allen and Earland) (GC666_002). (3–4) *Bulimina aculeata* d'Orbigny (GC666_002). (5–7) *Globocassidulina crassa* (d'Orbigny) subsp. *rossensis* Kennett (GC666_002). (8) *Trifarina earlandi* (Parr (GC666_002)). (9–10) *Bulimina* sp. 1 (GC666_119). (11–12) *Cibicides* sp. 1 (BC737; BC738 (D) 0–1 cm). (13–14) *Fursenkoina fusiformis* (Cushman) (GC666_002). (15–16) *Discorbis vilardeboanus* (d'Orbigny) (GC666_002). (14–16) *Nonionella bradii* (Chapman) (GC666_002). (Scale bar 100 µm unless otherwise indicated.)

2001 *Cassidulinoides porrectus* (Heron-Allen & Earland); Igarashi et al.: 153, pl. 10, fig. 11.
2005 *Cassidulinoides porrectus* (Heron-Allen & Earland); Majewski: 204, fig. 23(3).
2013 *Cassidulinoides porrectus* (Heron-Allen & Earland); Rodrigues et al.: p. 214, fig. 3 (3).

Material. Overall, 1452 specimens from 37 samples.

Description. Test small, planispirally enrolled in early stages, uncoiling to become biserial; commonly 2–4 chambers in the biserial part but can be as many as 10. Chambers subglobose, inflated, with small overlap at the periphery; sutures slightly depressed. Thick, calcareous, perforate, hyaline wall, covered in distinctive large pores. Interiomarginal, loop-shaped aperture, subterminal.

Occurrence. Originally described from various subantarctic locations (Heron-Allen and Earland, 1932a), subsequently in numerous additional Antarctic studies (Milam and Anderson, 1981; Violanti, 1996; Igarashi et al., 2001; Majewski, 2005; Rodrigues et al., 2013).

Genus *Globocassidulina* Voloshinova, 1960

Globocassidulina crassa* (d'Orbigny) subsp. *rossensis Kennett, 1967
(Fig. 13:5–7)

1967 *Globocassidulina crassa* (d'Orbigny) subsp. *rossensis* Kennett 134, pl. 11, figs. 4–6.
1981 *Globocassidulina crassa rossensis* Kennett; Milam & Anderson: 312, pl. 10, fig. 1.
1993 *Globocassidulina rossensis* Kennett; Mackensen et al.: 56, pl. 2, figs. 7–8.
1996 *Globocassidulina rossensis* Kennett; Violanti: p. 65, pl. 9, fig. 7.
2006 *Globocassidulina rossensis* Kennett; Hromic et al.: 124, pl. 1, fig. 5.

Material. Overall, 727 specimens from 32 samples.

Description. Oval to circular, involute, slightly compressed test; rounded, slightly lobulate, planispiral coil of biserial, inflated chambers that gradually increase in size; four to five pairs in the last whorl. Thin, smooth, calcareous wall. Aperture a narrow, interiomarginal slit with an aerial branch that extends perpendicular to the main slit approximately halfway up the apertural face, surrounded by a narrow rim.

Occurrence. Originally described from the Ross Sea (Kennett, 1967); subsequently described from other Antarctic locations (Milam and Anderson, 1981; Mackensen et al., 1993; Violanti, 1996; Hromic et al., 2006).

Remarks. Distinguished from other subspecies of *Globocassidulina crassa* (d'Orbigny) by an aerial branch that extends from the main part of the aperture.

Subfamily **Ehrenbergininae** Cushman, 1927

Genus *Ehrenbergina* Reuss, 1850

Ehrenbergina glabra Heron-Allen & Earland, 1922

1922 *Ehrenbergina hystrix* var. *glabra* Heron-Allen & Earland: 140, pl. 5, figs. 1–6.
1981 *Ehrenbergina glabra* Heron-Allen & Earland; Milam & Anderson: 311, pl. 9, fig. 7.
1990 *Ehrenbergina glabra* Heron-Allen & Earland; Mackensen et al.: 254, pl. 1, figs. 5–6.
1996 *Ehrenbergina glabra* Heron-Allen & Earland; Violanti: 65, pl. 9, fig. 9.
2001 *Ehrenbergina glabra* Heron-Allen & Earland; Igarashi et al.: 154, pl. 11, fig. 1.
2013 *Ehrenbergina glabra* Heron-Allen & Earland; Majewski: 182, fig. 10(13).

Material. Two specimens from one sample.

Description. Biserial test, initially enrolled rapidly uncoiling; lenticular in section with a convex dorsal side; flatter ventral side with a median furrow. Chambers are low and broad with considerable overlap at the peripheral midline. Spinose lateral margins; sutures curved, flush. Calcareous, smooth wall. Curved, elongate, slit-like aperture that runs parallel to the peripheral margin, perpendicular to the base of the apertural face.

Occurrence. Recorded from a number of locations around Antarctica (Milam and Anderson, 1981; Mackensen et al., 1990; Violanti, 1996; Igarashi et al., 2001; Majewski, 2013).

Remarks. Heron-Allen and Earland (1922) distinguished this species from *E. hystrix* Brady by the absence of spines on the early chambers, the more flattened oral face, the more marginal position of the aperture, and the near absence of striations around the aperture.

Family **Buliminidae** Jones in Griffith and Henfrey, 1875

Genus *Bulimina* d'Orbigny, 1826

Bulimina aculeata d'Orbigny, 1826
(Fig. 13:3–4)

1826 *Bulimina aculeata* d'Orbigny: 269 (no type figure).
1990 *Bulimina aculeata* d'Orbigny; Mackensen et al.: 255, pl. 2, figs. 1–3.

1993 *Bulimina aculeata* d'Orbigny; Mackensen et al.: 54, pl. 1, figs. 3–4.
1994 *Bulimina aculeata* d'Orbigny; Ishman & Domack: 152, pl. 2, fig. 8.
2001 *Bulimina aculeata* d'Orbigny; Igarashi et al.: 154, pl. 11, fig. 4.
2013 *Bulimina aculeata* d'Orbigny; Majewski: 181, fig. 9(8–9).

Material. Fifty-nine specimens from 20 samples.

Description. Elongate, triserial test, strongly tapered towards base. Globular, inflated chambers rapidly increase in size; distinct, depressed sutures. Smooth, finely perforate, calcareous wall. Early chambers ornamented with long, tapering spines that extend dorsally; fragile and often partially or completely broken. Loop-shaped aperture extends up the face of the final chamber from the basal margin; well-developed, elevated rim.

Occurrence. Originally described from the Adriatic (d'Orbigny, 1826) but more recently from various Antarctic localities (Mackensen et al., 1990, 1993; Ishman and Domack, 1994; Igarashi et al., 2001; Majewski, 2013).

Bulimina subteres Brady, 1881

1881 *Bulimina subteres* Brady: 55, pl. 50, figs. 17–18.

Material. Three specimens from three samples.

Description. Elongate, triserial, ovate test, rounded at the distal end and tapering to a point at the basal end; slightly inflated chambers; depressed sutures; curved, slit-like aperture extending up the face of the terminal chamber.

Occurrence. Originally described from the Recent of Fiji and the Caribbean (Brady, 1881).

***Bulimina* sp. 1**
(Fig. 13:9–10)

Material. Twenty-four specimens from 11 samples.

Description. Near spherical test, wider than high; only the three chambers of the final whorl visible. Inflated, globular chambers; depressed sutures. Calcareous, smooth, perforate wall; loop-shaped aperture extending from the base up the face of the final chamber, with a raised rim.

Family **Uvigerinidae** Haeckel, 1894

Subfamily **Angulogerininae** Galloway, 1933

Genus *Trifarina* Cushman, 1923

Trifarina earlandi (Parr, 1950)
(Fig. 13:8)

1950 *Angulogerina earlandi* Parr: 341, pl. 12, fig. 21.
2001 *Angulogerina earlandi* Parr; Igarashi et al.: 154, pl. 11, fig. 7.
2005 *Angulogerina earlandi* Parr; Majewski: 203, fig. 22(8–9).
2013 *Angulogerina earlandi* Parr; Majewski: 181, fig. 9(13–14).

Material. Overall, 204 specimens from 22 samples.

Description. Elongate, fusiform test, triserial, becoming uniserial; triangular cross section becoming rectilinear with rounded to sub-acute corners. Base rounded; slightly lobulate margins. Numerous inflated chambers ornamented with narrow, high costae that generally do not cross the sutures; in some specimens final chambers lack ornamentation. Terminal, ovate aperture, with internal hemicylindrical tooth plate, produced on a neck with a phialine lip.

Occurrence. Recorded from a number of locations around Antarctica (Parr, 1950; Igarashi et al., 2001; Majewski, 2005, 2013).

Remarks. Parr (1950) placed this species within *Angulogerina*. However, Loeblich and Tappan (1988) define *Angulogerina* as triserial throughout, whilst this species is triserial, becoming uniserial, diagnostic of *Trifarina*. The high narrow costae of *Trifarina earlandi* (Parr) distinguish it from the otherwise similar *T. angulosa* (Williamson).

Family **Fursenkoinidae** Loeblich & Tappan, 1961

Genus *Fursenkoina* Loeblich & Tappan, 1961

Fursenkoina fusiformis (Cushman, 1930)
(Fig. 13:13–14)

1930 *Virgulina fusiformis* Cushman: 45, pl. 8, fig. 8.
1981 *Fursenkoina fusiformis* (Cushman); Milam & Anderson: 311, pl. 9, fig. 6.
1994 *Fursenkoina fusiformis* (Cushman); Ishman & Domack: 152, pl. 2, fig. 7.
1996 *Fursenkoina fusiformis* (Cushman); Violanti: 65, pl. 9, figs. 14–15.
2005 *Fursenkoina fusiformis* (Cushman); Majewski: 204, fig. 23(9–12).
2009 *Fursenkoina fusiformis* (Cushman); Majewski & Anderson: 139, fig. 4.

Material. Overall, 1260 specimens from 34 samples.

Description. Narrow, elongate test, ovate in section. High, narrow, slightly inflated chambers, biserial, twisted

around the test axis. Oblique, depressed sutures; calcareous, hyaline, finely perforate wall, with smooth surface. Narrow, elongate aperture; basal part of the aperture may be closed in adult specimens, leaving an areal comma-shaped opening.

Occurrence. Recorded from a range of Antarctic locations (Milam and Anderson, 1981; Ishman and Domack, 1994; Violanti, 1996; Majewski, 2005; Majewski and Anderson, 2009).

Remarks. Very similar to *Stainforthia fusiformis* (Williamson), a species common in the high, northern latitudes. *F. fusiformis* (Cushman) can be distinguished from this species by the shape of the aperture and by being biserial throughout. *F. fusiformis* (Cushman) is common throughout the high, southern latitudes.

Family **Discorbidae** Ehrenberg, 1838

Genus *Discorbis* Lamarck, 1804

Discorbis vilardeboanus (d'Orbigny, 1839b)
(Fig. 13:15–16)

1839b *Rosalina vilardeboana* d'Orbigny: 44, pl. 6, figs. 13–15.
1932a *Discorbis vilardeboana* (d'Orbigny); Heron-Allen & Earland: 409, pl. 13, figs. 37–39.
1975 *Rosalina vilardeboana* d'Orbigny; Anderson: 88, pl. 8, fig. 10.
2001 *Rosalina globularis* d'Orbigny; Igarashi et al.: 154, pl. 11, fig. 13.
2005 *Rosalina globularis* d'Orbigny; Majewski: 205, fig. 24(1–4).
? 2009 *Rosalina* Majewski & Anderson: 139, fig. 4 (14).
2013 *Rosalina globularis* d'Orbigny; Majewski: 183, fig. 11(1).

Material. Twelve specimens from nine samples.

Description. Trochospiral test; spiral side convex; umbilical side flattened; 2.5 whorls; seven chambers in the final whorl; strongly curved, depressed sutures. Small chamberlets formed in umbilical region below triangular alar projections that protrude from the umbilical margin of each chamber. Thin, calcareous, finely perforate wall. Low, interiomarginal, extra-umbilical, arch-shaped aperture, with a secondary opening at the posterior margin of the umbilical flap.

Occurrence. Originally described from the Falkland Islands (d'Orbigny, 1839b), subsequently from various locations on the Antarctic shelf (Heron-Allen and Earland, 1932a; Anderson, 1975; Igarashi et al., 2001; Majewski, 2005, 2013; Majewski and Anderson, 2009).

Remarks. Chambers less inflated and alar projections more angular than those of *Rosalina globularis* d'Orbigny, with which it may sometimes be confused.

Family **Cibicididae** Cushman, 1927

Subfamily **Cibicidinae** Cushman, 1927

Genus *Cibicides* de Montfort, 1808

***Cibicides* sp. 1**
(Fig. 13:11–12)

Material. Four specimens from four samples.

Description. Trochospiral, planoconvex test; flat, slightly involute spiral side with somewhat thickened sutures; strongly convex, completely involute umbilical side. Sutures flush except around final chamber; rounded periphery; calcareous wall, coarsely perforate on spiral side with five large pores in each chamber; pores in earlier chambers filled by lamellar thickening; umbilical side finely perforate; keel and apertural face imperforate. Low, interiomarginal, equatorial aperture extending along the spiral side suture and slightly onto the umbilical side, with a narrow lip.

***Cibicides* sp. 2**

Material. One specimen from one sample.

Description. Trochospiral, planoconvex test; flat, slightly involute spiral side with somewhat thickened sutures; strongly convex, completely involute umbilical side. Calcareous wall, coarsely perforate on spiral side; umbilical side finely perforate; keel and apertural face imperforate; aperture not preserved.

Family **Nonionidae** Schultze, 1854

Subfamily **Nonioninae** Schultze, 1854

Genus *Nonionella* Cushman, 1926

Nonionella bradii (Chapman, 1916)
(Fig. 14:2–4)

1916 *Nonionina scapha* (Fichtel & Moll) var. *bradii* Chapman: 71, pl. 5, fig. 42.
1990 *Nonionella bradii* (Chapman); Mackensen et al.: 254, pl. 1, fig. 4.
1994 *Nonionella bradii* (Chapman); Ishman & Domack: 152, pl. 2, figs. 10 & 12.
1994 *Nonionella bradii* (Chapman); Jones: 108, pl. 109, fig. 16.
1996 *Nonionella bradii* (Chapman); Violanti: 67, pl. 10, figs. 8, 13, 17.

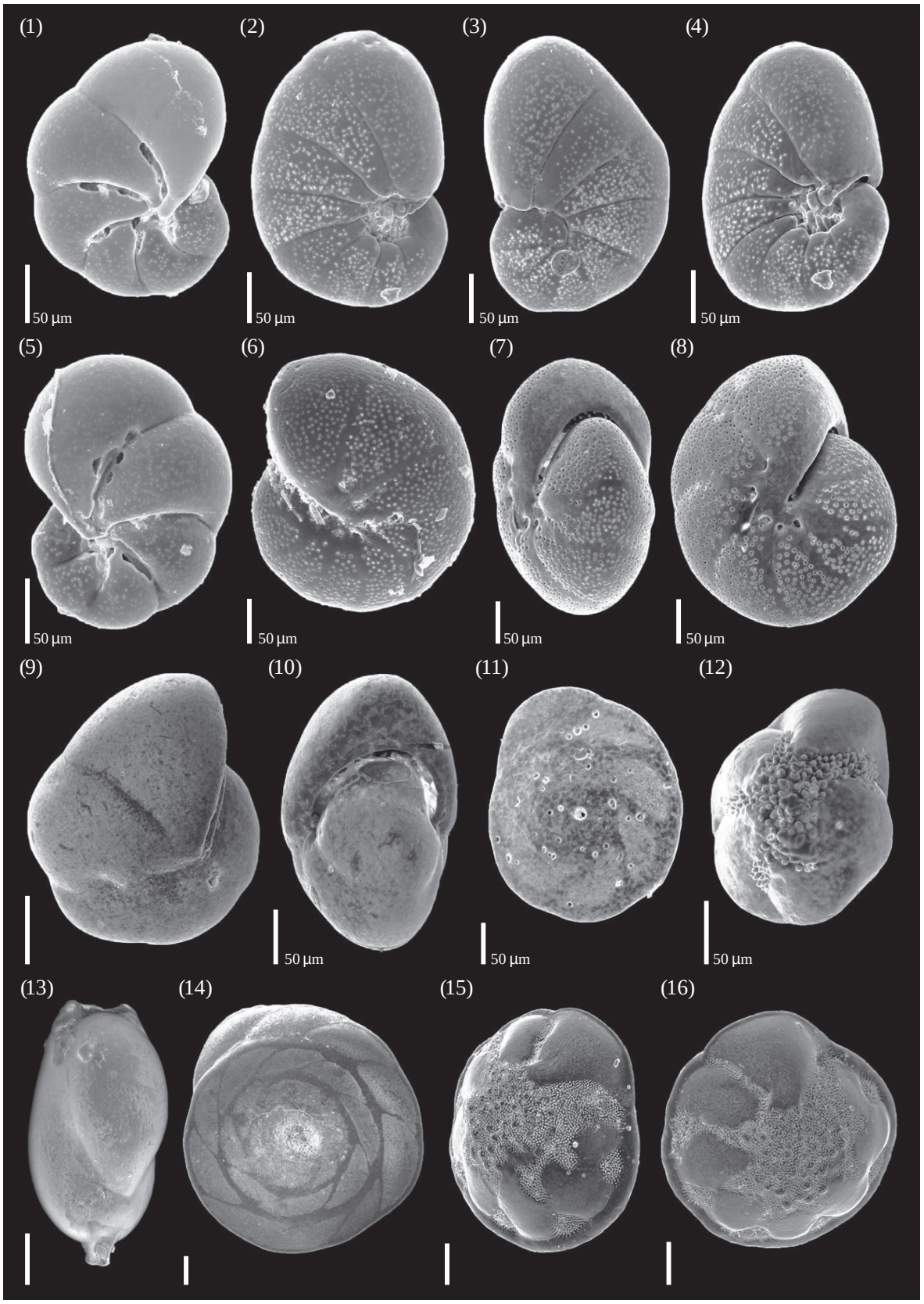


Figure 14. (1 and 5) *Nonionella iridea* Heron-Allen and Earland (GC666_002). (2–4) *Nonionella bradii* (Chapman) (GC666_002). (6–8) *Astrononion echolsi* Kennett (GC666_002). (9–10) *Pullenia subcarinata* (d'Orbigny) (GC666_002). (11–12) *Buccella* sp. 2 (GC666_002). (13) *Chilostomella* sp. 1 (BC671). (14–16) *Buccella* sp. 1 (GC666_002). (Scale bar 100 µm unless otherwise indicated.)

2001 *Nonionella bradii* (Chapman); Igarashi et al.: 155, pl. 12, fig. 5.
2005 *Nonionella bradii* (Chapman); Majewski: 206, fig. 25(4–5).
2009 *Nonionella bradii* (Chapman); Majewski & Anderson: 139, fig. 4.

Material. Sixty-seven specimens from 17 samples.

Description. Low trochospiral, compressed test with rounded periphery; involute umbilical side; partially evolute spiral side. Low, broad chambers that widen towards the periphery; 9–10 in the final whorl; chambers rapidly enlarge in the final whorl to produce a flared test. Flap-like projections from each chamber overhang the umbilicus. Slightly curved, narrow, depressed sutures. Calcareous, hyaline, finely perforate wall with a smooth surface. Aperture a low arch, interiomarginal, equatorial.

Occurrence. First described from the Ross Sea (Chapman, 1916); subsequently reported from numerous other Antarctic localities (Mackensen et al., 1990; Ishman and Domack, 1994; Jones, 1994; Violanti, 1996; Igarashi et al., 2001; Majewski, 2005; Majewski and Anderson, 2009).

Nonionella iridea Heron-Allen & Earland, 1932a
(Fig. 14:1 and 5)

1932a *Nonionella iridea* Heron-Allen & Earland: 438, pl. 16, figs. 14–16.
1990 *Nonionella iridea* Heron-Allen & Earland; Mackensen et al.: 254, pl. 1, figs. 7–9.
1994 *Nonionella iridea* Heron-Allen & Earland; Ishman & Domack: 152, pl. 2, fig. 11.
1996 *Nonionella iridea* Heron-Allen & Earland; Violanti: 67, pl. 10, figs. 9, 14, 18.
2001 *Nonionella iridea* Heron-Allen & Earland; Igarashi et al.: 155, pl. 12, fig. 6.
2005 *Nonionella iridea* Heron-Allen & Earland; Majewski: 206, fig. 25(2–3).
2009 *Nonionella iridea* Heron-Allen & Earland; Majewski & Anderson: 139, fig. 4.
2013 *Nonionella iridea* Heron-Allen & Earland; Majewski: 182, fig. 10(8).

Material. Overall, 323 specimens from 28 samples.

Description. Low trochospiral, compressed test, with rounded periphery; involute umbilical side; partially evolute spiral side. Low, broad, somewhat inflated chambers that widen towards the periphery; six to seven in the final whorl. Chambers enlarge in the final whorl to produce a slightly flared test; flap-like projections from each chamber overhang the umbilicus and overlap each other. Slightly curved, narrow, depressed sutures. Calcareous, hyaline, finely perforate wall with a smooth surface. Aperture a low arch; interiomarginal, equatorial, supplementary apertures develop in later chambers along the sutures from the umbilicus approximately halfway to the periphery (not visible in all specimens).

Occurrence. Originally described from the subantarctic, in particular South Georgia and the Falkland Islands (Heron-Allen and Earland, 1932a); subsequently reported from locations around Antarctica (Mackensen et al., 1990; Ishman and Domack, 1994; Violanti, 1996; Igarashi et al., 2001; Majewski, 2005, 2013; Majewski and Anderson, 2009).

Subfamily **Astrononioninae** Saidova, 1981

Genus *Astrononion* Cushman and Edwards, 1937

Astrononion echolsi Kennett, 1967
(Fig. 14:6–8)

1967 *Astrononion echolsi* Kennett: 134, pl. 11, figs. 7–8.
1981 *Astrononion echolsi* Kennett; Milam & Anderson: 313, pl. 11, fig. 3.
1994 *Astrononion echolsi* Kennett; Ishman & Domack: 152, pl. 2, fig. 3.
1996 *Astrononion echolsi* Kennett; Violanti: 67, pl. 10, fig. 16.
2001 *Astrononion echolsi* Kennett; Igarashi et al.: 155, pl. 12, fig. 11.
2005 *Astrononion echolsi* Kennett; Majewski: 206, fig. 25(6–7).
2009 *Astrononion echolsi* Kennett; Majewski & Anderson: 139, fig. 4
2013 *Astrononion echolsi* Kennett; Majewski: 182, fig. 10(7).

Material. Overall, 1216 specimens from 39 samples.

Description. Involute, planispiral, slightly compressed test, with a rounded periphery. Size of chambers gently increases as they are added; eight to nine in the final whorl; somewhat inflated in some specimens but more commonly not. Slightly limbate, curved sutures; slightly depressed to flush. Indistinct, tube-like supplementary chambers extend from the umbilical region, only visible as sunken pits on the sutural lines. Calcareous, hyaline, finely perforate, smooth wall, often with slightly yellow colour. Primary aperture a low, interiomarginal, equatorial arch.

Occurrence. Abundant in the Ross Sea and Scotia Sea, where it was first described (Kennett, 1967); also recorded from various other Antarctic locations (Milam and Anderson, 1981; Ishman and Domack, 1994; Violanti, 1996; Igarashi et al., 2001; Majewski, 2005, 2013; Majewski and Anderson, 2009).

Subfamily **Pulleniinae** Schwager, 1877

Genus *Pullenia* Parker & Jones in Carpenter et al., 1862

Pullenia subcarinata (d'Orbigny, 1839b)
(Fig. 14:9–10)

1839b *Nonionina subcarinata* d'Orbigny: 28, pl. 5, figs. 23–24.
1932a *Pullenia subcarinata* (d'Orbigny); Heron-Allen & Earland: 403, pl. 13, figs. 14–18.
1981 *Pullenia subcarinata* (d'Orbigny); Milam & Anderson: 313, pl. 11, fig. 5.
1993 *Pullenia subcarinata* (d'Orbigny); Mackensen et al.: 58, pl. 3, figs. 8–9.
? 1994 *Pullenia quinqueloba* (Reuss); Jones: 92, pl. 84, figs. 14–15.
1996 *Pullenia subcarinata* (d'Orbigny); Violanti: 48, pl. 10, fig. 19.

Material. Thirty-nine specimens from 18 samples.

Description. Involute, planispiral, slightly compressed test with a rounded periphery. Chambers slightly inflated, giving the test a slightly lobulate outline; five to six in the final whorl; face of final chamber has a somewhat triangular shape. Near-radial, slightly depressed sutures. Calcareous, smooth, very finely perforate wall. Aperture a low, interiomarginal, equatorial, crescentic slit, bordered on the upper margin by a raised lip.

Occurrence. Originally described from recent deposits from the Falkland Islands (d'Orbigny, 1839b); subsequently recorded from around Antarctica (Heron-Allen and Earland, 1932a; Milam and Anderson, 1981; Mackensen et al., 1993; Jones, 1994; Violanti, 1996).

Remarks. *Pullenia quinqueloba* (Reuss) is morphologically very similar to *P. subcarinata* (d'Orbigny), and Jones (1994) assigns the *Challenger* specimens to *P. quinqueloba* (Reuss). However, *Pullenia quinqueloba* (Reuss) was originally described from German Eocene deposits, and we therefore assign our specimens to *P. subcarinata* (d'Orbigny), which was originally described from Recent deposits from the Falkland Islands.

Family **Chilostomellidae** Brady, 1881

Subfamily **Chilostomellinae** Brady, 1881

Genus *Chilostomella* Reuss, 1849

***Chilostomella* sp. 1**
(Fig. 14:13)

Material. One specimen from one sample.

Description. Ovoid, planispiral, involute test; near-circular cross section. Two strongly embracing, inflated chambers in final whorls; final chamber significantly larger. Calcareous, finely perforate wall; smooth surface; equatorial, interiomarginal, narrow slit-shaped aperture, with a raised margin. Distinctive spine-like structure on basal end.

Family **Trichohyalidae** Saidova, 1981

Genus *Buccella* Andersen, 1952

***Buccella* sp. 1**
(Fig. 14:14–16)

Material. Overall, 241 specimens from 31 samples.

Description. Large, biconvex, carinate, trochospiral test; spiral side low convex and evolute; umbilical side higher and involute. Numerous rhomboidal chambers with curved sides, slightly inflated on the umbilical side; three and a half whorls; 8–10 chambers in the final whorl. Sutures on spiral side flush, slightly limbate, swept back towards periphery, straighter and depressed on the umbilical side. Umbilical region and sutural fissures on umbilical side filled with a mixture of fine and coarse granules; spiral side surface smooth, finely perforate on the chamber faces; periphery very slightly lobate, with a distinct keel. Aperture not visible in any of the specimens examined; may be covered by the abundant granules.

Remarks. Openings at the end of the sutural fissures that are common in members of this genus are not visible in any of the specimens examined here.

***Buccella* sp. 2**
(Fig. 14:11–12)

Material. Twenty-five specimens from 12 samples.

Description. Test small for this genus; trochospiral, biconvex; spiral side flatter and evolute; umbilical side convex and involute. Chambers almost semi-circular; two whorls; six to seven chambers in the final whorl; sutures limbate, flush, slightly curved on the spiral side, very depressed on the umbilical side. Umbilical region and sutural fissures on umbilical side filled with granules; spiral side surface smooth, finely perforate on the chamber faces; periphery slightly lobate and thickened but not carinate. Aperture not visible in any of the specimens examined and may be covered by the abundant granules.

Remarks. Bears some similarity to *Epistominella exigua* (Brady), especially in light microscope.

Genus *Neogloboquadrina* Bandy, Frerichs & Vincent, 1967

Neogloboquadrina pachyderma (Ehrenberg, 1861)

1861 *Aristerospira pachyderma* Ehrenberg: 276, 277, 303.
1932a *Globigerina pachyderma* Ehrenberg; Heron-Allen & Earland: 401, pl. 13, figs. 9–13.
1975 *Globigerina pachyderma* Ehrenberg; Anderson: 90, pl. 9, fig. 4.
1996 *Neogloboquadrina pachyderma* (Ehrenberg); Violanti: 62, pl. 8, figs. 17 and 21.
2001 *Neogloboquadrina pachyderma* (Ehrenberg); Igarashi et al.: 152, pl. 10, figs. 8–9.

Material. Overall, 209 specimens from 27 samples.

Description. Globular, low trochospiral test; globular chambers that rapidly enlarge as added; five to six in the final whorl. Straight to slightly curved, depressed, radial sutures; rounded periphery; open umbilical region. Calcareous, perforate wall; interiomarginal, extra-umbilical to umbilical aperture with bordering lip (may be absent in later stages).

Data availability. All the data analysed in this paper are available in the tables provided within the paper or in the Supplement.

The Supplement related to this article is available online at https://doi.org/10.5194/jm-37-25-2018-supplement.

Competing interests. The authors declare that they have no conflict of interest.

Acknowledgements. This study forms part of a doctoral project carried out by Rowan Dejardin, funded by the Centre for Environmental Geochemistry (University of Nottingham and the British Geological Survey) and supported by BGS-University Funding Initiative (BUFI). We thank the officers, crew, and scientific party on board the RRS *James Clark Ross* during scientific cruises JR257 and JC15002. Participation in cruise JR15002 by Rowan Dejardin was funded by the British Antarctic Survey Collaborative Gearing Scheme. We thank Hilary Sloane and Jack Lacey (BGS) for analytical assistance and Tony Milodowski and Gren Turner for their assistance generating the SEM images. We also thank the editor, Laia Alegret, one anonymous reviewer, and Wojciech Majewski for their insightful comments, which helped to strengthen this paper. This project was supported by NERC Isotope Geoscience Facility grant IP/1495/1114 (RCUK).

Edited by: Laia Alegret
Reviewed by: Wojciech Majewski and one anonymous referee

References

Alekseychik-Mitskevich, L. S.: Towards the classification of the foraminiferal family Haplophragmiidae, Trudy Vsesoyuzznogo neftyanogo Nauchnoissledovatel'skogo Geologorazvedochnogo Instituta, 343, 12–44, 1973.

Andersen, H. V.: Buccella, a new genus of the rotalid foraminifera, Journal of the Washington Academy of Sciences, 42, 143–151, 1952.

Anderson, J. B.: Ecology and distribution of foraminifera in the Weddell Sea of Antarctica, Micropalaeontology, 21, 69–96, 1975.

Bailey, J. W.: Microscopical examination of soundings made by the U.S. Coast Survey of the Atlantic coast of the U.S., Smithsonian Contributions, 2, 1–48, 1851.

Bandy, O. L., Frerichs, W. E., and Vincent, E.: Origin, development, and geologic significance of *Neogloboquadrina* Bandy, Frerichs, and Vincent, gen. nov., Contributions from the Cushman Foundation for Foraminiferal Research, 18, 152–157, 1967.

Barker, R. W.: Taxonomic notes on the species figured by H.B. Brady in his report of the foraminifera dredged by HMS Challenger during the years 1873–1876, American Association of Petroleum Geologists Special Publication, 9, 10238, 2–240, 1960.

Bernhard, J. M.: Distinguishing live from dead foraminifera: Methods review and proper applications, Micropaleontology, 46, 38–46, 2000.

Brady, H. B.: Contributions to the knowledge of the foraminifera. – On the rhizopodal fauna of the Shetlands, Transactions of the Linnaean Society, 24, 463–476, https://doi.org/10.1111/j.1096-3642.1863.tb00170.x, 1864.

Brady, H. B.: Notes on some of the Reticularian Rhizopoda of the "Challenger" Expedition. I. On new or little known arenaceous types, Q. J. Microsc. Sci., 19, 20–62, 1879.

Brady, H. B.: Notes on some of the Reticularian Rhizopoda of the "Challenger" Expedition. Part III, Q. J. Microsc. Sci., 21, 31–71, 1881.

Brady, H. B.: Report on the scientific results of the voyage of H.M.S. Challenger during the years 1873–76, in: Zoology of the Challenger Expedition, edited by: Thompson, C. W. and Murray, J., London, Neill, Edinburgh, 1884.

Brandon, M. A., Murphy, E. J., Whitehouse, M. J., Trathan, P. N., Murray, A. W. A., Bone, D. G., and Priddle, J.: The shelf break front to the east of the sub-Antarctic island of South Georgia, Cont. Shelf Res., 19, 799–819, https://doi.org/10.1016/s0278-4343(98)00112-5, 1999.

Brandon, M. A., Murphy, E. J., Trathan, P. N., and Bone, D. G.: Physical oceanographic conditions to the northwest of the sub-Antarctic Island of South Georgia, J. Geophys. Res.-Oceans, 105, 23983–23996, 10.1029/2000jc900098, 2000.

Brönnimann, P.: Two new genera of Recent Trochamminidae (Foraminiferida), Achives des Sciences, Geneve, 29, 215–218, 1976.

Brönnimann, P. and Beurlen, G.: Recent benthonic foraminifera from Brasil. Morphology and ecology. Part I, Achives des Sciences, Geneve, 30, 77–89, 1977.

Brönnimann, P. and Whittaker, J. E.: The Trochamminacea of the Discovery Reports, British Museum, London, 1988.

Brönnimann, P., Zaninetti, L., and Whittaker, J. E.: On the classification of the Trochamminacea (Foraminiferida), J. Foramin. Res., 13, 202–218, 1983.

Caralp, M. H.: Abundance of *Bulimina exilis* and *Melonis barleeanum* – relationship to the quality of marine organic-matter, Geo-Marine Letters, 9, 37–43, https://doi.org/10.1007/bf02262816, 1989.

Carpenter, W. B.: On the rhizopodal fauna of the deep sea, Proceedings of the Royal Society of London, 18, 59–62, 1869.

Carpenter, W. B., Parker, W. K., and Jones, T. R.: Introduction to the study of the Foraminifera, Ray Society, London, 1862.

Caulle, C., Mojtahid, M., Gooday, A. J., Jorissen, F. J., and Kitazato, H.: Living (Rose-Bengal-stained) benthic foraminiferal faunas along a strong bottom-water oxygen gradient on the Indian margin (Arabian Sea), Biogeosciences, 12, 5005–5019, https://doi.org/10.5194/bg-12-5005-2015, 2015.

Chapman, F.: Report on the Foraminifera and Ostracoda from elevated deposits on the shores of the Ross Sea, British Antarctic Expedition 1907–9 under the command of Sir E. H. Shackleton, C.V.O.: Reports on the scientific investigations, Geology, Vol. II – Contributions to the palaeontology and petrology of South Victoria Land, edited by: Benson, W. N., Chapman, F., Cohen, F., Cotton, L. A., Hedley, C., Jensen, H. I., Mawson, D., Skeats, E. W., Thomson, J. A., Walkom, A. B., and Woolnough, W. G., William Heinemann, London, 1916.

Chapman, F., Parr, W. J., and Collins, A. C.: Tertiary Foraminifera of Victoria, Australia. The Balcombian deposits of Port Phillip, Journal of the Linnaean Society, 38, 553–576, 1934.

Clark, F. E., Patterson, R. T., and Fishbein, E.: Distribution of Holocene benthic foraminifera from the tropical southwest Pacific Ocean, J. Foramin. Res., 24, 241–267, 1994.

Corliss, B. H. and Emerson, S.: Distribution of Rose-Bengal stained deep-sea benthic foraminifera from the Nova Scotian continental-margin and Gulf of Maine, Deep-Sea Res. Pt. A, 37, 381–400, https://doi.org/10.1016/0198-0149(90)90015-n, 1990.

Cushman, J. A.: A monograph of the Foraminifera of the North Pacific Ocean. Part I. Astrorhizidae and Lituolidae, Bulletin of the United States National Museum, 71, 1–134, 1910.

Cushman, J. A.: A monograph of the foraminifera of the North Pacific Ocean. Pt. III. Lagenidae, Bulletin of the United States National Museum, 71, 1–125, 1913.

Cushman, J. A.: The foraminifera of the Atlantic Ocean, Part 4. Lagenidae, Bulletin United States National Museum, 104, 1–228, 1923.

Cushman, J. A.: Foraminifera of the typical Monerey of California, Cushman Foundation for Foraminiferal Research Special Publication, 2, 53–69, 1926.

Cushman, J. A.: An outline of a re-classification of the foraminifera, Contributions from the Cushman laboratory for foraminiferal research, 3, 1–105, 1927.

Cushman, J. A.: The foraminifera of the Atlantic Ocean, Part 7, Nonionidae, Camerinidae, Peneroplidae and Alveolinellidae, Bulletin United States National Museum, 104, 1–79, 1930.

Cushman, J. A.: Foraminifera, their classification and economic use Cushman Lab. Foram. Res., Special Publications Cushman Laboratory for Foraminiferal Research, 4, 1–349, 1933.

Cushman, J. A.: Foraminifera of the United States Antarctic Service Expedition 1939–1941, Proceedings, American Philosophical Society, 89, 285–288, 1945.

Cushman, J. A. and Edwards, P. G.: *Astrononion* a new genus of the foraminifera and its species, Contributions from the Cushman laboratory for foraminiferal research, 13, 29–36, 1937.

d'Orbigny, A.: Tableau méthodique de la classe des Céphalopodes, Ann. Sci. Nat., 7, 245–314, 1826.

d'Orbigny, A.: Foraminifères, in: Histoire Physique, Politique et Naturelle de l'île de Cuba, edited by: de la Sagra, R., A. Bertrand, Paris, 1–224, 1839a.

d'Orbigny, A.: Voyage dans l'Amérique Méridionale (le Brésil, la République orientale de l'Uruquay, la République Argentine, la Patagonie, la République du Chili, la République de Bolivia, la République du Pérou) éxécuté pendant les années 1826, 1827, 1832 et 1833 in: Foraminifères, edited by: Levrault, S., Bertrand, Paris, 1–86, 1839b.

Defrance, J. L. M.: Dictionnaire des Sciences Naturelles, F. G. Levrault, Strasbourg, 1824.

DeLaca, T. E.: The morphology and ecology of *Astrammina rara*, J. Foramin. Res., 16, 216–233, 1986.

Earland, A.: Foraminifera, Part II, South Georgia, London, 27–138, 1933.

Earland, A.: Foraminifera. Part III. The Falklands sector of the Antarctic (excluding South Georgia), London, 1–208, 1934.

Echols, R. J.: Distribution of foraminifera in sediments of the Scotia Sea area, Antarctic waters, in: Antarctic Oceanography I, edited by: Reid, J. L., American Geophysical Union, Washington, D.C., 93–168, 1971.

Ehrenberg, C. G.: Uber die Bildung der Kreidefelsen und des Kreidemergels durch unsichtbare Organismen, Physikalische Abhandlungen der Koniglichen Akademie der Wissenschaften zu Berlin, 1838, 59–147, 1838.

Ehrenberg, C. G.: Elemente des tiefen Meeresgrundes im Mexikanishen Golfstrome bei Florida: uber die Tiefgrund-Verhaltnisse des Oceans am eingange der Davisstrasse und bei Island, Monatsbericht der Koniglichen Preussichen Akademie der Wissenschaften zu Berlin, 1861, 275–315, 1861.

Elderfield, H., Yu, J., Anand, P., Kiefer, T., and Nyland, B.: Calibrations for benthic foraminiferal Mg / Ca paleothermometry and the carbonate ion hypothesis, Earth Planet. Sc. Lett., 250, 633–649, https://doi.org/10.1016/j.epsl.2006.07.041, 2006.

Elderfield, H., Greaves, M., Barker, S., Hall, I. R., Tripati, A., Ferretti, P., Crowhurst, S., Booth, L., and Daunt, C.: A record of bottom water temperature and seawater δ^{18}O for the Southern Ocean over the past 440 kyr based on Mg / Ca of benthic foraminiferal Uvigerina spp, Quaternary Sci. Rev., 29, 160–169, https://doi.org/10.1016/j.quascirev.2009.07.013, 2010.

Elderfield, H., Ferretti, P., Greaves, M., Crowhurst, S., McCave, I. N., Hodell, D., and Piotrowski, A. M.: Evolution of Ocean Temperature and Ice Volume Through the Mid-Pleistocene Climate Transition, Science, 337, 704–709, https://doi.org/10.1126/science.1221294, 2012.

Enge, A. J., Nomaki, H., Ogawa, N. O., Witte, U., Moeseneder, M. M., Lavik, G., Ohkouchi, N., Kitazato, H., Kucera, M., and Heinz, P.: Response of the benthic foraminiferal community to a simulated short-term phytodetritus pulse in the abyssal North Pacific, Mar. Ecol.-Prog. Ser., 438, 129–142, https://doi.org/10.3354/meps09298, 2011.

Fontanier, C., Jorissen, F. J., Chaillou, G., David, C., Anschutz, P., and Lafon, V.: Seasonal and interannual variability of benthic foraminiferal faunas at 550 m depth in the Bay of Biscay,

Deep-Sea Res. Pt. I, 50, 457–494, https://doi.org/10.1016/s0967-0637(02)00167-x, 2003.

Fontanier, C., Jorissen, F., Anschutz, P., and Chaillou, G.: Seasonal variability of benthic foraminiferal faunas at 1000 m depth in the Bay of Biscay, J. Foramin. Res., 36, 61–76, https://doi.org/10.2113/36.1.61, 2006a.

Fontanier, C., Mackensen, A., Jorissen, F. J., Anschutz, P., Licari, L., and Griveaud, C.: Stable oxygen and carbon isotopes of live benthic foraminifera from the Bay of Biscay: Microhabitat impact and seasonal variability, Mar. Micropaleontol., 58, 159–183, https://doi.org/10.1016/j.marmicro.2005.09.004, 2006b.

Fontanier, C., Jorissen, F. J., Michel, E., Cortijo, E., Vidal, L., and Anschutz, P.: Stable oxygen and carbon isotopes of live (stained) benthic foraminifera from Cap-Ferret Canyon (Bay of Biscay), J. Foramin. Res., 38, 39–51, https://doi.org/10.2113/gsjfr.38.1.39, 2008.

Fontanier, C., Garnier, E., Brandily, C., Dennielou, B., Bichon, S., Gayet, N., Eugene, T., Rovere, M., Grémare, A., and Deflandre, B.: Living (stained) benthic foraminifera from the Mozambique Channel (eastern Africa): Exploring ecology of deep-sea unicellular meiofauna, Deep-Sea Res. Pt. I, 115, 159–174, https://doi.org/10.1016/j.dsr.2016.06.007, 2016.

Frerichs, W. E.: Recent arenaceous foraminifers from Gulf of Mexico, Palaeontological Contributions, University of Kansas, 46, 1–2, 1969.

Galloway, J. J.: A manual of Foraminifera, Principia Press, Bloomington, 1933.

Gaździcki, A. and Majewski, W.: Recent foraminifera from Goulden Cove of King George Island, Antarctica, Pol. Polar Res., 24, 3–12, 2003.

Gehlen, M., Mucci, A., and Boudreau, B.: Modelling the distribution of stable carbon isotopes in porewaters of deep-sea sediments, Geochim. Cosmochim. Ac., 63, 2763–2773, https://doi.org/10.1016/s0016-7037(99)00214-8, 1999.

Geslin, E., Heinz, P., Jorissen, F., and Hemleben, C.: Migratory responses of deep-sea benthic foraminifera to variable oxygen conditions: laboratory investigations, Mar. Micropaleontol., 53, 227–243, https://doi.org/10.1016/j.marmicro.2004.05.010, 2004.

Glaessner, M. F.: Die Entfaltung der Foraminiferenfamilie Buliminidae, Problemy Palaeontologii, Palaeontologicheskaya Laboratoriya Moskovskogo Gosudarstvennogo Universiteta, 2–3, 411–422, 1937.

Goes, A.: A synopsis of the Arctic and Scandinavian Recent marine Foraminifera hitherto discovered, Kongl. svenka vetenskaps-Akademiens handlinger 25, 1–127, 1894.

Gooday, A. J.: A response by benthic foraminifera to the deposition of phytodetritus in the deep-sea, Nature, 332, 70–73, https://doi.org/10.1038/332070a0, 1988.

Gooday, A. J. and Hughes, J. A.: Foraminifera associated with phytodetritus deposits at a bathyal site in the northern Rockall Trough (NE Atlantic): seasonal contrasts and a comparison of stained and dead assemblages, Mar. Micropaleontol., 46, 83–110, https://doi.org/10.1016/s0377-8398(02)00050-6, 2002.

Gooday, A. J., da Silva, A. A., Koho, K. A., Lecroq, B., and Pearce, R. B.: The "mica sandwich"; a remarkable new genus of Foraminifera (Protista, Rhizaria) from the Nazare Canyon (Portuguese margin, NE Atlantic), Micropaleontology, 56, 345–357, 2010.

Griffith, J. W. and Henfrey, A.: The Micrographic Dictionary, van Voorst, London, 1875.

Gross, O.: Influence of temperature, oxygen and food availability on the migrational activity of bathyal benthic foraminifera: evidence by microcosm experiments, Hydrobiologia, 426, 123–137, https://doi.org/10.1023/a:1003930831220, 2000.

Haeckel, E.: Systematische Phylogenie. Entwurf eines Naturlichen Systems der Organismen auf Grund ihrer Stammesgeschichte. Theil 1, Systematische Phylogenie der Protisten und Pflanzen, Georg Reimer, Berlin, 1894.

Hayward, B. W., Kawagata, S., Sabaa, A. T., Grenfell, H. R., van Kerckhoven, L., Johnson, K., and Thomas, E.: The last global extinction (Mid-Pleistocene) of deep-sea benthic foraminifera (Chrysalogoniidae, Ellipsoidinidae, Glandulonodosariidae, Plectofrondicularіidae, Pleursostomellidae, Stilostomellidae), their Late Cretaceous-Cenozoic history and taxonomy, Cushman Foundation for Foraminiferal Research Special Publication, 43, 1–410, 2012.

Heron-Allen, E. and Earland, A.: On some Foraminifera from the North Sea, etc., dredged by the Fisheries Cruiser "Goldseeker" (International North Sea Investigations – Scotland). I. On some new Astrorhizidae and their shell-structure, Journal of the Royal Microscopical Society, 1912, 382–389, 1912.

Heron-Allen, E. and Earland, A.: Les Foraminifères des "Sables Rouges" du golfe de Ajaccio (Côte Nord), Bulletin de la Société des sciences historiques et naturelles de la Corse, 42, 109–149, 1922.

Heron-Allen, E. and Earland, A.: XXVII. – Some new Foraminifera from the South Atlantic, Journal of the Royal Microscopical Society, 49, 324–334, https://doi.org/10.1111/j.1365-2818.1929.tb00787.x, 1929.

Heron-Allen, E. and Earland, A.: Some new foraminifera from the South Atlantic, Part 3., Journal of the Royal Microscopical Society, 50, 38—45, 1930.

Heron-Allen, E. and Earland, A.: Foraminifera. Part 1. The ice-free area of the Falkland Islands and adjacent seas, Cambridge University Press, London, 291–460, 1932a.

Heron-Allen, E. and Earland, A.: Some new foraminifera from the South Atlantic, IV, Journal of the Royal Microscopical Society, 52, 253–261, 1932b.

Herb, R.: Distribution of Recent Benthonic Foraminifera in the Drake Passage, in: Biology of the Antarctic Seas IV, American Geophysical Union, 251–300, 1971.

Hermelin, J. O. R.: Pliocene benthic foraminifera from the Ontong-Java plateau (western equatorial Pacific Ocean): faunal response to changing paleoenvironments, Cushman Foundation for Foraminiferal Research Special Publication, 26, 1–143, 1989.

Hogg, O. T., Barnes, D. K. A., and Griffiths, H. J.: Highly Diverse, Poorly Studied and Uniquely Threatened by Climate Change: An Assessment of Marine Biodiversity on South Georgia's Continental Shelf, Plos One, 6, e19795, https://doi.org/10.1371/journal.pone.0019795, 2011.

Höglund, H.: Foraminifera in the Gullmar Fjord and the Skagerak, Zoologiska Bidrag fran Uuppsala, 26, 1–328, 1947.

Holsten, J., Stott, L., and Berelson, W.: Reconstructing benthic carbon oxidation rates using δ13C of benthic foraminifers, Mar. Micropaleontol., 53, 117–132, https://doi.org/10.1016/j.marmicro.2004.05.006, 2004.

Hoogakker, B. A. A., Elderfield, H., Schmiedl, G., McCave, I. N., and Rickaby, R. E. M.: Glacial-interglacial changes in bottom-water oxygen content on the Portuguese margin, Nat. Geosci., 8, 40–43, https://doi.org/10.1038/ngeo2317, 2015.

Hromic, T., Ishman, S., and Silva, N.: Benthic foraminiferal distributions in Chilean fjords: 47° S to 54° S, Mar. Micropaleontol., 59, 115–134, https://doi.org/10.1016/j.marmicro.2006.02.001, 2006.

Igarashi, A., Numanami, H., Tsuchiya, Y., and Fukucki, M.: Bathymetric distribution of fossil foraminifera within marine sediment cores from the eastern part of Lutzow-Holm Bay, East Antarctica, and its paleoceanographic implications, Mar. Micropaleontol., 42, 125–162, https://doi.org/10.1016/s0377-8398(01)00004-4, 2001.

Ishman, S. E. and Domack, E. W.: Oceanographic controls on benthic foraminifers from the Bellingshausen margin of the Antarctic Peninsula, Mar. Micropaleontol., 24, 119–155, https://doi.org/10.1016/0377-8398(94)90019-1, 1994.

Jones, A. F.: The Micrographic Dictionary, edited by: Griffith, J. W. and Henfrey, A., van Voorst, London, 1875.

Jones, R. W.: A revised classification of the unilocular Nodosariida and Buliminida (Foraminifera), Revista Espanola de Micropaleontologia, 16, 91–160, 1984.

Jones, R. W.: The Challenger Foraminifera, Oxford University Press, Oxford, 1994.

Jorissen, F. J., deStigter, H. C., and Widmark, J. G. V.: A conceptual model explaining benthic foraminiferal microhabitats, Mar. Micropaleontol., 26, 3–15, https://doi.org/10.1016/0377-8398(95)00047-x, 1995.

Jorissen, F. J., Fontanier, C., and Thomas, E.: Paleoceanographical Proxies Based on Deep-Sea Benthic Foraminiferal Assemblage Characteristics, in: Proxies in Late Cenozoic Paleoceanography, edited by: Hillaire-Marcel, C., and de Vernal, A., Developments in Marine Geology, Elsevier, Amsterdam, 263–325, 2007.

Kaminski, M. A.: The Year 2000 Classification of the Agglutinated Foraminifera, in: Proceedings of the Sixth International Workshop on Agglutinated Foraminifera (Prague, Czech Republic, 1–7 September 2001), edited by: Kaminski, M. A. and Bubik, M., Grzybowski Foundation Special Publication, London, UK, 237–255, 2004.

Kaminski, M. A. and Gradstein, F. M.: Atlas of Paleogene Cosmopolitan deep-water agglutinated foraminifera, Grzybowski Foundation Special Publication, Krakow, 2005.

Kanmacher, F.: Adam's Essays on the Microscope: the Second Edition, with Considerable Additions and Improvements, Dillon & Keating, London, 1798.

Kender, S. and Kaminski, M. A.: Modern deep-water agglutinated foraminifera from IODP Expedition 323, Bering Sea: ecological and taxonomic implications, J. Micropalaeontology, https://doi.org/10.1144/jmpaleo2016-026, 2017.

Kennett, J. P.: New Foraminifera from the Ross Sea, Antarctica, Contributions from the Cushman Foundation for Foraminiferal Research, 18, 133–135, 1967.

Kitazato, H., Shirayama, Y., Nakatsuka, T., Fujiwara, S., Shimanaga, M., Kato, Y., Okada, Y., Kanda, J., Yamaoka, A., Masuzawa, T., and Suzuki, K.: Seasonal phytodetritus deposition and responses of bathyal benthic foraminiferal populations in Sagami Bay, Japan: preliminary results from "Project Sagami 1996–1999", Mar. Micropaleontol., 40, 135–149, https://doi.org/10.1016/s0377-8398(00)00036-0, 2000.

Knight, R.: Apertural characteristics of certain unilocular foraminifera: methods of study, nomenclature and taxonomic significance, J. Micropaleontol., 5, 37–47, 1986.

Lamarck, J. B.: Suite des mémoires sur les fossiles des environs de Paris, Annales du Muséum d'Histoire Naturelle, 5, 105–115, 179-188, 1804.

Lamarck, J. B.: Extrait du course de zoologie du Museum d'Histoire Naturelle, sur les animaux sans vertebres, d'Hautel, Paris, 1812.

Le Coze, F. and Hayward, B.: Lagena striatopunctata Parker & Jones, 1865, in: World Foraminifera Database, edited by: Hayward, B. W., Cedhagen, T., Kaminski, M., and Gross, O., avaiable at: http://www.marinespecies.org/foraminifera./aphia.php?p=taxdetails&id=525593 (last access: 12 July 2017), 2017.

Linke, P. and Lutze, G. F.: Microhabitat preferences of benthic foraminifera – a static concept or a dynamic adaptation to optimize food acquisition, Mar. Micropaleontol., 20, 215–234, https://doi.org/10.1016/0377-8398(93)90034-u, 1993.

Linnaeus, C.: Systema Naturae per Regnia tria Naturae, secundum classes, ordines, genera, species, cum characteribus, differentiis, synonymis, locis, Stockholm, 823 pp., 1758.

Lipps, J. H., DeLaca, T. E., Krebs, W. N., and Stockton, W.: Shallow-water foraminifera studies, Antarctic Peninsula, 1971–1972, Foraminiferal ecology, Antarctic Peninsula, Antarctic, Journal of the United States, 7, 82–83, 1972.

Loeblich, A. R. and Tappan, H.: Revision of some recent foraminiferal genera, Smithsonian Miscellaneous Collections, 128, 1–37, 1955.

Loeblich, A. R. and Tappan, H.: Suprageneric classification of the Rhizopodea, J. Paleontol., 35, 245–330, 1961.

Loeblich, A. R. and Tappan, H.: Some new proteinaceous and agglutinated genera of Foraminiferida, J. Paleontol., 58, 1158–1163, 1984.

Loeblich, A. R. and Tappan, H.: Some new and redefined genera and families of Textulariina, Fusulinina, Involutinina and Miliolina (Foraminiferida), J. Foramin. Res., 16, 334–346, 1986.

Loeblich, A. R. and Tappan, H.: Foraminiferal genera and their classification, Van Nostrand Reinhold, New York, 1988.

Loeblich, A. R. and Tappan, H.: Foraminifera of the Sahul Shelf and Timor Sea, Cushman Foundation for Foraminiferal Research Special Publication, 31, 1–661, 1994.

Loubere, P., Meyers, P., and Gary, A.: Benthic foraminiferal microhabitat selection, carbon isotope values, and association with larger animals – a test with *Uvigerina peregrina*, J. Foramin. Res., 25, 83–95, 1995.

Loubere, P., Jacobsen, B., Klitgaard Kristensen, D., Husum, K., Jernas, P., and Richaud, M.: The structure of benthic environments and the paleochemical record of foraminifera, Deep-Sea Res. Pt. I, 58, 535–545, https://doi.org/10.1016/j.dsr.2011.02.011, 2011.

Luo, M., Chen, L. Y., Wang, S. H., Yan, W., Wang, H. B., and Chen, D. F.: Pockmark activity inferred from pore water geochemistry in shallow sediments of the pockmark field in southwestern Xisha Uplift, northwestern South China Sea, Mar. Petrol. Geol., 48, 247–259, https://doi.org/10.1016/j.marpetgeo.2013.08.018, 2013.

Mackensen, A., Grobe, H., Kuhn, G., and Futterer, D. K.: Benthic Foraminiferal Assemblages from the Eastern Weddell Sea Between 68 and 73° S – Distribution, Ecology and

Fossilisation Potential, Mar. Micropaleontol., 16, 241–283, https://doi.org/10.1016/0377-8398(90)90006-8, 1990.
Mackensen, A., Futterer, D. K., Grobe, H., and Schmiedl, G.: Benthic Foraminiferal Assemblages from the Eastern South-Atlantic Polar Front Region Between 35 and 57° S – Distribution, Ecology and Fossilization Potential, Mar. Micropaleontol., 22, 33–69, https://doi.org/10.1016/0377-8398(93)90003-g, 1993.
Majewski, W.: Benthic foraminiferal communities: distribution and ecology in Admiralty Bay, King George Island, West Antarctica, Pol. Polar Res., 26, 159–214, 2005.
Majewski, W.: Benthic foraminifera from West Antarctic fiord environments: An overview, Pol. Polar Res., 31, 61–82, https://doi.org/10.4202/ppres.2010.05, 2010.
Majewski, W.: Benthic foraminifera from Pine Island and Ferrero bays, Amundsen Sea, Pol. Polar Res., 34, 169–200, https://doi.org/10.2478/popore-2013-0012, 2013.
Majewski, W. and Anderson, J. B.: Holocene foraminiferal assemblages from Firth of Tay, Antarctic Peninsula: Paleoclimate implications, Mar. Micropaleontol., 73, 135–147, https://doi.org/10.1016/j.marmicro.2009.08.003, 2009.
Marie, P.: La foraminifères de la Craie à Belemnitella mucronata du Bassin de Paris, Mémoires de Museum Nationale d'Histoire Naturelle, 12, 1–296, 1941.
Maync, W.: Critical taxonomic study and nomenclatural revision of the Lituolidae based upon the prototype of the family, *Lituola nautiloidea* Lamarck 1804, Contributions from the Cushman Foundation for Foraminiferal Research, 3, 35–56, 1952.
McCorkle, D. C. and Emerson, S. R.: The relationship between pore water carbon isotopic composition and bottom water oxygen concentration, Geochim. Cosmochim. Ac., 52, 1169–1178, https://doi.org/10.1016/0016-7037(88)90270-0, 1988.
McCorkle, D. C., Emerson, S. R., and Quay, P. D.: Stable carbon isotopes in marine porewaters, Earth Planet. Sc. Lett., 74, 13–26, https://doi.org/10.1016/0012-821x(85)90162-1, 1985.
McCorkle, D. C., Keigwin, L. D., Corliss, B. H., and Emerson, S. R.: The influence of microhabitats on the carbon isotopic composition of deep-sea benthic foraminifera, Paleoceanography, 5, 161–185, https://doi.org/10.1029/PA005i002p00161, 1990.
McCorkle, D. C., Corliss, B. H., and Farnham, C. A.: Vertical distributions and stable isotopic compositions of live (stained) benthic foraminifera from the North Carolina and California continental margins, Deep-Sea Res. Pt. I, 44, 983–1024, https://doi.org/10.1016/S0967-0637(97)00004-6, 1997.
McCulloch, I.: Qualitative observations on Recent foraminiferal tests with emphasis on the eastern Pacific, University of Southern California, Los Angeles, 1977.
Meredith, M. P., Brandon, M. A., Murphy, E. J., Trathan, P. N., Thorpe, S. E., Bone, D. G., Chernyshkov, P. P., and Sushin, V. A.: Variability in hydrographic conditions to the east and northwest of South Georgia, 1996–2001, J. Marine Syst., 53, 143–167, https://doi.org/10.1016/j.jmarsys.2004.05.005, 2005.
Mikhalevich, V. I.: Systematics and evolution of forminifera in the light of new data on their cytology and ultrastructure, Trudy Zoologicheskogo Instituta Akademiya Nauk SSSR, 94, 42–61, 1980.
Mikhalevich, V. I.: A new classification of the class Astrorhizata, Zoosystematica Rossica, 3, 161–174, 1995.
Mikhalevich, V. I.: The general aspects of the distribution of Antarctic foraminifera, Micropaleontology, 50, 179–194, https://doi.org/10.1661/0026-2803(2004)050[0179:moeoti]2.0.co;2, 2004.
Miklukho-Maklay, A. D.: Upper Palaeozoic of Central Asia, Leningradskiy Universitet, Lenigrad, 1963.
Milam, R. W. and Anderson, J. B.: Distribution and Ecology of Recent Benthonic Foraminifera of the Adelie-George-V Continental-Shelf and Slope, Antarctica, Mar. Micropaleontol., 6, 297–325, 1981.
Montagu, G.: Testacea Britannica or Natural History of British Shells, Marine, Land, and Fresh-Water, Including the Most Minute, J. S. Hollis, Romsey, England, 1803.
Montfort, P. D. d.: Conchyliologie systématique et classification méthodique des coquilles, F. Schoell, Paris, 676 pp., 1808.
Moreman, W. L.: Arenaceous foraminifera from Ordovician and Silurian limestones of Oklahoma, J. Paleontol., 4, 42–59, 1930.
Murphy, E. J., Hofmann, E. E., Watkins, J. L., Johnston, N. M., Pinones, A., Ballerini, T., Hill, S. L., Trathan, P. N., Tarling, G. A., Cavanagh, R. A., Young, E. F., Thorpe, S. E., and Fretwell, P.: Comparison of the structure and function of Southern Ocean regional ecosystems: The Antarctic Peninsula and South Georgia, J. Marine Syst., 109, 22–42, https://doi.org/10.1016/j.jmarsys.2012.03.011, 2013.
Murray, J. W. and Bowser, S. S.: Mortality, protoplasm decay rate, and reliability of staining techniques to recognize "living" foraminifera: A review, J. Foramin. Res., 30, 66–70, https://doi.org/10.2113/0300066, 2000.
Murray, J. W. and Pudsey, C. J.: Living (stained) and dead foraminifera from the newly ice-free Larsen Ice Shelf, Weddell Sea, Antarctica: ecology and taphonomy, Mar. Micropaleontol., 53, 67–81, https://doi.org/10.1016/j.marmicro.2004.04.001, 2004.
Nomaki, H., Heinz, P., Hemleben, C., and Kitazato, H.: Behavior and response of deep-sea benthic foraminifera to freshly supplied organic matter: A laboratory feeding experiment in microcosm environments, J. Foramin. Res., 35, 103–113, https://doi.org/10.2113/35.2.103, 2005.
Ohga, T. and Kitazato, H.: Seasonal changes in bathyal foraminiferal populations in response to the flux of organic matter (Sagami Bay, Japan), Terra Nova, 9, 33–37, https://doi.org/10.1046/j.1365-3121.1997.d01-6.x, 1997.
Parker, F. L.: Foraminiferal distribution in the Long Island Sound – Buzzards Bay area, Bulletin of the Museum of Comparative Zoology, Harvard, 106, 428–473, 1952.
Parker, W. K. and Jones, T. R.: On some foraminifera from the North Atlantic and Arctic Oceans, including Davis Straits and Baffin's Bay, Philos. T. R. Soc., 155, 325–441, 1865.
Parr, W. J.: On *Torrresina*, a new genus of the foraminifera from eastern Australia, Journal of the Royal Microscopical Society, 64, 129–135, 1947.
Parr, W. J.: Foraminifera, in: Reports B.A.N.Z. Antarctic Research Expedition 1929–1931, 232–392, 1950.
Patterson, R. T. and Richardson, R. H.: A taxonomic revision of the unilocular Foraminifera, J. Foramin. Res., 17, 212–226, 1987.
Pearcey, F. G.: Foraminifera of the Scottish National Antarctic Expedition, T. Roy. Soc. Edin., 49, 991–1044, 1914.
Peck, V. L., Allen, C. S., Kender, S., McClymont, E. L., and Hodgson, D.: Oceanographic variability on the West Antarctic Peninsula during the Holocene and the influence of up-

per circumpolar deep water, Quaternary Sci. Rev., 119, 54–65, https://doi.org/10.1016/j.quascirev.2015.04.002, 2015.

Piña-Ochoa, E., Høgslund, S., Geslin, E., Cedhagen, T., Revsbech, N. P., Nielsen, L. P., Schweizer, M., Jorissen, F., Rysgaard, S., and Risgaard-Petersen, N.: Widespread occurrence of nitrate storage and denitrification among Foraminifera and Gromiida, P. Natl. Acad. Sci. USA, 107, 1148–1153, https://doi.org/10.1073/pnas.0908440107, 2010.

Puri, H. S.: Contribution to the study of the Miocene of teh Florida panhandle, Bulletin Florida State Geological Survey, 36, 1–345, 1954.

Rauzer-Chernousova, D. M. and Reytlinger, E. A.: On the suprageneric systematics of the Order Hormosinida (Foraminifera), Paleontologicheskiy Zhurnal, 1986, 15–20, 1986.

Ravelo, A. C. and Hillaire-Marcel, C.: The use of oxygen and carbon isotopes of foraminifera in paleoceanography, in: Proxies in Late Cenozoic Paleoceanography, edited by: Hillaire-Marcel, C. and De Vernal, A., Developments in Marine Geology, Elsevier, Amsterdam, 735–764, 2007.

Reuss, A. E.: Uber zwei neue Arten von Foraminiferen aus dem Tegel van Baden und Mollersdorf, in: Bericht uder die Mittheilungen Freunden der Naturwissenschaften in Wien, edited by: Czjzek, J., 50–56, 1849.

Reuss, A. E.: Neues Foraminiferen aus den Schichten des Osterreichischen Tertiarbeckens, Denkschriften der Akademie des Wissenschaften, 1, 365–390, 1850.

Reuss, A. E.: Die Foraminiferen der westphälischen Kreideformation, Sitzungsberichte der mathematisch-naturwissenschaflichen Classe der kaiserlichen Akademie der Wissenschaften, 40, 147–238, 1860.

Reuss, A. E.: Entwurf einer systematischen Zusammenstellung der Foraminiferen, Sitzungsberichte der Kaiserlichen Akademie der Wissenschaften in Wien. Mathematicsch-Naturwissenschaftliche Classe, 1861, 355–396, 1862.

Reuss, A. E.: Die Foraminiferen, Anthozoen und Bryozoen des deutschen Septarienthones, Denkschriften der Akademie des Wissenschaften, Wien, 25, 117–214, 1866.

Rhumbler, L.: Entwurf eines naturlichen systems der Thalamophoren, Nachrichten von der Gesellschaft der Wissenschaften zu Gottingen, Math-Physik Klasse, 1895, 51–98, 1895.

Rhumbler, L.: Die Foraminiferen (Thalamophoren) der Plankton-Expedition, Erster Teil, Die allgemein Organizationsverhaltnisse der Foraminiferen, Ergebnisse der Plankton-Expedition der Humboldt-Stiftung Kiel u Liepzig, 3, 1–331, 1911.

Rodrigues, A. R., Eichler, P. P. B., and Eichler, B. B.: Foraminifera in two inlets fed by a tidewater glacier, King George Island, Antarctic Peninsula, J. Foramin. Res., 43, 209–220, 2013.

Saidova, K. M.: Bentosnye Foraminifery rayona kurilo-Kamchatskogo zheloba (po materianlam 39-go reysa e/s "Vityaz") [Benthic foraminifera in the Kurile-Kamchatka region based on the data of the 39th cruise of the R/V "Vityaz."], Trudy Instituta Okeanologii, 86, 134–161, 1970.

Saidova, K. M.: Bentosniye foraminifery Tikhogo Okeana, P.P. Shirshov Institute of Oceanology, Academy of Sciences of the USSR, Moscow, 1975.

Saidova, K. M.: O sovremennom sostoyanii sistemy nadvidovykh taksonov Kaynozoyskikh bentosnykh foraminifer [On an up-to-date system of supraspecific taxonomy of Cenozoic benthonic foraminifera], Akademiya Nauk SSSR, Moscow, 1981.

Sars, M.: Fortsatte bemerkinger over det dyriske livs udbredning i havets dybder, Förhandlinger i Videnskabsselskabet i Kristiania, 1869, 246–275, 1869.

Schilman, B., Almogi-Labin, A., Bar-Matthews, M., and Luz, B.: Late Holocene productivity and hydrographic variability in the eastern Mediterranean inferred from benthic foraminiferal stable isotopes, Paleoceanography, 18, https://doi.org/10.1029/2002pa000813, 2003.

Schmiedl, G., Mitschele, A., Beck, S., Emeis, K. C., Hemleben, C., Schulz, H., Sperling, M., and Weldeab, S.: Benthic foraminiferal record of ecosystem variability in the eastern Mediterranean Sea during times of sapropel S-5 and S-6 deposition, Palaeogeogr. Palaeocl., 190, 139–164, https://doi.org/10.1016/s0031-0182(02)00603-x, 2003.

Schmiedl, G., Pfeilsticker, M., Hemleben, C., and Mackensen, A.: Environmental and biological effects on the stable isotope composition of recent deep-sea benthic foraminifera, from the western Mediterranean Sea, Mar. Micropaleontol., 51, 129–152, https://doi.org/10.1016/j.marmicro.2003.10.001, 2004.

Schultze, M. J. S.: Über den Organismus der Polythalamien (Foraminiferen), nebst Bemerkungen über die Rhizopoden im allgemeinen, Leipzig, Ingelmann, 1854.

Schulze, F. E.: Rhizopodenstudien. III., Archiv für Mikroskopische Anatomie 11, 94–139, 1875.

Schwager, C.: Saggio di una classificazione dei foraminiferi avuto riguardo alle loro famiglie naturali, Bolletino R. Comitato Geologico d'Italia, 7, 475–485, 1876.

Schwager, C.: Quadro del proposto sistema di classificazione dei foraminiferi con guscio, Bolletino R. Comitato Geologico d'Italia, 8, 18–27, 1877.

Seguenza, G.: Dei terreni Terziarii del distretto di Messina: Parte II – Descrizione dei foraminiferi monotalamici delle marne Mioceniche del distretto di Messina, T. Capra, Messina, 1862.

Setoyama, E. and Kaminski, M. A.: Neogene benthic foraminifera from the southern Bering Sea (IODP Expedition 323), Palaeontologia Electronica, 18.2.38A, 1–30, 2015.

Shchedrina, Z. G.: O nekotorykh izmeneniyakh v sisteme semeytv Astrorhizidae i Reophacidae (Foraminifera) [On some changes in the systematics of the families Astrorhizidae and Reopacidae (Foraminifera)], Voprosy Mikropaleontologii, 11, 157–170, 1969.

Silvestri, A.: Lo stipite della Elissoforme e le sue affinita, Memorie della Pontificia Accademia della Scienze, Nouvi Lincei, 6, 231–270, 1923.

Silvestri, O.: Saggio di studi sulla fauna microscopia fossile appartenente al terreno subappenino italiano. Mem. I – monografia delle Nodosarie, Academia Gioenia Scienze Naturali Catania 7, 108, 1872.

Stefanoudis, P. V., Bett, B. J., and Gooday, A. J.: Relationship between "live" and dead benthic foraminiferal assemblages in the abyssal NE Atlantic, Deep-Sea Res. Pt. I, 121, 190–201, https://doi.org/10.1016/j.dsr.2017.01.014, 2017.

Sweetman, A. K., Sommer, S., Pfannkuche, O., and Witte, U.: Retarded response by macrofauna-size foraminifera to phytodetritus in a deep Norwegian fjord, J. Foramin. Res., 39, 15–22, https://doi.org/10.2113/gsjfr.39.1.15, 2009.

Tachikawa, K. and Elderfield, H.: Microhabitat effects on Cd / Ca and δ^{13}C of benthic foraminifera, Earth Planet. Sc. Lett.,

202, 607–624, https://doi.org/10.1016/S0012-821X(02)00796-3, 2002.

Thalmann, H. E.: Nomenclator (Um- und Neubennungen) zu den Tafeln 1 bis 115 in H. B. Brady's Werk uber die Foraminferen der *Challenger*-Expedition, London 1884, Eclogae Geologicae Helvetiae, 25, 293–312, 1932.

Theodor, M., Schmiedl, G., and Mackensen, A.: Stable isotope composition of deep-sea benthic foraminifera under contrasting trophic conditions in the western Mediterranean Sea, Mar. Micropaleontol., 124, 16–28, https://doi.org/10.1016/j.marmicro.2016.02.001, 2016.

Thorpe, S. E., Heywood, K. J., Brandon, M. A., and Stevens, D. P.: Variability of the southern Antarctic Circumpolar Current front north of South Georgia, J. Marine Syst., 37, 87–105, https://doi.org/10.1016/s0924-7963(02)00197-5, 2002.

Uchio, T.: Ecology of living benthonic foraminifera from the San Diego, California area, Special Publications Cushman Laboratory for Foraminiferal Research, 5, 1–72, 1960.

Uchio, T.: Influence of the River Shinano on foraminifera and sediment grain size distribution, Publications of the Seto Marine Biological Laboratory, 10, 363–392, 1962.

Van Marle, L.: Eastern Indonesia Late Cenozoic smaller benthic foraminifera, Verhandeling Koninklijke Nederlandse Akademie van Wetenschappen, Afdeling Antuurkunde, Eerste Reeks, 34, 1–328, 1991.

Violanti, D.: Taxonomy and distribution of recent benthic foraminifers from Terra Nova Bay (Ross Sea, Antarctica), oceanographic campaign 1987/1988, Palaeontographica Italica, 83, 25–71, 1996.

Voloshinova, N. A.: Progress in micropalaeontology in the work of studying the inner structure of Foraminifera, Trudy Pervogo Seminara po Mikrofaune, 48–87, 1960.

Wang, F., Gao, M., Liu, J., Pei, S., Li, C., Mei, X., and Yang, S.: Distribution and environmental significance of live and dead benthic foraminiferal assemblages in surface sediments of Laizhou Bay, Bohai Sea, Mar. Micropaleontol., 123, 1–14, https://doi.org/10.1016/j.marmicro.2015.12.006, 2016.

Wedekind, P. R.: Einfuhrung in die Grundlagen der historischen Geologie. Band II. Mikrobiostratigraphie der Korallen- und Foraminiferenzeit, Ferdinand Enke, Stuttgart, 1937.

Weldeab, S., Arce, A., and Kasten, S.: Mg / Ca-Delta CO3pore2-(water)-temperature calibration for Globobulimina spp.: A sensitive paleothermometer for deep-sea temperature reconstruction, Earth Planet. Sc. Lett., 438, 95–102, https://doi.org/10.1016/j.epsl.2016.01.009, 2016.

Wiesner, H.: Die Foraminiferen der Deutschen Südpolar Expedition 1901–1903. Deutschen Südpolar Expedition, Berlin (Zoology), 20, 53–165, 1931.

Williamson, W. C.: On the Recent British species of the genus *Lagena*, Annals and Magazine of Natural History, 2, 1–20, 1848.

Witte, U., Wenzhofer, F., Sommer, S., Boetius, A., Heinz, P., Aberle, N., Sand, M., Cremer, A., Abraham, W. R., Jorgensen, B. B., and Pfannkuche, O.: In situ experimental evidence of the fate of a phytodetritus pulse at the abyssal sea floor, Nature, 424, 763–766, 2003.

Zahn, R., Winn, K., and Sarnthein, M.: Benthic foraminiferal $\delta^{13}C$ and accumulation rates of organic carbon: *Uvigerina peregrina* group and *Cibicidoides wuellerstorfi*, Paleoceanography, 1, 27–42, 1986.

Zheng, S. and Fu, Z.: Fauna Sinica, Phylum Granuloreticulosa, Class Foraminiferea, Agglutinated Foraminifera, Science Press, Beijing, 2001.

Appendix A6 – Surface sample BFA census counts

		Rhabdammina spp.	*Hippocrepinella alba*	*Rhizammina* spp.	*Lagenammina* cf. *sphaerica*	*Saccamina* spp.	*Astrammina rara*	*Psammospaera bowmanni*	*Psammospaera fusca*	*Ammodiscus incertus*	*Miliammina earlandi*	*Milammina lata*
BC656	Total	0	0	0	1	2	0	0	2	1	22	0
	Stained	0	0	0	0	0	0	0	0	0	4	0
BC660	Total	1	0	0	1	0	0	0	2	0	30	2
	Stained	0	0	0	0	0	0	0	0	0	8	0
BC667	Total	0	1	2	25	0	1	0	3	11	99	9
	Stained	0	0	0	0	0	0	0	0	0	1	0
BC671	Total	0	11	8	6	0	0	0	2	5	52	2
	Stained	0	11	0	2	0	0	0	1	0	2	0
BC737	Total	2	1	4	10	0	4	0	0	9	44	0
	Stained	0	1	0	0	0	2	0	0	1	11	0
BC738	Total	1	0	9	3	0	0	1	2	0	86	0
	Stained	0	0	0	2	0	0	0	0	0	14	0

		Hormosinelloides guttifer	*Reophax subdentaliniformis*	*Reophax subfusiformis*	*Haplophragmoides bradyi niigatensis*	*Haplophragmoide quadratus*	*Labrosprira scitula*	*Labrospira* sp. 1	*Glaphyrammina americana*	*Glaphyrammina rostrata*	*Recurvoides* sp. 1	*Pseudobolivina antarctica*
BC656	Total	0	13	0	0	0	7	3	0	18	0	0
	Stained	0	3	0	0	0	2	1	0	2	0	0
BC660	Total	0	11	0	0	0	4	7	3	13	1	0
	Stained	0	1	0	0	0	1	2	0	1	1	0
BC667	Total	21	23	5	1	15	20	37	0	21	2	2
	Stained	7	0	1	1	0	1	2	0	1	0	0
BC671	Total	0	18	3	0	7	5	13	0	2	0	0
	Stained	0	5	0	0	0	2	3	0	0	0	0
BC737	Total	0	33	0	0	0	32	1	0	6	2	1
	Stained	0	8	0	0	0	8	1	0	3	0	0
BC738	Total	6	77	0	0	0	55	4	1	24	0	0
	Stained	6	26	0	0	0	14	0	0	2	0	0

		Portatrochammina antarctica weisneri	*Deuterammina scoresbyi*	*Pseudotrochamina* **.sp. 1**	*Cyclammina* **cf** *contorta*	*Textularia earlandi*	*Cornuspira antarctica*	*Quniqueloculina* **cf.** *occidentalis*	*Quniqueloculina* **cf.** *sublineata*	*Triloculina* **sp. 1**	*Hyalinonetrion* **cf.** *gracillima*	*Procerolagena distoma*
BC656	Total	7	2	2	0	0	0	0	0	1	0	0
	Stained	3	0	0	0	0	0	0	0	0	0	0
BC660	Total	6	5	11	0	0	0	0	0	0	0	0
	Stained	1	0	3	0	0	0	0	0	0	0	0
BC667	Total	38	17	34	1	5	0	1	0	1	3	0
	Stained	0	0	0	0	0	0	1	0	0	0	0
BC671	Total	18	6	9	0	0	1	1	1	0	0	0
	Stained	5	0	0	0	0	0	0	0	0	0	0
BC737	Total	8	7	13	0	1	0	3	0	0	0	1
	Stained	0	1	0	0	0	0	3	0	0	0	0
BC738	Total	5	12	0	0	1	0	10	0	0	0	0
	Stained	0	3	0	0	0	0	6	0	0	0	0

		Pygmaeoseistron hispidulum	*Oolina globosa*	*Vasicostella striatopunctata*	*Fissurina* **sp. 2**	*Parafissurina fusiformis*	*Bolivinellina earlandi*	*Cassidulinoides parkerianus*	*Cassidulinoides porrectus*	*Globocassidulina crassa rossensis*	*Bulimina aculeata*	*Bulimina* **sp. 1**
BC656	Total	0	0	0	0	0	0	2	1	0	0	0
	Stained	0	0	0	0	0	0	1	1	0	0	0
BC660	Total	0	0	1	0	0	1	1	0	1	0	0
	Stained	0	0	0	0	0	0	0	0	0	0	0
BC667	Total	0	0	0	0	9	9	3	37	81	7	0
	Stained	0	0	0	0	0	0	0	0	42	0	0
BC671	Total	0	0	0	0	0	1	26	9	4	1	2
	Stained	0	0	0	0	0	0	1	1	0	0	0
BC737	Total	0	1	0	0	0	2	0	39	12	1	0
	Stained	0	0	0	0	0	0	0	5	0	0	0
BC738	Total	1	0	0	1	3	0	2	45	7	3	0
	Stained	0	0	0	0	0	0	0	3	0	0	0

		Trifarina earlandi	*Fursenkoina fusiformis*	*Cibicides* **Sp. 1**	*Cibicides* **sp. 2**	*Nonionella bradii*	*Nonionella iridea*	*Astrononio echolsi*	*Pullenia subcarinata*	*Chilostomella* **sp. 1**	*Buccella* **sp. 1**	*Buccella* **sp. 2**
BC656	Total	0	0	0	0	0	0	17	0	0	0	0
	Stained	0	0	0	0	0	0	2	0	0	0	0
BC660	Total	1	3	0	0	0	7	10	0	0	0	0
	Stained	1	0	0	0	0	0	2	0	0	0	0
BC667	Total	27	31	0	0	3	8	53	3	0	6	0
	Stained	0	0	0	0	0	0	0	0	0	1	0
BC671	Total	0	2	0	0	0	3	16	0	1	7	1
	Stained	0	0	0	0	0	0	2	0	0	0	0
BC737	Total	1	9	1	1	0	0	49	0	0	1	0
	Stained	0	0	0	0	0	0	0	0	0	0	0
BC738	Total	2	2	0	0	0	0	46	1	0	1	0
	Stained	0	0	0	0	0	0	5	0	0	1	0

Appendix A7 – BC737 and BC738 BFA census counts

		Rhabdammina spp.	*Hippocrepinella alba*	*Rhizammina* spp.	*Lagenammina sphaerica*	*Saccamina* spp	*Astrammina rara*	*Psammospaera bowmanni*	*Psammospaera fusca*	*Ammodiscus incertus*	*Miliammina earlandi*	*Miliammina lata*
BC737												
0-1cm	Total	0	5	5	7	0	2	0	8	11	108	0
	Stained	0	5	0	2	0	0	0	1	2	18	0
1-2cm	Total	3	2	5	7	0	1	0	6	8	132	5
	Stained	0	2	0	0	0	1	0	0	4	38	2
2-3cm	Total	0	0	0	1	0	2	0	2	15	181	2
	Stained	0	0	0	0	0	0	0	0	3	26	0
3-4cm	Total	0	0	0	3	0	0	0	1	7	186	3
	Stained	0	0	0	0	0	0	0	0	1	28	0
4-5cm	Total	0	0	0	1	0	0	1	0	5	156	1
	Stained	0	0	0	0	0	0	0	0	1	32	0
5-6cm	Total	0	0	0	0	0	0	0	0	4	148	0
	Stained	0	0	0	0	0	0	0	0	0	40	0
6-7cm	Total	0	0	0	0	0	0	0	1	0	174	1
	Stained	0	0	0	0	0	0	0	0	0	58	1
7-8cm	Total	0	0	0	0	1	0	0	0	1	118	0
	Stained	0	0	0	0	0	0	0	0	0	8	0
8-9cm	Total	0	0	0	0	0	0	0	1	3	98	4
	Stained	0	0	0	0	0	0	0	0	0	1	0
9-10cm	Total	0	0	0	0	0	0	0	0	3	96	4
	Stained	0	0	0	0	0	0	0	0	0	1	1
10-11cm	Stained	0	0	0	0	0	0	0	0	0	0	0
11-12cm	Stained	0	0	0	0	0	0	0	0	0	0	0
12-13cm	Stained	0	0	0	0	0	0	0	0	0	0	0
BC738												
0-1cm	Total	0	5	5	4	1	2	2	5	6	103	0
	Stained	0	5	0	0	0	0	0	0	1	14	0
1-2cm	Total	4	3	10	0	0	0	0	7	6	176	0
	Stained	0	3	0	0	0	0	0	0	2	23	0
2-3cm	Total	2	0	1	1	0	0	0	0	0	115	0
	Stained	0	0	0	0	0	0	0	0	0	8	0
3-4cm	Total	0	0	0	0	0	0	0	3	3	128	0
	Stained	0	0	0	0	0	0	0	0	2	10	0
4-5cm	Total	0	0	0	0	0	0	0	0	2	120	0
	Stained	0	0	0	0	0	0	0	0	0	3	0
5-6cm	Total	0	0	0	0	0	0	0	1	0	148	0
	Stained	0	0	0	0	0	0	0	0	0	0	0
6-7cm	Total	0	0	0	0	0	0	0	0	0	69	0
	Stained	0	0	0	0	0	0	0	0	0	2	0
7-8cm	Total	0	0	0	0	0	0	0	0	2	96	0
	Stained	0	0	0	0	0	0	0	0	0	0	0
8-9cm	Total	0	0	0	0	0	0	0	0	1	104	0
	Stained	0	0	0	0	0	0	0	0	0	0	0
9-10cm	Total	0	0	0	0	0	0	0	0	2	123	0
	Stained	0	0	0	0	0	0	0	0	0	0	0
10-11cm	Stained	0	0	0	0	0	0	0	0	0	0	0
11-12cm	Stained	0	0	0	0	0	0	0	0	0	0	0
12-13cm	Stained	0	0	0	0	0	0	0	0	0	0	0

		Hormosinella sp.	*Hormosinelloides guttifer*	*Nodulina dentaliniformis*	*Reophax subdentaliniformis*	*Reophax subfusiformis*	*Pseudotrochamina* sp. 1	*Haplophragmoides bradyi niigatensis*	*Haplophragmoide quadratus*	*Labrosprira scitula*	*Labrospira* sp. 1	*Glaphyrammina americana*
BC737												
0-1cm	Total	1	3	6	33	1	10	5	6	63	6	1
	Stained	0	0	0	14	0	2	2	0	52	0	0
1-2cm	Total	0	0	0	31	0	25	3	0	4	11	0
	Stained	0	0	0	2	0	3	3	0	4	0	0
2-3cm	Total	0	0	0	18	0	18	1	2	10	10	0
	Stained	0	0	0	0	0	0	0	0	0	0	0
3-4cm	Total	0	0	0	13	0	9	0	3	4	13	0
	Stained	0	0	0	0	0	0	0	0	0	2	0
4-5cm	Total	0	0	0	2	1	17	1	3	4	9	0
	Stained	0	0	0	0	0	0	0	0	0	2	0
5-6cm	Total	0	0	0	3	1	2	0	0	4	5	0
	Stained	0	0	0	0	0	0	0	0	0	1	0
6-7cm	Total	0	0	0	3	0	3	0	0	0	3	0
	Stained	0	0	0	0	0	0	0	0	0	1	0
7-8cm	Total	0	0	0	0	0	2	0	0	2	8	0
	Stained	0	0	0	0	0	0	0	0	0	0	0
8-9cm	Total	0	0	0	5	0	4	0	0	2	9	0
	Stained	0	0	0	0	0	0	0	0	0	1	0
9-10cm	Total	0	0	0	0	0	1	0	0	2	4	0
	Stained	0	0	0	0	0	0	0	0	0	0	0
10-11cm	Stained	0	0	0	0	0	0	0	0	0	0	0
11-12cm	Stained	0	0	0	0	0	0	0	0	0	0	0
12-13cm	Stained	0	0	0	0	0	0	0	0	0	0	0
BC738												
0-1cm	Total	3	0	0	38	1	9	5	0	48	4	1
	Stained	0	0	0	5	0	1	4	0	12	0	0
1-2cm	Total	0	0	0	37	1	2	0	0	15	11	0
	Stained	0	0	0	2	0	0	0	0	1	0	0
2-3cm	Total	0	1	0	35	1	6	0	0	9	15	0
	Stained	0	0	0	0	0	2	0	0	0	0	0
3-4cm	Total	0	0	0	22	0	0	0	0	10	13	0
	Stained	0	0	0	5	0	0	0	0	0	2	0
4-5cm	Total	0	0	0	21	0	1	2	0	12	8	0
	Stained	0	0	0	0	0	0	0	0	0	0	0
5-6cm	Total	0	0	0	1	2	3	0	0	6	7	0
	Stained	0	0	0	0	0	0	0	0	0	0	0
6-7cm	Total	0	0	0	9	0	0	0	0	2	2	0
	Stained	0	0	0	0	0	0	0	0	0	1	0
7-8cm	Total	0	0	0	6	1	1	0	0	3	4	0
	Stained	0	0	0	0	0	0	0	0	0	0	0
8-9cm	Total	0	0	0	2	0	0	0	0	5	6	0
	Stained	0	0	0	0	0	0	0	0	0	0	0
9-10cm	Total	0	0	0	2	0	0	0	0	1	7	0
	Stained	0	0	0	0	0	0	0	0	0	0	0
10-11cm	Stained	0	0	0	0	0	0	0	0	0	0	0
11-12cm	Stained	0	0	0	0	0	0	0	0	0	0	0
12-13cm	Stained	0	0	0	0	0	0	0	0	0	0	0

		Glaphyrammina rostrata	*Recurvoides* sp. 1	*Spiroplectammina biformis*	*Pseudobolivina antarctica*	*Portatrochammina antarctica weisneri*	*Deuterammina scoresbyi*	*Textularia earlandi*	*Quniqueloculina* cf *occidentalis*	*Quniqueloculina seminula*	*Triloculina* sp. 1	*Laevidentalina communis*
BC737												
0-1cm	Total	18	0	0	0	17	10	2	3	1	2	0
	Stained	5	0	0	0	1	6	0	3	0	2	0
1-2cm	Total	6	0	0	3	20	20	3	1	0	0	0
	Stained	2	0	0	0	2	9	1	0	0	0	0
2-3cm	Total	0	0	0	0	20	12	6	0	0	1	0
	Stained	0	0	0	0	3	1	0	0	0	0	0
3-4cm	Total	4	0	0	1	21	6	2	0	1	4	1
	Stained	0	0	0	0	4	0	0	0	0	2	0
4-5cm	Total	5	0	0	6	11	11	5	0	0	4	0
	Stained	0	0	0	0	1	2	0	0	0	3	0
5-6cm	Total	1	0	0	1	13	6	1	0	0	1	0
	Stained	0	0	0	0	1	4	0	0	0	1	0
6-7cm	Total	0	0	0	2	15	7	2	0	0	0	0
	Stained	0	0	0	0	0	5	0	0	0	0	0
7-8cm	Total	0	0	0	0	12	4	0	0	0	0	0
	Stained	0	0	0	0	0	1	0	0	0	0	0
8-9cm	Total	2	0	0	0	14	4	1	0	0	1	0
	Stained	0	0	0	0	1	0	0	0	0	0	0
9-10cm	Total	3	0	0	0	10	0	2	0	0	0	0
	Stained	0	0	0	0	1	0	0	0	0	0	0
10-11cm	Stained	0	0	0	0	0	0	0	0	0	0	0
11-12cm	Stained	0	0	0	0	2	0	0	0	0	0	0
12-13cm	Stained	0	0	0	0	1	0	0	0	0	0	0
BC738												
0-1cm	Total	44	8	0	0	11	25	0	3	0	0	0
	Stained	7	8	0	0	1	6	0	3	0	0	0
1-2cm	Total	28	0	0	0	9	11	7	0	0	0	0
	Stained	1	0	0	0	4	2	0	0	0	0	0
2-3cm	Total	9	0	0	1	11	13	0	0	0	0	0
	Stained	2	0	0	0	1	1	0	0	0	0	0
3-4cm	Total	11	0	0	0	13	4	1	0	0	0	0
	Stained	0	0	0	0	2	0	0	0	0	0	0
4-5cm	Total	26	0	0	3	14	5	1	0	0	0	0
	Stained	0	0	0	0	4	0	0	0	0	0	0
5-6cm	Total	9	0	0	0	7	2	1	0	0	0	0
	Stained	0	0	0	0	0	0	0	0	0	0	0
6-7cm	Total	9	0	0	0	9	1	0	0	0	0	0
	Stained	0	0	0	0	1	0	0	0	0	0	0
7-8cm	Total	7	0	0	0	14	1	2	0	0	0	0
	Stained	0	0	0	0	1	0	0	0	0	0	0
8-9cm	Total	6	0	0	0	10	1	0	0	0	0	0
	Stained	0	0	0	0	1	0	0	0	0	0	0
9-10cm	Total	6	0	1	1	10	4	1	0	0	0	0
	Stained	0	0	0	0	1	0	0	0	0	0	0
10-11cm	Stained	0	0	0	0	0	0	0	0	0	0	0
11-12cm	Stained	0	0	0	0	0	0	0	0	0	0	0
12-13cm	Stained	0	0	0	0	0	0	0	0	0	0	0

		Lotostomoides calomorphus	*Lagena substriata*	*Lagena multilatera*	*Procerolagena distoma*	*Pygmaeoseistron hispidulum*	*Pygmaeoseistron* sp.	*Fissurina subformosa*	*Oolina globosa*	*Oolina* spp.	*Fissurina* sp. 1	*Fissurina* sp. 2
BC737												
0-1cm	Total	0	0	0	1	0	0	0	0	1	0	2
	Stained	0	0	0	0	0	0	0	0	0	0	0
1-2cm	Total	8	0	0	0	0	0	0	0	0	0	1
	Stained	1	0	0	0	0	0	0	0	0	0	1
2-3cm	Total	2	0	0	2	0	0	1	0	0	3	0
	Stained	0	0	0	0	0	0	0	0	0	0	0
3-4cm	Total	0	0	0	3	0	0	0	0	0	0	2
	Stained	0	0	0	1	0	0	0	0	0	0	0
4-5cm	Total	0	1	0	1	0	0	0	0	0	0	3
	Stained	0	0	0	0	0	0	0	0	0	0	0
5-6cm	Total	0	0	0	1	0	0	0	0	0	0	1
	Stained	0	0	0	0	0	0	0	0	0	0	0
6-7cm	Total	0	0	0	1	0	0	0	0	0	0	2
	Stained	0	0	0	0	0	0	0	0	0	0	0
7-8cm	Total	0	2	0	2	0	0	0	0	0	0	1
	Stained	0	0	0	0	0	0	0	0	0	0	0
8-9cm	Total	1	0	0	0	0	0	0	0	0	0	1
	Stained	0	0	0	0	0	0	0	0	0	0	0
9-10cm	Total	0	0	0	0	0	0	0	0	0	0	0
	Stained	0	0	0	0	0	0	0	0	0	0	0
10-11cm	Stained	0	0	0	0	0	0	0	0	0	0	0
11-12cm	Stained	0	0	0	0	0	0	0	0	0	0	0
12-13cm	Stained	0	0	0	0	0	0	0	0	0	0	0
BC738												
0-1cm	Total	0	0	0	0	1	0	0	0	0	0	4
	Stained	0	0	0	0	0	0	0	0	0	0	2
1-2cm	Total	0	0	0	0	0	0	1	0	0	0	0
	Stained	0	0	0	0	0	0	0	0	0	0	0
2-3cm	Total	0	0	0	0	0	1	0	0	0	0	0
	Stained	0	0	0	0	0	0	0	0	0	0	0
3-4cm	Total	0	0	0	0	0	0	0	1	3	0	0
	Stained	0	0	0	0	0	0	0	0	0	0	0
4-5cm	Total	0	0	0	0	0	0	0	0	0	0	0
	Stained	0	0	0	0	0	0	0	0	0	0	0
5-6cm	Total	0	1	1	0	0	0	0	0	0	1	0
	Stained	0	0	0	0	0	0	0	0	0	0	0
6-7cm	Total	0	0	0	0	0	0	0	0	0	0	0
	Stained	0	0	0	0	0	0	0	0	0	0	0
7-8cm	Total	0	0	0	0	0	0	0	0	0	0	0
	Stained	0	0	0	0	0	0	0	0	0	0	0
8-9cm	Total	0	0	0	0	0	0	0	0	2	0	0
	Stained	0	0	0	0	0	0	0	0	0	0	0
9-10cm	Total	0	0	0	0	0	0	0	0	1	1	0
	Stained	0	0	0	0	0	0	0	0	0	0	0
10-11cm	Stained	0	0	0	0	0	0	0	0	0	0	0
11-12cm	Stained	0	0	0	0	0	0	0	0	0	0	0
12-13cm	Stained	0	0	0	0	0	0	0	0	0	0	0

		Parafissurina fusiformis	*Bolivinellina earlandi*	*Cassidulinoides parkerianus*	*Cassidulinoides porrectus*	*Globocassidulina crassa rossensis*	*Bulimina aculeata*	*Bulimina subteres*	*Bulimina* sp. 1	*Trifarina earlandi*	*Fursenkoina fusiformis*	*Discorbis vilardeboanus*
BC737												
0-1cm	Total	0	6	1	78	33	3	0	0	0	16	1
	Stained	0	0	0	18	0	0	0	0	0	0	0
1-2cm	Total	0	15	8	86	6	4	0	2	2	9	0
	Stained	0	0	0	20	0	1	0	1	1	7	0
2-3cm	Total	1	2	8	78	21	5	0	0	5	45	1
	Stained	0	0	0	16	0	1	0	0	1	6	0
3-4cm	Total	1	2	6	94	31	2	1	0	4	39	1
	Stained	0	0	0	12	0	0	0	0	1	3	1
4-5cm	Total	0	1	10	63	35	2	1	0	1	33	1
	Stained	0	0	0	21	1	0	0	0	0	4	0
5-6cm	Total	0	0	7	63	12	4	0	0	3	17	1
	Stained	0	0	0	18	1	3	0	0	1	9	0
6-7cm	Total	1	0	7	48	6	3	1	0	5	47	0
	Stained	0	0	0	10	1	0	0	0	4	9	0
7-8cm	Total	0	0	4	30	4	5	0	0	5	37	0
	Stained	0	0	1	5	0	1	0	0	3	4	0
8-9cm	Total	0	2	3	39	5	2	0	2	0	32	0
	Stained	0	1	0	7	0	0	0	0	0	2	0
9-10cm	Total	0	2	6	42	3	4	0	0	3	27	0
	Stained	0	0	0	6	0	2	0	0	1	2	0
10-11cm	Stained	0	0	0	2	1	0	0	0	1	2	0
11-12cm	Stained	0	0	0	2	0	0	0	0	0	1	0
12-13cm	Stained	0	0	0	2	0	0	0	0	0	0	0
BC738												
0-1cm	Total	0	1	8	46	5	1	0	0	0	4	2
	Stained	0	0	0	21	0	1	0	0	0	0	1
1-2cm	Total	1	10	20	49	3	0	0	1	1	23	0
	Stained	0	0	0	10	0	0	0	0	1	0	0
2-3cm	Total	1	2	26	43	8	0	0	1	0	13	1
	Stained	0	0	0	18	0	0	0	0	0	1	1
3-4cm	Total	0	0	20	59	5	0	0	0	7	11	0
	Stained	0	0	1	9	0	0	0	0	3	0	0
4-5cm	Total	0	0	37	47	3	0	0	0	3	5	0
	Stained	0	0	1	10	0	0	0	0	1	0	0
5-6cm	Total	1	0	45	38	4	0	0	0	1	15	0
	Stained	0	0	0	5	0	0	0	0	1	0	0
6-7cm	Total	0	0	31	19	1	2	0	1	2	2	0
	Stained	0	0	0	6	0	1	0	0	2	0	0
7-8cm	Total	0	0	34	22	2	1	0	2	0	8	0
	Stained	0	0	0	1	0	0	0	0	0	0	0
8-9cm	Total	0	1	48	26	1	0	0	2	0	3	0
	Stained	0	0	0	0	0	0	0	0	0	0	0
9-10cm	Total	1	0	42	18	0	2	0	2	1	9	0
	Stained	0	0	0	0	0	2	0	0	1	0	0
10-11cm	Stained	0	0	0	0	0	0	0	0	0	0	0
11-12cm	Stained	0	0	0	0	0	0	0	0	0	0	0
12-13cm	Stained	0	0	0	0	0	0	0	0	0	0	0

		Cibicides sp. 1	*Nonionella bradii*	*Nonionella iridea*	*Astrononion echolsi*	*Pullenia subcarinata*	*Buccella* sp. 1	*Buccella* sp. 2
BC737								
0-1cm	Total	0	4	1	62	1	7	0
	Stained	0	0	0	23	0	4	0
1-2cm	Total	0	2	4	85	0	11	2
	Stained	0	0	0	18	0	3	0
2-3cm	Total	0	7	27	70	0	15	0
	Stained	0	0	0	17	0	3	0
3-4cm	Total	0	2	27	39	1	15	2
	Stained	0	0	0	11	0	1	0
4-5cm	Total	0	8	28	41	0	15	1
	Stained	0	0	2	20	0	3	0
5-6cm	Total	0	0	20	33	0	17	1
	Stained	0	0	0	10	0	3	0
6-7cm	Total	0	1	21	23	0	14	0
	Stained	0	0	0	12	0	5	0
7-8cm	Total	0	1	11	28	0	10	0
	Stained	0	0	0	8	0	3	0
8-9cm	Total	0	3	11	30	0	15	0
	Stained	0	0	0	8	0	2	0
9-10cm	Total	0	0	8	27	0	6	2
	Stained	0	0	0	4	0	0	0
10-11cm	Stained	0	0	0	1	0	0	0
11-12cm	Stained	0	0	0	1	0	1	0
12-13cm	Stained	0	0	0	1	0	0	0
BC738								
0-1cm	Total	1	0	2	47	1	0	0
	Stained	0	0	0	19	0	0	0
1-2cm	Total	0	1	2	45	0	1	0
	Stained	0	0	0	17	0	0	0
2-3cm	Total	0	2	2	31	5	0	0
	Stained	0	0	0	15	2	0	0
3-4cm	Total	1	1	3	30	1	3	0
	Stained	1	0	0	13	0	1	0
4-5cm	Total	0	0	2	29	2	2	1
	Stained	0	0	0	9	2	1	0
5-6cm	Total	0	1	0	23	8	3	0
	Stained	0	0	0	9	3	0	0
6-7cm	Total	0	0	1	15	2	1	0
	Stained	0	0	0	2	2	1	0
7-8cm	Total	0	0	0	16	1	1	0
	Stained	0	0	0	1	0	0	0
8-9cm	Total	0	3	1	24	3	1	0
	Stained	0	0	0	1	1	0	0
9-10cm	Total	0	0	1	16	0	2	0
	Stained	0	0	0	0	0	0	0
10-11cm	Stained	0	0	0	0	0	0	0
11-12cm	Stained	0	0	0	0	0	0	0
12-13cm	Stained	0	0	0	1	0	0	0

Appendix A8 – GC666 BFA census counts

Sample No.	*Ammodiscus incertus*	*Miliammina earlandi*	*Milammina lata*	*Reophax subfusiformis*	*Portatrochammina antarctica wiesneri*	*Haplophragmoides quadratus*	*Labrospira* sp. 1	*Glaphyrammina rostrata*	*Pseudobolivina antarctica*	*Deuterammina scoresbyi*	*.Pseudotrochammina* sp. 1	*Textularia earlandi*	*Cornuspira antarctica*	*Triloculina* sp. 1
002	1	60	16	0	31	2	17	0	2	11	22	6	1	2
003	5	31	17	0	18	0	0	1	0	8	8	0	1	0
009	0	23	0	0	1	0	0	0	0	0	0	0	0	0
021	0	34	0	0	0	0	0	0	0	0	0	0	0	0
033	0	63	1	0	0	0	0	0	0	0	0	0	0	0
037	0	45	0	0	0	0	0	0	0	0	0	0	0	0
041	0	46	4	0	0	0	0	0	0	0	0	0	0	0
045	0	53	1	0	0	0	0	0	0	0	0	0	0	0
049	0	34	0	0	0	0	0	0	0	0	0	0	0	0
053	0	88	1	0	0	0	0	0	0	0	0	0	0	0
057	0	117	4	3	0	0	0	0	0	0	0	0	0	0
064	0	99	5	0	1	0	0	0	0	0	0	0	0	0
065	0	80	0	0	0	0	0	0	0	2	0	0	0	0
073	0	25	1	0	0	0	0	0	0	0	0	0	0	0
081	0	38	8	0	0	0	0	0	0	0	0	0	0	0
089	0	42	1	0	0	0	0	0	0	0	0	0	0	0
097	0	55	16	0	0	0	0	0	0	0	0	0	0	0
098	0	162	15	0	0	0	0	0	0	0	0	0	0	0
099	0	41	31	0	0	0	0	0	0	0	0	0	0	0
101	0	63	25	0	0	0	0	0	0	0	0	0	0	0
102	0	47	8	0	0	0	0	0	0	0	0	0	0	0
103	0	42	8	0	0	0	0	0	0	0	0	0	0	0
104	0	21	10	0	0	0	0	0	0	0	0	0	0	0
105	0	26	8	0	0	0	0	0	0	0	0	0	0	0
106	0	62	12	0	0	0	0	0	0	0	0	0	0	0
107	0	45	5	0	0	0	0	0	0	0	0	0	0	0
108	0	32	7	0	0	0	0	0	0	0	0	0	0	0
109	0	68	9	0	0	0	0	0	0	0	0	0	0	0
111	0	48	33	0	0	0	0	0	0	0	0	0	0	0
112	0	23	22	0	0	0	0	0	0	0	0	0	0	0
113	0	77	14	0	0	0	0	0	0	0	0	0	0	0
114	0	15	36	0	0	0	0	0	0	0	0	0	0	0
115	0	54	10	0	0	0	0	0	0	0	0	0	0	0
116	0	45	4	0	0	0	0	0	0	0	0	0	0	0
117	0	57	12	0	0	0	0	0	0	0	0	0	0	0
118	0	35	4	0	0	0	0	0	0	0	0	0	0	0
119	0	67	3	0	0	0	0	0	0	0	0	0	0	0
121	0	39	3	0	0	0	0	0	0	0	0	0	0	0
122	0	39	7	0	0	0	0	0	0	0	0	0	0	0
123	0	28	5	0	0	0	0	0	0	0	0	0	0	0
124	0	25	0	0	0	0	0	0	0	0	0	0	0	0
125	0	61	1	0	0	0	0	0	0	0	0	0	0	0
126	0	72	0	0	1	0	0	0	0	0	0	0	0	0
127	0	45	0	0	7	0	0	0	0	0	0	0	0	0
135	0	55	0	0	0	0	0	0	0	0	0	0	0	0

Sample No.	*Laevidentalina communis*	*Lotostomoides calomorphus*	*Nodosaria simplex*	*Lenticulina asterizans*	*?Astacolus*	*Lagena substriata*	*Lagena multilatera*	*Hyalinonetrion gracillimum*	*Procerolagena distoma*	*Pygmaeoseistron hispudulum*	*Oolina squamosa*	*Oolina* spp.	*Fissurina subformosa*	*Fissurina* sp. 1
002	1	1	0	0	0	0	2	0	0	0	0	0	1	2
003	0	1	0	0	0	0	2	2	0	0	0	0	0	1
009	0	0	0	0	0	0	0	3	0	1	0	0	0	0
021	0	0	0	0	0	0	0	2	0	0	0	0	0	0
033	0	0	0	0	0	0	0	1	0	0	0	0	0	0
037	0	0	0	0	0	0	0	0	0	0	0	0	0	0
041	0	0	0	0	0	0	0	0	0	0	0	0	0	0
045	0	0	0	0	0	0	0	0	0	0	0	0	0	0
049	0	0	0	0	0	0	0	0	0	0	0	0	0	0
053	0	0	0	0	0	1	0	0	0	0	0	0	0	0
057	0	0	0	0	0	0	0	0	0	0	0	0	0	0
064	0	0	0	0	0	0	0	0	0	1	0	0	0	0
065	0	0	0	0	0	0	0	0	0	0	0	0	0	0
073	0	0	0	0	0	0	0	0	0	0	0	0	0	0
081	0	0	0	0	0	0	0	0	0	0	0	0	0	0
089	0	0	0	0	0	0	0	0	0	0	0	0	0	0
097	0	0	0	0	0	0	0	0	0	0	0	0	0	0
098	0	0	0	0	0	0	0	0	0	0	0	0	0	0
099	0	0	0	0	0	0	0	0	0	0	0	0	0	0
101	0	0	0	0	0	0	0	0	0	0	0	0	0	0
102	0	0	0	0	0	0	0	0	0	0	0	0	0	0
103	0	0	0	0	0	0	0	0	0	0	0	0	0	0
104	0	0	0	0	0	0	0	0	0	0	0	0	0	0
105	0	0	0	0	0	0	0	0	0	0	0	0	0	0
106	0	0	0	0	0	0	0	0	0	0	0	0	0	0
107	0	0	0	0	0	0	0	0	0	0	0	0	0	0
108	0	0	0	0	0	0	0	0	0	0	0	0	0	0
109	0	0	0	0	0	0	0	0	0	0	0	0	0	0
111	0	0	0	0	0	0	0	0	0	0	0	0	0	0
112	0	0	0	0	0	0	0	0	0	0	0	0	0	0
113	0	0	0	0	0	0	0	1	0	0	0	0	0	0
114	0	0	0	0	0	0	0	0	0	0	0	0	0	0
115	0	0	0	0	0	0	1	2	0	0	0	0	0	1
116	2	0	0	0	0	0	0	4	0	0	0	0	0	0
117	1	0	0	0	0	0	0	0	0	0	0	0	0	1
118	0	0	0	0	0	0	0	2	0	0	0	0	0	0
119	0	0	1	0	0	0	0	0	0	0	0	0	0	0
121	0	0	0	0	0	0	0	2	0	0	0	0	0	0
122	2	0	0	0	0	0	0	1	0	1	0	0	0	0
123	1	0	0	0	0	0	0	5	0	0	0	0	0	0
124	0	0	0	0	0	0	0	1	0	0	1	0	0	0
125	2	0	0	0	0	1	0	5	0	0	0	0	0	0
126	0	0	0	0	0	3	0	8	0	0	0	0	0	0
127	0	0	0	1	0	0	0	5	1	0	0	0	0	0
135	1	0	0	0	0	0	0	6	0	0	0	0	0	1

Sample No.	*Fissurina* sp. 2	*Parafissurina fusiformis*	*Bolivinellina earlandi*	*Cassidulinoides parkerianus*	*Cassidulinoides porrectus*	*Globocassidulina crassa rossensis*	*Ehrenbergina glabra*	*Bulimina aculeata*	*Bulimina* sp. 1	*Trifarina earlandi*	*Fursenkoina fusiformis*	*Discorbis vilardeboanus*	*Cibicides* sp. 1	*Nonionella bradii*
002	2	6	3	10	25	261	2	7	0	22	175	2	0	16
003	4	3	1	5	23	162	0	3	3	8	16	1	0	3
009	0	0	0	4	14	11	0	0	0	2	18	0	0	2
021	1	1	0	15	31	2	0	0	1	1	16	0	0	0
033	3	0	0	57	24	2	0	1	7	4	58	0	0	1
037	0	0	0	5	0	0	0	0	0	0	0	0	0	0
041	0	0	0	24	4	2	0	2	1	0	2	0	0	1
045	0	1	0	14	11	1	0	1	0	5	1	0	0	1
049	0	0	0	5	1	0	0	0	0	0	0	0	0	0
053	2	0	0	25	12	1	0	3	0	1	9	0	0	0
057	0	0	0	3	0	0	0	0	0	0	0	0	0	0
064	0	1	2	7	5	4	0	7	0	1	8	0	0	0
065	0	0	0	10	3	1	0	0	0	0	0	0	0	0
073	0	0	0	3	1	1	0	0	0	0	0	0	0	0
081	0	0	0	7	7	0	0	1	2	0	1	0	0	0
089	1	0	0	12	3	1	0	11	0	6	0	0	0	0
097	0	0	0	9	0	0	0	0	0	0	0	0	0	0
098	0	0	0	0	1	0	0	0	0	0	0	0	0	0
099	0	0	0	40	2	0	0	0	0	1	0	0	0	0
101	0	0	0	0	0	0	0	0	0	0	0	0	0	0
102	0	0	0	1	0	0	0	0	0	0	0	0	0	0
103	0	0	0	0	0	0	0	0	0	0	0	0	0	0
104	0	0	0	0	0	0	0	0	0	0	0	0	0	0
105	0	0	0	0	0	0	0	0	0	0	0	0	0	0
106	0	0	0	1	0	0	0	0	0	0	0	0	0	0
107	0	0	0	0	0	0	0	0	0	0	0	0	0	0
108	0	0	0	0	0	0	0	0	0	0	0	0	0	0
109	0	0	0	0	0	0	0	0	0	0	0	0	0	0
111	0	0	0	0	0	0	0	0	0	0	0	0	0	0
112	0	0	0	1	0	0	0	0	0	1	0	0	0	0
113	0	0	0	40	3	2	0	2	0	4	0	0	0	0
114	0	0	0	38	7	35	0	1	1	5	0	0	0	0
115	0	3	1	46	35	67	0	0	7	25	26	0	0	1
116	2	0	1	28	27	57	0	0	7	20	23	0	0	0
117	2	1	0	13	36	36	0	1	10	49	4	0	0	0
118	0	2	0	32	14	16	0	0	5	50	2	0	0	0
119	0	2	0	49	56	12	0	0	6	76	54	0	0	0
121	0	9	0	79	60	20	0	0	7	39	9	0	0	1
122	1	1	1	81	25	6	0	0	3	55	6	0	0	2
123	1	1	0	50	62	6	0	0	5	38	11	0	0	0
124	7	6	4	87	47	74	0	1	3	1	45	0	0	0
125	0	3	0	25	39	4	0	0	4	7	8	0	0	2
126	4	13	1	13	60	19	0	0	3	11	88	0	0	3
127	2	2	3	13	24	91	0	0	0	9	66	2	0	10
135	7	1	0	7	28	25	0	0	1	29	14	2	0	1

Sample No.	*Nonionella iridea*	*Astrononion echolsi*	*Pullenia subcarinata*	*Buccella* sp. 1	*Bucella* sp. 2
002	70	44	3	8	1
003	3	15	0	0	1
009	11	10	0	6	0
021	0	18	0	12	2
033	0	53	0	23	0
037	0	1	0	5	0
041	0	4	0	13	0
045	0	31	0	29	1
049	0	4	0	7	0
053	0	17	0	33	2
057	0	12	0	8	0
064	1	20	0	18	0
065	0	1	0	10	0
073	0	4	0	3	0
081	0	6	0	14	0
089	0	18	0	21	1
097	0	0	0	4	0
098	0	0	0	3	0
099	0	4	0	23	3
101	0	0	0	0	0
102	0	0	0	0	0
103	0	0	0	0	0
104	0	0	0	0	0
105	0	1	0	0	0
106	0	1	0	0	0
107	0	0	0	0	0
108	0	0	0	0	0
109	0	0	0	0	0
111	0	0	0	0	0
112	0	0	0	0	0
113	0	3	0	7	0
114	1	14	0	20	1
115	2	42	0	20	0
116	1	29	3	6	0
117	0	48	1	4	1
118	0	22	0	2	0
119	5	32	1	10	4
121	5	17	4	19	4
122	1	35	3	28	0
123	1	64	3	16	2
124	10	35	0	3	0
125	1	51	2	24	0
126	2	54	12	28	4
127	28	54	3	8	6
135	8	21	8	3	0

Sample No.	*Ammodiscus incertus*	*Miliammina earlandi*	*Milammina lata*	*Reophax subfusiformis*	*Portatrochammina antarctica wiesneri*	*Haplophragmoides quadratus*	*Labrospira* sp. 1	*Glaphyrammina rostrata*	*Pseudobolivina antarctica*	*Deuterammina scoresbyi*	*.Pseudotrochammina* sp. 1	*Textularia earlandi*	*Cornuspira antarctica*	*Triloculina* sp. 1
143	0	88	11	0	0	0	0	0	0	0	0	0	0	0
151	0	58	0	0	0	0	0	0	0	0	0	0	0	0
159	0	33	8	0	0	0	0	0	0	0	0	0	0	0
167	0	69	4	0	0	0	0	0	0	0	0	0	0	0
175	0	70	3	0	0	0	0	0	0	0	0	0	0	0
183	0	61	3	0	0	0	0	0	0	0	0	0	0	0
191	0	45	7	0	0	0	0	0	0	0	0	0	0	0
199	0	82	1	0	0	0	0	0	0	0	0	0	0	0
211	0	27	0	0	0	0	0	0	0	0	0	0	0	0
223	0	53	8	0	0	0	0	0	0	0	0	0	0	1
235	0	50	0	0	0	0	0	0	0	0	0	0	0	0
247	0	46	4	0	0	0	0	0	0	0	0	0	0	0
255	0	16	0	0	0	0	0	0	0	0	0	0	0	0
256	0	17	4	0	1	0	0	0	0	0	0	0	0	0
263	0	25	0	0	0	0	0	0	0	0	0	0	0	0
271	0	29	0	0	0	0	0	0	0	0	0	0	0	0
279	0	18	2	0	0	0	0	0	0	0	0	0	0	0
287	0	19	0	0	0	0	0	0	0	0	0	0	0	0
295	0	9	0	0	0	0	0	0	0	0	0	0	0	0
303	0	5	0	0	0	0	0	0	0	0	0	0	0	0
311	0	8	0	0	0	0	0	0	0	0	0	0	0	0
319	0	1	0	0	0	0	0	0	0	0	0	0	0	0
324	0	19	3	0	4	0	0	0	0	0	0	0	0	0
335	0	24	0	0	0	0	0	0	0	0	0	0	0	0
351	0	62	0	0	4	0	0	0	0	0	0	0	0	0
367	0	8	0	0	0	0	0	0	0	0	0	0	0	0
383	0	19	0	0	1	0	0	0	0	0	0	0	0	0
384	0	32	0	0	0	0	0	0	0	0	0	0	0	0
395	0	9	0	0	0	0	0	0	0	0	0	0	0	0
407	0	80	0	0	0	0	0	0	0	0	0	0	0	0
419	0	59	0	0	0	0	0	0	0	0	0	0	0	0
431	0	14	0	0	0	0	0	0	0	0	0	0	0	0
443	0	27	0	0	0	0	0	0	0	0	0	0	0	0
445	0	144	0	0	2	0	0	0	0	0	0	0	0	0
455	0	34	0	0	0	0	0	0	0	0	0	0	0	0
467	0	15	0	0	0	0	0	0	0	0	0	0	0	0
479	0	30	0	0	0	0	0	0	0	0	0	0	0	0
491	0	12	0	0	0	0	0	0	0	0	0	0	0	0
504	0	13	0	0	0	0	0	0	0	0	0	0	0	0
516	0	135	0	0	0	0	0	0	0	0	0	0	0	0
576	0	145	7	0	0	0	0	0	0	0	0	0	0	0
640	0	4	0	0	0	0	0	0	0	0	0	0	0	0
704	0	21	0	0	0	0	0	0	0	1	0	0	0	0
768	0	29	0	0	0	0	0	0	0	0	0	0	0	0

Sample No.	*Laevidentalina communis*	*Lotostomoides calomorphus*	*Nodosaria simplex*	*Lenticulina asterizans*	*?Astacolus*	*Lagena substriata*	*Lagena multilatera*	*Hyalinonetrion gracillimum*	*Procerolagena distoma*	*Pygmaeoseistron hispudulum*	*Oolina squamosa*	*Oolina* spp.	*Fissurina subformosa*	*Fissurina* sp. 1
143	0	4	0	0	0	2	3	10	0	0	0	0	0	2
151	0	0	0	0	0	0	0	3	0	0	0	0	0	0
159	0	0	1	0	1	0	0	5	0	0	0	0	0	0
167	0	0	0	0	0	0	0	4	0	1	0	0	0	0
175	0	0	0	0	0	0	1	5	0	0	0	0	0	0
183	0	0	0	0	0	3	0	3	1	1	0	0	2	0
191	0	0	0	0	0	1	0	0	0	0	0	0	0	0
199	0	0	0	0	0	2	0	1	0	0	0	0	0	0
211	0	0	0	0	0	0	0	1	0	0	0	0	0	1
223	0	0	0	0	0	0	0	4	0	0	0	0	0	0
235	0	0	0	0	0	0	0	0	0	0	0	0	0	0
247	0	0	0	0	0	0	0	0	0	0	0	0	0	0
255	0	0	0	0	0	0	0	0	0	0	0	0	0	1
256	0	0	0	0	0	0	0	0	0	0	0	0	0	0
263	0	0	0	0	0	0	0	1	0	0	0	0	0	0
271	0	0	0	0	0	0	0	1	0	0	0	0	0	0
279	0	0	0	0	0	0	0	1	0	0	0	0	1	0
287	0	0	0	0	0	0	0	2	0	0	0	0	0	0
295	0	0	0	0	0	0	0	4	0	0	1	0	0	0
303	0	0	0	0	0	0	1	1	0	0	0	0	0	0
311	0	0	0	0	0	0	0	2	0	0	0	0	0	1
319	0	0	0	0	0	0	0	4	0	0	0	0	0	0
324	0	0	0	0	0	0	2	4	0	0	0	0	0	0
335	2	0	0	0	0	0	0	7	0	0	0	0	0	0
351	0	0	0	0	0	0	0	2	0	0	0	0	0	0
367	0	0	0	0	0	0	0	1	0	0	0	0	0	0
383	0	0	0	0	0	0	0	0	0	0	0	0	0	0
384	0	0	0	0	0	0	0	0	0	0	0	1	0	0
395	0	0	0	0	0	0	0	1	0	0	0	0	0	0
407	0	0	0	0	0	0	0	0	0	0	0	0	0	0
419	0	0	0	0	0	0	0	0	0	0	0	0	0	0
431	0	0	0	0	0	0	0	0	0	0	0	0	0	0
443	0	0	0	0	0	0	0	0	0	0	0	0	0	0
445	0	0	0	0	0	0	0	0	0	0	0	0	0	0
455	0	0	0	0	0	0	0	0	0	0	0	0	0	0
467	0	0	0	0	0	0	0	0	0	0	0	0	0	0
479	0	0	0	0	0	0	0	0	0	0	0	0	0	0
491	0	0	0	0	0	0	0	0	0	0	0	0	0	0
504	0	0	0	0	0	0	0	0	0	0	0	0	0	0
516	0	0	0	0	0	0	0	0	0	0	0	0	0	0
576	0	0	0	0	0	0	0	0	0	0	0	0	0	0
640	0	0	0	0	0	0	0	0	0	0	0	0	0	0
704	0	0	0	0	0	0	0	0	0	0	0	0	0	0
768	0	0	0	0	0	0	0	0	0	0	0	0	0	0

Sample No.	*Fissurina* sp. 2	*Parafissurina fusiformis*	*Bolivinellina earlandi*	*Cassidulinoides parkerianus*	*Cassidulinoides porrectus*	*Globocassidulina crassa rossensis*	*Ehrenbergina glabra*	*Bulimina aculeata*	*Bulimina* sp. 1	*Trifarina earlandi*	*Fursenkoina fusiformis*	*Discorbis vilardeboanus*	*Cibicides* sp. 1	*Nonionella bradii*
143	3	1	2	16	115	8	0	0	8	56	12	0	0	1
151	0	0	3	69	75	0	0	0	3	45	7	0	0	0
159	1	2	0	80	99	12	0	0	0	24	17	0	0	0
167	0	2	1	57	40	9	0	0	3	36	46	0	0	0
175	0	15	0	71	109	34	0	0	5	6	180	0	0	2
183	7	12	1	40	122	37	0	0	4	12	511	0	0	8
191	0	0	0	58	14	28	0	0	0	7	53	0	0	2
199	1	5	0	39	27	24	0	0	7	1	35	0	1	0
211	3	6	1	22	31	76	0	0	2	0	117	1	0	3
223	5	6	1	107	139	58	0	0	6	3	398	4	0	3
235	0	0	0	2	3	0	0	0	0	0	1	0	0	0
247	2	0	0	72	50	7	0	0	3	14	19	1	0	1
255	1	0	2	11	15	14	0	0	1	0	226	2	0	0
256	2	1	3	4	5	21	0	0	0	0	261	0	0	0
263	8	1	0	14	20	7	0	0	1	0	509	0	0	0
271	1	1	0	29	19	11	0	0	3	0	251	0	0	0
279	0	2	1	41	42	36	0	0	7	0	571	1	0	5
287	0	2	2	20	23	14	0	0	7	0	195	0	0	0
295	0	0	2	38	48	8	0	0	0	0	163	0	0	2
303	3	5	1	17	55	22	0	0	8	0	540	0	0	0
311	4	3	0	28	22	12	0	0	0	0	363	0	0	1
319	0	6	4	13	25	9	0	0	0	0	265	1	0	2
324	2	0	3	30	47	42	0	0	8	0	185	0	0	1
335	3	3	1	68	91	41	0	0	5	0	309	3	0	2
351	0	0	3	8	16	15	0	0	0	1	280	0	0	0
367	0	1	1	22	16	7	0	0	0	0	174	0	0	0
383	1	1	5	13	21	6	0	0	0	0	447	1	0	1
384	0	0	7	34	20	30	0	0	0	0	812	0	0	0
395	1	0	3	23	20	3	0	0	3	0	377	0	0	0
407	1	2	0	37	47	13	0	0	4	0	1183	0	0	3
419	0	0	0	18	6	3	0	0	1	0	103	0	0	0
431	0	1	0	27	5	0	0	0	0	0	257	0	0	0
443	2	0	1	6	2	0	0	0	0	0	317	0	0	1
445	0	0	0	0	0	0	0	0	0	0	0	0	0	0
455	0	0	0	30	5	3	0	0	0	0	290	0	0	0
467	0	0	0	10	1	0	0	0	0	0	52	0	0	0
479	0	0	1	9	2	1	0	0	0	0	303	1	0	0
491	0	0	0	0	0	0	0	0	0	0	0	0	0	0
504	0	0	0	3	0	0	0	0	0	0	1	0	0	0
516	0	0	0	4	3	1	0	0	0	0	290	0	0	0
576	0	0	0	2	1	2	0	0	0	0	322	0	0	0
640	0	3	1	0	0	2	0	0	0	0	38	9	0	0
704	0	1	3	0	0	1	0	0	0	0	117	10	0	2
768	0	0	0	0	0	0	0	0	0	0	0	0	0	0

Sample No.	*Nonionella iridea*	*Astrononion echolsi*	*Pullenia subcarinata*	*Buccella* sp. 1	*Bucella* sp. 2
143	2	112	3	9	6
151	0	19	4	29	2
159	0	40	0	33	3
167	4	61	0	28	1
175	12	89	1	51	5
183	34	89	2	51	2
191	1	30	1	30	1
199	1	11	0	19	0
211	31	36	1	17	0
223	47	127	0	123	10
235	0	0	0	0	0
247	3	55	5	59	0
255	26	50	0	3	0
256	9	28	0	2	2
263	23	46	0	2	0
271	10	10	0	10	0
279	24	59	0	15	0
287	37	23	0	2	0
295	13	40	1	7	0
303	13	36	0	10	0
311	10	39	0	7	0
319	15	31	0	3	0
324	20	46	0	2	3
335	17	75	1	25	0
351	4	13	0	5	0
367	6	9	0	3	0
383	17	10	0	2	0
384	31	42	0	1	0
395	6	12	0	1	0
407	10	25	0	2	0
419	0	6	0	0	0
431	2	9	0	0	0
443	9	1	0	0	0
445	0	0	0	0	0
455	0	0	0	0	0
467	0	0	0	0	0
479	1	1	0	0	0
491	0	0	0	0	0
504	0	0	0	0	0
516	0	0	0	0	0
576	0	0	0	0	0
640	0	0	0	0	0
704	0	0	0	0	0
768	0	0	0	0	0

Appendix A9 – GC673 BFA census counts

Sample No.	*Saccamina* spp.	*Miliammina earlandi*	*Miliammina lata*	*Hormosinelloides guttifer*	*Reophax subdentaliniformis*	*Reophax subfusiformis*	*Labrospira* sp. 1	*Glaphyrammina rostrata*	*Spiroplectammina biformis*	*Pseudobolivina antarctica*	*Portatrochammina antarctica wiesneri*	*Deuterammina scoresbyi*	*Textularia earlandi*	*Cornuspira antarctica*
001	1	85	0	1	8	0	13	0	0	1	3	0	6	1
016	0	132	0	0	2	0	25	1	0	1	9	8	3	0
032	0	73	0	0	5	0	19	0	0	1	5	0	4	0
064	0	52	0	0	0	0	0	0	0	1	6	5	3	0
096	0	85	0	0	0	0	9	9	0	0	7	0	4	0
128	0	61	0	0	3	1	1	0	0	0	1	0	1	0
160	0	105	0	0	0	0	2	1	0	0	2	0	0	0
192	0	26	0	0	1	0	0	0	0	0	2	0	0	0
224	0	159	0	0	0	0	3	0	0	0	2	0	4	0
256	0	24	0	0	0	0	0	0	0	0	0	2	0	0
288	0	41	0	0	0	0	0	0	0	0	1	3	0	0
304	0	104	1	0	0	0	0	1	2	0	2	1	0	0
308	0	100	0	0	0	0	0	0	0	0	0	0	0	0
312	0	91	0	0	0	0	0	0	0	0	0	0	0	0
316	0	132	0	0	0	0	0	0	0	0	0	0	0	0
320	0	79	0	0	0	0	0	0	0	0	0	0	0	0
324	0	59	0	0	1	0	0	0	0	0	0	0	0	0
328	0	52	0	0	0	0	0	0	0	0	0	0	0	0
332	0	97	0	0	0	0	0	0	0	0	0	0	0	0
336	0	117	0	0	0	0	2	0	0	0	0	0	2	0
352	0	35	1	0	0	0	0	1	0	0	1	0	0	0
368	0	68	3	0	0	0	0	1	0	0	0	0	0	0
384	0	31	0	0	0	0	0	0	0	1	0	0	0	0
416	0	89	0	0	1	0	0	1	0	0	1	0	0	0
448	0	35	0	0	0	0	0	0	0	0	0	0	0	0
480	0	91	0	0	0	0	0	0	0	0	0	0	0	0
512	0	31	0	0	0	0	0	0	0	0	1	0	0	0
544	0	78	0	0	1	0	0	0	0	0	0	0	0	0
576	0	44	1	0	0	0	0	0	0	0	0	0	0	0
608	0	46	0	0	0	0	0	0	0	0	0	0	0	0
640	0	70	0	0	0	0	0	0	0	0	0	0	0	0
672	0	108	1	0	0	0	0	0	0	0	0	0	0	0
704	0	33	0	0	0	0	0	0	0	0	1	0	0	0
736	0	77	0	0	0	0	0	0	0	0	0	0	0	0
768	0	32	0	0	0	0	0	0	0	0	0	0	0	0
800	0	44	0	0	0	0	0	0	0	0	0	0	0	0
832	0	86	0	0	0	0	0	0	0	0	0	0	0	0
864	0	146	0	0	0	0	0	0	0	0	1	0	0	0

Sample No.	*Quniqueloculina seminula*	*Pyrgo subpisum*	*Pyrgo patagonica*	*Lotostomoides calomorphum*	*Lagena substriata*	*Lagena multilatera*	*Hyalinonetrion* cf. *gracillimum*	*Procerolagena distoma*	*Pygmaeoseistron hispidulum*	*Pygmaeoseistron* sp. 1	*Oolina squamosa*	*Oolina* spp.	*Fissurina subformosa*	*Fissurina* sp. 1
001	0	0	0	0	0	1	0	1	0	0	0	0	0	1
016	0	0	0	0	0	0	0	0	0	0	0	0	0	0
032	0	0	0	0	0	0	1	0	0	0	0	1	0	0
064	0	0	0	0	0	0	0	0	0	0	0	0	0	0
096	0	0	0	0	0	0	1	0	0	0	0	1	0	0
128	0	0	0	0	0	0	0	0	0	0	0	0	0	0
160	0	0	0	0	0	0	0	0	0	0	0	0	0	0
192	0	0	0	0	4	0	0	0	0	0	0	0	0	0
224	0	0	0	0	0	0	0	0	0	0	0	0	0	0
256	0	0	0	0	0	0	0	0	0	0	0	0	0	0
288	0	0	0	0	0	0	1	0	0	0	0	0	0	0
304	0	0	0	0	0	0	0	0	0	0	0	0	0	0
308	0	0	0	0	1	0	0	1	0	0	0	2	0	0
312	0	0	0	0	0	0	0	1	0	0	1	0	0	0
316	0	0	0	0	1	0	0	0	0	0	0	2	0	0
320	0	0	0	0	2	0	1	0	0	0	0	0	0	0
324	0	0	0	0	0	0	0	0	0	0	0	0	0	0
328	0	0	0	0	0	0	0	0	0	0	0	0	0	0
332	0	0	0	0	0	0	0	2	0	0	0	0	0	0
336	0	0	0	1	0	0	0	1	0	0	0	0	0	0
352	0	0	0	0	0	0	0	0	2	0	0	0	0	0
368	0	0	0	0	0	0	0	0	0	0	0	0	0	0
384	0	0	0	0	0	0	1	0	0	0	0	0	0	0
416	0	0	0	0	0	0	0	0	0	0	0	0	0	0
448	0	0	0	0	0	0	1	0	0	0	0	0	0	0
480	0	0	0	0	0	2	0	0	3	0	0	0	0	0
512	0	0	0	0	0	0	0	0	0	0	0	0	0	1
544	0	1	1	0	0	2	0	0	0	0	0	0	0	0
576	0	0	0	3	1	0	1	0	0	0	0	0	0	2
608	0	0	0	0	0	0	2	0	1	0	0	0	0	0
640	0	0	0	0	0	0	1	0	0	0	0	0	0	0
672	0	0	0	0	0	0	1	0	0	0	0	0	0	0
704	0	0	0	0	0	0	0	1	0	0	0	0	0	0
736	1	0	0	6	0	1	0	1	0	1	1	0	0	2
768	0	0	0	0	0	0	2	0	0	0	0	0	0	0
800	0	0	0	0	0	0	1	3	0	0	0	0	0	0
832	0	0	0	0	0	0	0	0	0	0	0	0	0	0
864	0	0	0	0	0	0	0	0	0	0	0	0	0	0

Sample No.	*Fissurina* sp. 2	*Parafissurina fusiformis*	*Bolivinellina earlandi*	*Bolivinellina pseudopunctata*	*Cassidulinoides parkerianus*	*Cassidulinoides porrectus*	*Globocassidulina crassa rossensis*	*Bulimina* sp. 1	*Trifarina earlandi*	*Fursenkoina fusiformis*	*Discorbis vilardeboanus*	*Cibicides* sp. 1	*Nonionella bradii*	*Nonionella iridea*
001	1	0	0	0	17	15	5	0	1	156	0	0	0	7
016	5	0	1	0	42	16	25	0	0	584	0	0	0	7
032	0	1	1	0	23	2	1	2	0	159	0	0	0	1
064	1	0	0	0	12	1	0	1	0	207	0	0	0	0
096	0	0	0	0	13	1	1	0	0	278	0	0	0	2
128	0	0	0	0	22	1	0	0	0	96	0	0	0	1
160	0	1	0	0	49	9	9	2	0	352	0	0	0	3
192	1	0	0	0	30	10	5	1	0	36	0	0	1	3
224	0	0	0	0	22	0	1	0	0	830	0	0	0	1
256	0	0	0	0	35	1	0	3	0	3	0	0	0	1
288	2	0	1	0	12	1	4	0	0	334	0	0	0	5
304	1	0	0	0	23	5	4	0	0	103	0	0	4	0
308	0	0	0	0	43	10	12	0	1	87	0	0	4	0
312	0	0	0	0	42	14	1	0	1	186	0	0	1	0
316	0	0	0	0	36	4	0	0	0	123	0	1	2	0
320	0	0	0	0	40	2	1	0	0	15	0	0	0	0
324	0	0	0	0	48	1	1	1	0	8	0	0	1	0
328	0	0	0	0	6	1	0	0	0	32	0	0	3	0
332	0	0	0	0	16	1	1	0	1	144	0	1	0	1
336	0	0	0	0	16	0	6	0	0	58	0	0	7	0
352	0	0	0	0	36	7	5	0	4	250	0	0	0	2
368	3	0	0	0	70	19	8	0	2	197	1	0	2	8
384	0	0	0	0	4	0	0	0	0	1095	0	0	0	11
416	1	0	0	0	2	0	1	0	0	227	0	0	0	0
448	3	0	0	0	3	0	1	0	0	334	0	0	0	3
480	0	0	0	0	23	10	1	1	1	118	0	0	0	1
512	1	0	0	0	6	3	0	0	0	327	0	0	1	1
544	1	0	0	0	31	7	14	0	0	255	0	0	0	7
576	0	0	2	0	28	16	16	1	3	274	0	0	7	12
608	0	1	0	0	42	19	20	0	0	1170	0	0	13	36
640	2	0	1	0	36	5	13	4	1	114	0	0	3	0
672	0	0	0	0	49	13	40	19	0	93	1	0	3	6
704	0	0	0	0	9	1	67	2	0	211	0	0	0	15
736	4	2	8	1	90	54	25	17	0	82	6	3	5	10
768	0	1	0	0	26	2	42	1	0	156	3	0	1	2
800	2	3	3	0	53	20	10	20	0	170	0	0	1	5
832	0	0	0	0	17	0	7	0	0	19	0	0	0	0
864	0	3	0	0	38	3	17	0	0	248	0	0	1	7

Sample No.	*Astrononion echolsi*	*Pullenia subcarinata*	*Buccella* sp. 1	*Buccella* sp. 2
001	25	0	4	3
016	38	0	7	2
032	9	0	2	1
064	10	0	0	0
096	8	0	1	1
128	7	0	3	0
160	13	0	1	0
192	56	0	7	1
224	5	0	2	1
256	2	0	1	0
288	33	0	1	0
304	53	0	4	0
308	45	0	12	0
312	30	0	20	0
316	12	0	8	1
320	26	0	8	0
324	6	0	5	0
328	3	0	0	0
332	15	0	1	0
336	27	0	27	3
352	30	0	29	0
368	45	0	66	0
384	5	0	0	0
416	23	0	0	0
448	25	0	0	0
480	28	0	5	0
512	19	1	4	0
544	48	0	15	1
576	45	0	4	0
608	34	0	4	1
640	25	0	5	0
672	16	0	1	1
704	0	0	1	0
736	66	7	4	4
768	2	0	1	0
800	56	0	0	0
832	1	0	0	0
864	13	0	0	0

Appendix A10 – GC666 1 cm resolution interpolated ages

Depth (cm)	μ (cal. yr BP)	2σ (yr)
0	300	73
1	316	83
2	333	92
3	349	100
4	366	107
5	383	112
6	400	118
7	417	122
8	432	126
9	441	127
10	457	130
11	474	133
12	490	134
13	506	136
14	523	137
15	539	138
16	556	138
17	573	138
18	589	137
19	606	136
20	622	135
21	638	133
22	655	131
23	672	129
24	688	126
25	696	124
26	713	120
27	729	116
28	745	111
29	762	105
30	779	97
31	798	88
32	813	78
33	828	68
34	864	122
35	931	182
36	966	206
37	1002	223
38	1072	252
39	1108	264
40	1143	273
41	1214	287
42	1248	294
43	1281	296
44	1356	301
45	1388	303
46	1430	302
47	1497	297
48	1527	294
49	1561	288
50	1631	273
51	1668	265
52	1702	253
53	1771	225
54	1803	211
55	1840	187
56	1911	124
57	1948	71
58	1980	104
59	1996	115
60	2026	135
61	2041	144
62	2072	159
63	2106	172
64	2121	177
65	2152	187
66	2167	191
67	2197	199
68	2229	206
69	2246	209
70	2274	214
71	2288	216
72	2321	220
73	2350	223
74	2368	224
75	2401	225
76	2416	226
77	2447	227
78	2476	227
79	2491	226
80	2523	224
81	2539	224
82	2571	221
83	2603	217
84	2620	215
85	2652	209
86	2667	207
87	2696	201
88	2726	193
89	2742	188
90	2773	179
91	2787	174
92	2820	162
93	2851	147
94	2866	139
95	2898	119
96	2915	107
97	2945	79
98	3246	660
99	3517	889
100	3661	969
101	3956	1110
102	4264	1216
103	4593	1294
104	4749	1326
105	5015	1342
106	5251	1350
107	5558	1332
108	5826	1303
109	5978	1270
110	6272	1201
111	6541	1110
112	6828	975
113	6987	887
114	7284	626
115	7556	61
116	7595	113

Depth (cm)	μ (cal. yr BP)	2σ (yr)
117	7675	172
118	7712	190
119	7748	200
120	7831	215
121	7870	219
122	7913	217
123	7993	205
124	8027	196
125	8069	180
126	8144	133
127	8184	93
128	8208	116
129	8235	137
130	8260	153
131	8288	170
132	8316	183
133	8342	195
134	8369	206
135	8393	215
136	8420	224
137	8445	232
138	8473	240
139	8497	247
140	8524	254
141	8550	260
142	8576	265
143	8602	271
144	8615	273
145	8642	278
146	8668	282
147	8694	286
148	8719	289
149	8746	293
150	8771	295
151	8797	298
152	8824	301
153	8850	303
154	8876	304
155	8903	306
156	8928	307

Depth (cm)	μ (cal. yr BP)	2σ (yr)
157	8954	308
158	8982	309
159	9008	309
160	9033	310
161	9059	309
162	9086	309
163	9112	309
164	9138	308
165	9165	306
166	9191	305
167	9217	303
168	9243	301
169	9268	299
170	9293	296
171	9320	294
172	9345	291
173	9372	287
174	9398	283
175	9425	278
176	9439	277
177	9465	271
178	9491	267
179	9516	261
180	9542	255
181	9568	248
182	9593	242
183	9621	234
184	9648	226
185	9674	216
186	9701	207
187	9728	196
188	9752	185
189	9776	173
190	9802	159
191	9829	141
192	9857	121
193	9869	125
194	9882	130
195	9905	137
196	9918	140

Depth (cm)	μ (cal. yr BP)	2σ (yr)
197	9931	144
198	9942	146
199	9954	149
200	9978	154
201	9991	156
202	10003	159
203	10015	161
204	10028	163
205	10051	166
206	10063	167
207	10075	168
208	10087	170
209	10111	172
210	10123	173
211	10135	173
212	10148	174
213	10160	174
214	10185	175
215	10196	176
216	10209	176
217	10221	176
218	10233	175
219	10257	175
220	10269	174
221	10282	174
222	10294	173
223	10306	172
224	10330	170
225	10342	170
226	10354	168
227	10365	167
228	10378	165
229	10402	162
230	10414	160
231	10427	158
232	10439	156
233	10463	151
234	10476	148
235	10488	145
236	10499	142

Appendix A10 – GC666 1 cm resolution interpolated ages

Depth (cm)	μ (cal. yr BP)	2σ (yr)
237	10511	139
238	10536	132
239	10548	128
240	10560	124
241	10572	119
242	10585	114
243	10609	103
244	10621	97
245	10633	91
246	10659	112
247	10672	122
248	10699	139
249	10712	147
250	10739	161
251	10766	173
252	10779	179
253	10806	189
254	10833	199
255	10846	204
256	10874	212
257	10887	216
258	10915	224
259	10940	231
260	10953	234
261	10980	240
262	11007	246
263	11021	249
264	11047	254
265	11060	257
266	11087	261
267	11114	266
268	11127	267
269	11154	271
270	11181	275
271	11194	276
272	11222	280
273	11235	281
274	11262	283
275	11289	286
276	11302	287

Depth (cm)	μ (cal. yr BP)	2σ (yr)
277	11328	289
278	11341	289
279	11368	291
280	11394	292
281	11406	293
282	11434	294
283	11461	295
284	11475	295
285	11503	295
286	11517	296
287	11543	296
288	11569	295
289	11583	295
290	11609	294
291	11636	294
292	11649	293
293	11676	292
294	11689	291
295	11715	290
296	11743	288
297	11756	287
298	11784	284
299	11796	283
300	11822	280
301	11849	278
302	11862	276
303	11889	273
304	11917	269
305	11931	267
306	11958	262
307	11972	261
308	11997	256
309	12024	251
310	12038	248
311	12064	242
312	12090	236
313	12104	233
314	12131	226
315	12144	222
316	12171	214

Depth (cm)	μ (cal. yr BP)	2σ (yr)
317	12199	205
318	12212	201
319	12238	192
320	12266	181
321	12279	175
322	12306	163
323	12319	157
324	12345	144
325	12352	144
326	12360	144
327	12368	144
328	12376	144
329	12383	144
330	12391	144
331	12399	144
332	12414	144
333	12421	144
334	12429	144
335	12437	144
336	12444	143
337	12452	143
338	12460	143
339	12467	142
340	12476	142
341	12483	141
342	12490	141
343	12498	141
344	12506	140
345	12513	140
346	12521	139
347	12537	138
348	12545	137
349	12552	136
350	12560	136
351	12567	135
352	12575	134
353	12582	133
354	12590	132
355	12598	131
356	12605	130

Depth (cm)	μ (cal. yr BP)	2σ (yr)
357	12614	129
358	12621	129
359	12629	127
360	12636	126
361	12644	125
362	12660	123
363	12667	121
364	12675	120
365	12682	119
366	12690	117
367	12697	116
368	12705	115
369	12713	113
370	12720	112
371	12727	110
372	12735	108
373	12743	106
374	12751	104
375	12759	102
376	12766	100
377	12781	96
378	12787	94
379	12796	91
380	12805	88
381	12812	86
382	12819	83
383	12827	80
384	12835	76
385	12846	78
386	12857	79
387	12867	80
388	12876	81
389	12889	91
390	12916	109
391	12930	118
392	12943	124
393	12956	132
394	12983	144
395	12997	150
396	13009	155

Depth (cm)	μ (cal. yr BP)	2σ (yr)
397	13022	160
398	13049	169
399	13062	174
400	13075	178
401	13089	183
402	13114	190
403	13128	194
404	13142	198
405	13156	201
406	13183	208
407	13195	211
408	13209	214
409	13223	217
410	13249	222
411	13262	224
412	13276	227
413	13289	229
414	13315	234
415	13328	236
416	13341	238
417	13355	241
418	13381	244
419	13395	246
420	13408	248
421	13421	250
422	13448	253
423	13460	255
424	13474	256
425	13487	258
426	13514	260
427	13527	262
428	13539	263
429	13553	264
430	13580	266
431	13594	267
432	13608	268
433	13621	269
434	13647	271
435	13660	271
436	13674	272

Depth (cm)	μ (cal. yr BP)	2σ (yr)
437	13687	273
438	13714	274
439	13727	274
440	13741	275
441	13768	275
442	13780	276
443	13794	276
444	13808	276
445	13833	276
446	13846	276
447	13858	276
448	13872	276
449	13900	276
450	13913	276
451	13926	276
452	13939	276
453	13967	275
454	13979	275
455	13992	274
456	14006	274
457	14032	272
458	14046	272
459	14059	271
460	14073	270
461	14099	269
462	14112	268
463	14125	267
464	14138	266
465	14166	264
466	14179	263
467	14192	261
468	14205	261
469	14232	258
470	14245	256
471	14258	255
472	14273	253
473	14299	250
474	14311	249
475	14325	247
476	14339	245

Appendix A10 – GC666 1 cm resolution interpolated ages

Depth (cm)	μ (cal. yr BP)	2σ (yr)
477	14365	241
478	14377	239
479	14391	237
480	14405	235
481	14432	230
482	14445	228
483	14458	225
484	14471	223
485	14498	217
486	14511	214
487	14524	212
488	14537	208
489	14563	202
490	14577	199
491	14587	199
492	14606	201
493	14626	202
494	14635	203
495	14654	204
496	14674	205
497	14683	205
498	14702	206
499	14712	206
500	14731	206
501	14732	206
502	14734	206
503	14736	205
504	14736	205
505	14739	205
506	14740	205
507	14741	204
508	14743	204
509	14744	204
510	14746	204
511	14748	203
512	14749	203
513	14751	203
514	14753	203
515	14754	202
516	14756	202
517	14758	202
518	14758	202
519	14760	201
520	14762	201
521	14763	201
522	14765	201
523	14767	201
524	14769	200
525	14770	200
526	14771	200
527	14773	200
528	14774	200
529	14776	200
530	14778	199
531	14779	199
532	14781	199
533	14783	199
534	14784	199
535	14786	199
536	14787	199
537	14788	199
538	14790	198
539	14792	198
540	14793	198
541	14795	198
542	14797	198
543	14798	198
544	14799	198
545	14801	198
546	14802	198
547	14804	197
548	14806	197
549	14807	197
550	14809	197
551	14811	197
552	14813	197
553	14813	197
554	14815	197
555	14817	197
556	14818	197
557	14820	197
558	14822	197
559	14823	197
560	14825	197
561	14827	197
562	14827	197
563	14829	197
564	14831	197
565	14832	197
566	14834	197
567	14836	197
568	14837	197
569	14839	197
570	14840	197
571	14841	197
572	14843	197
573	14845	197
574	14846	197
575	14848	197
576	14850	197
577	14851	197
578	14853	197
579	14855	197
580	14856	197
581	14857	197
582	14859	197
583	14861	197
584	14862	197
585	14864	198
586	14866	198
587	14867	198
588	14869	198
589	14870	198
590	14872	198
591	14873	198
592	14875	198
593	14876	198
594	14878	198
595	14880	199
596	14881	199

Depth (cm)	μ (cal. yr BP)	2σ (yr)
597	14883	199
598	14884	199
599	14885	199
600	14887	199
601	14889	200
602	14890	200
603	14892	200
604	14894	200
605	14895	200
606	14897	200
607	14898	201
608	14900	201
609	14901	201
610	14903	201
611	14905	201
612	14906	202
613	14908	202
614	14910	202
615	14911	202
616	14912	202
617	14914	203
618	14915	203
619	14917	203
620	14919	203
621	14920	204
622	14922	204
623	14924	204
624	14925	204
625	14926	205
626	14928	205
627	14929	205
628	14931	205
629	14933	206
630	14934	206
631	14936	206
632	14938	207
633	14939	207
634	14940	207
635	14942	207
636	14943	208

Depth (cm)	μ (cal. yr BP)	2σ (yr)
637	14945	208
638	14947	208
639	14949	209
640	14950	209
641	14952	209
642	14954	210
643	14955	210
644	14956	210
645	14958	211
646	14959	211
647	14961	211
648	14963	212
649	14964	212
650	14966	212
651	14968	213
652	14969	213
653	14970	213
654	14972	214
655	14973	214
656	14975	215
657	14977	215
658	14978	215
659	14980	216
660	14982	216
661	14982	216
662	14984	217
663	14986	217
664	14988	218
665	14989	218
666	14991	218
667	14993	219
668	14994	219
669	14996	220
670	14997	220
671	14998	220
672	15000	221
673	15002	222
674	15003	222
675	15005	222
676	15007	223

Depth (cm)	μ (cal. yr BP)	2σ (yr)
677	15008	223
678	15010	224
679	15011	224
680	15012	224
681	15014	225
682	15016	226
683	15017	226
684	15019	226
685	15021	227
686	15022	227
687	15024	228
688	15025	228
689	15026	229
690	15028	229
691	15030	230
692	15032	230
693	15033	231
694	15035	231
695	15037	232
696	15037	232
697	15039	233
698	15041	233
699	15042	234
700	15044	234
701	15046	235
702	15047	235
703	15049	236
704	15051	236
705	15052	237
706	15053	237
707	15055	238
708	15056	238
709	15058	239
710	15060	240
711	15061	240
712	15063	240
713	15065	241
714	15066	241
715	15067	242
716	15069	243

Appendix A10 – GC666 1 cm resolution interpolated ages

Depth (cm)	μ (cal. yr BP)	2σ (yr)
717	15070	243
718	15072	244
719	15074	244
720	15076	245
721	15077	245
722	15078	246
723	15080	247
724	15081	247
725	15083	248
726	15085	248
727	15086	249
728	15088	249
729	15090	250
730	15091	250
731	15093	251
732	15094	252
733	15095	252
734	15097	253
735	15099	254
736	15100	254
737	15102	255
738	15104	255
739	15105	256
740	15106	256
741	15108	257
742	15109	258
743	15111	258
744	15113	259
745	15114	259
746	15116	260
747	15118	261
748	15119	261
749	15121	262
750	15122	263
751	15124	264
752	15125	264
753	15127	265
754	15129	265
755	15130	266
756	15132	266

Depth (cm)	μ (cal. yr BP)	2σ (yr)
757	15134	267
758	15134	268
759	15136	268
760	15138	269
761	15139	269
762	15141	270
763	15143	271
764	15144	271
765	15146	272
766	15147	273
767	15148	273
768	15150	274
769	15152	275
770	15153	275
771	15155	276
772	15157	277
773	15158	277
774	15160	278
775	15162	279
776	15163	280
777	15164	280
778	15166	281
779	15168	282
780	15169	282
781	15171	283
782	15173	284
783	15174	284
784	15175	285
785	15177	286
786	15178	286
787	15180	287
788	15182	288
789	15183	288
790	15185	289
791	15187	290
792	15188	290
793	15189	291
794	15191	292
795	15192	292
796	15194	293

Depth (cm)	μ (cal. yr BP)	2σ (yr)
797	15196	294
798	15197	294
799	15199	295
800	15201	296
801	15202	296
802	15203	297
803	15205	298
804	15207	299
805	15208	299
806	15210	300
807	15212	301
808	15213	301
809	15215	302
810	15217	303
811	15218	304
812	15219	304
813	15221	305
814	15222	306
815	15224	307

Appendix A11 – GC666 sediment data

Sample No.	% >63 µm	>63 µm AR (cm^{-2} kyr^{-1})	>250 µm (g^{-1})	>250 µm (cm^{-2} kyr^{-1})
002	NA	NA	2.06	86.30
003	2.48	1.11	0.94	41.77
009	2.19	0.92	1.38	57.73
021	5.75	3.24	2.47	138.96
033	6.17	1.04	3.92	65.78
037	5.42	0.95	1.45	25.33
041	5.58	1.07	9.38	179.24
045	5.20	0.99	1.93	36.87
049	4.70	0.90	0.60	11.47
053	7.06	1.44	4.04	82.41
057	8.47	2.45	9.30	269.06
064	5.15	2.03	1.32	51.97
065	3.98	1.57	0.68	26.93
073	4.48	1.59	0.37	12.96
081	7.76	3.04	4.50	176.39
089	9.55	3.74	3.97	155.74
097	8.81	0.28	5.59	17.63
098	18.29	0.89	11.00	53.61
099	16.52	0.70	15.29	64.99
101	13.11	0.63	5.98	28.64
102	12.52	0.59	4.16	19.66
103	11.92	0.57	4.04	19.19
104	17.52	0.82	7.52	35.16
105	16.65	0.78	2.94	13.85
106	15.56	0.73	4.93	23.15
107	12.36	0.58	3.32	15.63
108	13.80	0.65	5.54	25.92
109	14.68	0.70	6.31	30.09
111	20.10	1.02	28.39	143.97
112	18.60	0.94	43.76	221.89
113	21.86	1.33	57.76	350.90
114	19.50	0.66	73.47	249.78
115	9.76	1.72	40.50	712.74
116	4.70	1.34	7.71	219.59
117	4.21	1.03	4.97	121.29
118	3.85	0.90	3.94	92.53
119	4.30	0.97	3.91	88.37

Sample No.	% >63 µm	>63 µm AR (cm^{-2} kyr^{-1})	>250 µm (g^{-1})	>250 µm (cm^{-2} kyr^{-1})
121	4.97	0.73	13.12	193.30
122	6.32	0.93	8.90	131.12
123	5.96	0.90	13.40	201.17
124	3.51	0.47	6.05	81.32
125	4.29	0.97	1.95	43.89
126	4.56	0.51	1.23	13.83
127	NA	NA	4.84	115.72
135	5.61	1.72	2.12	64.95
143	9.71	3.19	2.67	87.85
151	18.12	7.02	7.99	309.63
159	20.84	8.08	5.42	210.27
167	10.43	4.53	1.34	58.28
175	7.37	2.96	1.75	70.14
183	5.37	1.53	1.49	42.48
191	6.91	1.56	2.18	49.27
199	8.75	4.62	0.41	21.45
211	9.35	5.77	1.92	118.59
223	11.89	7.55	4.62	293.49
235	5.68	3.12	0.48	26.15
247	7.73	3.26	3.61	152.35
255	4.35	1.82	0.67	28.01
263	5.89	2.59	0.79	34.91
271	9.55	4.26	4.84	215.84
279	6.54	3.06	2.81	131.40
287	4.78	2.07	0.36	15.47
295	4.96	2.29	0.66	30.33
303	4.54	2.28	0.00	0.00
311	3.49	1.56	0.00	0.00
319	2.87	1.17	2.34	95.54
324	NA	NA	0.69	83.43
335	6.96	9.24	2.20	291.31
351	5.98	7.13	0.32	38.52
367	6.50	9.54	2.26	332.60
383	3.64	4.50	2.29	282.80
384	7.36	7.23	3.30	324.64
395	5.62	3.39	6.58	397.02
407	4.18	2.46	1.49	87.49

Sample No.	% >63 µm	>63 µm AR (cm^{-2} kyr^{-1})	>250 µm (g^{-1})	>250 µm (cm^{-2} kyr^{-1})
419	4.76	2.71	2.76	157.28
431	15.25	9.50	30.04	1871.9
443	12.33	8.82	21.95	1568.9
445	NA	NA	23.22	1659.9
455	11.07	7.93	35.30	2528.9
467	2.60	1.71	3.73	244.99
479	4.74	2.50	9.41	496.05
491	2.12	2.22	7.23	756.51
504	2.29	1.32	4.58	264.64
516	1.44	8.15	1.57	889.29
576	2.58	11.33	1.59	698.23
640	1.33	5.46	9.23	3776.1
704	2.05	7.80	2.98	1130.4
768	2.20	10.39	4.15	1962.4

Appendix A12 – GC666 organic geochemistry data

Sample No.	% Carbon	C_{org} AR (g cm^{-2} kyr^{-1})	C:N	$\delta^{13}C_{org}$ (‰ VPDB)
002	1.01	0.42	6.87	-22.96
003	1.09	0.49	6.97	-23.06
007	0.97	0.41	7.07	-22.87
009	0.97	0.40	7.10	-23.11
011	1.01	0.45	7.15	-22.91
015	0.98	0.43	7.16	-22.81
019	0.90	0.40	7.17	-22.79
021	0.73	0.41	7.35	-23.15
023	0.77	0.43	7.38	-22.91
027	0.87	0.49	7.29	-22.94
031	0.82	0.56	7.34	-22.90
033	0.88	0.15	7.33	-22.97
035	0.80	0.16	7.42	-22.99
037	0.79	0.14	7.55	-23.38
039	0.75	0.13	7.45	-22.86
041	0.72	0.14	7.53	-23.45
043	0.82	0.16	7.43	-23.05
045	0.69	0.13	7.47	-23.90
047	0.85	0.16	7.40	-23.63
049	0.70	0.13	7.65	-24.03
051	0.67	0.13	7.63	-23.84
053	0.68	0.14	7.54	-24.15
055	0.74	0.17	7.83	-23.84
057	0.81	0.23	7.70	-24.04
059	0.80	0.30	7.72	-23.94
063	0.60	0.24	7.62	-23.66
064	0.90	0.36	7.44	-23.34
065	0.75	0.29	7.46	-23.68
067	0.76	0.30	7.48	-23.52
071	0.80	0.28	7.55	-23.45
073	0.68	0.24	7.67	-23.63
075	0.75	0.27	7.53	-23.32
079	0.73	0.26	7.55	-23.19
081	0.61	0.24	7.66	-23.56
083	0.65	0.24	7.87	-23.37
087	0.71	0.28	7.89	-23.34
089	0.63	0.25	7.63	-23.47

Sample No.	% Carbon	C_{org} AR (g cm^{-2} kyr^{-1})	C:N	$\delta^{13}C_{org}$ (‰ VPDB)
091	0.75	0.32	7.85	-23.31
095	0.84	0.46	8.25	-23.34
097	0.79	0.02	7.70	-22.78
098	0.72	0.04	7.70	-22.85
099	0.69	0.03	8.24	-23.03
101	0.63	0.03	7.95	-22.94
102	0.69	0.03	7.99	-22.80
103	0.71	0.03	8.16	-22.71
104	0.66	0.03	7.99	-22.99
105	0.69	0.03	7.92	-22.93
106	0.66	0.03	8.09	-22.84
107	0.66	0.03	8.19	-22.76
108	0.65	0.03	7.84	-22.96
109	0.62	0.03	7.86	-23.00
111	0.61	0.03	8.47	-22.93
112	0.68	0.03	8.11	-23.20
113	0.75	0.05	7.93	-23.17
114	0.77	0.03	7.94	-23.63
115	0.93	0.16	8.27	-23.92
116	0.98	0.28	7.82	-24.08
117	0.94	0.23	7.92	-24.13
118	0.93	0.22	7.87	-24.22
119	1.01	0.23	8.11	-24.03
121	0.89	0.13	8.01	-24.67
122	0.88	0.13	7.96	-24.67
123	0.98	0.15	8.12	-24.69
124	0.94	0.13	7.92	-24.84
125	0.87	0.20	7.58	-24.74
126	1.17	0.13	7.72	-24.82
127	0.99	0.24	7.92	-24.65
131	0.95	0.29	7.74	-24.62
135	0.99	0.30	7.98	-24.22
139	1.01	0.31	8.00	-23.80
143	0.89	0.29	8.05	-23.82
147	0.83	0.27	8.10	-23.90
151	0.66	0.26	8.38	-24.15
155	0.70	0.28	8.37	-24.30

Sample No.	% Carbon	C_{org} AR ($g\ cm^{-2}\ kyr^{-1}$)	C:N	$\delta^{13}C_{org}$ (‰ VPDB)
159	0.65	0.25	8.18	-24.11
163	0.68	0.29	8.07	-24.01
167	0.74	0.32	7.96	-23.78
171	0.70	0.27	8.12	-23.84
175	0.89	0.36	7.77	-23.48
179	0.94	0.38	7.78	-23.29
183	0.91	0.26	7.85	-23.14
187	0.87	0.28	7.90	-23.49
191	0.80	0.18	7.87	-23.76
192	0.93	0.43	7.85	-23.61
195	0.87	0.46	7.86	-23.64
199	0.80	0.42	7.89	-23.74
203	0.80	0.42	7.62	-23.56
207	0.81	0.46	7.76	-23.48
211	0.72	0.44	7.75	-23.39
215	0.89	0.55	7.70	-23.20
219	0.82	0.51	7.65	-23.00
223	0.76	0.48	7.78	-22.78
227	0.84	0.53	7.73	-22.72
232	0.82	0.45	7.86	-22.94
235	0.90	0.50	7.71	-22.73
239	0.95	0.49	7.77	-22.62
243	0.87	0.77	7.70	-22.74
247	0.68	0.29	7.86	-23.01
251	0.84	0.34	7.81	-22.85
255	0.90	0.38	7.78	-22.72
256	0.83	0.35	8.92	-22.75
258	0.84	0.37	7.80	-22.84
263	0.88	0.39	7.78	-22.98
267	0.89	0.39	7.83	-22.93
271	0.78	0.35	7.89	-23.12
275	0.69	0.29	8.15	-23.29
279	0.77	0.36	8.07	-23.31
283	0.82	0.37	8.11	-23.23
287	0.81	0.35	8.00	-23.12
291	0.74	0.34	8.11	-23.20
295	0.80	0.37	8.09	-23.02
299	0.76	0.37	8.01	-23.03

Sample No.	% Carbon	C_{org} AR ($g\ cm^{-2}\ kyr^{-1}$)	C:N	$\delta^{13}C_{org}$ (‰ VPDB)
303	0.88	0.44	8.08	-22.85
307	0.81	0.39	8.18	-22.75
311	0.84	0.38	8.09	-22.73
315	0.84	0.36	8.04	-22.85
319	0.84	0.34	8.13	-22.83
323	0.90	0.33	8.21	-22.57
324	0.89	1.07	8.01	-22.31
327	0.91	1.10	8.01	-22.45
332	0.71	0.94	8.29	-22.60
335	0.73	0.97	7.79	-22.70
339	0.67	0.89	8.41	-22.68
343	0.71	0.99	8.24	-22.56
347	0.78	1.09	7.89	-22.30
351	0.68	0.81	7.60	-22.80
355	0.54	0.65	7.65	-23.35
358	0.56	0.66	7.82	-23.39
363	0.47	0.69	7.80	-23.55
367	0.57	0.83	7.74	-23.45
371	0.60	0.77	7.84	-23.60
375	0.58	0.73	7.77	-23.54
379	0.57	0.73	8.04	-23.50
383	0.52	0.64	7.85	-23.57
384	0.66	0.65	8.10	-23.40
387	0.60	0.59	7.93	-23.51
391	0.65	0.39	7.77	-23.47
395	0.66	0.40	7.80	-23.49
399	0.70	0.42	7.80	-23.40
403	0.62	0.36	7.92	-23.48
407	0.68	0.40	7.66	-23.38
411	0.70	0.40	7.89	-23.28
415	0.75	0.43	7.62	-23.34
419	0.67	0.38	8.05	-23.43
423	0.62	0.36	7.84	-23.28
427	0.69	0.40	7.71	-23.19
431	0.51	0.32	8.24	-23.44
435	0.48	0.30	8.31	-23.33
439	0.51	0.32	8.21	-23.28
443	0.61	0.44	8.08	-23.22

Sample No.	% Carbon	C_{org} AR ($g\ cm^{-2}\ kyr^{-1}$)	C:N	$\delta^{13}C_{org}$ (‰ VPDB)
445	0.45	0.32	8.65	-23.23
447	0.50	0.35	8.13	-23.33
451	0.62	0.44	7.84	-23.16
455	0.66	0.48	7.81	-23.03
458	0.64	0.46	7.90	-23.08
463	0.76	0.50	7.93	-22.92
467	0.70	0.46	7.90	-22.97
471	0.83	0.44	7.98	-22.93
475	0.73	0.39	8.02	-22.96
479	0.74	0.39	7.79	-22.96
483	0.73	0.39	7.76	-22.95
487	0.76	0.41	7.64	-23.12
491	0.79	0.83	7.68	-23.16
495	0.76	0.79	7.79	-23.03
497	0.76	0.79	7.68	-23.42
504	0.84	0.48	7.81	-23.50
508	0.86	0.50	7.75	-23.17
512	0.87	4.90	7.81	-23.52
516	0.80	4.53	7.86	-22.93
576	1.02	4.49	7.98	-22.54
640	1.07	4.38	8.18	-22.87
704	1.19	4.52	7.87	-22.66
768	1.27	5.99	7.63	-22.10

Appendix A13 – GC666 biogenic silica data

Sample No.	BSi (wt. %)	BSi AR ($g\ cm^{-2}\ kyr^{-1}$)
003	21.45	9.57
009	24.53	10.26
021	23.85	13.44
033	15.39	2.58
037	19.39	3.40
041	16.73	3.20
045	16.34	3.12
049	17.48	3.34
053	18.07	3.68
057	10.13	2.93
064	10.33	4.08
065	17.24	6.80
073	16.58	5.88
081	7.79	3.05
097	6.20	0.20
098	7.54	0.37
101	7.52	0.36
102	6.06	0.29
104	4.94	0.23
105	8.62	0.41
107	6.08	0.29
108	3.41	0.16
111	8.07	0.41
112	5.71	0.29
114	6.95	0.24
115	15.85	2.79
117	18.18	4.44
118	15.68	3.68
121	16.86	2.48
122	9.85	1.45
124	16.25	2.18
125	14.54	3.27
129	17.13	4.86
135	14.45	4.42
151	3.94	1.53
159	11.90	4.61
175	19.43	7.80

Sample No.	BSi (wt. %)	BSi AR ($g\ cm^{-2}\ kyr^{-1}$)
183	17.02	4.84
199	18.36	9.68
211	8.40	5.18
235	15.19	8.36
247	6.89	2.90
255	6.91	2.89
256	8.91	3.73
271	6.25	2.79
279	8.96	4.19
295	5.03	2.32
303	8.96	4.49
319	5.72	2.33
324	8.17	9.81
351	9.57	11.40
367	7.95	11.68
385	9.60	9.44
395	8.71	5.25
419	12.04	6.85
431	6.53	4.07
445	6.72	4.81
455	7.89	5.65
479	9.51	5.01
491	8.69	9.09
515	16.39	92.64
576	14.04	61.70
640	18.06	73.92
704	21.90	83.18
768	19.60	92.69

Appendix A14 – GC666 foraminiferal stable isotope data

Sample No.	Benthic $\delta^{13}C$ (‰ VPDB)	Benthic $\delta^{18}O$ (‰ VPDB)	Evidence for alteration?	Planktonic $\delta^{13}C$ (‰ VPDB)	Planktonic $\delta^{18}O$ (‰ VPDB)	Evidence for alteration?
002	-0.22	3.76	N	0.73	2.96	N
003				1.05	3.07	N
009	1.01	4.62	N	1.20	3.07	N
021	0.56	3.80	N			
033	0.28	3.99	N			
037	-0.05	3.88	N			
041	0.53	3.93	N			
045	0.32	3.76	N			
049	-0.39	4.03	N			
053	0.35	3.89	N			
057	0.08	3.83	N			
064	0.71	3.91	N			
065	0.77	3.84	N			
073	0.77	4.20	N			
081	0.06	3.95	N			
089	0.74	3.85	N			
097	0.41	3.79	N			
098	0.54	3.89	N			
099	0.82	3.90	N			
102	-1.31	3.92	N			
112	0.25	3.64	N			
113	0.70	3.79	N	0.89	3.13	N
114	0.58	3.87	N			
115	0.21	3.84	N			
116	0.43	3.82	N			
117	0.22	3.85	N			
118	0.34	3.71	N			
119	0.51	3.77	N			
121	0.03	3.75	N			
122	0.27	3.82	N			
123	0.47	3.93	N			
124	0.54	4.11	N	0.93	2.89	N
125	0.21	3.98	N	0.00	3.34	N
126	-0.23	3.70	N			
127	0.22	3.86	N	0.83	2.71	N
143	0.47	4.06	N	0.96	2.96	N
151	0.81	3.91	N	0.78	3.03	N
159	0.34	3.85	N	0.86	3.07	N

Sample No.	Benthic $\delta^{13}C$ (‰ VPDB)	Benthic $\delta^{18}O$ (‰ VPDB)	Evidence for alteration?	Planktonic $\delta^{13}C$ (‰ VPDB)	Planktonic $\delta^{18}O$ (‰ VPDB)	Evidence for alteration?
167	0.17	3.87	N			
175	0.35	3.95	N	0.39	3.26	N
183	0.37	3.88	N			
191	0.07	3.86	N			
199	0.00	3.89	N			
211	-0.50	3.87	Y	-6.78	3.51	Y
223	-2.10	4.24	Y	-5.02	3.44	Y
235	0.75	4.22	N			
247	0.40	4.13	N	-3.20	3.07	N
255	-1.53	4.13	Y	-8.69	3.71	Y
256	-6.33	4.26	Y			
263	-4.60	4.21	Y	-6.97	3.83	Y
271	-1.26	4.13	Y			
279	-1.96	4.14	Y			
287	-5.64	4.08	Y			
295	-3.34	4.14	Y	-10.77	3.88	Y
303	-2.95	4.16	Y	-6.34	3.33	Y
311	-4.44	4.46	Y	-8.17	3.91	Y
319	-2.94	4.70	Y	-8.48	3.81	Y
324	-3.80	4.27	Y			
335	-3.47	4.43	Y			
351	-0.34	4.16	Y			
367	-6.32	4.64	Y	-10.37	4.47	Y
383	-2.16	4.69	Y			
384	-4.02	4.70	Y			
395	-2.82	4.86	Y			
407	-3.38	4.85	Y	-11.43	4.32	Y
419	-2.44	4.75	Y			
431	-6.35	5.11	Y			
443	-3.03	4.91	Y			
455	-3.85	5.03	Y			
467	-0.09	5.14	?			
479	-0.31	4.95	N			
504	-7.90	5.66	Y			
516	-1.62	5.03	N	-2.99	3.76	Y
576	-0.76	5.13	Y	0.19	3.59	Y
640				0.89	4.15	N
704	1.07	4.98	Y	3.74	4.30	Y

Appendix A15 – GC666 alkenone data

Sample No.	$C_{37:4}$ area	$C_{37:3}$ area	$C_{37:2}$ area	% $C_{37:4}$	$U^{k'}_{37}$	SST (Muller et al., 1998)	SST (Sikes et al., 1997)
003	29396	4360151	488382	0.60	0.10	1.72	4.81
009	NA	397938	37956	NA	0.09	1.31	4.45
021	14358	2488732	238533	0.52	0.09	1.32	4.46
032	4322	467222	53351	0.82	0.10	1.77	4.85
037	15635	2103808	243442	0.66	0.10	1.81	4.89
041	5265	742244	77595	0.64	0.09	1.53	4.65
045	15300	2064452	184736	0.68	0.08	1.16	4.32
049	2721	335472	29128	0.74	0.08	1.09	4.26
053	7338	839151	82400	0.79	0.09	1.38	4.51
058	5804	693700	67834	0.76	0.09	1.37	4.50
065	10825	1765228	197656	0.55	0.10	1.72	4.81
073	5560	933403	93339	0.54	0.09	1.42	4.55
081	12536	2393837	268066	0.47	0.10	1.72	4.81
089	NA	163902	19172	NA	0.10	1.84	4.91
096	6770	982338	114028	0.61	0.10	1.82	4.89
099	6375	665079	79292	0.85	0.11	1.89	4.96
101	6072	632420	82642	0.84	0.12	2.17	5.20
102	7513	755151	91928	0.88	0.11	1.96	5.01
103	3874	341053	52830	0.97	0.13	2.73	5.69
104	4796	617910	87510	0.68	0.12	2.43	5.42
106	3154	415857	56327	0.66	0.12	2.28	5.30
107	3345	381995	47900	0.77	0.11	2.04	5.09
108	3896	443438	60829	0.77	0.12	2.32	5.33
109	5058	539878	68520	0.82	0.11	2.08	5.12
111	5046	516438	73277	0.85	0.12	2.43	5.43
112	2503	282042	43084	0.76	0.13	2.68	5.65
114	NA	198835	37311	NA	0.16	3.45	6.32
115	NA	31322	4819	NA	0.13	2.71	5.67
119	3501	302361	34009	1.03	0.10	1.73	4.82
121	4016	292056	33009	1.22	0.10	1.74	4.83
122	9280	1086105	116900	0.77	0.10	1.61	4.72
123	1843	156550	22113	1.02	0.12	2.42	5.41
124	12983	1350493	163876	0.85	0.11	1.95	5.01
127	5142	271281	31561	1.67	0.10	1.82	4.90
135	16800	2333377	271618	0.64	0.10	1.83	4.90
143	3365	254811	34374	1.15	0.12	2.27	5.29
151	NA	151296	17759	NA	0.11	1.85	4.92

Sample No.	$C_{37:4}$ area	$C_{37:3}$ area	$C_{37:2}$ area	% $C_{37:4}$	$U^{k'}_{37}$	SST (Muller et al., 1998)	SST (Sikes et al., 1997)
159	NA	28047	3360	NA	0.11	1.91	4.97
167	3418	295561	27186	1.05	0.08	1.22	4.37
175	815	59580	5143	1.24	0.08	1.07	4.25
183	NA	273025	33652	NA	0.11	1.99	5.05
199	NA	7417	925	NA	0.11	2.03	5.08
211	NA	76278	7244	NA	0.09	1.29	4.44
223	NA	7633	900	NA	0.11	1.86	4.93
235	NA	34893	4210	NA	0.11	1.93	4.99
247	NA	14113	NA	NA	NA	NA	NA
255	9274	42387	6625	15.91	0.14	2.76	5.72
263	4760	15872	3429	19.78	0.18	4.05	6.83
271	15306	32061	5034	29.21	0.14	2.78	5.73
279	3209	7099	NA	NA	NA	NA	NA
287	NA	7875	2350	NA	0.23	5.63	8.21
295	NA	7246	NA	NA	NA	NA	NA
303	NA	8236	NA	NA	NA	NA	NA
311	NA	7218	NA	NA	NA	NA	NA
319	NA	4555	NA	NA	NA	NA	NA
324	NA	6500	NA	NA	NA	NA	NA
335	NA	7749	NA	NA	NA	NA	NA
351	NA	8118	NA	NA	NA	NA	NA
367	3738	18472	NA	NA	NA	NA	NA
382	4226	11500	2038	23.79	0.15	3.23	6.12
395	7013	15558	2118	28.41	0.12	2.30	5.31
407	9173	18030	3069	30.30	0.15	3.07	5.99
419	3443	9899	NA	NA	NA	NA	NA
431	1669	4799	NA	NA	NA	NA	NA
443	NA	5110	NA	NA	NA	NA	NA
445	NA	2929	NA	NA	NA	NA	NA
455	NA	NA	NA	NA	NA	NA	NA
467	2986	5776	NA	NA	NA	NA	NA
479	3271	6315	NA	NA	NA	NA	NA
491	NA	NA	NA	NA	NA	NA	NA
504	6659	15887	NA	NA	NA	NA	NA
516	NA	NA	NA	NA	NA	NA	NA
576	12959	17644	NA	NA	NA	NA	NA
640	16152	18012	NA	NA	NA	NA	NA
704	51381	39090	NA	NA	NA	NA	NA
768	8676	12918	NA	NA	NA	NA	NA

Appendix A16 – GC673 1 cm resolution interpolated ages

Depth (cm)	Min. 95% (cal. yr BP)	Max. 95% (cal. yr BP)	Best (cal. yr BP)
16	268	428	341
17	271	430	344
18	275	432	347
19	278	435	349
20	281	438	353
21	285	441	356
22	288	444	359
23	292	447	362
24	296	450	366
25	300	453	369
26	304	456	373
27	308	460	377
28	312	463	381
29	316	467	385
30	321	470	389
31	325	474	393
32	330	478	397
33	334	482	402
34	339	486	406
35	344	490	410
36	349	494	415
37	354	498	420
38	359	503	424
39	364	507	429
40	369	511	434
41	374	516	439
42	379	520	444
43	385	525	449
44	390	530	454
45	395	535	460
46	401	539	465
47	407	544	470
48	412	549	476
49	418	555	481
50	424	560	487
51	430	565	493
52	435	571	498
53	441	576	504
54	447	582	510
55	453	587	516

Depth (cm)	Min. 95% (cal. yr BP)	Max. 95% (cal. yr BP)	Best (cal. yr BP)
56	459	593	522
57	465	598	527
58	471	604	533
59	478	610	540
60	484	616	546
61	490	622	552
62	496	628	558
63	503	633	564
64	509	640	570
65	515	646	577
66	521	652	583
67	527	658	589
68	534	665	596
69	540	671	602
70	547	677	609
71	553	683	615
72	560	690	622
73	566	696	628
74	572	703	635
75	579	709	641
76	585	715	648
77	591	722	655
78	598	729	661
79	604	735	668
80	611	742	675
81	617	749	681
82	623	755	688
83	630	762	695
84	636	769	701
85	642	776	708
86	648	782	715
87	655	789	721
88	661	796	728
89	667	803	735
90	674	810	742
91	680	817	748
92	687	824	755
93	693	831	762
94	699	838	768
95	706	845	775

Depth (cm)	Min. 95% (cal. yr BP)	Max. 95% (cal. yr BP)	Best (cal. yr BP)
96	712	852	782
97	718	859	788
98	724	866	795
99	730	873	802
100	737	880	808
101	743	887	815
102	749	893	822
103	755	900	828
104	761	907	835
105	767	914	841
106	773	921	848
107	779	928	854
108	785	935	861
109	790	942	867
110	796	949	873
111	802	956	880
112	808	963	886
113	813	970	892
114	819	976	898
115	824	983	905
116	829	990	911
117	834	996	917
118	840	1003	923
119	845	1009	929
120	850	1016	935
121	855	1022	941
122	861	1028	947
123	866	1035	952
124	871	1041	958
125	876	1047	964
126	881	1054	969
127	886	1060	975
128	890	1066	980
129	895	1072	986
130	900	1078	991
131	904	1083	997
132	909	1089	1002
133	913	1095	1007
134	917	1101	1012
135	922	1106	1017
136	926	1111	1022
137	930	1117	1027

Depth (cm)	Min. 95% (cal. yr BP)	Max. 95% (cal. yr BP)	Best (cal. yr BP)
138	934	1122	1032
139	938	1127	1037
140	942	1133	1041
141	946	1138	1046
142	950	1143	1050
143	954	1148	1055
144	958	1153	1059
145	962	1158	1063
146	965	1162	1067
147	969	1167	1072
148	972	1171	1075
149	975	1176	1079
150	979	1180	1083
151	982	1184	1087
152	985	1188	1090
153	988	1192	1094
154	991	1196	1097
155	993	1200	1101
156	996	1203	1104
157	999	1206	1107
158	1001	1210	1110
159	1004	1213	1113
160	1006	1216	1115
161	1009	1219	1118
162	1012	1223	1122
163	1016	1227	1126
164	1020	1232	1131
165	1026	1238	1136
166	1031	1244	1142
167	1037	1250	1148
168	1044	1257	1155
169	1051	1265	1162
170	1059	1273	1170
171	1067	1282	1179
172	1076	1291	1188
173	1085	1301	1197
174	1095	1311	1207
175	1106	1322	1218
176	1117	1333	1229
177	1128	1344	1240
178	1140	1356	1252
179	1152	1369	1265

Appendix A16 – GC673 1 cm resolution interpolated ages

Depth (cm)	Min. 95% (cal. yr BP)	Max. 95% (cal. yr BP)	Best (cal. yr BP)
180	1165	1382	1278
181	1179	1396	1291
182	1193	1409	1305
183	1207	1424	1320
184	1222	1439	1335
185	1237	1454	1350
186	1253	1470	1366
187	1269	1486	1382
188	1286	1502	1399
189	1303	1520	1416
190	1321	1537	1433
191	1339	1555	1451
192	1357	1573	1470
193	1376	1592	1488
194	1396	1611	1508
195	1415	1631	1527
196	1436	1650	1547
197	1456	1671	1568
198	1477	1692	1588
199	1499	1712	1610
200	1521	1734	1631
201	1543	1755	1653
202	1566	1777	1675
203	1589	1800	1698
204	1612	1823	1721
205	1636	1846	1744
206	1660	1870	1768
207	1684	1893	1792
208	1709	1917	1817
209	1734	1942	1841
210	1759	1967	1867
211	1785	1992	1892
212	1811	2017	1918
213	1837	2043	1944
214	1864	2069	1970
215	1891	2095	1997
216	1918	2122	2024
217	1946	2149	2051
218	1974	2176	2078
219	2002	2203	2106
220	2031	2231	2134
221	2059	2259	2163

Depth (cm)	Min. 95% (cal. yr BP)	Max. 95% (cal. yr BP)	Best (cal. yr BP)
222	2088	2287	2191
223	2118	2316	2220
224	2147	2345	2249
225	2177	2373	2279
226	2208	2403	2308
227	2238	2432	2338
228	2269	2462	2368
229	2300	2492	2399
230	2331	2522	2429
231	2362	2552	2460
232	2394	2583	2491
233	2426	2614	2523
234	2458	2645	2554
235	2490	2676	2586
236	2522	2708	2618
237	2555	2740	2650
238	2587	2772	2682
239	2620	2803	2714
240	2654	2835	2747
241	2687	2868	2780
242	2720	2900	2813
243	2754	2933	2846
244	2788	2965	2879
245	2822	2998	2912
246	2855	3031	2946
247	2890	3065	2980
248	2924	3098	3013
249	2958	3131	3047
250	2993	3165	3081
251	3028	3199	3116
252	3063	3233	3150
253	3098	3267	3184
254	3132	3301	3219
255	3167	3336	3254
256	3202	3370	3288
257	3237	3404	3323
258	3272	3439	3358
259	3308	3474	3393
260	3343	3508	3428
261	3379	3543	3463
262	3414	3578	3498
263	3449	3613	3534

Depth (cm)	Min. 95% (cal. yr BP)	Max. 95% (cal. yr BP)	Best (cal. yr BP)
264	3485	3648	3569
265	3520	3683	3604
266	3556	3718	3640
267	3592	3754	3675
268	3628	3789	3711
269	3663	3824	3746
270	3699	3860	3782
271	3735	3895	3817
272	3770	3931	3853
273	3806	3966	3889
274	3842	4002	3924
275	3877	4037	3960
276	3913	4073	3995
277	3949	4108	4031
278	3985	4144	4066
279	4020	4179	4102
280	4056	4214	4137
281	4091	4250	4173
282	4127	4285	4208
283	4162	4321	4244
284	4198	4356	4279
285	4233	4391	4314
286	4269	4427	4350
287	4304	4462	4385
288	4339	4498	4420
289	4374	4532	4455
290	4409	4568	4490
291	4443	4603	4525
292	4478	4637	4560
293	4512	4672	4594
294	4547	4707	4629
295	4582	4742	4664
296	4616	4776	4698
297	4650	4810	4732
298	4684	4845	4766
299	4718	4879	4800
300	4752	4913	4834
301	4785	4947	4868
302	4819	4981	4902
303	4852	5015	4935
304	4885	5048	4969
305	4918	5081	5002

Depth (cm)	Min. 95% (cal. yr BP)	Max. 95% (cal. yr BP)	Best (cal. yr BP)
306	4951	5115	5035
307	4984	5148	5068
308	5016	5181	5101
309	5048	5213	5133
310	5080	5246	5165
311	5112	5278	5198
312	5144	5311	5230
313	5175	5343	5261
314	5207	5374	5293
315	5238	5406	5324
316	5269	5437	5356
317	5300	5469	5387
318	5330	5500	5417
319	5360	5531	5448
320	5390	5561	5478
321	5420	5591	5508
322	5449	5622	5538
323	5478	5651	5568
324	5507	5681	5597
325	5536	5710	5626
326	5564	5740	5655
327	5592	5769	5684
328	5620	5797	5712
329	5648	5826	5740
330	5675	5854	5768
331	5702	5881	5795
332	5729	5909	5822
333	5756	5936	5849
334	5782	5963	5876
335	5808	5990	5902
336	5833	6016	5928
337	5858	6042	5953
338	5883	6067	5979
339	5908	6093	6004
340	5932	6118	6028
341	5956	6143	6053
342	5980	6167	6077
343	6003	6191	6100
344	6026	6215	6124
345	6049	6238	6147
346	6071	6261	6169
347	6093	6283	6191

Appendix A16 – GC673 1 cm resolution interpolated ages

Depth (cm)	Min. 95% (cal. yr BP)	Max. 95% (cal. yr BP)	Best (cal. yr BP)
348	6114	6306	6213
349	6135	6327	6235
350	6156	6349	6256
351	6176	6369	6276
352	6196	6390	6297
353	6215	6411	6316
354	6234	6430	6336
355	6253	6450	6355
356	6271	6468	6374
357	6289	6487	6392
358	6306	6505	6410
359	6323	6523	6427
360	6340	6540	6444
361	6356	6557	6461
362	6372	6574	6477
363	6387	6590	6493
364	6402	6605	6508
365	6417	6620	6522
366	6431	6635	6537
367	6445	6649	6551
368	6458	6662	6564
369	6471	6675	6577
370	6483	6689	6590
371	6496	6702	6603
372	6509	6715	6616
373	6521	6728	6629
374	6534	6741	6642
375	6547	6754	6654
376	6559	6767	6667
377	6571	6780	6680
378	6584	6793	6692
379	6596	6806	6705
380	6608	6819	6718
381	6621	6831	6730
382	6633	6844	6743
383	6645	6857	6755
384	6657	6869	6767
385	6670	6882	6780
386	6682	6894	6792
387	6694	6907	6804
388	6706	6919	6816
389	6718	6932	6828

Depth (cm)	Min. 95% (cal. yr BP)	Max. 95% (cal. yr BP)	Best (cal. yr BP)
390	6730	6944	6840
391	6742	6956	6853
392	6753	6968	6864
393	6765	6980	6876
394	6777	6992	6888
395	6789	7004	6900
396	6800	7016	6912
397	6812	7028	6924
398	6824	7040	6935
399	6835	7052	6947
400	6847	7063	6959
401	6858	7075	6970
402	6870	7087	6982
403	6881	7098	6993
404	6892	7110	7005
405	6904	7121	7016
406	6915	7133	7028
407	6926	7145	7039
408	6938	7156	7050
409	6949	7167	7061
410	6960	7178	7073
411	6971	7190	7084
412	6982	7201	7095
413	6993	7212	7106
414	7004	7223	7117
415	7015	7234	7128
416	7026	7245	7139
417	7037	7256	7150
418	7047	7267	7161
419	7058	7278	7171
420	7069	7288	7182
421	7080	7299	7193
422	7090	7310	7203
423	7101	7321	7214
424	7112	7331	7225
425	7122	7342	7235
426	7133	7352	7246
427	7143	7363	7256
428	7153	7373	7267
429	7164	7383	7277
430	7174	7394	7287
431	7185	7404	7298

Depth (cm)	Min. 95% (cal. yr BP)	Max. 95% (cal. yr BP)	Best (cal. yr BP)
432	7195	7414	7308
433	7205	7424	7318
434	7215	7435	7328
435	7225	7445	7338
436	7235	7455	7348
437	7245	7465	7358
438	7255	7475	7368
439	7265	7485	7378
440	7275	7494	7388
441	7285	7504	7398
442	7295	7514	7408
443	7305	7524	7418
444	7315	7534	7428
445	7325	7543	7437
446	7335	7553	7447
447	7344	7562	7457
448	7354	7572	7466
449	7364	7581	7476
450	7373	7591	7485
451	7383	7600	7495
452	7392	7610	7504
453	7402	7619	7514
454	7411	7628	7523
455	7421	7638	7532
456	7430	7647	7542
457	7439	7656	7551
458	7449	7665	7560
459	7458	7674	7569
460	7467	7683	7579
461	7476	7692	7588
462	7486	7701	7597
463	7495	7710	7606
464	7504	7719	7615
465	7513	7728	7624
466	7522	7737	7633
467	7531	7746	7642
468	7540	7755	7650
469	7548	7764	7659
470	7557	7772	7668
471	7566	7781	7677
472	7575	7789	7685
473	7584	7798	7694

Depth (cm)	Min. 95% (cal. yr BP)	Max. 95% (cal. yr BP)	Best (cal. yr BP)
474	7593	7807	7703
475	7601	7815	7711
476	7610	7824	7720
477	7619	7832	7728
478	7627	7840	7737
479	7636	7849	7745
480	7644	7857	7754
481	7653	7865	7762
482	7661	7873	7770
483	7670	7881	7779
484	7678	7890	7787
485	7687	7898	7795
486	7695	7906	7803
487	7703	7914	7812
488	7711	7922	7820
489	7720	7930	7828
490	7728	7938	7836
491	7736	7946	7844
492	7744	7953	7852
493	7752	7961	7860
494	7760	7969	7868
495	7768	7977	7876
496	7776	7985	7884
497	7784	7992	7891
498	7792	8000	7899
499	7800	8007	7907
500	7808	8015	7915
501	7816	8022	7922
502	7824	8030	7930
503	7832	8037	7938
504	7839	8045	7945
505	7847	8052	7953
506	7855	8060	7960
507	7863	8067	7968
508	7870	8074	7975
509	7878	8081	7983
510	7885	8089	7990
511	7893	8096	7997
512	7900	8103	8005
513	7908	8110	8012
514	7915	8117	8019
515	7923	8124	8027

Depth (cm)	Min. 95% (cal. yr BP)	Max. 95% (cal. yr BP)	Best (cal. yr BP)
516	7930	8131	8034
517	7937	8138	8041
518	7945	8145	8048
519	7952	8152	8055
520	7959	8159	8062
521	7966	8166	8069
522	7974	8172	8076
523	7981	8179	8083
524	7988	8186	8090
525	7995	8193	8097
526	8002	8199	8104
527	8009	8206	8111
528	8016	8213	8118
529	8023	8220	8125
530	8031	8226	8132
531	8037	8233	8138
532	8044	8239	8145
533	8051	8246	8152
534	8058	8252	8158
535	8065	8259	8165
536	8072	8265	8172
537	8078	8271	8178
538	8085	8278	8185
539	8092	8284	8191
540	8098	8290	8198
541	8105	8297	8204
542	8112	8303	8211
543	8118	8309	8217
544	8125	8315	8223
545	8131	8322	8230
546	8138	8328	8236
547	8144	8334	8242
548	8151	8340	8249
549	8157	8346	8255
550	8163	8352	8261
551	8170	8358	8267
552	8176	8364	8273
553	8183	8370	8280
554	8189	8376	8286
555	8195	8382	8292
556	8201	8387	8298
557	8207	8393	8304

Depth (cm)	Min. 95% (cal. yr BP)	Max. 95% (cal. yr BP)	Best (cal. yr BP)
558	8213	8399	8310
559	8219	8405	8316
560	8225	8411	8322
561	8232	8416	8328
562	8237	8422	8334
563	8244	8428	8339
564	8250	8434	8345
565	8255	8439	8351
566	8261	8445	8357
567	8267	8451	8363
568	8273	8457	8368
569	8279	8462	8374
570	8285	8468	8380
571	8291	8473	8385
572	8297	8478	8391
573	8302	8484	8397
574	8308	8489	8402
575	8314	8495	8408
576	8319	8500	8413
577	8325	8505	8419
578	8330	8511	8424
579	8336	8516	8430
580	8341	8521	8435
581	8347	8527	8441
582	8352	8532	8446
583	8358	8537	8451
584	8363	8542	8457
585	8368	8548	8462
586	8374	8553	8467
587	8379	8558	8473
588	8385	8563	8478
589	8390	8568	8483
590	8395	8573	8488
591	8401	8578	8494
592	8406	8584	8499
593	8411	8589	8504
594	8417	8594	8509
595	8422	8599	8514
596	8427	8604	8519
597	8432	8609	8524
598	8437	8614	8529
599	8442	8619	8534

Depth (cm)	Min. 95% (cal. yr BP)	Max. 95% (cal. yr BP)	Best (cal. yr BP)
600	8448	8623	8539
601	8453	8628	8544
602	8457	8633	8549
603	8463	8638	8554
604	8468	8643	8559
605	8472	8648	8564
606	8477	8653	8569
607	8482	8657	8574
608	8487	8662	8578
609	8492	8667	8583
610	8497	8671	8588
611	8501	8676	8593
612	8506	8681	8598
613	8511	8686	8602
614	8515	8690	8607
615	8520	8694	8612
616	8525	8699	8616
617	8529	8703	8621
618	8534	8707	8626
619	8539	8712	8630
620	8543	8717	8635
621	8548	8721	8639
622	8552	8726	8644
623	8557	8730	8648
624	8561	8734	8653
625	8566	8739	8657
626	8570	8743	8662
627	8575	8747	8666
628	8579	8752	8671
629	8583	8756	8675
630	8588	8761	8680
631	8592	8765	8684
632	8596	8769	8688
633	8600	8774	8693
634	8605	8778	8697
635	8609	8782	8701
636	8613	8786	8706
637	8617	8791	8710
638	8621	8795	8714
639	8625	8799	8718
640	8629	8804	8723
641	8633	8808	8727

Depth (cm)	Min. 95% (cal. yr BP)	Max. 95% (cal. yr BP)	Best (cal. yr BP)
642	8637	8812	8731
643	8642	8816	8735
644	8646	8820	8739
645	8649	8824	8743
646	8654	8828	8748
647	8657	8832	8752
648	8661	8837	8756
649	8665	8841	8760
650	8669	8845	8764
651	8673	8849	8768
652	8677	8853	8772
653	8681	8857	8776
654	8685	8861	8780
655	8688	8865	8784
656	8692	8869	8788
657	8696	8873	8792
658	8699	8877	8796
659	8703	8881	8800
660	8707	8885	8804
661	8711	8889	8808
662	8714	8893	8811
663	8718	8897	8815
664	8722	8900	8819
665	8726	8904	8823
666	8729	8908	8827
667	8733	8912	8831
668	8736	8916	8834
669	8740	8920	8838
670	8743	8923	8842
671	8747	8927	8846
672	8751	8931	8849
673	8754	8935	8853
674	8758	8939	8857
675	8761	8943	8861
676	8765	8946	8864
677	8768	8950	8868
678	8772	8954	8872
679	8775	8958	8875
680	8778	8961	8879
681	8782	8965	8883
682	8785	8969	8886
683	8789	8972	8890

Depth (cm)	Min. 95% (cal. yr BP)	Max. 95% (cal. yr BP)	Best (cal. yr BP)
684	8792	8976	8893
685	8795	8980	8897
686	8798	8983	8901
687	8802	8987	8904
688	8805	8991	8908
689	8808	8994	8911
690	8811	8998	8915
691	8814	9001	8918
692	8817	9005	8922
693	8821	9009	8925
694	8824	9012	8929
695	8827	9016	8932
696	8830	9019	8936
697	8833	9023	8939
698	8836	9026	8943
699	8839	9030	8946
700	8842	9033	8949
701	8845	9037	8953
702	8848	9040	8956
703	8852	9043	8960
704	8855	9047	8963
705	8858	9050	8966
706	8861	9054	8970
707	8864	9057	8973
708	8867	9061	8976
709	8870	9064	8980
710	8873	9068	8983
711	8876	9071	8986
712	8879	9075	8990
713	8882	9078	8993
714	8885	9082	8996
715	8888	9085	9000
716	8891	9088	9003
717	8894	9092	9006
718	8897	9095	9009
719	8899	9098	9013
720	8903	9102	9016
721	8905	9105	9019
722	8908	9108	9022
723	8911	9112	9026
724	8914	9115	9029
725	8917	9118	9032

Depth (cm)	Min. 95% (cal. yr BP)	Max. 95% (cal. yr BP)	Best (cal. yr BP)
726	8920	9122	9035
727	8923	9125	9038
728	8926	9128	9042
729	8929	9132	9045
730	8932	9135	9048
731	8935	9138	9051
732	8938	9142	9054
733	8940	9145	9057
734	8943	9148	9061
735	8946	9152	9064
736	8949	9155	9067
737	8952	9158	9070
738	8955	9162	9073
739	8957	9165	9076
740	8960	9168	9079
741	8962	9171	9083
742	8965	9175	9086
743	8968	9178	9089
744	8971	9181	9092
745	8973	9185	9095
746	8976	9188	9098
747	8979	9191	9101
748	8982	9194	9104
749	8985	9198	9107
750	8988	9201	9110
751	8990	9204	9113
752	8993	9207	9117
753	8996	9210	9120
754	8998	9214	9123
755	9001	9217	9126
756	9004	9220	9129
757	9006	9223	9132
758	9009	9226	9135
759	9012	9230	9138
760	9014	9233	9141
761	9017	9236	9144
762	9020	9239	9147
763	9022	9242	9150
764	9025	9246	9153
765	9028	9249	9156
766	9031	9252	9159
767	9034	9255	9162

Depth (cm)	Min. 95% (cal. yr BP)	Max. 95% (cal. yr BP)	Best (cal. yr BP)
768	9036	9258	9165
769	9039	9261	9168
770	9042	9265	9171
771	9044	9268	9174
772	9047	9271	9177
773	9050	9274	9180
774	9052	9277	9183
775	9055	9280	9186
776	9058	9283	9189
777	9060	9287	9192
778	9063	9290	9195
779	9066	9293	9198
780	9068	9296	9201
781	9071	9299	9204
782	9074	9302	9207
783	9077	9305	9210
784	9080	9309	9213
785	9082	9312	9216
786	9085	9315	9219
787	9088	9318	9222
788	9091	9321	9225
789	9093	9325	9228
790	9096	9328	9231
791	9099	9331	9234
792	9101	9334	9237
793	9104	9337	9240
794	9107	9341	9243
795	9109	9344	9246
796	9112	9347	9249
797	9115	9350	9252
798	9118	9353	9255
799	9120	9356	9258
800	9123	9360	9261
801	9126	9363	9264
802	9129	9366	9268
803	9132	9369	9271
804	9134	9372	9274
805	9137	9375	9277
806	9140	9379	9280
807	9143	9382	9283
808	9146	9385	9286
809	9149	9388	9289

Depth (cm)	Min. 95% (cal. yr BP)	Max. 95% (cal. yr BP)	Best (cal. yr BP)
810	9152	9391	9292
811	9155	9394	9295
812	9157	9398	9298
813	9160	9401	9301
814	9163	9404	9304
815	9166	9407	9307
816	9169	9410	9310

Appendix A17 – GC673 sediment data

Sample No.	% >63 µm	>63 µm AR (cm^{-2} kyr^{-1})	>250 µm (g^{-1})	>250 µm (cm^{-2} kyr^{-1})
001	4.15	9.68	14.06	32.82
016	4.05	12.32	10.85	33.02
032	4.60	10.39	36.57	82.51
048	2.55	4.02	NA	NA
064	3.89	5.59	1.05	1.51
080	4.22	5.83	NA	NA
096	2.49	3.09	3.08	3.82
112	3.73	5.53	NA	NA
128	4.68	8.72	40.55	75.59
144	4.41	9.73	NA	NA
160	2.20	6.09	14.77	40.94
176	7.84	6.95	NA	NA
192	5.39	2.89	20.95	11.22
208	4.40	1.66	NA	NA
224	9.28	2.97	3.46	1.11
240	11.38	3.80	NA	NA
256	16.40	5.14	25.81	8.09
272	1.86	0.61	NA	NA
288	4.92	1.31	1.01	0.27
304	8.71	2.55	3.42	1.00
308	12.77	3.81	20.43	6.09
312	14.95	5.99	40.30	16.16
316	18.06	7.44	37.41	15.40
320	31.67	13.43	90.33	38.30
324	45.13	19.79	185.77	81.45
328	38.22	17.40	84.14	38.30
332	29.52	14.38	52.15	25.40
336	22.33	11.40	52.46	26.77
352	14.10	8.71	89.08	55.04
368	13.60	12.38	134.15	122.14
384	5.09	4.32	8.51	7.21
400	3.05	2.87	NA	NA
416	2.33	2.29	7.65	7.54
432	2.83	2.70	NA	NA
448	2.52	2.54	4.39	4.43
464	12.87	13.10	NA	NA
480	3.88	4.84	5.52	6.88
496	3.13	4.36	NA	NA
512	1.97	2.60	3.49	4.60
528	3.39	4.84	NA	NA
544	3.13	4.65	50.30	74.73
560	3.46	5.58	NA	NA
576	2.41	3.91	6.13	9.95
592	1.86	3.55	NA	NA
608	2.91	5.11	35.75	62.87
624	1.85	3.69	NA	NA
640	2.74	6.85	4.50	11.26
656	4.27	11.22	NA	NA
672	3.84	10.26	4.30	11.48
688	2.88	8.59	NA	NA
704	2.87	8.52	1.45	4.33
720	2.07	5.04	NA	NA
736	2.98	10.31	7.80	26.96
752	5.27	18.53	NA	NA
768	3.55	11.43	3.31	10.66
784	2.50	7.59	NA	NA
800	5.56	19.04	6.66	22.81
816	6.57	21.66	NA	NA
832	2.88	8.08	1.02	2.86
848	2.44	7.11	NA	NA
864	2.05	4.63	4.02	9.09

Appendix A18 – GC673 organic geochemistry data

Sample No.	% Carbon	C_{org} AR (g cm^{-2} kyr^{-1})	C:N	$\delta^{13}C_{org}$ (‰ VPDB)
001	0.81	1.89	7.21	-23.12
016	0.75	2.27	7.16	-22.95
032	0.82	1.85	7.27	-22.94
048	0.73	1.15	7.34	-22.86
064	0.61	0.88	7.39	-23.12
080	0.65	0.90	7.33	-22.89
096	0.67	0.83	7.36	-22.68
112	0.61	0.90	7.34	-23.08
128	0.72	1.35	7.61	-22.95
144	0.75	1.65	7.63	-22.81
160	0.87	2.42	7.34	-22.46
176	0.53	0.47	7.90	-22.65
192	0.58	0.31	7.96	-23.16
208	0.78	0.30	7.39	-22.58
224	0.53	0.17	7.72	-23.39
240	0.49	0.16	7.94	-23.73
256	0.42	0.13	8.29	-23.57
272	0.90	0.29	7.65	-22.80
288	0.80	0.21	7.66	-22.55
304	0.68	0.20	7.86	-22.69
308	0.75	0.22	7.69	-22.81
312	0.67	0.27	7.46	-22.99
316	0.58	0.24	7.68	-23.06
320	0.54	0.23	8.12	-23.08
324	0.44	0.19	7.89	-23.19
328	0.55	0.25	7.52	-22.71
332	0.60	0.29	7.45	-22.77
336	0.72	0.37	7.93	-22.67
352	0.60	0.37	8.46	-23.57
368	0.56	0.51	8.37	-23.49
384	0.70	0.59	8.15	-23.59
400	0.70	0.66	8.15	-23.47
416	0.88	0.86	8.10	-23.33
432	0.83	0.79	8.14	-23.61
448	0.72	0.72	8.07	-23.48
464	0.78	0.79	7.78	-23.95
480	0.59	0.74	7.99	-23.78

Sample No.	% Carbon	C_{org} AR (g cm^{-2} kyr^{-1})	C:N	$\delta^{13}C_{org}$ (‰ VPDB)
496	0.68	0.95	7.91	-23.88
512	0.79	1.04	7.60	-23.72
528	0.88	1.25	7.50	-23.56
544	0.71	1.05	7.86	-23.80
560	0.84	1.36	7.74	-24.01
576	0.87	1.42	7.86	-24.45
592	0.75	1.43	7.82	-24.14
608	0.70	1.23	8.12	-24.35
624	0.74	1.48	7.45	-24.47
640	0.78	1.96	7.75	-24.25
656	0.64	1.67	7.84	-23.71
672	0.64	1.71	7.54	-23.52
688	0.64	1.90	7.94	-23.67
704	0.73	2.18	7.41	-23.76
720	0.68	1.67	7.43	-23.77
736	0.65	2.24	7.61	-23.87
752	0.53	1.85	7.75	-24.01
768	0.65	2.08	7.60	-23.86
784	0.65	1.98	7.59	-23.53
800	0.60	2.04	7.86	-23.77
816	0.80	2.62	7.36	-24.35
832	0.80	2.25	7.36	-23.68
848	0.72	2.10	7.61	-23.66
864	0.77	1.74	7.46	-23.56

Appendix A19 – GC673 biogenic silica data

Sample No.	BSi (wt. %)	BSi AR ($g\ cm^{-2}\ kyr^{-1}$)
001	14.85	34.67
032	16.42	37.06
064	14.25	20.48
096	15.69	19.46
128	9.90	18.45
160	16.86	46.74
192	12.52	6.70
224	11.93	3.82
256	9.58	3.00
288	20.53	5.45
320	7.76	3.29
352	8.42	5.20
384	10.76	9.13
416	11.31	11.14
448	11.04	11.13
480	11.68	14.57
512	11.26	14.86
544	13.68	20.33
576	11.93	19.37
608	14.07	24.74
640	12.22	30.55
672	14.72	39.33
704	17.27	51.36
736	11.87	41.03
768	11.47	36.97
800	12.28	42.05
832	16.14	45.28
864	15.30	34.60

Appendix A20 – GC673 foraminiferal stable isotope data

Sample No.	Benthic $\delta^{13}C$ (‰ VPDB)	Benthic $\delta^{18}O$ (‰ VPDB)	Evidence for alteration?
001	0.31	3.86	N
016	0.55	3.79	N
032	0.67	3.89	N
064	0.52	3.84	N
096	0.43	3.85	N
128	0.70	3.90	N
160	0.57	3.81	N
192	0.56	3.77	N
224	0.20	3.77	N
256	0.59	3.87	N
288	0.37	3.75	N
304	0.18	3.72	N
308	0.55	3.77	N
312	0.61	3.69	N
316	0.19	3.64	N
320	0.37	3.80	N
324	0.50	3.72	N
328	0.40	3.64	N
332	0.42	3.70	N
336	0.34	3.67	N
352	-0.78	3.84	N
368	0.05	3.79	N
384	-0.84	3.44	N
416	0.48	3.88	N
448	-0.17	3.48	N
480	0.35	3.85	N
512	-0.99	3.39	N
544	0.18	3.78	N
576	-1.21	3.89	Y
608	-3.21	4.00	Y
640	-0.25	3.78	N
704	-1.92	3.90	N
768	-6.30	4.11	Y
832	-0.92	3.85	N
864	0.01	3.97	N